UNIVERSITY OF CALIFORNIA

Los Angeles

Taming Radicals in the Crystalline Solid State:

Discovery and Total Synthesis of Psychotriadine

A dissertation submitted in partial satisfaction of the

requirements for the degree Doctor of Philosophy

in Chemistry

by

Jordan James Dotson

2020

ABSTRACT OF THE DISSERTATION

Taming Radicals in the Crystalline Solid State:

Discovery and Total Synthesis of Psychotriadine

by

Jordan James Dotson

Doctor of Philosophy in Chemistry

University of California, Los Angeles, 2020

Professor Neil Kamal Garg, Co-Chair

Professor Miguel A. Garcia-Garibay, Co-Chair

This dissertation describes studies on the use of solid-state photochemistry to construct challenging carbon–carbon bonds in alkaloid natural products, as well as a novel methodology to synthesize peripherally functionalized pentiptycenequinones. Solid-state photochemistry represents a promising but underutilized method to assemble the synthetically daunting vicinal quaternary stereocenter motif. This dissertation details the use of this methodology to forge the vicinal quaternary stereocenters present in cyclotryptamine and bis(cyclotryptamine) alkaloids. Additionally, a separate study focusing on the modular construction of pentiptycenequinones with promising materials applications is described.

Chapter One is a perspective on the solid-state Norrish type I photodecarbonylation to assemble vicinal quaternary stereocenters. This chapter describes early, proof-of-concept studies that demonstrate the feasibility of the transformation and details the thermochemical and structural parameters required for ketone substrates. The reaction scope, scalability, and applications in total synthesis are also discussed.

Chapter Two focuses on the evaluation of the solid-state photodecarbonylation reaction to install reverse prenyl moieties on the pyrrolidinoindoline scaffold. These studies include progress toward the total synthesis of debromoflustramine A. Furthermore, a workflow to optimize the physical state of ketone substrates for the photodecarbonylation reaction is also discussed.

Chapters Three and Four describe the use of the solid-state photodecarbonylation reaction to synthesize the bis(cyclotryptamine) alkaloid psychotriadine. These efforts culminated in an understanding of how crystalline substrate conformation influences the success or failure of the photodecarbonylative reaction. Furthermore, this work allowed for the first total synthesis of "psychotriadine", bearing the elusive piperidinoindoline framework. This alkaloid was subsequently identified in the extracts of the flower *Psychotria colorata* suggesting that it is a previously overlooked natural product.

Chapter Five focuses on a modular route to synthesize diverse, octakis-substituted pentiptycenequinone molecules. Our strategy was enabled by a sequential iron-mediated bromination reaction followed by a high-yielding palladium-catalyzed cross-coupling to form eight new C–C bonds. These endeavors enabled the construction of diverse pentiptycenequinone-based structures that could be promising candidates for materials science applications.

The dissertation of Jordan James Dotson is approved.

Ellen May Sletten

Patrick G. Harran

Miguel A. Garcia-Garibay, Committee Co-Chair

Neil Kamal Garg, Committee Co-Chair

University of California, Los Angeles

2020

For my parents, James and Deborah

and for my brother, Noah

TABLE OF CONTENTS

LIST OF FIGURES

CHAPTER ONE

CHAPTER TWO

CHAPTER THREE

CHAPTER FOUR

CHAPTER FIVE

LIST OF SCHEMES

CHAPTER ONE

CHAPTER TWO

LIST OF TABLES

CHAPTER ONE

CHAPTER THREE

CHAPTER FOUR

CHAPTER FIVE

LIST OF ABBREVIATIONS

[H]	reduction
[O]	oxidation
°C	degrees Celsius
Å	angstrom
Ac	acetyl, acetate
AcOH	acetic acid
Ad	adamantyl
AgOAc	silver acetate
APCI	atmospheric pressure chemical ionization
aq.	aqueous
BDE	bond-dissociation energy
Bn	benzyl
Boc	*tert*-butoxycarbonyl
Boc_2O	di-*tert*-butyl dicarbonate
br	broad
Bu	butyl
Bz	benzoyl
calcd	calculated
CAN	cerium (IV) ammonium nitrate
cat.	catalytic
CCDC	Cambridge Crystallographic Data Centre
CT	charge transfer
d	doublet
DART	direct analysis in real time
DDQ	2,3-dichloro-5,6-dicyano-1,4-benzoquinone
DMAP	4-dimethylaminopyridine
DMF	*N*,*N*-dimethylformamide
DMSO	dimethyl sulfoxide
dr	diastereomeric ratio
ee	enantiomeric excess
equiv	equivalent

ESI	electrospray ionization
Et	ethyl
EtOAc	ethyl acetate
g	gram(s)
Glc	glucosyl
h	hour(s)
HRMS	high resolution mass spectroscopy
Hz	hertz
hν	light
i-Bu	isobutyl
i-Pr	isopropyl
IR	infrared (spectroscopy)
isc	intersystem crossing
J	coupling constant
L	liter
LDA	lithium diisopropylamide
LiHMDS	lithium hexamethyldisilazide
m	meta
m	multiplet or milli
M	molecular mass or molarity
m/z	mass to charge ratio
MALDI	matrix-assisted laser desorption/ionization
Me	methyl
MeI	iodomethane
MHz	megahertz
min	minute(s)
mol	mole(s)
MOM	methoxymethyl ether
mp	melting point
MS	molecular sieves
n-Bu	butyl (linear)
NaOAc	sodium acetate
NMO	4-methylmorpholine *N*-oxide
NMO	*N*-methylmorpholine-*N*-oxide

NMR	nuclear magnetic resonance
o	ortho
ORTEP	Oak Ridge thermal ellipsoid plot
p	para
Pd/C	palladium on activated carbon
pH	hydrogen ion concentration in aqueous solution
Ph	phenyl
$PhSO_2Cl$	phenylsulfonyl chloride
Piv	pivaloyl
PMB	4-methoxybenzyl
PPh_3	triphenyl phosphine
ppm	parts per million
ppts	pyridinium *p*-toluenesulfonate
Pr	propyl
pyr	pyridine
q	quartet
quint.	quintet
R_f	retention factor
RP	radical pair
RSE	radical-stabilization energy
s	singlet
sat.	saturated
sext.	sextet
t	triplet
t-Bu	*tert*-butyl
TBS	*tert*-butyldimethylsilyl
TFA	trifluoroacetic acid
THF	tetrahydrofuran
TLC	thin layer chromatography
TMS	trimethylsilyl
TMSOTf	trimethylsiyl triflate
TMSOTf	trimethylsilyl trifluoromethanesulfonate
TOF	time of flight
TPAP	tetrapropylammonium perruthenate
Ts	*p*-toluenesulfonyl (tosyl)

UV	ultraviolet

ACKNOWLEDGEMENTS

One's academic advisor can make or break their graduate career. I owe the incredible five years and the successes that I have had while at UCLA to my two doctoral advisors, Neil and Miguel. Becoming a joint student under your combined mentorship was the best decision that I made throughout my educational process. Miguel, you are one of the most enthusiastic and excitable scientists that I have ever met and were an amazing mentor. You are an eternal optimist and are infinitely curious. Despite the fact that you are the Dean, you've always made time for me and supported me in every endeavor I undertook. Whether it was me coming to your office with an idea to start a photochemistry class, wanting to pursue total synthesis, or even becoming a joint student, you were always supportive and always made time for me. I have learned so much from the way you look at science. You view every problem as an interesting, fundamental question that a physical organic chemist can answer. That is why your students pursue projects ranging from solid-state NMR and amphidynamic crystals to natural product synthesis. Your eternal curiosity is infectious and inspiring. Neil, I cannot imagine having a more attentive and dedicated mentor. In my opinion, there are two key things that you do which make you a fantastic advisor. First, you hold incredibly high standards for every member of your lab (science, presentation, publication, etc.) Second, you spend so much of your own time and effort helping us all to achieve those standards. One (of many) examples of this, was when you took me to breakfast the week before I started writing my NIH F32 fellowship application. Despite your busy schedule, you were aware that I had a lot on my plate. You could have sent an email or texted me and that would have been supportive in and of itself. Instead, you got up early and set aside time to talk me through the process, brainstorm how I could manage my time, prioritize the application documents and also

buy me breakfast. I cannot adequately list or thank you for all of the time and dedication that you spent helping me and pushing me to be a better scientist; you spent countless hours meeting with me, guiding me, and generally helping me even before I was your student. I am truly grateful.

I also want to thank the other two members of my committee who made my education as rich as it was: Ellen and Patrick. Ellen, you welcomed me into your lab, office, lab parties, Superbowl parties, Santa Monica Brew Works visits, and even group Dodgers games throughout my time at UCLA. On more than one occasion when I was facing a difficult decision in graduate school, I knew that you would be there to give me advice and to be a source of support. I was always able to walk into your office without an email warning and you were happy to help me in any way that you could. You were a mentor to me even though I was not your student. Patrick, I have never met anyone with a more encyclopedic knowledge of organic chemistry. Yet somehow you are also an incredible teacher and your ability to convey that knowledge is second to none. Furthermore, you were always willing to help me and lend a hand in my own research challenges. On many occasions, when I was stuck on a problem that had nothing to do with your research, you were happy to set aside the time to discuss the chemistry and give me suggestions. Thank you also for allowing me to TA for your synthesis II course. Playing a role in that class was an absolute blast that was made even more enjoyable by Friday morning bagels.

While I owe much of my graduate education (professional and scientific) to my committee members, I would not have even gotten into graduate school in the first place if it were not for my undergraduate mentors. While I was impacted by many of the faculty at Western Washington University, I want to particularly thank Chris Markworth and Jim Vyvyan. Dr. Markworth, you were the first person to introduce me to organic chemistry. While I was a student in your o-chem lecture classes, you were happy to spend hours answering my long lists of questions and being

patient as I learned the basics. Dr. Vyvyan, you welcomed me into your research group when I was an undergraduate and had absolutely no experience working in a lab. You were the chair of the chemistry department but still found the time to come into lab and teach me how to run a column, set up a reaction, and to "flute" filter paper. You were also there to help me through the grad school application process and give me advice when I started my Ph.D. studies.

I would not have even been in a position to study at UCLA and pursue my Ph.D. if it were not for the love and support of my family back in Washington. Mom, you gave up your own career to homeschool Noah and I and make sure that we had an awesome education. Throughout that process, you always made sure to encourage our curiosity and to make every topic interesting and worthwhile. The most important thing to you was that we knew how to learn and were always interested in the world. You always found ways to work field trips into every vacation and expose us to as much as you could to encourage our curiosity. Dad, as a kid you were always the one I could turn to and ask how things worked. Pistons, camshafts, airplanes, helicopters, propellers, generators, dams, electricity, guns, finances, and just about anything else that I could think of. Some of my best memories growing up were hanging out in the garage and getting your take on how stuff worked. Thank you, Mom and Dad, for raising me and helping me get to where I am today. I love you both.

Noah, growing up we became interested in science together. Despite that we work in dramatically different fields, we maintain the exact same sense of humor, hair, height, and many other attributes. Also, your ability to train cats to hike off leash will never cease to amaze me. I look forward to you visiting me in Salt Lake City. Chad, we have not lived in the same place since high school, yet you have remained one of my closest friends for over ten years now. I know that

whenever I can visit home, I will enjoy spending as much time as I can golfing and hanging out with you. Hopefully, we can eventually live in the same state as one another.

In August of 2015, I flew to Los Angeles with a few suitcases and without knowing anyone or ever having been to the city. Now that I am about to leave, I feel like I am saying goodbye to a second home. The incredible friends that I made during my time in Los Angeles made that possible. I have so many people that have made an impact on my life so, while I cannot list everyone, I'll try to list a few. First and foremost, thank you to the "4235 boys" (Marcus, Vince, and Trevor) for making my lab room a joy to be in. We spent many long hours and late nights in lab and at the hood. Continuous jokes and friendship made those hours a pleasure. Marcus, when we decided to room together despite being in the same lab, I was extremely concerned that both living with you and working with you nonstop would be way too much for any reasonable person to handle. I worried that the grinning for no reason, humming, and general "Wisconsin-ness" might be excessive. Yet, after two years of non-stop interaction, you have somehow become an even better friend. I sincerely enjoyed the book clubs, road trips, cocktail nights, and the occasional "gaslighting." I even forgave you for taking me to a bar with 500+ die-hard Packers fans for the Packers-Seahawks playoff game while I was wearing a Seahawks jersey. I'll miss you when I move to Utah, buddy. Also, we were all glad you introduced Shima to the lab. It has been a pleasure getting to know her. Maly, you were the first person I met at UCLA and the only one willing to go with me to the La Brea Tar Pits the week before starting classes. Since then, we have gone through every phase of grad school together. Your friendship over the last few years has truly been a joy and I look forward to seeing what you do with your career (and life) after we graduate. Also, as long as we know each other, I will never let you live down your explanation of electrophilic aromatic substitution to a class of undergrads. Vince, despite the tiny size of your apartment, you

were always down to host whiskey hour, Liar's Dice, movie night, Beef Wellington cook night, and just about every other group activity. It has been awesome getting to know you and Roxann over the last few years. You also made a great hood buddy. Trevor, it was awesome being friends with you. Also, I have been blown away at how much you have grown as a scientist since you showed up in the summer of 2016. You started with no lab experience in organic chemistry at all, battled a difficult project, and through it all have grown into a very talented "hardcore synth guy." Ieva, I am thrilled that you decided to be the resident computational chemist in the MGG group. You are so skilled at what you do and such a pleasure to work with. To Geeta, Jin, Tim, Vanessa, Xing, Salvador, and Jean Luc: thank you for welcoming me into the lab as a first-year graduate student and always being available to answer questions, show me procedures, or just generally lend a hand.

Equally important to all the people that I worked with in the MGG lab, I also want to thank all of the folks that I had the pleasure of getting to know in the Garg lab. When I joined the group at the end of my second year, everyone truly went out of their way to make me feel welcome. Jacob, Michael, and Rob (aka "The Fellas"), I could not have asked for three better compatriots. Michael, you are always willing to talk about any random chemistry ideas. I had an absolute blast on every Vegas trip and ice-skating outing that you planned. I also had a pretty great time in North Carolina (despite being stranded at the airport overnight). Thank you for teaching me to play craps. Jacob, you are such a good conversationalist and just a generally interesting dude. I especially enjoyed the political discussions that we had into the early hours of the morning in Orlando. Rob, you had the patience to teach me how to run and assign 2D NMR spectra, get grease out of compounds for characterization, and set up my Schlenk with "spaghetti tubes." Thanks for always being willing to help. Logan, it was a blast working with you on photochemistry and total synthesis

when you joined the lab. Also, thank you so much for helping me out with the F32 application process. You were really a lifeline to me for the entire application. Your experience, advice, and encouragement made the whole process so much smoother than it could have been. Veronica, you are a very talented chemist and it has been cool to see you tackle really challenging late stage chemistry after a background of methodology. Tim, you are one of the most enthusiastic and intelligent chemists I know. I cannot wait to see where you go in your career: I am sure it will be outstanding. Sarah, your general enthusiasm and (especially musical enthusiasm) are unmatched. Melissa, I enjoyed getting to know you and James during grad school and I look forward to seeing you start an awesome postdoc. Jason, you are one of the nicest and most generous people I know. You also have insane attention to detail. I don't think I gave a presentation or sent out an important document without you reading it first. I look forward to you visiting me in Utah! Francesca, it was nice working with you and getting to know you. Remember that you are not the only one who Michael refers to as "almost Canadian." Rachel, I have enjoyed getting to know you especially during the many molecule-of-the-month presentations we worked together on. Milauni, although I pick on you regularly, it has been so much fun having you in the lab. You've also grown so much as a chemist through the last two years. Katie, I have overlapped with you for a short while, but you are clearly a smart and talented chemist. Andrew, I am continually impressed with your general knowledge and love for chemistry. It was awesome overlapping with you during the last year or so. Laura, Matt, and Ana, we have only worked together for a short while, but it has been a pleasure getting to know you three. While I cannot list all of the former lab members that impacted me during my time in grad school, I have to mention two. Evan and Eli, you two are both truly exceptional scientists and I looked up to both of you as a grad student. You were both always willing to help, lend advice or encouragement, and generally be great lab mates. I learned so much

by watching how both of you conducted yourselves as scientists and it was a pleasure to have met both of you.

In addition to the people that I got to know through UCLA, I consider myself incredibly fortunate to have met Marcin, Tiran, Donny, Roland, Leon, Sylvia, Aram, Steve, Javi, Anita, and Karo. I have enjoyed all of the various birthday parties, road trips, weddings, and New Year's Eve celebrations that I've been a part of. Marcin, you are an exceptionally smart person and it has been a pleasure becoming friends with you. I hope I can rely on you to eventually give me ethically questionable, but valuable legal advice. Tiran, you made so many trips to Westwood to hang out; I always had such a great time during your visits. Roland, you went out of your way to drop by UCLA on your way home from work on numerous occasions. I always appreciated you making the time to hang out. Leon, somehow you know far more about Salt Lake City than I do. I appreciate your brewery advice and I look forward to having you visit during the winter in your Subaru. Aram and Sylvia, thank you for your friendship and for including me in all of the traditional Armenian celebrations. Karo, your cold brew advice has changed my average level of caffeination for the worse. Despite that, I appreciate the tips. Javi, you are a genuinely nice person and I enjoy talking to you every time we meet. Donny, you have such an interesting career and are an interesting person. I cannot wait to eventually brag to other people that I "know the guy who wrote this movie." Thank you so much to all of you for making Los Angeles feel like home.

Lesya and Slava, both of you welcome me into your home on a regular basis and have invited me to your Thanksgivings, birthday parties, and almost every barbecue you host. Despite the fact that I am always the only one who does not speak Ukrainian or Russian, you always make sure to speak to me in English and translate every conversation for me. Slava, you are an incredible

cook and a warm and generous person. Lesya, you are always kind, inviting, and always welcoming. Thank you both for everything.

Finally, I cannot get through this without thanking my biggest support through this entire process: Nataliya. I cannot even imagine what the last five years would have been like had I not met you. No matter what happened in lab or what kind of setbacks I faced you were a constant source of support and encouragement. You were there to celebrate with me in all of my victories and were also the first one to lift me up in when I faced hardship. Although I can still only say about five words in Ukrainian (and my accent is atrocious) I have enjoyed every bit of Ukrainian culture that you and your family have shared with me. It was a joy bringing you to Washington, flying to see you in Nevada every chance I got, and spending every minute I could with you during your visits to LA. You made even the sketchiest of redeye Greyhound trips to Henderson worth it. Graduate school was a wonderful chapter of my life and I think that is largely because you were in it. Lastly, I am so excited that you succeeded in your own education and I cannot wait to see you start your career as a "real doctor" in just a few short weeks. Thank you for making my time in Los Angeles the joy that it was. I love you.

Chapter One is a version of Jordan J. Dotson, Salvador Perez-Estrada, Miguel A. Garcia-Garibay. *J. Am. Chem. Soc.* **2018**, *140*, 8359–8371. Dotson, Perez-Estrada, and Garcia-Garibay were responsible for writing.

Chapter Two is a version of Jordan J. Dotson, Neil K. Garg, and Miguel A. Garcia-Garibay. Dotson was responsible for the experimental work. Dotson, Garg, and Garcia-Garibay were responsible for writing.

Chapter Three describes unpublished studies. Dotson and Bachman were responsible for experimental work. Dotson, Bachman, Garcia-Garibay, and Garg were responsible for writing.

Chapter Four describes unpublished studies. Dotson and Bachman were responsible for experimental work. Hipwell and Khan were responsible for crystallographic analysis. Liepuoniute was responsible for computational work. Dotson, Bachman, Houk, Garg, and Garcia-Garibay were responsible for writing.

Chapter Five is a version of Vadhera, G. S. Jiang, X.; Dotson, J. J.; Chu, G.; Garcia-Garibay, M. A. *Org. Lett.* **2017**, *19*, 1838–1841. Vadhera, Jiang, Dotson, and Chu were responsible for experimental work. Vadhera, Jiang, Dotson, and Garcia-Garibay were responsible for writing.

These studies were supported by the UCLA Dissertation Year Fellowship.

BIOGRAPHICAL SKETCH

Education:

University of California, Los Angeles, CA

- Ph.D. in Chemistry, anticipated Spring 2020
- Graduate Research Assistant, September 2015 – May 2020
- Current GPA: 3.96/4.0

Western Washington University, Bellingham, WA

- Bachelor of Science in Biochemistry, June 2015
- Undergraduate Research Assistant, January 2014 – June 2015
- Cumulative GPA: 3.56/4.00

Professional and Academic Experience:

Graduate Research Assistant: University of California, Los Angeles, CA

- September 2015 – May 2020, under the direction of Professors Neil K. Garg and Miguel A. Garcia-Garibay
- Completed the first total syntheses of psychotriadine using a key photodecarbonylation reaction to access vicinal quaternary stereocenters in a diastereoselective fashion.
- Discovered the presence of psychotriadine in extracts of the flower *Psychotria colorata.*
- Developed a model for conformational control of reactivity and chemoselectivity for the solid-state photodecarbonylation reaction in the context of alkaloid total synthesis.
- Made progress toward the regiodivergent total syntheses of debromoflustramines A & B.
- Assisted in the development of a divergent strategy for the synthesis of octakis-substituted pentiptycenequinones.

Undergraduate Research Assistant: Western Washington University, Bellingham, WA

- January 2014 – June 2015, under the direction of Professor James R. Vyvyan
- Developed gold(III) catalyzed intramolecular S_N2' cycloetherifications for the diastereoselective synthesis of disubstituted tetrahydropyran and tetrahydrofuran motifs.

Honors and Awards:

- UCLA Majeti–Alapati Dissertation Award, 2020.
- UCLA Dissertation Year Fellowship, 2019.
- ACS Division of Organic Chemistry Graduate Research Symposium, 2019.
- UCLA Research Showcase Travel Award, 2017.
- Western Washington University Award for Research in Organic Chemistry, 2014.
- Western Washington University Chemistry Scholarship, 2015.
- Kaiser-Borsari STEM Scholarship, 2013.

Publications:

6. **Crystalline Control of Reactivity and Selectivity in the Total Synthesis of Psychotriadine.** Jordan J. Dotson, Ieva Liepuoniute, J. Logan Bachman, Vince H. Hipwell, Saeed I. Khan, K. N. Houk, Neil K. Garg, and Miguel A. Garcia-Garibay. *Manuscript in preparation.*

5. **Discovery and Total Synthesis of a Bis(Cyclotryptamine) Alkaloid Bearing the Elusive Piperidinoindoline Scaffold.** Jordan J. Dotson, J. Logan Bachman, Miguel A. Garcia-Garibay, and Neil K. Garg. *Manuscript submitted*.

4. **Evaluation of the Photodecarbonylation of Crystalline Ketones for the Installation of Reverse Prenyl Groups on the Pyrrolidinoindoline Scaffold.** Jordan J. Dotson, Neil K. Garg, and Miguel A. Garcia-Garibay. *Tetrahedron* Just Accepted, DOI: 10.1016/j.tet.2020.131181.

3. **Scalable Synthesis of Vicinal Quaternary Stereocenters via the Solid-State Photodecarbonylation of a Crystalline Hexasubstituted Ketone.** Trevor Y. Chang, Jordan J. Dotson, and Miguel A. Garcia-Garibay. *Manuscript in preparation*.

2. **Taming Radical Pairs in Nanocrystalline Ketones: Photochemical Synthesis of Compounds with Vicinal Stereogenic All-Carbon Quaternary Centers.** Jordan J. Dotson, Salvador Perez-Estrada, and Miguel A. Garcia-Garibay. *J. Am. Chem. Soc.* **2018**, *140*, 8359–8371.

1. **A High-Yielding and Divergent Paradigm for the Synthesis of D2h-Symmetric Octakis-Substituted Pentiptycenequinones.** Geeta S. Vadhera, Xing Jiang, Gong M. Chu, and Miguel A. Garcia-Garibay. *Org. Lett.* **2017**, *19*, 1838–1841.

CHAPTER ONE

Taming Radical Pairs in Nanocrystalline Ketones: Photochemical Synthesis of Compounds with Vicinal Quaternary Stereocenters

Adapted from: Jordan J. Dotson, Salvador Perez-Estrada, Miguel A. Garcia-Garibay.

J. Am. Chem. Soc. **2018**, *140*, 8359–8371.

1.1 Abstract

Here we describe the use of crystalline ketones to control the fate of the radical pair intermediates generated in the Norrish type I photodecarbonylation reaction to render it a powerful tool in the challenging synthesis of sterically congested carbon-carbon bonds. This methodology makes the synthetically more accessible hexasubstituted ketones ideal synthons for the construction of adjacent, quaternary stereocenters. We describe here the structural and thermochemical parameters required of the starting ketone in order to react in the solid state. Finally, the scope and scalability of the reaction and its application in the total synthesis of two natural products are described.

1.2 Introduction

Vicinal quaternary stereocenters (VQSs) represent an important structural motif that is present in numerous secondary metabolites (Scheme 1.1). While their relatively exotic structures tend to attract a great deal of academic attention, little is generally known about their biological

roles as a result of their natural scarcity and their limited synthetic availability. However, there is a growing demand for drug candidates to feature dense stereochemical complexity and low molecular weight. This makes VQSs an appealing motif to explore within the realm of active pharmaceutical ingredients (APIs), as they cover a region of chemical space that has not been widely analyzed because of its inherent inaccessibility.[1] In fact, VQSs are remarkably absent in pharmaceuticals and fine chemicals. Of the 200 top-selling small molecule-based drugs, none contain VQSs, and only 14 bear single quaternary stereocenters.[2] While elegant solutions have been found for the installation of vicinal quaternary stereocenters in the total synthesis of several natural products, a general, scalable and stereoselective methodology remains elusive.[3] To this end, we have shown that solid-state photodecarbonylation of crystalline ketones represents an attractive way to access this challenging functionality. The method relies on a wealth of synthetic tools for the stereoselective preparation of a wide range of ketones[4] (Scheme 1.2, Part 1), their tendency to crystallize, the predictable formation of highly reactive radical-pair intermediates upon photochemical excitation, and the extraordinary preservation of the original ketone stereochemistry in selective bond-forming reactions (Scheme 1.2, Part 2). While reactions in solution are hampered by the numerous side products available to the intermediate radical pairs, we have shown that reactions in crystals can occur with high stereochemical control and in high chemical yields. The key role played by the crystal is to limit the number of reaction pathways by reducing the configurational (statistical) entropy of the reactant and reaction intermediates. It is well known that reactions in crystals are preferred when they feature a minimum of atomic and molecular motion[5]; this phenomenon can be thought of as the crystalline phase "taming" the otherwise highly reactive radical species. In this chapter, we will highlight the development of solid-state photodecarbonylation reaction as a viable synthetic tool, describe a predictive model

for the solid-state reaction based on the structure of the substrate, and describe the use of this approach for the total synthesis of several natural products.

Scheme 1.1. Representative natural products featuring vicinal quaternary stereocenters.

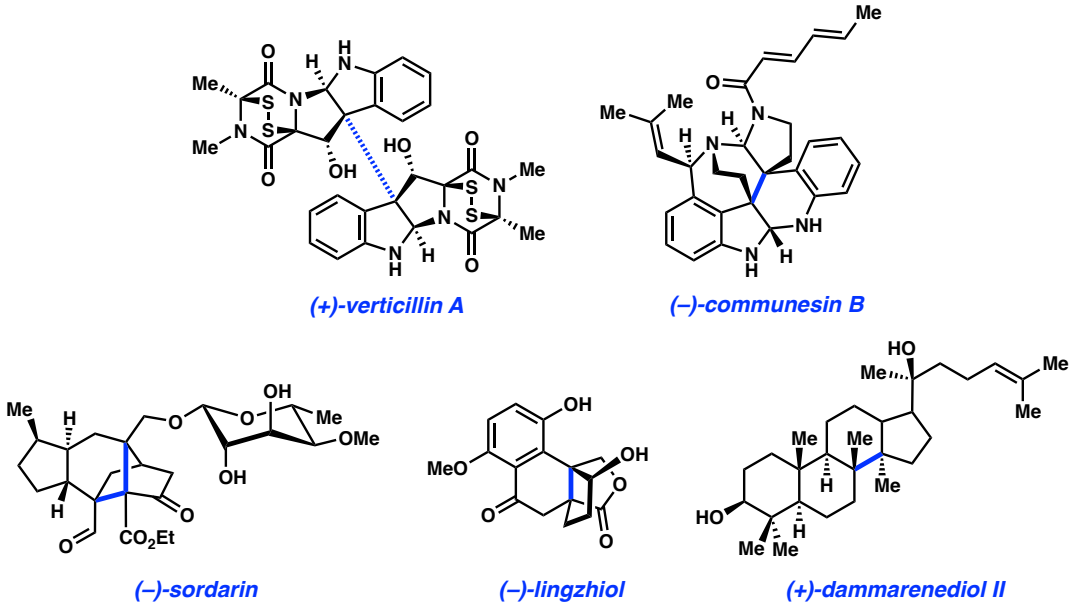

Scheme 1.2. Enantioselective synthesis of hexasubstituted ketones and photodecarbonylation in crystals as a general strategy for the synthesis of vicinal quaternary stereocenters.

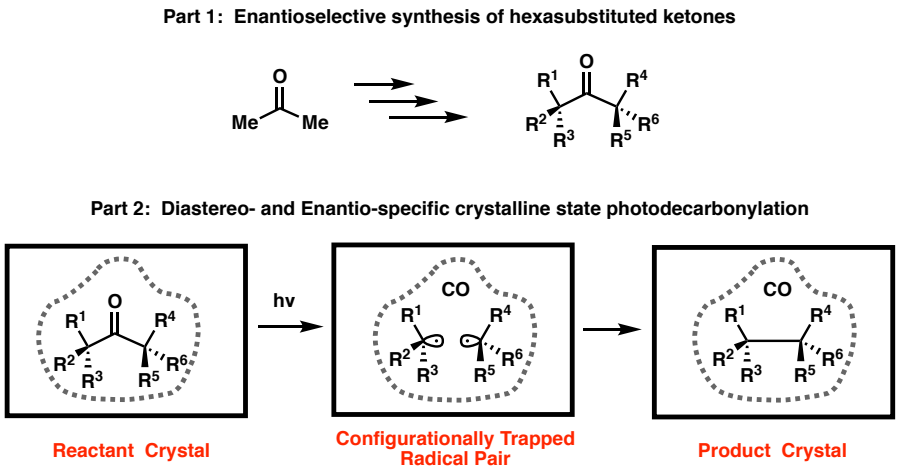

1.3 Free Radicals and Radical Pairs in the Synthesis of Vicinal Quaternary Stereocenters

Though a general and reliable method is not yet available for the synthesis of VQSs, many strategies have been explored, and numerous ad-hoc solutions have been encountered. As elegantly covered by Gong and Yang[3a] and by Overman[3b], examples of successful transformations include the use of intramolecular pericyclic rearrangements, intermolecular Diels-Alder reactions, alkylations of highly reactive nucleophiles and electrophiles, transition metal-catalyzed reactions, photochemical rearrangements, and some radical coupling reactions.[3] Among these, radical coupling reactions represent a particularly promising strategy, as the formation of the hindered bond is made possible by the exothermicity of its bond construction. Given that bond energies are on the order of 60–90 kcal/mol, the potential for overcoming unfavorable steric interactions is probably better by radical coupling than by any other synthon and synthetic disconnection.

The use of radical coupling strategies for the construction of VQSs in the synthesis of natural products in solution has been pioneered by Movassaghi and coworkers.[8,9,10a,11] They selected the C_2-symmetric bis(cyclotryptamine) alkaloids, (+)-chimonanthine **1.4**, (+)-folicanthine **1.5** and (-)-calycanthine **1.6** as test models to explore the synthesis of this structural motif.[6] Their approach was based on a biosynthetically inspired oxidative dimerization of tryptamines.[6b,7] They posited that the C3-C3' bond in these C_2-symmetric structures could be formed by the dimerization of the enantioenriched, benzylic pyrrolidinoindolyl radical **1.2**, where the configuration at the aminal stereocenter would impose a high degree of stereoselectivity and act to preserve the chiral information of the radical (Scheme 1.3). To that end, *tris*(triphenylphosphine)-cobalt(I)chloride [$CoCl(PPh_3)_3$] was shown to effectively reduce the tricyclic bromide **1.1** to the corresponding tertiary benzylic free radical **1.2**, which can subsequently dimerize to afford compound **1.3** in 60% yield and 99% *ee*. With the VQSs set at carbon, C3 and C3', compound **1.3** was then used as a

common intermediate in the synthesis of (+)-chimonanthine **1.4**, (+)-folicanthine **1.5**, and (-)-calycanthine **1.6** (Scheme 1.3).[8,9]

Scheme 1.3. Benzylic pyrrolidinoindolyl radical dimerization for the stereocontrolled synthesis of the C3-C3' quaternary carbons.

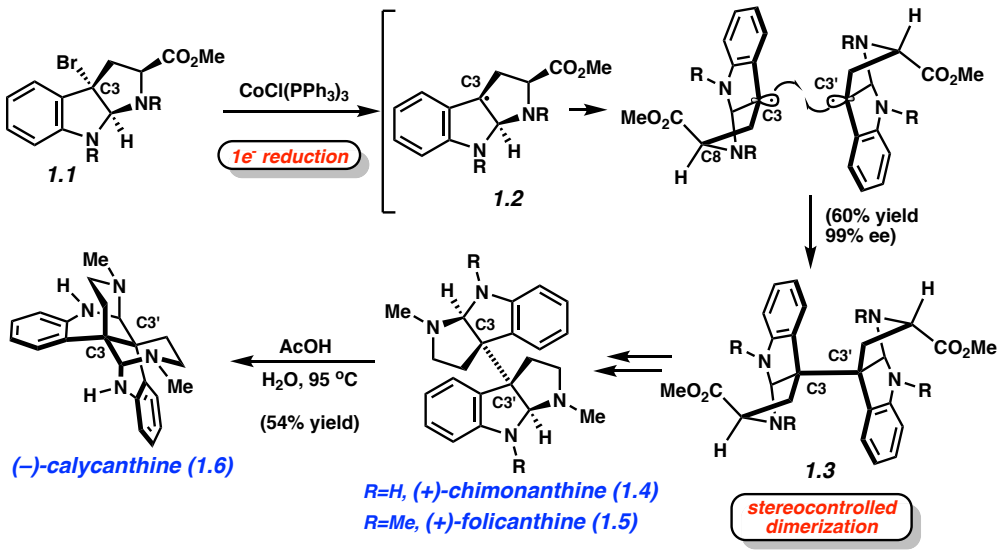

The cobalt-catalyzed radical dimerization strategy could not be extended to the synthesis of heterodimers because of the poor selectivity of heterodimerization versus homodimerization. The combination of free radicals in solution is random and one can generally expect statistical mixtures of the two distinct homocoupling products (25% each) plus the heterocoupling (in ca. 50% yield). In order to circumvent this problem in the total synthesis of (-)-communesin F **1.10**, a diazene precursor that yields a singlet radical pair was synthesized by linking the two indoline halves of the molecule through the two benzylic carbons, which are the target of the intended VQS bond (Scheme 1.4). This strategy was also applied to several related natural products. Ultraviolet irradiation of diazene **1.7** resulted in the expected bond cleavage reaction, furnishing the singlet geminate radical pair **1.8** and molecular nitrogen. The geminate radical pair was shown to recombine to form the heterodimeric coupling product **1.9** in 38% yield, which was subsequently

elaborated to furnish the natural product **1.10** (Scheme 1.4).[8] It should be noted that the key to this process is the geminate recombination of the singlet radical pair to assure high selectivity in the heterodimerization step. As in the cobalt catalyzed benzylic radical homodimerization, the absolute configuration of neighboring stereocenters along with the strain imposed by the *cis*-fusion of the two five-membered rings assures retention of the absolute stereochemistry, an experimental observation that is often referred to as "memory of chirality".[9]

Scheme 1.4. Photodenitrogenation to effect heterodimeric coupling of tertiary benzyl radicals.

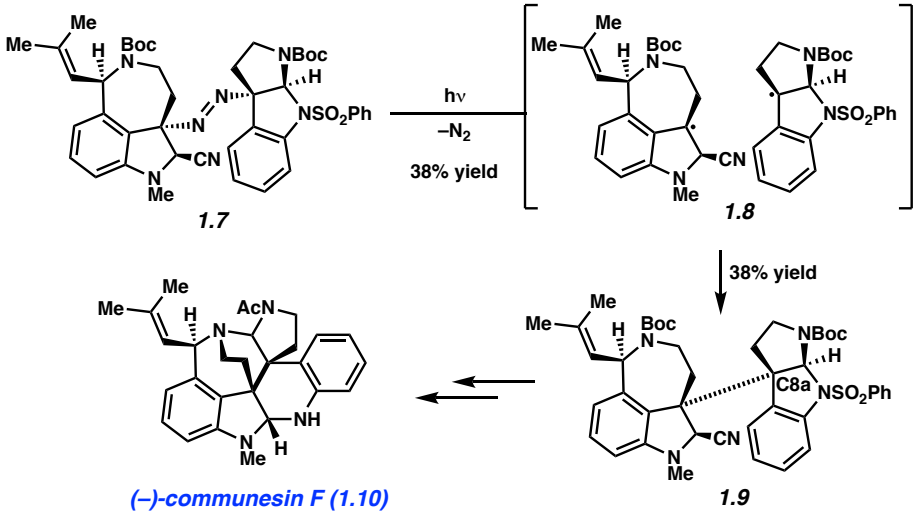

The examples in Schemes 1.3 and 1.4 are impressive and demonstrate the potential of radical coupling for the synthesis of VQSs displaying excellent face selectivity primarily as a result of an excellent substrate design. This includes stereogenic influences by the aminal stereocenter, a strong preference for *cis* ring fusion in the product, and the steric influence of the α-cyano group in the coupling partner (Scheme 1.4).[10] However, intermediates lacking strongly directing stereogenic elements are known to result in complex product mixtures in solution. By contrast, as suggested in Scheme 1.2 and illustrated in the examples below, radical pairs generated in

crystalline solids display highly selective bond-forming reactions where the rigidity of the solid assures an excellent "memory of chirality".[9a,11]

1.4 Engineering Reactions in Crystals Part I: Molecular Information Determines Solid-State Photochemical Reactivity

Part 1 of the synthetic strategy shown in Scheme 1.2, while far from trivial, relies on organic synthesis acumen and a strong intuition developed by trends that arise from thousands of reactions in solution.[12] By contrast, the viability and predictability of Part 2 in Scheme 1.2 have not been widely recognized. To that effect, we have shown that a key consideration in engineering photochemical reactions in crystals[5a] is the selection of excited-state transformations that display a downward staircase energy profile (Scheme 1.5), which is reminiscent of the strategies used by nature in photobiology. In fact, stable molecules that absorb UV or visible light "instantaneously" increase their energy content by 60–90 kcal/mol, which makes the formation of a wide range of reactive intermediates accessible. We have shown that crystals of diazo compounds,[13] diazenes,[14] pyrazolines[15] and triazolines[16] can be exposed to UV light to generate carbenes, dialkyl radical pairs, 1,3-dialkyl biradicals and 1,3-alkyl-aminyl radical pairs, respectively, which can go on to give clean products in the solid state. In the case of crystalline ketones (**K**, Scheme 1.5), excitation to the n,π* excited state followed by intersystem crossing leads to the triplet state ^{3}**K***, which is able to undergo an α-cleavage reaction to form of a triplet acyl-alkyl radical pair (^{3}**RP-1**) with energetics that depend on the radical-stabilizing abilities of the α-substituents (R_1-R_3). The more stable the two radical centers in ^{3}**RP-1**, the more exothermic and efficient the reaction is. The second step depends on the nature of the substituents at the other α-carbon (R_4-R_6) and consists of a second bond-cleavage reaction where the acyl radical loses a CO molecule to form a triplet radical pair ^{3}**RP-2**, which is able to form the desired product after intersystem crossing to the

singlet ^{1}RP-2 (not shown). The reaction occurs along a high-energy profile following the arrows and intermediates shown in green. It must be pointed out that reaction from **^{3}RP-1** to **^{3}RP-2** must be faster than intersystem crossing to ^{1}RP-1 (not shown), which would rapidly go back to the starting ketone as indicated by the blue arrow. It should be noted that the energetic information that determines the reaction is contained in the structure of the starting material and the role of the crystal is simply to control the fate of the highly reactive radical pairs.

Scheme 1.5. Engineering ketone photodecarbonylations in crystals.

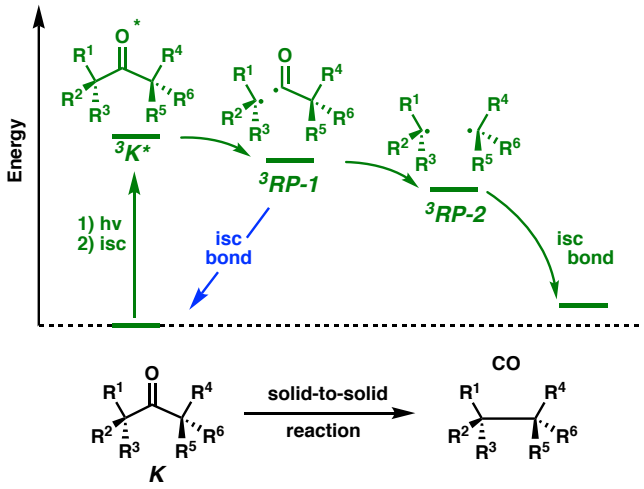

We have shown that energetic profiles such as the one represented in Scheme 1.5 are helpful for reactions to occur in the crystalline state.[17] Due to the absence of collisions, rotations, and conformational motions, reactions in crystals must be nearly barrierless in order to occur. Furthermore, if one considers the Hammond postulate, low barriers and reactant-like transition states are more likely when reactions are highly exothermic, which is often made possible when excited states are 60–90 kcal/mol above the stable reactants and products. Another key consideration comes from the fact that molecular motion and structural changes in the solid state are minimal, implying that changes in entropy do not play a very large role in activation free

energies. We propose that based on these relatively simple considerations, *one should be able to predict reactions in crystals based on simple enthalpic factors*.

In order to develop a general and predictive model for the photodecarbonylation reaction, one can take acetone as a standard and look at the effects of α,α'-substituents on the intermediates along the reaction coordinate (Scheme 1.6). The values indicated in parentheses include the heats of formation for acetone (–51.9 kcal/mol), acetyl and methyl radicals (32.6 kcal/mol), and CO plus two methyl radicals (43.6 kcal/mol) at ambient conditions. The singlet and triplet excitation energies of acetone were added to the ground state value to estimate the heats of formation of the singlet (36.1 kcal/mol) and triplet (28.1 kcal/mol) excited states.

Scheme 1.6. Effect of radical stabilization of the α–substituents on the photodecarbonylation reaction.[a]

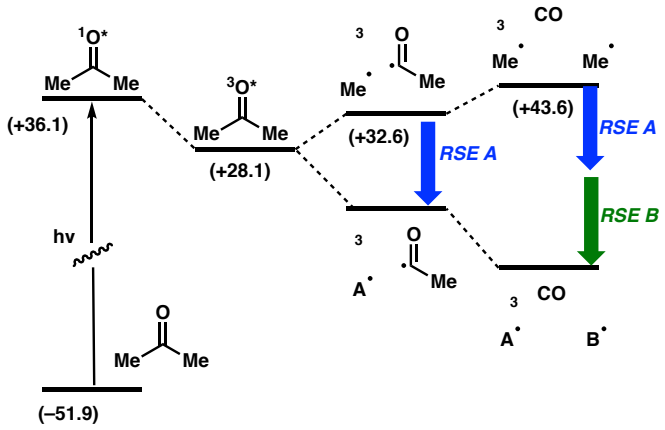

[a] Energy values in parenthesis are in units of kcal/mol.

Analysis of the heats of formation in the photoreaction of acetone in Scheme 1.6 shows that cleavage of the α-bond from the triplet excited state is endothermic by 4.5 kcal/mol, and that the loss of CO from the acetyl radical would be endothermic by 11 kcal/mol. While this makes it difficult for acetone to undergo this reaction in solution, the reaction is virtually impossible in the solid state. Since the loss of CO to form two methyl radicals is the most endergonic step, it is also

the one that determines whether or not the reaction occurs in a crystal. If the loss of CO cannot occur, the alkyl and acyl radicals in **^{3}RP-1** can flip a spin into the singlet **^{1}RP-1** and go back to the starting ketone, as shown by the blue arrow in Scheme 1.5.

Knowing that the excitation energy of substituted acetones do not change appreciably as a function of α-substituents, one should be able predict changes in the relative stability of the acyl-alky and alkyl-alkyl radical pairs. As shown in Scheme 1.6, we will consider the reaction energetics of ketones where the methyl groups of acetone are substituted by groups "A" and "B". For example, an increasing number of methyl groups in the two α-position of acetone leads to ketones where the A and B become ethyl CH_3-CH_2, *iso*-propyl $(CH_3)_2CH$, and *tert*-butyl $(CH_3)_3C$ radicals. The radical stabilization energies [RSE(X)] of these substituents (X), defined as the decrease in the bond dissociation energy of the H-CH_2X bond as compared to H-CH_3, have been documented in the literature. From a small selection of RSE values shown in Table 1.1 one can see that the stabilization provided by one, two or three methyl groups has values of 4.5 kcal/mol, 6.9 kcal/mol and 9.3 kcal/mol, respectively, such that the α-cleavage reaction (relying on RSE-A) should be thermoneutral for ketones with primary α-alkyl substituent (R-CH_2), and slightly exothermic for ketones with secondary or tertiary α-alkyl groups (i.e., R_2CH and R_3C). However, we can predict that even a tertiary α-alkyl substituted radical (RSE-B) would not be sufficient to render the loss of CO exothermic. Based on this hypothesis, one can predict that trialkyl substituted ketones should be photostable in the crystalline state, even when they are known to be highly photoreactive in solution. That is the case of di-*tert*-butyl ketone, which reacts efficiently in solution but it is photostable in the solid state.[18] In fact, we proposed that values of RSE > 11 kcal/mol would be required on both α-carbons for ketones to be reactive in the crystalline state. We also predicted

that the larger the values of the RSE-A and RSE-B, the greater the quantum efficiency of the solid-state reaction.

Table 1.1. Bond dissociation energies (BDE) and radical stabilization energies (RSE) of several α-substituents.

Descriptor	α-substituent(s)	BDE[a] (kcal/mol)	RSE (kcal/mol)
Methyl	—**CH_3**	105.0	—
1ry alkyl	—**CH_2-CH_3**	100.5	4.5
2ry alkyl	—**$CH(CH_3)_2$**	98.1	6.9
3ry alkyl	—**$C(CH_3)_3$**	95.7	9.3
1ry benzylic	—**CH_2-Ph**	88.5	16.5
2ry benzylic	—**$CH(CH_3)$Ph**	85.4	19.6
3ry benzylic	—**$C(CH_3)_2$Ph**	83.5	21.5
2ry-hydoxy-benzylic	—**CH(OH)Ph**	87.5	17.5
3ry-hydroxy-benzilic	—**$C(CH_3)$OHPh**	88.3	16.7
2ry bisbenzylic	—**$CH(Ph)_2$**	84.5	20.5
3ry bisbenzylic	—**$C(CH_3)Ph_2$**	82.8	22.2
1ry enol (ester)	—**CH_2-COOR**	97.1	7.9
2ry enol (ester)	—**CH(Me)COOR**	94.0	11.0
3ry enol (ester)	—**$C(Me)_2$COOR**	92.6	12.4

[a]Defined as the energy difference between the heats of formation of the radical plus that of a hydrogen atom [ΔH_f (R.)] – [ΔH_f (H.)] compared with the heat of formation of the hydrocarbon [ΔH_f (R-H)].

One of the earlier tests of the relationship between radical stabilization and solid-state photoreactivity included a series of acetone diadamantyl esters, **1.11a-e** (Scheme 1.7). These compounds were all crystalline, and by increasing the number of methyl groups on the two α-positions we were able to change the RSE values from –8.9 kcal/mol for **1.11a** to –19.79 kcal/mol for **1.11e**.[19] In order to compare the effect of radical stabilizing substituents, each of these ketones were irradiated in dilute benzene solutions and as fine crystalline powder. In solution, it was observed that, while **1.11a** only showed trace reaction, ketones **1.11b–1.11e** all showed

conversions greater than 80% after 4 hours, but they all produced very complex product mixtures. This lack of selectivity is consistent with the expected chemical behavior of free radicals in solution, where multiple reaction pathways are accessible.

Scheme 1.7. Solid-state photochemistry of several substituted acetone dicarboxylates.

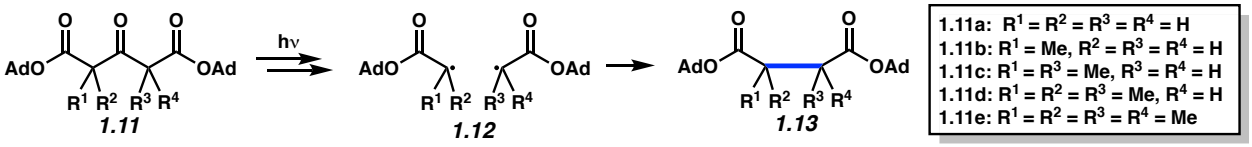

Figure 1.1. Photodecarbonylation reaction of ketones **1.11a-1.11e** as a function time in the solid state (adapted from Ref. 19).

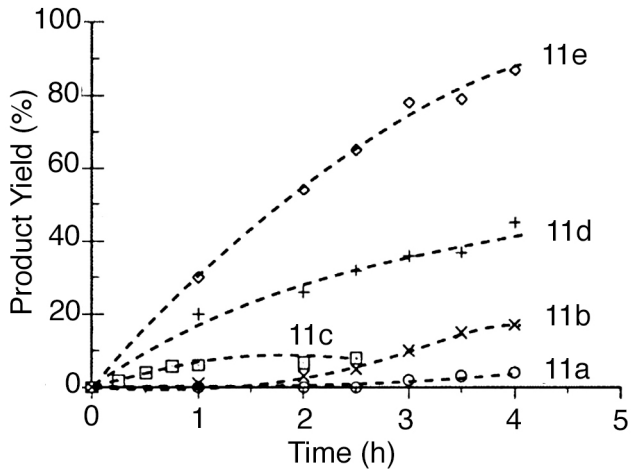

As shown in Figure 1.1, the reactivity of the different crystalline solids varied dramatically. After irradiation for 1h, ketones **1.11e**, **1.11d**, **1.11c**, **1.11b**, and **1.11a** reached 30%, 20%, 6%, 0%, and 0% conversion, respectively (Figure 1.1). Only products corresponding to radical recombination were observed. The lack of reactivity of **1.11b** and **1.11a** was consistent with our hypothesis that the rate of the second α-cleavage (k_{-CO}), and thereby solid-state reactivity, are dependent on substantial radical stabilization on both α-carbons. The more reactive ketones **1.11e** and **1.11d** generated radicals with stabilization energies of –19.79 kcal/mol and –15.07 kcal/mol

respectively. It should be noted that while ketones **1.11a** and **1.11b** showed no observable reaction in the first hour, irradiation for 3h revealed a sigmoidal conversion as a function of time (Figure 1.1). This behavior was attributed to photoreactions occurring at defect sites in the crystal. Additionally, **1.11c** showed a sudden loss of selectivity at around 10-12% conversion, when the melting point decreased and liquids began to form.

1.5 Reaction Homology in Crystal Photochemistry

One of the fundamental principles of organic chemistry is that different functional groups undergo reactions with characteristic mechanisms, rules, and exceptions that translate across a range of structural variations.[20,21] The high level of predictability of these mechanisms provides much of the basis for the organic chemists' "chemical intuition" and allows us to predict reaction outcomes by simple inspection of the molecular structure.

The reliability of our thermochemical hypothesis was first tested with a set of cyclohexanones with various α-phenyl substitution patterns that covered a range of RSE values, which are indicated on the two sides of the carbonyl group in Scheme 1.8.[22] Also shown are the structures of the solid-state photoproducts with a measure of the relative reaction yield values, which are obtained upon exposure to light under identical experimental conditions. It should be pointed out that while all solid-state reactions are chemoselective and stereospecific, reactions in solution yielded mixtures of bond formation and disproportionation products with loss stereochemical information. The only products observed in crystals come from radical-radical bond formation, and the only stereochemistry observed was the one of the reactant. RSE values greater than 11 kcal/mol are indicated in blue and range from 16.7 for tertiary hydroxybenzylic substitution in ketones **1.16** and **1.18** , to 21.5 kcal/mol for quaternary benzylic substituents in ketones **1.17** and **1.19**. α-Phenyl cyclohexanone **1.14** has a reactive α-carbon that forms a

secondary benzylic radical (shown in blue) and an unreactive α-carbon that would form a primary alkyl group, shown in red. While this compound is reactive in solution, it is completely stable in the solid state, suggesting that α-cleavage may occur on the more substituted side, but the endothermic loss of CO in the less substituted side is disfavored. Except for **1.14**, all the compounds in the set are reactive and selective in the solid state. However, there is a reactivity difference of ca. 100-fold between **1.15** (relative yield 0.01) compared to the highly reactive ketone **1.19** (relative yield 1.0), supporting the reactivity models in Schemes 1.5 and 1.6.

Scheme 1.8. Solid-state photochemistry of several phenyl-substituted cyclohexanones.[a]

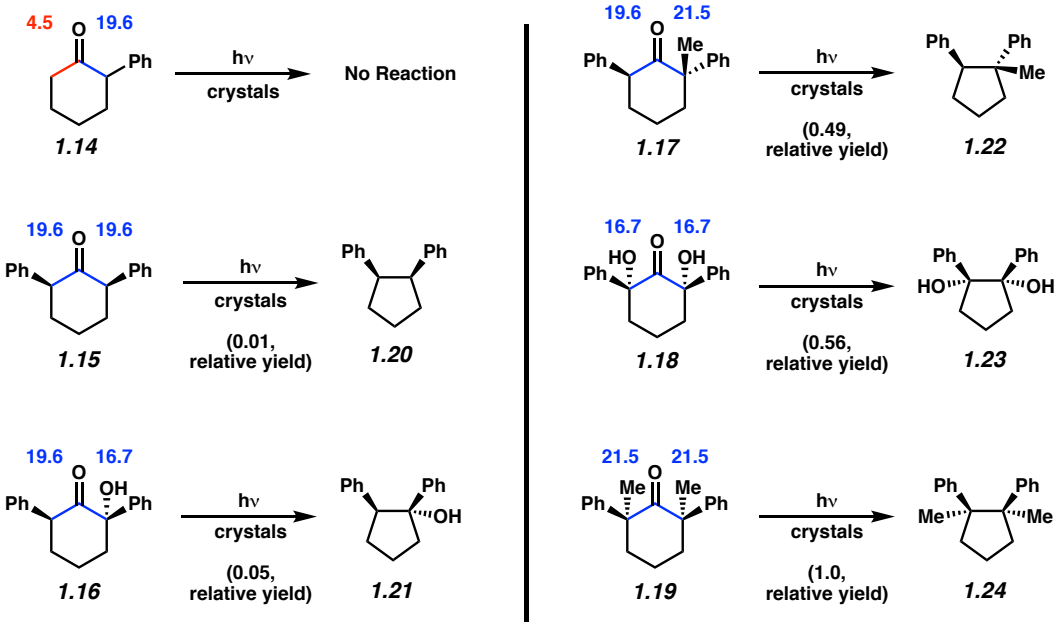

[a]Energy values above α-carbons are in kcal/mol.

Similar observations can be made with the cyclopentanones and 2-indanones in Schemes 1.9 and 1.10, respectively. The importance of having substituents with RSE > 11 kcal/mol is highlighted by observations of ketones **1.25**–**1.27**, all of which are highly reactive and give relatively complex product mixtures in solution. The tetraalkyl substituted ketone **1.25** can

generate tertiary alkyl radicals and, as expected, is reactive in solution but completely stable in the crystalline state. Ketone **1.26** has two phenyl groups in one α-carbon and is expected to undergo the first α-cleavage reaction efficiently by forming a relatively stable tertiary diphenyl methyl radical. However, two methyl groups on the other α-position make the loss of CO difficult and crystals are photostable. Finally, the reaction of tetraphenyl cyclopentanone **1.27** generates tertiary diphenylmethyl radicals in both α-carbons and the reaction goes to completion upon relatively short ultraviolet light exposure times. Notably, the intermediate 1,4-biradical in crystals gives the cyclobutane product **1.28** exclusively, while the solution reaction has a large preference to form 2 moles of 1,1-diphenyl ethylene **1.29** by cleavage of the 3-4 bond. The reaction-enabling effect of α-aryl substituents is related to their ability to stabilize the radical center through π-conjugation. This can be established by comparison of photostable 2-indanone **1.30** in Scheme 1.9 with the photoreactive diastereomeric indanones **1.31** and **1.32**, and the dicumyl ketones in Scheme 1.11. The photostability of crystals of **1.30** is the result of the coplanar orientation of the two aryl-α-sigma bonds, which prevent benzylic delocalization of the radical center formed upon α-bond cleavage. The orthogonal orientation between the aromatic ring π-system and σ-bond orbital prevents electronic communication, such that the corresponding RSE values may be viewed as analogous to those of a tertiary alkyl radical center. By contrast, as reported by Quinkert et al.,[23] crystals of *cis*- and *trans*-1,3-diphenyl-2-indanones **1.31** and **1.32** react efficiently and in a highly stereospecific manner to form the corresponding benzocyclobutanes **1.34** and **1.35**. In a subsequent study, it was shown that α,α-dialkoxy substitution in 2-indanone **1.33** also leads to an efficient solid-state photodecarbonylation to form benzocyclobutane **1.36**.

Scheme 1.9. Solid-state photochemistry of several substituted cyclopentanones.

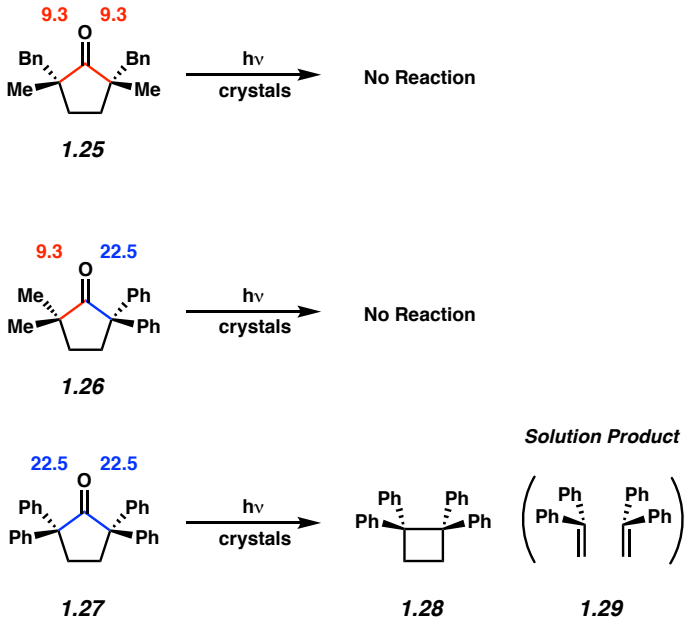

Scheme 1.10. Solid-state photochemistry of 2-indanones.

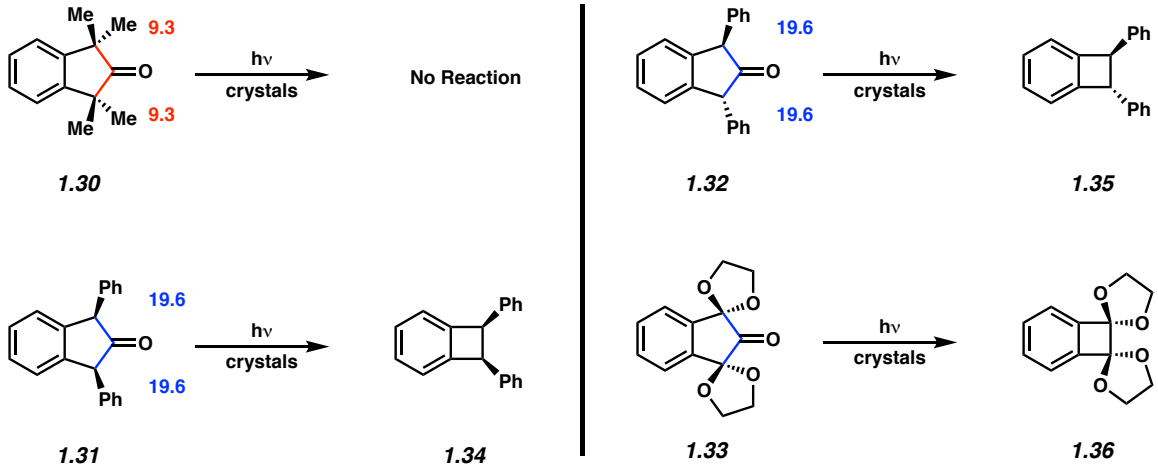

That the solid-state photodecarbonylation reaction is quite general and with reactivity that follows reasonably predictable patterns was also demonstrated with acyclic 2,4-diaryl-substituted-2,4-dimethyl-3-pentanones **1.37a**–**1.37f**. As shown in Scheme 1.11, all the compounds in the set were crystalline solids that reacted in a chemoselective manner to give the corresponding 2,3-diarylbutanes. It should be pointed out that the modest effect of the substituents, with relative

reactivities that range by a factor of ca. 2, is consistent with a radical-mediated process. Furthermore, that the structure of pentanones **1.37** can extend beyond substituted phenyl groups was demonstrated with pentanone **1.38**, which cleanly transforms photochemically into diarylbutane **1.39**.

Scheme 1.11. Solid-state photochemistry of several acyclic 3-pentanones **1.37**.

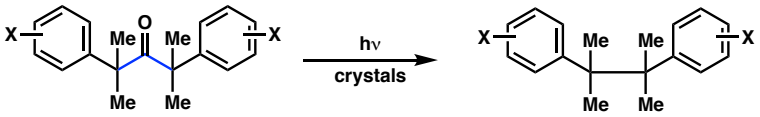

X	Ketone	Relative reactivity
4-H	1.37a	1.0
4-MeO	1.37b	1.55
4-Me	1.37c	1.14
4-F	1.37d	1.05
4-CF_3	1.37e	2.18
3,4-MeO	1.37f	1.08

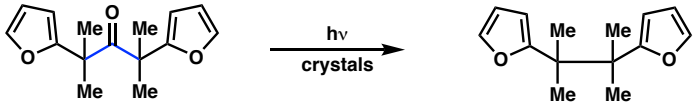

1.38 ***1.39***

The structures in the examples shown in Schemes 1.6–1.11 are limited but give credence to the premise that thermodynamic information can be used to predict whether or not the corresponding crystals are going to be photoreactive. Exceptions should be expected for ketones that have internal quenching mechanisms and/or alternative photochemical pathways that are faster than α-cleavage and the loss of CO. Scheme 1.12 includes some examples that appear to be suitable candidates for a solid-state photodecarbonylation reaction but are not. *Cis*- and *trans*-cyclohexanones **1.40** have phenyl groups at both α-positions along with vinyl and alkyl (benzyl) substituents, which should make them reactive in the solid state. However, while the α-phenyl

groups enable the reaction, it is well known that β-phenyl groups provide a very efficient quenching of the ketone excited state that has been proposed to operate either through an intramolecular charge transfer or a transient radical addition of the triplet ketone to the aryl group followed by ketone reformation.[25b] Thus *cis*- and *trans*- ketones **1.40** are photochemically stable both in solution and in crystals.[24]

Scheme 1.12. Crystalline ketones with quenching or competing pathways that fail to photodecarbonylate.

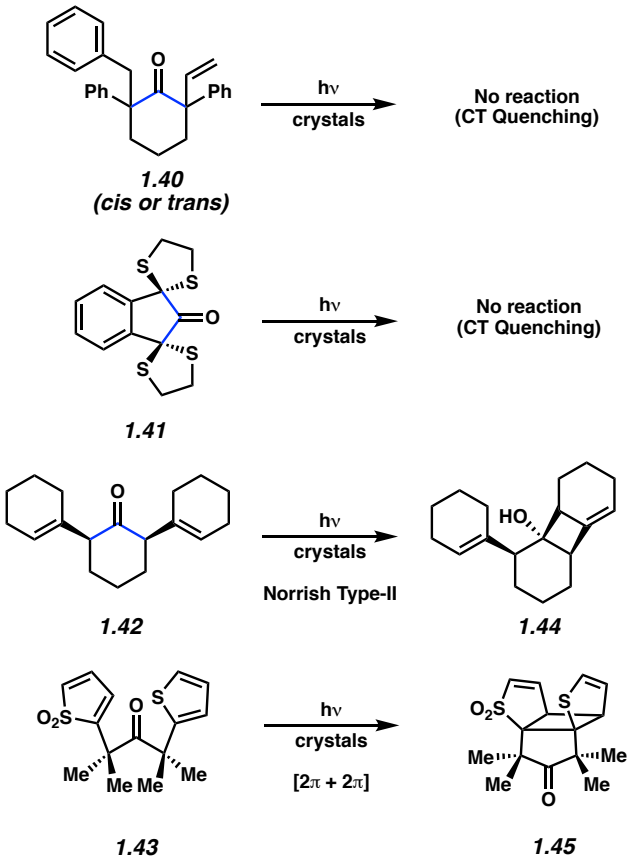

Similarly, while it is well known that α-thioethers are good radical stabilizing substituents and have reactivity similar to that of **1.33**, experiments have revealed that *bis*(thioketal)ketone **1.41** is photostable as a result of a similar intramolecular charge transfer quenching mechanism. With

vinyl groups at the two α-carbons, ketone **1.42** possesses a large RSE of ca. 25.9 kcal/mol. However, in lieu of an α-cleavage reaction, compound **1.42** reacts by a much faster γ-hydrogen transfer reaction to give a 1,4-biradical that closes to give the cyclobutanol **1.44** by a competing Norrish type II photoreaction.[25] Finally, ketone **1.43** flanked with thiophene and thiophene dioxide groups should be reactive towards a photodecarbonylation process, but the two heteroaromatics adopt a parallel orientation that is ideal for a 2π+2π photocycloaddition reaction that leads to quantitative yields of product **1.45**.[26]

1.6 Engineering Reactions in Crystals Part II: Selectivity and Specificity Under Entropic Control

While molecular structure and substituent effects determine whether or not a reaction is possible in the solid state, the selectivity and specificity of the reaction are dictated by the structural characteristic and integrity of the crystal lattice.[5a, 27] While rigidity restricts the translational, rotational, and conformational freedom of excited states and reactive intermediates, crystal homogeneity helps assure that all reaction events occur under the same structural influences, such that reactions in crystals often display the levels of chemo- and stereoselectivity that are commonly observed with enzymes.

To reach the highest possible level of reaction control, one must ensure that reactions take place without melting. In simple terms, the best conditions will occur when both the reactant and the product form high melting crystals, so that reactions can be carried out under ambient conditions. One needs to be mindful of the two-component phase diagram that describes the presence of different solid and liquid phases as a function of temperature and composition, which, in this case, is the reaction progress (Figure 1.2). It is important to recognize that the accumulation of the product can be seen as a growing impurity that depresses the melting point of the pure

reactant [$T_m(R)$], thus following the solid-blue line. While a more detailed description of the changes that take place in a solid-to-solid reaction can be found elsewhere,[17b] suffice it to say that the success of a solid-state reaction relies on the use of temperatures that are below the eutectic point (T_{Eut}, black open circle in Figure 1.2) of the phase diagram, which is the lowest temperature where liquid phases can exist at normal pressure. If we execute our reaction above T_{Eut}, in zone A, our sample will melt, and radical reactions in the liquid will lead to multiple byproducts. By contrast, if we carry out our reaction in zone B, below the eutectic point, and we expose our crystals to UV light at a temperature such as that indicated with a green asterisk (*), we will start with the pure reactant in its own crystal phase, **{R}R**. As the product accumulates the original crystal becomes a solid solution of the product in the crystal of the reactant in the mixed crystal zone indicated as {**R+P**}**R**. Once the solubility limit of the product in the crystal of the reactant is attained at the point indicated with green circle 1, there will be a reconstructive phase transition to the crystal phase of the product **{R+P}P** with a composition that matches the one corresponding to green circle 2. As the reaction continues, the product can be obtained almost pure in its own crystal phase, **{P}P**. Crystal-to-crystal reactions that occur by a reconstructive phase transition are characterized by the destruction of the original crystal of the reactant and the nucleation and growth of the crystal phase of the product in microscopic domains. Single crystals undergoing a reaction by a reconstructive phase transition change from translucent to opaque and their X-ray diffraction changes from that of a single crystal to one of an ordered powdered.

Figure 1.2. Phase diagram of reactant (R) and product (P) as a function of reaction progress.

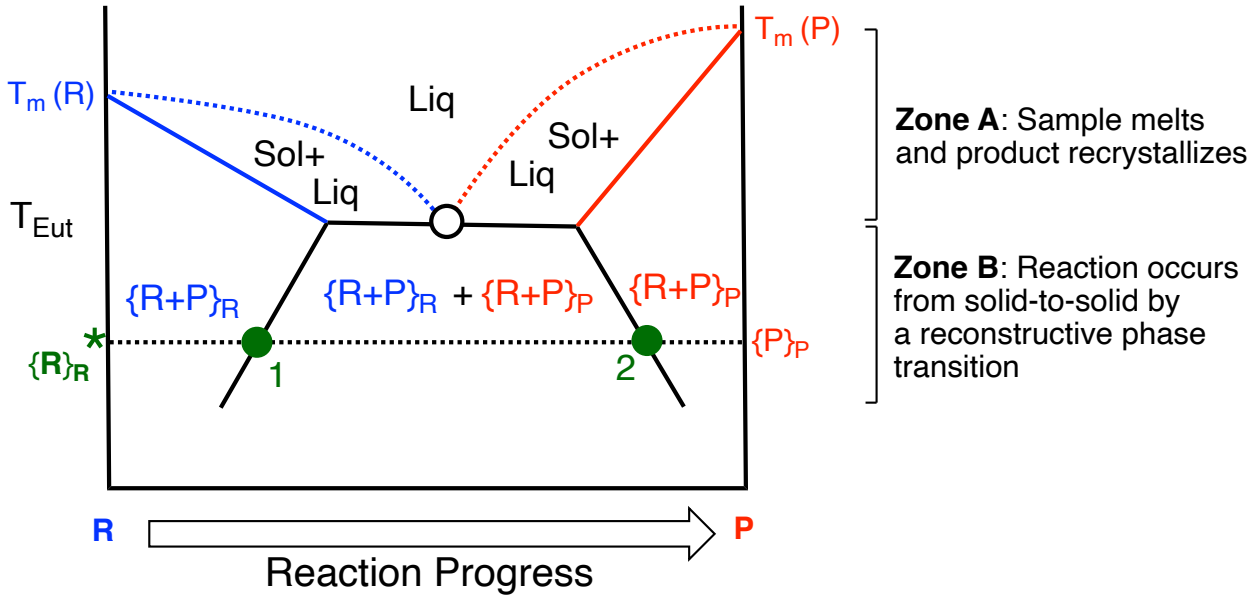

1.7 Reaction Selectivity and Scope

As discussed above, radical pairs generated in close proximity are able to undergo bond-forming reactions that make it possible to target the synthesis of the coveted VQSs (Scheme 1.2). However, a competing reaction that is commonly observed in solution is the disproportionation of the two radicals to give products that are formed by transferring a hydrogen atom that is adjacent to one of the radicals to the other, to form alkane and alkene products (Scheme 1.13). Based on a large number of examples of reactions in crystals where radical combination has been observed, one may conclude that the bond-forming reaction is the path that requires the least amount of atomic and molecular motion. To a rough approximation, the distance between the two α–carbons in a ground state ketone is approximately 2.7Å, which is significantly smaller than the sum of the Van der Waals radii between two carbon atoms (3.4 Å).[14] While the distance between the carbon-centered radical and the hydrogen that would participate in the disproportionation event are often similar, two carbon-centered radicals held at a 2.7 Angstrom distance from one another are likely

already at the steep descent component of the C-C sigma bond potential energy curve. Once the two carbon-centered radicals assume the required singlet state multiplicity, bond formation in the solid state is likely to be a barrierless process.

Scheme 1.13. Example of a radical disproportionation reaction.

Bicyclic ketone **1.46** (Scheme 1.14) was selected to test and challenge the ability of the crystalline phase to control the chemoselectivity of the recombination vs. disproportionation reactions.[28] This compound had been shown to exclusively undergo disproportionation reactions in solution, with the *cis*- and *trans*- isomers of **1.48** observed as the only products (Scheme 1.14).[29] It should be noted that ketone **1.46** was viewed a promising substrate for a solid-state reaction because the carbonyl group is flanked by quaternary carbons with ester groups and have RSE = 12.4 kcal/mol (Table 1.1, tertiary enol, ester), which is more than the required 11 kcal/mol. Furthermore, given that the radicals centers in **BR-2** cannot diffuse apart, one can assign differences in reactivity to the different reaction phases. As expected, when ketone **1.46** was irradiated as a crystalline solid, it formed the recombination photoproduct **1.47** in quantitative yield, suggesting that topochemical considerations play an important role in determining the outcomes of the photodecarbonylation.

Scheme 1.14. Photodecarbonylation of ketone **1.46** in solution and in crystals.

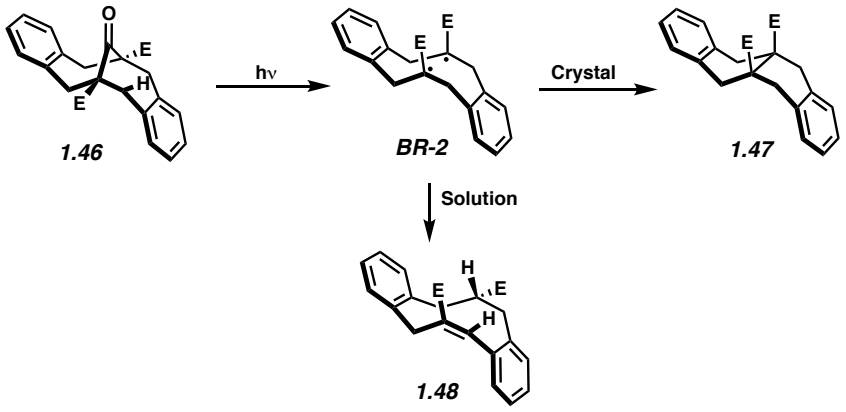

It is expected that an increase in the density of functional groups will result in more reaction pathways that lead to the formation of additional photoproducts. An interesting case that helps address this concern is the photodecarbonylation of the *cis*- and *trans*- 2,6-divinyl substituted ketones **1.49**.[30] As suggested in Scheme 1.15, in addition to the photochemical α-cleavage and decarbonylation reaction leading to an intermediate dialkyl radical pair that can go on to give various modes of radical combination (**1.50**–**1.53**) and disproportionation (**1.54**) reactions. Additionally, excited states of β,γ-unsaturated ketones such as *cis*- and *trans*-**1.49** are prone to undergo 1,3-acyl shifts (**1.55**) and the oxa-di-π–methane rearrangement (**1.56**).[31]

Scheme 1.15. Photochemical reaction pathways available for *cis*- and *trans*- divinyl ketones **1.49** in solution.

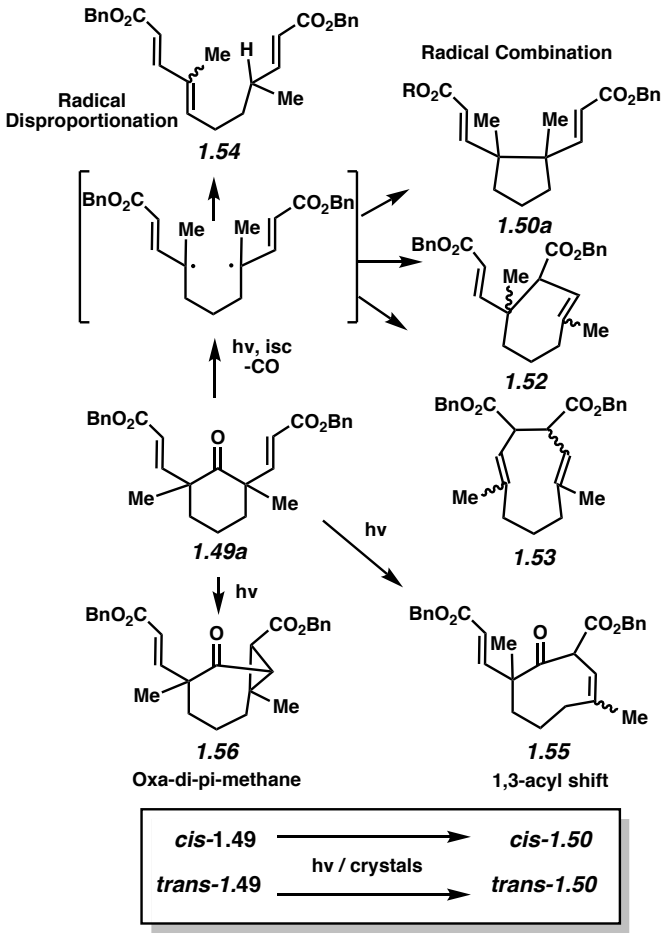

Photochemical experiments carried out in benzene solutions with benzylic esters *cis*-**1.49a** or *trans*-**1.49a** gave complex product mixtures, suggesting that the pathways in Scheme 1.15 (and others) are probably available. In contrast, reactions carried out in the solid state with the same two compounds reacted cleanly to yield exclusively the five membered-ring diesters *cis*-**1.50a** and *trans*-**1.50a** in a highly chemoselective and stereospecific photoreaction. However, high selectivity in these cases was only observed until the reaction had reached ca. 20% conversion. At that point, the solid mixture of reactants and products melted and subsequent reaction gave a complex mixture

similar to that observed in the solution-phase experiments. To facilitate a reaction with higher conversion in the crystalline phase, the benzyl esters were cleaved and the resulting carboxylic acids were converted to the corresponding benzylammonium salts *cis*-**1.49b** and *trans*-**1.49b** by the simple addition of two equivalents of benzyl amine (Scheme 1.16). These organic salts were then irradiated as a crystalline suspensions in hexanes to yield the ring-contraction product in nearly quantitative yield.

Scheme 1.16. Solid-state photochemistry of ketobenzylammonium salts *cis*-**1.49b** and *trans*-**1.49b**.

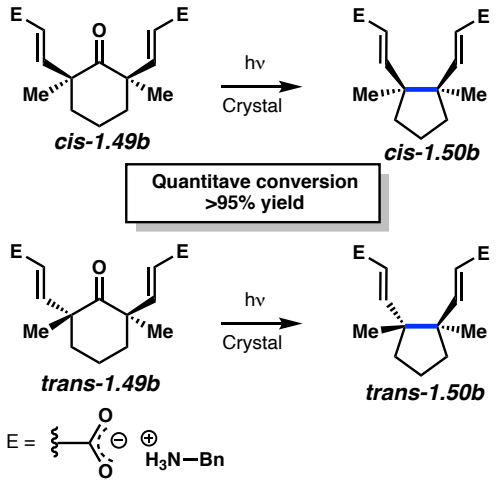

It is well known that stereochemical control of acyclic substrates is more challenging than analogous processes with cyclic structures, in part because the latter tend to have fewer conformations as they are more rigid. One may expect that such a distinction should not play a role in the solid state because the stereochemical control, in this case, comes from the rigidity of the medium. This was confirmed with the photodecarbonylation of C_2 symmetric ketones **1.57a** and **1.57b**, which were investigated both in solution and in the solid state (Scheme 1.17).[32] When irradiated in solution, it was shown that disproportionation does not occur for either substrate and

that the selectivity for two compounds in solution is very similar but not identical, with the *d,l*-**1.58** slightly favored in both cases. By contrast, the selectivity of the photochemical reactions in the crystalline state was dramatically improved, with both ketones proceeding to full conversion and full retention of stereochemistry. This study supports the notion that acyclic ketones may display diastereoselectivities just as high as those of their cyclic counterparts.

Scheme 1.17. Solution and solid-state photochemistry of *C2*-symmetric acyclic ketones.

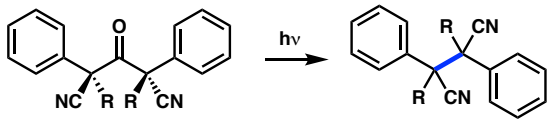

R = Me, 1.57a ***R = Et, 1.57b*** ***R = Me, 1.58a*** ***R = Et, 1.58b***

Ketone	Medium	Conversion	*d,l* -**1.58:** *meso*-**1.58:** Disprop.
d,l- **1.57a**	C_6D_6	99	64 : 35 : 0
	Crystal	100	~100 : 0 : 0
d,l- **1.57b**	C_6D_6	100	53 : 47 : 0
	Crystal	100	~100 : 0 : 0

Considering that the rigidity of the crystal lattice is responsible for the exceptional diastereoselectivity, it would be reasonable to expect crystalline enantiomerically pure ketones with radical stabilizing α-substituents to display a high memory of chirality. To test this hypothesis, enantiomerically pure ketones **1.59** and **1.61** were prepared and their photochemical reactivity was investigated (Scheme 1.18).[33] As expected, solution-phase irradiation afforded complex product mixtures with loss of stereochemical information. However, irradiation in the solid state quantitatively converted the penta-substituted ketone **1.59** to **1.60** in >95% d.r. and ca. 100% e.e., and the hexasubstituted substituted ketone **1.61** to compound **1.62** in ca. 100% d.r. and ca. 100% ee (Scheme 1.18). While these diastereoselectivities were consistent with prior

observations, it was gratifying to confirm that the chirality of the reactant is fully preserved in a manner that resembles enzymatic processes. We feel that the exceptional enantioselectivity of these transformations will render them useful tools for synthetic chemistry.

Scheme 1.18. Solid-state photochemistry of homochiral ketones.

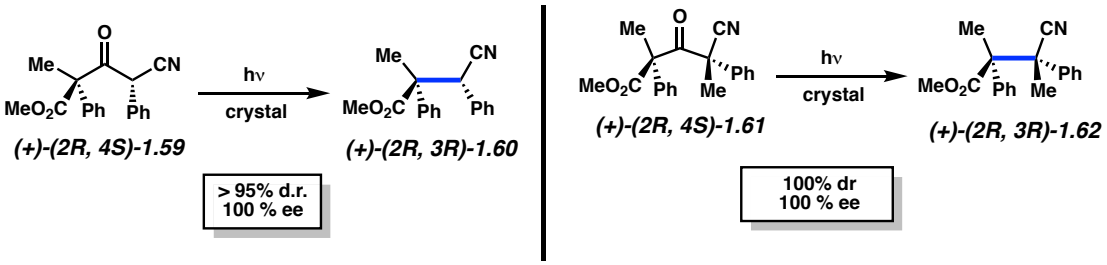

1.8 Scalability and Green Chemistry

In order to take advantage of the promising stereochemical control available from reactions in crystals, it is essential for the reaction to be amenable to multigram and eventually kilogram scale. The main practical challenge for the execution of photochemical reactions in crystalline solids is related to the need to provide at least one photon (and often more depending on the quantum yield), to every molecule in the solid. Since large crystals and dry powders are able to absorb light to a penetration depth that typically reaches only a few microns, we suggested that a possible solution would be the use of crystals that are even smaller, in the range of 100–500 nm. We reasoned that crystals of this size would retain the structural information of the large specimens but allow for the electric field of UV/Visible photons, with the wavelength in the 200–500 nm range, to completely surround an entire nanocrystal. We recognized that this idea could be easily tested by taking advantage of the simple formation of nanocrystalline suspensions in water by the "re-precipitation" method, which has been reported by Nakanishi in 2002.[34] In fact, nanocrystalline suspensions are easy to prepare in many cases by preparing a concentrated solution of the

compound of interest in a water-miscible fluid (acetone, MeCN, THF, EtOH, etc.) and rapidly adding it into stirring water. If the compound loading is high (e.g., 5 g per liter), the resulting suspension has a milky white appearance. Photochemical reactions with nanocrystals can be carried out using the equipment that is commonly used for photochemical reactions in liquids and can be conveniently carried out by immersing the light source into the stirring suspension.[35]

One of the benefits of efficient light penetration into the crystalline material was shown with the solid-state photodecarbonylation of bis(3-thiophenyl) ketone **1.63** (Scheme 1.19). It was discovered that UV irradiation of **1.63** as a bulk powder gave the expected 2,3-dithiophenylbutane **1.64** as the main product, but under various conditions, the reaction was not able to proceed beyond 8% conversion.[36] It was shown that highly absorbing unidentifiable trace impurities generated during the reaction acted as a filter and prevented further exposure of the substrate. When the reaction was conducted as a nanocrystalline suspension in water, however, **1.63** proceeded to **1.64** in quantitative yield. This observation indicates that UV light is indeed available to all the molecules in the nanocrystals.

Scheme 1.19. Dry solid suspension photochemistry of ketone **1.63**.

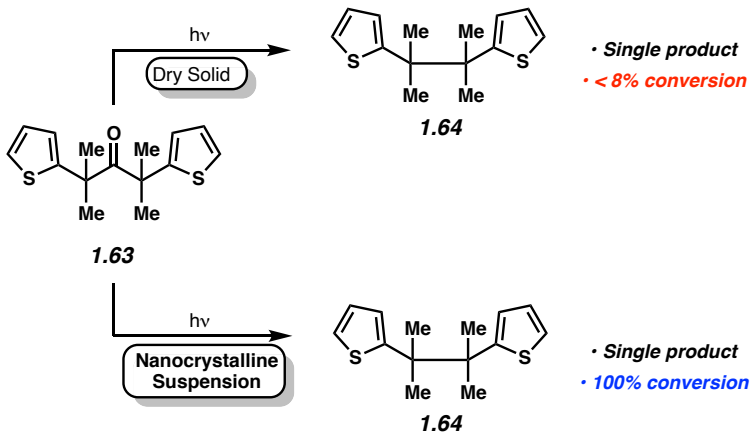

The first example where the scalability of the solid-state reaction was explored involved the photochemistry of readily available dicumyl ketone (DCK) **1.65** (Scheme 1.20). It was confirmed that single crystals and powders of DCK resulted in the highly selective formation of dicumene (DC) **1.66**, but as expected, the reaction occurred with a largely reduced efficiency when compared to reactions in solution.[35b]

Scheme 1.20. Solid-state photodecarbonylation of dicumyl ketone (**1.65**).

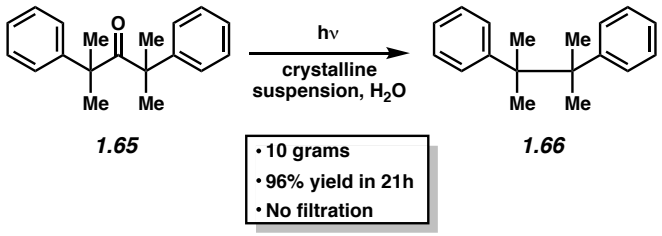

Aqueous suspensions of DCK were generated by the reprecipitation method using a saturated solution in acetone, which was injected in an aqueous solution of sodium dodecyl sulfate (SDS) at submicellar concentrations. Small amounts of surfactant help stabilize the nanocrystals in the suspension, which otherwise tends to aggregate and precipitate. This procedure afforded nanocrystals with sizes in the range of 800–1500 nm, as determined by dynamic light scattering (DLS).[35b] Employing immersion well photoreactors equipped with a Pyrex glass filter (λ>290 nm) and a 400 W medium-pressure Hg lamp, photolysis of stirred suspensions were efficiently scaled up to 10 g by taking advantage of a flow system that consists of a large reservoir and 1 L reactor, where reaction velocities of ca. 0.5 g/h were attained. This reactor featured an 8 L reservoir equipped with a submersible pump which cycled the suspension through a photoreactor (Figure 1.3).[35b]

Figure 1.3. Experimental set up for batch- and stepped-flow preparative-scale solid-state photochemistry using nanocrystalline suspensions.

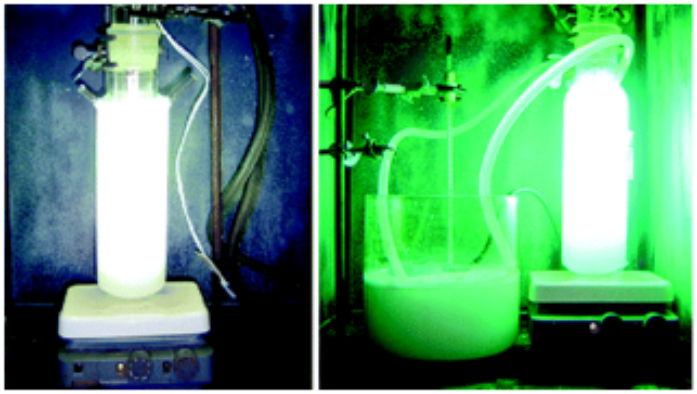

Knowing that the solid-state photodecarbonylation reaction can be executed on multigram scales to generate vicinal quaternary centers, the next test was to conduct a large scale synthesis of a homochiral compound containing VQSs. With that in mind, optically pure ketone (+)-**1.69** was readily prepared in three steps starting from malonic ester **1.67** (Scheme 1.21). Enzymatic hydrolysis/desymmetrization of **1.67** with pig liver esterase (PLE) afforded the enantiomerically pure acid (+)-**1.68**, which was then converted to the corresponding acid chloride, *via* treatment with oxalyl chloride.

Scheme 1.21. Synthesis and crystallization of the homochiral ketone **1.69**.

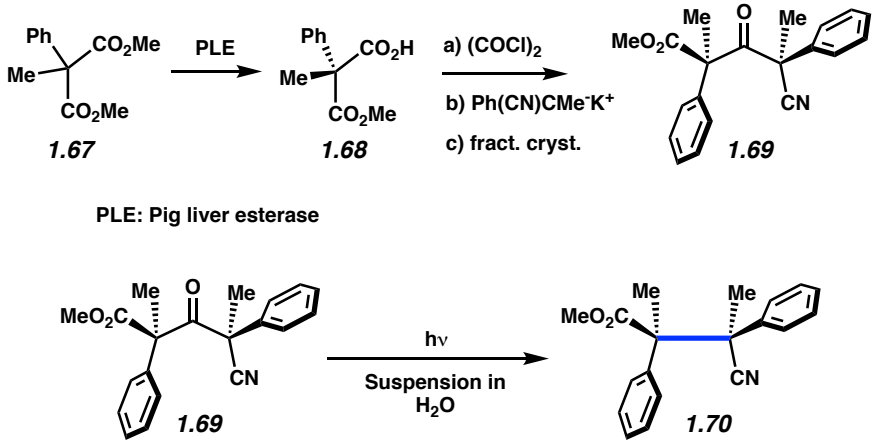

This acid chloride was then treated with a tertiary potassium enolate, to furnish homochiral (+)-**1.69**, in 80% yield following column chromatography and fractional recrystallization. The *S* configuration of the newly formed stereocenter was assigned by single-crystal X-ray diffraction. Using the known configuration of the acid (+)-(*R*)-**1.68**, the absolute configuration of the ketone product was established as (+)-(2*R*,4*S*)-**1.69**. Upon irradiation as an aqueous suspension, **1.69** was smoothly converted to **1.70** in quantitative yield and ca. 100% ee and dr. Due to the ease of preparation of the hexasubstituted homochiral ketone (+)-(2*R*,4*S*)-**1.69** and its clean transformation into (+)-(2*R*,3*R*)-**1.70**, we felt that this system would be ideal to demonstrate the synthetic utility and robust nature of the photodecarbonylation toward the synthesis of VQSs. As such we repeated the reaction on 15 g scale. A nanocrystalline suspension was prepared using the reprecipitation method and irradiated using the stepped flow system described above but with two reactors in series. Suspensions of nanocrystals in water with submicellar SDS were prepared with 2, 4, and 15 g of (+)-(2*R*,4*S*)- **1.69** that corresponds to loadings of 0.6 up to 4 g/L. In each case, the suspension was circulated through the photoreactors and reservoir until full conversion was observed. Just as in earlier examples, this reaction proceeded quantitatively with full retention of enantio- and diastereochemical information from the ketone, therefore demonstrating the ease of conducting this reaction on a multigram scale.[33b]

1.9 Application to Natural Product Synthesis

In addition to promising efficiency, scalability, and selectivity, there are some examples that illustrate the potential of the solid-state photodecarbonylation reaction for the total synthesis of small molecule natural products, including the sesquiterpene herbertenolide **1.75**. While the structure of herbertenolide is relatively simple, the main synthetic challenge is the construction of the central VQS core (Scheme 1.22).[37] Starting from commercially available 2-bromo-4-

methylanisole (**1.71**) and cyclohexane oxide, ketone **1.72** was prepared on gram scale in 96% overall yield in two steps by lithiation of arene **1.71**, followed by an epoxide opening C–C bond formation, and finally, a Swern oxidation of the resultant alcohol. Ketone **1.73** was then prepared in 43% yield over three steps by conventional enolate methylation/acylation methodology (Scheme 1.22). At this point, photodecarbonylation was conducted both in solution (0.1M, degassed benzene) and as finely powdered crystals. In solution, the photodecarbonylation of **1.73** performed poorly and yielded a complex mixture of decomposition products. No desired radical combination product was detected in the product mixture; however, the presence of vinyl protons in the crude ^{1}H NMR spectrum suggested that the primary pathway might have been disproportionation. In sharp contrast, **1.73** proceeded smoothly to **1.74** in the solid state and displayed 76% yield at up to 20% conversion. The reaction could not be continued past 20% conversion because the accumulation of **1.74** in the starting material crystals lowered the melting point of the mixture such that it melted at ambient conditions. Photoproduct **1.74**, was then treated with BBr_3 to affect a demethylation/intramolecular transesterification cascade to furnish herebertenolide **1.75** in 60% yield.

Scheme 1.22. Synthesis of *rac*-Herbertenolide (**1.75**).

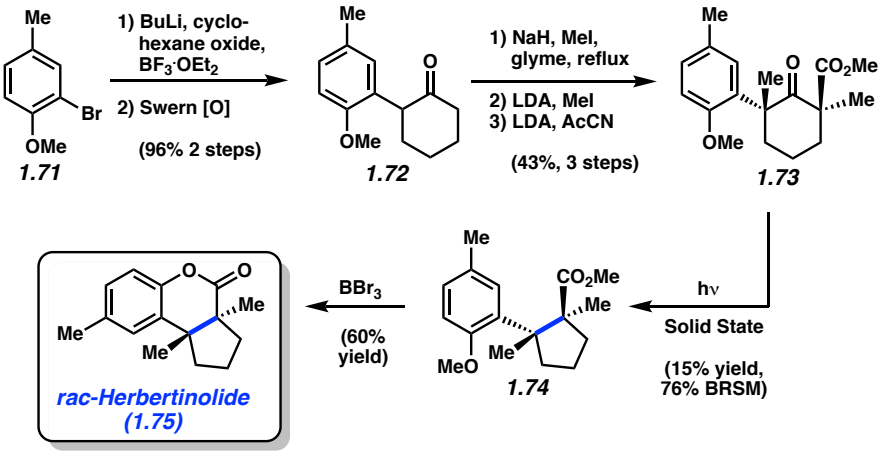

While the results of the photodecarbonylation were dramatically improved in the solid state in comparison to solution, the limited conversion required in this example necessitated iterative starting material purification/photolysis to generate useful quantities of **1.75**. This example illustrates the fact that in order to obtain quantitative yields and high conversions it is desirable to devise strategies that involve crystalline substrates and photoproducts with high melting points. In this case, it is likely that derivatization of **1.73**, either through transesterification or use of a larger, rigid substituent in place of the methyl group on the aryl ester could provide a higher melting point and improved solid-state performance.

After the successful racemic synthesis of herbertenolide, **1.75**, we sought to utilize the solid-state photodecarbonylation in the asymmetric total synthesis of the two enantiomers of α-cuparenone **1.80** (Scheme 1.23).[38] Since the two enantiomers of this relatively simple secondary metabolite occur naturally from different plant specimens and have been the target of numerous synthetic methods for vicinal quaternary center construction, it was an ideal choice for comparison.[39] Starting from racemic diketone **1.76**, difluorodioxaborinane **1.77** was synthesized by α-acylation followed by the addition of BF_3•Et_2O. This compound was treated with homochiral, (*S*)-α-methylbenzylamine, to generate diastereomers (*S,S*)-**1.78** and (*S,R*)-**1.78**, which were easily separated *via* flash column chromatography. Both diastereomers were irradiated as a nanocrystalline suspension in water with cetrimonium bromide (CTAB) surfactant to generate (*R,S*)-**1.79** and (*S,S*)-**1.79**, respectively in ca. 80% yield. These borane complexes were then hydrolyzed by heating in a solution of sodium acetate in ethanol, and the corresponding β-ketoamides were hydrolyzed and decarboxylated to furnish both (+)- and (-)-cuperanone, **1.80**. We were gratified by the results in Scheme 1.23 as it represented the first enantioselective total synthesis using solid-state photochemistry, and, despite there having been 17 prior asymmetric

syntheses of this compound, our work provided the highest overall yield (36%) as well as the highest enantioselectivity (>99%).[38]

Scheme 1.23. Enantioselective synthesis of (+)- and (–)- α-cuparenone (**1.80**).

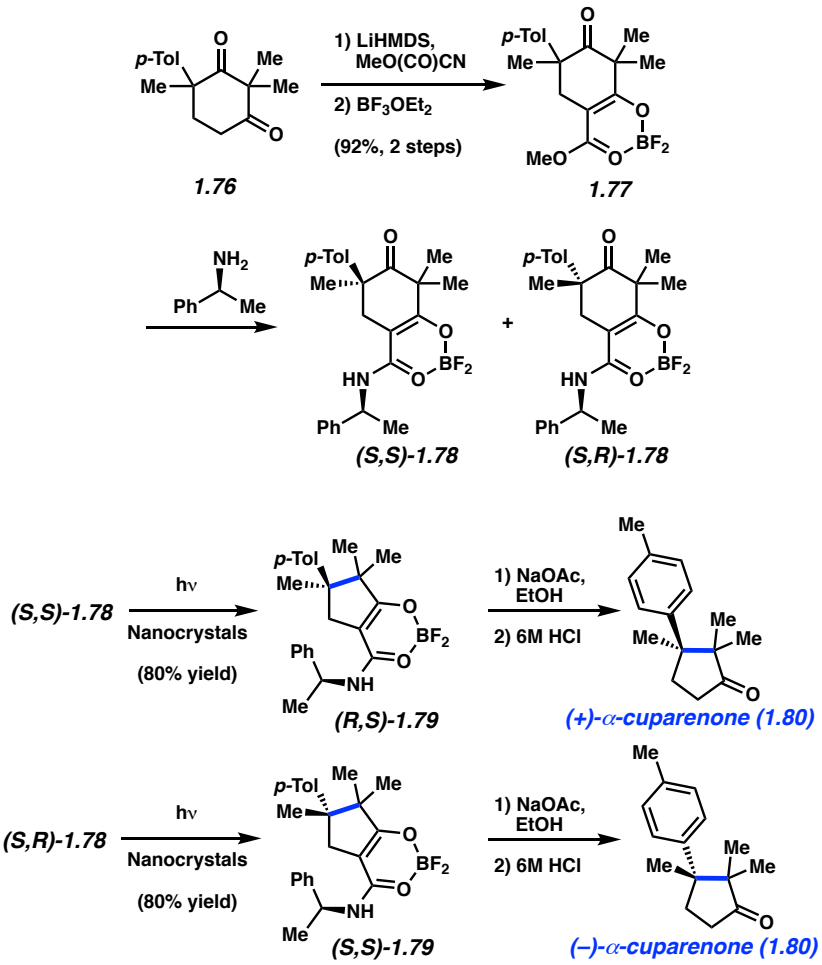

While our own lab has showcased the utility of the solid state in controlling the reactivity of Norrish type I photodecarbonylation reaction, the Baran lab recently showed that the solid state may also be used to help control the Norrish-Yang cyclobutanol formation as a useful step in complex molecule synthesis (Scheme 1.24).[40] In their elegant report of the total synthesis of ouabagenin (**1.85**) from commercially available adrenosterone, they sought to utilize the endogenous ketone at C11 of the protected aldresterone derivative **1.81** to direct oxygenation to

the angular methyl group, C19. They first attempted to conduct this transformation in solution phase and were met with only moderate yields. The desired cyclobutanol **1.82** was furnished in a modest 43% yield, the major product, **1.83**, resulted from a Norrish type I fragmentation followed by ketene formation and solvent-mediated esterification (Scheme 1.24). To circumvent this side reaction, Baran and coworkers carried out the reaction in the solid state. The substrate was irradiated as a crystalline suspension in water with SDS surfactant, leading to a markedly improved 68% yield of the desired product with 12% recovered starting material and a full suppression of the undesired Norrish type I product (100% relative yield of Norrish II vs Norrish I). As we have discussed in this report, is likely this suppression of the Norrish type I reaction, in this case, resulted from the lack of radical stabilizing substituents at either α-carbon.

Scheme 1.24. Use of solid-state Norrish-Yang cyclization in the total synthesis of ouabagenine.

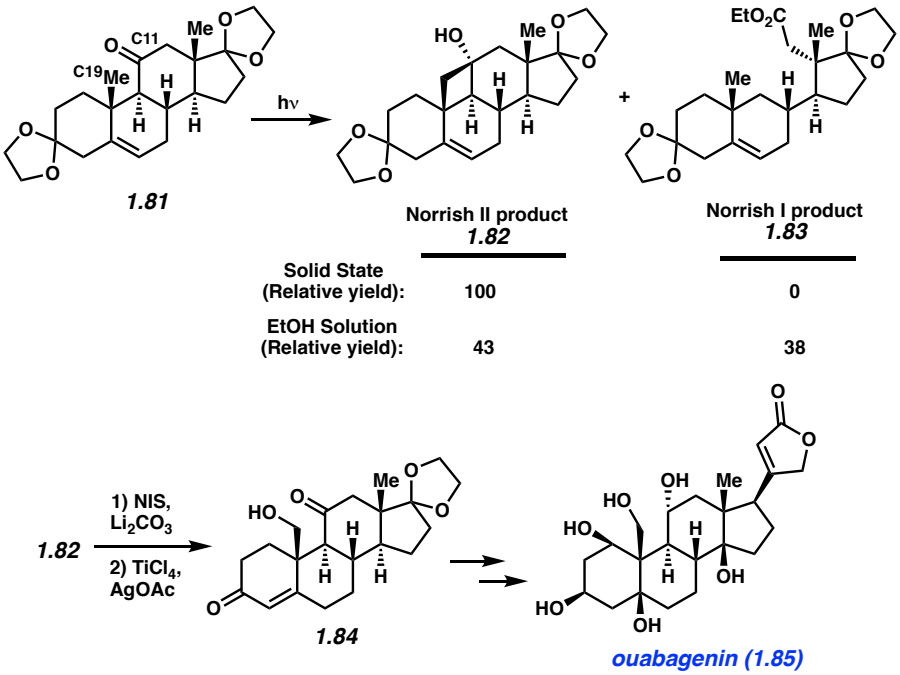

1.10 Conclusion

Although the Norrish type I photodecarbonylation has been known for over 100 years, it has seen little use in synthesis due to the highly reactive alkyl radical intermediates. The implementation of this reaction in the solid state provides an efficient and environmentally friendly alternative to access VQSs with high diastereoselectivity, enantioselectivity, and chemical yield. Importantly, our investigation of this reaction has displayed that not only are the intermediate alkyl radicals limited to caged radical reaction pathways, they also display a remarkable propensity to recombine in a stereoretentive fashion that is favored by the topochemical postulate. While not all ketones should be considered to be reactive in the solid state, we have demonstrated that the reactivity of a ketone in the solid state is determined by the radical stabilizing substituents at both α-carbons. If the resonance stabilizing energy is greater than 11 kcal/mol relative to methyl radical at each α-carbon, it is likely that the ketone will be photoreactive in the solid state. This thermochemical model has been shown to be quite general. It should be noted, however, that one key limitation of this methodology is the requirement for the substrate to both be crystalline and have a melting point sufficiently above room temperature. While this does make highly flexible aliphatic compounds and low molecular weight oils challenging substrates for this transformation, we have shown that the inclusion of an ionizable functional group (carboxylate, ammonium salt, etc.) which is inherently crystalline and high melting, may dramatically increase the substrate scope of this reaction. As such, the solid-state photodecarbonylation should be viewed as a reliable, strategy-level reaction, which may be used in complex molecule synthesis. Ultimately, the key strength of this reaction is its use of a chiral ketone as a synthon for difficult to construct carbon-carbon bonds. As there is a tremendous arsenal of methodology available to the synthetic chemist for the asymmetric α-functionalization of carbonyl compounds, ketones represent ideal substrates

to construct asymmetric, sterically encumbered stereocenters, which will ultimately be coupled together via the solid-state photodecarbonylation. While this reaction has not yet been widely adopted by the synthetic community, we feel that its successful employment in a handful of natural product syntheses demonstrates its utility. Furthermore, ongoing efforts in our lab toward the use of solid-state photodecarbonylation as the key step in the synthesis of increasingly complicated natural products will be reported in due course.

1.11 Notes and References

(1) (a) Clemons, P. A.; Bodycombe, N. E.; Carrinski, H. A.; Wilson, J. A.; Shamji, A. F.; Wagner, B. K.; Koehler, A. N.; Schreiber, S. L. *Proc. Natl. Acad. Sci. USA* **2010**, *107*, 18787–18792. (b) Schreiber, S. L. *Science* **2000**, *287*, 1964–1969. b) Lovering, F.; Bikker, J.; Humblet, C. *J. Med. Chem.* **2009**, *52*, 6752–6756.

(2) (a) Liu, Y.; Han, S.; Liu, W.; Stoltz, B. M. *Acc. Chem. Res.* **2015**, *48*, 740–751. (b) http://njardarson.lab.arizona.edu/sites/njardarson.lab.arizona.edu/files/Top200%20Pharmaceutical%20Products%20by%20US%20Prescription%20in%202012_0.pdf.

(3) (a) Long, R.; Huang, J.; Gong, J.; Yang, Z. *Nat. Prod. Rep.* **2015**, *32*, 1584–1601. (b) Peterson, E., Overman, L. E. *Proc. Natl. Acad. Sci. USA* **2004**, *101*, 11943–11948.

(4) Methods for the α-functionalization of ketones have been known since the late 1800s. (a) Garner, S. A. PhD Dissertation. UT Austin, 2007. (b) von Richter, V. *Ber. Deut. Chem. Ges.* **1869**, *2*, 552. (c) Würtz, A. *Bull. Soc. Chim. Fr.* **1872**, *17*, 436.

(5) (a) Ramamurthy, V.; Venkatesan, K. *Chem. Rev.* **1987**, *87*, 433–481. (b) Kohlshutter, H. W. Z. *Anorg. Allg. Chem.* **1918**, *105*, 121.

(6) (a) Movassaghi, M.; Schmidt, M. A. *Angew. Chem., Int. Ed.* **2007**, *46*, 3725–3728. (b) Schmidt, M. A.; Movassaghi, M. *Synlett* **2008**, 313–324.

(7) (a) Woodward, R. B.; Yang, N. C.; Katz, T. J.; Clark, V. M.; Harley-Mason, J.; Ingleby, R. F.; Sheppard, N. *Proc. Chem. Soc. London* **1960**, 76. (b) Robinson, R.; Teuber, H. J. *Chem. Ind. (London)* **1954**, 783. (d) May, J. A.; Stoltz, B. M. *Tetrahedron* **2006**, *62*, 5262–5271.

(8) Lathrop, S. P.; Pompeo, M.; Chang, W.-T. T.; Movassaghi, M. *J. Am. Chem. Soc.* **2016**, *138*, 7763–7769.

(9) (a) Kawabata, T.; Yahiro, K.; Fuji, K. *J. Am. Chem. Soc.* **1991**, *113*, 9694–9696. (b) Zhao, H.; Hsu, D. C.; Carlier, P. R., *Synthesis* **2005**, 1–16.

(10) Crich, D.; Banerjee, A. *Acc. Chem. Res.* **2007**, *40*, 151–161.

(11) Resendiz, M. J.; Natarajan A.; Garcia-Garibay, M. A. *Chem. Commun.* **2008**, 193–195.

(12) Kürti, L.; Czakó, B. *Strategic Applications of Name Reactions in Organic Synthesis*, 1st ed.; Elsevier Academic Press: Burlington, MA, 2005.

(13) Garcia-Garibay, M.A. *Acc. Chem. Res.* **2003**, *36*, 491–498.

(14) Hoijemberg, P. A.; Karlen, S. D.; Sanramé, C. N.; Aramendia, P. F.; Garcia-Garibay, M. A. *Photochem. Photobiol. Sc.* **2009**, *8*, 961–969.

(15) Shiraki, S.; Vogelsberg, C. S.; Garcia-Garibay, M. A. *Photochem. Photobiol. Sci*. **2012**, *11*, 1929–1937.

(16) (a) de Loera, D.; Garcia-Garibay, M. A. *Org. Lett*. **2012**, *14*, 3874–3877. (b) de Loera, D.; Stopin, A.; Garcia-Garibay, M. A. *J. Am. Chem. Soc*. **2013**, *135*, 6626–6632.

(17) (a) Garcia-Garibay, M. A. *Photochem. Photobiol. Sci.* **2010**, *9*, 1574–1588. (b) Shiraki, S.; Garcia-Garibay, M. A. in *Handbook of Synthetic Photochemistry*; Albini, A. and Fagnoni, M. Ed.; John Wiley: New York, 2010, p 25.

(18) Experiments carried out with di-*tert*-butyl ketone powder using a Rayonet reactor with λ = 300 nm light bulbs for 12 h.

(19) Campos, L. M.; Dang, H.; Ng, D.; Yang, Z.; Martinez, H. L.; Garcia-Garibay, M. A. *J. Org. Chem.* **2002**, *67*, 3749–3754.

(20) Grossman, R. B. *The Art of Writing Reasonable Organic Reaction Mechanisms*, 2nd ed.; Springer-Verlag Press; New York, 2003.

(21) Anslyn, E. V.; Dougherty, D. A. *Modern Physical Organic Chemistry*; University Science Books: Sausalito, CA, 2006; pp. 1–992.

(22) Choi, T.; Peterfy, K.; Khan, S. I.; Garcia-Garibay, M. A. *J. Am. Chem. Soc.* **1996**, *118*, 12477–12478.

(23) Quinkert, G.; Tabata, T.; Hickman, E. A. J.; Dobrat, W. *Angew. Chem. Int. Ed. Engl.* **1971**, *10*, 198–199.

(24) (a) Ng, D.; Yang, Z.; Garcia-Garibay, M. A. *Tetrahedron Lett.* **2001,** *42*, 9113–9116. (b) Bucher, G. *J. Phys. Chem. A.* **2008**, *112*, 5411–5417.

(25) Mortko, C. J.; Dang, D.; Campos. L. M.; Garcia-Garibay, M. A. *Tetrahedron Lett*. **2003**, *44*, 6133–6136.

(26) Resendiz, M. J. E.; Taing, J.; Khan, S. I.; Garcia-Garibay, M. A. *J. Org. Chem.* **2008**, *73*, 638–643.

(27) (a) Choi, T.; Cizmeciyan, D.; Khan, S. I.; Garcia-Garibay, M. A. *J. Am. Chem. Soc.* **1995**, *117*, 12893–12894. (b) Schmidt, J. M. J. in *Solid State Photochemistry*; Ginsburg, D., Ed.; Verlag Chemie: New York, 1976. (c) Cohen, M. D. *Angew. Chem. Int. Ed. Engl.* **1975**, *14*, 386. (d) Scheffer, J. R.; Garcia-Garibay, M. A.; Nalamasu, O. In *Organic Photochemistry*;

Padwa, A., Ed.; Marcel Dekker, Inc.: New York, 1987; pp 249–347. (e) Desiraju, G. R. *Organic Solid State Chemistry*; Elsevier: Amsterdam, 1987; p 550.

(28) Choe, T.; Khan, S. I.; Garcia-Garibay, M. A. *Photochem. Photobio. Sci.* **2006**, *5*, 449–451.

(29) Mataka, S.; Lee, S. T.; Tashiro, M. *J. Chem. Soc., Perkin Trans.* **1990**, *2*, 2017–2021.

(30) Mortko, C. J.; Garcia-Garibay, M. A. *J. Am. Chem. Soc.* **2005**, *127*, 7994–7995.

(31) Houk, K. N. *Chem. Rev.* **1976**, *76*, 1–74.

(32) Shiraki, S.; Natarajan, A.; Garcia-Garibay, M. A. *J. Am. Chem. Soc.* **2011**, *10*, 1480–1487.

(33) (a) Ellison, M. E.; Ng, D.; Dang, H.; Garcia-Garibay, M. A. *Org. Lett.* **2003**, *5*, 2531–2534. (b) Hernández-Linares, M. G. H.; Guerrero-Luna, G.; Pérez-Estrada, S.; Ellison, M.; Ortin, M. –M.; Garcia-Garibay, M. A. *J. Am. Chem. Soc.* **2015**, *137*, 1679–1684.

(34) (a) Takashi, S.; Miura, H.; Kasai, H.; Okada, H.; Oikawa, H.; Nakanishi, H. *J. Am. Chem. Soc.* **2002**, *124*, 10944–10945. (b) Bucar, D.-K.; MacGillivray, L. R. *J. Am. Chem. Soc.* **2007**, *129*, 32–33. (c) Al-Kaysi, R. O.; Bardeen, C. J. *Adv. Mater.* **2007**, *19*, 1276–1280.

(35) (a) Chin, K. K.; Natarajan, A.; Gard, M. N.; Campos, L. M.; Shepherd, H.; Johanson, E.; Garcia-Garibay, M. A. *Chem. Commun.* **2007**, 4266–4268. (b) Veerman, M.; Resendiz, M. J. E.; Garcia-Garibay, M. A. *Org. Lett.* **2006**, *8*, 2615–2617. (c) Kuzmanich, G.; Xue, J.; Netto-Ferreira, J.-C.; Scaiano, J. C.; Platz, M.; Garcia-Garibay, M. A. *Chem. Sci.* **2011**, *2*, 1497–1501.

(36) Resendiz, M. J. E.; Taing, J.; Garcia-Garibay, M. A. *Org. Lett.* **2007**, *9*, 4351–4354.

(37) Ng, D.; Yang, Z.; Garcia-Garibay, M. A. *Org. Lett.* **2004**, *6*, 645–647.

(38) Natarajan, A.; Ng, D.; Yang, Z.; Garcia-Garibay, M. A. *Angew. Chem. Int. Ed.* **2007**, *46*, 6485–6487.

(39) (a) Taber, D. F.; Petty, E. H.; Raman, K. *J. Am. Chem. Soc.* **1985**, *107*, 196–199. (b) Kametani, T.; Kawamura, K.; M. Tsubuki, Honda, T. *Chem. & Pharm. Bull.* **1985**, *33*, 4821–4828. (c) Meyers, A. I.; Lefker, B. A. *J. Org. Chem.* **1986**, *51*, 1541–1544. (d) Greene, A. E.; Charbonnier, F.; Luche, M. J.; Moyano, A. *J. Am. Chem. Soc.* **1987**, *109*, 4752–4753. (e) Asaoka, M.; Takenouchi, K.; Takei, H. *Tetrahedron Lett.* **1988**, *29*, 325–328. (f) Takano, S.; Inomata, K.; Ogasawara, K. *J. Chem. Soc., Chem. Commun.* **1989**, 271–272. (f) Gharpure, M. M.; Rao, A. S. *Synth. Commun.* **1989**, *19*, 1813–1823. (g) Fadel, A.; Canet, J. L.; Saluan, J. *Synlett* **1991**, 60–62. (g) Nemoto, H.; Ishibashi, N.; Nagamochi, M.; Fukumoto, K. *J. Org. Chem.* **1992**, *57*, 1707–1712. (h) Canet, J. –L.; Fadel, A.; Salaun, J. *J. Org. Chem.* **1992**, *57*, 3463–3473. (i) Honda, T.; Kimura, N.; Tsubuki, M., *Tetrahedron: Asymmetry* **1993**, *4*, 21–24. (j) Maruoka, K.; Oishi, M.; Yamamoto, H. *J. Am. Chem. Soc.* **1996**, *118*, 2289–2290. (k) Kosaka, T.; Bando, T.; Shishido, K. *J. Chem. Soc. Chem. Commun.* **1997**, 1167–1168. (l) Nakashima, H.; Sato, M.; Taniguchi, T.; Ogasawara, K. *Tetrahedron Lett.* **2000**, *41*, 2639–2642. (m) Satoh, T.; Yoshida, M.; Masaaki, T. Y.; Ota, H. *Tetrahedron Asymmetry* **2003**, *14*, 281–288. (n) Spino, C.; Godbout, C.; Beaulieu, C.; Harter, M.; Mwene-Mbeja, T. M.; Boisvert, L. *J. Am. Chem. Soc,* **2004**, *126*, 13312–13319.

(40) Renata, H.; Zhou, Q.; Baran, P. S. *Science* **2013**, *339*, 59–63.

CHAPTER TWO

Evaluation of the Photodecarbonylation of Crystalline Ketones for the Installation of Reverse Prenyl Groups on the Pyrrolidinoindoline Scaffold

Adapted from: Jordan J. Dotson, Neil K. Garg,* and Miguel A. Garcia-Garibay.*

Tetrahedron, DOI: 10.1016/j.tet.2020.131181.

2.1 Abstract

We report synthetic efforts toward the regiocontrolled installation of the prenyl moiety in debromoflustramine A by the regiospecific photodecarbonylation of a prenyl-substituted ketone. Synthetic approaches to access the plausible photodecarbonylation substrates beginning from tryptamine were evaluated. Initial attempts to synthesize a suitable substrate for photodecarbonylation were hampered by a lack of substrate crystallinity (a prerequisite for solid-state photochemistry). Ultimately, a crystalline substrate could be accessed to attempt the key step by judicious selection of *N*-substituents. Although the photodecarbonylation did not result in the desired reverse prenylation, this study highlights the troubleshooting and optimization required for crystal-phase photochemistry and underscores methods that can be used to control substrate crystallinity.

2.2 Introduction

The regiocontrolled introduction of prenyl or unsymmetrical allyl fragments is a challenging transformation in synthetic organic chemistry.[1] Despite this, prenyl and reverse prenyl

decoration is featured widely across diverse classes of biologically active natural products (e.g., **2.1**–**2.5**, Scheme 2.1).[2] As such, selective methods for their introduction are highly desirable. Successful methodologies leveraging nucleophilic addition into electrophilic Ir and Pd π-allyl complexes and Pd-catalyzed Suzuki-type prenylations have been developed; however, regiocontrolled prenylation of cationic or radical centers remains challenging.[3]

Scheme 2.1. Representative prenylated and reverse prenylated indole alkaloids **2.1**–**2.5**.

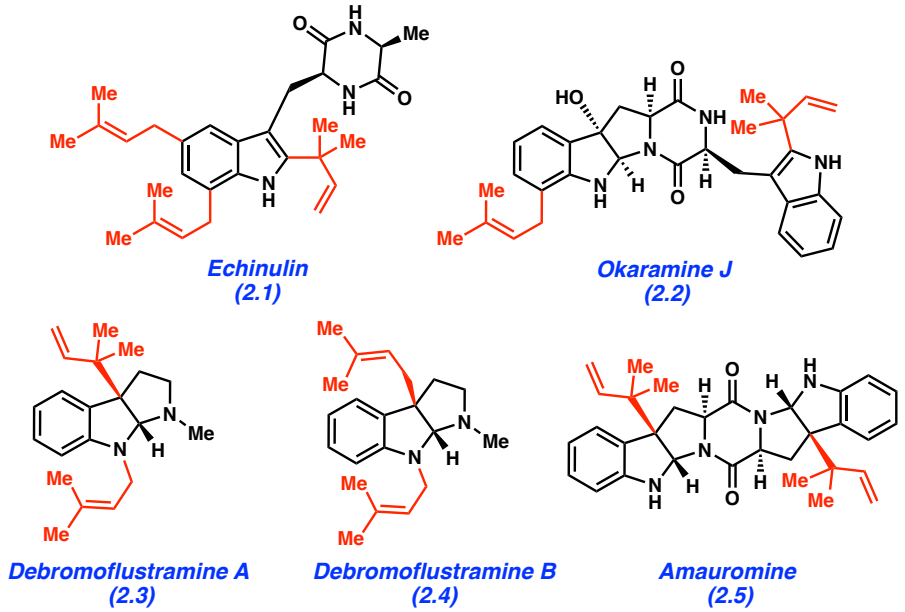

An attractive, albeit underexplored, means of regiocontrolled radical prenylation would involve a Norrish type I photodecarbonylation of isomeric ketones **2.6** or **2.7** to furnish prenylated compounds **2.8** or **2.9**, respectively (Scheme 2.2). This type of transformation would be valuable as it would allow regiochemical information to be encoded into ketones **2.6** and **2.7**. In turn, that information could be relayed to products **2.8** and **2.9**. The intrinsic difficulty of this approach, however, is the fact that radical pairs **2.10** and **2.11** differ only in their orientation with respect to one another. For this reason, rotation of the prenyl radical could allow facile interconversion of

2.10 and **2.11** leading to mixtures of regioisomers. Additionally, caged radical pairs **2.10** and **2.11** could also dissociate to form free radicals that could undergo deleterious side reactions.

Scheme 2.2. Radical prenylation using a regioselective Norrish type I photodecarbonylation.

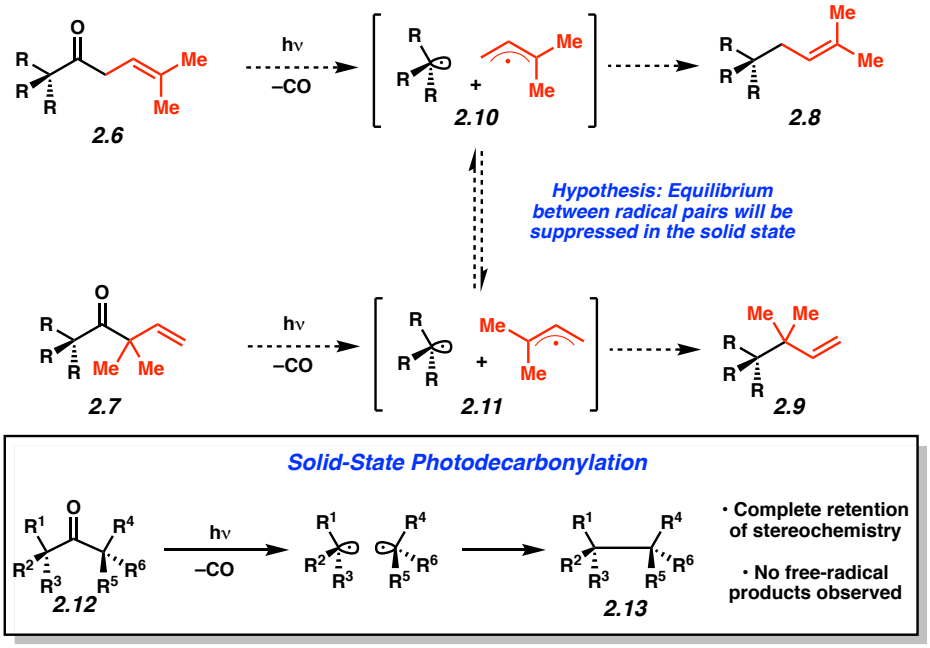

In order to address the aforementioned challenges, we sought to conduct these reactions in the crystalline solid state. It has been shown that Norrish type I photodecarbonylations of α-stereogenic ketones **2.12** provide recombination products **2.13** with exquisite stereochemical retention and without dissociation to form free-radicals (Scheme 2.2).[4] This selectivity results from restrictions on translational and rotational degrees of freedom imparted by the crystalline lattice. Efforts to manipulate unsymmetrical allylic radicals using solid-state photodecarbonylation have not been reported.

In order to investigate this approach in the context of complex molecule synthesis, we devised a strategy to access debromoflustramines A (**2.3**) and B (**2.4**), which possess reverse and

direct prenylated scaffolds, respectively (Scheme 2.3).[5,6] Debromoflustramines A (**2.3**) and B (**2.4**) possess sterically congested quaternary stereocenters, whereas **2.3** bears vicinal quaternary carbons.[7] As the construction of vicinal quaternary centers represents a long-standing challenge in organic synthesis, we prioritized the synthesis of debromoflustramine A (**2.3**). The brominated analogs of these alkaloids, isolated from the marine invertebrate *Flustra foliacea* in the North Atlantic Ocean, are known to act as skeletal and smooth muscle relaxants by blocking voltage-gated calcium channels.[8] Retrosynthetically, we envisioned accessing **2.3** and **2.4** from caged radical pairs **2.14** and **2.15**, respectively. In turn, these radical pairs would be generated from parent ketones **2.16** or **2.17**, with retention of regiochemistry arising from the use of solid-state photodecarbonylation. We hoped to access both ketones from the tricyclic aldehyde **2.18**, which was previously synthesized by Bisai and coworkers.[9]

Scheme 2.3. Retrosynthetic analysis of debromoflustramines A (**2.3**) & B (**2.4**) utilizing a key regioretentive solid-state photodecarbonylation.

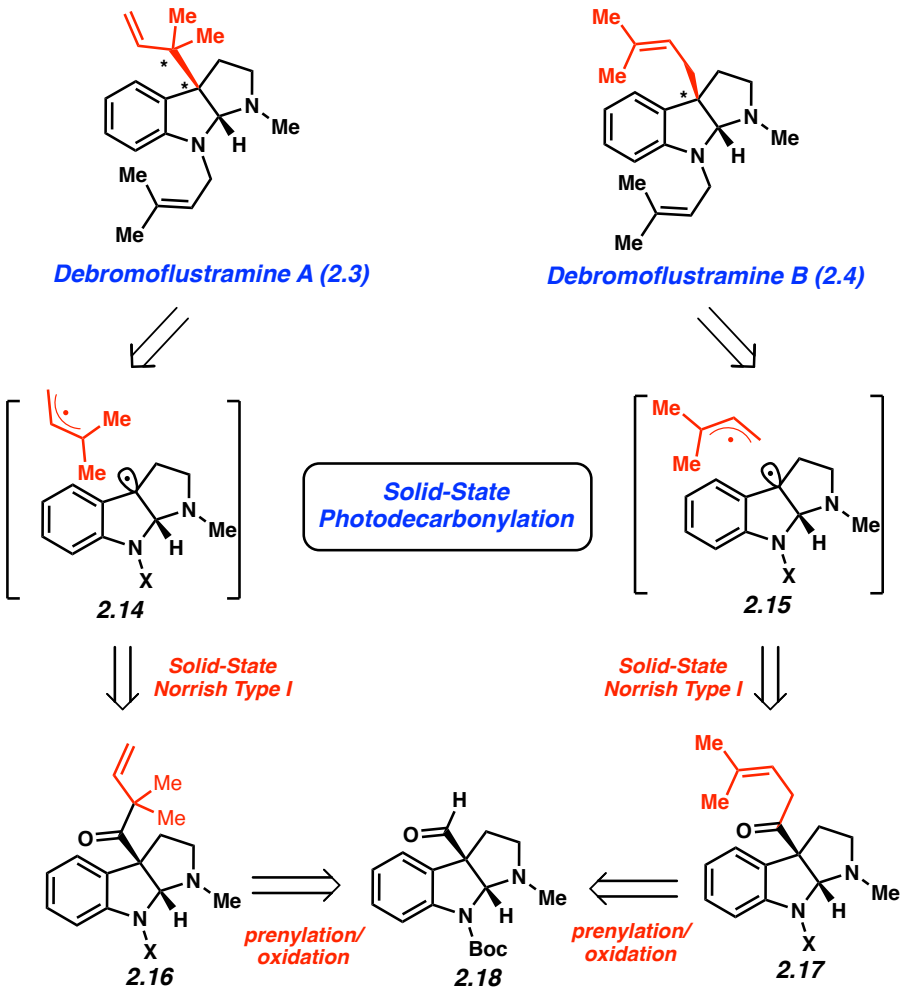

2.3 Results and Discussion

Our efforts commenced by synthesizing Boc-protected pyrrolidinoindoline ketone **2.19** using the sequence shown in Scheme 2.4. Beginning from commercially available tryptamine hydrochloride (**2.20**), aldehyde **2.18** was synthesized in 9 steps following the route reported by Bisai and coworkers.[9] With this aldehyde in hand, addition of prenylmagnesium bromide provided

secondary alcohol **2.21** as an inconsequential mixture of diastereomers. The structure of the major diastereomer was verified by X-ray crystallography. Oxidation of **2.21** under Ley-Griffith conditions furnished the target substrate for photodecarbonylation, ketone **2.19**.[10] Unfortunately, despite extensive attempts to nucleate crystallization, **2.19** remained a viscous oil at room temperature. While the physical state of the substrate would typically be inconsequential for a solution-phase photochemical reaction, substrate crystallinity is imperative for the solid-state photochemical reaction we desired. Nonetheless, irradiation of **2.19** as a neat oil was attempted but provided a complex mixture of products.

Scheme 2.4. Synthesis of ketone **2.19** and attempted photodecarbonylation of neat oil.

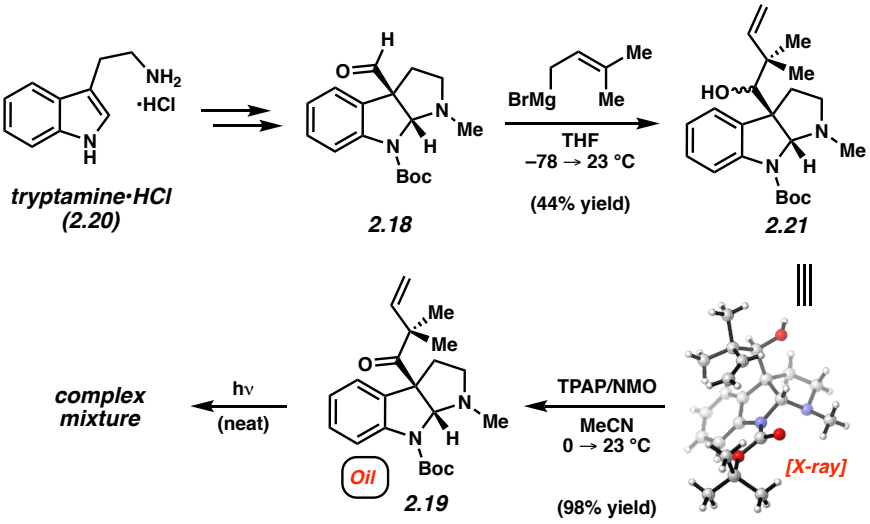

Several strategies were investigated to derivatize **2.19** to arrive at a crystalline substrate. Formation of ammonium salts by protonation of the pyrrolidine was unsuccessful and our attempts were accompanied by Boc cleavage with subsequent decomposition. To circumvent this issue, we envisioned exchanging the acid-labile Boc protecting group with a benzenesulfonamide. In addition to displaying greater stability to acid, the presence of a benzenesulfonyl protecting group is known to furnish crystalline solids when appended to pyrrolidinoindoline motifs.[11]

In order to synthesize a benzenesulfonyl-protected ketone, protecting group exchange was attempted on alcohol **2.21** (Scheme 2.5). Acetylation of the secondary alcohol to provide ester **2.22** followed by Lewis acid-mediated cleavage of the carbamate furnished **2.23** in good yield. With free *N*-H compounds in hand, we were optimistic that phenylsulfonamide formation could be accomplished as Rainier and coworkers reported successful sulfonylation on a closely related pyrrolidinoindoline scaffold.[12] To our surprise, upon subjecting **2.23** to phenylsulfonyl chloride, we observed structural rearrangement rather than the desired product **2.25**. The rearranged compound was isolated following acetate cleavage and was determined to be **2.24**. This product likely arises from a cationic aza-Prins-type cascade to give the 6,5,6-Strychnos scaffold. This type of aza-Prins cyclization to give hydrocarbazole ring systems has been reported on similar substrates by Reisman and coworkers.[13,14]

Scheme 2.5. Attempted protecting group exchange leads to an undesired aza-Prins rearrangement to give **2.24** bearing the Strychnos core.

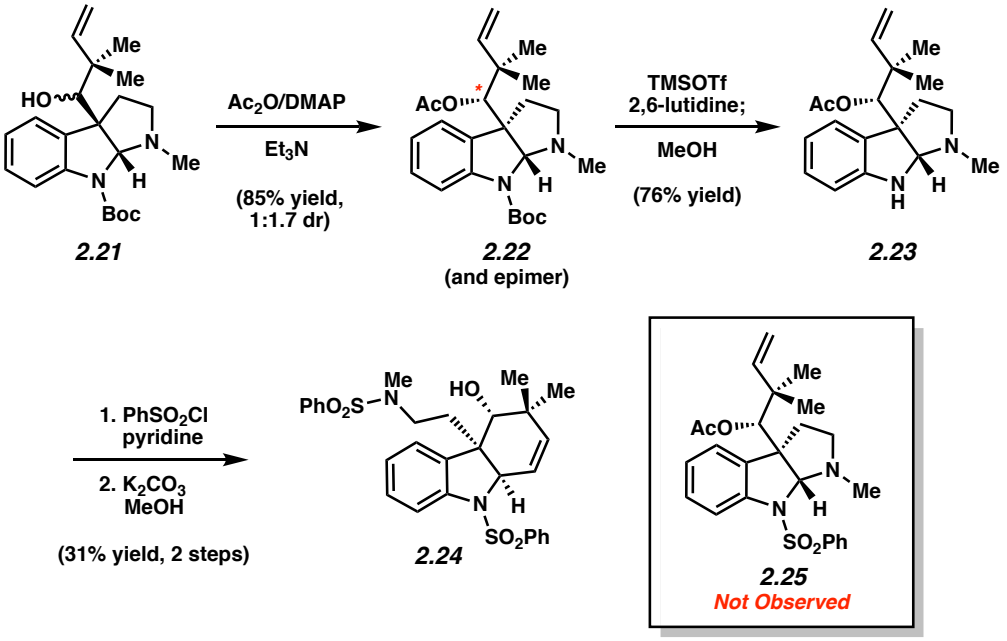

Finally, we explored a strategy involving earlier swapping of the Boc group with a benzenesulfonyl moiety (Scheme 2.6). From intermediate **2.26**, acetylation of neopentylic alcohol **2.26** and Boc cleavage provided oxindole **2.27**. Subsequent treatment with sodium hydride and benzenesulfonyl chloride allowed for the desired *N*-sulfonylation. Next, a two-step reduction sequence involving carbonyl reduction and Cbz removal furnished pyrrolidinoindoline **2.28**. Treatment of **2.28** with K_2CO_3/methanol, followed by a three-step oxidation-prenylation-oxidation sequence, furnished **2.29**.

Scheme 2.6. Synthesis of crystalline ketone **2.30** and attempted photodecarbonylation.

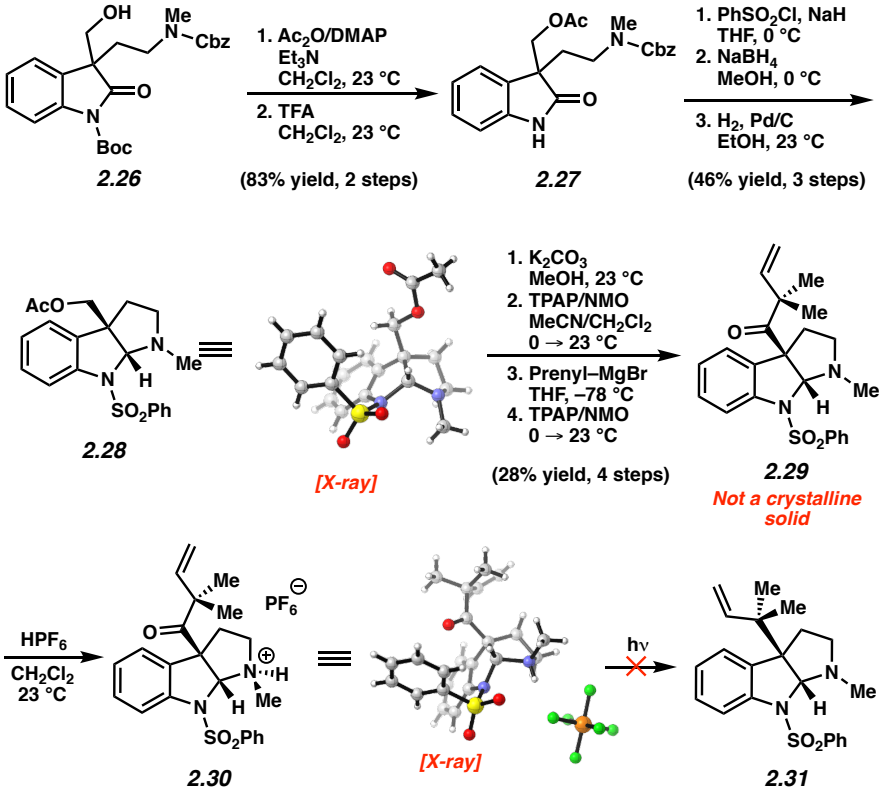

With **2.29** in hand, we explored methods to achieve crystallinity and attempt the desired solid-state photodecarbonylation (Scheme 2.6). Although ketone **2.29** was not a crystalline solid, the benzenesulfonamide group proved stable to acid, which allowed us to attempt the synthesis of crystalline ammonium salts. Indeed, an extensive survey of Brønsted acids gave rise to ammonium

hexafluorophosphate salt **2.30**, which was a crystalline solid. The structure of **2.30** was verified using single-crystal X-ray diffraction. Eager to test the solid-state photodecarbonylation reaction, salt **2.30** was exposed to UV irradiation. Unfortunately, various UV light irradiation conditions gave a complex mixture of products rather than the expected photodecarbonylation product **2.31**. We suspect that the reaction fails due to competitive photochemical decomposition of the phenylsulfonyl group.[15] Future studies will allow us to test the introduction of the prenyl group present in debromoflustramine B using an analogous approach.

2.4 Conclusion

In summary, we have devised a strategy for the introduction of reverse prenyl and prenyl groups using solid-state photodecarbonylation. Our synthetic efforts focused on the former en route to the natural product debromoflustramine A (**2.3**). Although our initial synthetic efforts were thwarted by difficulties in accessing a crystalline substrate and undesired structural rearrangements, we were ultimately able to access a crystalline substrate using multistep synthesis. The attempted photodecarbonylation, however, was unfortunately unsuccessful. Although disappointing, it is plausible that an alternative substrate may prove more successful in solid-state reverse prenylation. We hope future studies will determine the viability of using regiocontrolled reverse prenylation and prenylation reactions in the solid state to access complex indole alkaloids. Furthermore, this endeavor highlights a workflow and troubleshooting strategy that can be used to surmount one of the key challenges intrinsic to solid-state chemistry, namely, achieving substrate crystallinity.

2.5 Experimental Section

2.5.1 Materials and Methods

Unless stated otherwise, reactions were conducted in flame-dried glassware under an atmosphere of argon using anhydrous solvents (either freshly distilled or passed through activated alumina columns). All commercially available reagents were used as received unless otherwise specified. Tetrapropylammonium perruthenate (TPAP), trifluoroacetic acid (TFA), *N*-methylmorpholine-*N*-oxide (NMO), acetic anhydride, 4-dimethylaminopyridine (DMAP), trimethylsilyl trifluoromethanesulfonate (TMSOTf), 2,6-lutidine, phenylsulfonyl chloride, sodium hydride (60% dispersion in mineral oil), sodium borohydride, and palladium on activated carbon (Pd/C) were obtained from Sigma-Aldrich. Hexafluorophosphoric acid (60 wt% in water) was purchased from Fisher Scientific. Prenylmagnesium bromide was prepared from a known literature procedure.[16] Unless stated otherwise, reactions were performed at room temperature (approximately 23 °C). Thin-layer chromatography (TLC) was conducted with EMD gel 60 F254 pre-coated plates (0.25 mm) and visualized using a combination of UV, ceric ammonium molybdate, and potassium permanganate staining. Silicycle silica gel 60 (particle size 0.040–0.063 mm) was used for flash column chromatography. ^{1}H NMR spectra were recorded on Bruker spectrometers (at 500 MHz) and are reported relative to deuterated solvent signals. Data for ^{1}H NMR spectra are reported as follows: chemical shift (δ ppm), multiplicity, coupling constant (Hz) and integration. ^{13}C NMR spectra are reported in terms of chemical shift (125 MHz). High-resolution mass spectra were obtained on Thermo ScientificTM Exactive Mass Spectrometers with

DART ID-CUBE. X-ray crystallographic images in Schemes 2.4 and 2.6 were rendered using CYLview.[17]

2.5.2 Experimental Procedures

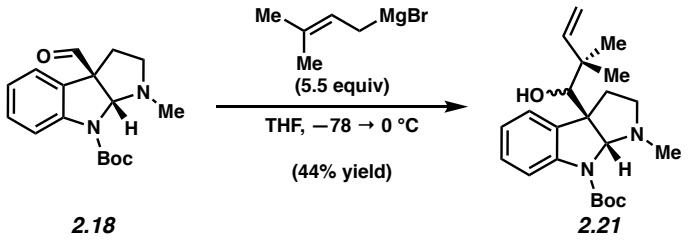

2.18 *2.21*

Alcohol 2.21. To a solution of aldehyde **2.18**[9] (110 mg, 0.36 mmol, 1.0 equiv) at –78 °C, prenylmagnesium bromide (10.1 mL, 0.18 M in THF, 1.82 mmol, 5.0 equiv) was added dropwise over 1 min. The reaction was then allowed to warm to 23 °C over 10 min before being quenched by the dropwise addition of sat. aq. NH_4Cl (0.5 mL) over 1 min. 1.0 M aq. NaOH (50 mL) was added, the layers were separated, and the aqueous layer was extracted with CH_2Cl_2 (2 x 15 mL). The combined organic layers were dried over $MgSO_4$ and concentrated under reduced pressure. The crude mixture was purified via column chromatography (7:3 → 1:1 Hexanes:EtOAc) to afford alcohol **2.21** (99 mg, 44% yield) as a white solid in a 2:1 mixture of diastereomers. Crystals of the major diastereomer suitable for X-ray diffraction studies (CCDC 1987254) were obtained using slow evaporation of the diastereomeric mixture from $CDCl_3$. R_f 0.19 (1:1 Hexanes:EtOAc); ^{1}H NMR (500 MHz, C_6D_6): δ 8.02 (m, 3H), 7.37–7.35 (m, 1H), 7.15–7.08 (m, 3H), 6.89–6.80 (m, 5H), 5.68–5.56 (m, 6H), 4.84–4.72 (m, 6H), 3.50 (s, 2H), 3.44 (s, 1H), 2.61–2.50 (m, 14H), 2.45–2.40 (m, 2H), 2.32–2.23 (m, 2H), 2.14–2.08 (m, 1H), 1.83–1.76 (m, 2H), 1.48 (m, 27H), 0.82–0.81 (m, 12H), 0.76 (s, 6H); ^{13}C NMR (125 MHz, C_6D_6): δ 153.1, 145.6, 145.3, 143.2, 135.5, 128.3, 125.1, 122.7, 116.4, 115.7, 113.1, 84.0, 83.2, 82.7, 81.2, 80.1, 61.3, 52.4, 51.8, 43.5, 43.3, 40.5, 39.4, 38.0, 36.8, 28.5, 28.5, 26.2 23.3; HRMS-APCI (*m/z*) $[M + H]^+$ calcd for $C_{22}H_{33}N_2O_3^+$,

373.2485; found 373.2467. Note: **2.21** was obtained as a mixture of rotamers of two diastereomers. The ^{1}H and ^{13}C NMR spectra reported were collected at 70 °C to sharpen the observed peaks, however, broad resonances in the ^{13}C NMR spectrum due to rotation on the NMR timescale resulted in overlapping carbon signals. The empirical spectra are reported.

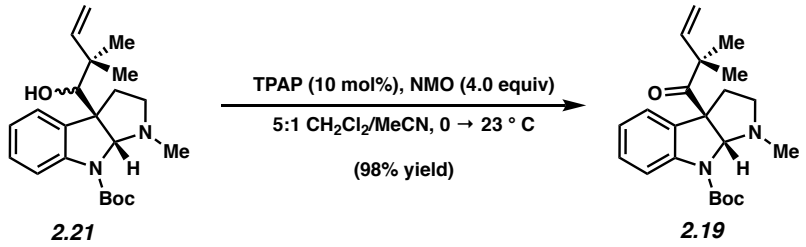

2.21 *2.19*

Ketone 2.19. Finely ground 4Å molecular sieves (160 mg), NMO (93 mg, 0.79 mmol, 4.0 equiv) and alcohol **2.21** (74 mg, 0.20 mmol, 1.0 equiv) were suspended in a mixture of CH_2Cl_2 (30 mL) and MeCN (4 mL). The mixture was cooled to 0 °C and a solution of TPAP (12.7 mg, 0.036 mmol, 18 mol%) in MeCN (2 mL), also cooled to 0 °C, was then added to the reaction dropwise over 1 min. The reaction was warmed to 23 °C. After stirring for 2 hours, the reaction mixture was filtered over silica gel (~2 x 5 cm) using EtOAc as the eluent (100 mL). The crude reaction mixture was concentrated under reduced pressure and purified via column chromatography (9:1 → 4:1 Hexanes:EtOAc) to afford ketone **2.19** (72 mg, 98% yield) as a yellow oil. R_f 0.32 (4:1 Hexanes:EtOAc); ^{1}H NMR (500 MHz, C_6D_6): δ 7.90 (s, 1H), 7.08–7.00 (m, 2H), 6.76 (t, *J* = 7.5 Hz, 1H), 5.98 (s, 1H), 5.62 (dd, *J* = 17.5, 10.6 Hz, 1H), 4.90–4.85 (m, 2H), 4.82 (d, *J* = 10.7 Hz, 1H), 2.76 (ddd, *J* = 12.2, 10.5, 6.5 Hz, 1H), 2.48 (s, 3H), 2.42 (ddd, *J* = 8.8, 6.5, 2.0 Hz, 1H), 2.26 (td, *J* = 9.9, 5.0 Hz, 1H), 1.91 (ddd, *J* = 12.2, 5.0, 2.0 Hz, 1H), 1.43 (s, 9H), 1.15 (s, 3H), 1.03 (s, 3H); ^{13}C NMR (125 MHz, C_6D_6): δ 207.7, 153.0, 144.3, 141.8, 133.2, 128.5, 123.8, 122.8, 115.8, 114.2, 84.2, 80.4, 68.5, 51.5, 50.9, 38.6, 36.9, 27.9, 25.4, 25.3. HRMS-APCI (*m/z*) $[M + H]^+$ calcd

for $C_{22}H_{31}N_2O_3^+$, 371.2329; found 371.2317. Note: NMR spectra of ketone **2.19** were obtained at 70 °C.

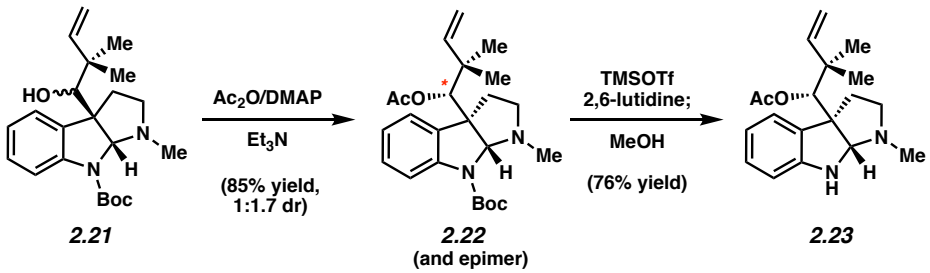

Pyrrolidinoindoline 2.23. To a solution of alcohol **2.21** (131 mg, 0.35 mmol, 1.0 equiv) in CH_2Cl_2 (12 mL) were added sequentially Et_3N (0.49 mL, 3.5 mmol, 10 equiv), Ac_2O (0.32 mL, 3.5 mmol, 10 equiv), followed by DMAP (43 mg, 0.25 mmol, 0.7 equiv). The resulting reaction mixture was allowed to stir for 1 h at 23 °C before being poured into a solution of sat. aq. $NaHCO_3$ (20 mL). The layers were separated and the aqueous layer was extracted with CH_2Cl_2 (2 x 15 mL). The combined organic layers were dried over $MgSO_4$ and then concentrated under reduced pressure. The resulting residue was purified by column chromatography (9:1 Hexanes:EtOAc) to give ester **2.22** and its epimer as a white foam (125 mg, 85% yield, 1.7:1 dr).

A solution of 2,6-lutidine (51 μL, 47 mg, 0.44 mmol, 13 equiv) and **2.22** (14.3 mg, 0.035 mmol, 1.0 equiv) in CH_2Cl_2 (0.36 mL) was cooled to 0 °C and then TMSOTf (80 μL, 0.44 mmol, 13 equiv) was added. After 105 min, 1 drop of sat. aq. $NaHCO_3$ followed by MeOH (1 mL) were added, the reaction mixture was flushed through a plug of Na_2SO_4, and then concentrated under reduced pressure. The resulting residue was purified via column chromatography (9:1 Hexanes:EtOAc with 5% v/v Et_3N) to provide pyrrolidinoindoline **2.23** (8.2 mg, 76% yield, 2 steps) as a colorless oil. R_f 0.39 (1:1 Hexanes:EtOAc with 5% v/v Et_3N); ^1H NMR (500 MHz, C_6D_6): δ 6.97 (t, J = 7.7 Hz, 1H), 6.75 (d, J = 7.4 Hz, 1H), 6.60 (t, J = 7.4 Hz, 1H), 6.33 (d, J = 7.7 Hz, 1H), 5.82 (dd, J = 17.4, 10.7 Hz, 1H), 5.54 (s, 1H), 4.80–4.64 (m, 3H), 3.53 (s, 1H), 2.43–2.32

(m, 1H), 2.32–2.19 (m, 2H), 2.16 (s, 3H), 1.93–1.82 (m, 4H), 0.92 (s, 3H), 0.88 (s, 3H); ^{13}C NMR (125 MHz, C_6D_6): δ 170.4, 151.2, 145.6, 132.4, 128.5, 125.9, 118.4, 110.5, 109.0, 82.3, 81.2, 62.5, 51.5, 43.3, 39.9, 37.0, 25.7, 25.4, 20.8. HRMS-APCI (*m/z*) $[M + H]^+$ calcd for $C_{19}H_{27}N_2O_2^+$, 315.2067; found 315.2056.

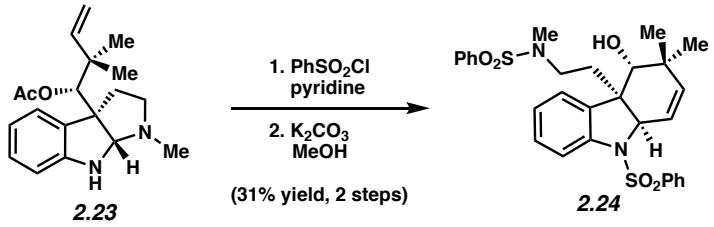

Tricycle 2.24. Pyrrolidinoindoline **2.23** (4.2 mg, 0.013 mmol, 1.0 equiv) was dissolved in pyridine (0.18 mL) and cooled to 0 °C. Phenylsulfonyl chloride (17 μL, 0.13 mmol, 10 equiv) was added and the reaction was warmed to 23 °C and allowed to stir for 16 h before being diluted with CH_2Cl_2 (4 mL) and washed with 1 M HCl (4 mL). The layers were separated and the organic layer was concentrated under reduced pressure. The resulting residue was purified by column chromatography (7:3 Hexanes:EtOAc) and the tricycle was carried on to the subsequent step.

The tricycle from the previous step (2.3 mg, 0.0051 mmol, 1.0 equiv) was dissolved in MeOH (2.0 mL) and K_2CO_3 (38 mg, 0.28 mmol, 55 equiv) was added. The reaction mixture was submerged in a preheated 57 °C oil bath and stirred for 5 min. The reaction was cooled to 23 °C and then diluted with EtOAc (15 mL) and washed sequentially with deionized H_2O (10 mL) and sat. aq. NaCl (10 mL). The layers were separated and the organic layer was dried over $MgSO_4$ and then concentrated under reduced pressure. The resulting residue was purified via column chromatography (7:3 Hexanes:EtOAc) to afford tricycle **2.24** (2.3 mg, 31% yield, 2 steps) as an off-white foam. R_f 0.15 (7:3 Hexanes:EtOAc); ^{1}H NMR (500 MHz, C_6D_6): δ 8.00 (d, J = 8.1 Hz, 1H), 7.71–7.58 (m, 2H), 7.58–7.46 (m, 2H), 6.93–6.81 (m, 5H), 6.77–6.63 (m, 4H), 6.20 (dd, J =

10.3, 4.0 Hz, 1H), 5.34 (d, J = 10.3 Hz, 1H), 4.19 (t, J = 4.1, 1.0 Hz, 1H), 3.31 (d, J = 6.6 Hz, 1H), 2.87–2.77 (m, 1H), 2.14–1.98 (m, 6H), 0.91–0.81 (m, 4H), 0.50 (s, 3H); ^{13}C NMR (125 MHz, C_6D_6): δ 141.1, 138.8, 138.0, 137.6, 135.3, 132.6, 131.7, 128.7, 128.6, 128.3, 127.2, 125.4, 123.3, 122.7, 116.1, 115.0, 76.0, 65.9, 49.9, 45.9, 36.8, 34.2, 32.8, 30.0, 24.6; HRMS-APCI (*m/z*) [M + H]$^+$ calcd for $C_{29}H_{33}N_2O_5S_2^+$, 553.1825; found 553.1829.

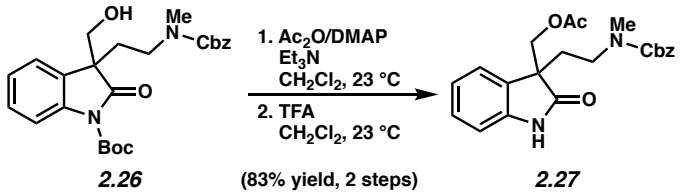

Oxindole 2.27. A solution of alcohol **2.26**[9] (1.10 g, 2.4 mmol, 1.0 equiv) was dissolved in CH_2Cl_2 (60 mL) and cooled to 0 °C. Et_3N (3.0 mL, 22 mmol, 9.0 equiv), Ac_2O (2.0 mL, 21 mmol, 9.0 equiv), and DMAP (263 mg, 2.1 mmol, 0.9 equiv) were added sequentially and the reaction mixture was allowed to stir at 0 °C for 15 min before being poured into sat. aq. $NaHCO_3$ (40 mL). The layers were separated and the aqueous layer was extracted with CH_2Cl_2 (2 x 20 mL). The combined organic layers were dried over Na_2SO_4 and then concentrated under reduced pressure. The resulting residue was purified by column chromatography (4:1 Hexanes:EtOAc) and the acetate-protected oxindole was carried on to the subsequent step.

The acetate protected oxindole from the previous step (557 mg, 1.1 mmol, 1.0 equiv) and anisole (0.12 mL, 1.1 mmol, 1.0 equiv) were dissolved in CH_2Cl_2 (18 mL) and cooled to 0 °C. TFA (2 mL) was added. The mixture was warmed to 23 °C and stirred for 30 min before being quenched with a solution of sat. aq. $NaHCO_3$ (100 mL) and diluted with CH_2Cl_2 (50 mL). The layers were separated and the aqueous layer was extracted with CH_2Cl_2 (2 x 10 mL). The combined organic layers were dried over Na_2SO_4 and concentrated under reduced pressure. The resulting residue was purified via column chromatography (7:3 → 1:1 Hexanes:EtOAc) to furnish **2.27** as a

white foam (550 mg, 83% yield, 2 steps). R_f 0.26 (1:1 Hexanes:EtOAc); ^{1}H NMR (500 MHz, $CDCl_3$): δ 8.37–8.06 (m, 1H), 7.48–7.27 (m, 5H), 7.24–7.17 (m, 1H), 7.09–6.91 (m, 2H), 6.89–6.80 (m, 1H), 5.12–4.85 (m, 2H), 4.60–4.37 (m, 1H), 4.30–4.08 (m, 1H), 3.30–2.89 (m, 2H), 2.83–2.69 (m, 3H), 2.30–1.98 (m, 2H), 1.95–1.82 (m, 3H); ^{13}C NMR (125 MHz, $CDCl_3$): δ 178.9, 178.8, 170.5, 170.5, 156.0, 141.1, 137.0, 136.7, 129.1, 129.0, 128.8, 128.6, 128.5, 128.1, 128.0, 123.9, 123.8, 122.9, 122.9, 110.0, 67.6, 67.5, 67.3, 67.1, 51.5, 51.4, 44.9, 44.4, 34.8, 34.2, 31.2, 30.6, 20.7; HRMS-APCI (*m/z*) $[M + H]^+$ calcd for $C_{22}H_{25}N_2O_5^+$, 397.1758; found 397.1744. Note: **2.27** was obtained as a mixture of rotamers. These data represent empirically observed chemical shifts from the ^{1}H and ^{13}C NMR spectra.

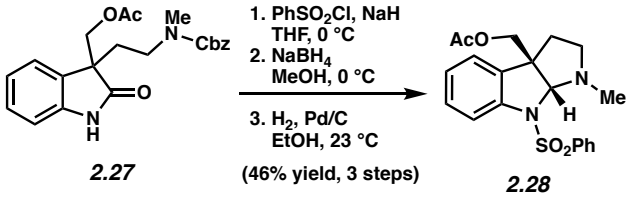

2.27 *2.28*

Pyrrolidinoindoline 2.28. NaH (240 mg, 60 wt% dispersion in mineral oil, 6.1 mmol, 6.0 equiv) was suspended in THF (6 mL) and cooled to 0 °C. Oxindole **2.27** (400 mg, 1.0 mmol, 1.0 equiv) was dissolved in THF (12 mL) and added to the stirring suspension of NaH. After stirring for 15 min, phenylsulfonyl chloride (0.25 mL, 2.0 mmol, 2.0 equiv) was added and the solution was warmed to 23 °C. After stirring at 23 °C for 10 min, the reaction mixture was quenched with a solution of sat. aq. NH_4Cl (1 mL) and diluted with CH_2Cl_2 (10 mL) and deionized H_2O (10 mL). The layers were separated and the aqueous layer was extracted with CH_2Cl_2 (2 x 5 mL). The combined organic layers were washed with sat. aq. NaCl (10 mL), dried over Na_2SO_4, and concentrated under reduced pressure. The resulting residue was purified via column

chromatography (7:3 → 1:1 Hexanes:EtOAc) and the resultant phenylsulfonyl oxindole was carried forward to the subsequent step.

The phenylsulfonyl oxindole from the previous step (230 mg, 0.43 mmol, 1.0 equiv) was dissolved in MeOH (6 mL) and cooled to 0 °C. $NaBH_4$ (32 mg, 0.85 mmol, 2.0 equiv) was added and the solution was allowed to stir for 15 min before more $NaBH_4$ (32 mg, 0.85 mmol, 2.0 equiv) was added. The reaction was allowed to stir for 10 min before being quenched with a solution of sat. aq. $NaHCO_3$ (25 mL) and diluted with CH_2Cl_2 (25 mL). The layers were separated and the aqueous layer was extracted with CH_2Cl_2 (2 x 25 mL). The combined organic layers were dried over $MgSO_4$ and concentrated under reduced pressure. The resulting residue was carried on to the subsequent step.

The residue from the previous step was dissolved in EtOH (10 mL). Pd/C (75 mg) was added and the suspension was stirred for 10 min before being sparged with H_2 for 10 min. After stirring under H_2 (1 atm) for 16 h, the reaction was filtered over a short silica plug (~2 x 5 cm) and then rinsed with EtOAc (100 mL). The reaction mixture was then concentrated under reduced pressure and the resultant residue was purified by flash chromatography (4:1 → 7:3 Hexanes:EtOAc) to afford pyrrolidinoindoline **2.28** (87 mg, 46% yield, 3 steps) as a white crystalline solid. Crystals suitable for X-ray diffraction studies (CCDC 1987257) were obtained using slow evaporation from 1:2 Benzene/CH_2Cl_2. R_f 0.25 (4:1 Hexanes:EtOAc); ^{1}H NMR (500 MHz, C_6D_6): δ 7.92 (d, *J* = 8.1 Hz, 1H), 7.61–7.58 (m, 2H), 6.94 (ddd, *J* = 8.2, 7.5, 1.3 Hz, 2H), 6.79–6.75 (m, 1H), 6.72 (td, *J* = 7.5, 1.0 Hz, 1H), 6.68 (t, *J* = 7.7 Hz, 2H), 6.63–6.58 (m, 1H), 5.18 (s, 1H), 3.48 (d, *J* = 11.2 Hz, 1H), 3.19 (d, *J* = 11.3 Hz, 1H), 2.76 (s, 3H), 2.38 (ddd, *J* = 9.7, 6.8, 3.1 Hz, 1H), 2.28 (td, *J* = 8.9, 5.4 Hz, 1H), 1.89 (ddd, *J* = 11.8, 8.7, 6.5 Hz, 1H), 1.52–1.48 (m, 1H), 1.45 (s, 3H); ^{13}C NMR (125 MHz, C_6D_6): δ 169.3, 142.7, 138.5, 135.7, 132.6, 128.6, 128.5,

127.0, 124.8, 124.0, 117.3, 88.6, 66.6, 56.5, 51.8, 36.2, 34.9, 19.8. HRMS-APCI (*m/z*) $[M + H]^+$ calcd for $C_{20}H_{23}N_2O_4S^+$, 387.1373; found 387.1357.

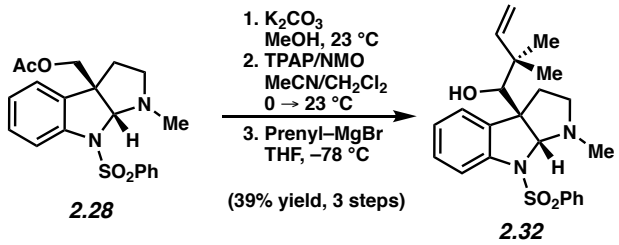

Alcohol 2.32. Pyrrolidinoindoline **2.28** (74 mg, 0.19 mmol, 1.0 equiv) was dissolved in MeOH (3.5 mL) and K_2CO_3 (270 mg, 2.0 mmol, 11 equiv) was added. After stirring for 5 min, the reaction was diluted with CH_2Cl_2 (10 mL), filtered over a short silica plug (~1 x 1 cm), and then rinsed with EtOAc (20 mL). The reaction mixture was then concentrated under reduced pressure and the resultant residue was carried forward without further purification.

The alcohol from the previous step (65 mg, 0.19 mmol, 1.0 equiv) was dissolved in a mixture of CH_2Cl_2 (16 mL) and MeCN (4 mL). NMO (44 mg, 0.38 mmol, 2.0 equiv) and finely ground 4Å molecular sieves (72 mg) were added and the reaction mixture was cooled to 0 °C. TPAP (15 mg, 0.038 mmol, 10 mol%) was then added as a solution in MeCN (1 mL). The reaction was warmed to 23 °C, stirred for 15 min. The mixture was then diluted with EtOAc (30 mL), flushed through a short silica plug (~2 x 5 cm), and rinsed with EtOAc (30 mL) as eluent. The mixture was concentrated under reduced pressure and the resultant residue was purified via column chromatography (1:1 Hexanes:EtOAc) to furnish the corresponding pyrrolidinoindoline aldehyde.

A solution of the pyrrolidinoindoline aldehyde from the last step (15 mg, 0.044 mmol, 1.0 equiv) was dissolved in THF (2 mL) and cooled to 0 °C. Prenylmagnesium bromide (0.5 mL, 0.34 M in THF, 0.17 mmol, 3.9 equiv) was added and the reaction was stirred 5 min before being quenched by the addition of solid NH_4Cl (~15 mg), followed by acetone (10 mL). The suspension

was then concentrated directly onto silica under reduced pressure. The resultant residue (adsorbed onto silica gel) was then purified by flash chromatography (4:1 → 3:1 Hexanes:EtOAc) to furnish alcohol **2.32** (9 mg, 39% yield, 3 steps) in >20:1 diastereomeric excess. R_f 0.37 (7:3 Hexanes:EtOAc); ^{1}H NMR (500 MHz, $CDCl_3$): δ 7.96–7.89 (m, 2H), 7.56–7.50 (m, 1H), 7.46–7.38 (m, 3H), 7.23–7.15 (m, 2H), 6.99 (td, *J* = 7.5, 1.1 Hz, 1H), 5.87 (dd, *J* = 17.5, 10.8 Hz, 1H), 5.47 (s, 1H), 5.06 –4.94 (m, 2H), 3.11 (d, *J* = 4.9 Hz, 1H), 2.68 (ddd, *J* = 9.1, 6.7, 2.0 Hz, 1H), 2.61 (m, 4H), 2.34 (td, *J* = 9.7, 5.1 Hz, 1H), 1.79 (ddd, *J* = 11.8, 5.1, 2.0 Hz, 1H), 1.67 (d, *J* = 5.4 Hz, 1H), 1.00 (s, 3H), 0.84 (s, 3H); ^{13}C NMR (125 MHz, $CDCl_3$): δ 145.2, 142.1, 140.1, 135.7, 132.9, 129.0, 128.6, 127.6, 126.8, 123.6, 115.0, 113.3, 89.3, 79.1, 63.0, 52.4, 43.4, 38.4, 36.9, 29.9, 26.6, 24.1; HRMS-APCI (*m/z*) $[M + H]^+$ calcd for $C_{23}H_{29}N_2O_3S^+$, 413.1893; found 413.1908.

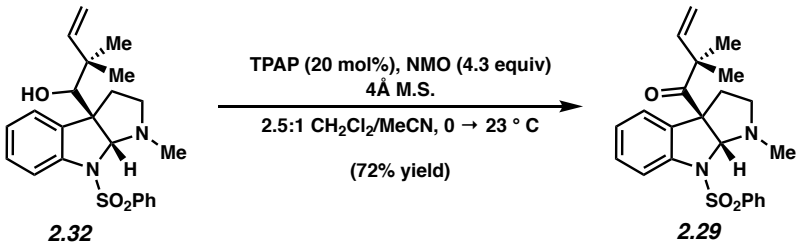

Ketone 2.29. **2.32** (9.1 mg, 0.022 mmol, 1.0 equiv) was dissolved in a mixture of CH_2Cl_2 (0.8 mL) and MeCN (0.1 mL). NMO (11 mg, 0.094 mmol, 4.3 equiv) and 4Å molecular sieves (10 mg) were added and the reaction mixture was cooled to 0 °C. TPAP (1.7 mg, 0.005 mmol, 20 mol%) was added as a solution in MeCN (0.2 mL). The reaction was warmed to 23 °C and stirred for 1h. The reaction was then diluted with a 1:1 mixture of Hexanes and EtOAc (5 mL), filtered through a silica plug (~ 1 x 1 cm), and rinsed with a 1:1 mixture of Hexanes and EtOAc (30 mL) as the eluent. The mixture was concentrated under reduced pressure and the resultant residue was purified via column chromatography (9:1 → 4:1 Hexanes:EtOAc) to furnish the ketone **2.29** (6.4 mg, 72% yield). R_f 0.52 (7:3 Hexanes:EtOAc). ^{1}H NMR (500 MHz, $CDCl_3$): δ 7.92 (dd, *J* = 8.5, 1.3 Hz,

2H), 7.56–7.49 (m, 1H), 7.48–7.40 (dd, *J* = 8.2, 0.8 Hz, 3H), 7.20 (ddd, *J* = 8.0, 7.4, 1.4 Hz, 1H), 7.06 (dd, *J* = 7.6, 1.3 Hz, 1H), 6.98 (td, *J* = 7.6, 1.1 Hz, 1H), 5.81 (s, 1H), 5.77 (dd, *J* = 17.5, 10.6 Hz, 1H), 5.13 (dd, *J* = 10.6, 0.5 Hz, 1H), 5.05 (d, *J* = 17.5 Hz, 1H), 2.79–2.67 (m, 2H), 2.61 (s, 3H), 2.51–2.39 (m, 1H), 2.02–1.80 (m, 1H), 1.09 (s, 3H), 1.04 (s, 3H); ^{13}C NMR (125 MHz, $CDCl_3$) δ 209.1, 142.1, 141.8, 140.0, 133.3, 133.1, 129.0, 129.0, 127.6, 125.3, 123.8, 115.6, 114.6, 90.5, 69.7, 51.9, 39.0, 38.5, 29.9, 26.1, 25.5; HRMS-APCI (*m/z*) $[M + H]^+$ calcd for $C_{23}H_{27}N_2O_3S^+$, 411.1740; found 411.1761.

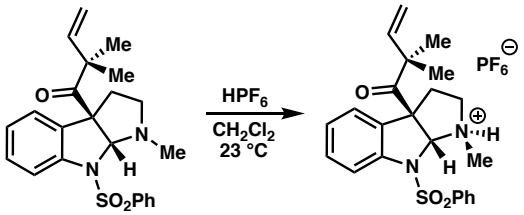

2.29 *2.30*

Salt 2.30. Ketone **2.29** (19 mg, 0.046 mmol) was dissolved in CH_2Cl_2 (5 mL). DI H2O (1.5 mL) followed by aq. HPF_6 (60 wt%, 5 drops from glass Pasteur pipette) were added, the layers were separated, the aqueous layer was rinsed with CH_2Cl_2, and the combined organic layers were concentrated under reduced pressure. The resultant residue was dissolved in $CDCl_3$ (0.5 mL) and salt **2.30** crashed out of solution as a white crystalline powder within 15 min. Crystals suitable for X-ray diffraction studies (CCDC 1987258) were obtained as follows. First, the salt was dissolved in $CHCl_3$ (2 mL). Then, nHexane (6 mL) was added carefully to avoid disturbing the $CHCl_3$ layer. Finally, the layers were allowed to diffuse together over ~16 hours until crystals suitable for single-crystal X-ray diffraction were observed.

2.6 Spectra Relevant to Chapter Two:

Evaluation of the Photodecarbonylation of Crystalline Ketones for the Installation of Reverse Prenyl Groups on the Pyrrolidinoindoline Scaffold

Adapted from: Jordan J. Dotson, Neil K. Garg,* and Miguel A. Garcia-Garibay.*

Tetrahedron, https://doi.org/10.1016/j.tet.2020.131181.

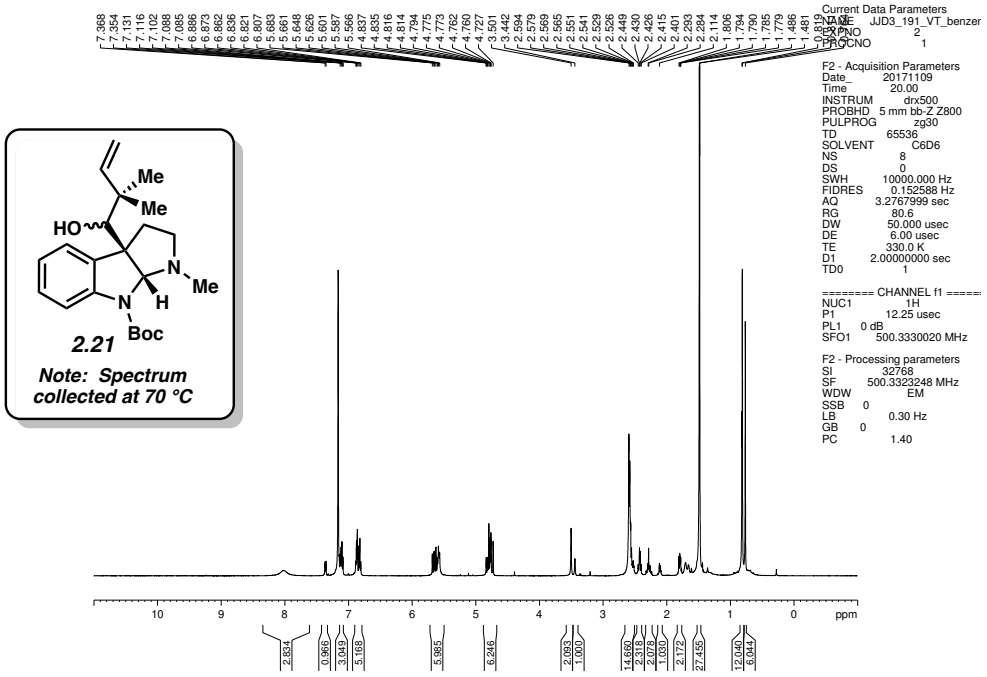

Figure 2.1 ^{1}H NMR (500 MHz, C_6D_6) of compound **2.21**.

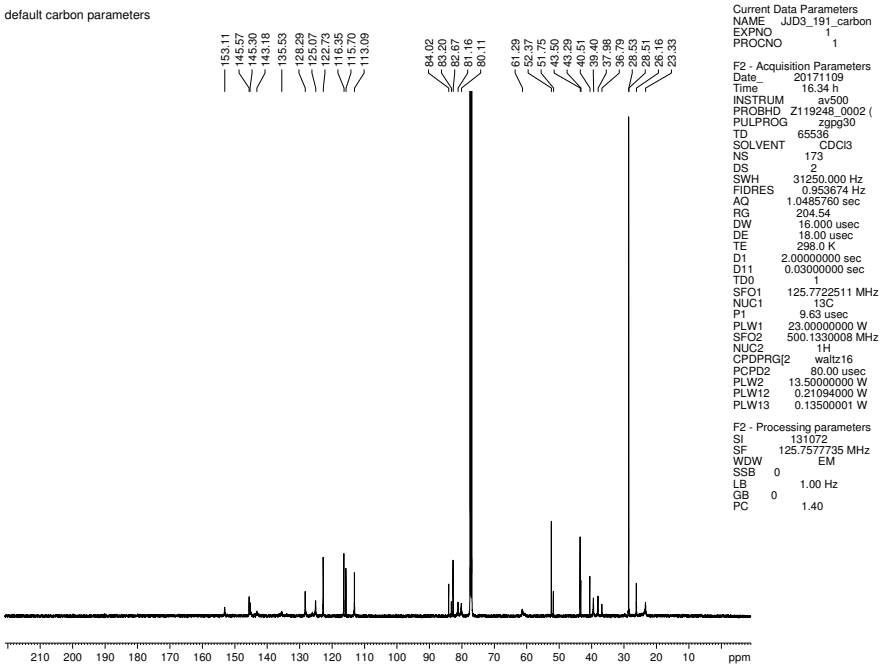

Figure 2.2 ^{13}C NMR (125 MHz, C_6D_6) of compound **2.21**.

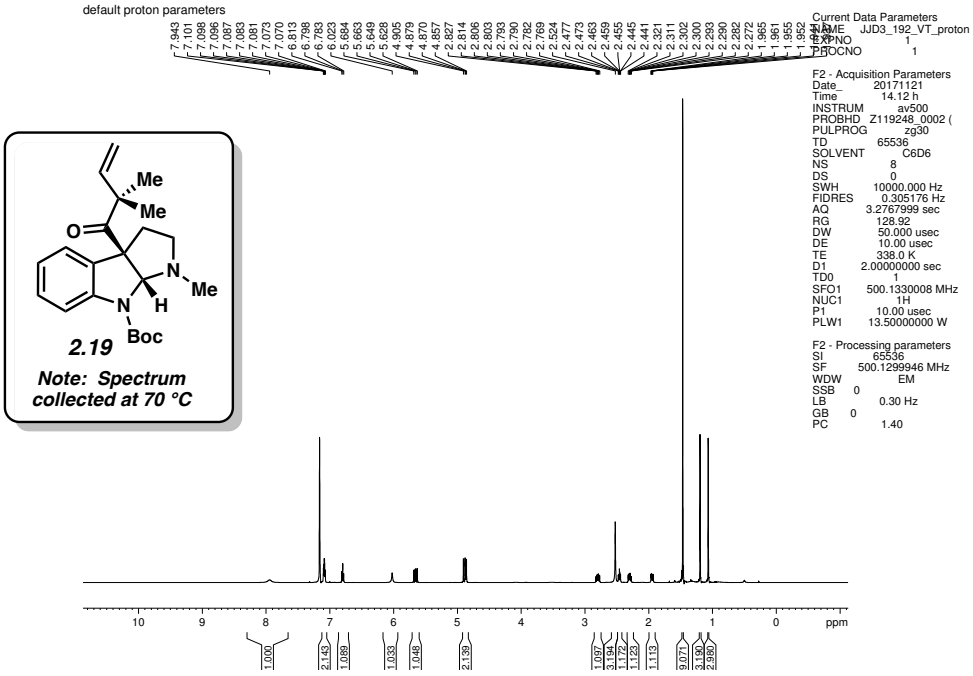

Figure 2.3 ^{1}H NMR (500 MHz, C_6D_6) of compound **2.19**.

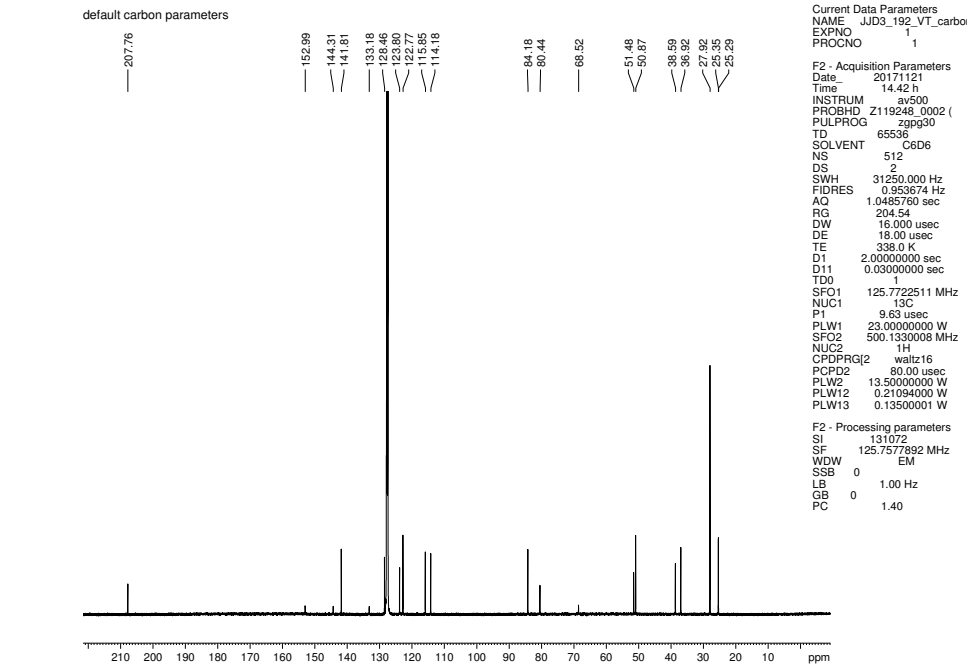

Figure 2.4 ^{13}C NMR (125 MHz, C_6D_6) of compound **2.19**.

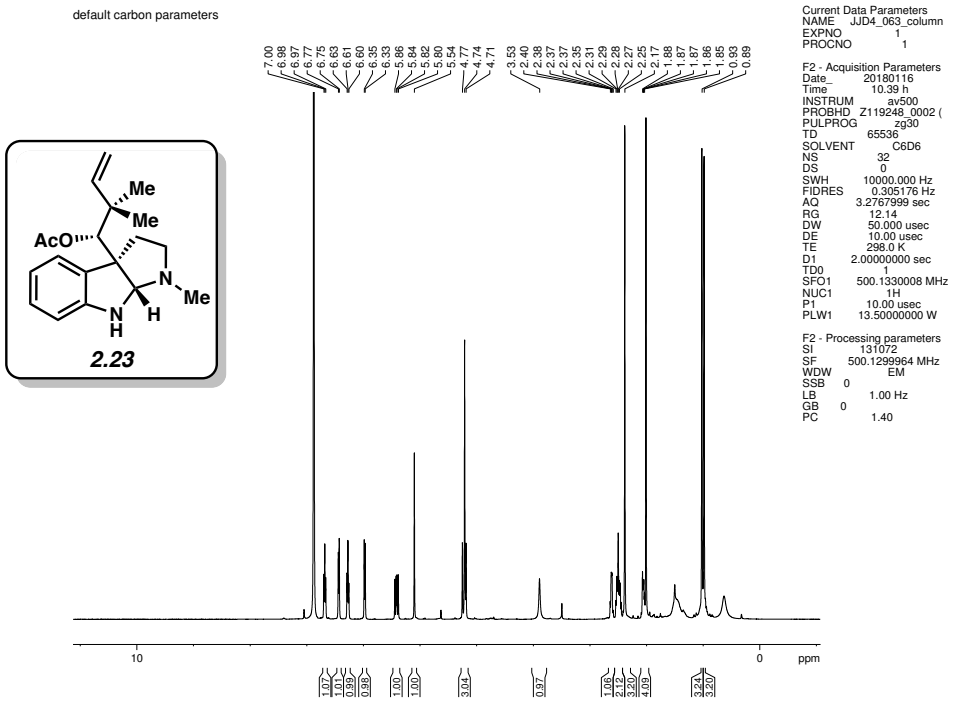

Figure 2.5 ^{1}H NMR (500 MHz, C_6D_6) of compound **2.23**.

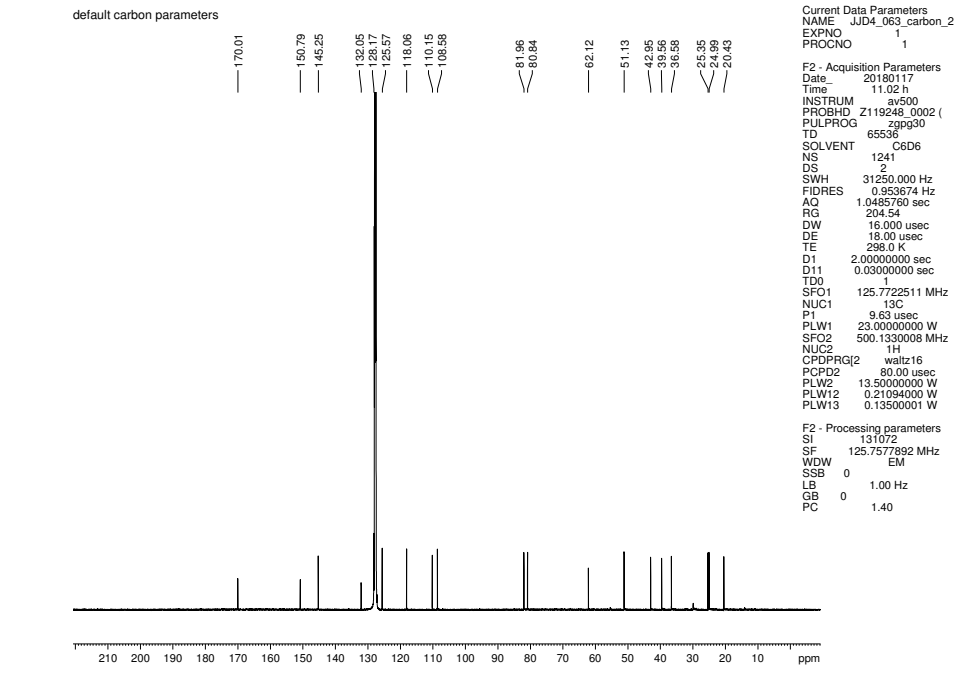

Figure 2.6 ^{13}C NMR (125 MHz, C_6D_6) of compound **2.23**.

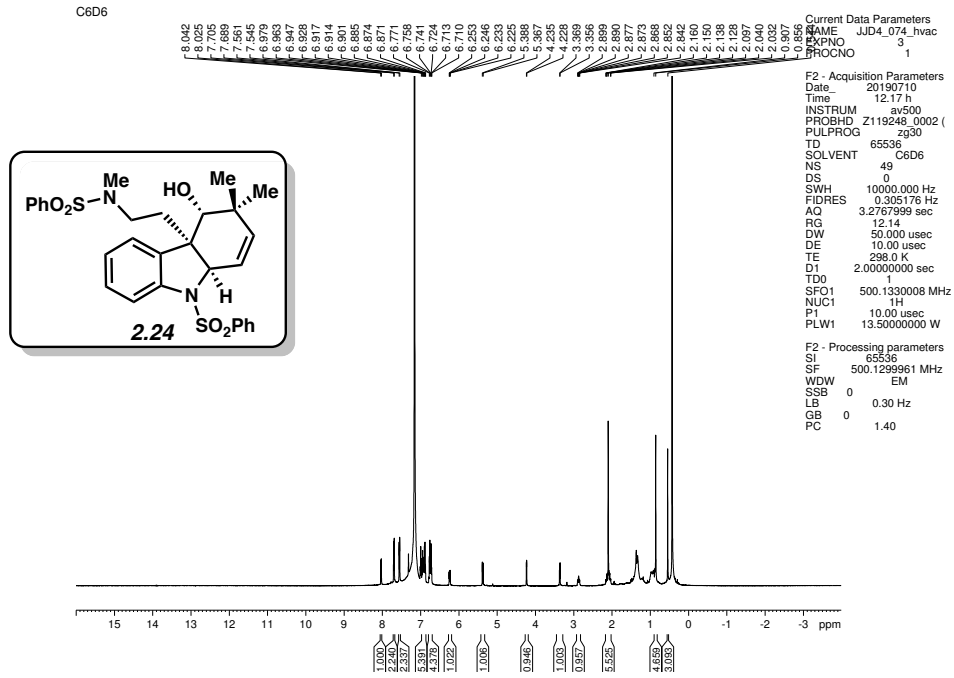

Figure 2.7 ^{1}H NMR (500 MHz, C_6D_6) of compound **2.24**.

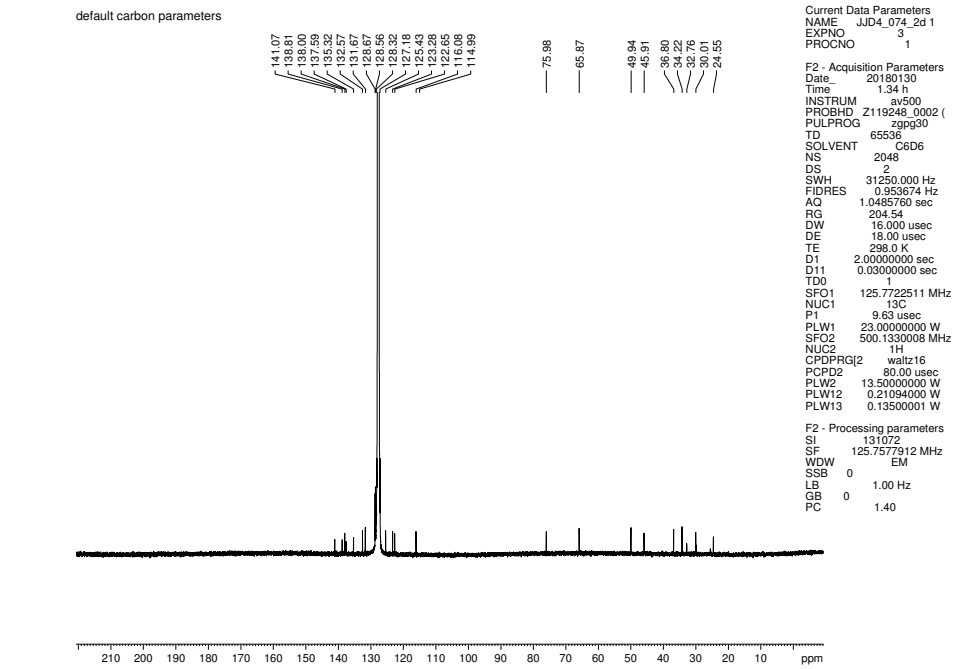

Figure 2.8 ^{13}C NMR (125 MHz, C_6D_6) of compound **2.24**.

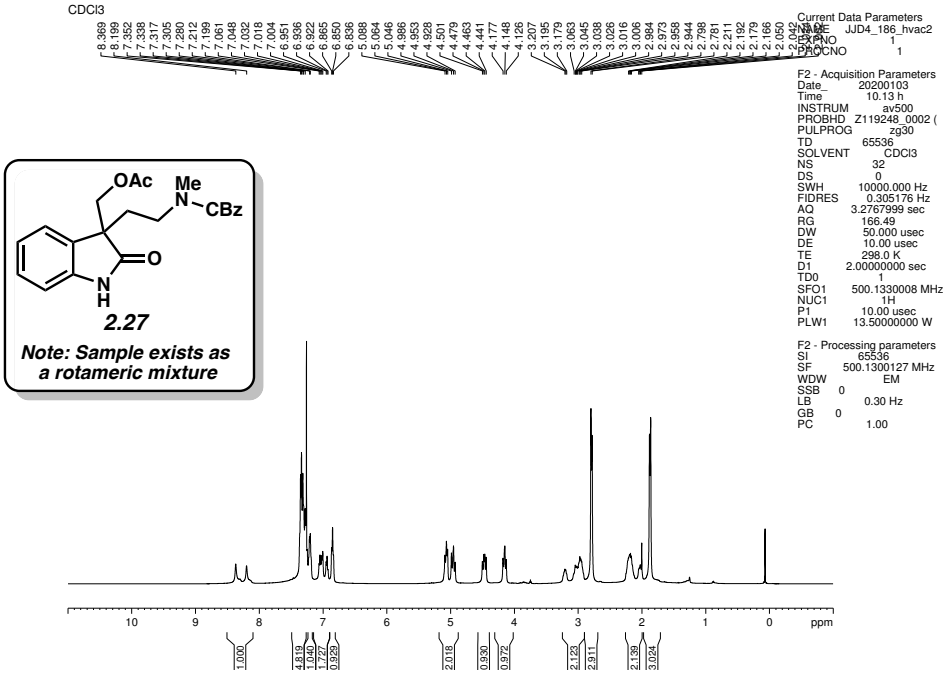

Figure 2.9 ^{1}H NMR (500 MHz, $CDCl_3$) of compound **2.27**.

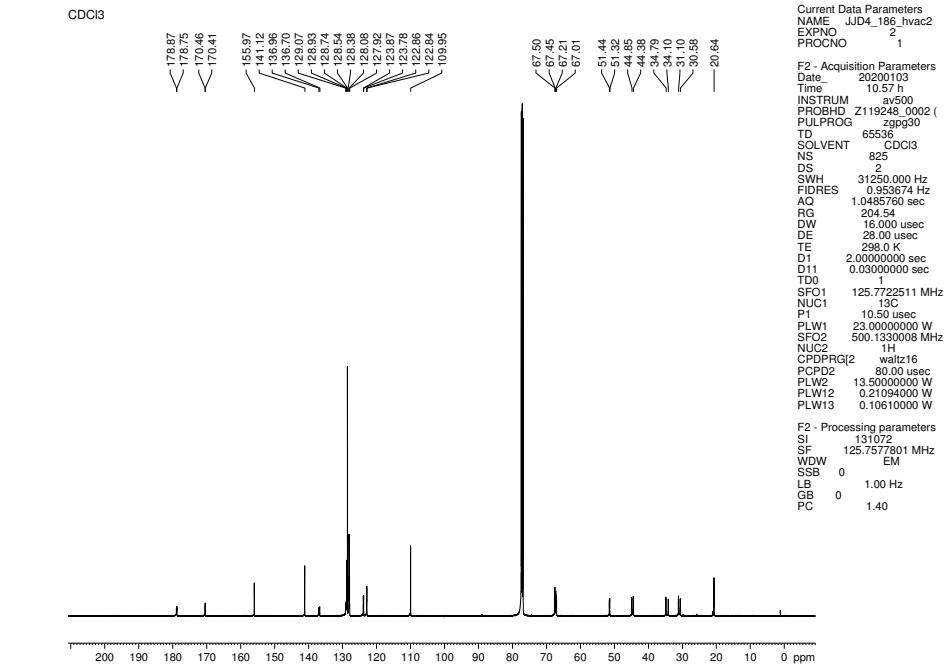

Figure 2.10 ^{13}C NMR (125 MHz, $CDCl_3$) of compound **2.27**.

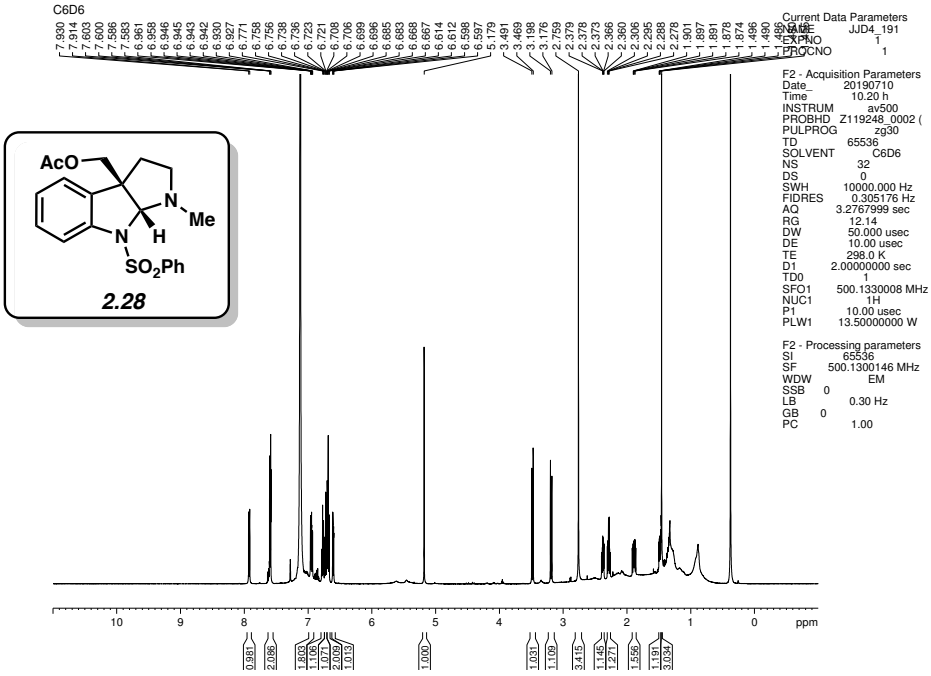

Figure 2.11 ^{1}H NMR (500 MHz, C_6D_6) of compound **2.28**.

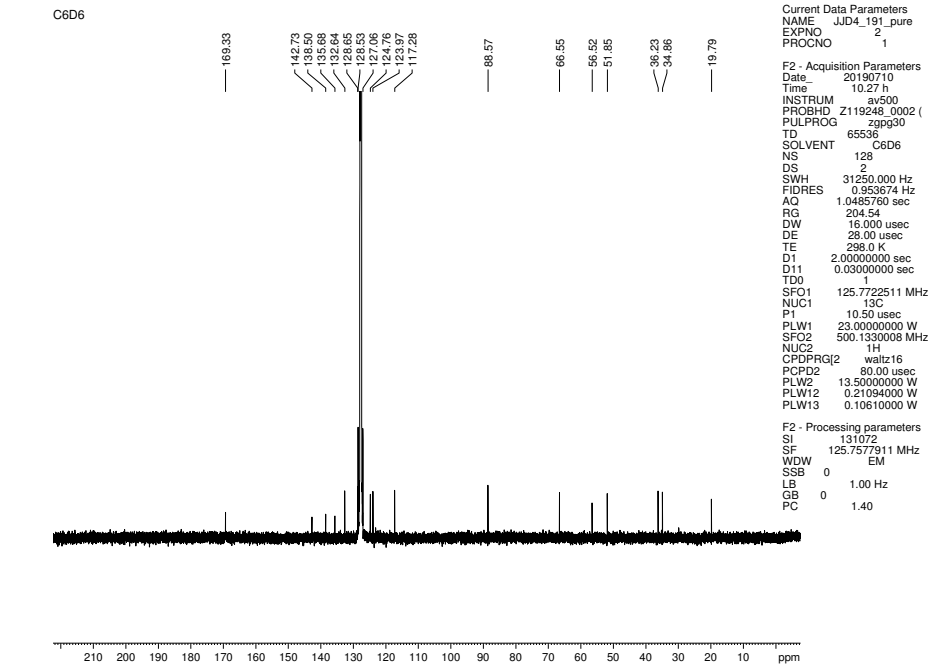

Figure 2.12 ^{13}C NMR (125 MHz, C_6D_6) of compound **2.28**.

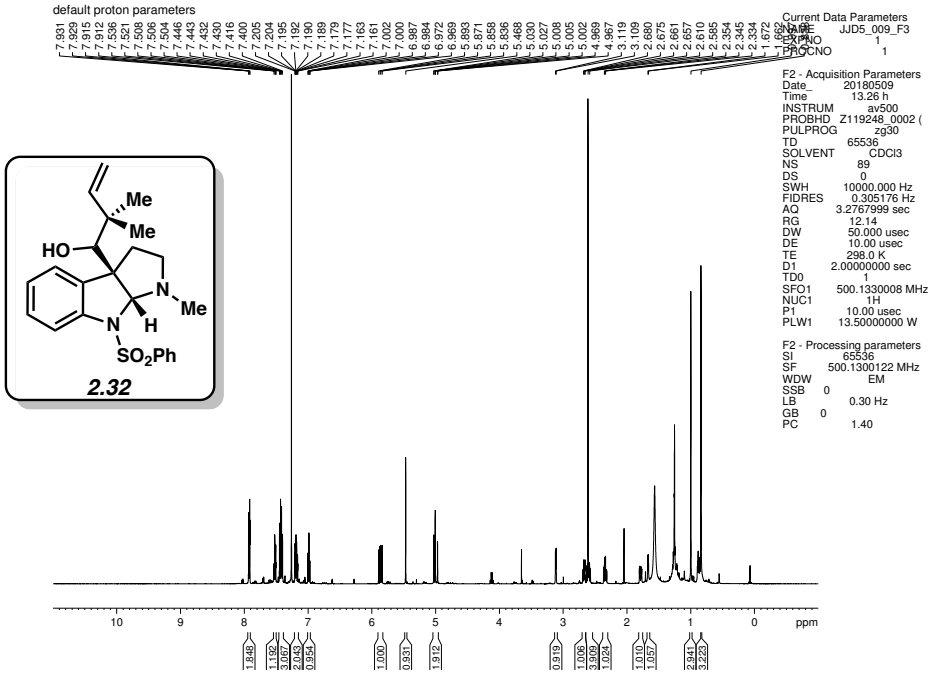

Figure 2.13 ^{1}H NMR (500 MHz, $CDCl_3$) of compound **2.32**.

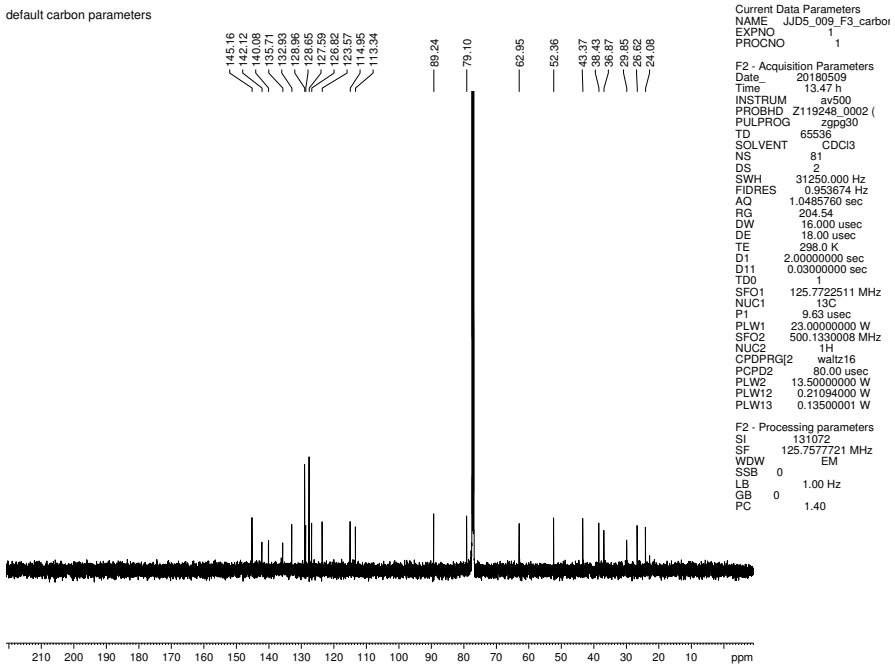

Figure 2.14 ^{13}C NMR (125 MHz, $CDCl_3$) of compound **2.32**.

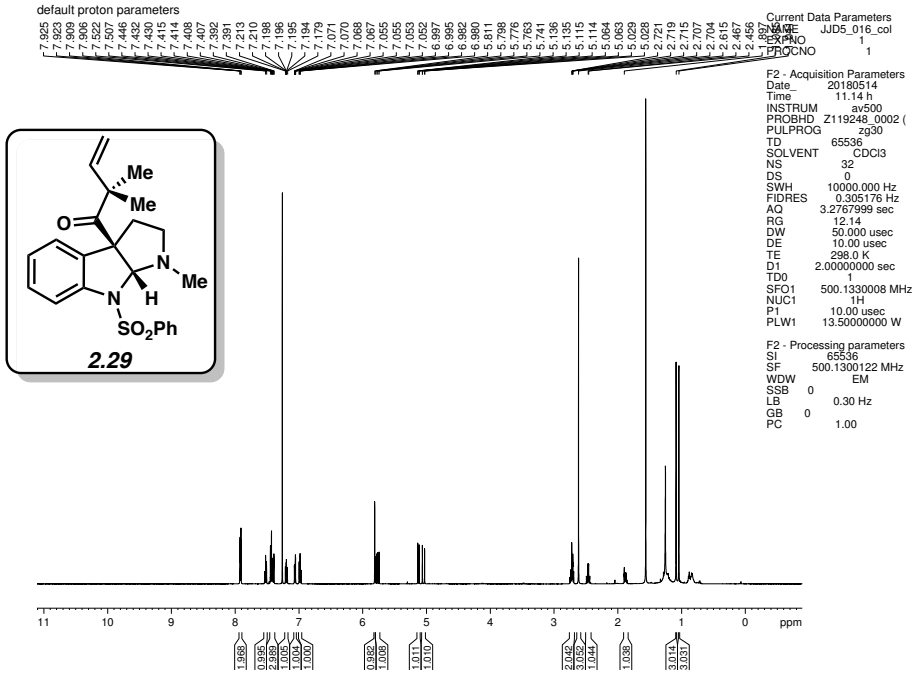

Figure 2.15 ^{1}H NMR (500 MHz, $CDCl_3$) of compound **2.29**.

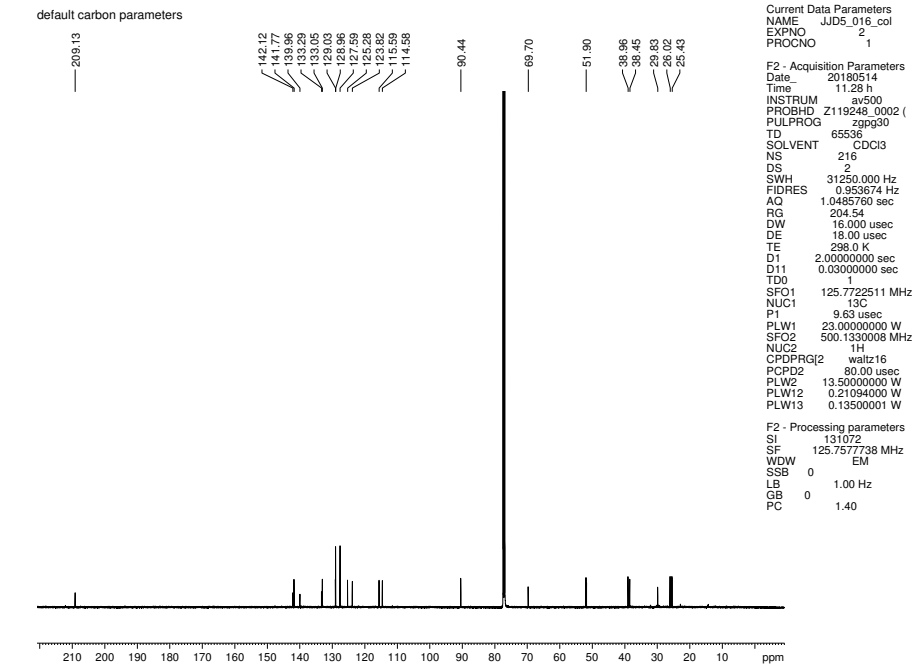

Figure 2.16 ^{13}C NMR (125 MHz, $CDCl_3$) of compound **2.29**.

2.7 Notes and References

(1) Lu, Z.; Ma, S. *Angew. Chem., Int. Ed.* **2008**, *47*, 258–297.

(2) Razzak, M.; De Brabander, J. K. *Nat. Chem. Biol.* **2011**, *7*, 865–875.

(3) (a) Yang, Y.; Buchwald, S. L. *J. Am. Chem. Soc.* **2013**, *135*, 10642–10645; (b) Ruchti, J.; Carreira, E. M. *J. Am. Chem. Soc.* **2014**, *136*, 16756–16759; (c) Trost, B. M.; Malhotra, S.; Chan, W. H. *J. Am. Chem. Soc.* **2011**, *133*, 7328–7331; (d) Müller, J. M.; Stark, C. B. W. *Angew. Chem., Int. Ed.* **2016**, *55*, 4798–4802.

(4) (a) Dotson, J. J.; Perez-Estrada, S.; Garcia-Garibay, M. A. *J. Am. Chem. Soc.* **2018**, *140*, 8359–8371; (b) Hernández-Linares, M. G.; Guerrero-Luna, G.; Pérez-Estrada, S.; Ellison, M.; Ortin, M. M.; Garcia-Garibay, M. A. *J. Am. Chem. Soc.* **2015**, *137*, 1679–1684.

(5) For previous syntheses of Flustramines A and B, see: (a) Adla, S. K.; Sasse, F.; Kelter, G.; Fiebig, H. H.; Lindel, T. *Org. Biomol. Chem.*, **2013**, *11*, 6119–6130; (b) Trost, B. M.; Malhotra, S.; Chan, W. H. *J. Am. Chem. Soc.* **2011**, *133*, 7328–7331; (c) Kawasaki, T.; Shinada, M.; Kamimura, D.; Ohzono, M.; Ogawa, A. *Chem. Commun.* **2006**, 420–422; (e) Fuchs, J. R.; Funk, R. L. *Org. Lett.* **2005**, *7*, 677–680.

(6) For previous syntheses of debromoflustramines A or B, see: (a) Morales-Ríos, M. S.; Suarez-Castíllo, O. R.; Joseph-Nathan, P. *J. Org. Chem.* **1999**, *64*, 1086–1087; (b) Kawesake, T.; Shinada, M.; Ohzono, M.; Ogawa, A.; Terashima, R.; Sakamoto, M. *J. Org. Chem.* **2008**, *73*, 5959–5964; (c) Ignatenko, V. A.; Zhang, P.; Viswanathan, R. *Tetrahedron Lett.*, **2011**, *52*, 1269–1272. (d) (c) Schammel, A. W.; Boal, B. W.; Zu, L.; Mesganaw, T.; Garg, N. K. *Tetrahedron* **2010**, *66*, 4687–4695.

(7) For select synthetic strategies to form C3 quaternary pyrrolidinoindoline ring systems, see: (a) Repka, L. M.; Reisman, S. E. *J. Org. Chem.* **2013**, *78*, 12314–12320; (b) Schmidt, M. A.;

Movassaghi, M. *Synlett* **2008**, 313–324; (c) Susick, R. B.; Morrill, L. A.; Picazo, E.; Garg, N. K. *Synlett* **2017**, *28*, 1–11; (d) Crich, D.; Banerjee, A. *Acc. Chem. Res.* **2007**, *40*, 151–161; (e) Furst, L.; Narayanam, J. M. R.; Stephenson, C. R. J. *Angew. Chem., Int. Ed.* **2011**, *50*, 9655–9659; (f) Overman, L. E.; Larrow, J. F.; Stearns, B. A.; Vance, J. M. *Angew. Chem., Ind. Ed.* **2000**, *39*, 213–215; (g) Wang, H.; Reisman, S. E. *Angew. Chem., Int. Ed.* **2014**, *53*, 6206–6210; (h) Jamison, C. R.; Badillo, J. J.; Lipshultz, J. M.; Comito, R. J.; Macmillan, D. W. C. *Nat. Chem.* **2017**, *9*, 1165–1169; (i) Gentry, E. C.; Rono, L. J.; Hale, M. E.; Matsuura, R.; Knowles, R. R. *J. Am. Chem. Soc.* **2018**, *140*, 3394–3402; (j) Verotta, L.; Orsini, F.; Sbacchi, M.; Scheildler, M. A.; Amador, T. A.; Elisabetsky, E. *Bioorg. Med. Chem.* **2002**, *10*, 2133–2142.

(8) (a) Carié, J. S.; Christophersen, C. *J. Org. Chem.* **1980**, *45*, 1586–1589; (b) Sjoblom, T.; Bholin, L.; Christophersen, C. *Acta Pharm. Suec.* **1979**, *20*, 415–418; (c) Peters, L.; König, G. M.; Terlau, H.; Wright, A. D. *J. Nat. Prod.* **2002**, *65*, 1633–1637.

(9) De, S.; Das, M. K.; Bhunia, S.; Bisai, A. *Org. Lett.* **2015**, *17*, 5922–5925.

(10) (a) Griffith, W. P.; Ley, S. L.; Whitcombe, G. P.; White, A. D. *J. Chem. Soc., Chem. Commun.* **1987**, 1625–1627; (b) Griffith, W. P. *Chem. Soc. Rev.*, **1992**, *21*, 179–185.

(11) (a) Bruncko, M.; Crich, D.; Samy, R. *J. Org. Chem.* **1994**, *59*, 5543–5549; (b) Crich, D.; Banerjee, A. *Acc. Chem. Res.* **2007**, *40*, 151–161.

(12) Sabahi, A.; Rainier, J. D. *Arkivoc* **2010**, *8*, 116–125.

(13) An identical protection strategy was attempted on the epimer of **2.23** and and also resulted in an aza-Prins rearrangement.

(14) Daniels, B. E.; Ni, J.; Reisman, S. E. *Angew. Chem., Int. Ed.* **2016**, *55*, 3398–3402.

(15) Weiss, B.; Durr, H.; Haas, H. J. *Angew. Chem., Int. Ed. Engl.* **1980**, *19*, 648–650.

(16) Lipshutz, B. H.; Hackmann, C. *J. Org. Chem.* **1994**, *59*, 7437–7444.

(17) Legault, C.Y. *CYLview*, 1.0b; Université de Sherbrooke: Quebec, 2009; http://www.cylview.org.

CHAPTER THREE

Discovery and Total Synthesis of a Bis(Cyclotryptamine) Alkaloid Bearing the Elusive Piperidinoindoline Scaffold

3.1 Abstract

Bis(cyclotryptamine) alkaloids have been popular topics of study for many decades. Five possible scaffolds for bis(cyclotryptamine) alkaloids were originally postulated in the 1950s, but only four of these scaffolds have been observed in natural products to date. We describe synthetic access to the elusive fifth scaffold, the piperidinoindoline, through syntheses of compounds now termed "dihydropsychotriadine" and "psychotriadine." The latter of these compounds was subsequently identified in extracts of the flower *Psychotria colorata*. Our synthetic route features a stereospecific solid-state photodecarbonylation reaction to introduce the key vicinal quaternary stereocenters.

3.2 Introduction

Since the initial isolation of calycanthine in 1888,[1] bis(cyclotryptamine) alkaloids[2] have captivated the attention of scientists worldwide. Interest in these natural products has been fueled by a combination of their biological activities and intricate structures. With regard to the latter, the identification and structural elucidation of bis(cyclotryptamine) alkaloids has a rich history.[2a,b] For example, although calycanthine was isolated in 1888, its structure remained a mystery until 1954,

when Robert Robinson and H. J. Teuber first proposed a plausible structural identity.[3] At that time, they suggested the existence of five possible distinct ring systems, depicted as **3.1**–**3.5**, arising from common biosynthon **3.6** (Figure 3.1). On the basis of degradation studies, piperidinoindoline **3.5** was postulated as the constitutional isomer for calycanthine. However, in 1960, studies by Woodward[4] and Hamor[5] identified bridged bicycle **3.1** as the correct structure.

Figure 3.1. Possible bis(cyclotryptamine) alkaloid constitutional isomers **3.1**–**3.5** arising from common biosynthon **3.6**.

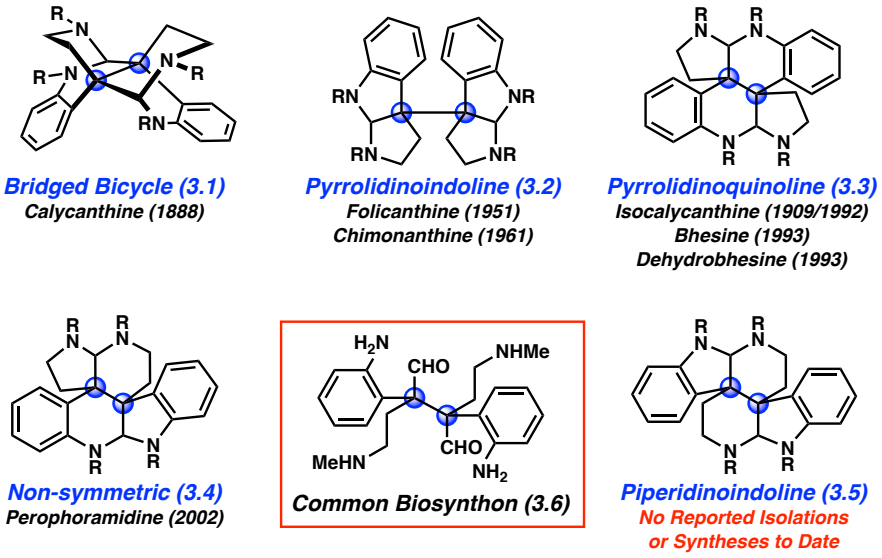

Over the subsequent six decades, many isolation reports,[6] biosynthetic studies,[7] and synthetic efforts have been disclosed.[2] This has led to the discovery of more than 20 bis(cyclotryptamine) alkaloids to date.[2] Interestingly, of the five possible isomeric scaffolds originally proposed, only four have been confirmed to exist (i.e., **3.1**–**3.4**) in isolated natural products.[6] With regard to synthetic studies, completed total syntheses of natural products bearing scaffolds **3.1**, **3.2**, and **3.4** have been most common over the past few decades while efforts to

access piperidinoindoline scaffold **3.5** have been rare. In a seminal study, however, Scott and coworkers are believed to have accessed a meso compound bearing scaffold **3.5** in 1967.[8] More recently, compounds bearing substituted piperidinoindoline scaffolds have been accessed in the context of communesin studies, as shown independently by our and Tang's group[9] and by Movassaghi's group.[10] Scaffold **3.5** has not been observed naturally.

Like many laboratories, we were drawn to the bis(cyclotryptamine) alkaloids due to their remarkable structures. These compounds typically feature four nitrogen atoms, vicinal quaternary stereocenters (arising biosynthetically from the dimerization of a tryptamine derivative[2a–c,7]), and six interwoven rings. With the aim of potentially accessing the various isomeric members of the family, we targeted biosynthon **3.6**. Overman,[11] Movassaghi,[12] and others,[2,13] have elegantly demonstrated the success of this general approach to access pyrrolidinoindoline isomer **3.2** from pre-formed indoline (or related) ring systems.[14] In this manuscript, we demonstrate an alternative approach to **3.6** that relies on the stereospecific photodecarbonylation of a crystalline ketone to access the requisite vicinal quaternary centers, ultimately leading to the synthesis of an alkaloid bearing the elusive piperidinoindoline scaffold **3.5** and its identification in *Psychotria colorata* flower extracts.

3.3 Results and Discussion

Our retrosynthetic approach targeted biosynthon **3.6** as a potential means to access various bis(cyclotryptamine) scaffolds (Scheme 3.1). As **3.6** itself would not be isolable, we targeted a synthetic equivalent or congener by reduction of bis(lactam) **3.7** and late-stage C–N bond formation. In turn, brominated compound **3.7** would arise from ketone **3.9** via a solid-state photodecarbonylation reaction. This key step would proceed by Norrish type I

photodecarbonylation of **3.9**, followed by coupling of radical pair **3.8**. Due to conformational restrictions imposed by the rigid reaction cavity of the crystal lattice, illustrated by the dotted lines, the conversion of **3.9** to **3.7** was expected to occur stereoretentively. We have previously shown the success of such solid-state photodecarbonylation reactions in simpler systems.[15,16,17] Moreover, this key step would complement the elegant radical-based approach to accessing cyclotryptamine alkaloids pioneered by Movassaghi and coworkers.[12] Ketone **3.9** would be prepared from acid chloride **3.10** and enolate **3.11**.[18]

Scheme 3.1. Retrosynthetic analysis of biosynthon **3.6** with key stereospecific radical combination in the crystalline state.

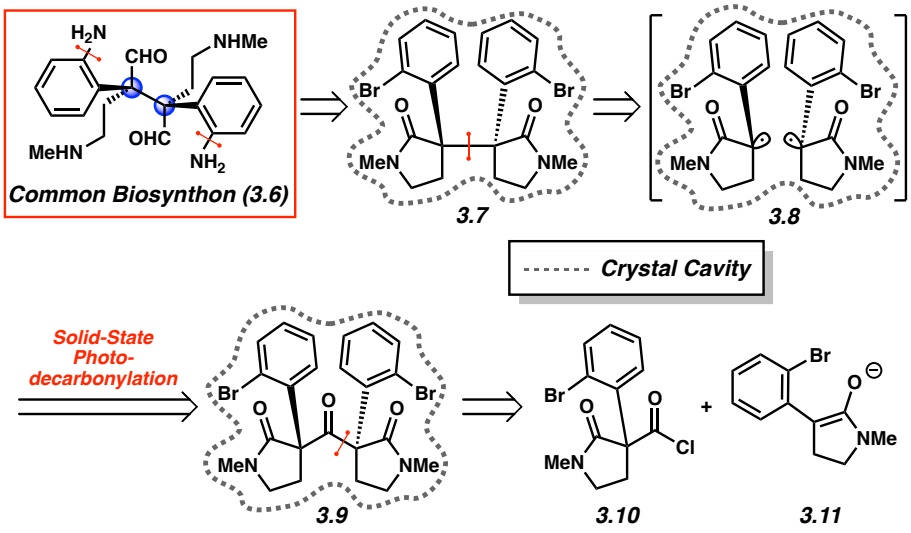

Scheme 3.2 summarizes our synthesis of ketone substrate **3.9** and the attempted photodecarbonylation reaction. Arylmalonic ester **3.12** was converted to pyrrolidinone **3.13** through alkylation with bromoacetonitrile followed by a reductive cyclization. Subsequent methylation furnished pyrrolidinone **3.14**, which served as a point of divergence. In one pathway, **3.14** was converted to acid chloride **3.10** through a two-step sequence involving saponification and

treatment of the resultant carboxylic acid with oxalyl chloride and catalytic DMF. In the other sequence, **3.14** was saponified and then thermally decarboxylated to provide amide **3.15** in 79% yield. To unite the fragments, amide **3.15** was converted to its lithium enolate by deprotonation with LiHMDS. In situ trapping with acid chloride **3.10** delivered ketone **3.9**, the desired substrate for photodecarbonylation, as validated by X-ray crystallography.[19] Of note, only the *d,l*-diastereomer of **3.9** was observed, which we attribute to a highly ordered transition state mediated by Li^+ chelation, given prior literature reports.[16b] With crystalline substrate **3.9** in hand, we attempted the key solid-state photodecarbonylation. However, only a small quantity of the desired product **3.7** was formed. Instead, the mass balance was attributed to competitive disproportionation, giving products **3.15** and **3.16**, as well as substantial non-specific decomposition.[20] Although the yield of **3.7** was low, thus limiting late-stage efforts, the formation of **3.7** served as a proof-of-principle that a solid-state photodecarbonylation could forge the critical vicinal quaternary stereocenters with easily modifiable functional groups in place on the aromatic rings.

Scheme 3.2. Synthesis and photodecarbonylation of ketone **3.9**.

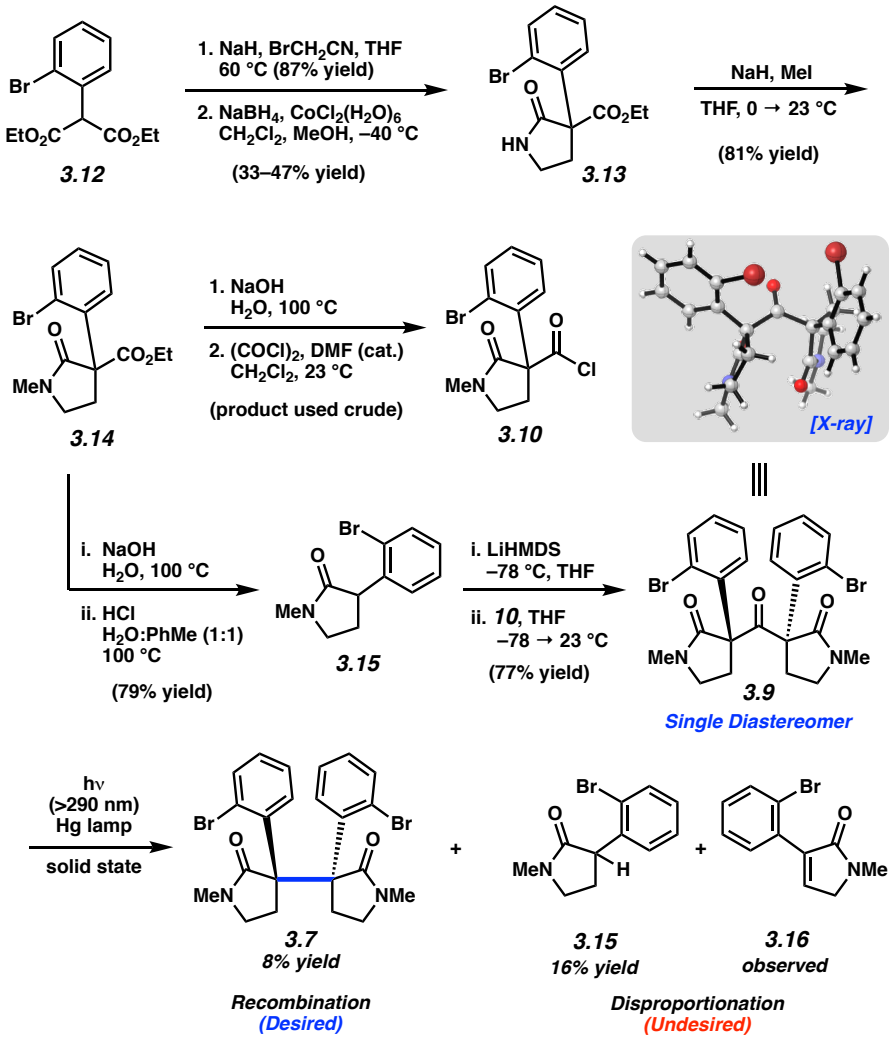

To improve the efficiency of the photodecarbonylation reaction, we explored structural derivatives of ketone substrate **3.9**. Our most promising findings are shown in Figure 3.2.[17] In four linear steps, pyrrolidinone **3.13** was converted to ketone **3.17**, bearing removable *para*-methoxybenzyl (PMB) protecting groups (Figure 3.2A). With the hope of being able to introduce other *N*-substituents and identify a crystalline substrate, we then attempted to enact oxidative cleavage of the PMB moieties using ceric ammonium nitrate (CAN). However, this led to the formation of imide products **3.18** and **3.19**. Given that both compounds were high-melting

crystalline solids, we tested them in the solid-state photodecarbonylation reaction (Figure 3.2B). Whereas symmetrical ketone **3.18** proved completely unreactive, even under prolonged irradiation, we were delighted to find that hemiacyl ketone **3.19** underwent the desired reaction to furnish **3.21** after *N*-deprotection. Of note, despite going through the intermediacy of a radical pair with no configurationally inert stereocenters, this decarbonylative C–C bond forming reaction proceeded with high diastereoselectivity and established the vicinal quaternary stereocenters present in biosynthon **3.6**.[16c,21]

Figure 3.2. Preparation of substrates **3.18** and **3.19**, solid-state photodecarbonylation studies, and explanation for reaction outcomes (the R groups on imides **3.18** and **3.19** are removed from the X-ray renderings for clarity).

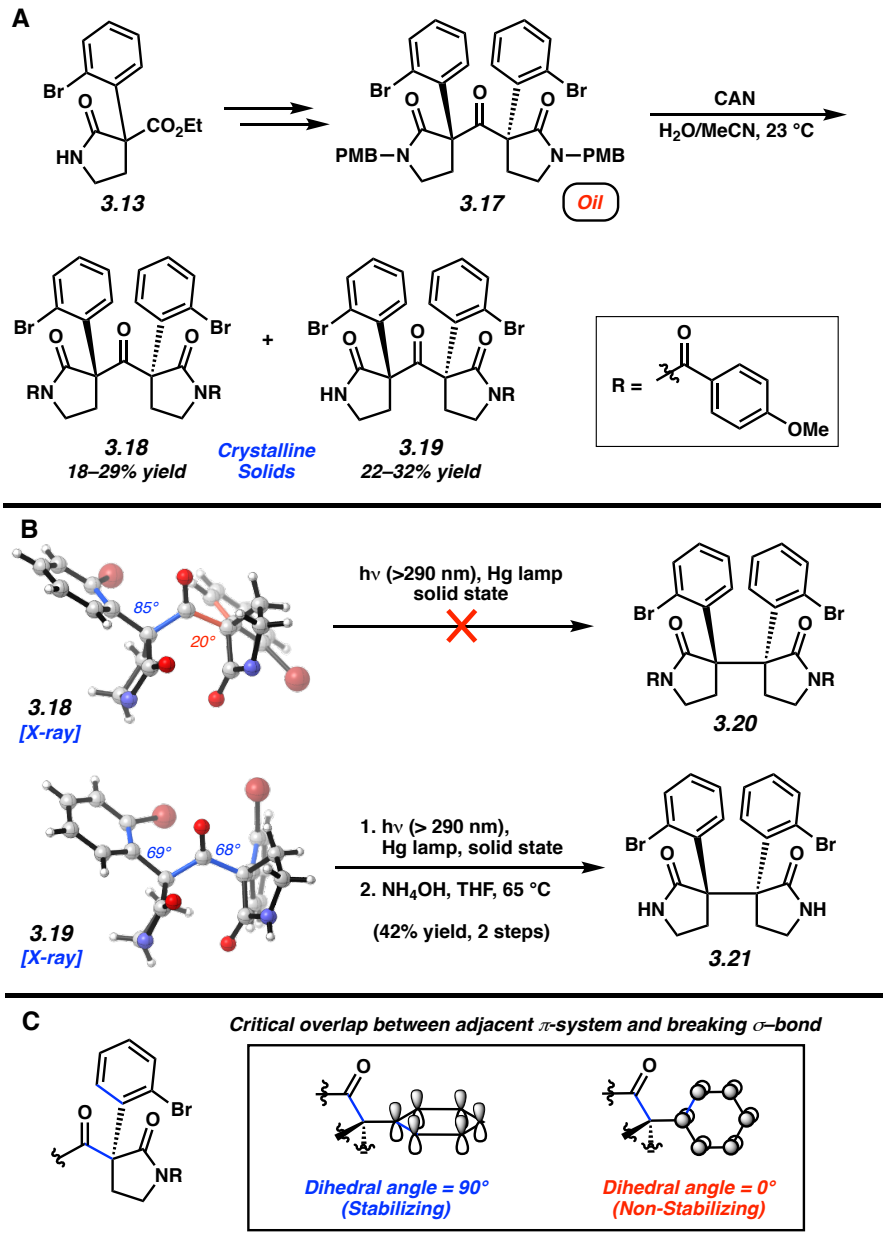

The dramatically different reactivities of ketones **3.18** and **3.19** can be rationalized based on the analysis shown in Figure 3.2C and inspection of the single crystal X-ray structures (see

Figure 3.2B)[19] for both compounds. Solid-state photodecarbonylation requires stabilization of the breaking C–C sigma bonds by neighboring π-systems.[15,22] The extent of these hyperconjugative interactions in substrates **3.18** and **3.19** can be correlated to the dihedral angle between the breaking C–C sigma bond and the nearest C–C bond of the aromatic π-system (see bonds highlighted in blue in Figure 3.2C). A dihedral angle of 90° is ideal, allowing for maximum orbital overlap. Alternatively, if the dihedral angle is 0°, the C–C sigma bond and π-system will be orthogonal, resulting in no electronic stabilization. In considering ketone **3.18**, the two relevant dihedral angles are 85° and 20°, the latter of which presumably leads to negligible orbital overlap and failed bond homolysis. On the other hand, the relevant dihedral angles in ketone **3.19** are 69° and 68°, which we surmise provide sufficient orbital overlap to facilitate decarbonylation.

Having installed the key vicinal quaternary stereocenters, we turned our attention to the elaboration of **3.21** to a bis(cyclotryptamine) alkaloid (Scheme 3.3). *N*-Methylation of **3.21** proceeded smoothly to furnish **3.7** in 84% yield. Next, several attempts to affect double C–N bond formation were put forth, but most were deemed unsuccessful, presumably due to the highly sterically hindered nature of the C–Br bonds in **3.7**. Eventually, we found that a modification of Ma's copper-catalyzed azidation procedure could be implemented to furnish bis(azide) **3.22**.[23] Bis(azide) **3.22** could not be isolated cleanly, despite significant effort, and had to be used directly in the subsequent step.[24] With the requisite nitrogen atoms installed, we then attempted a challenging reduction cascade by treating **3.22** with $LiAlH_4$ at 90 °C. To our surprise, this led to the formation of **3.25** bearing the elusive piperidinoindoline scaffold.[25,26] The structure of **3.25**, a compound we have termed "dihydropsychotriadine," was ultimately confirmed by single crystal X-ray diffraction.[19] Interestingly, bhesine (**3.26**), or variants thereof, were not observed. One plausible pathway from **3.22** to **3.25** involves double azide reduction to furnish intermediate **3.23**,

double 5-exo-trig cyclization / transamidation to give **3.24**, double cyclization to give the piperidine rings,[27] and mono amidine reduction.[28] Despite the mechanistic possibilities for the formation of other isomers (e.g. scaffolds **3.1**–**3.4**) during the reduction of **3.22**, we did not observe any major byproducts by ^{1}H NMR analysis. However, the formation of other isomeric products cannot be ruled out at this time.

Scheme 3.3. Total synthesis of "psychotriadine" (**3.28**) bearing the piperidinoindoline scaffold (the chloride counterion of the X-ray structure of **3.25** is omitted for clarity).

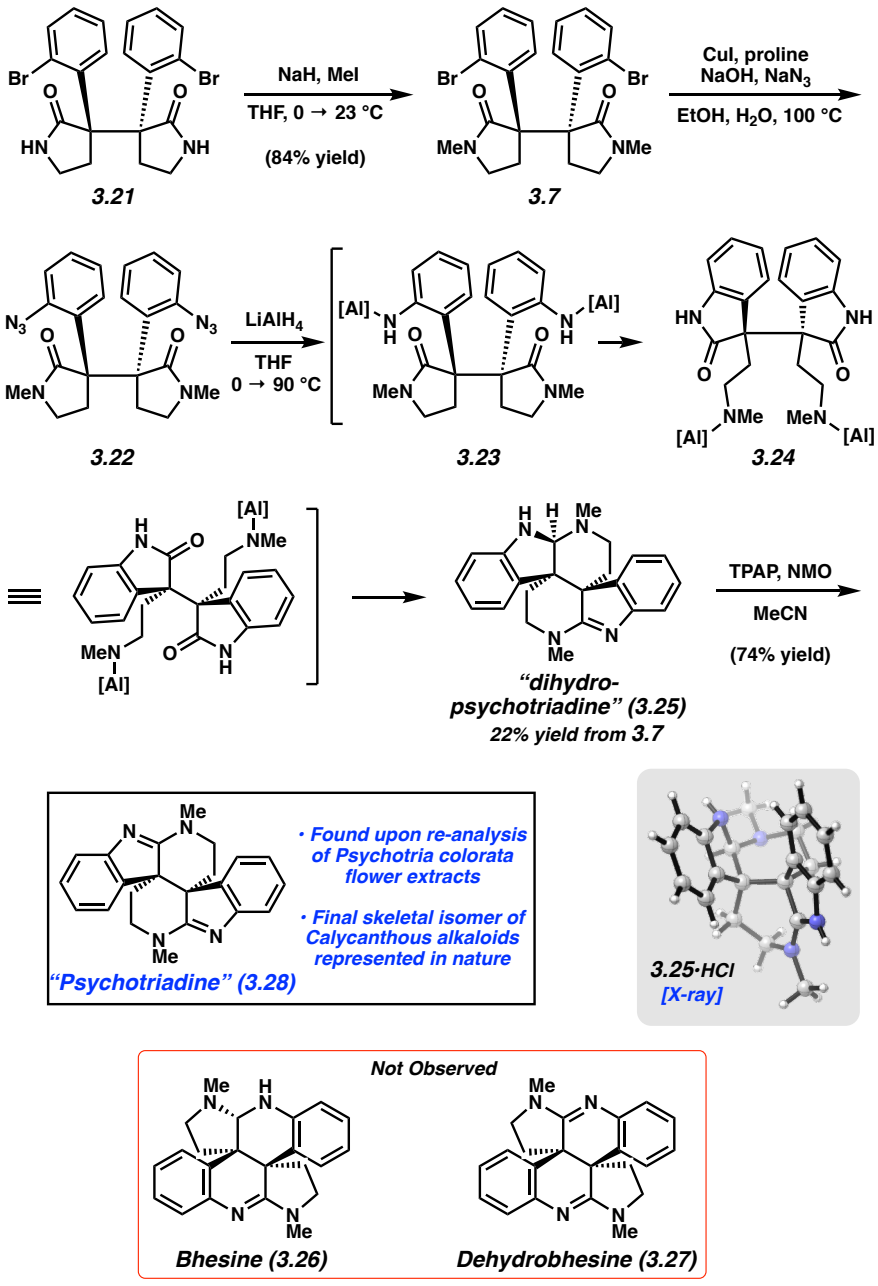

Prior to unambiguously establishing the structure of **3.25** by X-ray diffraction, we had surmised that **3.25** could be an aminal stereoisomer of bhesine (**26**). As such, **3.25** was treated under Ley–Griffith oxidation conditions to ablate the aminal stereocenter.[29] The product, which

we obtained in 74% yield, was compared to an authentic sample of dehydrobhesine (**3.27**) obtained from the extracts from *Psychotria colorata*.[6a] Although our synthetic sample did not match **3.27**, the isolation sample also contained a previously unidentified compound representing ~10% of the sample mass. This compound was found to spectroscopically match our synthetic oxidation product. On the basis of crystallographic characterization of **3.25** and NMR analysis of the oxidation product, we propose the depicted piperidinoindoline structure for compound **3.28**. Because of its presence in the extracts from *Psychotria colorata*, **3.28** is presumed to be a naturally occurring metabolite that we have now termed "psychotriadine."[30]

3.4 Conclusion

In summary, we have developed a synthetic route to access "psychotriadine," a previously unknown bis(cyclotryptamine) alkaloid bearing the elusive piperidinoindoline scaffold. Our approach features a stereospecific solid-state photodecarbonylation reaction to convert fully substituted ketone substrate **3.19** into **3.21** bearing vicinal quaternary stereocenters. The success or failure of this key step correlates to the solid-state geometry of the ketone substrate. Following late-stage C–N bond formation and a reduction cascade, the piperidinoindoline framework could be accessed. Re-analysis of *Psychotria colorata* flower extracts revealed the presence of "psychotriadine," suggesting it is likely a naturally occurring alkaloid. These studies not only underscore the value of solid-state photodecarbonylation chemistry in total synthesis, but also demonstrate that all five of the distinct bis(cyclotryptamine) alkaloid frameworks originally proposed are represented in nature.

3.5 Experimental Section

3.5.1 Materials and Methods

Unless stated otherwise, reactions were conducted in flame-dried glassware under an atmosphere of nitrogen using anhydrous solvents (either freshly distilled or passed through activated alumina columns). All commercially available reagents were used as received unless otherwise specified. Tetrapropylammonium perruthenate (TPAP), trifluoroacetic acid, *N*-methylmorpholine *N*-oxide, 4-dimethylaminopyridine, sodium hydride (60% dispersion in mineral oil), oxalyl chloride, iodomethane (MeI), bromoacetonitrile, iodomethane, lithium bis(trimethylsilyl)amide (LiHMDS), ceric ammonium nitrate, copper(I) iodide, sodium azide, L-proline, and sodium borohydride were obtained from Sigma-Aldrich. Cobalt(II) chloride hexahydrate and 4-methoxybenzyl chloride were purchased from TCI America. CH_2Cl_2 saturated with NH_3 was prepared by sparging a glass bottle of CH_2Cl_2 with gaseous NH_3 for 10 minutes. Unless stated otherwise, reactions were performed at room temperature (rt, approximately 23 °C). Thin-layer chromatography (TLC) was conducted with EMD gel 60 F254 pre-coated plates (0.25 mm) and visualized using a combination of UV, ceric ammonium molybdate, and potassium permanganate staining. Silicycle silica gel 60 (particle size 0.040–0.063 mm) was used for flash column chromatography. Compounds **3.18** and **3.19** were purified using a Teledyne ISCO Combi*Flash*® NextGen™ instrument using Redi*Sep*®Rf high-performance silica gold columns (24 g, catalog No. 692203346, 12 g, catalog No. 692203345). ^{1}H NMR spectra were recorded on Bruker spectrometers (at 300 MHz, 500 MHz, or 600 MHz) and are reported relative to deuterated solvent signals. Data for ^{1}H NMR spectra are reported as follows: chemical shift (δ ppm), multiplicity, coupling constant (Hz) and integration. ^{13}C NMR spectra are reported in terms of chemical shift (at 125 MHz). High-resolution mass spectra were obtained on Thermo Scientific™ Exactive Mass

Spectrometers with DART ID-CUBE. X-ray structures shown in Figure 3.2 and Schemes 3.2 and 3.3 of the manuscript were created using CYLview.

3.5.2 Experimental Procedures

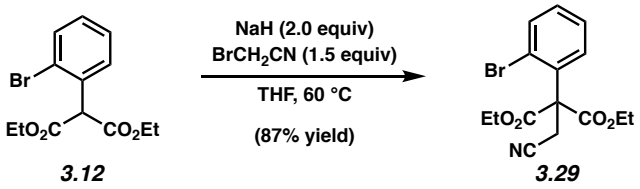

Nitrile 3.29. To a solution of malonate ester **3.12**[31] (42.0 g, 136 mmol, 1.00 equiv) in THF (330 mL), was added NaH (10.7 g, 60% dispersion in mineral oil, 268 mmol, 1.97 equiv) in 3 portions over 10 min with stirring. Bromoacetonitrile (13.9 mL, 14.2 g, 204 mmol, 1.50 equiv) was added dropwise via syringe over 1 minute. The reaction was submerged in an oil bath preheated to 60 °C and stirred for 15 h. Then the reaction was cooled to 23 °C and poured into a biphasic mixture of sat. aq. NH_4Cl (500 mL) and CH_2Cl_2 (500 mL). The layers were separated and the aqueous layer was extracted with CH_2Cl_2 (2 x 200 mL). The combined organic layers were dried over Na_2SO_4 and concentrated directly onto silica gel (120 g) under reduced pressure. The crude product was purified by flash column chromatography (120 g silica gel, 9:1 Hexanes:EtOAc → 7:3 Hexanes:EtOAc) to yield **3.29** as a white solid (40.9 g, 87% yield). Nitrile **3.29**: mp: 84.7–85.6 °C, R_f 0.42 (7:3 Hexanes:EtOAc); ^{1}H NMR (300 MHz, $CDCl_3$) δ 7.63 (dd, J = 7.9, 1.4 Hz, 1H), 7.37 (td, J = 7.6, 1.4 Hz, 1H), 7.25 (td, J = 7.7, 1.7 Hz, 1H), 7.17 (dd, J = 7.8, 1.7 Hz, 1H), 4.48 – 4.17 (m, 4H), 3.53 (s, 2H), 1.32 (t, J = 7.1 Hz, 6H); ^{13}C NMR (125 MHz, $CDCl_3$) δ 167.8, 135.1, 135.0, 130.6, 130.4, 128.1, 122.9, 116.9, 63.5, 63.1, 24.0, 13.9; HRMS-APCI (m/z) $[M + H]^+$ calcd for $C_{15}H_{17}NO_4Br^+$, 354.0341; found 354.0337.

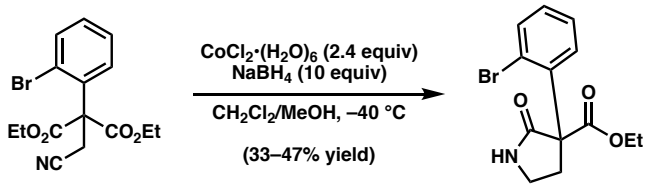

3.29 *3.13*

Pyrrolidinone 3.13. Nitrile **3.29** (20.6 g, 58.2 mmol, 1.00 equiv) was split into two reactions which were run in parallel as follows: To a solution of nitrile **3.29** (10.3 g, 29.1 mmol, 1.00 equiv) in CH_2Cl_2 (50 mL) was added MeOH (320 mL) followed by $CoCl_2 \cdot (H_2O)_6$ (16.3 g, 68.5 mmol, 2.35 equiv) and the solution was then cooled to –40 °C. $NaBH_4$ (10.7 g, 282 mmol, 9.69 equiv) was added in small aliquots (~300 mg) every 1 minute for the course of 36 minutes. Following this addition, aq. HCl (3.0 M, 200 mL) was added and the resultant mixture was stirred for 5 minutes. Sat. aq. NH_4OH (250 mL) was then added and the reaction was stirred for another 25 minutes. The two parallel reactions were combined and poured into a biphasic mixture of sat. aq. NaCl (200 mL) and EtOAc (500 mL). The layers were separated, and the aqueous layer was extracted with EtOAc (2 x 200 mL). The combined organic layers were diluted with CH_2Cl_2 (500 mL), dried over Na_2SO_4, and concentrated under reduced pressure. The crude oil was dissolved in EtOAc (10 mL), seeded with a small amount of crystalline pyrrolidinone **3.13**, and allowed to recrystallize overnight. The crystalline solid was rinsed with 0 °C EtOAc (~10 mL) to furnish pyrrolidinone **3.13** as a white solid (6.76 g, 38% yield). Note that the yield of **3.13** ranges from 33–47%. Pyrrolidinone **3.13**: mp: 127.2–127.6 °C; R_f 0.43 (2:8 Hexanes:EtOAc); ^{1}H NMR (500 MHz, $CDCl_3$) δ 7.75 (s, 1H), 7.59 (dd, *J* = 7.9, 1.3 Hz, 1H), 7.46 (dd, *J* = 7.9, 1.7 Hz, 1H), 7.31 (td, *J* = 7.6, 1.4 Hz, 1H), 7.16 (td, *J* = 7.7, 1.6 Hz, 1H), 4.29 (dq, *J* = 10.8, 7.1 Hz, 1H), 4.22 (dq, *J* = 10.8, 7.1 Hz, 1H), 3.54 – 3.42 (m, 2H), 3.27 – 3.13 (m, 1H), 2.47 – 2.31 (m, 1H), 1.24 (t, *J* = 7.1 Hz, 3H); ^{13}C NMR (125 MHz, $CDCl_3$) δ 174.1, 170.2, 138.5, 134.2, 129.2, 129.0, 127.7, 124.0, 62.7,

62.6, 39.4, 33.7, 13.9; HRMS-APCI (m/z) $[M + H]^+$ calcd for $C_{13}H_{15}NO_3Br^+$, 312.0235; found 312.0223.

Note 1: It is critical to maintain rapid stirring and efficient cooling for the duration of this reaction to mitigate the formation of side products (reduction of the C–Br to C–H). For this reason, reactions on >10 g scale were run in parallel and combined for workup and purification. The remaining over-reduced product is cleanly removed during the recrystallization.

Note 2: It is critical that $NaBH_4$ is added slowly, the reaction vigorously releases H_2 gas.

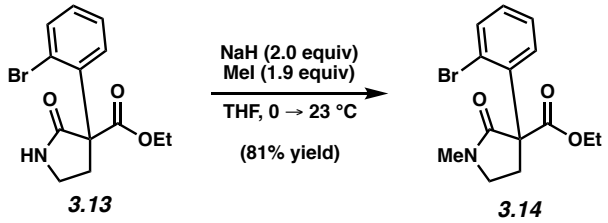

Pyrrolidinone 3.14. To a solution of pyrrolidinone **3.13** (1.50 g, 4.81 mmol, 1.00 equiv) in THF (50 mL), was added NaH (0.390 g, 60% dispersion in mineral oil, 9.75 mmol, 2.03 equiv). The reaction mixture was stirred at 23 °C for 10 minutes before it was cooled to 0 °C. MeI (0.450 mL, 1.30 g, 9.16 mmol, 1.91 equiv) was added dropwise over 2 minutes and the reaction was stirred for a further 15 minutes at this temperature. The ice bath was removed, and the reaction was stirred for 25 minutes at 23 °C. The reaction was then poured into a biphasic mixture of sat. aq. NH_4Cl (100 mL) and CH_2Cl_2 (200 mL). The layers were separated, and the aqueous layer was extracted with CH_2Cl_2 (2 x 50 mL). The combined organic layers were dried over $MgSO_4$ before being concentrated under reduced pressure directly onto silica gel (2.5 g). The crude product was purified by flash column chromatography (8 g silica gel, 7:3 Hexanes:EtOAc → 1:1 Hexanes:EtOAc) to give pyrrolidinone **3.14** (1.27 g, 81% yield) as a white solid. Pyrrolidinone **3.14**: mp: 121.1–121.6 °C; R_f 0.44 (3:7 Hexanes:EtOAc); ^{1}H NMR (300 MHz, CDCl3) δ 7.59 (dd, J = 7.9, 1.3 Hz, 1H), 7.34 – 7.25 (m, 2H), 7.15 (td, J = 7.6, 1.9 Hz, 1H), 4.39 – 4.11 (m, 2H), 3.65 – 3.35 (m, 2H), 3.35

– 3.19 (m, 1H), 3.00 (s, 3H), 2.33 – 2.15 (m, 1H), 1.24 (t, J = 7.1 Hz, 3H); ^{13}C NMR (125 MHz, $CDCl_3$) δ 174.5, 170.3, 138.6, 134.3, 129.3, 129.1, 127.8, 124.1, 63.0, 62.7, 62.2, 39.6, 33.8, 14.0; HRMS-APCI (m/z) $[M + H]^+$ calcd for $C_{14}H_{17}NO_3Br^+$, 326.0392; found 326.0384.

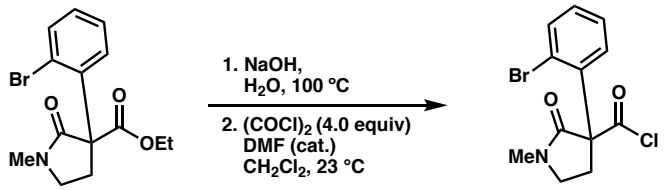

3.14 *3.10*

Acid Chloride 3.10. A suspension of pyrrolidinone **3.14** (0.830 g, 2.54 mmol, 1.00 equiv) in aq. NaOH (1.0 M, 15 mL) was heated at reflux until the solution became homogeneous (5 min) and then was allowed to cool to 23 ºC. The reaction was poured into aq. HCl (0.5 M, 50 mL) and the aqueous layer was extracted with CH_2Cl_2 (3 x 100 mL). The combined organic layers were dried over $MgSO_4$ and concentrated under reduced pressure. The resultant crude carboxylic acid was carried directly to the next step.

To a solution of the crude carboxylic acid in CH_2Cl_2 (20 mL) with two drops of DMF from a glass Pasteur pipette, oxalyl chloride (0.870 mL, 10.1 mmol, 3.98 equiv) was added dropwise over 1 minute. The reaction was stirred for 1 h at 23 ºC before being concentrated under reduced pressure. The resultant oil was dissolved in PhMe (20 mL) and concentrated under reduced pressure (x2). The crude oil was then put under vacuum (< 1 mbar) for 1 h. Crude acid chloride **3.10** was used immediately without further purification.

Note 1: It is critical that this set-up is kept anhydrous and excess oxalyl chloride is fully removed at the end of the reaction. Each time the acid chloride was concentrated under rotary evaporation (both from CH_2Cl_2 and then from PhMe) the water bath was maintained at 50 °C and the vacuum was maintained at the highest setting (~15 mbar) for 15 minutes. The oil was left under high vacuum (< 1 mbar) for 1 h to ensure complete removal of the oxalyl chloride.

Note 2: The carboxylic acid does not completely dissolve in CH_2Cl_2. Once the oxalyl chloride has been added all of the solids dissolve within 30 minutes.

Note 3: In order to ensure water is not introduced between rotary evaporations, the rotary evaporator is backfilled with a balloon of dry Ar for this step (see image below).

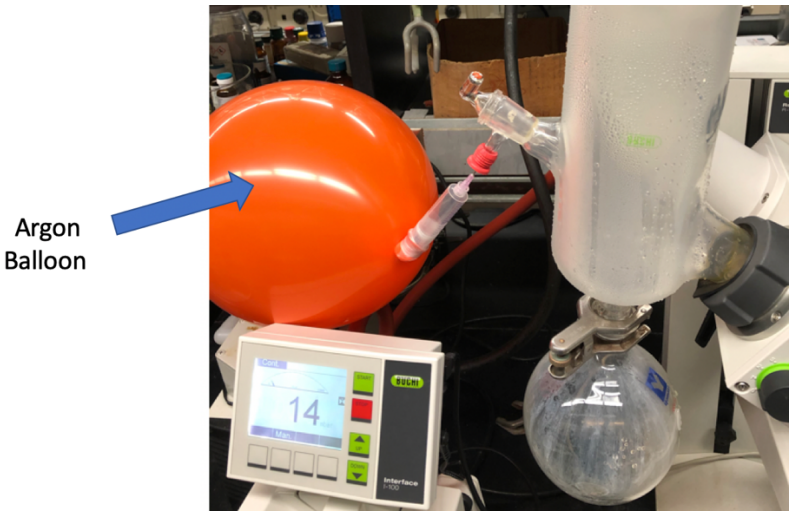

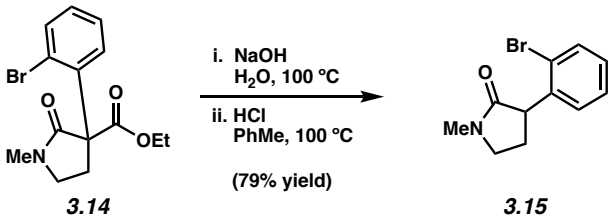

3.14 *3.15*

Amide 3.15. A suspension of pyrrolidinone **3.14** (0.550 g, 1.69 mmol, 1.00 equiv) in aq. NaOH (1.0 M, 30 mL) was submerged in an oil bath preheated to 115 °C and stirred for 30 minutes before being allowed to cool to 23 °C. Aq. HCl (12 M) was added over 1 minute until the solution reached pH 1. PhMe (30 mL) was added and the reaction was submerged in an oil bath preheated to 115 °C and stirred for 1 h. The reaction was then cooled to 23 °C and poured into a biphasic mixture of DI H_2O (100 mL) and CH_2Cl_2 (100 mL). The layers were separated, and the aqueous layer was extracted with CH_2Cl_2 (2 x 100 mL). The combined organic layers were dried over $MgSO_4$ and concentrated under reduced pressure. The crude product was purified by flash column

chromatography (15 g silica gel, 1:1 Hexanes:EtOAc) to provide amide **3.15** (0.340 g, 79% yield) as a white solid. Amide **3.15**: mp: 69.4–70.0 °C; R_f 0.30 (EtOAc); ^{1}H NMR (500 MHz, $CDCl_3$) δ 7.56 (dd, *J* = 8.0, 1.2 Hz, 1H), 7.29 (td, *J* = 7.5, 1.2 Hz, 1H), 7.19 (dd, *J* = 7.8, 1.8 Hz, 1H), 7.11 (td, *J* = 7.6, 1.8 Hz, 1H), 4.12 (t, *J* = 9.2 Hz, 1H), 3.64 – 3.26 (m, 2H), 2.97 (s, 3H), 2.73 – 2.56 (m, 1H), 1.93 (dq, *J* = 12.9, 8.6 Hz, 1H); ^{13}C NMR (125 MHz, $CDCl_3$) δ 174.3, 139.9, 133.1, 129.4, 128.7, 128.1, 125.0, 48.4 47.6, 30.3, 27.7; HRMS (DART) calcd for $C_{11}H_{13}BrNO$ $[M+H]^+$, 254.0175; found 254.0169.

Note: The ester starting material is not soluble in aqueous NaOH. The ester completely dissolves over the course of the reaction and the mixture should be homogenous at the end of heating.

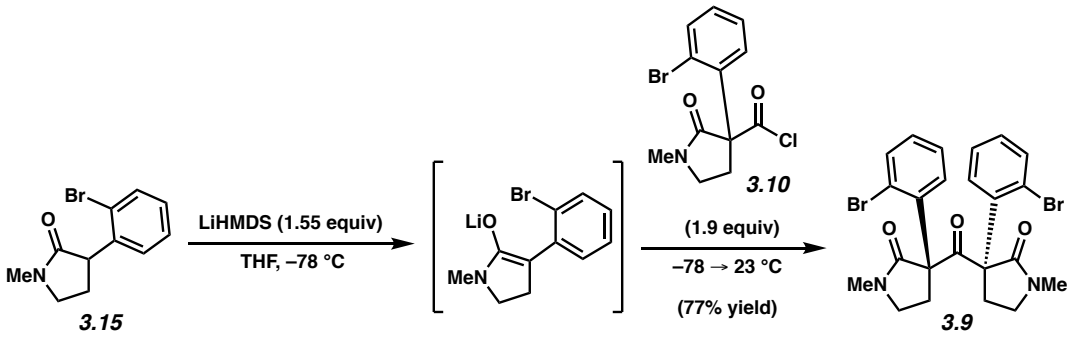

Ketone 3.9. To a solution of LiHMDS (1.0 M in THF, 2.0 mL, 340 mg, 2.0 mmol, 1.6 equiv) was added THF (10 mL) and the mixture was cooled to –78 °C. A solution of amide **3.15** (328 mg, 1.29 mmol, 1.00 equiv) in THF (10 mL) was added dropwise over 15 minutes and the reaction was stirred for at –78 °C for 1 h. A solution of freshly prepared acid chloride **3.10** (420 mg, 1.6 mmol, 1.9 equiv) in THF (10 mL) was added dropwise over 5 minutes. The reaction was immediately removed from the –78 °C bath and stirred at 23 °C for 30 minutes. The reaction was quenched by pouring it into a biphasic mixture of sat. aq. NaCl (50 mL) and aq. HCl (1.0 M, 50 mL). The layers were separated and the aqueous layer was extracted with CH_2Cl_2 (3 x 100 mL). The combined organic layers were dried over $MgSO_4$ and concentrated directly onto silica gel (3.5 g). The crude

product was purified by flash column chromatography (15 g silica gel, 7:3 Hexanes:EtOAc → 1:1 Hexanes:EtOAc) to give ketone **3.9** (533 mg, 77% yield) as a white solid. Crystals suitable for X-ray diffraction studies were obtained using slow evaporation from a mixture of CH_2Cl_2/Hexanes. Ketone **3.9**: mp: 195.0–195.2 °C; R_f 0.30 (1:1 Hexanes:EtOAc); ^{1}H NMR (500 MHz, $CDCl_3$) δ 7.83 (dd, *J* = 8.0, 1.7 Hz, 2H), 7.62 (dd, *J* = 7.9, 1.4 Hz, 2H), 7.29 – 7.23 (m, 2H), 7.13 (td, *J* = 7.6, 1.7 Hz, 2H), 3.62 (ddd, *J* = 13.1, 8.3, 4.7 Hz, 2H), 3.37 (ddd, *J* = 9.6, 8.3, 5.6 Hz, 2H), 3.13 (ddd, *J* = 9.5, 8.1, 4.8 Hz, 2H), 2.88 (s, 6H), 2.42 (ddd, *J* = 13.4, 8.1, 5.6 Hz, 2H); ^{13}C NMR (125 MHz, $CDCl_3$) δ 197.4, 171.1, 138.6, 135.7, 131.2, 129.2, 127.2, 123.9, 70.3, 46.8, 31.1, 30.9; HRMS-APCI (m/z) $[M + H]^+$ calcd for $C_{23}H_{23}N_2O_3Br_2^+$, 535.0050; found 535.0039.

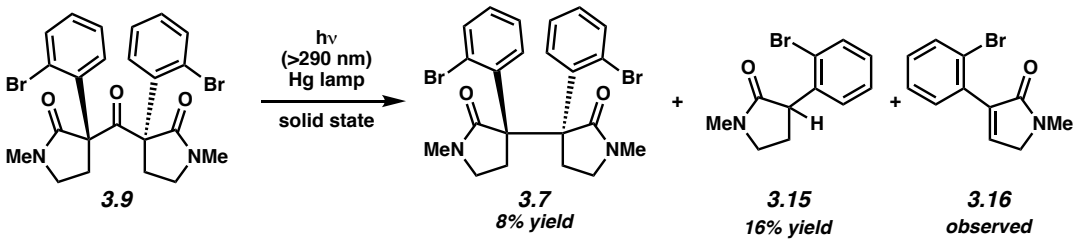

***N*–Me Bis(arylbromide) 3.7**. Ketone **3.9** (30–50 mg) was dissolved in CH_2Cl_2 (~5 mL) and Hexanes (~3 mL) were added until the mixture became cloudy. This was allowed to evaporate over ~16 h. Once crystals had formed, the residual solvent was removed using a glass Pasteur pipette. The resultant crystalline solid was put under high vacuum (<1 mbar) for 1 h. A small sample of crystalline **3.9** (4.50 mg, 8.42 μmol) was placed between two glass microscope slides. The two slides were rubbed together for 10 seconds to crush **3.9** into a thin layer of crystalline powder (Note 1). The two glass slides were then clamped together using two binder clips. The solid sample was irradiated with a 450 W medium pressure Hg Hanovia UV lamp placed inside a water-cooled immersion-well Pyrex filter (Ace Glass, model 7857-05, $\lambda \geq 290$ nm; 53 mm external diameter, 220 mm full length, 150 mm depth) for 7 h (see Note 3 for reaction monitoring). At this time, the sample was flipped over (to expose the other side of the solid to light) and then irradiated

for another 18 h. The binder clips were then removed and a metal spatula was used to scrape the solid off of the glass slides into a vial. The slides and spatula were then rinsed with $CDCl_3$ (~5 mL) to give a mixture of *N*–Me bis(arylbromide) **3.7** (0.32 mg, 8% yield) and disproportionation product **3.15** (0.33 mg, 16% yield). (Yield determined by ^1H QNMR with 1,4-dinitrobenzene as the external standard). Characterization data for **3.7** is reported later in this document.

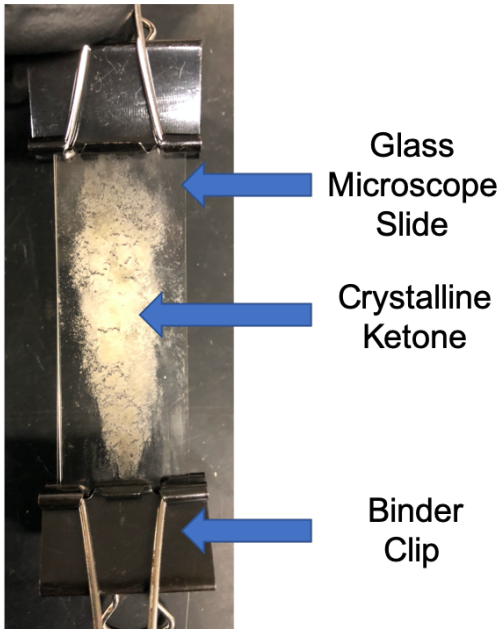

Note 1: It is critical that the solid is crushed into a very thin layer to ensure adequate light penetration.

Note 2: The 450W Hg lamp produces significant heat. This is mitigated by the jacket of cooling water and fans to circulate warm air out of the box containing the irradiation setup.

*Note 3: This particular reaction was not monitored by TLC in order to ensure accurate yield determination. In general, to monitor the reaction by TLC, a very small aliquot (<0.1 mg) of solid is removed with the tip of a glass Pasteur pipette. This solid is then dissolved in ~1 drop of CH_2Cl_2 and analyzed by TLC. Since the product **3.7** is difficult to visualize, conversion is determined by loss of the spot corresponding to ketone **3.9**.*

Note 4: While some of the mass balance is attributed to disproportionation and unidentified decomposition products, a substantial amount of insoluble yellow solid is produced. The identity of this material is unknown.

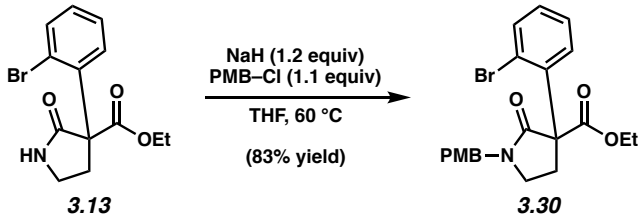

PMB Pyrrolidinone 3.30. To a solution of pyrrolidinone **3.13** (6.70 g, 25.0 mmol, 1.00 equiv) in THF (250 mL) was added NaH (1.21 g, 60% dispersion in mineral oil, 30.3 mmol, 1.21 equiv, 60%) in one portion and the reaction was stirred for 5 minutes. 4-Methoxybenzyl chloride (3.75 mL, 4.35 g, 27.8 mmol, 1.11 equiv) was added dropwise over 1 minute and the reaction was submerged in an oil bath preheated to 60 °C. The reaction was stirred for 5 h and then allowed to cool to 23 °C. The reaction was poured into a biphasic mixture of sat. aq. NH_4Cl (300 mL) and EtOAc (200 mL). The layers were separated, and the aqueous layer was extracted with EtOAc (2 x 100 mL). CH_2Cl_2 (250 mL) was added to the combined organic layers and the solution was dried over Na_2SO_4 and concentrated under reduced pressure directly onto silica gel (20 g). The crude product was purified by flash column chromatography (80 g silica gel, 9:1 Hexanes:EtOAc → 7:3 Hexanes:EtOAc) to give pyrrolidinone **3.30** as a glassy solid (7.91 g, 83% yield). Pyrrolidinone **3.30**: R_f 0.69 (2:3 Hexanes:EtOAc); ^{1}H NMR (500 MHz, $CDCl_3$) δ 7.58 (d, J = 7.9 Hz, 1H), 7.33 (d, J = 8.0 Hz, 1H), 7.28 – 7.25 (m, 1H), 7.24 – 7.20 (m, 2H), 7.14 (t, J = 7.6 Hz, 1H), 6.92 – 6.73 (m, 2H), 4.59 (d, J = 14.5 Hz, 1H), 4.47 (d, J = 14.4 Hz, 1H), 4.35 – 4.15 (m, 2H), 3.80 (s, 3H), 3.44 – 3.25 (m, 2H), 3.17 – 2.96 (m, 1H), 2.33 – 2.03 (m, 1H), 1.25 (t, J = 7.1 Hz, 3H); ^{13}C NMR (125 MHz, $CDCl_3$) δ 170.5, 170.2, 159.4, 139.1, 134.2, 129.8, 129.3, 129.0, 128.0, 127.7, 124.1,

114.3, 63.7, 62.6, 55.4, 47.1, 43.8, 31.3, 14.1; HRMS-APCI (m/z) $[M + H]^+$ calcd for $C_{21}H_{23}BrNO_4^+$, 432.0805; found, 432.0805.

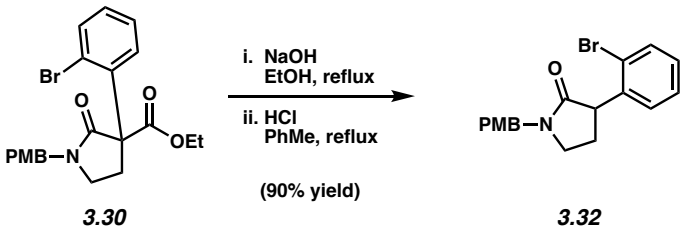

3.30 *3.32*

PMB Amide 3.32. A solution of pyrrolidinone **3.30** (3.16 g, 7.82 mmol, 1.00 equiv) in EtOH (140 mL) was submerged in an oil bath preheated to 100 °C and stirred until all the solids had dissolved (~10 minutes). Aq. NaOH (1.0 M, 70 mL) was added and the refluxing solution was stirred for 30 minutes and then allowed to cool to 23 °C. Aq. HCl (12 M, 16 mL) and PhMe (80 mL) were added sequentially. The reaction was then submerged in an oil bath preheated to 100 °C, stirred for 6 h, and then allowed to cool to 23 ºC. The reaction mixture was poured into DI H_2O (200 mL) and the layers were separated. The aqueous layer was extracted with CH_2Cl_2 (2 x 60 mL). The combined organic layers were dried over Na_2SO_4 and then concentrated under reduced pressure to give PMB amide **3.32** (2.54 g, 90% yield) as a glassy solid. This was used without further purification. Amide **3.32**: R_f 0.41 (1:1 Hexanes:EtOAc); ^{1}H NMR (500 MHz, $CDCl_3$) δ 7.56 (d, *J* = 8.0 Hz, 1H), 7.29 (t, *J* = 7.5 Hz, 1H), 7.26 – 7.23 (m, 2H), 7.20 (d, *J* = 7.6 Hz, 1H), 7.11 (t, *J* = 7.7 Hz, 1H), 6.92 – 6.85 (m, 2H), 4.57 (d, *J* = 14.4 Hz, 1H), 4.44 (d, *J* = 14.4 Hz, 1H), 4.16 (t, *J* = 9.2 Hz, 1H), 3.82 (s, 3H), 3.35 – 3.18 (m, 2H), 2.58 (dddd, *J* = 10.9, 9.5, 5.6, 3.4 Hz, 1H), 1.88 (dq, *J* = 12.9, 8.6 Hz, 1H); ^{13}C NMR (125 MHz, $CDCl_3$) δ 173.9, 159.2, 139.7, 133.0, 129.7, 129.3, 128.6, 128.5, 128.0, 124.9, 114.1, 55.3, 48.7, 46.6, 44.6, 27.5; HRMS-APCI (m/z) $[M + H]^+$ calcd for $C_{18}H_{19}BrNO_2^+$, 360.0594; found, 360.0593.

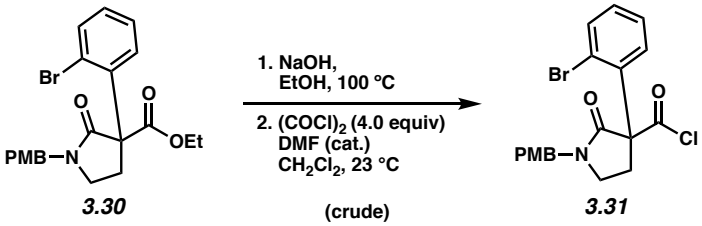

PMB Acid Chloride 3.31. A solution of pyrrolidinone **3.30** (4.74 g, 11.0 mmol, 1.00 equiv) in EtOH (60 mL) was submerged in an oil bath preheated to 100 °C and stirred until all the solids had dissolved (~10 min). Aq. NaOH (1.0 M, 60 mL) was added to the refluxing solution and the mixture was stirred for 15 minutes before the mixture was allowed to cool to 23 °C. The reaction mixture was poured into a biphasic mixture of aq. HCl (200 mL, 1.0 M) and CH_2Cl_2 (150 mL) and the layers were separated. The aqueous layer was extracted with CH_2Cl_2 (100 mL). The combined organic layers were dried over $MgSO_4$ and then concentrated under reduced pressure directly onto silica gel (12 g). The crude product was purified using a (12 g RediSep Gold, 1:1 Hexanes:EtOAc → 100% EtOAc) to provide the corresponding carboxylic acid (3.95 g, 89% yield) as a white solid.

To the solid carboxylic acid (3.95 g, 9.77 mmol, 1.00 equiv) was added two drops of DMF (using a glass Pasteur pipette) and CH_2Cl_2 (100 mL). Oxalyl chloride (2.25 mL, 4.96 g, 39.0 mmol, 3.99 equiv) was added to the mixture dropwise over 5 minutes. The reaction was stirred at 23 ºC for 16 h and then concentrated under reduced pressure. The oil was dissolved in PhMe (30 mL) and concentrated under reduced pressure (x2). The crude oil was then put under high vacuum (< 1 mbar) for 1 h. Crude acid chloride **3.31** was used directly in the next step without further purification.

Note 1: It is critical that this set up is kept anhydrous and that the excess oxalyl chloride is fully removed at the end of the reaction. Each time the acid chloride was concentrated under rotary evaporation (both from CH_2Cl_2 and then from PhMe) the water bath was maintained at 50 °C and

the vacuum was maintained at the highest setting (~15 mbar) for 15 minutes. After this, it is recommended that the oil be put under high vacuum (< 1 mbar) for 1 h.

Note 2: In order to ensure that undue water is not introduced between rotary evaporations, the rotary evaporator is backfilled with a balloon of dry Ar (see image below).

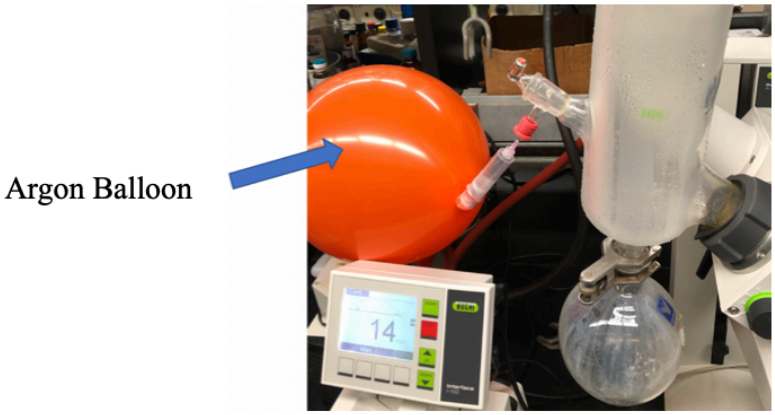

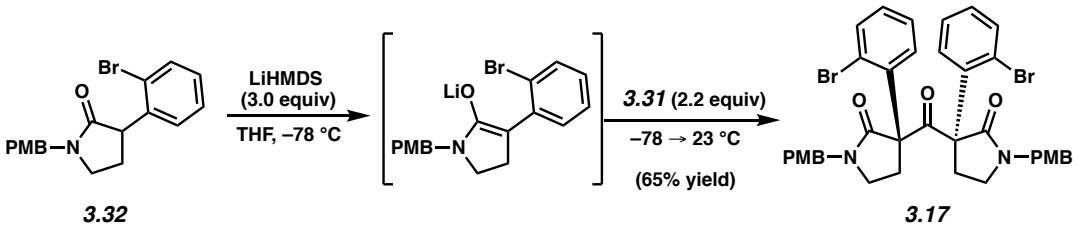

Ketone 3.17. To a solution of amide **3.32** (0.710 g, 2.00 mmol, 1.00 equiv) in THF (30 mL) at –78 °C was added a solution of LiHMDS (1.0 M in THF, 5.9 mL, 990 mg, 5.9 mmol, 3.0 equiv) dropwise over 1 minute. The reaction was stirred for 1 h and then a solution of acid chloride **3.31** (2.0 g, 2.4 mmol, 2.2 equiv) in THF (16 mL) was added dropwise over 1 minute and the reaction was immediately removed from the –78 °C bath, placed in a 0 °C bath, and the reaction was stirred for 35 minutes. The reaction was quenched at 0 °C by the addition of aq. HCl (0.5 M, 6 mL) and poured into a biphasic mixture of DI H_2O (100 mL), sat. aq. NaCl (100 mL), and CH_2Cl_2 (100 mL). The layers were separated, and the aqueous layer was extracted with CH_2Cl_2 (2 x 100 mL). The combined organic layers were dried over Na_2SO_4 and concentrated under reduced pressure

directly onto silica gel (2 g). The crude product was purified by flash column chromatography (20 g silica gel, 4:1 Hexanes:EtOAc) to give ketone **3.17** (963 mg, 65% yield) as a white foam. Ketone **3.17**: R_f 0.44 (3:2 Hexanes:EtOAc); ^{1}H NMR (500 MHz, $CDCl_3$) δ 7.89 (d, *J* = 8.0 Hz, 2H), 7.64 (d, *J* = 7.9 Hz, 2H), 7.36 – 7.23 (m, 6H), 7.15 (td, *J* = 7.7, 1.5 Hz, 2H), 6.93 – 6.73 (m, 4H), 4.99 (d, *J* = 14.6 Hz, 2H), 4.00 (d, *J* = 14.6 Hz, 2H), 3.79 (s, 6H), 3.62 (ddd, *J* = 13.2, 8.1, 5.0 Hz, 2H), 3.27 (td, *J* = 8.7, 5.3 Hz, 2H), 3.00 (td, *J* = 8.5, 5.0 Hz, 2H), 2.43 (ddd, *J* = 13.2, 7.9, 5.3 Hz, 2H); ^{13}C NMR (125 MHz, $CDCl_3$) δ 197.0, 171.0, 159.1, 138.1, 135.6, 131.2, 130.0, 129.1, 128.0, 127.1, 123.7, 114.0, 70.7, 55.3, 47.6, 44.2, 30.8; HRMS-APCI (m/z) $[M + H]^+$ calcd for $C_{37}H_{35}Br_2N_2O_5^+$, 747.0887; found, 747.0892.

*Note 1: It is critical that amide **3.32** is completely dry. To ensure this, **3.32** was concentrated from anhydrous benzene before the reaction was set up to remove residual water.*

*Note 2: In the event that residual enolate precursor **3.32** remains after the reaction, separation of ketone **3.17** and pyrrolidinone **3.32** is tedious. To circumvent this, **3.32** can be decomposed by treating the mixture of **3.32** and **3.17** with LiHMDS in THF at –78 °C (see conditions to form ketone above) and then quenching the resultant enolate with $(CH_2O)_n$ (5 equiv). This cleanly hydroxymethylated any residual **3.32**. The resultant impurity that now bears a hydroxymethyl group is sufficiently polar that it can be easily removed from ketone **3.17** via column chromatography.*

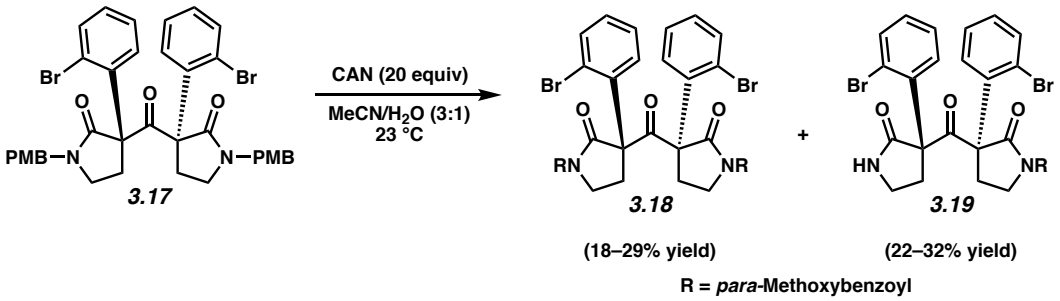

Ketones 3.18 & 3.19. To a solution of ketone **3.17** (2.01 g, 2.69 mmol, 1.00 equiv) in MeCN (285 mL) were added DI H_2O (95 mL) followed by ceric ammonium nitrate (CAN) (29.4 g, 53.9 mmol, 20.0 equiv) in one portion. The reaction mixture was stirred at 23 °C for 90 minutes. The resultant solution was poured into a biphasic mixture of DI H_2O (800 mL) and CH_2Cl_2 (400 mL). The layers were separated, and the aqueous layer was extracted with CH_2Cl_2 (2 x 300 mL). The combined organic layers were dried over $MgSO_4$ and concentrated directly onto silica gel (4 g). The crude product was purified by flash column chromatography (24 g RediSep Gold, 7:3 Hexanes:EtOAc → 100% EtOAc) to give a ketone **3.18** (375 mg, 18% yield) and ketone **3.19** (550 mg, 32% yield). Note that these the yield of **3.18** ranges from 18–29% and the yield of **3.19** ranges from 22–32%. Crystals of both **3.18** and **3.19** suitable for X-ray diffraction studies (**3.18**, CCDC 1999793; **3.19**, CCDC 1999794) were obtained as follows: pure ketone (15 mg) was dissolved in minimal $CHCl_3$ (~2 mL) *n*Hexane (~6 mL) was layered on top of $CHCl_3$ solution and the layers were allowed to slowly diffuse together over 3 days. This furnished high quality single crystals that were amenable to X-ray diffraction. Ketone **3.18**: R_f 0.48 (1:1 Hexanes:EtOAc); ^{1}H NMR (500 MHz, $CDCl_3$) δ 7.76 – 7.68 (m, 4H), 7.66 – 7.61 (m, 4H), 7.33 (td, *J* = 7.7, 1.4 Hz, 2H), 7.22 (td, *J* = 7.6, 1.6 Hz, 2H), 6.82 – 6.75 (m, 4H), 3.89 (ddd, *J* = 10.2, 7.3, 5.2 Hz, 2H), 3.75 (s, 6H), 3.59 (dt, *J* = 13.5, 7.0 Hz, 2H), 3.45 (dt, *J* = 10.8, 6.8 Hz, 2H), 2.70 (ddd, *J* = 12.9, 7.1, 5.5 Hz, 2H); ^{13}C NMR (125 MHz, $CDCl_3$) δ 194.5, 172.5, 169.3, 162.8, 136.1, 135.7, 131.8, 131.0, 129.9, 127.5, 125.9, 123.3, 113.2, 72.1, 55.3, 45.1, 30.0; HRMS-APCI (m/z) $[M + H]^+$ calcd for $C_{37}H_{31}Br_2N_2O_7^+$, 775.0472;

found, 775.0476. Ketone **3.19**: R_f 0.30 (3:2 Hexanes:EtOAc); ^{1}H NMR (500 MHz, $CDCl_3$) δ 7.91 (d, *J* = 8.0 Hz, 1H), 7.88 – 7.82 (m, 2H), 7.72 – 7.62 (m, 2H), 7.59 (dd, *J* = 8.0, 1.7 Hz, 1H), 7.32 (td, *J* = 7.7, 1.5 Hz, 1H), 7.29 – 7.26 (m, 1H), 7.23 – 7.14 (m, 2H), 6.99 – 6.88 (m, 2H), 5.46 (s, 1H), 3.97 – 3.83 (m, 4H), 3.63 – 3.44 (m, 3H), 3.29 – 3.21 (m, 1H), 3.04 (dt, *J* = 9.4, 6.8 Hz, 1H), 2.79 – 2.61 (m, 2H); ^{13}C NMR (125 MHz, $CDCl_3$) δ 195.8, 174.7, 172.2, 169.9, 162.8, 136.5, 136.4, 136.1, 135.9, 131.9, 131.5, 131.4, 129.72, 129.70, 127.6, 127.4, 126.9, 124.0, 123.3, 113.1, 72.8, 69.0, 55.5, 44.6, 39.6, 33.4, 29.8; HRMS-APCI (m/z) $[M + H]^+$ calcd for $C_{29}H_{25}Br_2N_2O_5^+$, 641.0104; found, 641.0104.

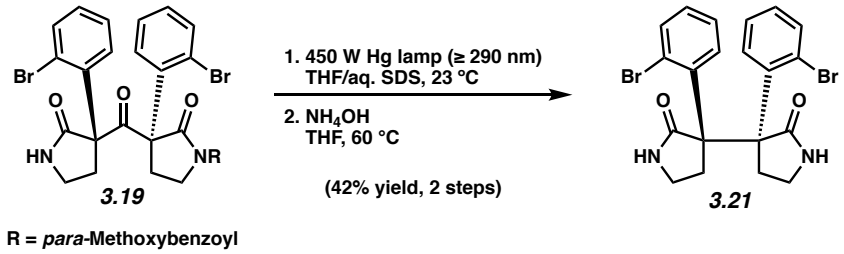

Bis(arylbromide) 3.21. Ketone **3.19** (235 mg, 0.367 mmol, 1.00 equiv) was dissolved in THF (18 mL). An aliquot (3 mL) was added dropwise into a vortexing aqueous solution of sodium dodecyl sulfate (0.7 mg/mL, 30 mL) (see Note 1 for vortexing procedure). This was repeated a total of six times and the resultant suspensions were combined in a 300 mL Pyrex tube (5 cm diameter) with rapid stirring, giving a suspension of ketone **3.19** (total volume of aq. SDS = 180 mL). This suspension was irradiated with a 450 W medium pressure Hg Hanovia UV lamp placed inside a water-cooled immersion-well Pyrex filter (Ace Glass, model 7857-05, $\lambda \geq 290$ nm; 53 mm external diameter, 220 mm full length, 150 mm depth) for 49 h (see Note 3 for reaction monitoring). The reaction was poured into a biphasic mixture of sat. aq. NaCl (150 mL) and EtOAc (100 mL). The layers were separated, and the aqueous layer was extracted with EtOAc (3 x 75 mL). The combined organic layers were diluted with CH_2Cl_2 (100 mL) and dried over Na_2SO_4 before being concentrated under reduced pressure. Residual SDS was removed by flushing the crude oil over a

short silica plug (5 cm) with EtOAc (100 mL) and the resultant solution was concentrated under reduced pressure and used without further purification.

To a solution of the crude photoproduct in THF (30 mL) in a heavy-walled tube, NH_4OH (30–32% w/v, 2.9 mL) was added. The vessel was sealed with a Teflon screwcap, submerged in an oil bath preheated to 65 °C and stirred for 90 minutes. The reaction was allowed to cool to 23 °C and was diluted with CH_2Cl_2 (75 mL). Sat. aq. NaCl (100 mL) was added and the layers were separated. The aqueous layer was extracted with CH_2Cl_2 (2 x 75 mL) and the combined organic layers were dried over Na_2SO_4 and then concentrated under reduced pressure directly onto silica gel (0.5 g). The crude product was purified by flash column chromatography (4 g silica gel, 1:1 Hexanes:EtOAc → 100% EtOAc) to give the bis(arylbromide) **3.21** as a glassy solid (105 mg, 47% yield). Average yield over 2 runs (43% yield). Bis(arylbromide) **3.21**: R_f 0.35 (EtOAc); ^{1}H NMR (600 MHz, $CDCl_3$) δ 8.06 (s, 2H), 7.71 (d, J = 7.6 Hz, 2H), 7.30 – 7.27 (m, 2H), 7.14 – 7.00 (m, 4H), 3.61 (t, J = 9.6 Hz, 2H), 3.51 – 3.33 (m, 4H), 2.81 (td, J = 11.7, 9.5, 3.9 Hz, 2H); ^{13}C NMR (125 MHz, $CDCl_3$) δ 178.2, 140.5, 136.3, 135.7, 128.6, 125.4, 124.2, 61.1, 41.4, 33.6; HRMS-APCI (m/z) $[M + H]^+$ calcd for $C_{20}H_{19}Br_2N_2O_2^+$, 478.9787; found, 478.9775.

Note 1: Vortexing SDS solution: A 50 mL graduated cylinder containing 30 mL SDS solution (0.7 mg/mL in DI H_2O) was placed on a Thermo-Fischer Maxi-Mix® 0.5 W, 60 Hz vortex mixer. Once the aq. solution was rapidly vortexing, the solution of ketone in SDS was added dropwise from a syringe (see image below).

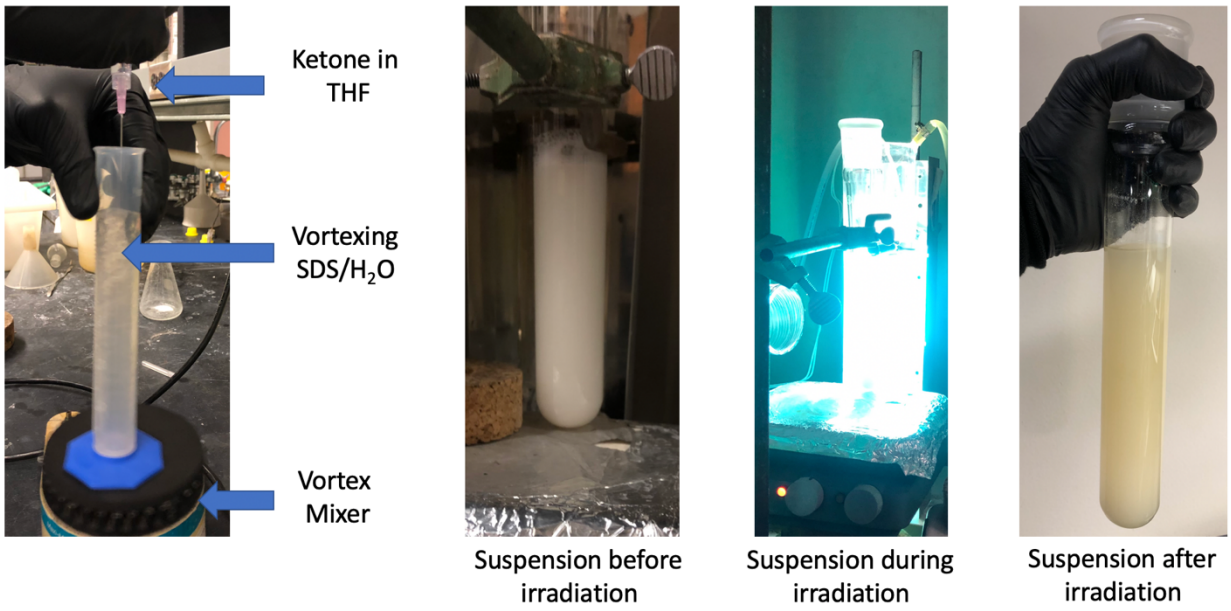

Note 2: During the reaction, the solids have a tendency to become clumped on the side of the glass. This aggregation limits surface area and slows reaction progress. To mitigate this problem, the reaction is stopped every ~4–8 h and the aggregated solid broken up by swirling the solution rapidly with a glass pipette.

Note 3: It is critical to monitor this reaction by aliquots using ^{1}H NMR analysis as reaction times can vary based on how much solid adheres to the glass. Aliquots are collected as follows: 1 mL of the suspension was removed from the reaction mixture and poured into a culture tube with sat. aq. NaCl (2 mL). This mixture was extracted with EtOAc (2 x 2 mL). The combined organic layers were dried over Na_2SO_4 and then flushed through a plug of silica gel (~3 cm) with EtOAc (10 mL). It is important to flush through silica gel prior to collection of NMR spectrum as it removes residual SDS. If this is not done, the ^{1}H NMR resonances become very broad as a result of the SDS and it is difficult to ascertain reaction conversion.

Note 4: It is critical to maintain rapid stirring so the solids remain suspended throughout the course of the reaction.

Note 5: The 450W Hg lamp produces significant heat. This is mitigated by the jacket of cooling water and fans to circulate warm air out of the box containing the irradiation setup.

Note 6: Bis(arylbromide) ***3.21*** *is difficult to visualize by TLC analysis. Very concentrated solutions may be visualized on TLC with a 254 nm handheld UV-lamp.*

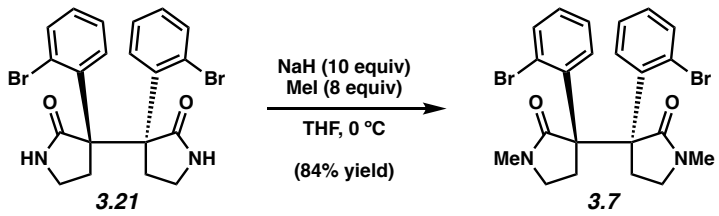

3.21 ***3.7***

***N*–Me Bis(arylbromide) 3.7.** THF (2.8 mL) was added to a vial containing neat bis(arylbromide) **3.21** (40.0 mg, 0.0790 mmol, 1.00 equiv) and NaH (32 mg, 60% dispersion in mineral oil, 0.80 mmol, 10 equiv) and stirred for 5 minutes. The reaction mixture was cooled to 0 °C, MeI (40 μL, 0.091 mg, 0.64 mmol, 8.1 equiv) was added dropwise over 1 minute, and then stirred for 45 minutes. The reaction was quenched by pouring into a biphasic mixture of sat. aq. NH_4Cl (30 mL) and CH_2Cl_2 (30 mL). The aqueous layer was extracted with CH_2Cl_2 (4 x 30 mL). The combined organic layers were dried over Na_2SO_4 and concentrated under reduced pressure directly onto silica gel (300 mg). The crude product was purified by flash chromatography (2 g silica gel, 9:1 Hexanes:EtOAc → 100% EtOAc) to give *N*–Me bis(arylbromide) **3.7** as a white solid (34 mg, 84% yield). *N*–Me Bis(arylbromide) **3.7**: R_f 0.47 (EtOAc); ^{1}H NMR (600 MHz, $CDCl_3$) δ 7.74 – 7.58 (m, 2H), 7.23 (dd, *J* = 7.1, 2.7 Hz, 2H), 7.13 – 6.96 (m, 4H), 3.59 (td, *J* = 9.6, 9.1, 4.9 Hz, 2H), 3.52 – 3.31 (m, 4H), 2.79 (s, 6H), 2.71 – 2.58 (m, 2H); ^{13}C NMR (125 MHz, $CDCl_3$) δ 173.2, 141.2, 136.1, 135.4, 128.4, 125.4, 124.0, 60.6, 48.4, 30.8, 30.5; HRMS-APCI (m/z) $[M + H]^+$ calcd for $C_{22}H_{23}Br_2N_2O_2^+$, 505.0121; found, 505.0104.

Note 1: Bis(arylbromide) ***3.7*** *is difficult to visualize by TLC analysis. Very concentrated solutions may be visualized on TLC with a 254 nm handheld UV-lamp.*

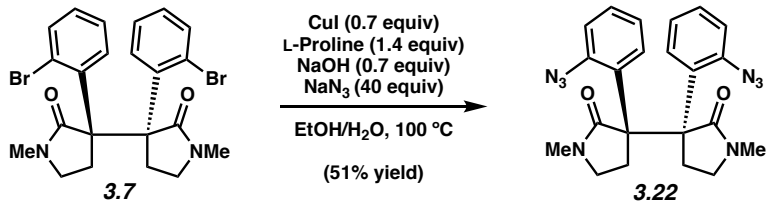

Bis(azide) 3.22-Optimized Procedure. A dram vial was charged with *N*–Me Bis(arylbromide) **3.7** (8.6 mg, 0.017 mmol, 1.00 equiv) and sodium azide (44 mg, 0.68 mmol, 40 equiv) and placed under a flow of N_2. Copper(I) iodide (2.26 mg, 0.0119 mmol, 0.706 equiv) and L-proline (2.73 mg, 0.0237 mmol, 1.41 equiv) were charged to the vial which was then evacuated and backfilled with N_2 (3x). DI H_2O (0.125 mL), EtOH (0.385 mL), and NaOH (2.0 M, 0.012 mL, 0.71 equiv) (which had been each been sparged with N_2 for 20 min) were added via syringe and the reaction was placed in a preheated 100 ºC aluminum heating block and stirred for 20 h. After allowing the reaction to cool to 23 ºC, it was poured into a biphasic mixture of aq. NaOH (1.0 M, 5 mL) and CH_2Cl_2 (3 mL). The layers were separated, and the aqueous layer was extracted with CH_2Cl_2 (3 x 4 mL). The combined organic layers were dried over Na_2SO_4 and concentrated under reduced pressure. After the crude product was further dried under high vacuum for 2 h, it was re-subjected to identical reaction conditions as described above to give bis(azide) **3.22** (3.4 mg, 47% yield) as a cream colored solid without further purification. (Yield determined by ^1H QNMR with 1,3,5-trimethoxybenzene as the external standard; average yield over two identical runs (51%)).

Note 1: The CuI used in the optimized reaction conditions was purified from refluxing aq. NaI prior to use.[32]

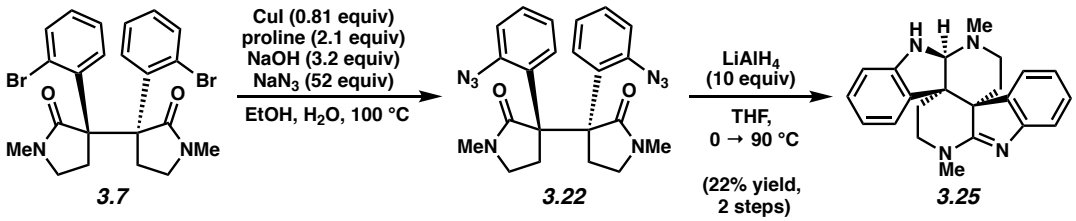

Dihydropsychotriadine 3.25. A vial was charged with *N*–Me bis(arylbromide) **3.7** (40.2 mg, 0.0790 mmol, 1.00 equiv), CuI (12.2 mg, 0.0641 mmol, 0.811 equiv), L-proline (20.0 mg, 0.173 mmol, 2.18 equiv), NaOH (10.1 mg, 0.252 mmol, 3.19 equiv), and NaN_3 (226 mg, 4.09 mmol, 51.8 equiv) and then taken into a glovebox under N_2 atmosphere. EtOH (1.4 mL) and DI H_2O (0.6 mL) that had been sparged for 20 minutes with argon were added via syringe and the vial was sealed with a Teflon screwcap, removed from the glovebox, and placed in an aluminum block preheated to 100 °C. The reaction was stirred at 100 °C for 24 h, cooled to 23 °C, and then diluted with aq. NaOH (0.20 M, 4 mL). The reaction mixture was washed with CH_2Cl_2 (3 x 3 mL) and the combined organic layers were dried over Na_2SO_4 and concentrated under reduced pressure directly onto silica gel (400 mg). The crude product was purified by flash column chromatography (2 g silica gel, 6:4 Hexanes:EtOAc → 1:1 Hexanes:EtOAc) to give semi-pure bis(arylazide) **3.22** which was used without further purification in the next step.

The semipure bis(arylazide) **3.22** from the previous step (24 mg) was dissolved in THF (3.0 mL) and cooled to 0 °C. To the stirring mixture was added $LiAlH_4$ (24 mg, 0.63 mmol, 10 equiv) in one portion and then sealed with a Teflon screwcap. The mixture was stirred at 0 °C for 20 min, then warmed to 23 °C and stirred for another 20 min. The reaction mixture was then placed in an aluminum block preheated to 90 °C and stirred for 1 h. The reaction was then cooled to 23 °C, diluted with EtOAc (1 mL), aq. NaOH (0.20 M, 2 mL), and CH_2Cl_2 (3 mL). The layers were separated and the aqueous layer was extracted with CH_2Cl_2 (2 x 3 mL). The combined organic layers were dried over Na_2SO_4 and concentrated under reduced pressure. The crude mixture was

purified via preparative thin layer chromatography (3% MeOH in CH_2Cl_2 saturated with NH_3) to afford dihydropsychotriadine **3.25** (6.0 mg, 22% yield, two steps). Crystals suitable for X-ray diffraction studies (CCDC 1999795) were obtained using slow evaporation from $CDCl_3$ over 3 days. Dehydropsychotriadine **3.25**: R_f 0.19 (5% MeOH in CH_2Cl_2 saturated with NH_3); ^{1}H NMR (500 MHz, $CDCl_3$) δ 7.79 (d, *J* = 7.5 Hz, 1H), 7.07 (d, *J* = 7.7 Hz, 1H), 6.98 (t, *J* = 7.5 Hz, 1H), 6.83 (t, *J* = 7.6 Hz, 1H), 6.64 (d, *J* = 7.5 Hz, 1H), 6.58 (dt, *J* = 7.5, 3.6 Hz, 2H), 6.39 (t, *J* = 7.4 Hz, 1H), 4.54 (s, 1H), 4.22 (br s, 1H), 3.80 (dt, *J* = 12.4, 6.3 Hz, 1H), 3.48 (dt, *J* = 13.1, 6.6 Hz, 1H), 3.31 – 3.17 (m, 4H), 2.62 (d, *J* = 10.1 Hz, 5H), 2.29 (td, *J* = 12.8, 4.2 Hz, 1H), 2.25 – 2.16 (m, 1H), 1.21 (dd, *J* = 13.3, 2.8 Hz, 1H); ^{13}C NMR (125 MHz, $CDCl_3$) δ 177.8, 154.0, 148.0, 139.2, 134.2, 128.1, 127.6, 123.9, 122.0, 120.4, 119.8, 116.5, 110.8, 86.1, 56.0, 49.5, 46.2, 44.3, 42.7, 38.7, 33.2, 33.1; HRMS-APCI (m/z) $[M + H]^+$ calcd for $C_{22}H_{25}N_4^+$, 345.2074; found, 345.2079.

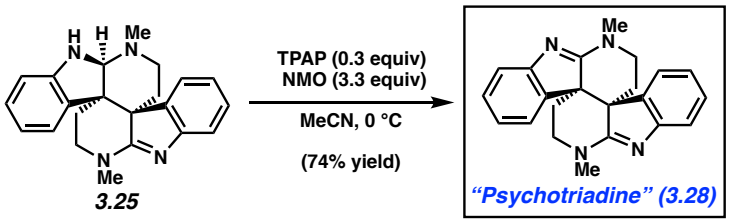

Psychotriadine 3.28. A stock solution of TPAP (4.2 mg, 0.010 mmol, 0.91 equiv) and NMO (12.3 mg, 0.105 mmol, 10.0 equiv) in MeCN (1.80 mL) was prepared. To a separate vial containing dehydropsychotriadine **3.25** (3.9 mg, 0.011 mmol, 1.0 equiv) dissolved in MeCN (1.10 mL) at 0 °C was added 0.600 mL of the aforementioned stock solution dropwise over 1 minute. The reaction was stirred at 0 °C for 1 h before being diluted with CH_2Cl_2 saturated with NH_3 (3 mL). The mixture was flushed through a silica plug (2 cm), then the silica plug was rinsed with CH_2Cl_2 saturated with NH_3 (6 mL). The mixture was then concentrated under reduced pressure and the crude mixture was purified via preparative thin layer chromatography (3% MeOH in CH_2Cl_2 saturated with NH_3) to afford pysochotriadine **3.28** as a white solid (2.9 mg, 74% yield).

Psychotriadine **3.28**: R_f 0.22 (5% MeOH in CH_2Cl_2 saturated with NH_3); ^1H NMR (600 MHz, $CDCl_3$) δ 7.24 (d, *J* = 7.7 Hz, 2H), 7.09 (ddd, *J* = 7.7, 6.9, 1.9 Hz, 2H), 6.72 – 6.56 (m, 4H), 3.59 – 3.47 (m, 4H), 3.22 (s, 6H), 2.90 (ddd, *J* = 14.2, 11.9, 7.3 Hz, 2H), 1.49 (ddd, *J* = 14.2, 5.1, 1.6 Hz, 2H); ^{13}C NMR (125 MHz, $CDCl_3$) 176.8, 154.1, 136.6, 128.7, 121.6, 120.5, 117.7, 51.5, 49.4, 38.2, 33.3; HRMS-APCI (m/z) $[M + H]^+$ calcd for $C_{22}H_{23}N_4^+$, 343.1932; found, 343.1920.

Table 3.1. Comparison of ^{13}C NMR data for natural[6a] vs. synthetic psychotriadine.

Natural Psychotriadine (From Sample Provided by L. Verotta)[6a] ^{13}C, 500 MHz, $CDCl_3$	Synthetic Psychotriadine ^{13}C, 500 MHz, $CDCl_3$
176.8	176.8
154.1	154.1
136.6	136.6
128.7	128.7
121.5	121.6
120.5	120.5
117.6	117.7
51.5	51.5
49.4	49.4
38.2	38.2
33.3	33.3

Figure 3.3. Comparison of [1]H NMR data for natural[6a] vs. synthetic psychotriadine (full spectrum).

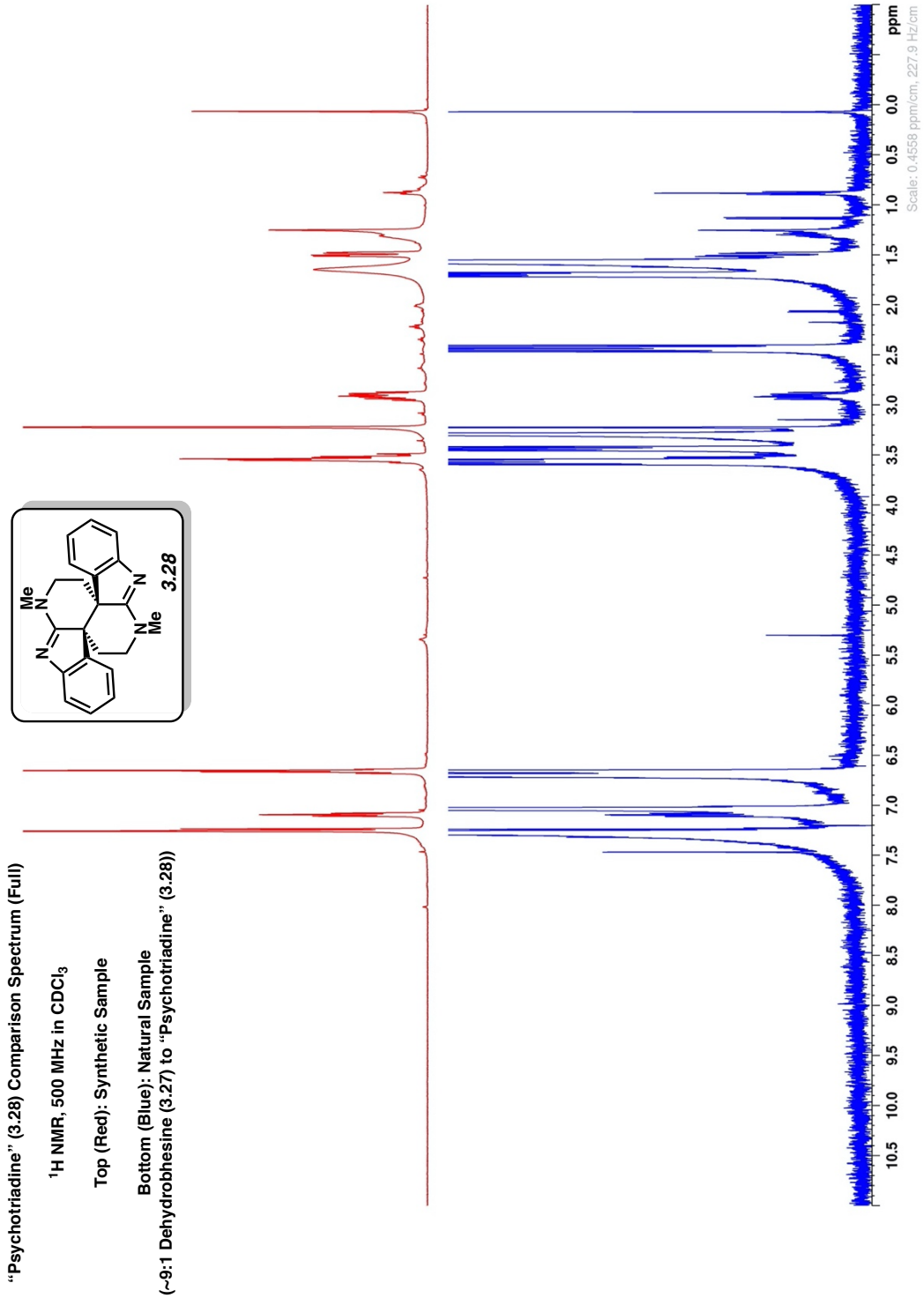

Figure 3.4. Comparison of ^{1}H NMR data for natural[6a] vs. synthetic psychotriadine (aliphatic region).

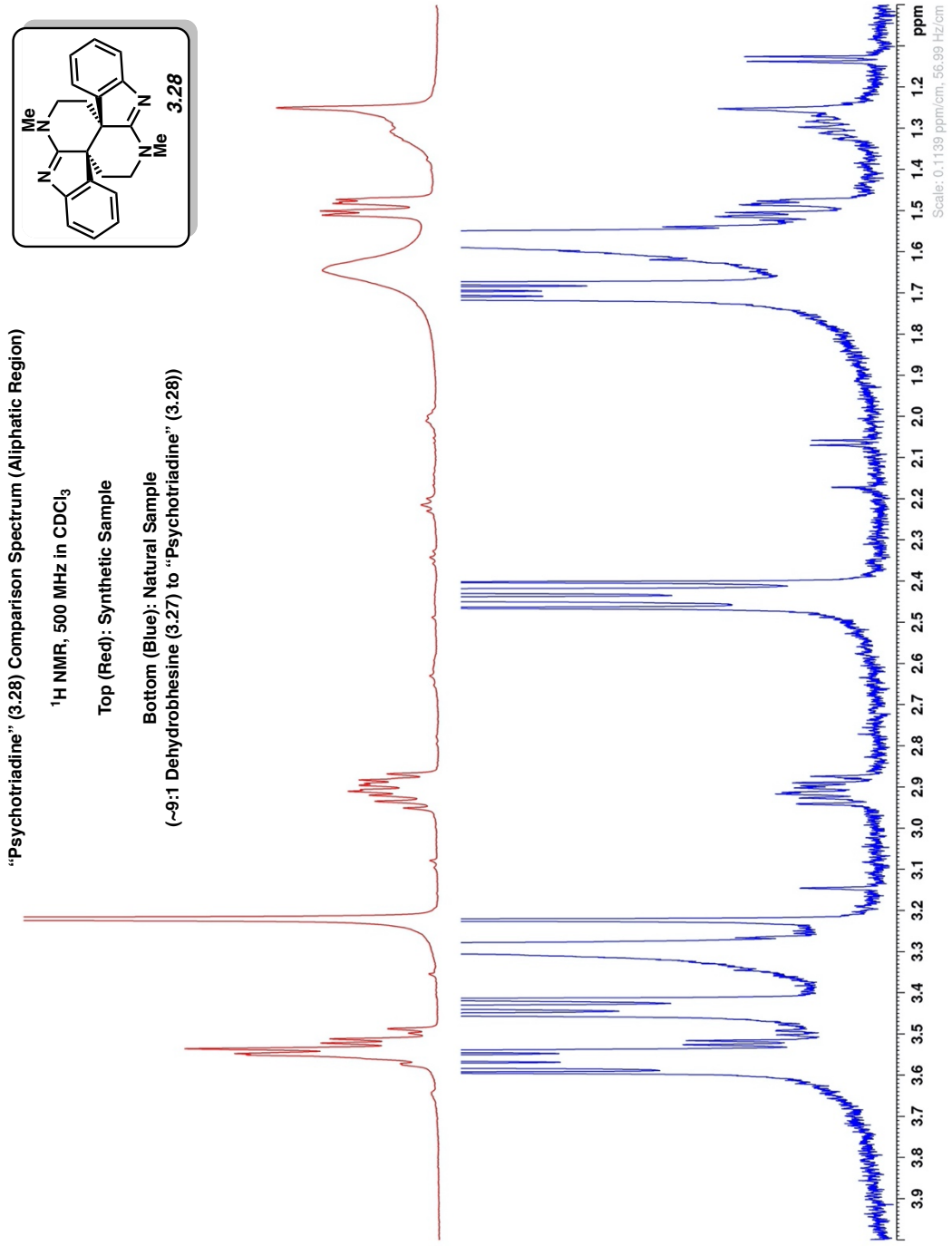

Figure 3.5. Comparison of ^{1}H NMR data for natural[6a] vs. synthetic psychotriadine (aromatic region).

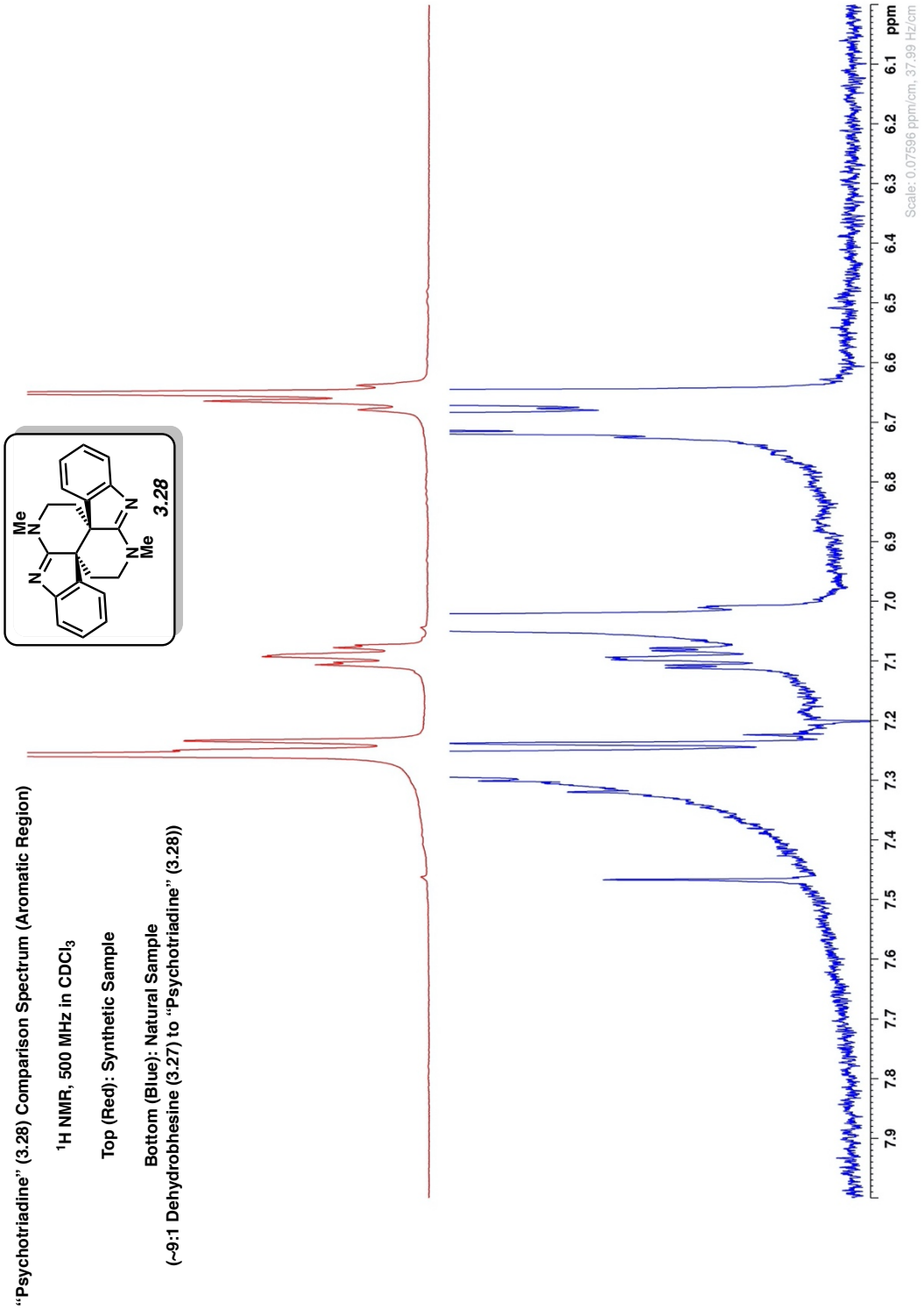

Figure 3.6. Comparison of ^{13}C NMR data for natural[6a] vs. synthetic psychotriadine.

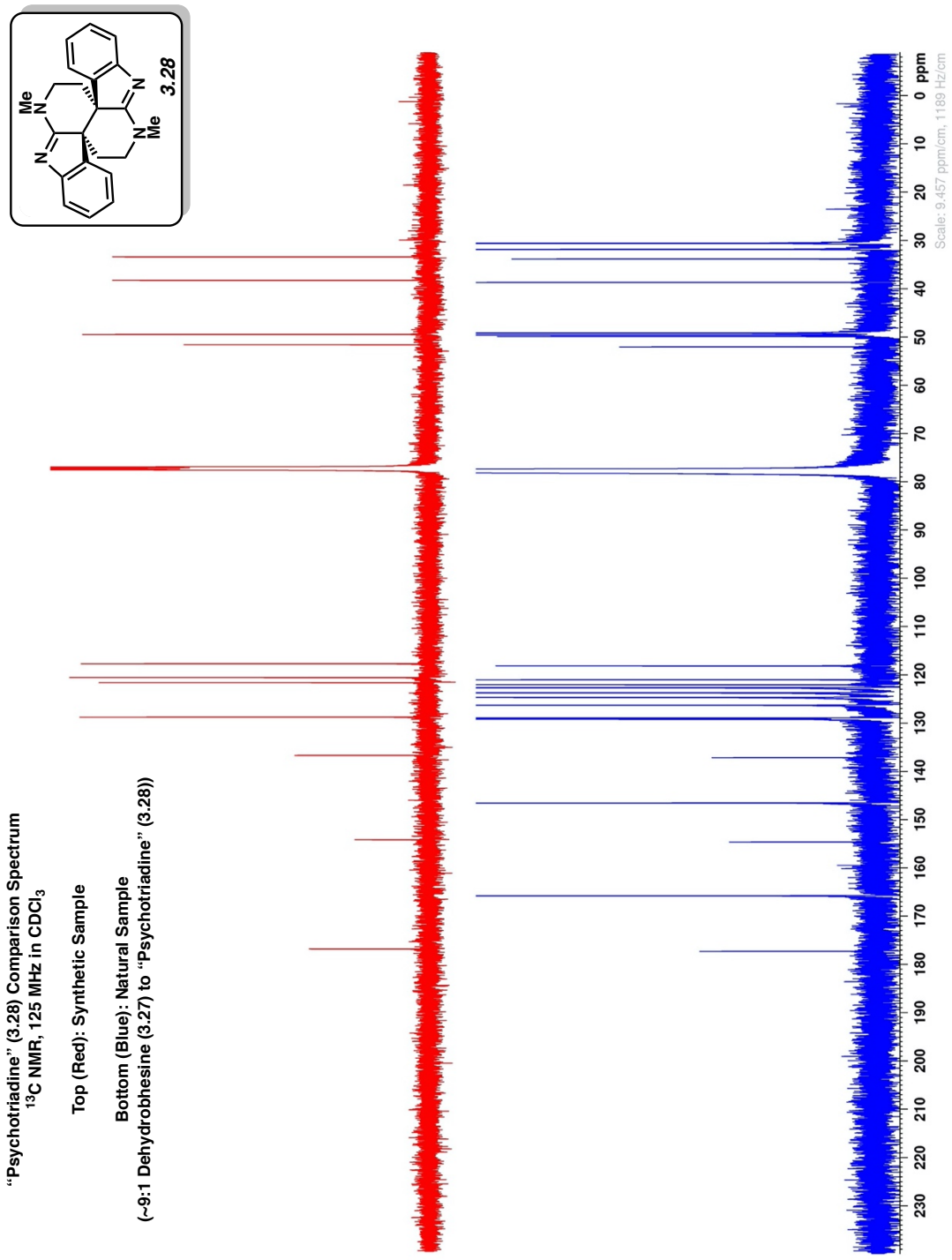

3.5.3. Alternative Routes Explored

Amine Installation Prior to Photodecarbonylation (Figure 3.7):

Having accessed compound **3.9**, we were interested in the possibility of carrying out C–N bond formation prior to the key photodecarbonylation step. To accomplish this, we subjected **3.9** to Cu-catalyzed azidation conditions and were delighted to find that **3.9** underwent double azidation to give **3.33** in 72% yield. Next, we attempted reduction of **33** using hydrogenolysis conditions. However, rather than the desired bis(amine) **3.34** for use in photodecarbonylation, we obtained spirocycle **3.36**, presumably via the intermediacy of **3.34**. We also attempted photodecarbonylation of bis(azide) **3.33** (not shown), which unfortunately led to substantial nonspecific decomposition. The results obtained from these studies led us to realize the requisite order of operations for access to the bis(cyclotryptamine) scaffolds: photodecarbonylation of a ketone bearing a modifiable *ortho*- substituent followed by installation of the amine moiety.

Figure 3.7. Amine installation prior to photodecarbonylation.

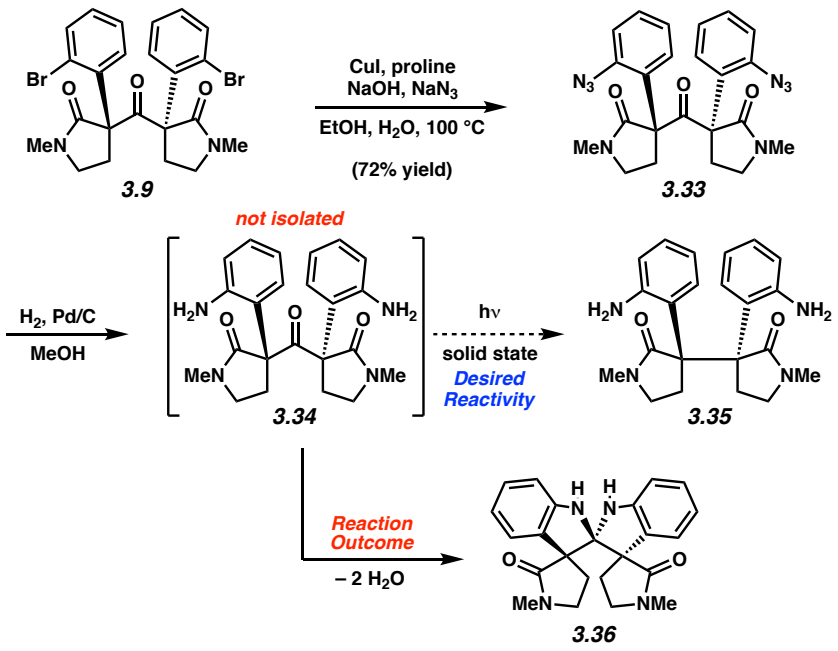

Use of directed *ortho*- metallation / amination to install requisite amine functional groups (Figure 3.8):

Given difficulties faced carrying *ortho*- substituents on the ketone substrate's aryl groups through the photodecarbonylation reaction, we sought to install the amine substituents through a late stage C–H activation of **3.38** (Figure 3.8). Compound **3.38** was accessed in 51% yield by exposing ketone **3.37** to ultraviolet light in the solid-state. We then attempted to introduce the *ortho*- functionality through an array of directed metalation / amination sequences. Experts in C–H functionalization also tried to achieve this transformation with material provided by our laboratories (using non-disclosed reaction conditions). Unfortunately, despite significant attempts, directed lithiation, transition metal-catalyzed functionalization, and nitration routes were uniformly deemed unsuccessful.

Figure 3.8. Use of directed *ortho*- metalation / amination to install requisite amine functional groups.

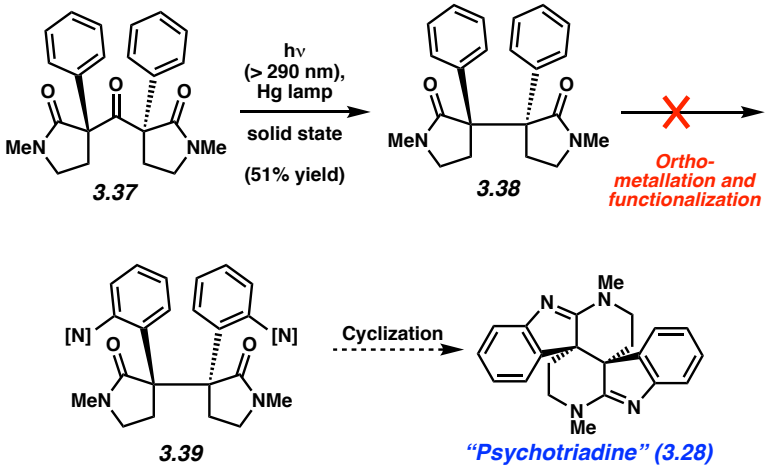

Use of *ortho*-chloro substituent to access bis(cyclotryptamines) (Figure 3.9):

We investigated using unsymmetrical, chlorinated ketone **3.40** to synthesize the bis(cyclotryptamine) alkaloids. Relative to the *ortho*-bromo substrate **3.19**, chloro-substituted compound **3.40** was more efficient in the photodecarbonylation reaction, proceeding in 61% yield over 2 steps to give **3.41** (compared with 41% yield for compound **3.19** to give **3.21**). Amide methylation of **3.41** proceeded cleanly to give **3.42**. However, all efforts to achieve activation of the C–Cl bond to generate **3.43** proved unsuccessful. Various catalysts and nucleophiles were investigated, but successful installation of nitrogen atoms from **3.42** was never realized.

Figure 3.9. Use of *ortho*-chloro substituent to access bis(cyclotryptamines).

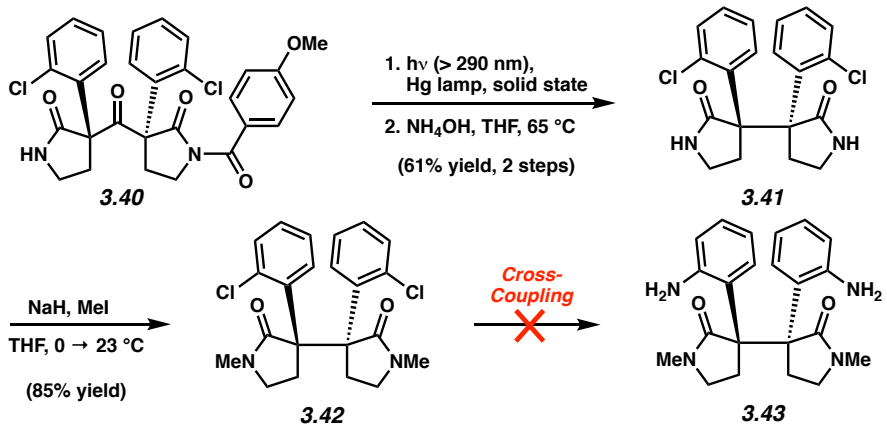

Reduction of dihydropsychotriadine (3.25) to access other members of the bis(cyclotryptamine) alkaloid family (Figure 3.10):

We were curious if **3.25** could be reduced to **3.44**. This would help us ascertain if **3.44** itself was a stable compound and if it could be isomerized to the alkaloids calycanthine (**3.45**) and chimonanthine (**3.46**). Unfortunately, attempts to reduce **3.25** to the corresponding geminal diamine **3.44** or an isomer thereof were either met with decomposition or led to recovered starting material.

Figure 3.10. Reduction of dihydropsychotriadine (**3.25**) to access other members of the bis(cyclotryptamine) alkaloid family.

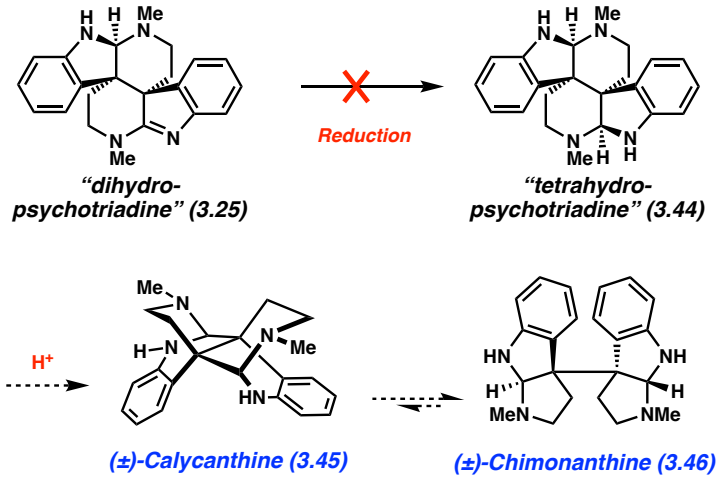

3.5.4. Alternative Mechanism for the Conversion of 3.22 to 3.25.

Although Scheme 3.3 provides one mechanistic possibility for the conversion of **3.22** to **3.25**, other mechanistic possibilities are feasible. One reasonable mechanism is shown in Figure 3.11. After reduction of the azide moieties in **3.22**, intermediate **3.23** could undergo intramolecular condensation to form the five membered amidine **3.47**. Upon reduction with another equivalent of $LiAlH_4$, **3.48** could rearrange to provide indolenine **3.49**. In turn, **3.49** could undergo a transamidation to give piperidinone **3.50**, which could give rise to **3.25** upon cyclization, dehydration, and aqueous workup.

Figure 3.11. Alternative mechanism for the conversion of **3.22** to **3.25.**

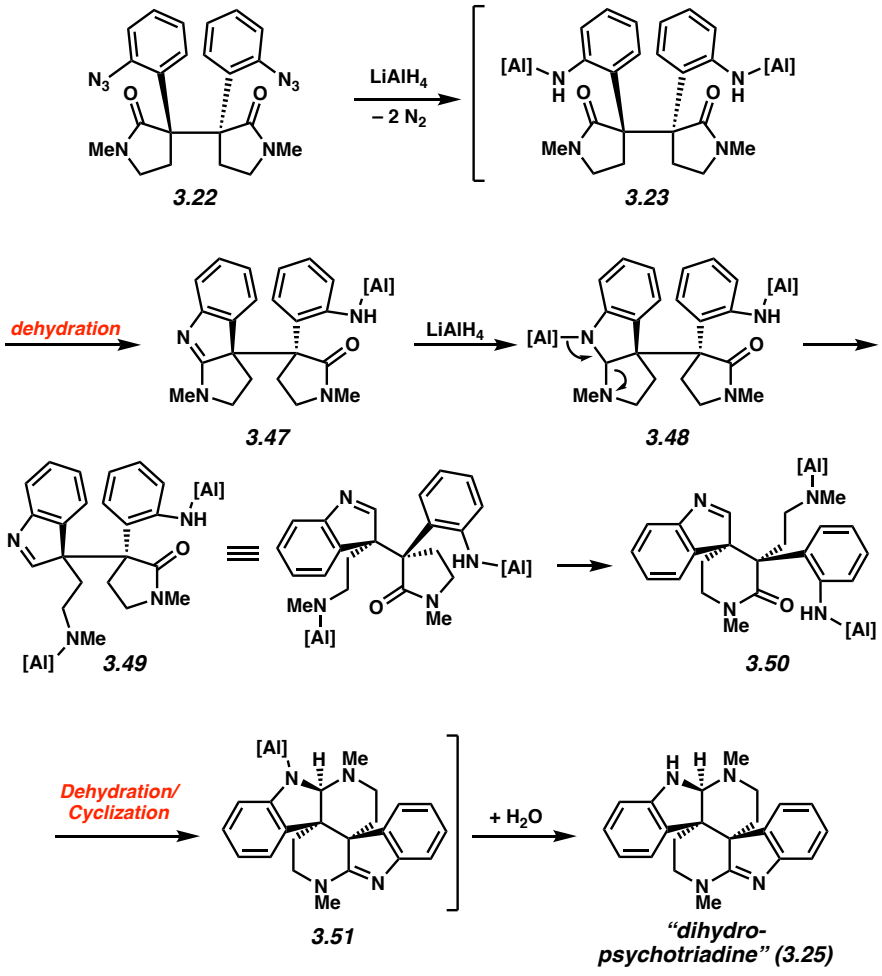

3.5.5. Crystal Structure Data

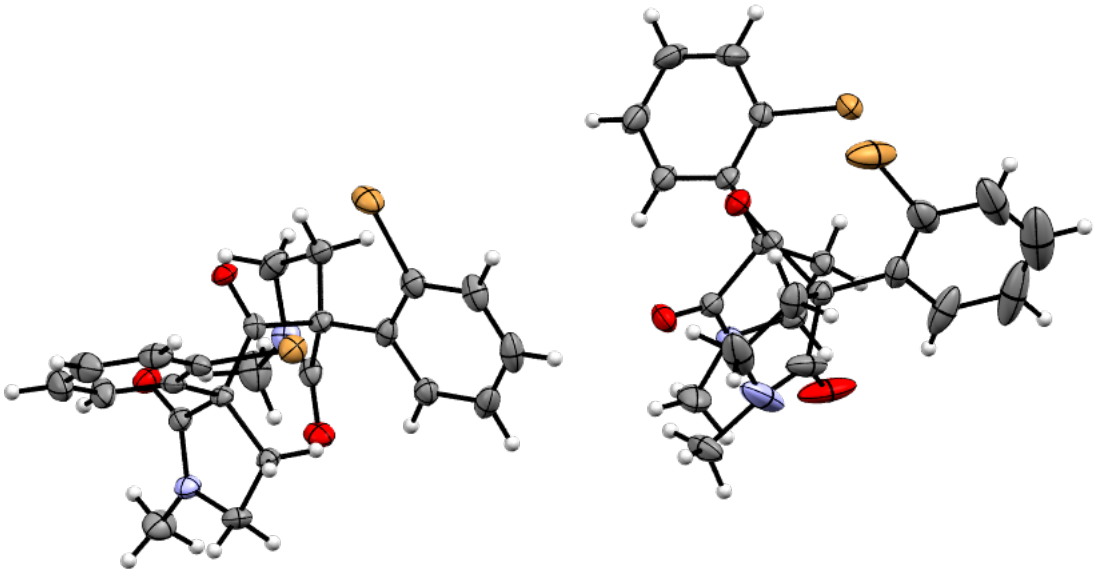

Table 3.2. Crystal data and structure refinement for **3.9**.

Identification code	cu_gg1622-twin5	
Empirical formula	C23 H22 Br2 N2 O3	
Formula weight	534.24	
Temperature	100(2) K	
Wavelength	1.54178 Å	
Crystal system	Triclinic	
Space group	P -1	
Unit cell dimensions	a = 8.2766(3) Å	a= 91.499(2)°.
	b = 12.5596(4) Å	b= 95.714(2)°.
	c = 21.0814(7) Å	g = 93.240(2)°.
Volume	2175.94(13) $Å^3$	
Z	4	
Density (calculated)	1.631 Mg/m^3	

Absorption coefficient	4.952 mm^{-1}
F(000)	1072
Crystal size	0.200 x 0.150 x 0.100 mm^3
Theta range for data collection	2.107 to 69.354°.
Index ranges	-9<=h<=9, -15<=k<=15, 0<=l<=25
Reflections collected	13102
Independent reflections	13102 [R(int) = ?]
Completeness to theta = 67.679°	99.3 %
Absorption correction	Semi-empirical from equivalents
Max. and min. transmission	0.75 and 0.49
Refinement method	Full-matrix least-squares on F^2
Data / restraints / parameters	13102 / 60 / 556
Goodness-of-fit on F^2	1.165
Final R indices [I>2sigma(I)]	R1 = 0.0457, wR2 = 0.1275
R indices (all data)	R1 = 0.0597, wR2 = 0.1325
Extinction coefficient	n/a
Largest diff. peak and hole	0.946 and -2.055 $e.Å^{-3}$

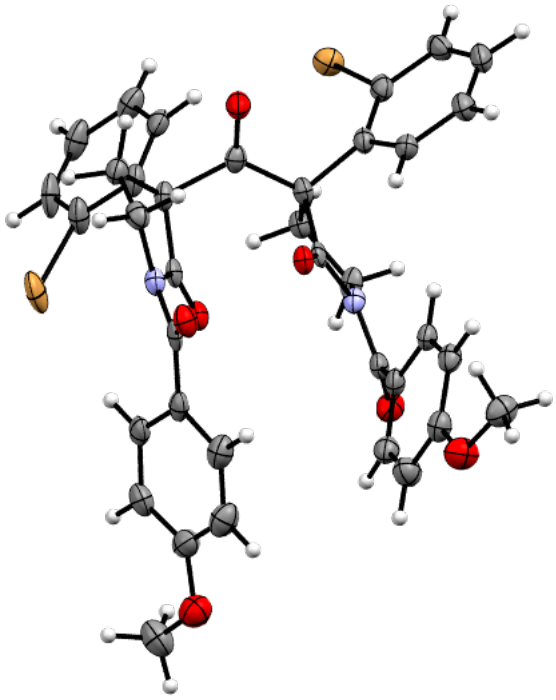

Table 3.3. Crystal data and structure refinement for **3.18**.

Identification code	cu_gg1916s_a	
Empirical formula	C37 H30 Br2 N2 O7	
Formula weight	774.45	
Temperature	100(2) K	
Wavelength	1.54178 Å	
Crystal system	Monoclinic	
Space group	P 21/c	
Unit cell dimensions	a = 13.2817(4) Å	α= 90°.
	b = 14.6241(4) Å	β= 90.198(2)°.
	c = 16.4472(4) Å	γ = 90°.
Volume	3194.57(15) Å^3	

Z	4
Density (calculated)	1.610 Mg/m^3
Absorption coefficient	3.684 mm^{-1}
F(000)	1568
Crystal size	0.080 x 0.040 x 0.020 mm^3
Theta range for data collection	3.327 to 70.277°.
Index ranges	-16<=h<=16, -17<=k<=17, -19<=l<=20
Reflections collected	25105
Independent reflections	5920 [R(int) = 0.0745]
Completeness to theta = 67.679°	99.1 %
Absorption correction	Semi-empirical from equivalents
Max. and min. transmission	0.75 and 0.63
Refinement method	Full-matrix least-squares on F^2
Data / restraints / parameters	5920 / 0 / 435
Goodness-of-fit on F^2	1.026
Final R indices [I>2sigma(I)]	R1 = 0.0475, wR2 = 0.1085
R indices (all data)	R1 = 0.0714, wR2 = 0.1199
Extinction coefficient	n/a
Largest diff. peak and hole	1.297 and -0.767 $e.Å^{-3}$

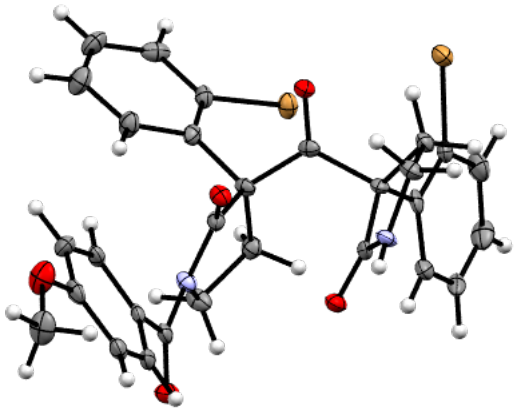

Table 3.4. Crystal data and structure refinement for **3.19**.

Identification code	cu_garg1913s_a	
Empirical formula	C29 H24 Br2 N2 O5	
Formula weight	640.32	
Temperature	100(2) K	
Wavelength	1.54178 Å	
Crystal system	Monoclinic	
Space group	P 21/c	
Unit cell dimensions	a = 14.9870(5) Å	α= 90°.
	b = 10.0874(3) Å	β= 104.245(2)°.
	c = 17.7928(6) Å	γ = 90°.
Volume	2607.20(15) $Å^3$	
Z	4	
Density (calculated)	1.631 Mg/m^3	
Absorption coefficient	4.309 mm^{-1}	
F(000)	1288	

Crystal size	0.180 x 0.060 x 0.020 mm^3
Theta range for data collection	3.042 to 69.895°.
Index ranges	-18<=h<=17, -11<=k<=12, -20<=l<=17
Reflections collected	20426
Independent reflections	4685 [R(int) = 0.0854]
Completeness to theta = 67.679°	96.1 %
Absorption correction	Semi-empirical from equivalents
Max. and min. transmission	0.75 and 0.60
Refinement method	Full-matrix least-squares on F^2
Data / restraints / parameters	4685 / 0 / 347
Goodness-of-fit on F^2	1.054
Final R indices [I>2sigma(I)]	R1 = 0.0437, wR2 = 0.0954
R indices (all data)	R1 = 0.0671, wR2 = 0.1022
Extinction coefficient	n/a
Largest diff. peak and hole	0.665 and -0.771 $e.Å^{-3}$

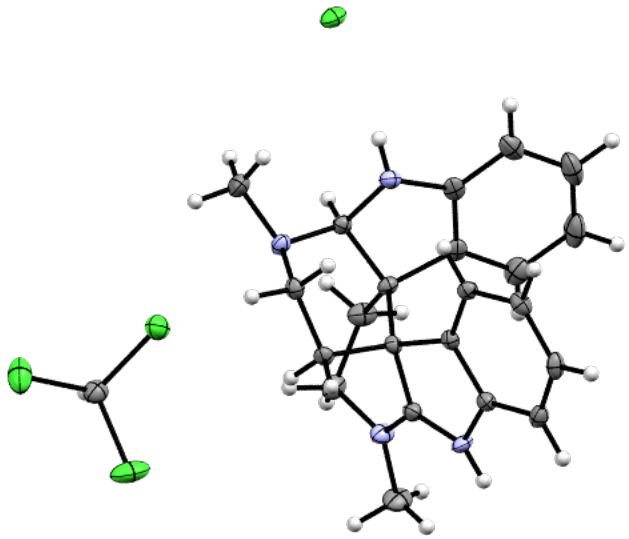

Table 3.5. Crystal data and structure refinement for **3.25**.

Identification code	garg2002s_a	
Empirical formula	C23 H26 Cl4 N4	
Formula weight	500.28	
Temperature	100(2) K	
Wavelength	1.54178 Å	
Crystal system	Triclinic	
Space group	P -1	
Unit cell dimensions	a = 9.6194(4) Å	α= 69.962(3)°.
	b = 11.4565(5) Å	β= 87.308(3)°.
	c = 12.5447(6) Å	γ = 66.232(2)°.
Volume	1181.94(9) $Å^3$	
Z	2	
Density (calculated)	1.406 Mg/m^3	

Absorption coefficient	4.693 mm^{-1}
F(000)	520
Crystal size	.20 x .10 x .04 mm^3
Theta range for data collection	3.772 to 69.534°.
Index ranges	-11<=h<=11, -13<=k<=13, -15<=l<=14
Reflections collected	16933
Independent reflections	4241 [R(int) = 0.0411]
Completeness to theta = 67.679°	96.3 %
Absorption correction	Semi-empirical from equivalents
Max. and min. transmission	0.75 and 0.59
Refinement method	Full-matrix least-squares on F^2
Data / restraints / parameters	4241 / 0 / 290
Goodness-of-fit on F^2	1.149
Final R indices [I>2sigma(I)]	R1 = 0.0327, wR2 = 0.0851
R indices (all data)	R1 = 0.0416, wR2 = 0.0881
Extinction coefficient	n/a
Largest diff. peak and hole	0.333 and -0.268 $e.Å^{-3}$

3.6 Spectra Relevant to Chapter Three:

Discovery and Total Synthesis of a Bis(Cyclotryptamine) Alkaloid Bearing the Elusive Piperidinoindoline Scaffold

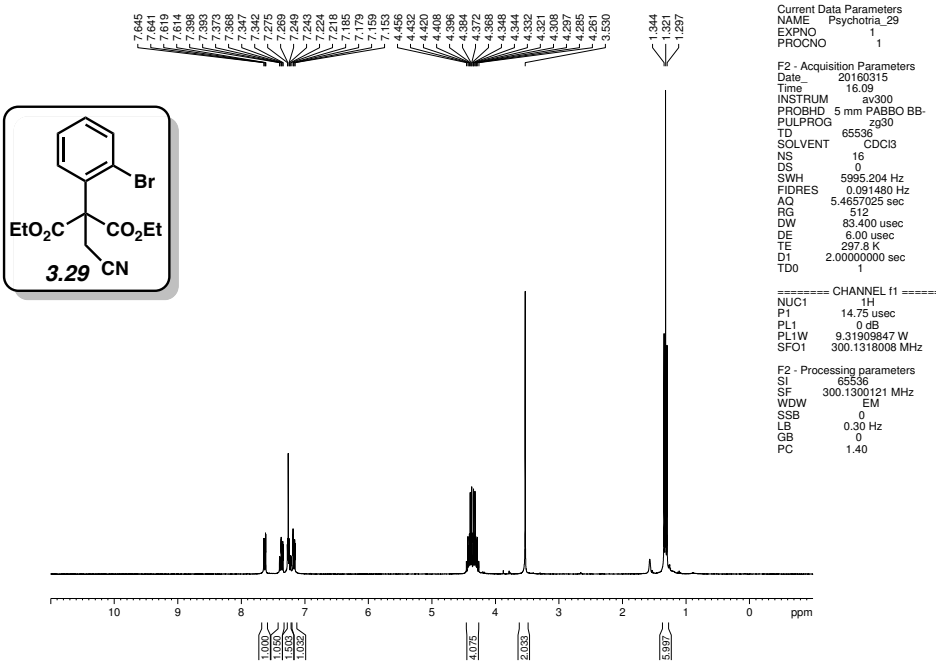

Figure 3.12 ^{1}H NMR (300 MHz, C_6D_6) of compound **3.29**.

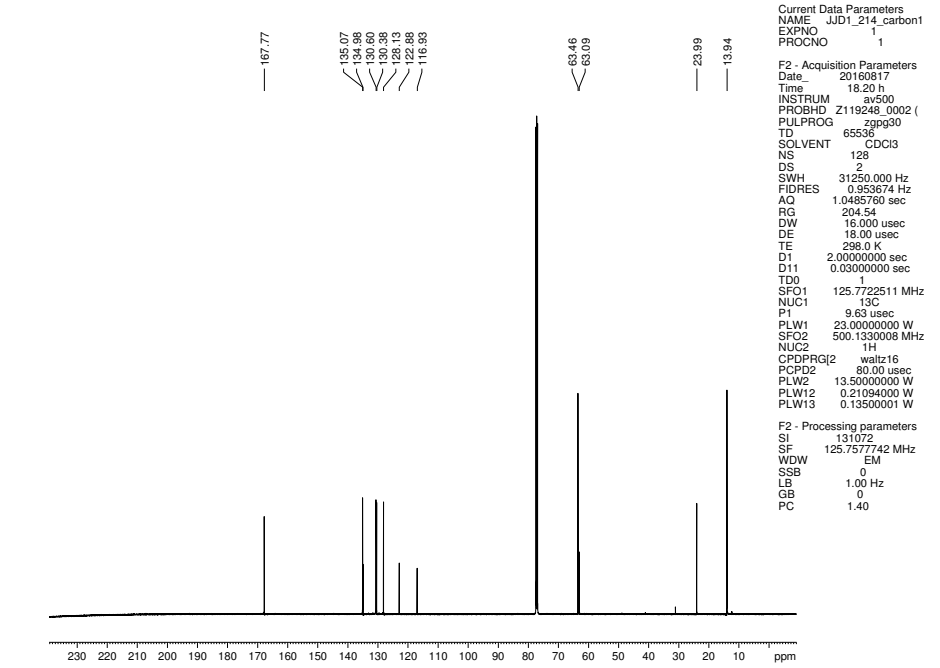

Figure 3.13 ^{13}C NMR (125 MHz, C_6D_6) of compound **3.29**.

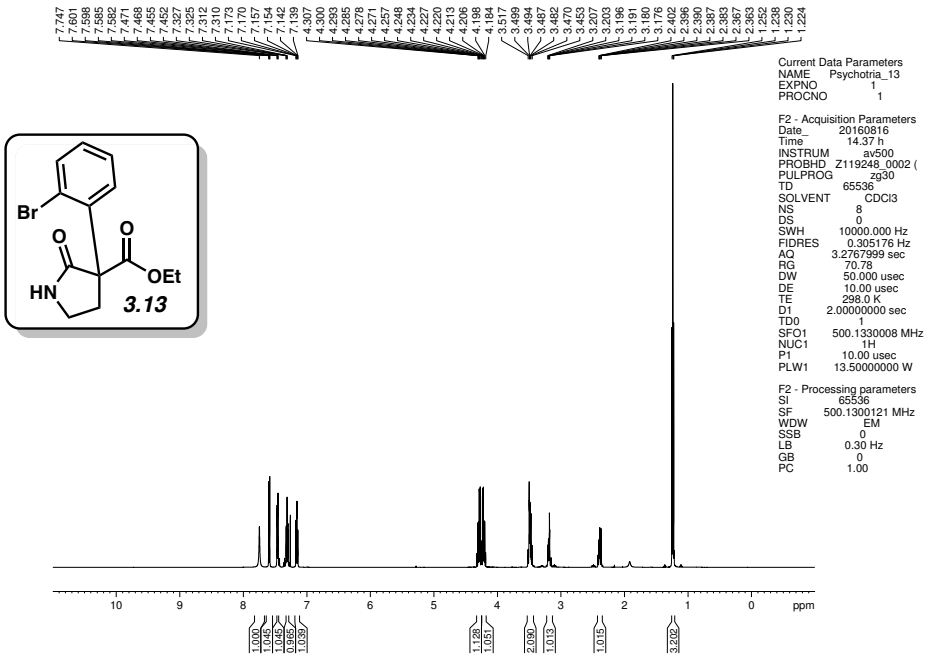

Figure 3.14 ^{1}H NMR (500 MHz, C_6D_6) of compound **3.13**.

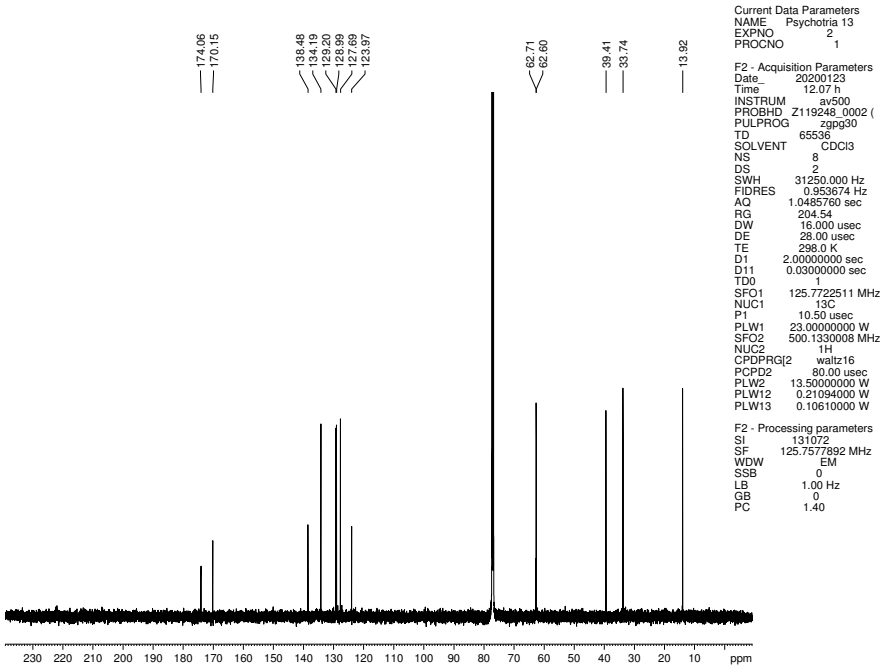

Figure 3.15 ^{13}C NMR (125 MHz, C_6D_6) of compound **3.13**.

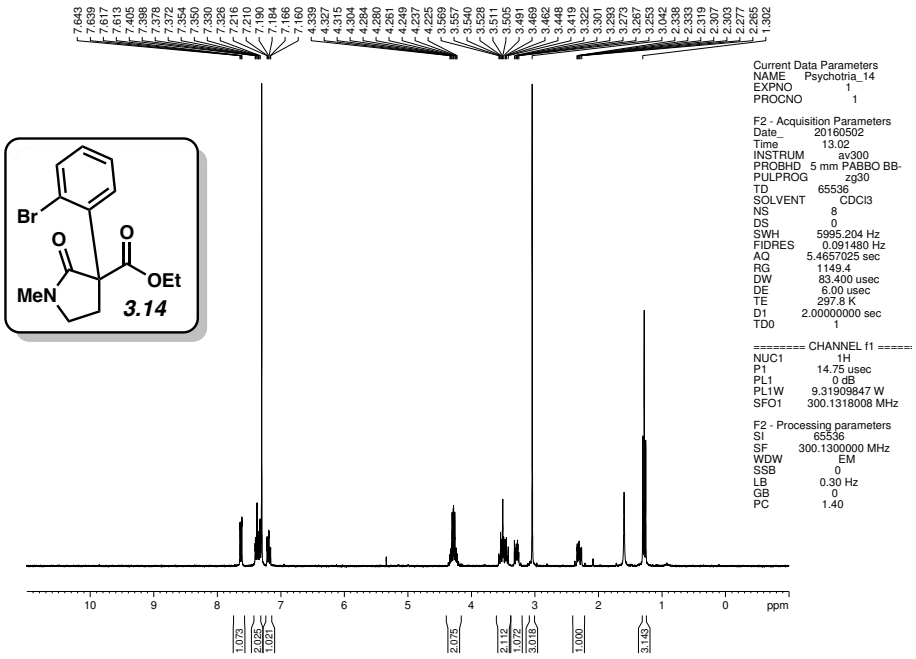

Figure 3.16 ^{1}H NMR (300 MHz, C_6D_6) of compound **3.14**.

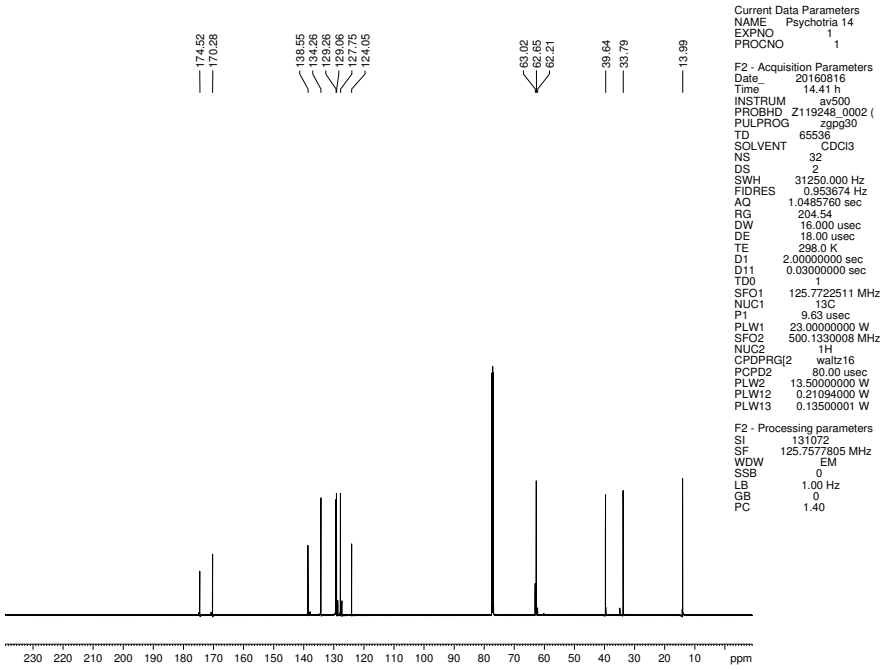

Figure 3.17 ^{13}C NMR (125 MHz, C_6D_6) of compound **3.14**.

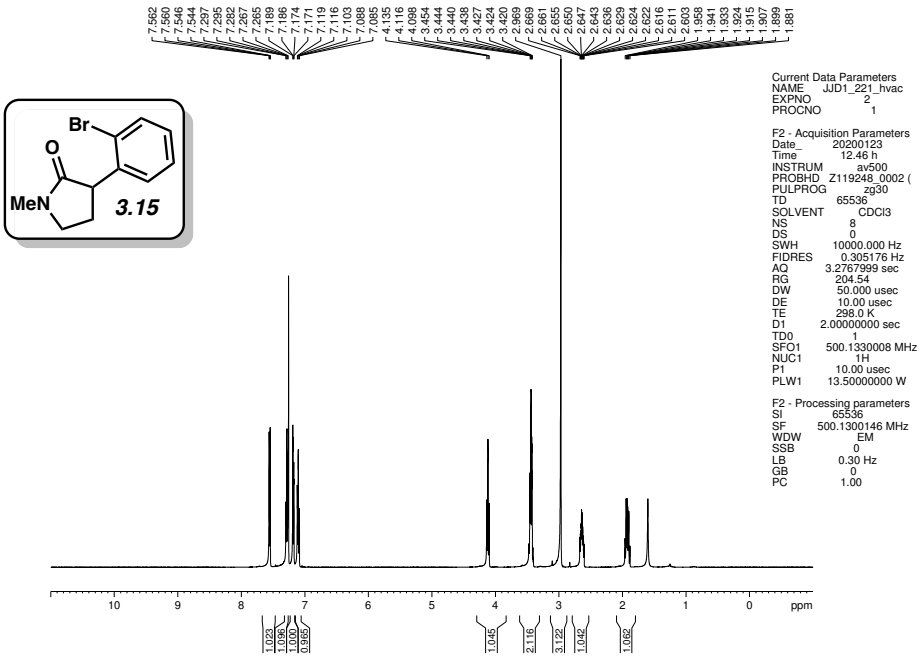

Figure 3.18 ^{1}H NMR (500 MHz, C_6D_6) of compound **3.15**.

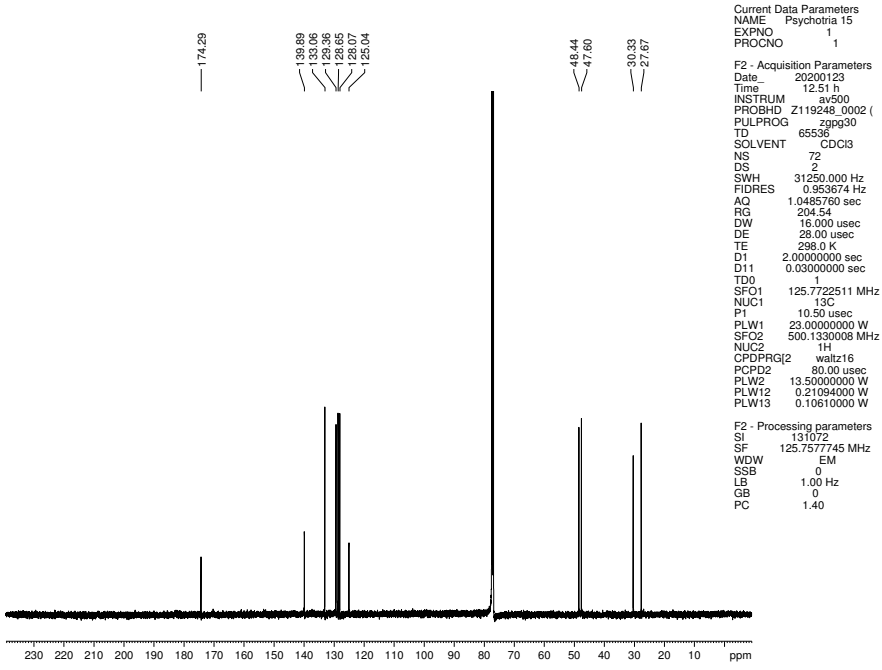

Figure 3.19 ^{13}C NMR (125 MHz, C_6D_6) of compound **3.15**.

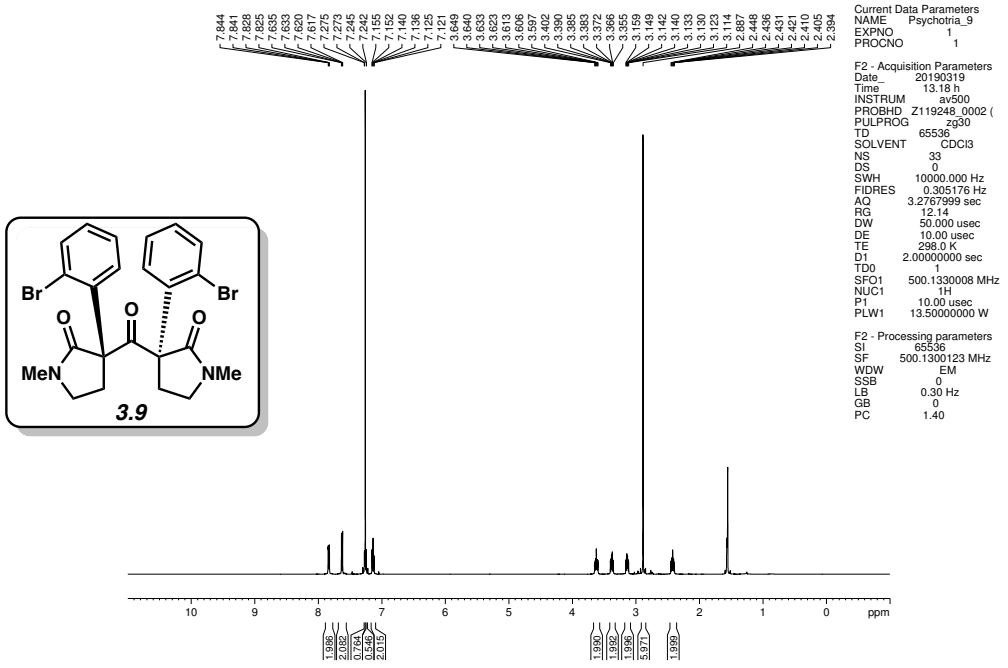

Figure 3.20 ^{1}H NMR (500 MHz, $CDCl_3$) of compound **3.9**.

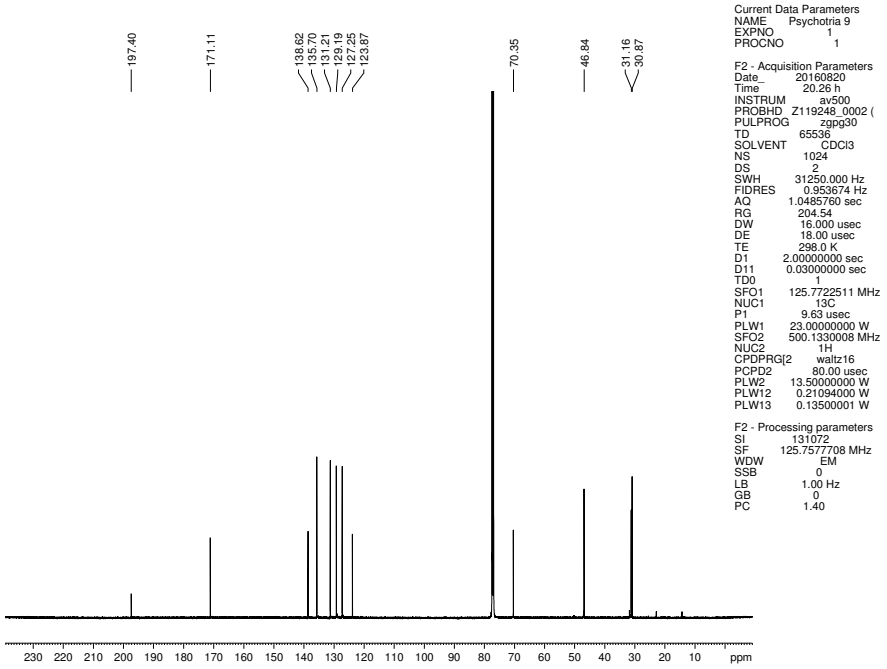

Figure 3.21 ^{13}C NMR (125 MHz, $CDCl_3$) of compound **3.9**.

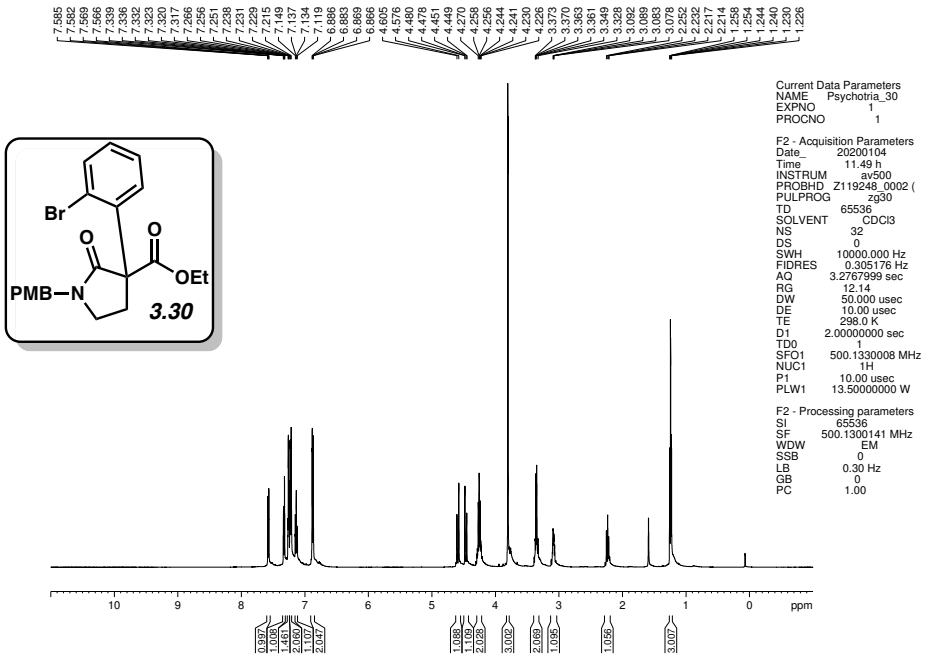

Figure 3.22 ^{1}H NMR (500 MHz, C_6D_6) of compound **3.30**.

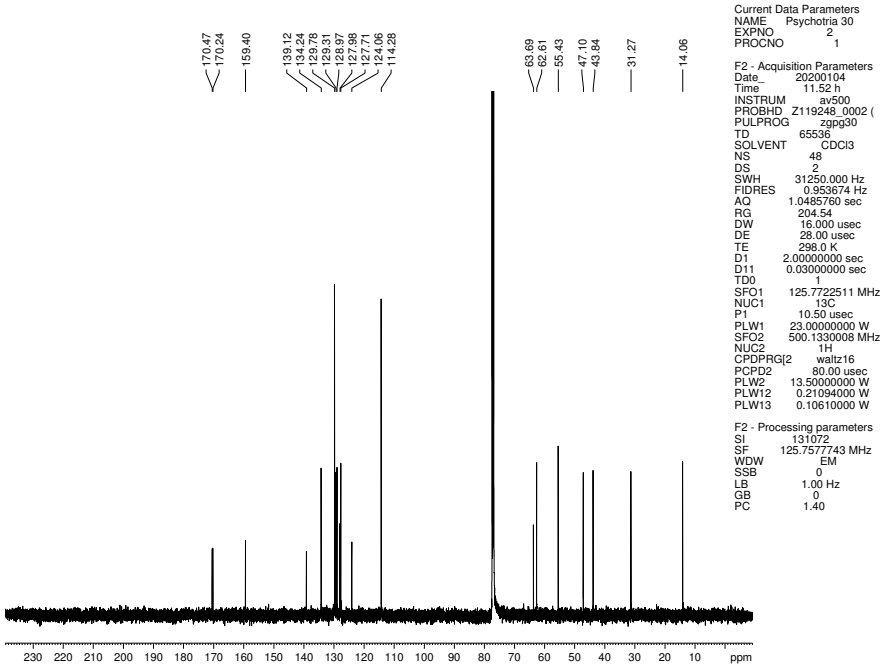

Figure 3.23 ^{13}C NMR (125 MHz, C_6D_6) of compound **3.30**.

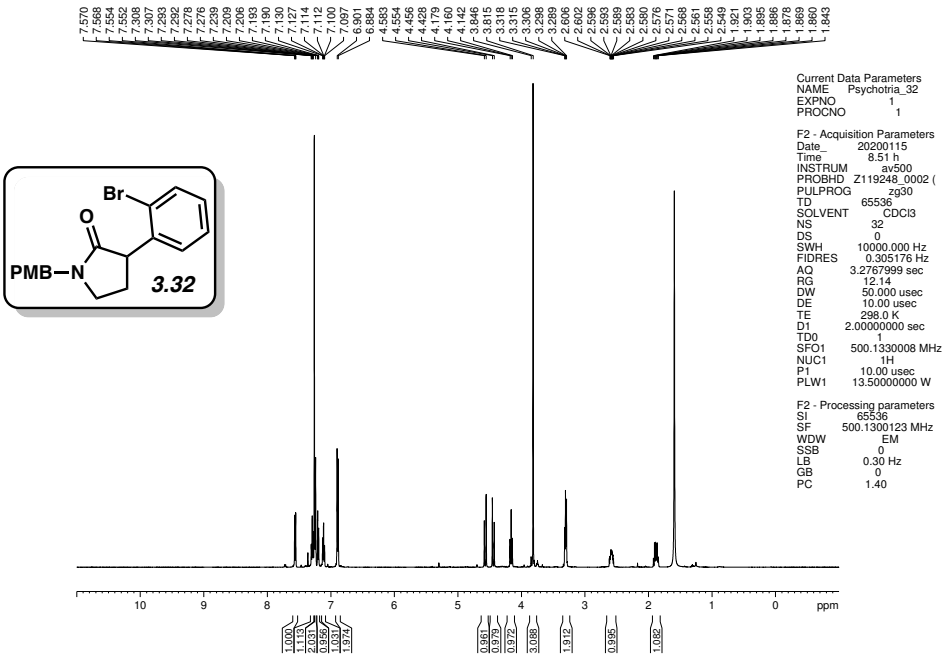

Figure 3.24 ^{1}H NMR (500 MHz, $CDCl_3$) of compound **3.32**.

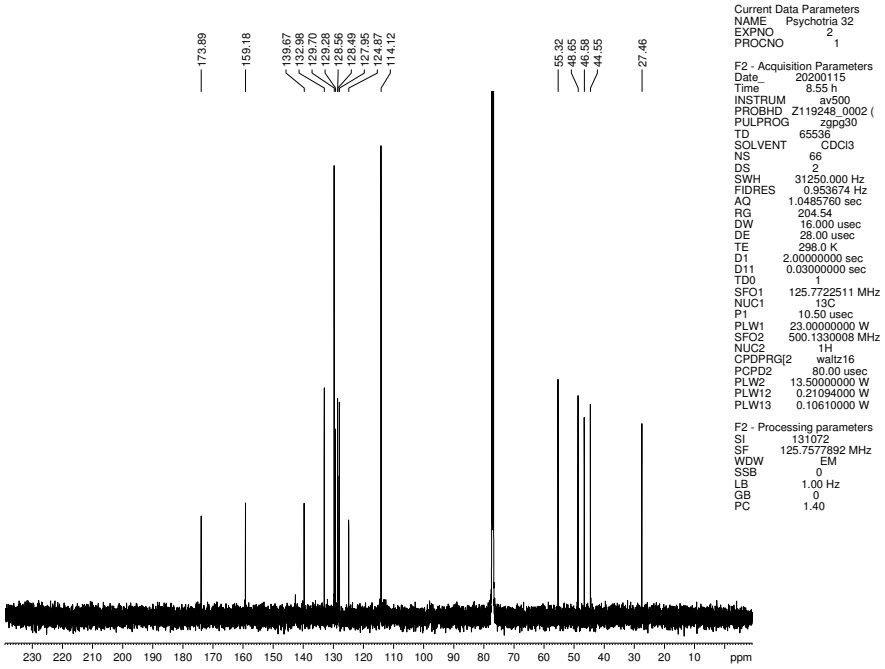

Figure 3.25 ^{13}C NMR (125 MHz, $CDCl_3$) of compound **3.32**.

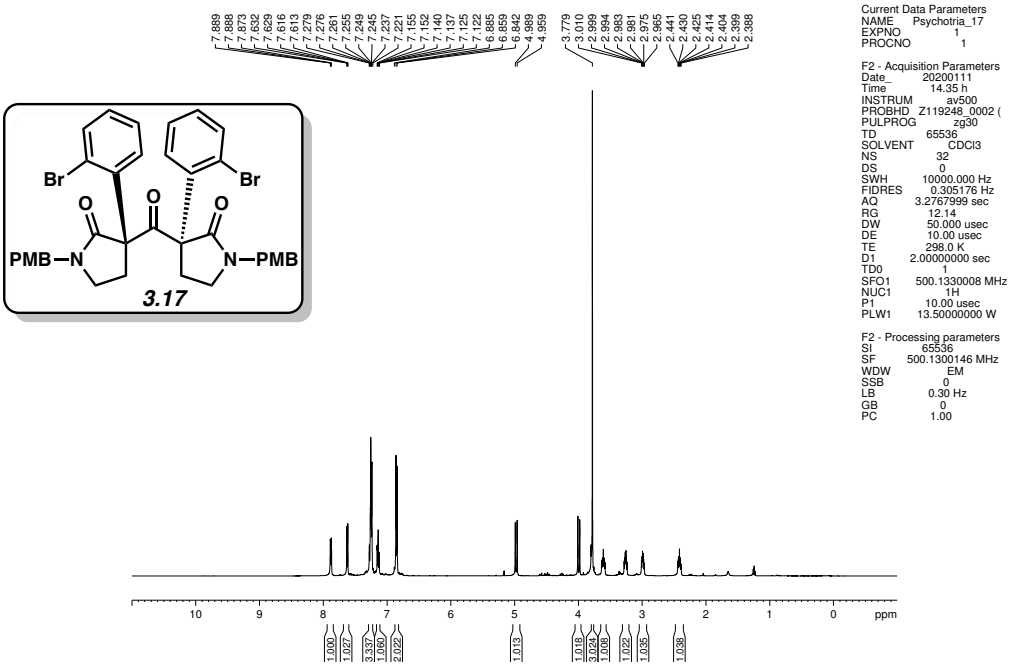

Figure 3.26 ^{1}H NMR (500 MHz, $CDCl_3$) of compound **3.17**.

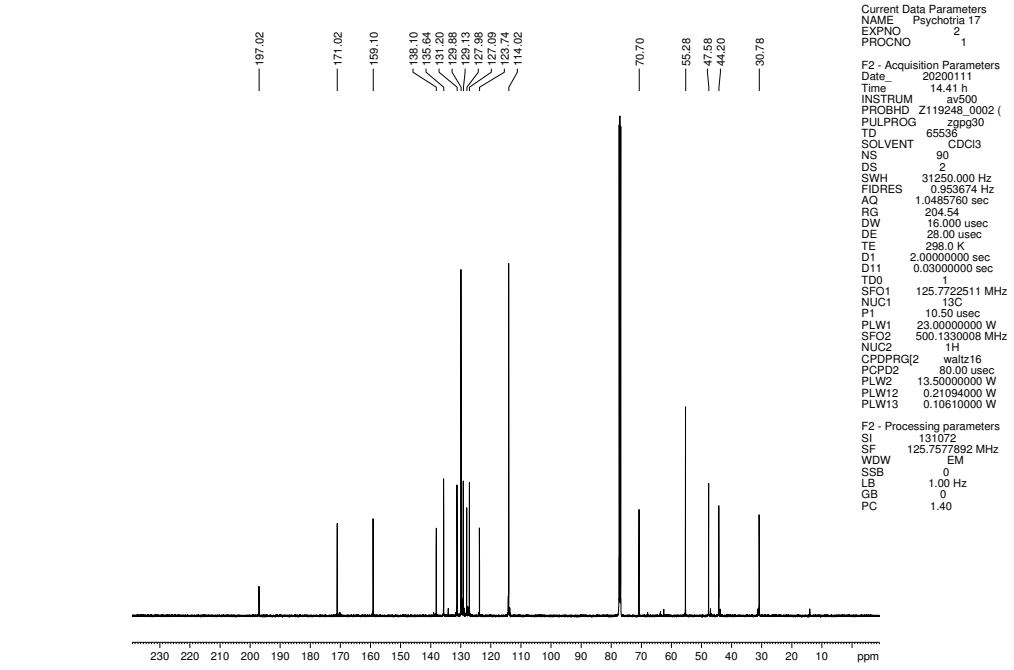

Figure 3.27 ^{13}C NMR (125 MHz, $CDCl_3$) of compound **3.17**.

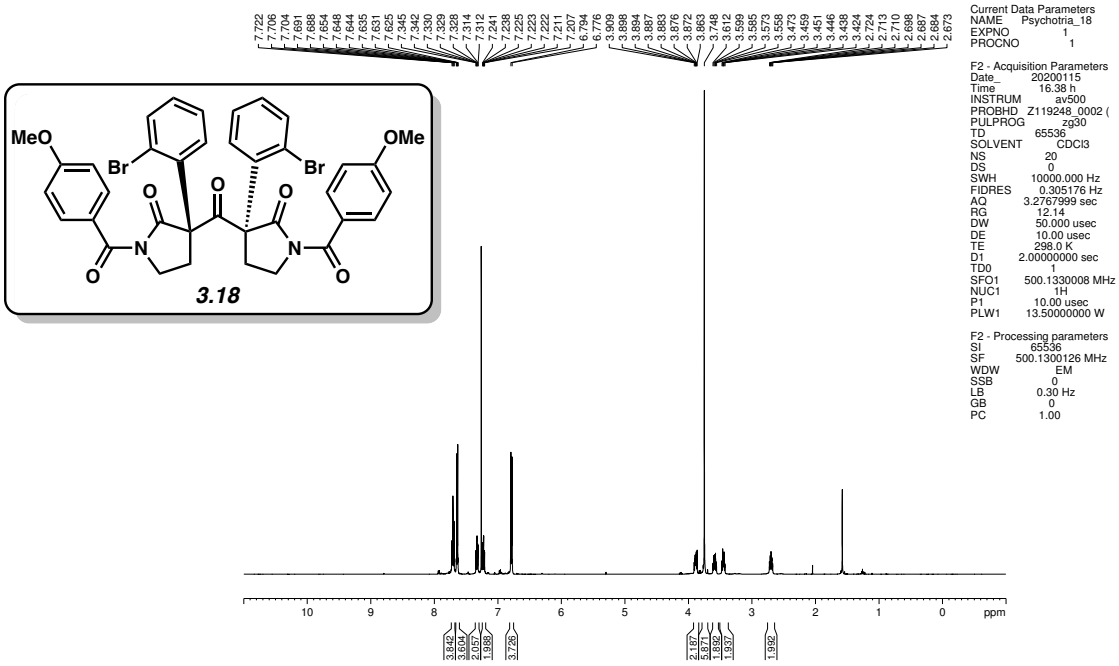

Figure 3.28 ^{1}H NMR (500 MHz, C_6D_6) of compound **3.18**.

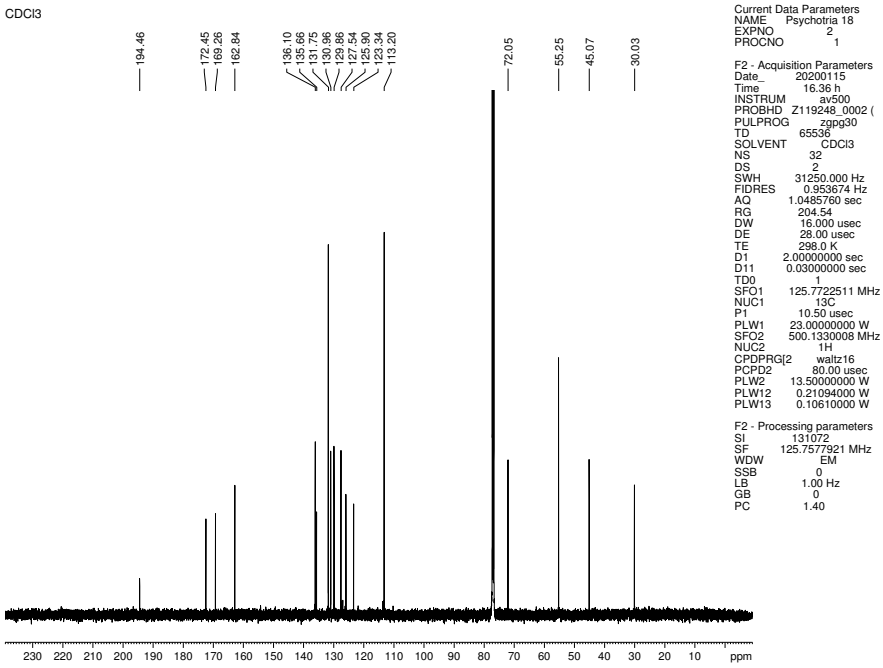

Figure 3.29^{13}C NMR (125 MHz, C_6D_6) of compound **3.18**.

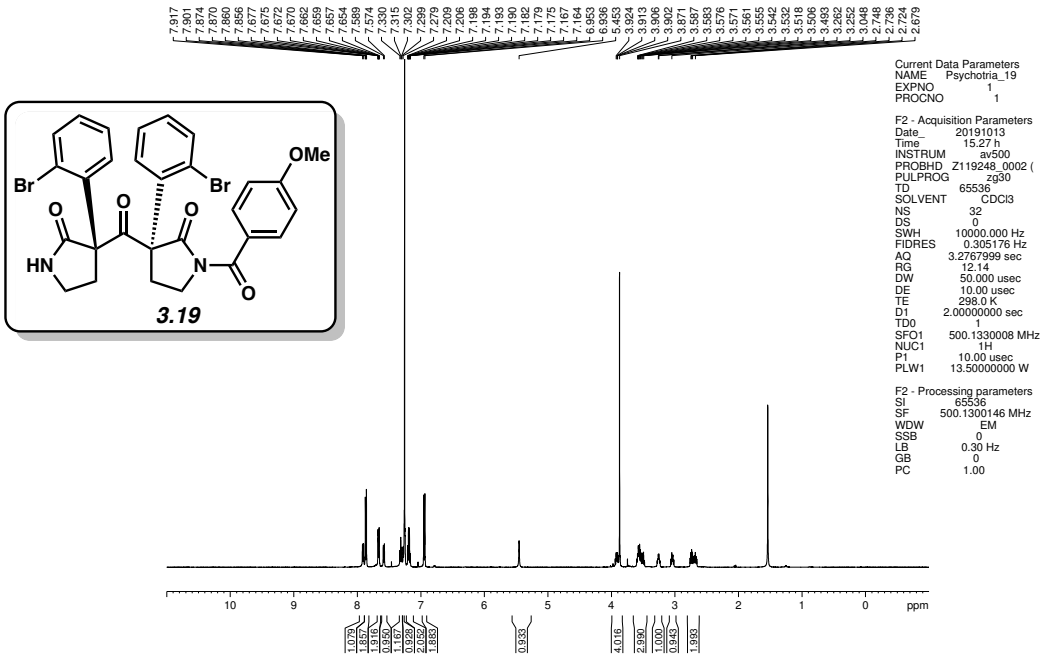

Figure 3.30 ^{1}H NMR (500 MHz, C_6D_6) of compound **3.19**.

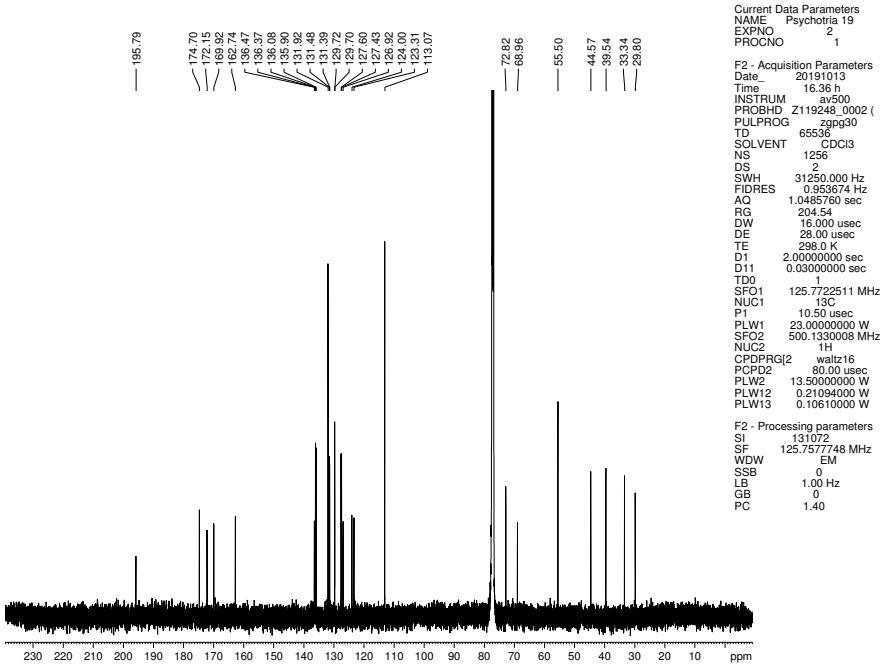

Figure 3.31 ^{13}C NMR (125 MHz, C_6D_6) of compound **3.19**.

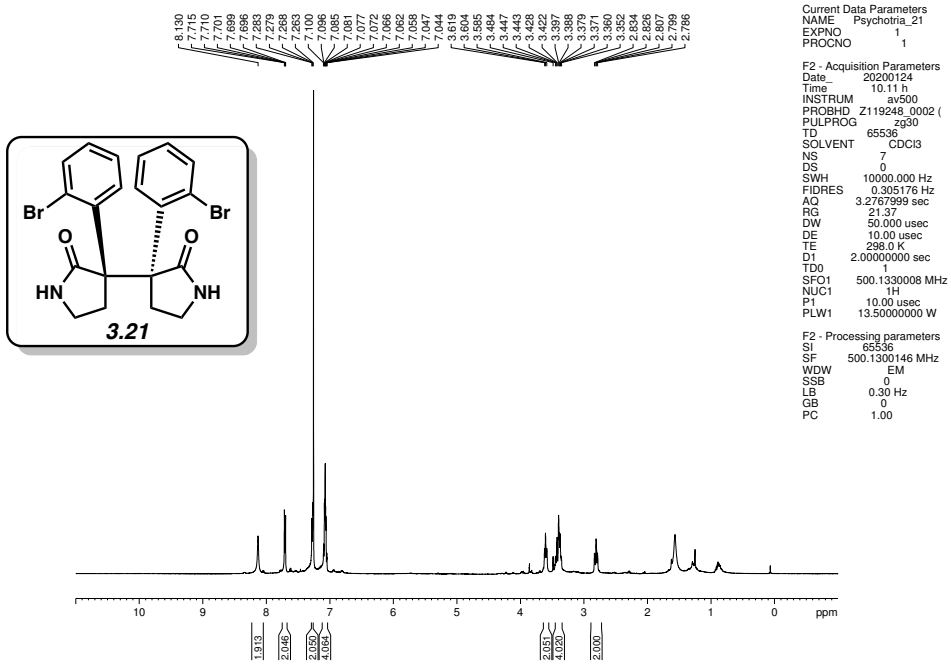

Figure 3.32 ^{1}H NMR (500 MHz, C_6D_6) of compound **3.21**.

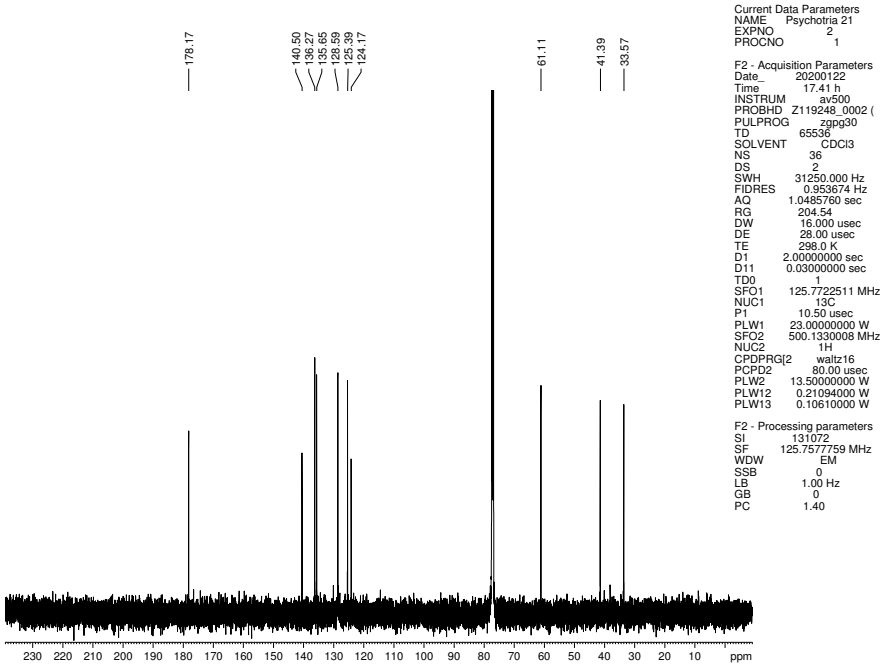

Figure 3.33 ^{13}C NMR (125 MHz, C_6D_6) of compound **3.21**

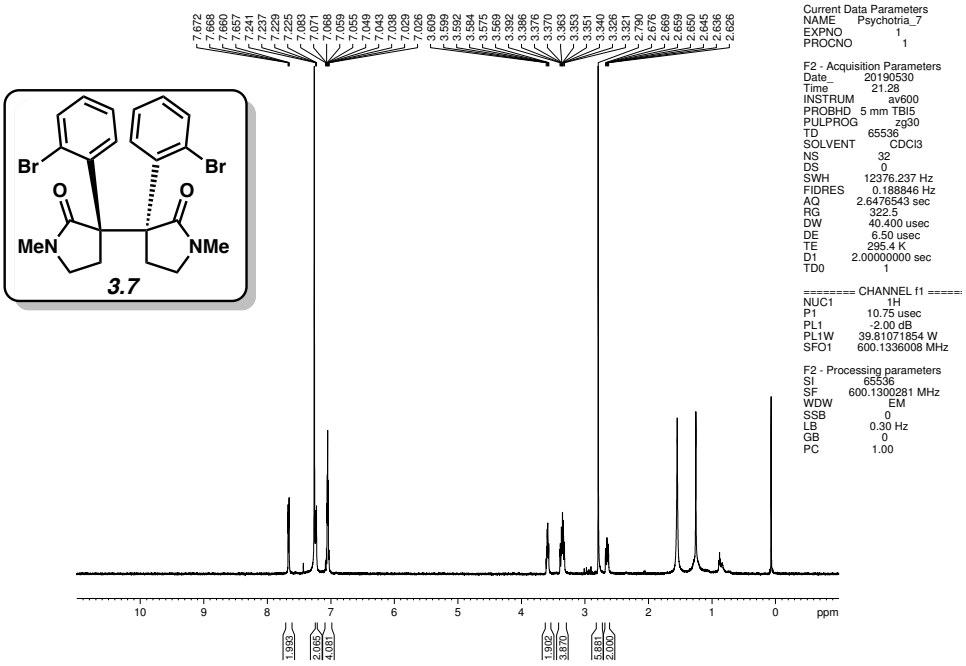

Figure 3.34 ^{1}H NMR (600 MHz, C_6D_6) of compound **3.7**.

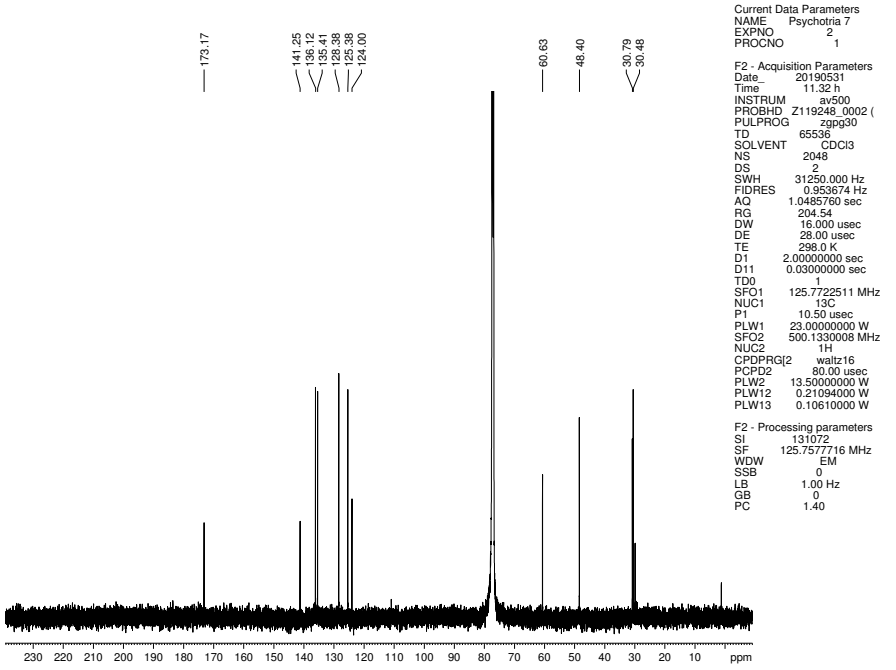

Figure 3.35 ^{13}C NMR (125 MHz, C_6D_6) of compound **3.7**.

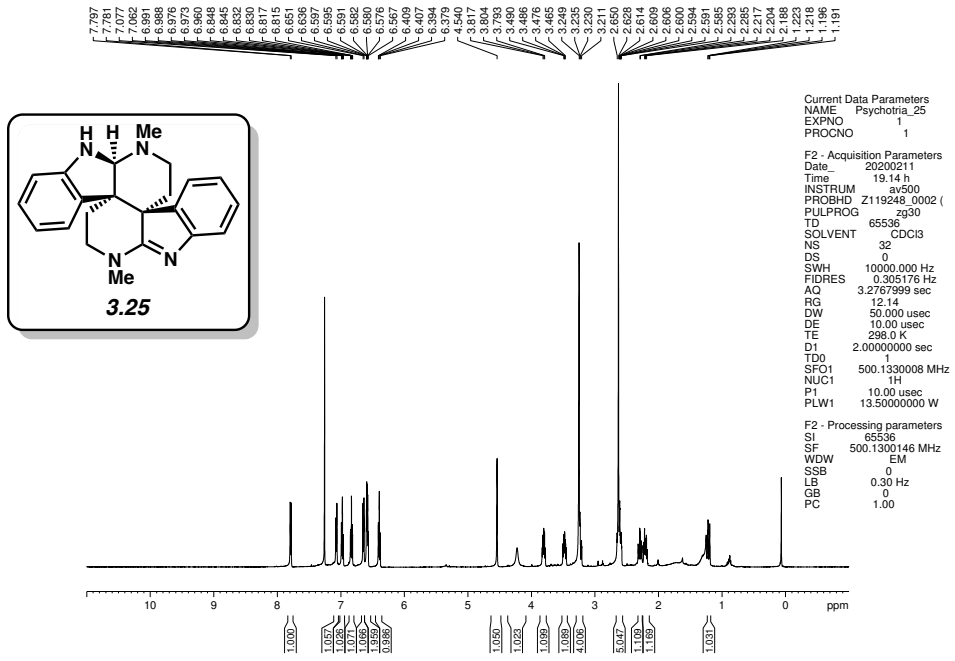

Figure 3.36 ^{1}H NMR (500 MHz, $CDCl_3$) of compound **3.25**.

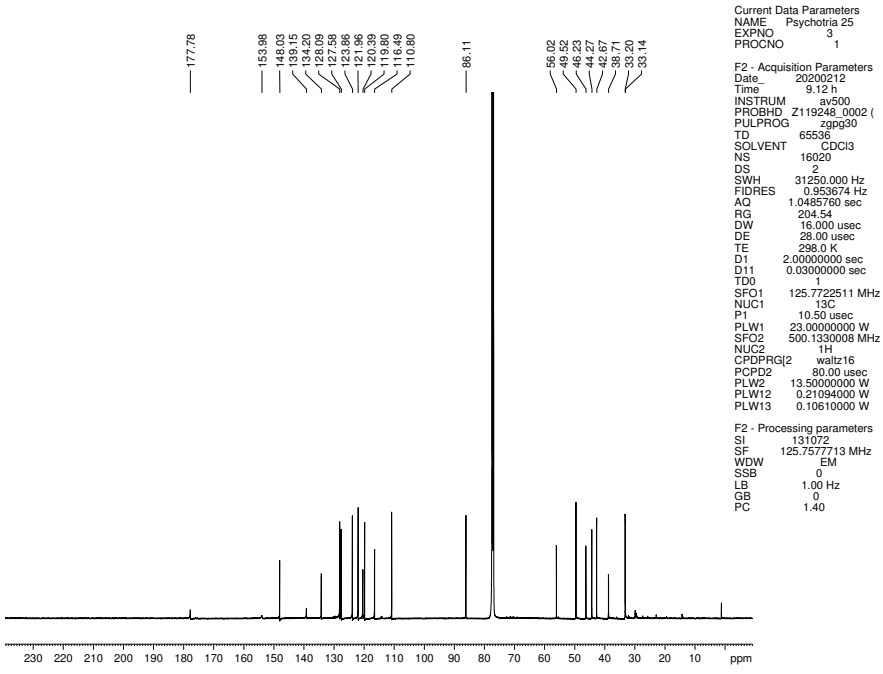

Figure 3.37 ^{13}C NMR (125 MHz, $CDCl_3$) of compound **3.25**.

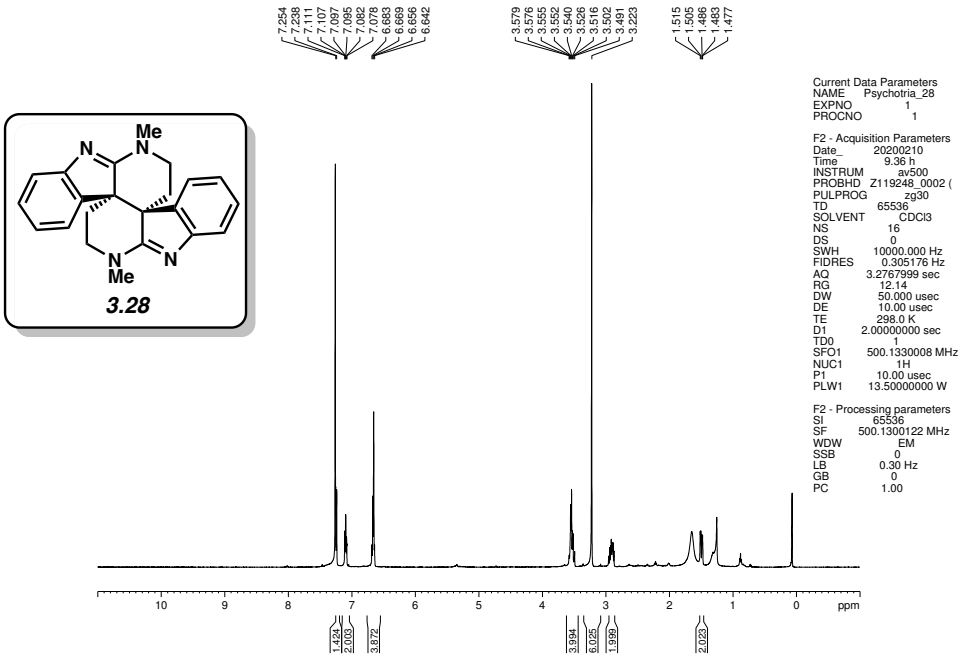

Figure 3.38 ^{1}H NMR (500 MHz, C_6D_6) of compound **3.28**.

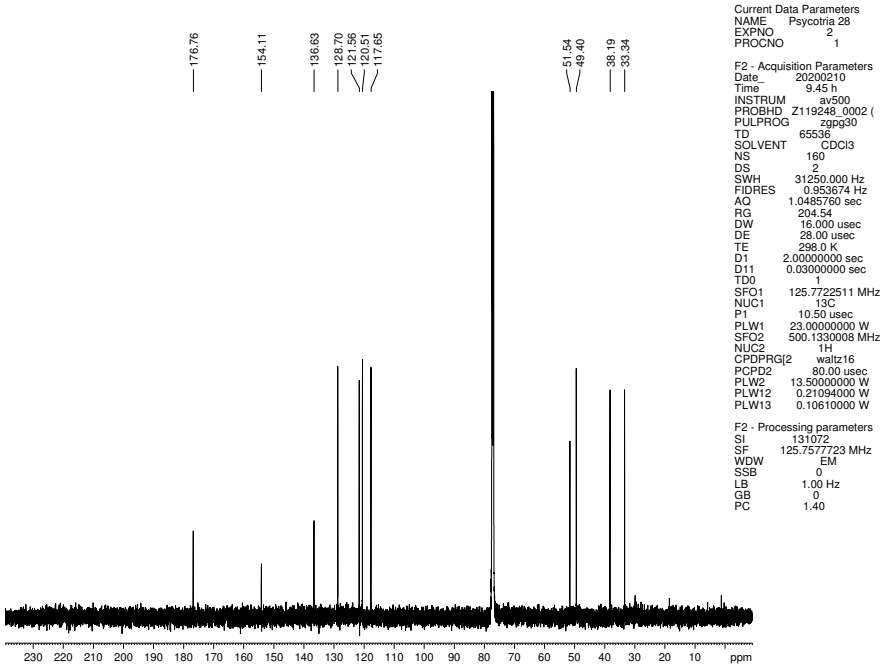

Figure 3.39 ^{13}C NMR (125 MHz, C_6D_6) of compound **3.28**.

3.7 Notes and References

(1) Eccles, R. G. Calycanthine. *Druggists' Circular and Chemical Gazette* **1888**, *32*, 65.

(2) For reviews, see: (a) May, J. A.; Stoltz, B. *Tetrahedron* **2006**, *62*, 5262–5271. (b) Schmidt, M. A.; Movassaghi, M. *Synlett* **2008**, 313–324. (c) Steven, A.; Overman, L. E. *Angew. Chem., Int. Ed.* **2007**, *46*, 5488–5508. (d) Trost, B. M.; Osipov, M. *Chem. Eur. J.* **2015**, *21*, 16318–16343. (e) Xu, J.-B.; Cheng, K.-J. *Molecules* **2015**, *20*, 6715–6738.

(3) (a) Robinson, R.; Teuber, H. J. *Chem. Ind. (London)* **1954**, 783–784. (b) Manske, R. H. *Alkaloids* **1965**, *8*, 581–589.

(4) Woodward, R. B.; Yang, N. C.; Katz, T. J.; Harley-Mason, J.; Ingelby, R. F.; Sheppard, N. *Proc. Chem. Soc., London* **1960**, 76–78.

(5) Hamor, T. A.; Robertson, J. M.; Shrivastava, H. N.; Silverton, J. V. *Proc. Chem. Soc., London* **1960**, 78–80.

(6) For select examples of bis(cyclotryptamine) alkaloid isolations, see: (a) Verotta, L.; Pilati, T.; Tató, M.; Elisabetsky, E.; Amaor, T. A.; Nunes, D. S. *J. Nat. Prod.* **1998**, *61*, 392–396. (b) Balayer, A.; Sévenet, T.; Schaller, H.; Haudi, A. H. A.; Chiaroni, A.; Riche, C.; Païs, M. *Nat. Prod. Lett.* **1993**, *2*, 61–67. (c) Adjibade, Y.; Weniger, B.; Quirion, J. C.; Kuballa, B.; Cabalion, P.; Anton, R. *Phytochemistry* **1992**, *31*, 317–319. (d) Verbitski, S. M.; Mayne, C. L.; Davis, R. A.; Concepcion, G. P.; Ireland, C. M. *J. Org. Chem.* **2002**, *67*, 7124–7126. (e) Gordin, H. M. *J. Am. Chem. Soc.* **1909**, *31*, 1305–1312.

(7) Kirby, G. W.; Shah, S. W.; Herbert, E. J. *J. Chem. Soc. C* **1969**, 1916–1919.

(8) Hall, E. S.; McCapra, F.; Scott, A. I. *Tetrahedron* **1967**, *23*, 4131–4141.

(9) Lin, H.-C.; McMahon, T. C.; Patel, A.; Corsello, M.; Simon, A.; Xu, W.; Zhao, M.; Houk, K. N.; Garg, N. K.; Tang, Y. *J. Am. Chem. Soc.* **2016**, *138*, 4002–4005.

(10) Pompeo, M. M.; Cheah, J. H.; Movassaghi, M. *J. Am. Chem. Soc.* **2019**, *141*, 14411–14420.

(11) For select studies from the Overman group pertaining to **3.1** and **3.2**, see: (a) Link, J. T.; Overman, L. E. *J. Am. Chem. Soc.* **1996**, *118*, 8166–8167. (b) Overman, L. E.; Paone, D. V; Stearns, B. A. *J. Am. Chem. Soc.* **1999**, *121*, 7702–7703. (c) Overman, L. E.; Larrow, J. F.; Stearns, B. A. *Angew. Chem., Int. Ed.* **2000**, *39*, 213–215. (d) Hoyt, S. B.; Overman, L. E. *Org. Lett.* **2000**, *2*, 3241–3244. (e) Lebsack, A. D.; Link, J. T.; Overman, L. E.; Stearns, B. A. *J. Am. Chem. Soc.* **2002**, *124*, 9008–9009. (f) Overman, L. E.; Peterson, E. A. *Angew. Chem., Int. Ed.* **2003**, *42*, 2525–2528. (g) Kodanko, J. J.; Overman, L. E. *Angew. Chem., Int. Ed.* **2003**, *42*, 2528–2531. (h) Ellis, J. M.; Overman, L. E.; Tanner, H. R.; Wang, J. *J. Org. Chem.* **2008**, *73*, 9151–9154. (i) Canham, S. M.; Hafensteiner, B. D.; Lebsack, A. D.; May-Dracka, T. L.; Nam, S.; Stearns, B. A.; Overman, L. E. *Tetrahedron* **2015**, *71*, 6424–6436.

(12) For select studies from the Movassaghi group pertaining to **3.1** and **3.2**, see: (a) Movassaghi, M.; Schmidt, M. A. *Angew. Chem., Int. Ed.* **2007**, *46*, 3725–3728. (b) Movassaghi, M.; Schmidt, M. A.; Ashenhurst, J. A. *Angew. Chem., Int. Ed.* **2008**, *47*, 1485–1487. (c) Kim, J.; Ashenhurst, J. A.; Movassaghi, M. *Science* **2009**, *324*, 238–241. (d) Movassaghi, M.; Ahmad, O. K.; Lathrop, S. P. *J. Am. Chem. Soc.* **2011**, *133*, 13002–13005. (e) Lathrop, S. P.; Movassaghi, M. *Chem. Sci.* **2014**, *5*, 333–340. (f) Linovska, P.; Movassaghi, M. *J. Am. Chem. Soc.* **2017**, *139*, 17590–17596.

(13) For select syntheses of calycanthine and chimonanthine, see: (a) Hendrickson, J. B.; Göschke, R.; Rees, R. *Tetrahedron* **1964**, *20*, 656–579. (b) Snell, R. H.; Woodward, R. L.; Willis, M. C. *Angew. Chem., Int. Ed.* **2011**, *50*, 9116–9119. (c) Mitsunuma, H.; Shibasaki, M.; Kanai, M.; Matsunaga, S. *Angew. Chem., Int. Ed.* **2012**, *51*, 5217–5221. (d) Trost, B. M.; Osipov, M. *Angew. Chem., Int. Ed.* **2013**, *52*, 9176–9181. (e) Ding, M.; Liang, K.; Pan, R.;

Zhang, H.; Xia, C. *J. Org. Chem.* **2015**, *80*, 10309–10316. (f) Babu, K. N.; Roy, A.; Singh, M.; Bisai, A. *Org. Lett.* **2018**, *20*, 6327–6331. (g) Gentry, E. C.; Rono, L. J.; Hale, M. E.; Matsura, R.; Knowles, R. R. J. Am. Chem. Soc. 2018, 140, 3394–3402. (h) Kumar, N.; Das, M. K.; Ghosh, S.; Bisai, A. *Chem. Commun.* **2017**, *53*, 2170–2173.

(14) A common related approach involves pre-formation of oxindoles instead of indoline ring systems; see ref 2.

(15) (a) Dotson, J. J.; Perez-Estrada, S.; Garcia-Garibay, M. A. *J. Am. Chem. Soc.* **2018**, *140*, 8359–8371. (b) Natarajan, A.; Ng, D.; Yang, Z.; Garcia-Garibay, M. A. *Angew. Chem., Int. Ed.* **2007**, *46*, 6485–6487.

(16) For select examples of solid-state photodecarbonylation reactions with retention of stereochemistry, see: (a) Hérnandez-Linares, M. G. H.; Guerrero-Luna, G.; Pérez-Estrada, S.; Ellison, M.; Ortin, M.-M.; Garcia-Garibay, M. A. *J. Am. Chem. Soc.* **2015**, *137*, 1679–1684. (b) Resendiz, M. J. E.; Natarajan, A.; Garcia-Garibay, M. A. *Chem. Commun.* **2008**, 193–195. (c) Resendiz, M. J. E.; Family, F.; Fuller, K.; Campos, L. M.; Khan, S. I.; Lebedeva, N. V.; Forbes, M. D. E.; Garcia-Garibay, M. A. *J. Am. Chem. Soc.* **2009**, *131*, 8425–8433. (d) Resendiz, M. *Photochemical Decarbonylation of Ketones in the Solid State and in Solution. Progress Towards The Synthesis Of Natural Products*, Ph. D. Thesis, UCLA, 2008.

(17) Although a non-brominated analog of **3.9** has been shown to undergo solid-state photodecarbonylation (see reference 16b), we have found that the presence of certain ortho-substituents on the aromatic rings is problematic for the photodecarbonylation reaction.

(18) An alternative strategy was explored involving the use of phosgene and two equivalents of an enolate species. However, this protocol was found to be unsuccessful. For the parent transformation being carried out on a non-brominated starting material, see references 16b,c.

(19) X-ray structures were rendered using CYLview; see: Legault, C.Y. *CYLview*, 1.0b; Université de Sherbrooke: Quebec, 2009; http://www.cylview.org.

(20) To our knowledge, this is the first documented case of disproportionation in a crystalline solid-state photodecarbonylation reaction. An explanation for this reactivity is currently under investigation and will be reported in due course.

(21) Although we cannot rule out the formation of the corresponding meso isomer of **3.21** to a minor extent, we estimate the selectivity to be >9:1.

(22) (a) Yang, Z.; Ng, D.; Garcia-Garibay, M. A. *J. Org. Chem.* **2001**, *66*, 4468–4475. (b) Campos, L. M.; Dang, H.; Ng, D.; Yang Z.; Martinez, H. L.; Garcia-Garibay, M. A. *J. Org. Chem.* **2002**, *67*, 3749–3754. (c) Ng, D.; Yang, Z.; Garcia-Garibay, M. A. *Tetrahedron Lett.* **2002**, *43*, 7063–7066.

(23) Zhu, W.; Ma, D. *Chem. Commun.* **2004**, 888–889.

(24) Optimization efforts for this step were regrettably cut short because of COVID-19 related laboratory shutdowns, although preliminary optimization studies showed that the double azidation step could be achieved in 51% yield (according to ^{1}H NMR analysis with an external standard, average of two experiments).

(25) Although the two-step yield from **3.7** to **3.25** proceeds with a 78% loss of mass balance, we surmise that most of this (>65%) occurred during the cross-coupling step (based on ^{1}H NMR analysis of crude **3.22**). Therefore, if isomeric products resulted from the reduction of **3.22** they were present in <18% yield.

(26) "Dihydropsychotriadine" (**3.25**) has not yet been found in nature. Whether or not this compound is naturally-occurring remains an open question.

(27) Presumed intermediate **3.24** could plausibly undergo cyclization to form either a 6-membered ring (observed) or a 5-membered ring. It is surprising that the latter was not observed as related reductive cyclizations have been reported to form the 5-membered ring under similar conditions (see references 11a–c and 13h). Of note, the studies disclosed in references 11a–c and 13h, which include alkyl substituents on the oxindole nitrogens, presumably undergo reduction of the oxindole to aldehyde oxidation state followed by a reversible, thermodynamically controlled cyclization to form a 5-membered ring. We speculate that the system disclosed herein may undergo a kinetically controlled cyclocondensation of the amine onto the oxindole to form a 6-membered ring.

(28) Other possible mechanisms exist for the conversion of **3.22** to **3.25** that do not involve formation of bis(oxindole) **3.24**; see Figure 3.9.

(29) Oxidation conditions adapted from: Higuchi, K.; Sato, Y.; Tsuchimochi, M.; Sugiura, K.; Hatori, M.; Kawasaki, T. *Org. Lett.* **2009**, *11*, 197–199.

(30) Calculations suggest that **3.28** is 8.7 kcal/mol higher in energy than **3.27** (ωB97XD/6-31G(d,p)). As such, it is unlikely that **3.27** spontaneously rearranges to **3.28** during isolation. It is plausible that the substrate in a lower oxidation state, "tetrahydropsychotriadine," could readily isomerize to give calycanthine or chimonanthine. Related scaffolds reminiscent of "tetrahydropsychotriadine" have only been isolated previously when constrained due to the presence of additional ring systems (see references 9 and 10). Preliminary efforts aimed at reducing **3.25** to the corresponding geminal diamine were either met with decomposition or led to recovered starting material (see Figure 3.10).

(31) Zhang, D.; Yum, E. K.; Liu, Z.; Larock, R. C. *Org. Lett.* **2005**, *7*, 4963–4966.

(32) Armarego, W. L. F.; Chai, C. Purifications of Laboratory Chemicals, 6th ed.; Butterworth-Heinemann: Oxford, 2009; p 461.

CHAPTER FOUR

Taming Radicals in the Solid State: Discovery and Total Synthesis of Psychotriadine

4.1 Abstract

Solid-state photodecarbonylation is an attractive but underutilized methodology to forge hindered C–C bonds in complex molecules. This study discloses the use of this reaction to assemble the vicinal quaternary stereocenter motif present in bis(cyclotryptamine) alkaloids. Our strategy was enabled by experimental and computational investigations of the role of substrate conformation on the success or failure of the solid-state photodecarbonylation reaction. This informed a crystal engineering strategy to optimize the key step of the total synthesis. Ultimately, this endeavor culminated in the successful synthesis of the bis(cyclotryptamine) alkaloid "psychotriadine," which features the elusive piperidinoindoline framework. Psychotriadine, a previously unknown compound, was identified in the extracts of the flower *Psychotria colorata*, suggesting it is a naturally occurring metabolite.

4.2 Introduction

Photochemistry has become an increasingly powerful tool in modern organic synthesis.[1] One particularly interesting class of photochemical transformations with great potential is those conducted in the crystalline solid state. Such transformations are attractive because of the opportunity to control various selectivities (stereo-, regio-, and chemo-), potential for scalable green chemistry, and ability to form strained or congested frameworks.[2]

Our laboratory has been particularly interested in photodecarbonylation reactions that occur in the crystalline solid state, and have demonstrated their potential for the stereospecific assembly of vicinal quaternary centers (Figure 4.1a).[2a,3] The introduction of vicinal quaternary stereocenters has remained a long-standing challenge in organic synthesis.[4] An attractive approach to this motif, **4.1**, is via direct coupling of two prochiral aliphatic radicals **4.2**. In turn, radicals **4.2** can be generated from the photodecarbonylation of hexasubstituted ketone **4.3**. Whereas in solution the coupling of prochiral radicals can lead to complex product mixtures, the corresponding process in the crystalline solid state can result in high-yielding stereoretentive recombination.[2a] Despite promising investigations into fundamental reactivity, this solid-state approach has seen little use in natural product synthesis[3c,d] and has not been used to construct complex alkaloids. Moreover, the understanding of how substrate conformations relate to the success or failure of solid-state photodecarbonylation reactions has remained underexplored.

Figure 4.1. Solid-state photodecarbonylation to introduce vicinal quaternary stereocenters and overview of select bis(cyclotryptamine) alkaloids.

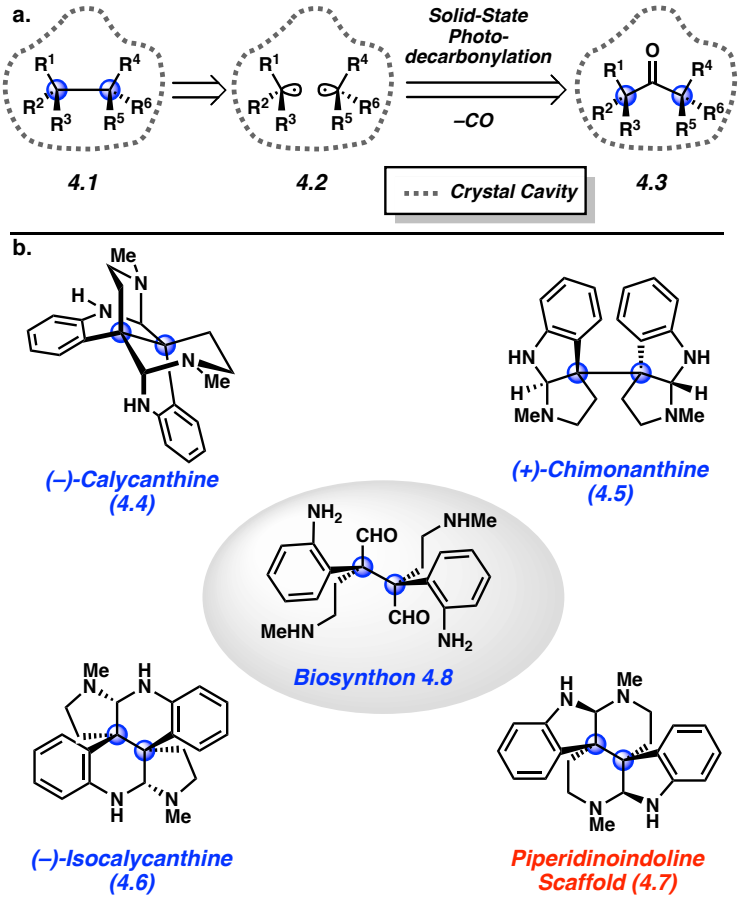

With the aforementioned motivations in mind, we sought to evaluate solid-state photodecarbonylation chemistry in the context of the bis(cyclotryptamine) alkaloids (Figure 4.1b). This class of natural products, arising from common biosynthon **4.8**, features vicinal quaternary stereocenters and has been popular amongst synthetic chemists for many decades.[5] In addition, this family of small molecules possesses a rich history, stemming from the isolation report of calycanthine (**4.4**) in 1888 and the subsequent discovery of related[6] natural products (e.g., **4.5** and **4.6**), representing a total of four unique constitutional isomers.[7] Interestingly, a fifth piperidinoindoline isomer **4.7** was proposed by Robinson in 1954, but has never been isolated from

a natural source.[8,9] Given the rich history of these compounds and their complex structures bearing vicinal quaternary stereocenters, we deemed the bis(cyclotryptamine) alkaloids an ideal arena to test the solid-state photodecarbonylation methodology.

Our laboratory recently described the successful application of photodecarbonylation chemistry in the context of the bis(cyclotryptamine) alkaloids (see Chapter 3). Here, we disclose our full investigation of the key photodecarbonylation step, including the evaluation of 11 different crystalline substrates. By analysis of substrate conformation via X-ray structures and computations, we provide the physical organic underpinnings that explain the success or failure of the key photodecarbonylation step. These efforts demonstrate that the overall transformation can be optimized by manipulating the crystalline conformation of the necessary hexasubstituted ketone substrate. Ultimately, our crystalline conformation-based approach enabled the formation of the challenging vicinal quaternary stereocenters present in biosynthon **4.8**. These efforts culminated in the total synthesis of a natural product that had previously been overlooked in nature and features the elusive piperidinoindoline scaffold of the bis(cyclotryptamine) alkaloids.

4.3 Results and Discussion

4.3.1 Retrosynthetic Analysis

Our retrosynthetic analysis of common biosynthon **4.8** is depicted in Figure 4.2. It was envisioned that **4.8**, or a dehydrated synthetic congener thereof, would arise from late-stage bis(amination) and reduction of intermediate **4.9**. In turn, **4.9**, bearing the requisite vicinal quaternary stereocenters, would be accessed via a key solid-state photodecarbonylation of hexasubstituted ketone **4.11** via the intermediacy of radical pair **4.10**. Although both radical centers would be stereochemically labile in intermediate **4.10**, it was anticipated that the rigidity of the

crystalline lattice would affect the transfer of stereochemical information from **4.11** to **4.9**.[2a] Finally, **4.11** would be constructed rapidly by the convergent coupling of two equivalents of lithium enolate **4.12** with an equivalent of phosgene (**4.13**).

Figure 4.2. Retrosynthetic analysis of biosynthon **4.8**.

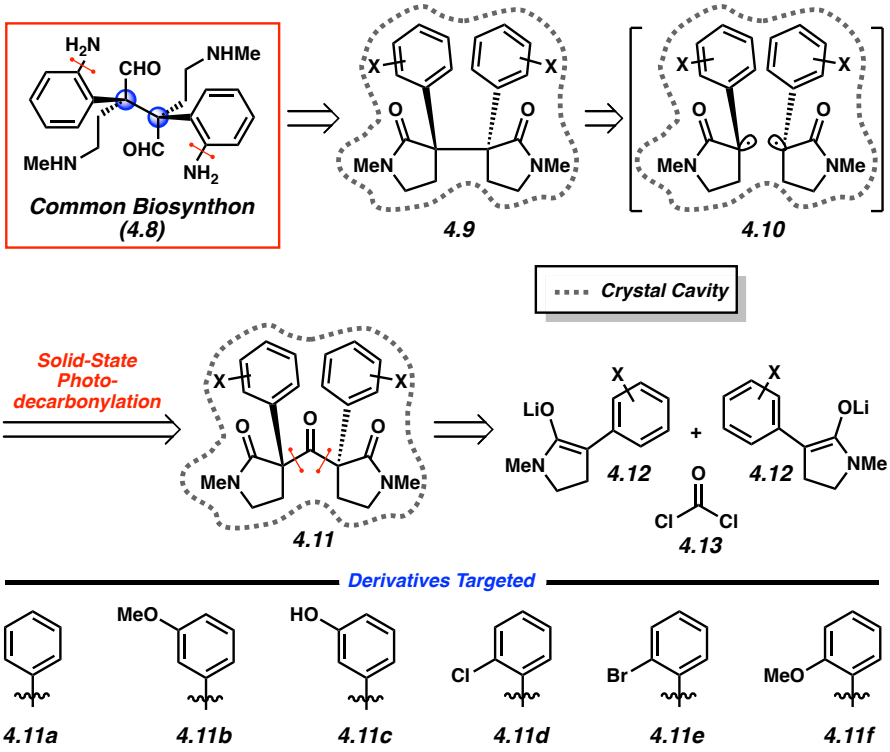

At the outset of this research pursuit, it was anticipated that a major challenge in our synthetic strategy would be the preparation of **4.9** bearing amines on the ortho position of the aromatic rings. Introduction of protected amines at the *ortho*- positions early in the synthesis would be ideal, but the steric crowding imparted by *ortho*- substituents in close proximity to the quaternary centers would make the assembly of the corresponding ketone challenging.[10] Additionally, it was envisioned that the increased steric bulk resulting from these substituents may also hinder C–C bond formation from radical pair **4.10**. To address these concerns, two classes of

ketone substrates (**4.11a–c** and **4.11d–f**; see Figure 4.2) were targeted that would be synthetically accessible from a common route. It was hypothesized that the photodecarbonylation of ketones **4.11a–c** would occur selectively and the resulting products **4.9a–c** could be functionalized by directed *ortho*- C–H metalation/amination. It was predicted that ketones **4.11d–f** could be competent substrates for photodecarbonylation to access **4.9d–f**, and that the *ortho*- Cl, Br, and OMe substituents could also function as synthetic handles for a metal-catalyzed amination.[11]

4.3.2 Synthesis and Photodecarbonylation of Crystalline Ketones

Photodecarbonylation substrates **4.11a–c** were prepared in a straightforward manner from readily available diesters **4.14** (Scheme 4.1).[12] Malonic esters **4.14** were subjected to a two-step alkylation/reductive cyclization sequence to furnish pyrrolidinones **4.15** in good yield. *N*-methylation of **4.15** under basic conditions provided **4.16** in 60–87% yield. In turn, *N*-methylpyrrolidinones **4.16** were cleanly converted to **4.17** via a one-pot protocol involving ester saponification and subsequent acid-mediated decarboxylation. Finally, treatment of lactams **4.17** with LiHMDS provided the corresponding enolates, which were coupled with phosgene to deliver **4.11** in 49–64% yield and with high diastereoselectivity. While **4.11a** was a high-melting crystalline solid, **4.11b** was a viscous oil at room temperature (and therefore not a candidate for a solid-state photodecarbonylation reaction).[13] However, after efficiently cleaving the aryl-methyl ethers of **4.11b** using BBr_3, we were delighted to find that phenolic ketone **4.11c** was a crystalline solid.

Scheme 4.1. Synthesis of ketone substrates **4.11a–c**.

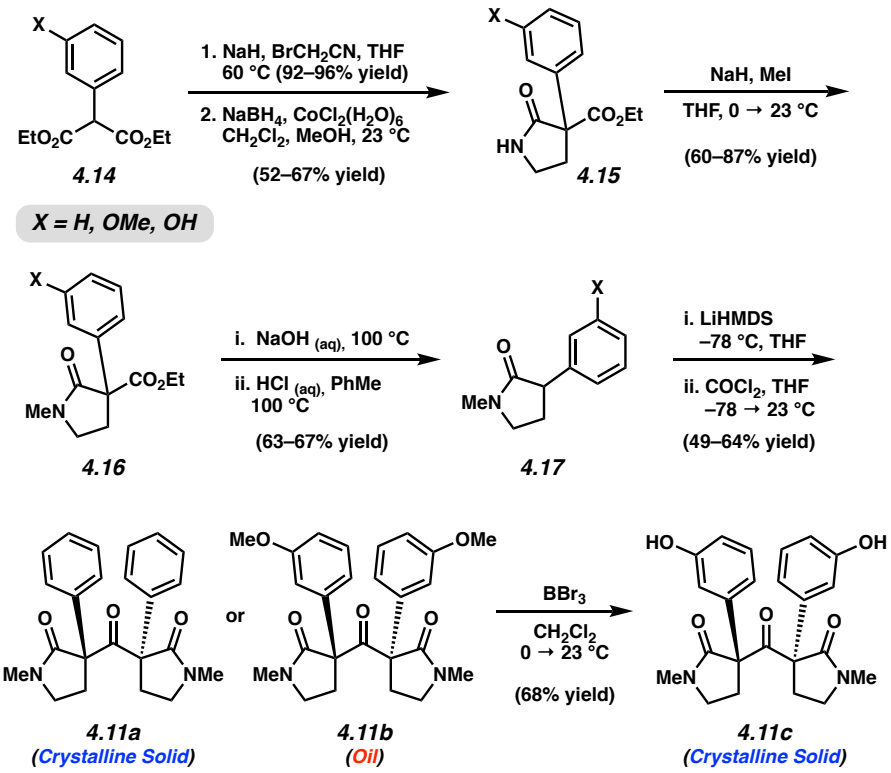

The preparation of ketones **4.11d–f** is shown in Scheme 4.2.[12] The beginning of this synthetic sequence mirrored that for ketones **4.11a–c**. A two-step annulation of malonic esters **4.14** and subsequent *N*-methylation cleanly furnished pyrrolidinones **4.16**. Saponification of the ester in **4.16**, followed by decarboxylation, provided enolate precursors **4.17** in 79–90% yield. Unfortunately, we observed that the reaction of **4.17d–f** with phosgene did not provide ketone **4.11** and instead resulted in substantial non-specific decomposition (not shown). To circumvent this issue, we constructed acid chloride **4.18** in a two-step sequence from pyrrolidinone **4.16**. This electrophile was then efficiently coupled with the lithium enolate derived from **4.17** to provide ketones **4.11d–f** in good to excellent yields and with high diastereoselectivity.

Scheme 4.2. Synthesis of ketone substrates **4.11d–f**.

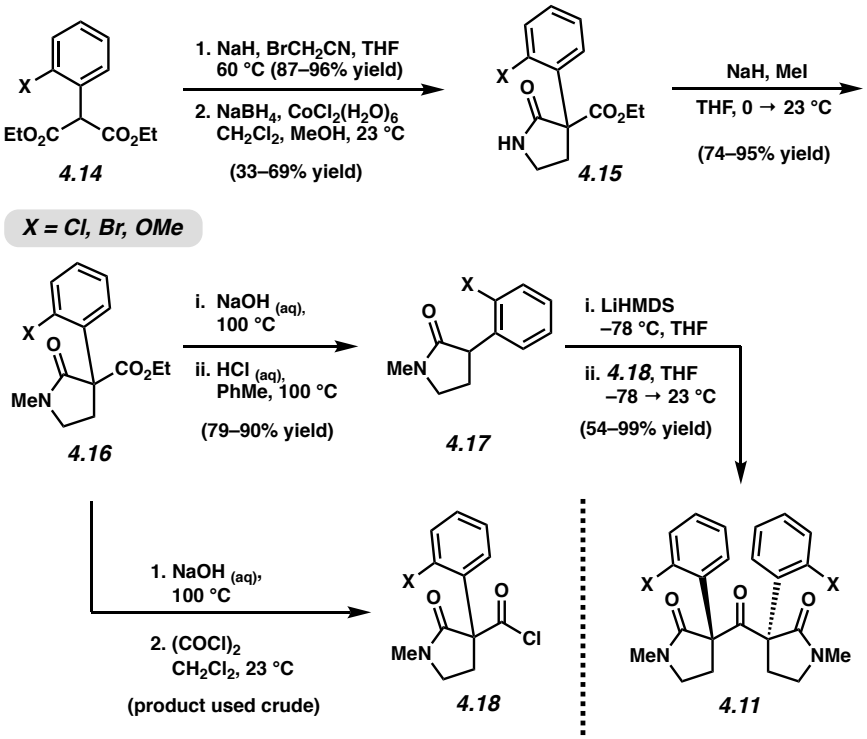

Once we had prepared ketones **4.11a–f**, we next turned our attention to the key solid-state photodecarbonylation reaction that forges the vicinal quaternary stereocenters present in the bis(cyclotryptamine) alkaloids (Figure 4.3). In exploring the photodecarbonylation of these, a wide range of reactivity was observed. Substrates **4.11a** and **4.11c** were irradiated in the solid-state and proceeded smoothly to provide **4.9a** and **4.9c** in 51% and 34% yield, respectively.[14] Although identifiable side products were not observed from the photodecarbonylation of **4.11c**,[15] the reaction of **4.11a** also gave rise to products **4.17a** and **4.19a**, presumably via a competing disproportionation process.[16] Unfortunately, *ortho*-substituted ketones **4.11d–f** performed poorly in the desired C–C bond formation. Solid-state irradiation of ketones **4.11d** and **4.11e** resulted in 9% and 8% yields of **4.9d** and **4.9e**, respectively, while irradiation of ketone **4.11f** gave no identifiable recombination product **4.9f**.[17] As was the case for ketone **4.11a**, the

photodecarbonylation of ketones **4.11d–f** displayed a competitive disproportionation reaction pathway that was the major reaction outcome for these substrates.[18]

Figure 4.3. Photodecarbonylation of ketones **4.11** (yields resulting from decarbonylation of substrates **4.11c–f** determined using qNMR).

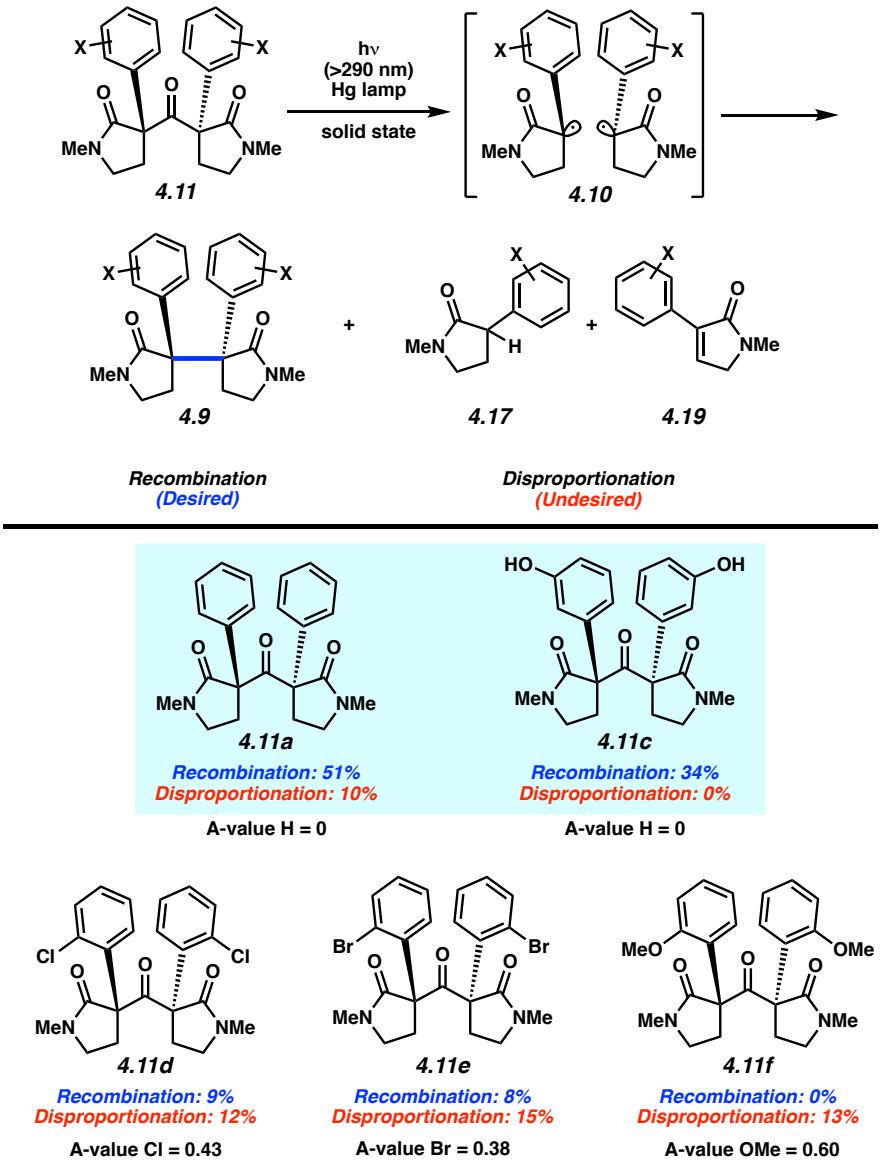

Interestingly, we noted a correlation between the relative selectivity of radical pair **4.10** undergoing recombination over disproportionation to the size of the *ortho*- substituent (quantified by the A-value).[19] Ketones **4.11a** and **4.11c** bearing only a hydrogen atom (A-value = 0) at the *ortho*- position underwent recombination to give **4.9a** and **4.9c**, respectively, as the major products. Ketones **11d**–**f**, bearing *ortho*- substituents, displayed lower yields of **4.9d–f**, and showed a higher incidence of disproportionation. Intrigued by these results, we sought to understand the structural factors that guide the outcome of the solid-state photodecarbonylation reaction.

Based on close inspection of substrate X-ray crystal structures, we offer the analysis shown in Figure 4.4 to explain the sensitivity of the photodecarbonylation reaction to aromatic substituents. We postulate that radical pair **4.10** is prevented from forming a C–C bond due to steric clash between the *ortho*- substituent on one radical fragment and the aromatic ring on the other (Figure 4.4a). The proposed repulsive interactions can further be observed in the X-ray crystal structures of the substrates (Figure 4.4b & c). For ketones **4.11d**–**f**, steric congestion is observed in the interaction between the *ortho*- substituent on one half of the molecule and the aryl ring on the other (interaction depicted with a red arrow). Notably, such interactions are not present in ketones without *ortho*- functionality, (i.e., **4.11a** and **4.11c**).[20] Since the radical centers in **4.10** must move closer to one another by approximately 1.2 Å to generate a C–C bond, these close interactions in the substrate are likely to become strongly repulsive at the transition state. It is important to note that reactions that take place in the crystalline solid state are governed by the topochemical principle and favor reaction pathways with minimal atomic motion.[21] As such, the conformational features observed in the X-ray crystal structures of the substrate are likely to also be present in the reactive intermediates and transition state structures.

Figure 4.4. Crystalline conformation blocks radical–radical recombination trajectory.

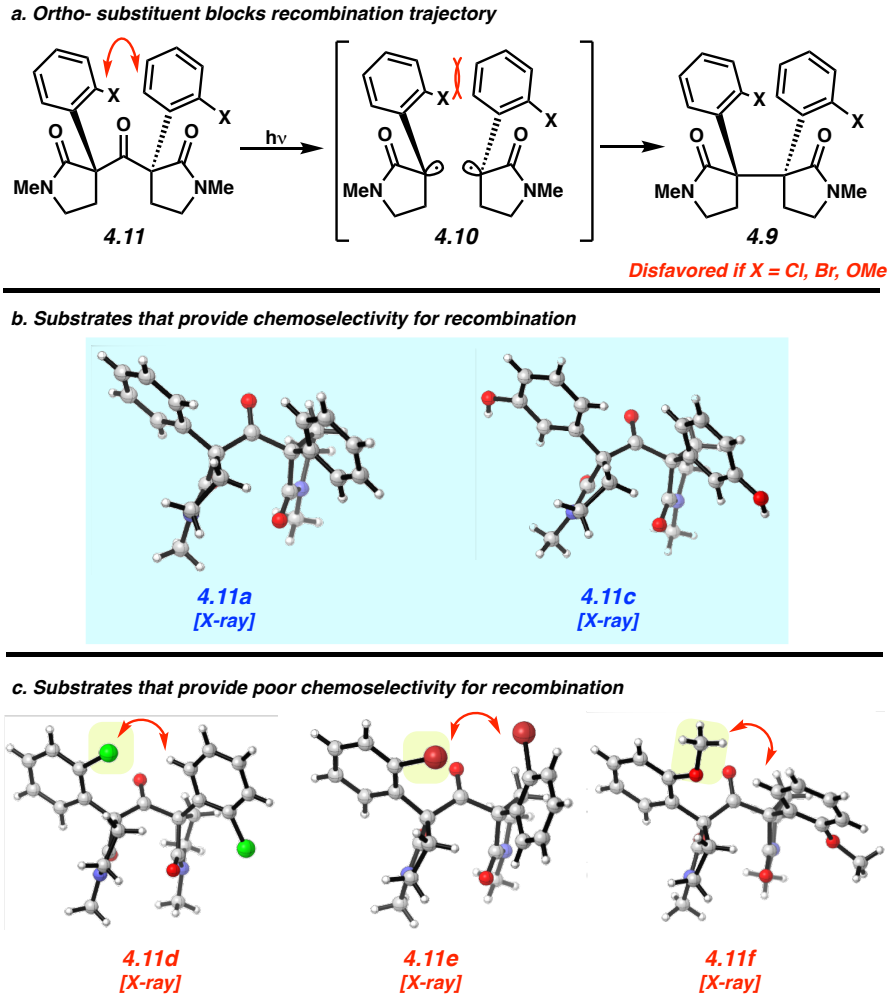

Given the efficiency of the solid-state photodecarbonylation of **4.11a** to give **4.9a**, we pursued a C–H functionalization approach to install the requisite C–N bonds in **4.9a** (Scheme 4.3).[22] We hypothesized that the pyrrolidinone oxygens may function as convenient directing groups for either transition metal-catalyzed *ortho*- functionalization[23] or directed lithiation.[24] Unfortunately, despite extensive experimentation, we were unable to functionalize the arene and most attempts either returned starting material or resulted in substantial non-specific decomposition. Interestingly, we found that the use of alkyllithium bases resulted in deprotonation

of the *N*-methyl groups on **4.9a** to give the corresponding primary carbanion (not shown).[25] In order to circumvent this issue, we sought to construct a derivative of **4.9a** with cleavable protecting groups on the nitrogen. This would allow for the introduction of *N*-substituents that would not undergo competitive activation.

Scheme 4.3. Attempted directed *ortho*-metalation / functionalization.

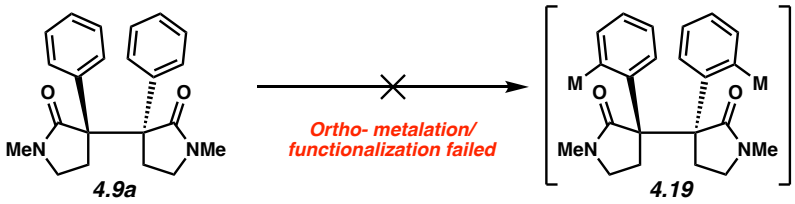

In pursuit of a derivative of **4.9a** with cleavable *N*-substituents, ketone precursor **4.20** (Figure 4.5) was prepared.[26] To our surprise, inspection of the X-ray crystal structure of **4.20** revealed a different ketone conformation compared to our previous observations, leading us to suspend our efforts toward C–H activation, and instead focus on manipulating the conformation of the ketone substrate to optimize the solid-state photodecarbonylation reaction (Figure 4.5). As noted previously, it is likely that the solid-state conformations of ketones **4.11d–f** prevent successful decarbonylative C–C bond formation due to a growing steric clash in radical pair **4.10**. Based on the striking change in crystalline conformation between **4.11a** and **4.20** (Figure 4.5a), we hypothesized that the conformation of an *ortho*- functionalized ketone **4.21** could also be altered by modifying the *N*-substituents. An alternative conformation of **4.21** could lead to hypothetical radical pair **4.22** that does not feature a steric clash that prevents the formation of **4.23**. Therefore, we sought to explore whether conformational manipulation could be used to give a ketone that both includes latent aryl electrophiles for late-stage metal-catalyzed amination and

the ability to undergo efficient solid-state photodecarbonylation to forge the desired vicinal quaternary stereocenters.

Figure 4.5. Conformational change could enhance chemoselectivity of the photodecarbonylation reaction.

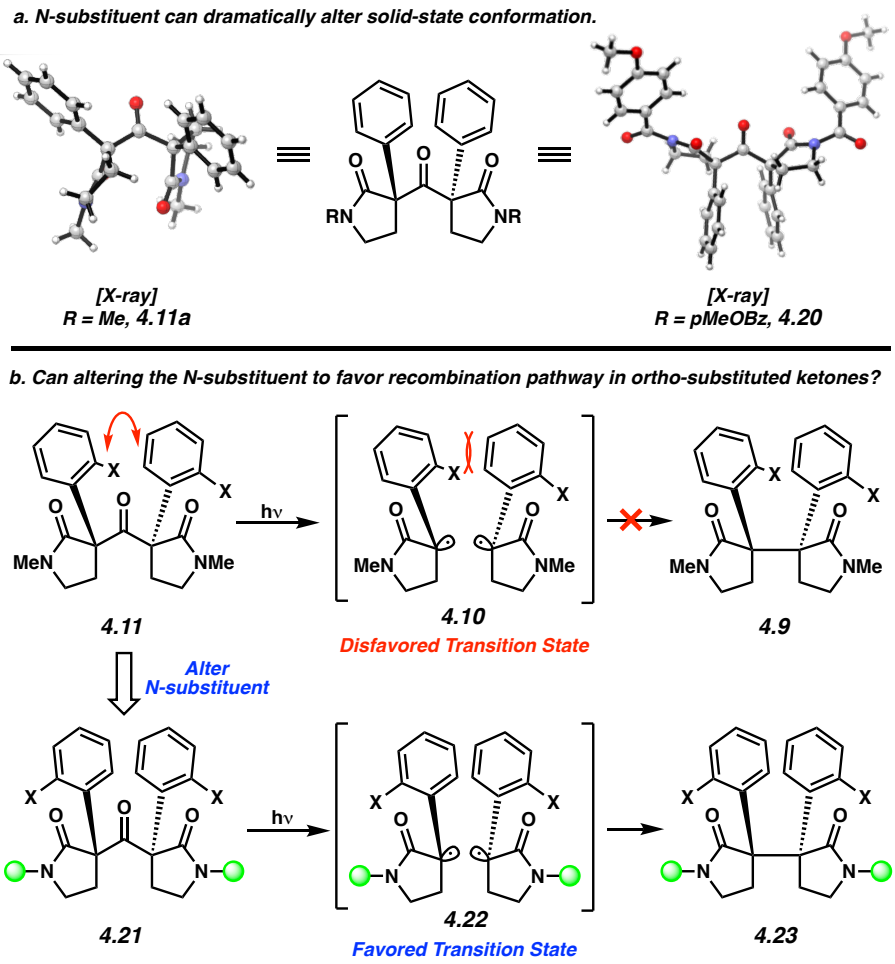

In order to prepare ketones **4.21** bearing modifiable *N*-substituents, we conducted the synthetic sequence depicted in Scheme 4.4.[27] First, *ortho*-chloro and *ortho*-bromo pyrrolidinones **4.15** were cleanly converted to *para*-methoxybenzyl (PMB) protected substrates **4.24** under basic conditions. At this point the synthesis diverged. Esters **4.24** were saponified and then thermally

decarboxylated to provide **4.25** in 79–90% yield. Esters **4.24** were also converted to acid chlorides **4.26** by a two-step saponification / dehydrochlorination protocol. Pyrrolidinones **4.25** were then deprotonated with LiHMDS and the resultant enolates were coupled with acid chlorides **4.26** to furnish PMB-protected ketones **4.27**. As was observed in the construction of **4.11**, formation of **4.27** occurred with exquisite diastereoselectivity, presumably due to a highly ordered transition state mediated by Li^+ chelation.[26] In efforts to cleave the PMB protecting groups, ketones **4.27** were then treated with ceric ammonium nitrate (CAN), which unexpectedly furnished a mixture of imide products **4.28** and **4.29**. Interestingly, ketones **4.28** and **4.29** were both high-melting point crystalline solids. Given this observation, we then sought to test their efficiency in the solid-state photodecarbonylation reaction.

Scheme 4.4. Synthesis of ketones **4.28** and **4.29**.

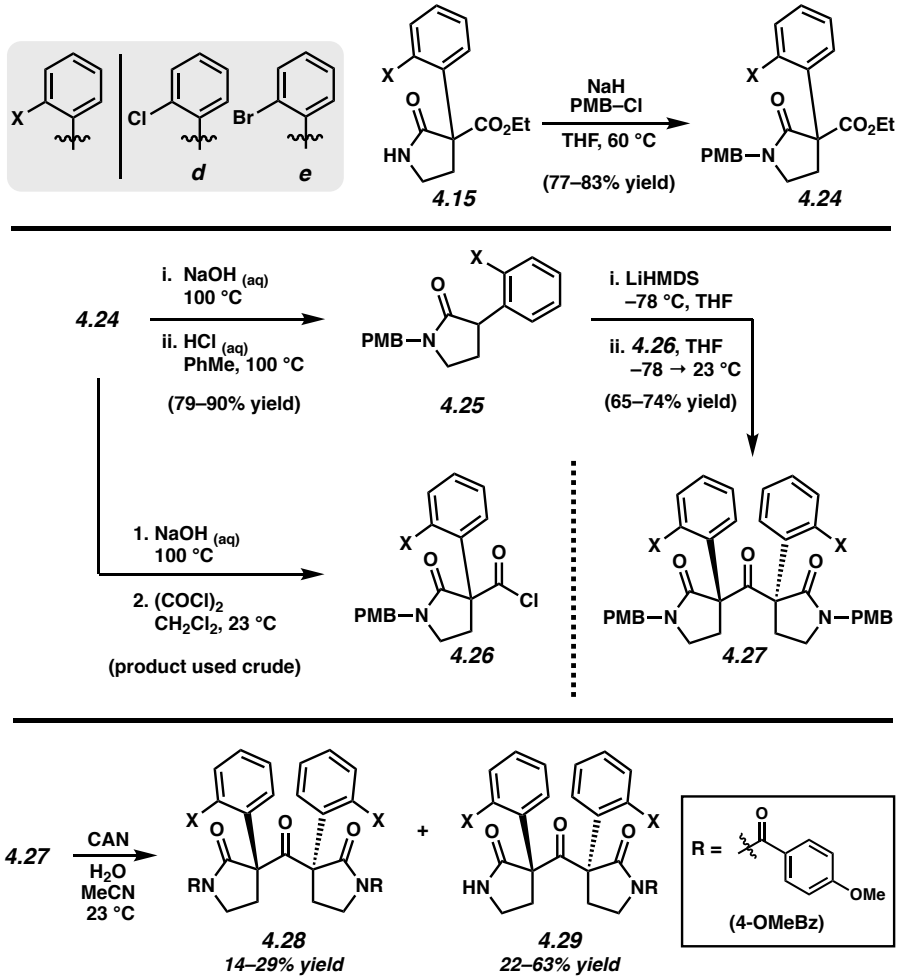

The results of the solid-state photodecarbonylation of symmetric chloride-containing ketone **4.28d** are depicted in Figure 4.6a. We were pleased to find that initial efforts toward the conversion of **4.28d** to **4.30d** proceeded smoothly and with retention of stereochemistry, as verified by single-crystal X-ray diffraction. Furthermore, a competing disproportionation reaction pathway was not observed in the photodecarbonylation of **4.28d**. This result validated our hypothesis that exchanging the *N*-substituents could alter the chemoselectivity of the photodecarbonylation reaction, presumably due to the new conformation of **4.28d** relative to ketone **4.11d**. Furthermore, the efficiency of the reaction demonstrated that solid-state

photodecarbonylation is a competent transformation to forge the vicinal quaternary stereocenter motif present in the bis(cyclotryptamine) alkaloids.

Figure 4.6. Solid-state photochemistry of ketones **4.28d** and **4.28e** (the R-groups on imides **4.28d** and **4.28e** were removed from the X-ray renderings for clarity).

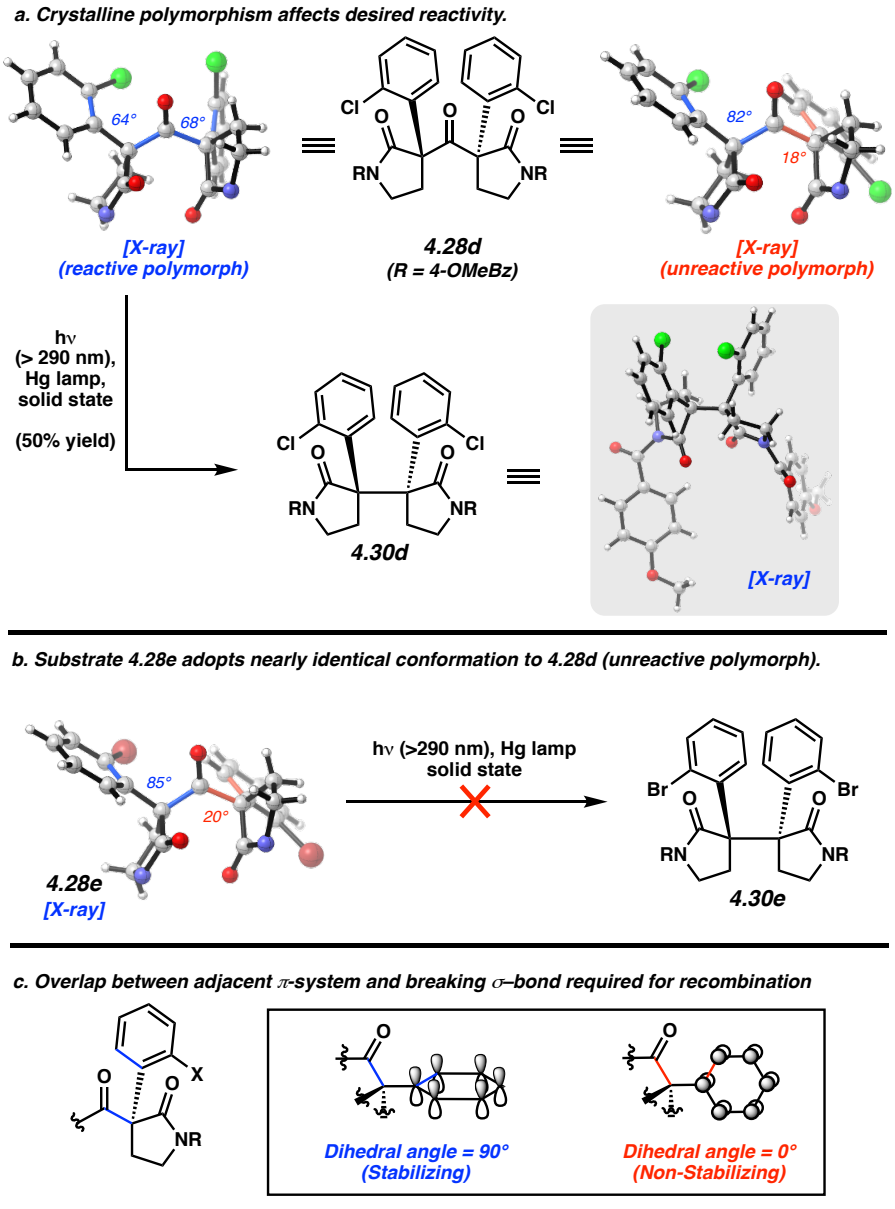

Despite initial success, it was found that the solid-state photodecarbonylation reaction was difficult to reproduce with new batches of **4.28d** (Figure 4.6a). While exposure of **4.28d** to ultraviolet light initially led to full consumption of starting material within 24–48 h, similar irradiation of new samples of **4.28d** only resulted in recovered starting material. After verifying the robustness of the light source and ruling out the possibility of impurities being present in the substrate, it was realized that a new, more stable polymorph of **4.28d**, termed "unreactive polymorph," had formed. Single-crystal X-ray diffraction revealed that this new polymorph adopts a different conformation than the "reactive polymorph" (see X-ray crystal structures in Figure 4.6a). Unfortunately, once the unreactive polymorph was present, it was exceedingly difficult to prepare the reactive polymorph, despite extensive screening of crystallization conditions. These results suggest that the reactive polymorph was likely formed kinetically, while the unreactive polymorph was thermodynamically favored.[28] Trace quantities of the unreactive polymorph that form likely act as seed crystals in subsequent recrystallization attempts, thereby preventing further preparation of the reactive polymorph.[29]

Due to the poor reaction reproducibility stemming from the conformational polymorphism of **4.28d**, we turned our attention to evaluating the *ortho*-bromo substrate **4.28e** (Figure 4.6b). Whereas two conformationally distinct polymorphs were observed for **4.28d**, we only identified a single polymorph of **4.28e**. The conformation observed in the X-ray structure was almost identical to that of the **4.28d** unreactive polymorph. As was expected based on the similar conformation, **4.28e** was also unreactive under solid-state irradiation.

The dramatically different behavior of **4.28d** (reactive polymorph) relative to **4.28d** (unreactive polymorph) and **4.28e** is likely controlled by substrate conformation in the crystalline solid state (Figure 4.6c). Solid-state photodecarbonylation requires stabilization of the breaking

C–C sigma bonds by neighboring π-systems. The extent of these hyperconjugative interactions in substrate **4.28d** (both reactive and unreactive polymorphs) and **4.28e** can be correlated to the dihedral angle between the breaking C–C sigma bond and the nearest C–C bond of the aromatic π-system. A dihedral angle of 90° is ideal, allowing for maximum orbital overlap (see bonds highlighted in blue). Alternatively, if the dihedral angle is 0°, the C–C σ-bond and π-system will be orthogonal, resulting in no electronic stabilization (see bonds highlighted in red). In considering substrate **4.28d** (unreactive polymorph) and **4.28e**, the relevant dihedral angles are 82° and 18° in the former and 85° and 20° in the latter. The smaller of the two dihedral angles for each substrate, 18° and 20°, presumably lead to negligible orbital overlap and failed bond homolysis. On the other hand, the relevant dihedral angles in **4.28d** (reactive polymorph) are 64° and 68°, which we surmise provide sufficient orbital overlap to facilitate decarbonylation.

Having explored the reactivity of symmetric ketones **4.28** in solid-state photochemistry, we next investigated non-symmetrical ketones **4.29** (Figure 4.7). To our delight, both **4.29d** and **4.29e** underwent productive photodecarbonylation. Upon exposure to UV light and subsequent pyrrolidinone deprotection, **4.29d** and **4.29e** efficiently provided **4.31d** and **4.31e**, respectively. Unlike substrate **4.28d**, the solid-state transformations of **4.29d** and **4.29e** were reproducible even when performed on >300 mg scale.[30] These results were consistent with our understanding of the role of solid-state conformation and photochemical lability of the ketone carbonyl. The relevant dihedral angles between breaking C–C bonds and the nearest C–C bond of the aromatic π-system (see bonds highlighted in blue in the X-ray structures) are 67° and 68° for **4.29d**, and 69° and 68° for **4.29e**. These values, which were similar to those seen in the reactive polymorph of **4.28d**, presumably provide enough hyperconjugative stabilization to the breaking C–C bonds to facilitate decarbonylation. Fortuitously, we have only observed reactive polymorphs of **4.29d** and **4.29e**.

Figure 4.7. Solid-state photochemistry of ketones **4.29d** and **4.29e** (the R-groups on imides **4.29d** and **4.29e** were removed from the X-ray renderings for clarity).

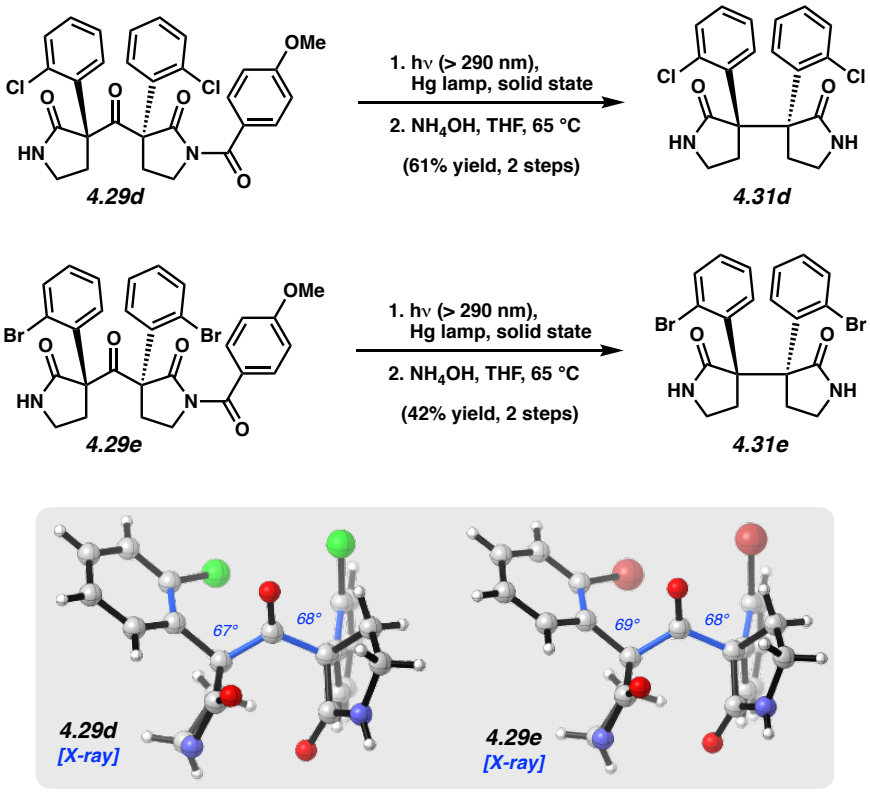

4.3.3 Computational Analysis of C–C Bond Formation

In order to better understand the role of substrate conformation in reaction selectivity, we conducted a computational study of the radical pairs **4.10a** and **4.10c–d** (Figure 4.8 and 4.9). At the outset, we recognized that effective computational simulation of the crystalline lattice would be critical in achieving meaningful results. While gas-phase and simple solvation models would be unlikely to accurately simulate the crystalline environment, full density functional theory (DFT) treatment of the crystalline lattice would be untenable due to prohibitive computational cost. Therefore, the ONIOM[31] approach within the hybrid QM/MM[32] method was employed, which would reliably account for the intermolecular interactions within the crystal lattice environment.[33]

The central layer consisted of a single molecule described at the unrestricted closed-shell dispersion-corrected ωB97X-D/6-311G(d,p) level of theory.[34] The surrounding shell of molecules, extracted from the experimentally determined crystal structure, was used as the low layer with electronically embedded UFF.[35]

Figure 4.8. QM/MM hybrid approach to model radical–radical recombination in the crystalline solid state. "Ball-and-stick" representation was used for the atoms treated by the DFT method (ωB97X-D/6-311G(d,p) level of theory) and a "wireframe" representation for the atoms in the low-level layer (UFF).

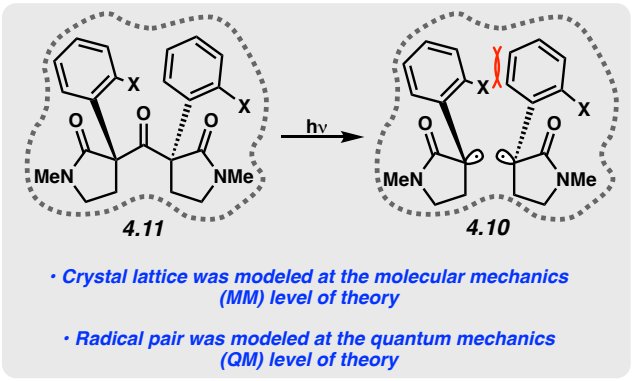

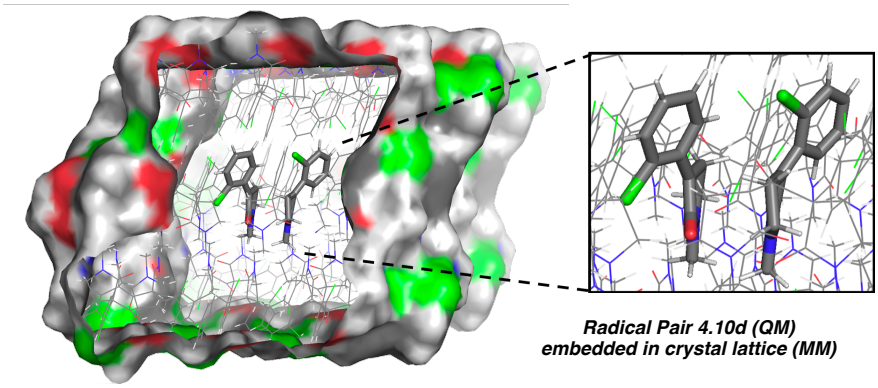

Using this methodology, we investigated the recombination barriers for radical pairs **4.10** in the solid state (Figure 4.9). Radical pairs **4.10** were generated computationally by removing the

carbonyls from ketone **4.11** and then performing an energy minimization calculation. Interestingly, the success of the ground-state optimization for radical fragments was critically dependent on embedding them in their respective crystal cavities. In the gas phase, the radical pair would spontaneously recombine to form the C–C bond. However, when conformationally restrained by the crystal cavity, the radical pair was an energetic minimum and existed as a discrete species. Transition states for the recombination reaction were then identified for each of the radical pairs in their respective lattices. Radical pairs **4.10a** and **4.10c**, which lack *ortho*- substitution, displayed the lowest barriers of 1.7 and 4.8 kcal/mol, respectively. Recombination barriers for *ortho*-functionalized ketones **4.11d–f** were uniformly higher, with values between 6.1 and 6.8 kcal/mol. Given the successful calculation of transition states for C–C bond formation from radical pairs **4.10**, we were additionally interested in probing the competing disproportionation process. Unfortunately, we were unable to obtain meaningful results, despite extensive efforts, and therefore did not include these calculations in our analysis.[36]

Figure 4.9. Computational investigation of radical pair **4.10**.

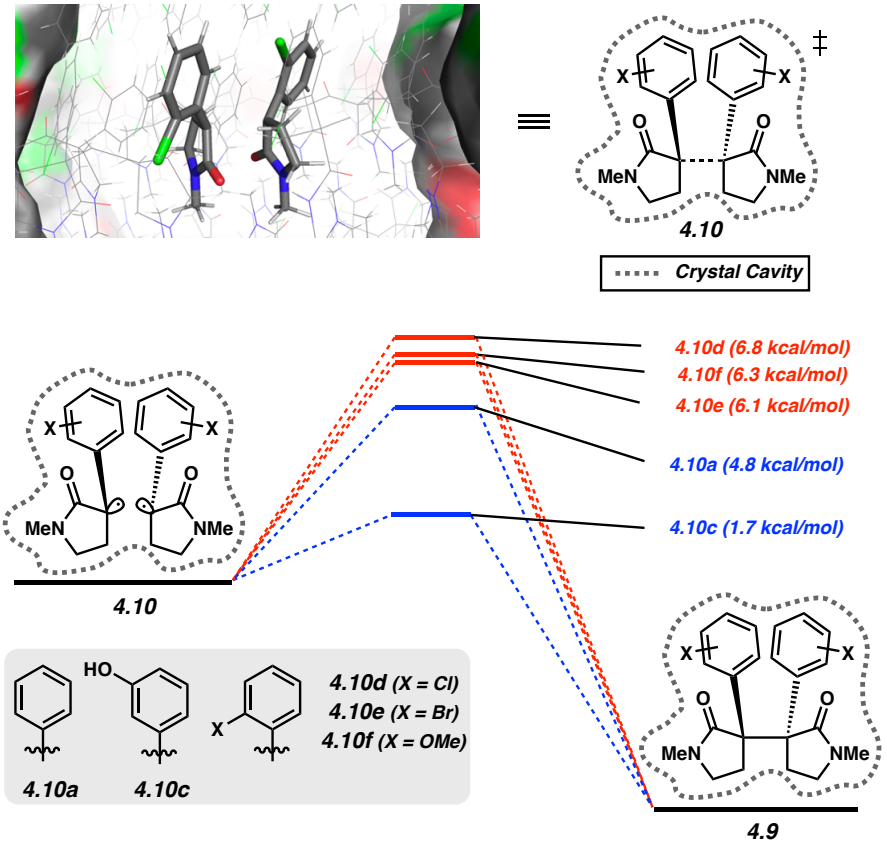

After determining the recombination barriers for radical pairs **4.10**, we turned our attention to radical pair **4.21d** (arising from decarbonylation of ketone **4.28d**) (Figure 4.10). For this calculation, we used the coordinates derived from the reactive polymorph of **4.28d**. Whereas radical pairs **4.10** all displayed small, but non-negligible barriers to C–C bond formation, the corresponding process for radical pair **4.21** was barrierless. In fact, all attempts at energy minimization of **4.21** resulted in radical recombination to form the C–C bond. This result was consistent with experimental results described previously, which demonstrated that photodecarbonylation of ketone **4.28d** (reactive polymorph) could result in efficient C–C bond formation (Figure 4.6a).

Figure 4.10. Computational investigation of radical pair **4.21**.

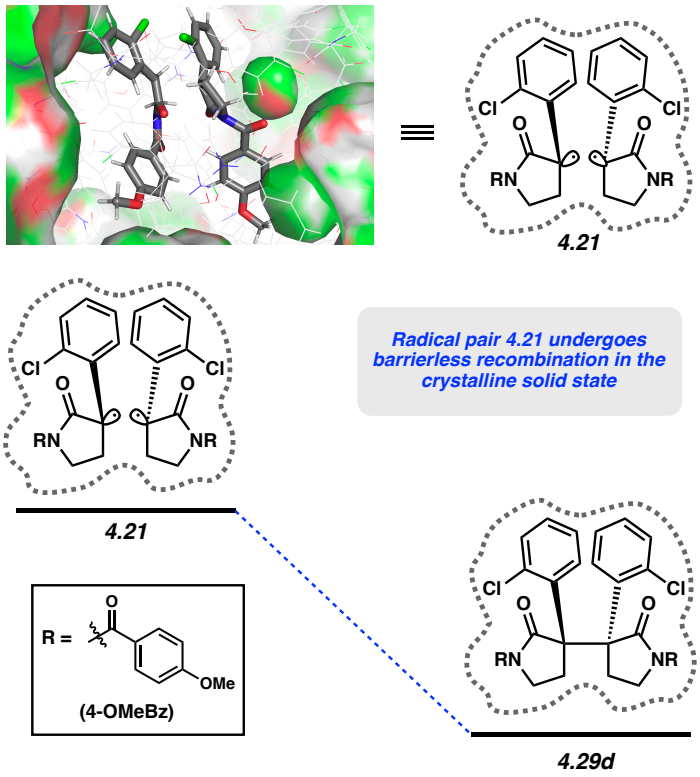

Based on the computational results depicted in Figures 4.9 and 4.10, and the experimental results previously discussed, we were able to draw a number of conclusions about the key photodecarbonylation reaction. Conformational restriction can sometimes lead to activation barriers for recombination. In the photodecarbonylation reaction of ketones **4.11a** and **4.11c–f**, the computationally generated radical pairs **4.10a** and **4.10c–f** were not energetic minima unless they were confined by the crystalline lattice. This is consistent with our hypothesis that in the solid state, unfavorable ground-state substrate conformations can lead to repulsive interactions in the course of the reaction, realized by the presence of an activation barrier. Comparatively, the reactive polymorph of ketone **4.28d** likely undergoes a barrierless recombination due to a favorable ground

state conformation. This is reflected both by the barrierless recombination observed in computational analysis, and by the high-yielding formation of photoproduct **4.30d**. Additionally, the magnitude of the barrier to radical recombination for radical pairs derived from ketones **4.11** is related to the presence of an *ortho*- substituent. The computational results clearly show a higher activation energy for recombination when an *ortho*- substituent is present (6.1–6.8 kcal/mol) and a diminished barrier for radical pairs that lack *ortho*- substitution (1.7–4.8 kcal/mol).[37]

4.3.4 Summary of the Optimization and Mechanistic Analysis of the Solid-State Photodecarbonylation Reaction

The optimization and analysis en route to the bis(cyclotryptamine) alkaloids gave insight into the role of substrate conformation on the success or failure of the solid-state photodecarbonylation reaction. It was found that the performance of the transformation was highly sensitive to remote substituent effects. While low yielding for *N*-methyl ketones **4.11d**–**f**, the solid-state photodecarbonylation reaction of *N*-acyl ketones **4.28d** and **4.29d**,**e** gave up to 61% yield of the desired vicinal quaternary stereocenter-containing product. We hypothesize that changes to the solid-state conformation of the substrate underpin these dramatic substituent effects on photodecarbonylation. This hypothesis was further supported computationally through study of the C–C bond forming events for radical pairs **4.10a**, **4.10c**–**f**, and **4.21**. Additionally, a key stereoelectronic relationship between the conformation of the substrate and the photolability of the ketone carbonyl was identified. This led to dramatically different reactivity of two polymorphic forms of **4.28d**, the failed reaction of **4.28e**, and efficient decarbonylative C–C bond formation from **4.29d**,**e**. Ultimately, this optimization employed crystal engineering of the solid-state

conformation to improve the key step of our synthetic endeavor. To our knowledge this is the first use of a crystal engineering-based optimization in a natural product total synthesis campaign.

4.3.5 Total Synthesis of a Bis(Cyclotryptamine) Alkaloid with the Piperidinoindoline Framework

Having optimized the solid-state photochemical methodology to assemble the daunting vicinal quaternary stereocenter motif, we were poised to elaborate **4.31** to access members of the bis(cyclotryptamine) alkaloid family. We first focused our efforts on synthetic elaboration of **4.31d** (Scheme 4.5). It was found that treatment of **4.31d** with sodium hydride and iodomethane furnished *N*-methylamide **4.9d** in 85% yield. Next, we attempted to install the requisite nitrogen substituents on the aromatic rings through a metal-catalyzed double amination reaction. Although robust methods for amination of hindered aryl chlorides have been reported,[38] attempts at amination of **4.9d** were uniformly unsuccessful. We surmise that the dense steric encumbrance of the vicinal quaternary stereocenters and the potential for the amide carbonyls in **4.9d** to chelate catalysts in a bidentate fashion is responsible for the poor reactivity.

Scheme 4.5. Failed cross-coupling attempts using bis(arylchloride) **4.9d**.

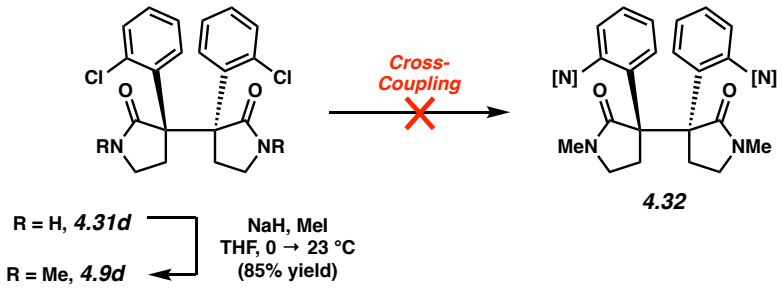

Unabated by the difficulty of functionalizing the C–Cl bond of **4.9d**, we turned our efforts to the potentially more reactive *ortho*-bromo variant, **4.9e** (Scheme 4.6). Efficient *N*-methylation of **4.31e** was realized through a base-mediated alkylation to provide **4.9e**. After subjecting **4.9e** to a variety conditions to effect amination of the aryl bromides, it was found that a modification of Ma's copper-catalyzed azidation conditions yielded the desired double azidation product, **4.33**.[39] We then subjected **4.33** to $LiAlH_4$ to enact a global reduction in an effort to access an equivalent of biosynthon **4.8**, and thereby the bis(cyclotryptamine) framework. To our surprise, under strongly reducing conditions, **4.33** underwent a skeletal rearrangement to provide piperidinoindoline **4.36**.[40] While there are several mechanistic possibilities to explain this reaction, one plausible pathway involves double azide reduction to give **4.34**, followed by Lewis acid-mediated transamidation to generate bis(oxindole) **4.35**. Finally, reductive cyclocondensation of **4.35** resulted in formation of piperidinoindoline **4.36**. Although single-crystal X-ray diffraction ultimately confirmed the structure, we were initially unsure if the correct structural assignment of **4.36** was the piperidinoindoline depicted. As shown in Scheme 4.7, it was plausible that intermediate **4.34** could have undergone double cyclodehydration to provide dehydrobhesine (**4.37**), followed by monoamidine reduction to give bhesine (**4.38**).[41]

Scheme 4.6. Cross-coupling and assembly of "tetrahydropsychotriadine" (**4.36**).

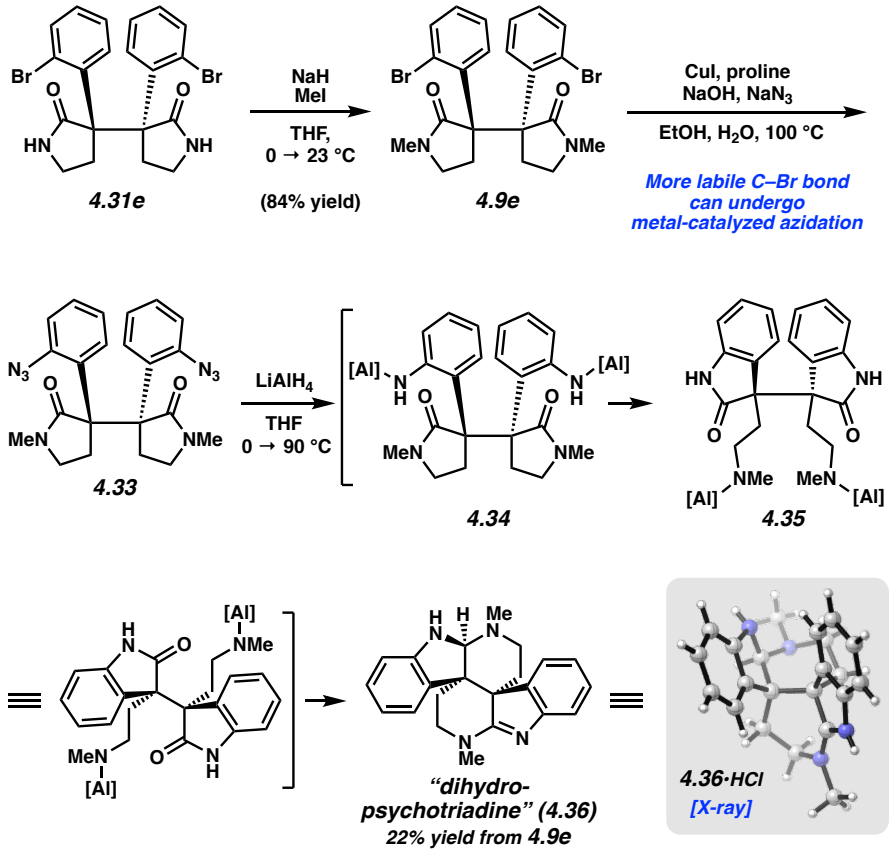

Scheme 4.7. Possible competing pathway to give **4.37** or **4.38** (not observed).

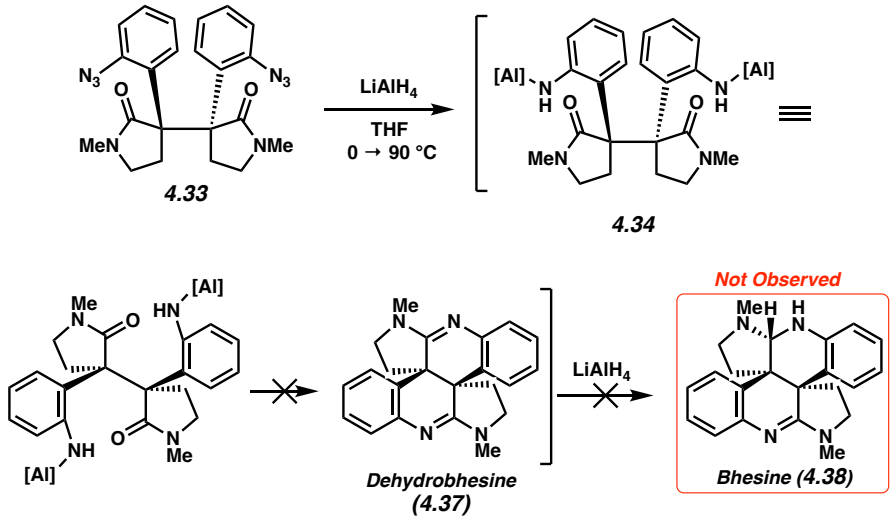

Before we ultimately obtained the single-crystal X-ray structure of **4.36**, we sought to confirm the structural identity of **4.36** by oxidizing the aminal to the corresponding amidine (Scheme 4.8). To accomplish this transformation, **4.36** was converted to bis(amidine) **4.39** under Ley-Griffith oxidation conditions.[42] Initially surmising that we may have generated dehydrobhesine (**4.37**), we compared our synthetic material to an authentic sample of **4.37** extracted from the leaves of the *Psychotria colorata* flower.[43] Upon NMR spectroscopic analysis, it was observed that the natural sample contained a 7:1 mixture of **4.37** and a second, unknown isomeric alkaloid. Surprisingly, the spectrum of our synthetic material **4.39** matched that of the unknown alkaloid present in the natural material. Based on this analysis, and the unambiguous crystallographic characterization of **4.36**, we propose that our synthetic material bears the depicted piperidinoindoline scaffold. Furthermore, its presence in the extracts of *Psychotria colorata* suggests it is a naturally occurring alkaloid that we have termed "psychotriadine."

Scheme 4.8. Total synthesis of "psychotriadine" (**4.39**).

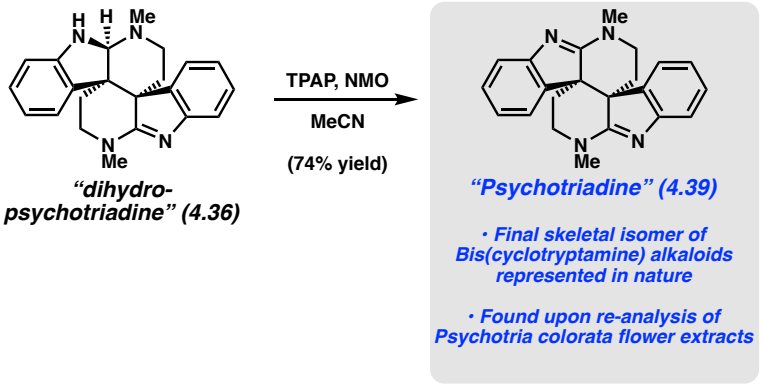

4.4 Conclusion

We have completed the first total synthesis of a naturally occurring bis(cyclotryptamine) alkaloid featuring the elusive piperidinoindoline scaffold and have confirmed its natural occurrence in the *Psychotria colorata* flower. These studies demonstrate that all five of the structurally distinct bis(cyclotryptamine) ring systems originally proposed by R. B. Woodward and Robert Robinson are, in fact, seen in natural products. Essential to the success of this endeavor was the use of the solid-state photodecarbonylation reaction to stereoselectively forge the daunting vicinal quaternary sterecenter motif and a fortuitous reductive rearrangement of bis(azide) **4.33** to give piperidinoindoline **4.36**.

Psychotriadine marks the most complex, synthetically challenging natural product accessed by solid-state photochemistry to date. In deploying the key photodecarbonylation reaction, two primary hurdles were faced: poor chemoselectivity for recombination and a lack of substrate reactivity. Both of these were overcome by manipulation of the substrate conformation. To our knowledge, this is the first use of crystal engineering to optimize a reaction in a total synthesis endeavor. While these efforts showcase the power of crystal engineering as a tool to optimize solid-state reactions, the unpredictability of crystallization remains a major challenge. As is reflected in this work, optimization of the crystalline conformation of a substrate currently relies on trial-and-error based experimentation. Although the use of easily modifiable motifs expedites this process, de novo prediction of crystal conformation represents the ideal solution. As such, the advent of computational prediction of crystal structures would offer a rapid means of predictive control of reactivity and selectivity in solid-state organic reactions.

4.5 Experimental Section

4.5.1 Materials and Methods

Unless stated otherwise, reactions were conducted in flame-dried glassware under an atmosphere of nitrogen using anhydrous solvents (either freshly distilled or passed through activated alumina columns). All commercially available reagents were used as received unless otherwise specified. Sodium hydride (60% dispersion in mineral oil), oxalyl chloride, iodomethane (MeI), bromoacetonitrile, lithium bis(trimethylsilyl)amide (LiHMDS), ceric ammonium nitrate, and sodium borohydride were obtained from Sigma-Aldrich. Cobalt(II) chloride hexahydrate and 4-methoxybenzyl chloride were purchased from TCI America. Unless stated otherwise, reactions were performed at room temperature (rt, approximately 23 °C). Thin-layer chromatography (TLC) was conducted with EMD gel 60 F254 pre-coated plates (0.25 mm) and visualized using a combination of UV, ceric ammonium molybdate, and potassium permanganate staining. Silicycle silica gel 60 (particle size 0.040–0.063 mm) was used for flash column chromatography. Compounds **4.9a**, **4.17f**, and **4.16f** were purified using a Teledyne ISCO Combi*Flash*® NextGen™ instrument using Redi*Sep*®Rf high-performance silica gold columns (24 g, catalog No. 692203346). ^{1}H NMR spectra were recorded on Bruker spectrometers (at 500 MHz or 600 MHz) and are reported relative to deuterated solvent signals. Data for ^{1}H NMR spectra are reported as follows: chemical shift (δ ppm), multiplicity, coupling constant (Hz) and integration. ^{13}C NMR spectra are reported in terms of chemical shift (at 125 MHz). High-resolution mass spectra were obtained on Thermo Scientific™ Exactive Mass Spectrometers with DART ID-CUBE. X-ray structures shown in Figures 4.4, 4.5, 4.6, and 4.7 and Scheme 4.7 of this chapter were created using CYLview.

4.5.2 Experimental Procedures

4.5.2.1 Synthesis of Ketones 4.11.

Note: For experimental information on compounds **4.9e**, **4.11e**, **4.15e**, **4.16e**, **4.17e**, **4.18e**, **4.24e**, **4.25e**, **4.26e**, **4.27e**, **4.28e**, **4.29e**, **4.31e**, **4.34**, **4.36**, **4.39**, and **4.40e**, see Chapter 3. For experimental data on **4.15a**, **4.16a**, **4.17a**, **4.11a**, and **4.9a**, see reference 26.

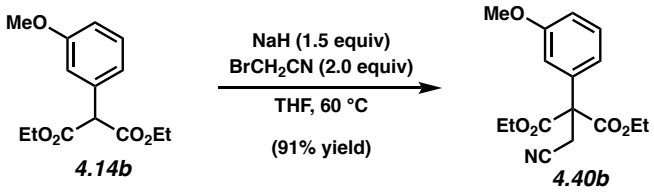

Nitrile 4.40b. To a suspension of NaH (2.78 g, 60% w/w, 69.5 mmol, 1.50 equiv) was added a solution of *m*-methoxyphenyl malonate ester **4.14b** (11.1 g, 41.7 mmol, 1.00 equiv) in THF (100 mL) via canula. Bromoacetonitrile (5.8 mL, 10 g, 83 mmol, 2.00 equiv) was then added dropwise over 1 min via syringe. The reaction was stirred for 10 min and then submerged in an oil bath preheated to 60 °C and stirred for 15 min. The reaction was then cooled to 23 °C and then quenched with aq. HCl (0.5 M, 20 mL). The reaction mixture was poured into a biphasic mixture of aq. HCl (0.5 M, 50 mL) and EtOAc (75 mL). The layers were then separated and the aqueous layer was extracted with EtOAc (2 x 100 mL). The combined organic layers were washed with sat. aq. NaCl (100 mL), dried over Na_2SO_4, and concentrated under reduced pressure directly onto silica gel (20 g). The crude product was then purified by flash column chromatography (80 g silica gel, 9:1 Hexanes:EtOAc → 7:3 Hexanes:EtOAc) to yield **4.40b** as a white solid (11.5 g, 91% yield). Nitrile **4.40b**: R_f 0.41 (7:3 Hexanes:EtOAc); ^{1}H NMR (500 MHz, $CDCl_3$) δ 7.31 (td, J = 7.4, 1.8 Hz, 1H), 6.97 – 6.81 (m, 3H), 4.42 – 4.25 (m, 4H), 3.81 (s, 3H), 3.23 (s, 2H), 1.31 (t, J = 7.1 Hz, 6H); ^{13}C

NMR (125 MHz, $CDCl_3$) δ 168.2, 159.8, 136.5, 129.9, 119.5, 116.8, 113.9, 113.9, 63.1, 60.8, 55.4, 26.4, 14.1; HRMS-APCI (m/z) $[M + H]^+$ calcd for $C_{16}H_{20}NO_5^+$, 306.1336; found 306.1321.

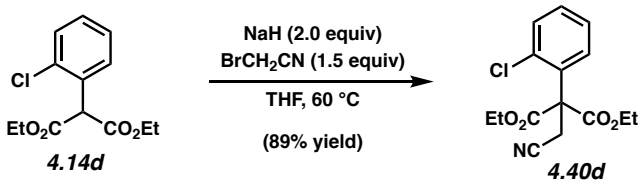

Nitrile 4.40d. To a solution of *o*-chlorophenyl malonate ester **4.14d** (20.0 g, 73.9 mmol, 1.00 equiv) in THF (250 mL), was added NaH (5.91 g, 60 % w/w, 150 mmol, 2.00 equiv) in two portions over 5 min with stirring. Bromoacetonitrile (7.73 mL, 10.2 g, 85.0 mmol, 1.50 equiv) was added dropwise over 1 minute via syringe. The reaction was submerged in an oil bath preheated to 60 °C and stirred for 2 h. After cooling the mixture to 23 °C, an additional aliquot of bromoacetonitrile (2.0 mL, 3.4 g, 29 mmol, 0.39 equiv) was added dropwise via syringe over 1 minute. The reaction was placed in an oil bath preheated to 60 °C and stirred for 18 h. The mixture was then cooled to 23 °C and poured into a biphasic mixture of sat. aq. NH_4Cl (400 mL) and CH_2Cl_2 (300 mL). The layers were separated and the aqueous layer was extracted with CH_2Cl_2 (2 x 100 mL). The organic layers were combined and dried over $MgSO_4$ and concentrated under reduced pressure directly onto silica gel (30 g). The crude product was then purified by flash column chromatography (30 g silica gel, 9:1 Hexanes:EtOAc) to yield **4.40d** as a white solid (20.5 g, 89% yield). Nitrile **4.40d**: mp: 63.7–68.0 °C; R_f 0.46 (7:3 Hexanes:EtOAc); ^1H NMR (500 MHz, $CDCl_3$) δ 7.45 – 7.41 (m, 1H), 7.37 – 7.30 (m, 2H), 7.22 – 7.16 (m, 1H), 4.46 – 4.19 (m, 4H), 3.46 (s, 2H), 1.31 (t, J = 7.1 Hz, 6H); ^{13}C NMR (125 MHz, $CDCl_3$) δ 167.7, 133.5, 133.1, 131.4, 130.3, 130.2, 127.6, 116.9, 63.4, 61.8, 23.8, 13.9; HRMS-APCI (m/z) $[M + H]^+$ calcd for $C_{15}H_{17}NO_4Cl^+$, 310.0846; found 310.0830.

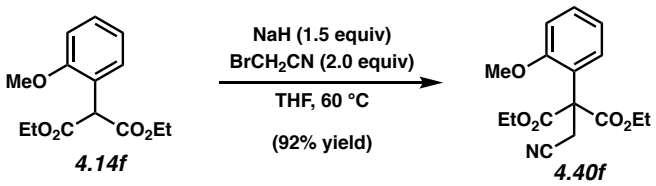

Nitrile 4.40f. To a solution of *o*-methoxyphenyl malonate ester **4.14f** (11.2 g, 42.1 mmol, 1.00 equiv) in THF (140 mL), was added NaH (2.52 g, 60 % w/w, 63 mmol, 1.5 equiv) with stirring. Bromoacetonitrile (5.90 mL, 10.1 g, 84.2 mmol, 2.00 equiv) was added dropwise over 1 min via syringe. The reaction was submerged in an oil bath preheated to 60 °C and stirred for 50 min. The reaction was cooled to 23 °C and poured into a biphasic mixture of sat. aq. NH_4Cl (100 mL) and EtOAc (100 mL). The layers were separated, and the aqueous layer was extracted with EtOAc (2 x 100 mL). The combined organic layers were washed with sat. aq. NaCl (100 mL), dried over $MgSO_4$, and concentrated under reduced pressure directly onto silica gel (20 g). The crude product was then purified by flash column chromatography (80 g silica, 9:1 Hexanes:EtOAc → 3:2 Hexanes:EtOAc) to yield **4.40f** as a white solid (11.8 g, 92% yield). Nitrile **4.40f**: R_f 0.55 (1:1 Hexanes:EtOAc); ^{1}H NMR (500 MHz, $CDCl_3$) δ 7.35 (t, J = 7.8 Hz, 1H), 7.10 (d, J = 7.7 Hz, 1H), 6.99 (t, J = 7.6 Hz, 1H), 6.92 (d, J = 8.2 Hz, 1H), 4.40 – 4.22 (m, 4H), 3.79 (s, 3H), 3.31 (s, 2H), 1.29 (t, J = 7.1 Hz, 6H); ^{13}C NMR (125 MHz, $CDCl_3$) δ 168.6, 156.4, 130.3, 128.8, 124.9, 121.3, 117.7, 111.6, 62.8, 59.7, 55.5, 24.0, 14.1; HRMS-APCI (m/z) $[M + H]^+$ calcd for $C_{16}H_{20}NO_5$, 306.1336; found 306.1332.

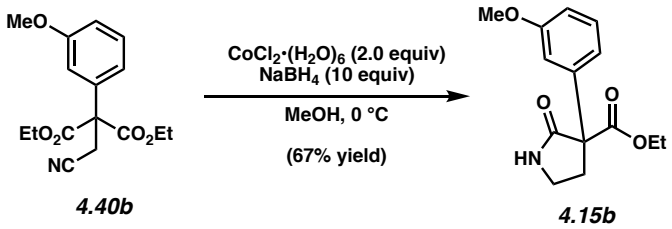

Pyrrolidinone 4.15b. To a solution of nitrile **4.40b** (6.50 g, 21.3 mmol, 1.00 equiv) in MeOH (210 mL), was added $CoCl_2(H_2O)_6$ (10.1 g, 43.6 mmol, 2.00 equiv) with stirring. The reaction was then

cooled to 0 °C and $NaBH_4$ (8.05 g, 213 mmol, 10.0 equiv) was added portionwise (Note 1) over 10 min. The reaction was allowed to warm to 23 °C and was poured into a biphasic mixture of sat. aq. NH_4Cl (260 mL), sat. aq. NaCl (200 mL), and EtOAc (400 mL). The layers were separated and the aqueous layer was extracted with EtOAc (1 x 200 mL). The combined organic layers were dried over $MgSO_4$ and concentrated under reduced pressure directly onto silica gel (8 g). The crude product was purified by flash column chromatography (30 g silica gel, 1:1 Hexanes:EtOAc → 1:4 Hexanes:EtOAc) to give pyrrolidinone **4.15b** (3.75 g, 67% yield) as a viscous oil. Pyrrolidinone **4.15b**: R_f 0.42 (1:4 Hexanes:EtOAc); ^{1}H NMR (500 MHz, $CDCl_3$) δ 7.32 (dd, *J* = 7.7, 1.7 Hz, 1H), 7.30 – 7.24 (m, 1H), 7.20 (s, 1H), 6.95 (td, *J* = 7.6, 1.2 Hz, 1H), 6.88 (dd, *J* = 8.2, 1.1 Hz, 1H), 4.30 (dq, *J* = 10.7, 7.1 Hz, 1H), 4.13 (dq, *J* = 10.8, 7.1 Hz, 1H), 3.78 (s, 3H), 3.52 – 3.40 (m, 1H), 3.32 (ddd, *J* = 13.0, 8.2, 6.8 Hz, 1H), 3.26 – 3.15 (m, 1H), 2.19 (ddd, *J* = 13.0, 7.5, 4.2 Hz, 1H), 1.19 (t, *J* = 7.1 Hz, 3H); ^{13}C NMR (125 MHz, $CDCl_3$) δ 174.2, 170.6 159.8, 139.4, 129.6, 119.7, 113.5, 113.0, 62.3, 59.8, 55.4, 39.4, 34.9, 14.2; HRMS-APCI (m/z) $[M + H]^+$ calcd for $C_{14}H_{18}NO_4^+$, 264.1230; found 264.1218.

Note 1: It is critical that $NaBH_4$ is added slowly, the reaction vigorously releases H_2 gas. The solid was added in roughly equal quantities every ~30 seconds for 10 min to prevent the mixture from erupting out of the flask.

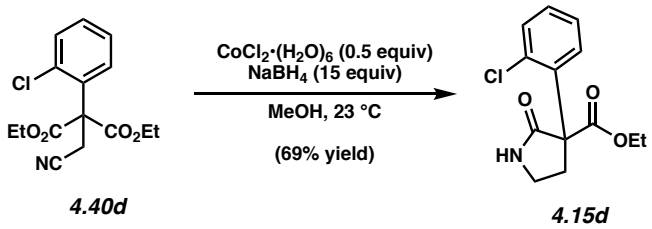

4.40d *4.15d*

Pyrrolidinone 4.15d. To a solution of nitrile **4.40d** (10.4 g, 33.6 mmol, 1.00 equiv) in MeOH (400 mL), was added $CoCl_2$•$(H_2O)_6$ (4.0 g, 17 mmol, 0.50 equiv) with stirring. $NaBH_4$ (19 g, 500 mmol, 15.0 equiv) was added portionwise (Note 1) over 10 min and the reaction was stirred a further 10

min at 23 °C. Aq. HCl (2 M, 200 mL) was added and the reaction was stirred for 10 min. Aq. NH_4OH (30–32% w/v, 300 mL) was then added and stirred for 10 min before the reaction mixture was poured into a biphasic mixture of sat. aq. NaCl (200 mL) and EtOAc (400 mL). The layers were separated and the aqueous layer was extracted with EtOAc (2 x 200 mL). The combined organic layers were washed with sat. aq. NaCl (100 mL), dried over $MgSO_4$, and concentrated under reduced pressure directly onto silica gel (20 g). The crude product was then purified by flash column chromatography (50 g silica gel, 3:2 Hexanes:EtOAc → 3:7 Hexanes:EtOAc) to yield **4.15d** as a viscous oil (6.16 g, 69% yield). Pyrrolidinone **4.15d**: R_f 0.19 (1:1 Hexanes:EtOAc); ^{1}H NMR (500 MHz, $CDCl_3$) δ 7.33 (s, 1H), 7.28 (dd, *J* = 7.3, 2.2 Hz, 1H), 7.20 (dd, *J* = 7.2, 2.1 Hz, 1H), 7.11 – 7.01 (m, 2H), 4.11 (dq, *J* = 10.8, 7.1 Hz, 1H), 4.00 (dq, *J* = 10.8, 7.1 Hz, 1H), 3.39 – 3.20 (m, 2H), 3.08 – 2.95 (m, 1H), 2.14 (ddd, *J* = 13.2, 7.6, 3.3 Hz, 1H), 1.03 (t, *J* = 7.1 Hz, 3H); ^{13}C NMR (125 MHz, $CDCl_3$) δ 174.4, 170.3, 137.2, 133.9, 130.7, 128.9, 128.7, 127.2, 62.6, 61.4, 39.7, 33.5, 14.0; HRMS-APCI (m/z) $[M + H]^+$ calcd for $C_{13}H_{15}NO_3Cl^+$, 268.0740; found 268.0727.

Note 1: It is critical that $NaBH_4$ is added slowly, the reaction vigorously releases H_2 gas. The solid was added in roughly equal quantities every ~30 seconds for 10 min to prevent the mixture from erupting out of the flask.

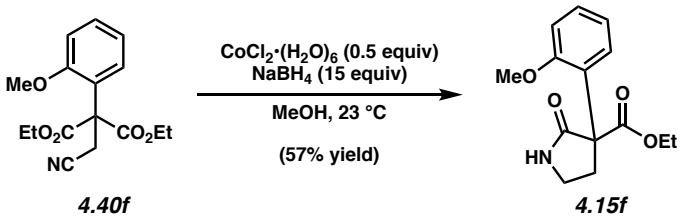

4.40f *4.15f*

Pyrrolidinone 4.15f. To a solution of nitrile **4.40f** (5.87 g, 19.2 mmol, 1.00 equiv) in MeOH (200 mL), was added $CoCl_2(H_2O)_6$ (2.45 g, 10.3 mmol, 0.50 equiv) with stirring. $NaBH_4$ (11.0 g, 291 mmol, 15.0 equiv) was added portionwise (Note 1) over 20 min. Aq. HCl (1 M, 200 mL) was then

added and the reaction was allowed to stir for 5 min before being poured into a biphasic mixture of aq. NH_4OH (30–32% w/v, 200 mL), sat. aq. NaCl (150 mL), and EtOAc (300 mL). The layers were separated, and the aqueous layer was extracted with CH_2Cl_2 (2 x 150 mL). The combined organic layers were dried over $MgSO_4$ and concentrated under reduced pressure directly onto silica gel (20 g). The crude product was then purified by flash column chromatography (50 g silica gel, 7:3 Hexanes:EtOAc → 1:1 Hexanes:EtOAc → 1:1 CH_2Cl_2/EtOAc) to yield **4.15f** as a white solid (3.04 g, 57% yield). Pyrrolidinone **4.15f**: R_f 0.41 (2:8 Hexanes:EtOAc); ^{1}H NMR (500 MHz, $CDCl_3$) δ 7.32 – 7.23 (m, 1H), 7.11 – 6.94 (m, 2H), 6.84 (dd, *J* = 8.3, 2.5 Hz, 1H), 6.64 (s, 1H), 4.31 – 4.15 (m, 2H), 3.81 (s, 3H), 3.51 – 3.38 (m, 1H), 3.36 – 3.25 (m, 1H), 3.12 (ddd, *J* = 12.8, 7.4, 5.2 Hz, 1H), 2.49 (ddd, *J* = 13.2, 7.3, 6.0 Hz, 1H), 1.25 (t, *J* = 7.1 Hz, 3H); ^{13}C NMR (125 MHz, $CDCl_3$) δ 175.0, 171.0, 156.9, 128.8, 128.2, 127.7, 120.9, 110.9, 61.8, 58.9, 55.3, 39.7, 33.6, 14.2; HRMS-APCI (m/z) $[M + H]^+$ calcd for $C_{14}H_{18}NO_4^+$, 264.1230; found 264.1229.

Note 1: It is critical that $NaBH_4$ is added slowly, the reaction vigorously releases H_2 gas. The solid was added in roughly equal quantities every ~30 seconds for 20 min to prevent the mixture from erupting out of the flask.

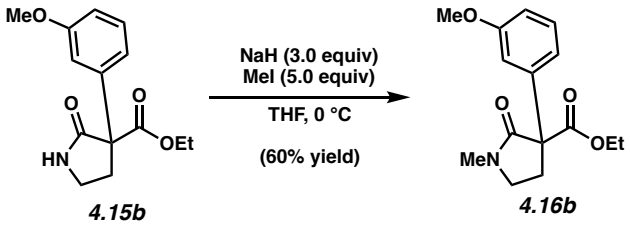

4.15b *4.16b*

Pyrrolidinone 4.16b. A solution of pyrrolidinone **4.15b** (940 mg, 3.57 mmol, 1.0 equiv) in THF (25 mL) was added over 5 min via syringe to a 0 °C suspension of NaH (430 mg, 10.7 mmol, 3.0 equiv, 60% dispersion in mineral oil) in THF (10 mL). The reaction was stirred for 20 min before MeI (1.1 mL, 2.5 g, 18 mmol, 5.0 equiv) was added dropwise over 1 min. The reaction was stirred at 0 °C for 45 min and then poured into a slurry of sat. aq. NH_4Cl (50 mL) and ice. EtOAc (100

mL) was added, the layers were separated, and the aqueous layer was further extracted with EtOAc (2 x 30 mL). The combined organic layers were washed with sat. aq. NaCl (30 mL), dried over Na_2SO_4, and concentrated under reduced pressure directly onto silica gel (1.5 g). The crude product was purified by flash column chromatography (7 g silica gel, 4:1 Hexanes:EtOAc → 1:1 Hexanes:EtOAc) to provide pyrrolidinone **4.16b** (940 mg, 60% yield) as a viscous oil. Pyrrolidinone **4.16b**: R_f 0.47 (1:4 Hexanes:EtOAc); ^{1}H NMR (500 MHz, $CDCl_3$) δ 7.39 – 7.30 (m, 1H), 7.12 – 7.09 (m, 1H), 7.09 – 7.01 (m, 1H), 6.94 – 6.86 (m, 1H), 4.48 – 4.14 (m, 2H), 3.87 (s, 3H), 3.57 – 3.46 (m, 1H), 3.42 – 3.30 (m, 1H), 3.09 (ddd, *J* = 12.9, 7.7, 5.1 Hz, 1H), 3.02 (s, 3H), 2.46 (dt, *J* = 13.3, 6.9 Hz, 1H), 1.30 (t, *J* = 7.1 Hz, 3H); ^{13}C NMR (125 MHz, $CDCl_3$) δ 170.9, 170.7, 159.7, 139.9, 129.5, 119.6, 113.4, 113.00, 62.2, 60.5, 55.4, 46.5, 32.3, 30.6, 14.2; HRMS-APCI (m/z) $[M + H]^+$ calcd for $C_{15}H_{20}NO_4^+$, 278.1387; found 278.1375.

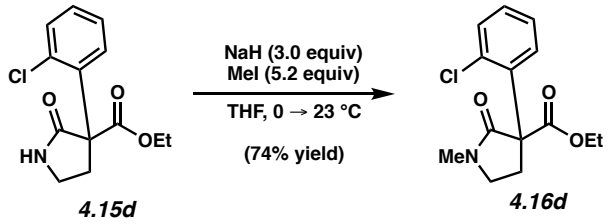

Pyrrolidinone 4.16d. To a 0 °C suspension of NaH (420 mg, 11 mmol, 3.0 equiv, 60% dispersion in mineral oil) in THF (20 mL) was added a solution of pyrrolidinone **4.15d** (935 mg, 3.49 mmol, 1.00 equiv) in THF (20 mL). The reaction was stirred for 45 min at 0 °C and MeI (0.90 mL, 2.6 g, 18 mmol, 5.2 equiv) was added dropwise over 1 min via syringe. The reaction was removed from the 0 °C bath, stirred for 15 min, and then poured into a slurry of aq. HCl (0.5 M, 100 mL) and ice. The crude mixture was extracted with EtOAc (3 x 100 mL) and the combined organic layers were dried over $MgSO_4$ before being concentrated under reduced pressure directly onto silica gel (2.5 g). The crude product was then purified by flash column chromatography (15 g silica gel, 7:3 Hexanes:EtOAc → 1:1 Hexanes:EtOAc) to provide pyrrolidinone **4.16d** (731 mg, 74% yield) as a

viscous oil. Pyrrolidinone **4.16d**: R_f 0.19 (7:3 Hexanes:EtOAc); ^{1}H NMR (500 MHz, $CDCl_3$) δ 7.28 – 7.20 (m, 2H), 7.14 – 7.06 (m, 2H), 4.20 – 4.11 (m, 1H), 4.10 – 4.01 (m, 1H), 3.46 – 3.32 (m, 1H), 3.26 (ddd, *J* = 13.4, 8.6, 6.3 Hz, 1H), 3.19 – 3.06 (m, 1H), 2.87 (s, 3H), 2.09 (ddd, *J* = 12.6, 8.0, 4.2 Hz, 1H), 1.09 (t, *J* = 7.1 Hz, 3H); ^{13}C NMR (125 MHz, $CDCl_3$) δ 170.5, 170.2, 137.9, 133.9, 130.6, 129.0, 128.8, 127.2, 62.5, 61.9, 46.7, 31.1, 30.7, 14.1; HRMS-APCI (m/z) $[M + H]^+$ calcd for $C_{14}H_{17}NO_3Cl^+$, 282.0897; found 282.0888.

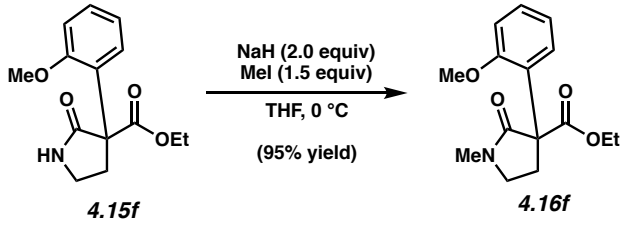

4.15f *4.16f*

Pyrrolidinone 4.16f. To a solution of pyrrolidinone **4.15f** (1.50 g, 5.70 mmol, 1.00 equiv) in THF (50 mL), was added NaH (460 mg, 11 mmol, 2 equiv, 60% dispersion in mineral oil) in 2 portions over 5 min with stirring. The reaction was stirred at 23 °C for 15 min before being placed in a 0 °C bath. MeI (0.53 mL, 1.21 g, 8.6 mmol, 1.5 equiv) was added dropwise over 1 min via syringe. The reaction was stirred at 0 °C for 2 h and then poured into a biphasic mixture of sat. aq. NH_4Cl (100 mL) and CH_2Cl_2 (200 mL). The layers were separated, and the aqueous layer was extracted with CH_2Cl_2 (2 x 100 mL). The combined organic layers were dried over $MgSO_4$ before being concentrated under reduced pressure. The crude product was purified by flash column chromatography (RediSep Gold 25 g silica gel, 9:1 Hexanes:EtOAc → 7:3 Hexanes:EtOAc) to provide pyrrolidinone **4.16f** (1.50 g, 95% yield) as a white solid. Pyrrolidinone **4.16f**: R_f 0.47 (3:7 Hexanes:EtOAc); ^{1}H NMR (500 MHz, $CDCl_3$) δ 7.32 – 7.22 (m, 1H), 7.20 (d, *J* = 7.6 Hz, 1H), 6.92 (t, *J* = 7.5 Hz, 1H), 6.86 (d, *J* = 8.1 Hz, 1H), 4.32 – 4.19 (m, 1H), 4.19 – 4.04 (m, 1H), 3.77 (s, 3H), 3.54 – 3.38 (m, 1H), 3.29 – 3.16 (m, 2H), 2.97 (s, 3H), 2.05 (td, *J* = 10.8, 10.3, 6.7 Hz, 1H), 1.17 (t, *J* = 7.1 Hz, 3H); ^{13}C NMR (125 MHz, $CDCl_3$) δ 171.4, 170.9, 156.89, 129.0, 128.7,

127.7, 120.9, 110.9, 61.8, 59.5, 55.3, 46.8, 31.2, 30.6, 14.2; HRMS-APCI (m/z) $[M + H]^+$ calcd for $C_{15}H_{20}NO_4^+$, 278.1387; found 278.1384.

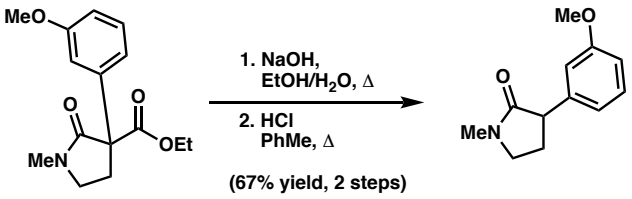

4.16b *4.17b*

Pyrrolidinone 4.17b. To a solution of pyrrolidinone **4.16b** (750 mg, 5.10 mmol, 1.00 equiv) in EtOH (10 mL), was added aq. NaOH (1 M, 17 mL). The reaction was placed in a preheated 110 °C oil bath, stirred at reflux for 20 min, and then cooled to 23 °C. The reaction was poured into aq. HCl (0.5 M, 100 mL), the layers were separated, and the aqueous layer was extracted with EtOAc (3 x 75 mL). The combined organic layers were washed with sat. aq. NaCl (75 mL), dried over Na_2SO_4, and concentrated under reduced pressure directly onto silica gel (1.7 g). The crude product was purified by flash column chromatography (8 g silica gel, 4:1 Hexanes:EtOAc → 2:3 Hexanes:EtOAc) to provide the corresponding carboxylic acid, which was carried crude to the next step.

To a suspension of the crude carboxylic acid prepared in the previous step (465 mg, 2.27 mmol, 1.00 equiv) in PhMe (20 mL), was added aq. HCl (0.5 M, 25 mL). The reaction was placed in a preheated 110 °C oil bath and stirred at reflux for 2 h before being allowed to cool to 23 °C. The reaction was poured into a biphasic mixture of DI H_2O (100 mL) and CH_2Cl_2 (100 mL). The layers were separated, and the aqueous layer was extracted with CH_2Cl_2 (2 x 100 mL). The combined organic layers were dried over $MgSO_4$ and concentrated under reduced pressure directly onto silica gel (1 g). The crude product was purified by flash column chromatography (5 g silica gel, 7:3 Hexanes:EtOAc) to provide pyrrolidinone **4.17b** (299 mg, 67% yield, 2 steps) as a viscous oil. Pyrrolidinone **4.17b**: R_f 0.22 (2:8 Hexanes:EtOAc); ^1H NMR (500 MHz, $CDCl_3$) δ 7.28 – 7.20

(m, 1H), 6.85 – 6.70 (m, 3H), 3.79 (s, 3H), 3.62 (t, J = 8.7 Hz, 1H), 3.51 – 3.36 (m, 2H), 2.93 (s, 3H), 2.51 (dtd, J = 12.8, 8.5, 3.9 Hz, 1H), 2.12 (dq, J = 12.9, 8.1 Hz, 1H); ^{13}C NMR (125 MHz, $CDCl_3$) δ 174. 9, 160.0, 141.7, 129.9, 120.3, 113.9, 112.4,5 55.4, 48.2, 47.9, 30.3, 28.0; HRMS-APCI (m/z) $[M + H]^+$ calcd for $C_{12}H_{16}NO_2^+$, 206.1176; found 206.1167.

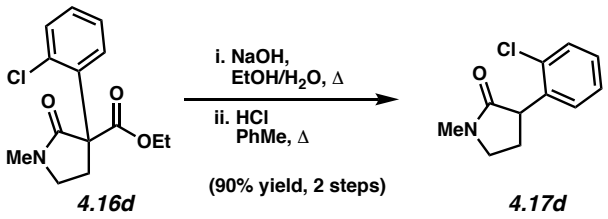

Pyrrolidinone 4.17d. To a solution of pyrrolidinone **4.16d** (290 mg, 1.03 mmol, 1.0 equiv) in EtOH (5 mL), was added aq. NaOH (1 M, 15 mL). The reaction was placed in a preheated 110 °C oil bath, stirred at reflux for 45 min, and then cooled to 23 °C. Aq. HCl (2 M, 15 mL) was added followed by PhMe (20 mL). The reaction was placed in a preheated 110 °C oil bath and stirred at reflux for 2 h before being allowed to cool to 23 °C. The reaction was poured into a biphasic mixture of DI H_2O (100 mL) and CH_2Cl_2 (100 mL), the layers were separated, and the aqueous layer was extracted with CH_2Cl_2 (2 x 100 mL). The combined organic layers were dried over $MgSO_4$ and concentrated under reduced pressure directly onto silica gel (2.5 g). The crude product was purified by flash column chromatography (15 g silica gel, 1:1 Hexanes:EtOAc → 1:3 Hexanes:EtOAc) to provide pyrrolidinone **4.17d** (195 mg, 90% yield) as a glassy solid. Pyrrolidinone **4.17d**: R_f 0.40 (EtOAc); ^{1}H NMR (500 MHz, $CDCl_3$) δ 7.42 – 7.33 (m, 1H), 7.26 – 7.16 (m, 3H), 4.11 (t, J = 9.2 Hz, 1H), 3.53 – 3.39 (m, 2H), 2.97 (s, 3H), 2.61 (dddd, J = 13.4, 9.4, 6.7, 4.3 Hz, 1H), 1.96 (dq, J = 13.0, 8.6 Hz, 1H); ^{13}C NMR (125 MHz, $CDCl_3$) δ 174.3, 138.1, 134.4, 129.8, 129.5, 128.4, 127.4, 47.7, 46.1, 30.3, 27.4; HRMS-APCI (m/z) $[M + H]^+$ calcd for $C_{11}H_{13}NOCl^+$, 210.0686; found 210.0672.

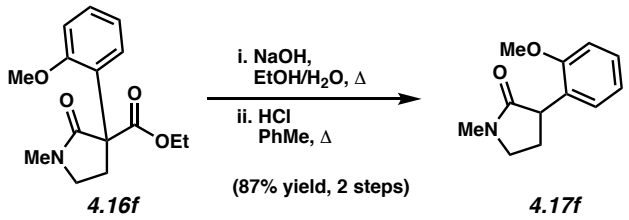

4.16f *4.17f*

Pyrrolidinone 4.17f. To a solution of pyrrolidinone **4.16f** (1.42 g, 5.10 mmol, 1.0 equiv) in EtOH (10 mL), was added aq. NaOH (1 M, 17 mL). The reaction was placed in a preheated 115 °C oil bath, stirred at reflux for 15 min, and then cooled to 23 °C. To the reaction was added, aq. HCl (1 M, 30 mL) followed by PhMe (30 mL). The reaction was placed in a preheated 115 °C oil bath and stirred at reflux for 3 h before being allowed to cool to 23 °C. The reaction was poured into a biphasic mixture of DI H_2O (100 mL) and CH_2Cl_2 (100 mL), the layers were separated, and the aqueous layer was extracted with CH_2Cl_2 (2 x 100 mL). The combined organic layers were dried over $MgSO_4$ and concentrated under reduced pressure. The crude product was purified by flash column chromatography (RediSep Gold 25 g silica gel, 3:7 Hexanes:EtOAc) to provide pyrrolidinone **4.17f** (909 mg, 87% yield) as a glassy solid. Pyrrolidinone **4.17f**: R_f 0.40 (EtOAc); ^{1}H NMR (600 MHz, $CDCl_3$) δ 7.22 (ddd, *J* = 8.2, 7.5, 1.7 Hz, 1H), 7.12 (dd, *J* = 7.5, 1.7 Hz, 1H), 6.92 (td, *J* = 7.4, 1.2 Hz, 1H), 6.87 (dd, *J* = 8.2, 1.1 Hz, 1H), 3.91 (t, *J* = 9.0 Hz, 1H), 3.80 (s, 3H), 3.48 – 3.35 (m, 2H), 2.94 (s, 3H), 2.46 (dddd, *J* = 13.1, 9.6, 7.7, 4.0 Hz, 1H), 2.00 (dtd, *J* = 12.8, 8.7, 7.5 Hz, 1H); ^{13}C NMR (125 MHz, $CDCl_3$) δ 175.5, 157.5, 129.5, 128.9, 128.3, 121.0, 111.0, 55.7, 48.0, 43.7, 30.3, 27.1; HRMS-APCI (m/z) $[M + H]^+$ calcd for $C_{12}H_{16}NO_2^+$, 206.1176; found 206.1173.

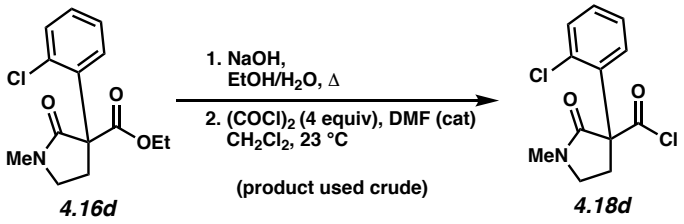

Acid Chloride 4.18d. To a solution of pyrrolidinone **4.16d** (440 mg, 1.56 mmol, 1.00 equiv) in EtOH (5 mL), was added aq. NaOH (1 M, 15 mL). The reaction was placed in a preheated 115 °C oil bath, stirred at reflux until all solid had dissolved (~ 5 min), and then cooled to 23 °C. The reaction mixture was poured into aq. HCl (0.5 M, 50 mL) and extracted with EtOAc (3 x 100 mL). The combined organic layers were washed with sat. aq. NaCl (100 mL), dried over Mg_2SO_4, and concentrated under reduced pressure. The resultant crude carboxylic acid was carried on directly to the next step.

To neat crude carboxylic acid from the previous step was added one drop of DMF from a glass Pasteur pipette, followed by CH_2Cl_2 (16 mL) via syringe. Oxalyl chloride (0.54 mL, 6.2 mmol, 4.0 equiv) was then added dropwise over 1 min. The reaction was stirred at 23 °C for 16 h and then concentrated under reduced pressure. The resultant oil was dissolved in PhMe (10 mL) and concentrated under reduced pressure (x2). The crude oil was then put under vacuum (< 1 mbar) for 1 h. Crude acid chloride **4.18d** was used immediately without further purification.

Note 1: It is critical that this set up is kept both anhydrous and that the oxalyl chloride is fully removed. Each time the acid chloride was concentrated under rotary evaporation (both from CH_2Cl_2 and then from PhMe) the water bath was maintained at 50 °C on full vacuum (~15 mbar) for > 15 min. After this, it is recommended that the oil be put under high vacuum for > 1 h.

Note 2: In order to ensure that undue water is not introduced between rotary evaporations, the rotary evaporator is backfilled with a balloon of dry Ar.

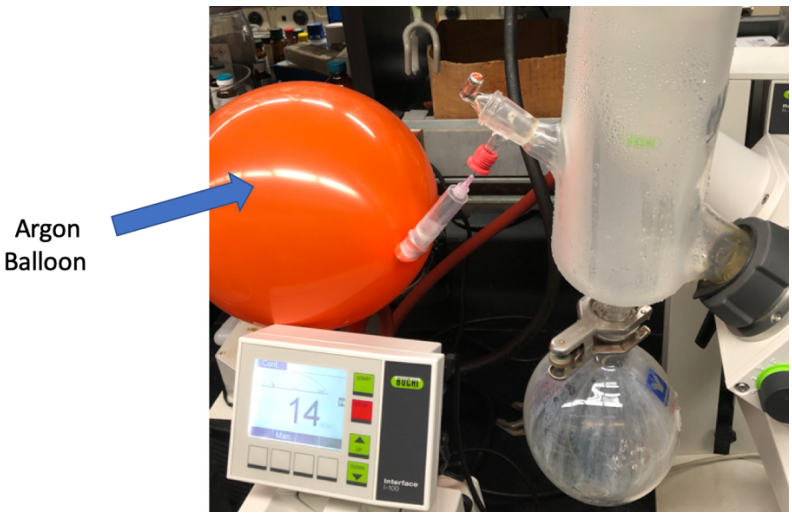

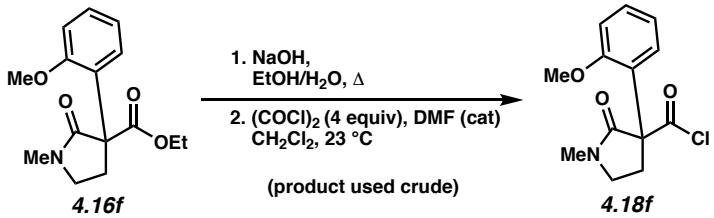

Acid Chloride 4.18f. To a solution of pyrrolidinone **4.16f** (2.0 g, 7.2 mmol, 1.0 equiv) in EtOH (30 mL), was added aq. NaOH (1 M, 50 mL). The reaction was placed in a preheated 105 °C oil bath, stirred at reflux for 15 min, and then cooled to 23 °C. The reaction mixture was poured into aq. HCl (2 M, 60 mL) and extracted with CH_2Cl_2 (3 x 100 mL). The combined organic layers were dried over Mg_2SO_4, and then concentrated under reduced pressure. The resultant crude carboxylic acid was carried on directly to the next step.

To neat crude carboxylic acid from the previous step (926 mg, 3.71 mmol, 1.0 equiv), was added one drop of DMF from a glass Pasteur pipette followed by CH_2Cl_2 (35 mL) via syringe. Oxalyl chloride (1.27 mL, 14.9 mmol, 4.0 equiv) was then added dropwise over 1 min. The reaction was stirred at 23 °C for 1 h and then concentrated under reduced pressure. The resultant

oil was dissolved in PhMe (20 mL) and concentrated under reduced pressure (x2). The crude oil was then put under vacuum (< 1 mbar) for 1 h. Crude acid chloride **4.18f** was used immediately without further purification.

*See the preparation of **4.18d** for experimental notes.*

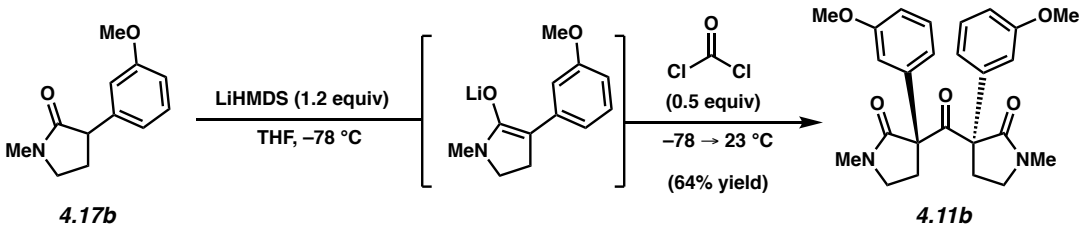

4.17b *4.11b*

Ketone 4.11b. A solution of amide **4.17b** (470 mg, 1.41 mmol, 1.0 equiv) in THF (10 mL) was cooled to –78 °C. A solution of LiHMDS (270 mg, 1.61 mmol, 1.15 equiv) in THF (1 mL) was added dropwise over 5 min and the reaction was stirred for 45 min. Phosgene (15 wt% in PhMe, 0.50 mL, 0.70 mmol, 0.5 equiv) was added dropwise over 5 min and the reaction was immediately transferred to a 0 °C bath and stirred for 20 min. The mixture was then quenched by the addition of aq. HCl (0.1 M, 10 mL) and the aqueous layer was extracted with CH_2Cl_2 (2 x 75 mL). The combined organic layers were dried over $MgSO_4$ and concentrated under reduced pressure directly gel (0.5 g). The crude product was purified by flash column chromatography (5 g silica gel, CH_2Cl_2 → 7:3 CH_2Cl_2:EtOAc) to provide ketone **4.11b** (198 mg, 64% yield) as a viscous oil. Ketone **4.11b**: R_f 0.20 (1:4 Hexanes:EtOAc); ^{1}H NMR (500 MHz, $CDCl_3$) δ 7.28 – 7.17 (m, 2H), 6.84 – 6.74 (m, 6H), 3.77 (s, 6H), 3.37 – 3.25 (m, 4H), 3.11 – 3.05 (m, 2H), 2.86 (s, 6H), 1.95 – 1.88 (m, 2H); ^{13}C NMR (125 MHz, $CDCl_3$) δ 200.49, 171.08, 159.91, 140.52, 129.70, 119.78, 113.32, 112.88, 67.84, 55.33, 46.69, 33.12, 30.65; HRMS-APCI (m/z) $[M + H]^+$ calcd for $C_{25}H_{29}N_2O_5^+$, 437.2071; found 437.2053.

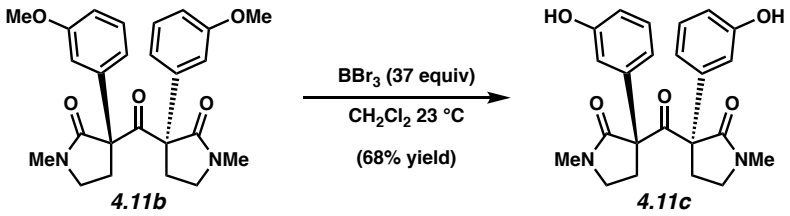

Ketone 4.11c. To a solution of ketone **4.11b** (297 mg, 0.68 mmol, 1.00 equiv) in CH_2Cl_2 (50 mL), was added BBr_3 (2.4 mL, 6.3 g, 25 mmol, 37 equiv) dropwise over 3 min. The reaction mixture was stirred at 23 °C for 50 min and then cooled to –78 °C. The reaction was quenched by the addition of a mixture of Et_3N (4.5 mL) in MeOH (15 mL) dropwise over 1 min, warmed 23 °C, and then poured into EtOAc (50 mL). The mixture was washed with sat. aq. $NaHCO_3$ (40 mL) followed by sat. aq. NaCl (40 mL), dried over Na_2SO_4, and concentrated under reduced pressure directly onto silica gel (1.2 g). The crude product was purified by flash column chromatography (10 g silica gel, 3:7 Hexanes:EtOAc → EtOAc) to provide ketone **4.11c** (189 mg, 68% yield) as a white solid. Crystals suitable for X-ray diffraction studies (CCDC 2006463) were obtained by slow evaporation from MeOH. Ketone **4.11c**: R_f 0.49 (EtOAc); ^{1}H NMR (500 MHz, Methanol-d_4) δ 7.17 (t, J = 7.9 Hz, 2H), 6.72 (dd, J = 8.1, 2.3 Hz, 2H), 6.67 – 6.58 (m, 4H), 3.28 – 3.20 (m, 4H), 3.17 – 3.07 (m, 2H), 2.86 (s, 6H), 1.99 – 1.88 (m, 2H); ^{13}C NMR (125 MHz, Methanol-d_4) δ 200.4, 171.7, 157.49, 140.0, 129.4, 117.9, 114.1, 114.0, 67.9, 46.2, 32.9, 29.2; HRMS-APCI (m/z) $[M + H]^+$ calcd for $C_{23}H_{25}N_2O_5^+$, 409.1758; found 409.1742.

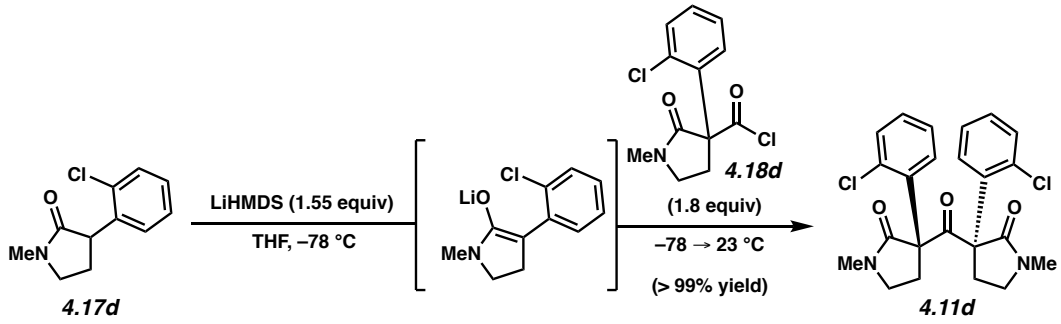

Ketone 4.11d. A solution of pyrrolidinone **4.17d** (179 mg, 0.853 mmol, 1.00 equiv) in THF (5 mL) was added dropwise over 5 min to a pre-cooled –78 °C solution of LiHMDS (6.32 mL, 221 mg, 1.32 mmol, 1.55 equiv) in THF (6.32 mL). The mixture was allowed to stir for 1 h before acid chloride **4.18d** (420 mg, 1.6 mmol, 1.8 equiv) was added dropwise over 5 min. The reaction was then removed from the –78 °C bath and stirred at 23 °C for 2 h before being poured into a mixture of sat. aq. NaCl (50 mL) and aq. HCl (1 M, 50 mL). The layers were separated and the aqueous layer was extracted with CH_2Cl_2 (3 x 100 mL). The combined organic layers were dried over $MgSO_4$ and concentrated under reduced pressure directly onto silica gel (2.5 g). The crude product was purified by flash column chromatography (15 g silica gel, CH_2Cl_2 → 9:1 CH_2Cl_2:EtOAc) to provide ketone **4.11d** (387 mg, > 99% yield) as a white solid. Crystals suitable for X-ray diffraction studies (CCDC 2006461) were obtained using slow evaporation from a mixture of CH_2Cl_2/Hexanes. Ketone **4.11d**: mp: 151.0–151.1 °C; R_f 0.56 (EtOAc); ^{1}H NMR (500 MHz, $CDCl_3$) δ 7.72 (dd, J = 7.1, 2.5 Hz, 2H), 7.47 – 7.36 (m, 2H), 7.24 – 7.19 (m, 4H), 3.57 (ddd, J = 13.1, 8.2, 4.8 Hz, 2H), 3.36 (td, J = 8.8, 5.5 Hz, 2H), 3.13 (td, J = 8.6, 4.7 Hz, 2H), 2.89 (s, 6H), 2.31 (ddd, J = 13.4, 8.0, 5.6 Hz, 2H); ^{13}C NMR (125 MHz, $CDCl_3$) δ 197.4, 171.1, 137.4, 134.0, 131.9, 130.6, 129.0, 126.8, 69.3, 46.9, 30.9, 30.8; HRMS-APCI (m/z) $[M + H]^+$ calcd for $C_{23}H_{23}N_2O_3Cl_2^+$, 445.1086; found 445.1086.

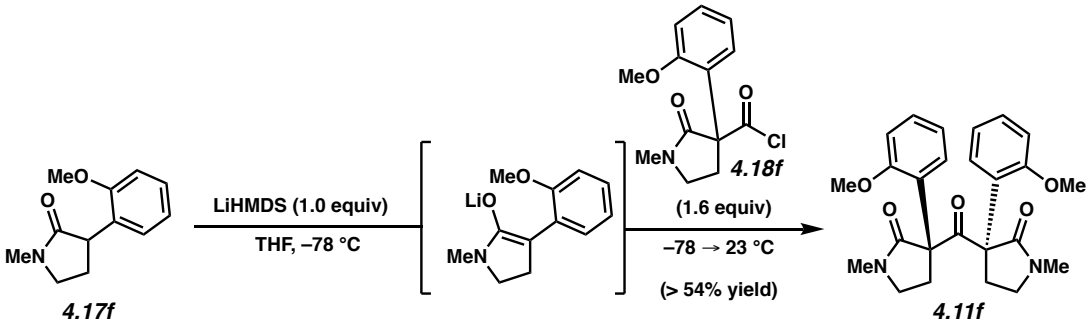

Ketone 4.11f. LiHMDS (1 M in THF, 2.29 mL, 383 mg, 2.29 mmol, 1.00 equiv) was added dropwise to a –78 °C solution of amide **4.17f** (470 mg, 2.29 mmol, 1.00 equiv) in THF (24 mL) and the mixture was then stirred for 45 min. A solution of acid chloride **4.18f** (990 mg, 3.7 mmol, 1.6 equiv) in THF (10 mL) was added dropwise over 5 min, the reaction was removed from the –78 °C bath, and then stirred at 23 °C for 15 min. The reaction was then poured into aq. HCl (0.5 M, 25 mL), the layers were separated, and the aqueous layer was extracted with CH_2Cl_2 (2 x 75 mL). The combined organic layers were dried over $MgSO_4$ and concentrated under reduced pressure directly onto silica gel (2 g). The crude product was then purified by flash column chromatography (15 g silica gel, 9:1 CH_2Cl_2:EtOAc → 7:3 CH_2Cl_2:EtOAc) to provide ketone **4.11f** (543 mg, 54% yield) as a white solid. Crystals suitable for X-ray diffraction studies (CCDC 2006463) were obtained as follows: pure ketone (30 mg) was dissolved in minimal $CHCl_3$ (~2 mL). *n*Hexane (~6 mL) was layered on top of $CHCl_3$ solution and the layers were allowed to slowly diffuse together over 3 days. Ketone **4.11f**: mp: 249.2–251.0 °C; R_f 0.20 (1:4 Hexanes:EtOAc); ^{1}H NMR (500 MHz, $CDCl_3$) δ 7.36 (dd, *J* = 7.7, 1.7 Hz, 2H), 7.30 (ddd, *J* = 8.2, 7.4, 1.7 Hz, 2H), 6.95 (dd, *J* = 8.2, 1.1 Hz, 2H), 6.92 (td, *J* = 7.6, 1.2 Hz, 2H), 3.85 (s, 6H), 3.37 – 3.24 (m, 4H), 3.15 – 3.05 (m, 2H), 2.87 (s, 6H), 2.26 – 2.12 (m, 2H); ^{13}C NMR (125 MHz, $CDCl_3$) δ 200.6, 172.1, 157.0, 129.4, 129.2, 128.9, 120.4, 112.0, 67.9, 55.4, 47.2, 31.3, 30.6; HRMS-APCI (m/z) $[M + H]^+$ calcd for $C_{25}H_{29}N_2O_5^+$, 437.2071; found 437.2028.

4.5.2.2 Photochemistry of Ketones 4.11.

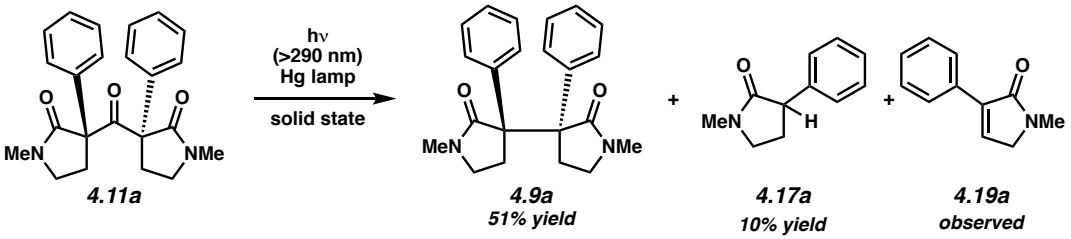

Bis(pyrrolidinone) 4.9a. Ketone **4.11a** (~ 1g) was dissolved in CH_2Cl_2 (~50 mL) and Hexanes (~30 mL) were added until the mixture became cloudy. This was allowed to evaporate over ~16 h. Once crystals had formed, the residual solvent was removed using a glass Pasteur pipette. The resultant crystalline solid was put under high vacuum (<1 mbar) for 1 h. A sample of crystalline **4.11a** (204mg, 0.542 mmol, 1.0 equiv) was placed between glass microscope slides. The slides were rubbed together for 10 seconds to crush **4.11a** into a thin layer of crystalline powder (Note 1). The glass slides were then clamped together using two binder clips. The solid sample was irradiated with a 450 W medium pressure Hg Hanovia UV lamp placed inside a water-cooled immersion-well Pyrex filter (Ace Glass, model 7857-05, $\lambda \geq 290$ nm; 53 mm external diameter, 220 mm full length, 150 mm depth) for 14 h. At this time, the sample was flipped over (to expose the other side of the solid to light) and then irradiated for another 12 h. The binder clips were then removed and a metal spatula was used to scrape the solid off of the glass slides into a vial. The slides and spatula were then rinsed with $CDCl_3$ (~15 mL) and the combined organics were concentrated under reduced pressure. The crude product was purified by flash column chromatography (24 g RediSep Gold, $CH_2Cl_2 \rightarrow$ 1:1 CH_2Cl_2:EtOAc) to give a bis(pyrrolidinone) **4.9a** (124 mg, 51% yield) and pyrrolidinone **4.17** (9.5 mg, 10% yield) (Note 2 & 3). Characterization data for **4.9a** and **4.17a** matched those previously reported in the literature.[26]

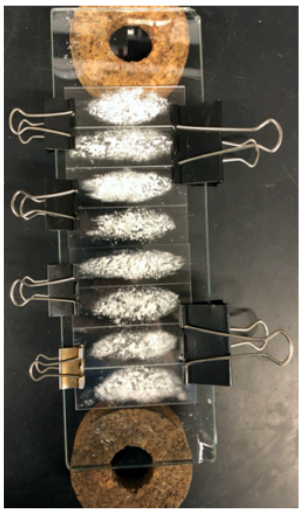

Before Irradiation

During Irradiation

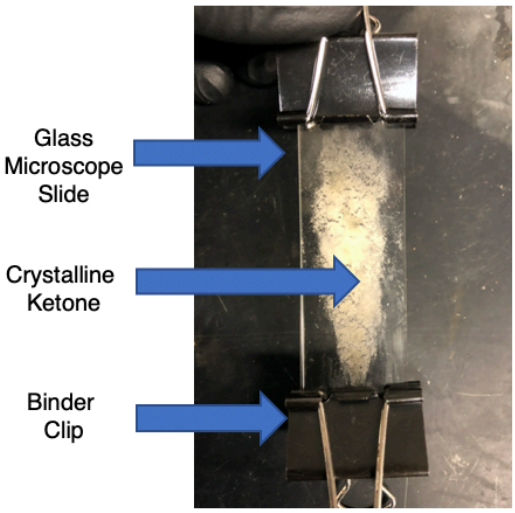

After Irradiation

Note 1: It is critical that the solid is crushed into a very thin layer to ensure adequate light penetration. In order to prevent overloading, several slides are irradiated in parallel w/ 20–30 mg of substrate between each pair of slides.

Note 2: Column chromatography is not sufficient to completely remove residual ***4.17a*** *from* ***4.9a****. In order to completely purify* ***4.9a*** *the partially pure material from the flash column is subjected to the following recrystallization conditions: Semi-pure* ***4.9*** *(oil) is dissolved in minimal* Et_2O *(~10 mL per 100 mg of semi-pure* ***4.9a****) and is placed in a –20 °C freezer for 1h. Mother liquor is removed with a Pasteur pipette and the resultant crystals are then rinsed with minimal –20 °C* Et_2O *(~1 mL). The mother liquor is then concentrated and resubjected to the same crystallization conditions (1x).*

Note 3: Due to difficulty of purifying ***4.17a*** *from the reaction mixture, an isolated yield was not obtained. The reported yield was determined based on the relative yield of* ***4.9a*** *in the* ^1H *NMR spectrum of the crude material and the isolated yield of* ***4.9a***

Note 4: In order to ensure that the crystal polymorph being irradiated was the same as the polymorph observed in the X-ray crystal structure, PXRD data was collected from the crystalline powder prior to irradiation.

General Procedure A (Photochemistry of 4.11c is used as an example).

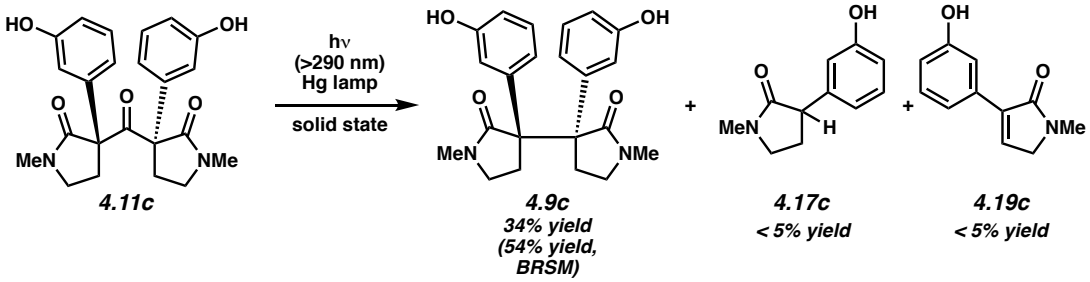

Bis(pyrrolidinone) 4.9c. Ketone **4.11c** (100–150 mg) was dissolved in MeOH (~10 mL). This was allowed to evaporate over ~16 h. A small sample of crystalline **4.11c** (22.7 mg, 55.7 μmol, 1.00 equiv) was placed between glass microscope slides. The slides were rubbed together for 10 seconds to crush **4.11c** into a thin layer of crystalline powder (Note 1). The two glass slides were then clamped together using two binder clips. The solid sample was irradiated with a 450 W medium pressure Hg Hanovia UV lamp placed inside a water-cooled immersion-well Pyrex filter (Ace Glass, model 7857-05, $\lambda \geq 290$ nm; 53 mm external diameter, 220 mm full length, 150 mm depth) for 14 h (see Note 3 for reaction monitoring). At this time, the sample was flipped over (to expose the other side of the solid to light) and then irradiated for another 12 h. The binder clips were then removed and a metal spatula was used to scrape the solid off of the glass slides into a vial. The slides and spatula were then rinsed with $CDCl_3$ (~15 mL) and the resultant solution was concentrated under reduced pressure to give a bis(pyrrolidinone) **4.9c** (7.46 mg, 35% yield, 54% yield based on recovered starting material). (Yield determined by ^{1}H QNMR with dimethyl terephthalate as the external standard). Bis(pyrrolidinone) **4.9c**: R_f 0.49 (EtOAc); ^{1}H NMR (500

MHz, Methanol-d_4) δ 7.10 (t, J = 7.9 Hz, 2H), 6.76 (t, J = 2.2 Hz, 2H), 6.73 (ddd, J = 8.0, 2.4, 0.8 Hz, 2H), 6.69 (ddd, J = 7.8, 1.7, 0.7 Hz, 2H), 3.21 – 3.13 (m, 2H), 2.91 – 2.82 (m, 2H), 2.80 (s, 6H), 1.79 (dd, J = 12.4, 5.5 Hz, 2H); ^{13}C NMR (125 MHz, Methanol-d_4) δ 178.0, 158.0, 139.3, 129.6, 121.4, 117.4, 115.5, 57.1, 46.8, 30.9, 30.3; HRMS-APCI (m/z) $[M + H]^+$ calcd for $C_{22}H_{25}N_2O_4^+$, 381.1809; found 318.1800.

One methylene proton is obscured by residual MeOH-d_4 signal but is inferred by HSQC spectrum.

Note 1: It is critical that the solid is crushed into a very thin layer to ensure adequate light penetration. In order to prevent overloading, no more than 14 mg is placed between two slides. For larger scale reactions, several slides are run in parallel w/ 10–15 mg of substrate between each pair of slides.

Note 2: The 450W Hg lamp produces significant heat. This is mitigated by the jacket of cooling water and fans to circulate warm air out of the box containing the irradiation setup.

Note 3: This particular reaction was not monitored by TLC in order to ensure accurate yield determination. In general, to monitor the reaction by TLC, a very small aliquot (<0.1 mg) of solid is removed with the tip of a glass Pasteur pipette. This solid is then dissolved in ~1 drop of MeOH and analyzed by TLC.

Note 4: While some of the mass balance is attributed to unidentified decomposition products, a substantial amount of insoluble yellow solid is produced. The identity of this material is unknown.

Note 5: In order to ensure that the crystal polymorph being irradiated was the same as the polymorph observed in the X-ray crystal structure, PXRD data was collected from the crystalline powder prior to irradiation.

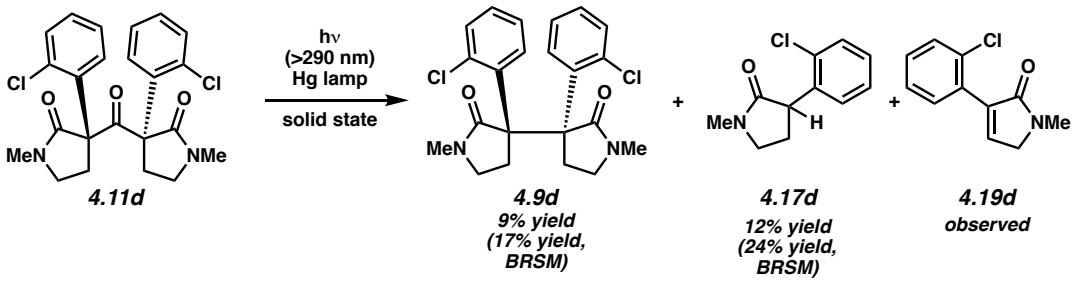

Bis(pyrrolidinone) 4.9d. Followed General Procedure A using ketone **4.11d** (39.3 mg, 73.5 μmol, 1.00 equiv) to afford bis(pyrrolidinone) **4.9d** (5.60 mg, 9% yield, 17% yield based on recovered starting material) and pyrrolidinone **4.17d** (3.80 mg, 12% yield, 24% yield based on recovered starting material). (Yields determined by ^{1}H QNMR with dimethyl terephthalate as the external standard). Bis(pyrrolidinone) **4.9d**: R_f 0.25 (1:1 Hexanes:EtOAc); ^{1}H NMR (500 MHz, $CDCl_3$) δ 7.43 (dd, *J* = 8.0, 1.5 Hz, 2H), 7.23 (d, *J* = 8.1 Hz, 2H), 7.16 (td, *J* = 7.7, 1.6 Hz, 2H), 7.01 (td, *J* = 7.9, 1.5 Hz, 2H), 3.58 (td, *J* = 9.0, 4.8 Hz, 2H), 3.50 – 3.26 (m, 4H), 2.81 (s, 6H), 2.62 (ddd, *J* = 13.1, 10.2, 4.8 Hz, 2H); ^{13}C NMR (125 MHz, $CDCl_3$) δ 173.4, 140.1, 134.7, 134.3, 132.23, 128.2, 124.9, 59.4, 48.1, 30.7, 30.4; HRMS-APCI (m/z) $[M + H]^+$ calcd for $C_{22}H_{23}N_2O_2Cl_2^+$, 417.1131; found 417.1117.

Note 1: Prior to conducting the solid-state photodecarbonylation, ***4.11d*** *was crystallized as follows: An amorphous sample of* ***4.11d*** *(~100 mg) was dissolved in minimal Et_2O (~50 mL) and then sonicated until the solution became cloudy (due to precipitation of crystals). The sample was allowed to evaporate under ambient conditions and the resultant white powder was put under high vacuum (< 1 mbar) for 1 h to ensure complete removal of the solvent.*

Note 2: While some of the mass balance is attributed to disproportionation and unidentified decomposition products, a substantial amount of insoluble yellow solid is produced. The identity of this material is unknown.

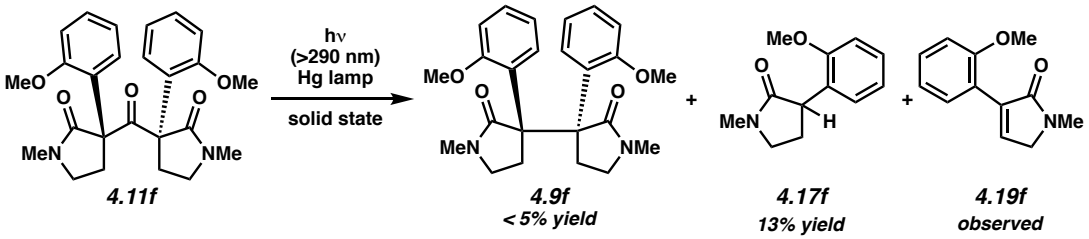

Photochemistry of 4.11f. Ketone **4.11f** (100–150 mg) was dissolved in CH_2Cl_2 (~15 mL) and Hexanes (~5 mL) were added until the mixture became cloudy. This was allowed to evaporate over ~16 h. Once crystals had formed, the residual solvent was removed using a glass Pasteur pipette. The resultant crystalline solid was put under high vacuum (< 1 mbar) for 1 h. Crystalline **4.11f** (48.8 mg, 0.111 mmol, 1.00 equiv) was split into two portions and each was added to a separate 4-dram vial (Note 1). To each vial, an aqueous solution of SDS (0.7 mg/mL, 10 mL) was added in one portion and the suspension was sonicated for 5 min at 23 °C (Note 2). The vials were equipped with stirbars, sealed with screwcaps, and irradiated (with rapid stirring) with a 450 W medium pressure Hg Hanovia UV lamp placed inside a water-cooled immersion-well Pyrex filter (Ace Glass, model 7857-05, $\lambda \geq 290$ nm; 53 mm external diameter, 220 mm full length, 150 mm depth) for 26 h. The mixture was then poured into sat. aq. NaCl (30 mL) and extracted with EtOAc (3 x 20 mL). The combined organic layers were dried over $MgSO_4$ and concentrated under reduced pressure to provide disproportionation product **4.17f** (2.90 mg, 13% yield). (Yield determined by ^{1}H QNMR with dimethyl terephthalate as the external standard).

Note 1: It is important that the crystalline solid be crushed into a fine powder before solvent is added. This can be done with a metal spatula.

*Note 2: This reaction proceeds exceptionally slowly. In order to obtain appreciable conversion, it is necessary to maximize substrate surface area. Sonication in SDS $_{(aq)}$ gives **4.11f** crystals a well-suspended, powdery consistency.*

Note 3: While some of the mass balance is attributed to disproportionation and unidentified decomposition products, a substantial amount of insoluble yellow solid is produced. The identity of this material is unknown.

Note 4: In order to ensure that the crystal polymorph being irradiated was the same as the polymorph observed in the X-ray crystal structure, PXRD data was collected from the crystalline powder prior to irradiation.

4.5.2.3 Synthesis of Ketones 4.27, 4.28, & 4.29.

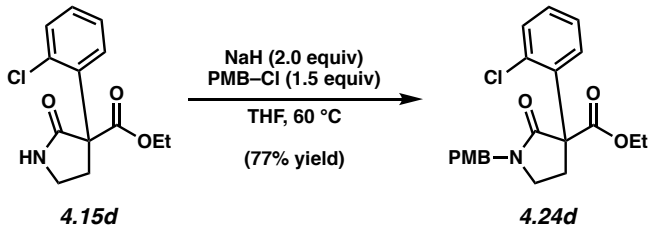

4.15d *4.24d*

PMB Pyrrolidinone 4.24d. To a solution of pyrrolidinone **4.15d** (3.01 g, 11.2 mmol, 1.00 equiv) in THF (110 mL), was added NaH (900 mg, 23 mmol, 2.0 equiv, 60% dispersion in mineral oil) with stirring. The reaction was stirred at 23 °C for 5 min and 4-methoxybenzyl chloride (2.27 mL, 2.63 g, 16.8 mmol, 1.50 equiv) was added dropwise over 3 min via syringe. The reaction was placed in a preheated 60 °C oil bath and stirred for 100 min before being removed from heat. The reaction was cooled to 0 °C and quenched by the addition of aq. HCl (0.5 M, 50 mL). The reaction mixture was poured into sat. aq. NaCl (200 mL) and the layers were separated. The aqueous layer was extracted with CH_2Cl_2 (2 x 100 mL) and the combined organic layers were dried over $MgSO_4$ and concentrated under reduced pressure directly onto silica gel (6 g). The crude product was purified by flash column chromatography (12 g silica gel, 9:1 Hexanes:EtOAc → 7:3 Hexanes:EtOAc) to provide the protected PMB pyrrolidinone **4.24d** as a viscous oil (3.35 g, 77%

yield). PMB Pyrrolidinone **4.24d**: R_f 0.58 (1:1 Hexanes:EtOAc); ^{1}H NMR (500 MHz, $CDCl_3$) δ 7.39 – 7.35 (m, 1H), 7.35 – 7.32 (m, 1H), 7.24 – 7.18 (m, 4H), 6.92 – 6.82 (m, 2H), 4.58 (d, *J* = 14.5 Hz, 1H), 4.46 (d, *J* = 14.5 Hz, 1H), 4.32 – 4.16 (m, 2H), 3.79 (s, 3H), 3.40 – 3.25 (m, 2H), 3.15 – 2.99 (m, 1H), 2.23 – 2.10 (m, 1H), 1.22 (t, *J* = 7.1 Hz, 3H); ^{13}C NMR (125 MHz, $CDCl_3$) δ 170.4, 170.2, 159.4, 137.7, 133.8, 130.6, 129.8, 128.9, 128.8, 128.0, 127.1, 114.3, 62.5, 62.2, 55.4, 47.1, 43.9, 31.0, 14.1; HRMS-APCI (m/z) $[M + H]^+$ calcd for $C_{21}H_{23}NO_4Cl^+$, 388.1310; found 388.1294.

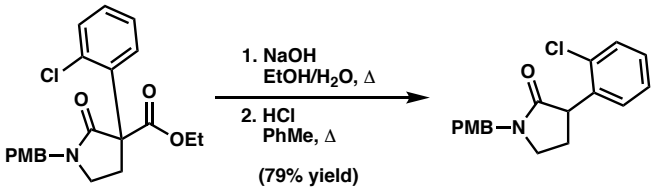

4.24d *4.25d*

PMB Pyrrolidinone 4.25d. To a solution of pyrrolidinone **4.24d** (0.46 g, 1.20 mmol, 1.0 equiv) in EtOH (10 mL), was added aq. NaOH (1 M, 15 mL). The reaction was placed in a preheated 100 °C oil bath, stirred at reflux for 20 min, and then cooled to 23 °C. Aq. HCl (1.5 mL, 12 M) was added followed by PhMe (12 mL). The reaction was placed in a preheated 100 °C oil bath, stirred at reflux for 3 h, and then cooled to 23 °C. The reaction was diluted with CH_2Cl_2 (100 mL) and the layers were separated. The aqueous layer was extracted with CH_2Cl_2 (2 x 50 mL) and the combined organic layers were dried over $MgSO_4$ and then concentrated under reduced pressure directly onto silica gel (1 g). The crude product was purified by flash column chromatography (5 g silica gel, 9:1 Hexanes:EtOAc → 3:2 Hexanes:EtOAc) to provide the PMB pyrrolidinone **4.25d** as a viscous oil (297 mg, 79% yield). PMB pyrrolidinone **4.25d**: R_f 0.59 (1:1 Hexanes:EtOAc); ^{1}H NMR (500 MHz, $CDCl_3$) δ 7.37 (dd, *J* = 7.8, 1.4 Hz, 1H), 7.26 – 7.17 (m, 5H), 6.95 – 6.84 (m, 2H), 4.58 (d, *J* = 14.4 Hz, 1H), 4.43 (d, *J* = 14.3 Hz, 1H), 4.15 (t, *J* = 9.2 Hz, 1H), 3.82 (s, 3H), 3.41 – 3.18 (m, 2H), 2.62 – 2.44 (m, 1H), 1.93 (dq, *J* = 12.9, 8.6 Hz, 1H); ^{13}C NMR (125 MHz,

$CDCl_3$) δ 174.0, 159.3, 138.0, 134.4, 129.9, 129.8, 129.6, 128.7, 128.5, 127.4, 114.2, 55.5, 46.7, 46.5, 44.7, 27.3; HRMS-APCI (m/z) $[M + H]^+$ calcd for $C_{18}H_{19}NO_2Cl^+$, 316.1099; found 316.1086.

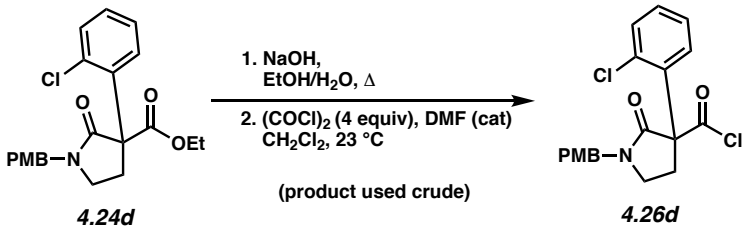

4.24d *4.26d*

PMB Acid Chloride 4.26d. To a solution of pyrrolidinone **4.24d** (550 mg, 1.4 mmol, 1.0 equiv) in EtOH (10 mL), was added aq. NaOH (1 M, 15 mL). The reaction was placed in a preheated 100 °C oil bath, stirred at reflux for 10 min, and then cooled to 23 °C. The reaction mixture was poured into aq. HCl (1 M, 30 mL). The layers were separated, the aqueous layer was extracted with CH_2Cl_2 (3 x 75 mL), and the combined organic layers were dried over $MgSO_4$ and concentrated under reduced pressure. The resultant carboxylic acid was carried forward to the next step.

To neat carboxylic acid from the previous step, was added 1 drop of DMF from a glass Pasteur pipette followed by CH_2Cl_2 (16 mL). Oxalyl chloride (0.54 mL, 790 mg, 6.2 mmol, 4.0 equiv) was added dropwise over 1 min, the reaction was stirred at 23 °C for 90 min, and then the mixture was concentrated under reduced pressure. The resultant oil was dissolved in PhMe (20 mL) and concentrated under reduced pressure (x2). The crude oil was then put under vacuum (< 1 mbar) for 1 h. Crude acid chloride **4.26d** was used immediately without further purification.

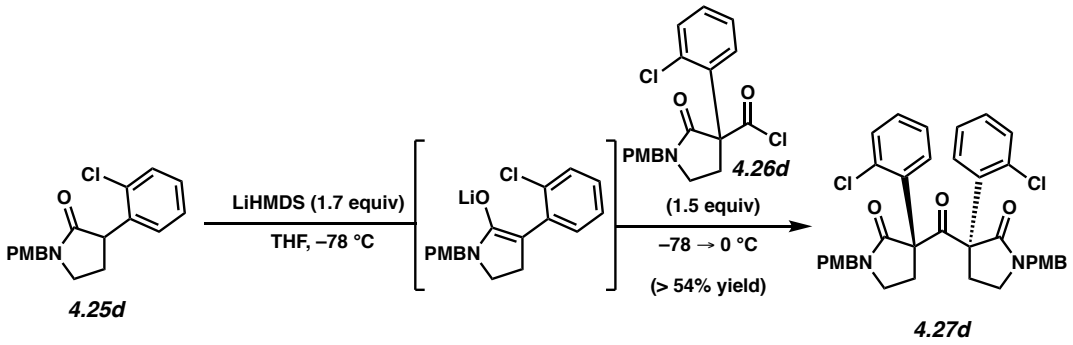

PMB Ketone 4.27d. To a solution of pyrrolidinone **4.25d** (287 mg, 0.909 mmol, 1.00 equiv) in THF (10 mL) at –78 °C was added a solution of LiHMDS (1 M in THF, 1.55 mL, 260 mg, 1.55 mmol, 1.70 equiv) dropwise over 1 minute. The reaction was stirred for 30 min and then a solution of acid chloride **4.26d** (540 mg, 1.4 mmol, 1.5 equiv) in THF (5 mL) was added dropwise over 5 min and the reaction was immediately removed from the –78 °C bath, placed in a 0 °C bath, and the reaction was stirred for 5 min. The reaction was quenched at 0 °C by the addition of aq. HCl (0.5 M, 5 mL) and poured into a biphasic mixture of DI H_2O (50 mL) and CH_2Cl_2 (75 mL). The layers were separated, and the aqueous layer was extracted with CH_2Cl_2 (2 x 50 mL). The combined organic layers were dried over $MgSO_4$ and concentrated under reduced pressure directly onto silica gel (2 g). The crude product was purified by flash column chromatography (20 g silica gel, 4:1 Hexanes:EtOAc) to give ketone PMB ketone **4.27d** (443 mg, 74% yield) as a white foam. PMB ketone **4.27d**: R_f 0.58 (1:1 Hexanes:EtOAc); ^{1}H NMR (500 MHz, $CDCl_3$) δ 7.77 (dd, *J* = 7.1, 2.4 Hz, 2H), 7.53 – 7.37 (m, 2H), 7.34 – 7.07 (m, 8H), 6.99 – 6.72 (m, 4H), 4.98 (d, *J* = 14.6 Hz, 2H), 4.00 (d, *J* = 14.6 Hz, 2H), 3.79 (s, 6H), 3.56 (ddd, *J* = 13.2, 8.1, 5.1 Hz, 2H), 3.26 (td, *J* = 8.7, 5.4 Hz, 2H), 2.99 (ddd, *J* = 9.5, 8.0, 5.1 Hz, 2H), 2.32 (ddd, *J* = 13.3, 7.9, 5.4 Hz, 2H); ^{13}C NMR (125 MHz, $CDCl_3$) δ 197.4, 171.1, 159.2, 137.0, 134.0, 131.9, 130.7, 129.9, 129.1, 128.2, 126.7, 114.2, 69.8, 55.4, 47.6, 44.4, 30.7; HRMS-APCI (m/z) $[M + H]^+$ calcd for $C_{37}H_{35}N_2O_5Cl_2^+$, 657.1918; found 657.1902.

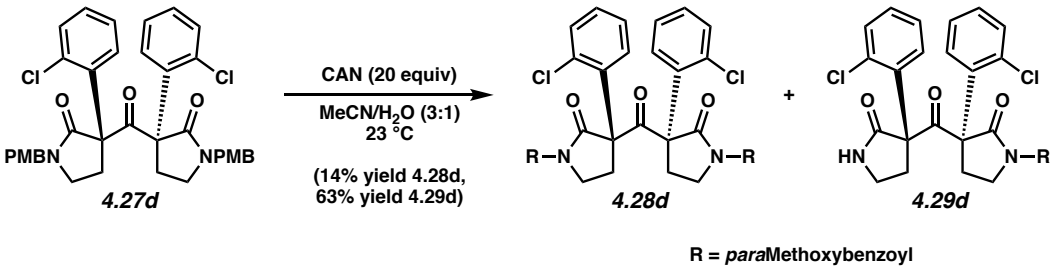

Ketones 4.28d & 4.29d. Ketone **4.27d** (1.70 g, 2.59 mmol, 1.00 equiv) was dissolved in MeCN (275 mL). Once solid was completely dissolved, DI H_2O (90 mL) was added. To this stirring mixture was added CAN (28.1 g, 51.3 mmol, 20.0 equiv) in a single portion and the reaction was allowed to stir at 23 °C for 105 min before being poured into a biphasic mixture of H_2O (800 mL) and CH_2Cl_2 (400 mL). The layers were separated and the aqueous layer was washed with CH_2Cl_2 (2 x 300 mL). The combined organic layers were dried over $MgSO_4$ and concentrated directly onto silica gel (4 g). The crude product was then purified by flash column chromatography (20 g silica gel, 4:1 Hexanes:EtOAc → 3:1 Hexanes:EtOAc) to furnish ketone **4.28d** (241 mg, 14% yield) and ketone **4.29d** (1.11g, 63% yield). Crystals of both **4.28d** (reactive polymorph, CCDC 2006465) and **4.29d** (CCDC 2006466) suitable for X-ray diffraction studies were obtained as follows: pure ketone (30 mg) was dissolved in minimal $CHCl_3$ (~2 mL) *n*Hexane (~6 mL) was layered on top of $CHCl_3$ solution and the layers were allowed to slowly diffuse together over 3 days. Crystal of **4.28d** (unreactive polymorph, CCDC 2006467) was grown via slow evaporation from CH_2Cl_2.

Ketone 4.28d: R_f 0.58 (1:1 Hexanes:EtOAc); ^{1}H NMR (500 MHz, $CDCl_3$) δ 7.67 – 7.59 (m, 6H), 7.48 (dd, *J* = 7.7, 1.7 Hz, 2H), 7.32 (td, *J* = 7.5, 1.8 Hz, 2H), 7.28 (td, *J* = 7.6, 1.7 Hz, 2H), 6.86 – 6.76 (m, 4H), 3.94 – 3.83 (m, 2H), 3.76 (s, 6H), 3.54 (dt, *J* = 13.3, 7.0 Hz, 2H), 3.45 (dt, *J* = 10.8, 6.8 Hz, 2H), 2.55 (ddd, *J* = 12.7, 7.0, 5.5 Hz, 2H); ^{13}C NMR (125 MHz, $CDCl_3$) δ 194.7, 172.5, 169.4, 163.0, 134.7, 133.8, 132.4, 131.9, 130.4, 129.9, 127.2, 126.0, 113.4, 71.2, 55.4, 45.3, 30.0; HRMS-APCI (m/z) $[M + H]^+$ calcd for $C_{37}H_{31}N_2O_7Cl_2^+$, 685.1503; found 685.1516.

Ketone 4.29d: R_f 0.51 (1:1 Hexanes:EtOAc); ^{1}H NMR (500 MHz, $CDCl_3$) δ 7.92 – 7.79 (m, 3H), 7.52 – 7.39 (m, 3H), 7.32 – 7.26 (m, 3H), 7.22 (td, *J* = 7.6, 1.5 Hz, 1H), 6.99 – 6.92 (m, 2H), 5.56 (s, 1H), 3.95 – 3.82 (m, 4H), 3.59 – 3.43 (m, 3H), 3.26 (tdd, *J* = 8.0, 4.9, 1.6 Hz, 1H), 3.05 (ddd, *J* = 9.4, 7.4, 5.8 Hz, 1H), 2.64 – 2.49 (m, 2H); ^{13}C NMR (125 MHz, $CDCl_3$) δ 195.7, 174.5, 172.0, 169.8, 162.7, 135.2, 135.1, 134.2, 133.4, 132.1, 131.9, 131.9, 130.7, 130.5, 129.5, 129.4, 127.0, 126.9, 126.7, 113.0, 71.6, 67.7, 55.4, 44.5, 39.5, 33.1, 29.5; HRMS-APCI (m/z) $[M + H]^+$ calcd for $C_{29}H_{25}N_2O_5Cl_2^+$, 551.1135; found 551.1141.

Note 1: The workup in this reaction makes a very challenging emulsion. This was partially mitigated by simply collecting all three organic layers (from three washes) as somewhat of an emulsion and only discarding the layer that was mostly aqueous and did not contain substantial organic emulsion. To this emulsion was added copious $MgSO_4$. This caused emulsion to dissipate. The organic layer here was collected.

Note 2: It is absolutely critical for the subsequent solid-state photochemistry that this solid is completely pure. It is recommended that, after chromatography, this be recrystallized. This can be done either from 1:1 Hexanes:EtOAc or via layer diffusion (Bottom layer = CH_2Cl_2, top layer = n-Hexane).

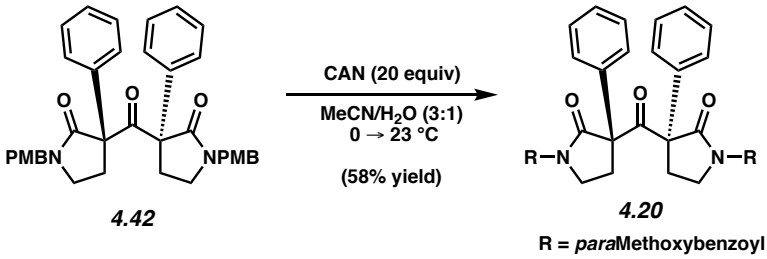

4.42 ***4.20***

R = *para*Methoxybenzoyl

Ketone 4.20. A solution of ketone **4.42**[26] (90 mg, 0.15 mmol, 1.0 equiv) was dissolved in MeCN (15 mL) and DI H_2O (5 mL) and cooled to 0 °C. CAN (1.7 g, 3.0 mmol, 20 equiv) was added and the reaction was stirred for 90 min before being allowed to warm to 23 °C. After being stirred at

23 °C for 30 min, the reaction was poured into a mixture of H_2O (100 mL) and CH_2Cl_2 (100 mL). The layers were separated and the organic layer was washed with CH_2Cl_2 (2 x 100 mL). The combined organic layers were dried over $MgSO_4$ and concentrated directly onto silica gel. The crude product was then purified by flash column chromatography (9:1 Hexanes:EtOAc → 7:3 Hexanes:EtOAc) to furnish ketone **4.20** (55 mg, 58% yield). Crystals suitable for X-ray diffraction analysis were grown via slow evaporation from $CDCl_3$/n–Hexane (CCDC 2006460), EtOAc/*n*–Hexane (CCDC 2006464), and EtOH (CCDC 2006468). Ketone **4.20**: R_f 0.55 (1:1 Hexanes:EtOAc); ^{1}H NMR (500 MHz, $CDCl_3$) δ 7.68 – 7.63 (m, 4H), 7.35 – 7.29 (m, 6H), 7.19 – 7.12 (m, 4H), 6.92 – 6.85 (m, 4H), 3.94 – 3.78 (m, 8H), 3.55 (ddd, *J* = 10.7, 8.5, 6.8 Hz, 2H), 3.15 (dt, *J* = 13.2, 8.1 Hz, 2H), 2.20 (ddd, *J* = 13.1, 6.5, 3.6 Hz, 2H); ^{13}C NMR (125 MHz, $CDCl_3$) δ 200.1, 171.9, 169.7, 163.3, 134.9, 132.0, 129.2, 128.5, 127.4, 125.9, 113.4, 69.3, 55.6, 44.1, 30.8; HRMS-APCI (m/z) $[M + H]^+$ calcd for $C_{37}H_{33}N_2O_7^+$, 617.2282; found 617.2268.

4.5.2.4 Photodecarbonylation of Ketones 28d and 29d.

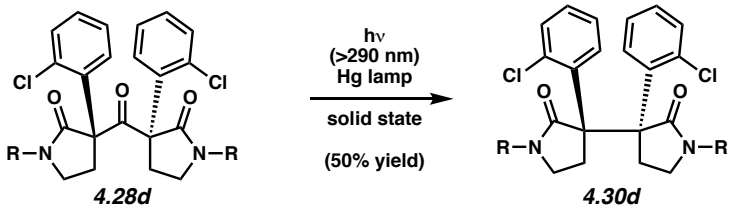

R = *para*-Methoxybenzoyl

Bis(pyrrolidinone) 4.30d. Ketone **4.28d** (96 mg) was suspended in Et_2O (~15 mL) and sonicated for 1 min. During sonication, clear suspension rapidly turned white/cloudy. This was allowed to evaporate under ambient conditions until visible Et_2O was gone at which point the resultant white solid was placed under high vacuum (< 1 mbar) for 2h. A small portion of **4.28d** (18.6 mg, 27.1 μmol, 1.00 equiv) was suspended in THF (1.0 mL) (Note 1) and added to a vortexing solution of aq. SDS (0.7 mg/mL, 7mL) (Note 2). The reaction was transferred to a 4-dram vial with rapid

stirring, giving a suspension of ketone **4.28d**. This suspension was irradiated with a 450 W medium pressure Hg Hanovia UV lamp placed inside a water-cooled immersion-well Pyrex filter (Ace Glass, model 7857-05, $\lambda \geq 290$ nm; 53 mm external diameter, 220 mm full length, 150 mm depth) for 21 h. The reaction was poured into a biphasic mixture of sat. aq. NaCl (20 mL) and EtOAc (20 mL). The layers were separated, and the aqueous layer was extracted with EtOAc (2 x 20 mL). The combined organic layers were dried over $MgSO_4$ before being concentrated under reduced pressure directly onto silica gel (200 mg). The crude product was purified by flash column chromatography (2 g silica gel, 9:1 Hexanes:EtOAc → 7:3 Hexanes:EtOAc) to give the bis(pyrrolidinone) **4.30d** as a white solid (9.01 mg, 50% yield). Crystals suitable for X-ray diffraction studies (CCDC 2006469) were prepared by evaporation for toluene-d_8 (Note 3). Bis(pyrrolidinone) **4.30d**: R_f 0.56 (1:1 Hexanes:EtOAc); ^{1}H NMR (600 MHz, Toluene-d_8) δ 7.83 – 7.74 (m, 4H), 7.31 (s, 2H), 7.14 (dd, J = 7.9, 1.5 Hz, 2H), 6.78 (td, J = 7.6, 1.5 Hz, 2H), 6.76 – 6.71 (m, 6H), 3.97 – 3.75 (m, 4H), 3.42 (dt, J = 13.7, 8.1 Hz, 2H), 3.32 (s, 6H), 2.82 (s, 2H); ^{13}C NMR (151 MHz, Toluene-d_8) δ 175.0, 169.8, 163.5, 135.6, 134.4, 133.3, 132.5, 132.2, 128.4, 126.0, 113.7, 62.0, 55.1, 44.2, 28.9; HRMS-APCI (m/z) $[M + H]^+$ calcd for $C_{37}H_{31}N_2O_6Cl_2^+$, 657.1554; found 657.1538.

*Note 1: Solid **4.28d** did not fully dissolve in THF prior to being added into the aq. solution of SDS and was instead a milky-white suspension.*

Note 2: Vortexing SDS solution: A 25 mL culture tube containing 7 mL SDS solution (0.7 mg/mL in DI H_2O) was placed on a Thermo-Fischer Maxi-Mix® 0.5 W, 60 Hz vortex mixer. Once the aq. solution was rapidly vortexing, the solution of ketone in SDS was added dropwise from a syringe.

Note 3: After collecting NMR spectra at 100 °C a small amount of in toluene-d_8 evaporated and resulted in the growth of high-quality crystals (on the walls of the NMR tube) which were submitted directly for X-ray diffraction analysis.

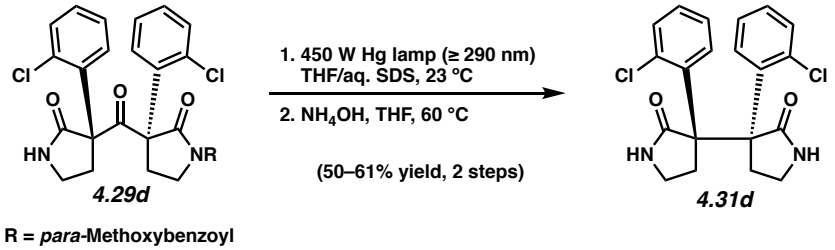

R = *para*-Methoxybenzoyl

Bis(pyrrolidinone) 4.31d. A solution of ketone **4.29d** (77.1 mg, 0.140 mmol, 1.00 equiv) dissolved in THF (6 mL) was added dropwise into a vortexing aqueous solution of sodium dodecyl sulfate (0.7 mg/mL, 40 mL) (see Note 1 for vortexing procedure). The resultant suspension was irradiated with a 450 W medium pressure Hg Hanovia UV lamp placed inside a water-cooled immersion-well Pyrex filter (Ace Glass, model 7857-05, $\lambda \geq 290$ nm; 53 mm external diameter, 220 mm full length, 150 mm depth) for 49 h (see Note 3 for reaction monitoring). The reaction was poured into a biphasic mixture of sat. aq. NaCl (50 mL) and EtOAc (50 mL). The layers were separated and the aqueous layer was extracted with EtOAc (3 x 25 mL). The combined organic layers were dried over Na_2SO_4 before being concentrated under reduced pressure. Residual SDS was removed by flushing the crude oil over a short silica plug (5 cm) with EtOAc (50 mL) and the resultant solution was concentrated under reduced pressure and used without further purification.

To a solution of the crude photoproduct in THF (20 mL) in a heavy-walled tube, NH_4OH (30–32% w/v, 1.0 mL) was added. The vessel was sealed with a Teflon screwcap, submerged in an oil bath preheated to 65 °C and stirred for 90 min. The reaction was allowed to cool to 23 °C and was diluted with CH_2Cl_2 (30 mL). H_2O (50 mL) was added and the layers were separated. The aqueous layer was extracted with CH_2Cl_2 (3 x 30 mL) and the combined organic layers were dried over Na_2SO_4 and then concentrated under reduced pressure directly onto silica gel (0.5 g). The

crude product was purified by flash column chromatography (4 g silica gel, 1:1 Hexanes:EtOAc → 100% EtOAc) to give the bis(pyrrolidinone) **4.31d** as a glassy solid (29.4 mg, 54% yield). Yields ranged from 50–61%. Bis(pyrrolidinone) **4.31d**: R_f 0.42 (EtOAc); ^{1}H NMR (600 MHz, $CDCl_3$) δ 8.48 (s, 2H), 7.47 (dd, *J* = 8.0, 1.3 Hz, 2H), 7.34 – 7.26 (m, 2H), 7.19 (t, *J* = 7.5 Hz, 2H), 7.03 (t, *J* = 7.4 Hz, 2H), 3.56 (td, *J* = 9.9, 3.2 Hz, 2H), 3.43 (ddd, *J* = 13.5, 9.9, 3.4 Hz, 2H), 3.35 (td, *J* = 9.2, 4.4 Hz, 2H), 2.75 (ddd, *J* = 14.2, 10.4, 4.4 Hz, 2H); ^{13}C NMR (125 MHz, $CDCl_3$) δ 178.4, 139.5, 135.0, 134.7, 132.4, 128.5, 125.0, 59.8, 41.1, 33.5; HRMS-APCI (m/z) $[M + H]^+$ calcd for $C_{20}H_{19}Cl_2N_2O_2^+$, 389.0818; found, 389.0810.

Note 1: Vortexing SDS solution: A 100 mL graduated cylinder containing 40 mL SDS solution (0.7 mg/mL in DI H_2O) was placed on a Thermo-Fischer Maxi-Mix® 0.5 W, 60 Hz vortex mixer. Once the aq. solution was rapidly vortexing, the solution of ketone in SDS was added dropwise from a syringe (see image below).

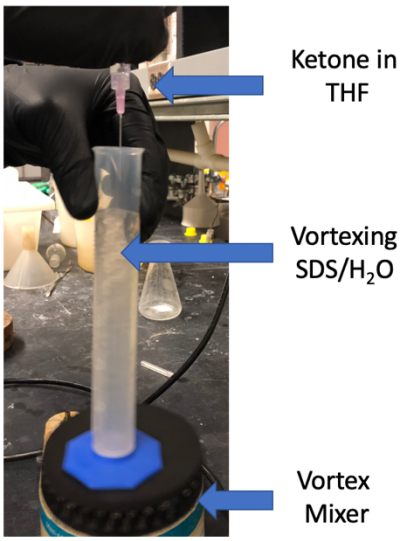

Note 2: During the reaction, the solids have a tendency to become clumped on the side of the glass. This aggregation limits surface area and slows reaction progress. To mitigate this problem, the

reaction is stopped every ~4–8 h and the aggregated solid broken up by swirling the solution rapidly with a glass pipette.

Note 3: It is critical to monitor this reaction by aliquots using ^{1}H NMR analysis as reaction times can vary based on how much solid adheres to the glass. Aliquots are collected as follows: 0.5 mL of the suspension was removed from the reaction mixture and poured into a culture tube with sat. aq. NaCl (1 mL). This mixture was extracted with EtOAc (2 x 2 mL). The combined organic layers were dried over Na_2SO_4 and then flushed through a plug of silica gel (~3 cm) with EtOAc (10 mL). It is important to flush through silica gel prior to collection of NMR spectrum as it removes residual SDS. If this is not done, the ^{1}H NMR resonances become very broad as a result of the SDS and it is difficult to ascertain reaction conversion.

Note 4: It is critical to maintain rapid stirring so that the solids remain suspended throughout the course of the reaction.

Note 5: The 450W Hg lamp produces significant heat. This is mitigated by the jacket of cooling water and fans to circulate warm air out of the box containing the irradiation setup.

*Note 6: Bis(pyrrolidinone) **4.30d** is difficult to visualize by TLC analysis. Very concentrated solutions may be visualized on TLC with a 254 nm handheld UV-lamp.*

4.5.3 Computational Section

The reaction mechanism was studied using density functional theory (DFT). All quantum mechanics calculations were performed with Gaussian 09.[44] Atomic coordinates were extracted from the X-ray diffraction data. The ONIOM[32] approach within the hybrid QM/MM[34] method was employed to account for the intermolecular interactions within the crystal lattice environment. The central layer was a single molecule described at unrestricted closed-shell dispersion-corrected ωB97X-D/6-311G(d,p) level. The surrounding shell of molecules extracted from the experimentally determined crystal structure was used as the low layer with electronically embedded UFF. We favor the employment of a molecular mechanics method to describe the low-level layer (over semiempirical methods or quantum chemical calculations with very small basis sets) since the MM force field by definition includes a description of dispersion effects between all atoms in the MM region and between QM and MM regions. Indeed, this hybrid approach has been shown to be accurate in computational studies of solid-state transformations of stilbene where crystalline environment calculations were included in the low-level layer. Vibrational frequencies were computed at the QM/MM level to determine if the optimized structures are minima or saddle points on the potential energy surface corresponding to minima and transition state geometries, respectively. Transition structures have been verified by intrinsic reaction coordinate (IRC) calculations. The partitioning of atoms into the two layers is shown in **Figure S1** using a "ball-and-stick" representation for the atoms treated by the DFT method and a "wire" representation for the atoms in the low-level layer.

Some initial energy minimization calculations were done on the isolated molecules in the gas phase. We mimicked Norrish Type I photodecarbonylation by removing carbonyl moiety and allowing the two radical fragments to relax to their ground state (GS) geometries. In all instances

geometry optimization led to radical recombination for all studied *ortho*- and *meta*-substituted systems. The success of GS optimization for radical fragments was critically dependent on embedding them in their respective crystal cavities. Our computational model entailed the two radical fragments surrounded by the shell of ketones, as determined by X-ray diffraction studies. Carbon monoxide moiety was excluded from the computational model. Performing energy minimization yielded a GS structure with the two fragments positioned at the ~2.7Å distance. A relaxed scan for bond association between the two fragments was performed to map out the potential energy profile for recombination and predict the transition state (TS) structure. Frequency calculations for the TS structures yielded one imaginary frequency corresponding to the in-plane asymmetric stretching of the two radical fragments. In all instances, the radicals were ~2.5Å distance apart. The calculated electronic barriers supported the experimental trend and were in the range of ~2–5 kcal/mol for systems that show high selectivity and 6–7 kcal/mol for systems that show low recombination selectivity. We hypothesize that the origin of the chemoselectivity is directly related to the conformation adopted by the reactants in the crystal cavity and the intramolecular steric hindrance, which creates a 2–7 kcal/mol barrier for radical recombination.

4.5.4 Powder X-ray Diffraction Data

Figure 4.11. Simulated and experimental PXRD patterns of ketone **4.11a** before solid-state irradiation.

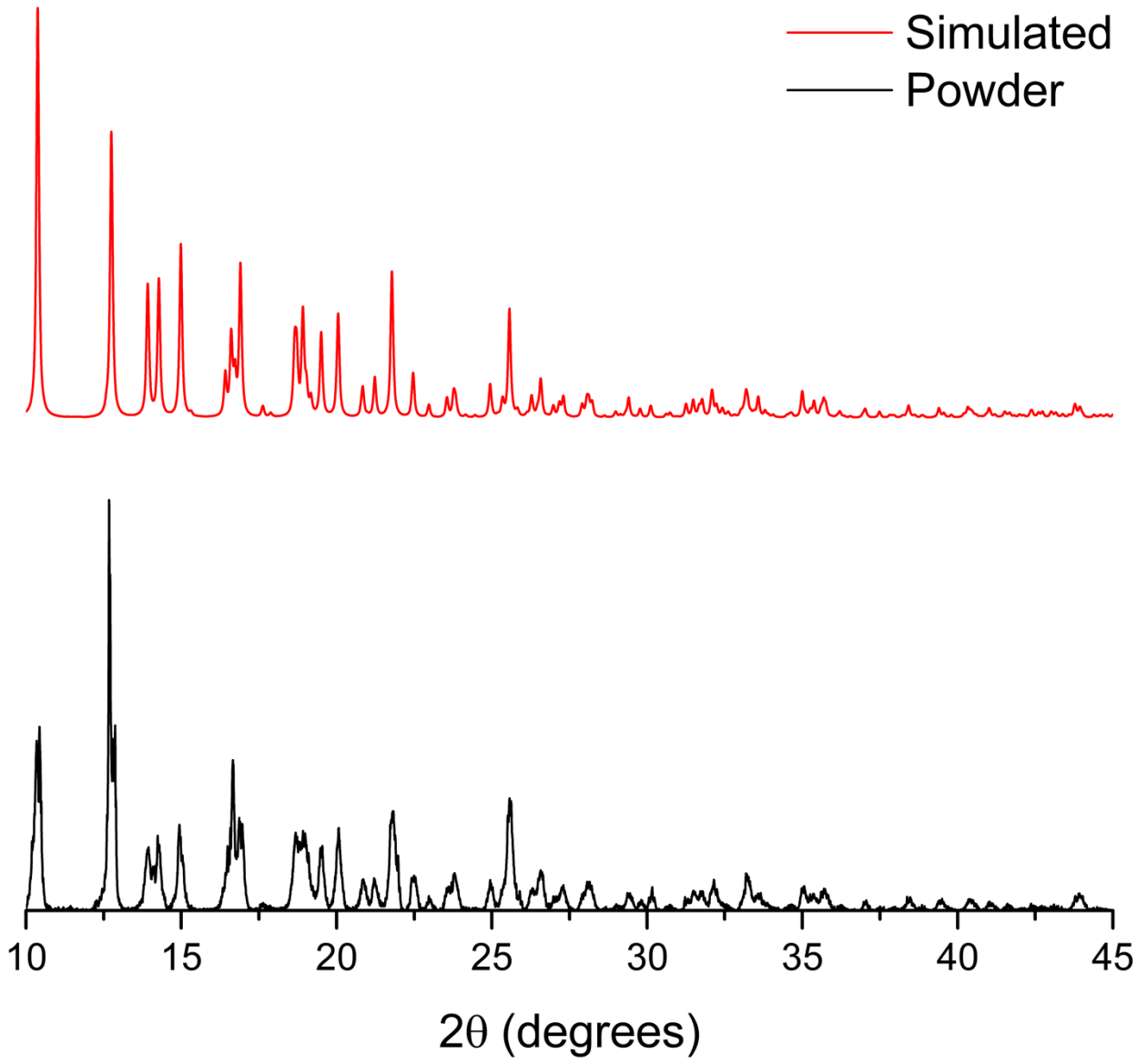

Figure 4.12. Simulated and experimental PXRD patterns of ketone **4.11c** before solid-state irradiation.

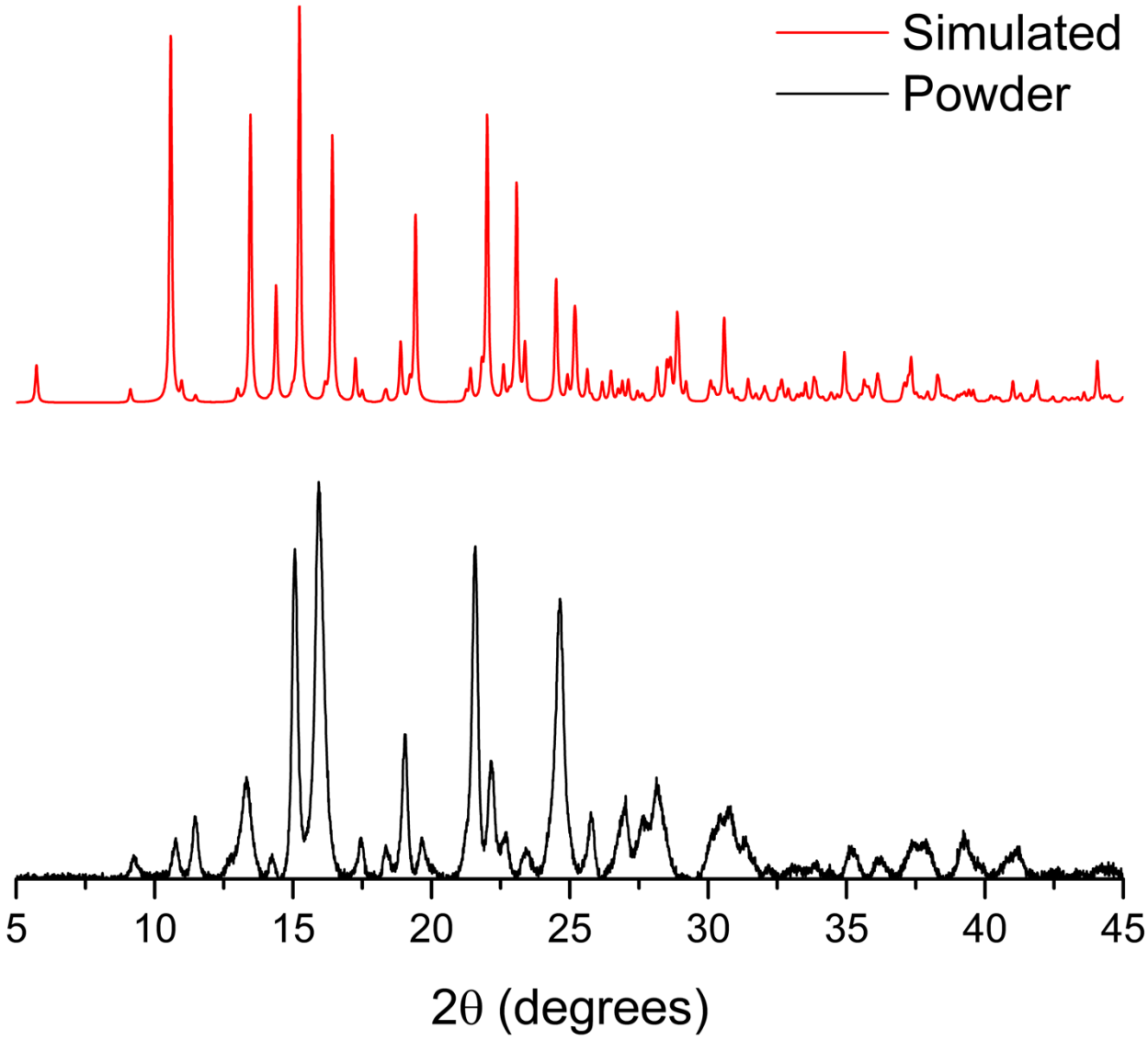

Figure 4.13. Simulated and experimental PXRD patterns of ketone **4.11d** before solid-state irradiation.

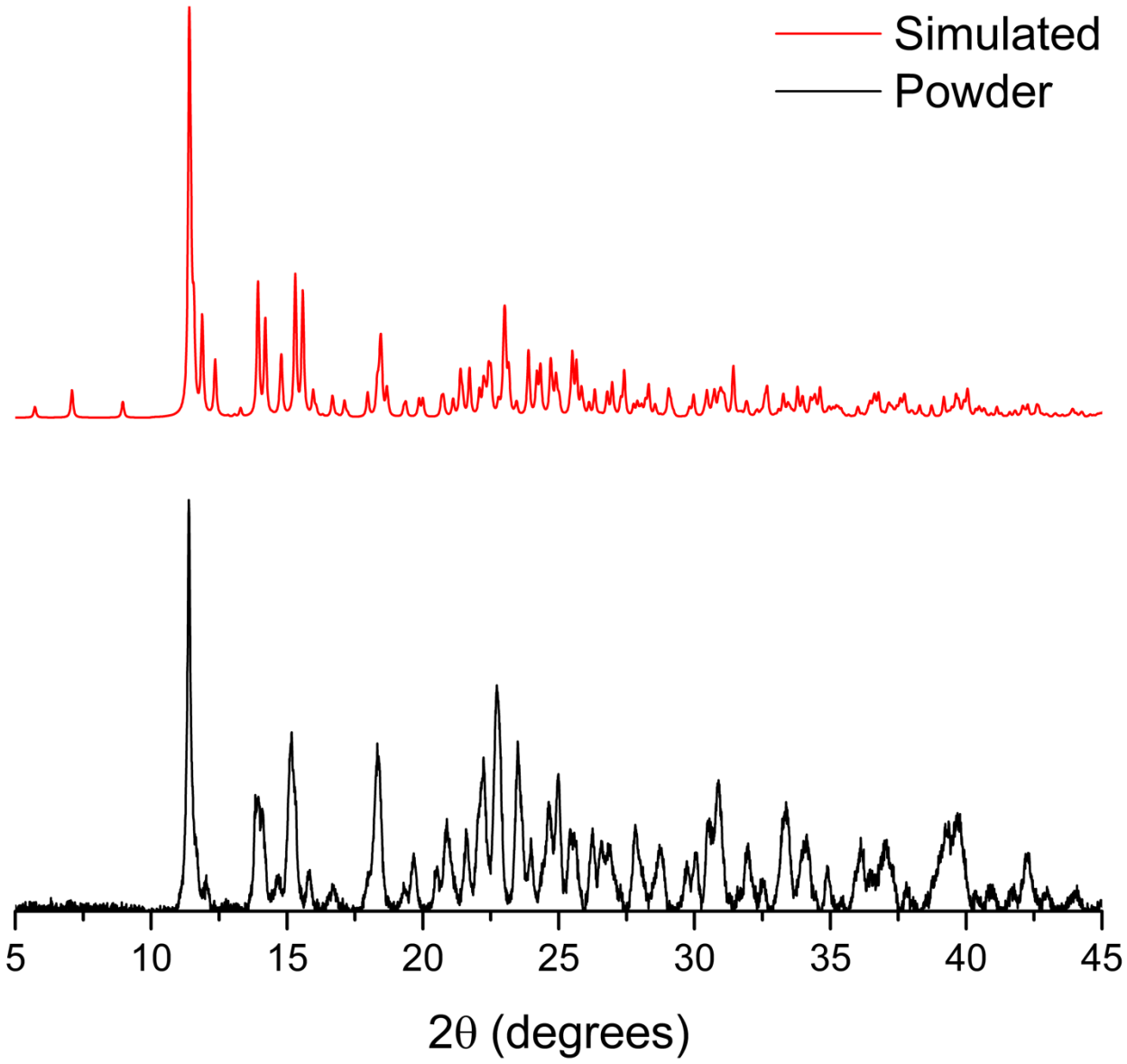

Figure 4.14. Simulated and experimental PXRD patterns of ketone **4.11f** before solid-state irradiation.

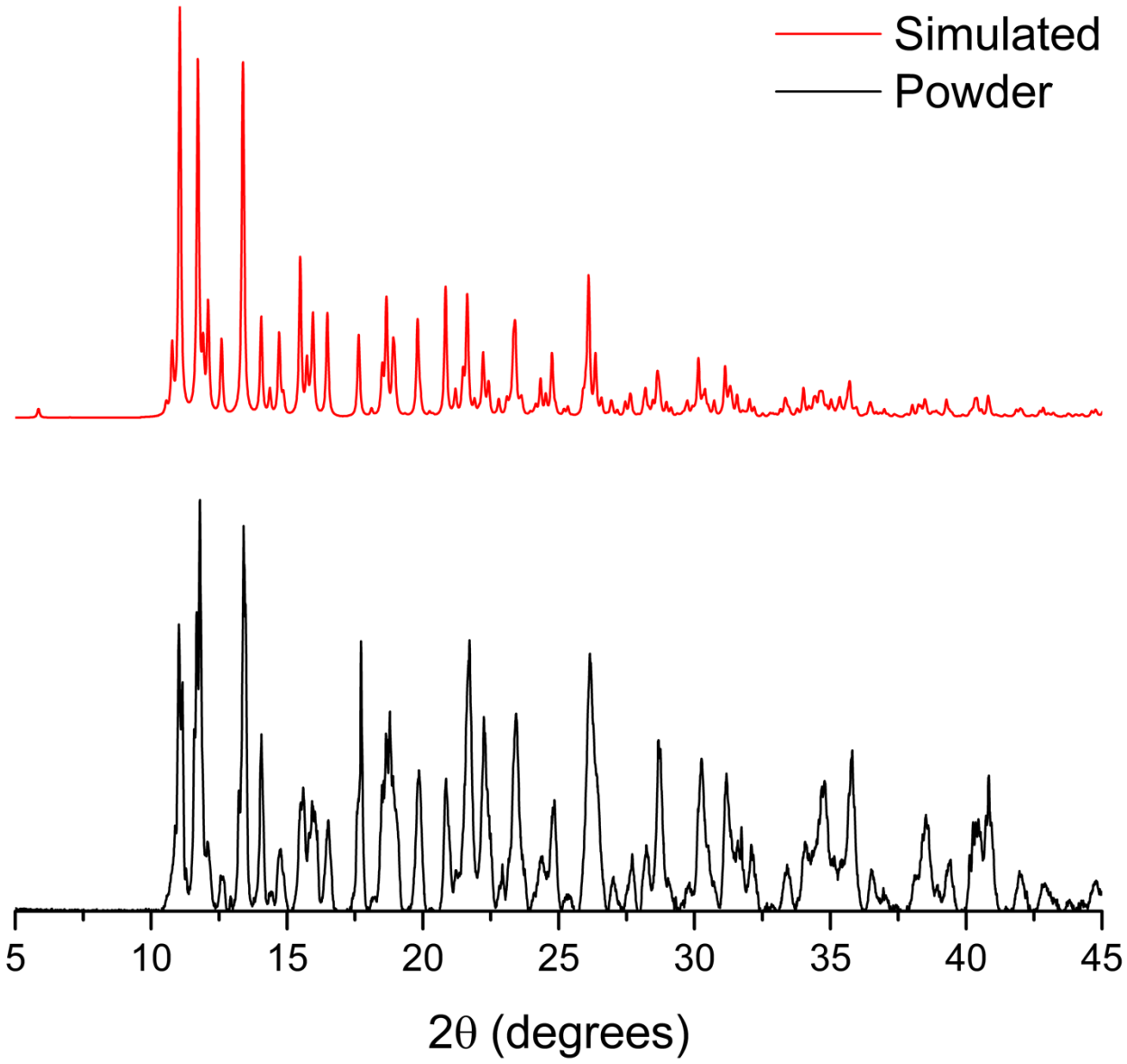

4.5.5 Crystal Structure Data

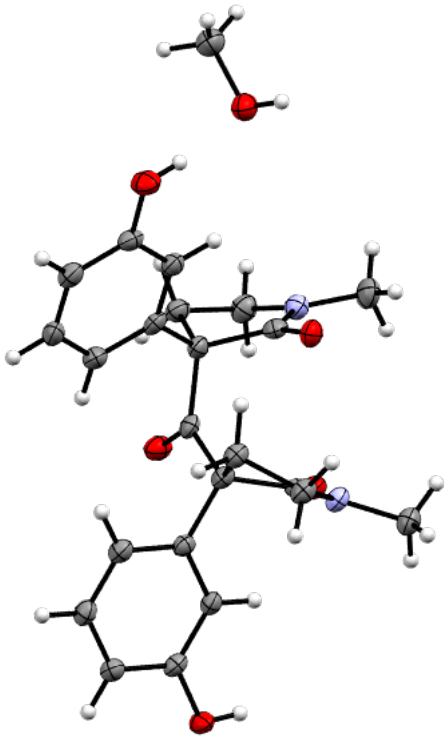

Table 4.1. Crystal data and structure refinement for **4.11c**.

Bond precision: C-C = 0.0030 A Wavelength=1.54178

Cell: a=15.4150(11) b=7.2655(6) c=19.3811(13)

alpha=90 beta=92.331(5) gamma=90

Temperature: 100 K

Volume 2168.8(3)

Space group P 21/c

Hall group -P 2ybc

Moiety formula C24 H28 N2 O6

Sum formula C24 H28 N2 O6

Mr 440.48

Dx,g cm-3 1.349

Z 4 4

Mu (mm-1) 0.802

F000 936.0

F000' 939.03

h,k,lmax 18,8,23

Nref 4037

Tmin,Tmax 0.490,0.750

Tmin' 0.908

Correction method= # Reported T Limits: Tmin=0.490

Tmax=0.750 AbsCorr = MULTI-SCAN

Data completeness= 0.968 Theta(max)= 70.952

R(reflections)= 0.0557(2779) wR2(reflections)= 0.1587(4037)

S = 1.005 Npar= 295

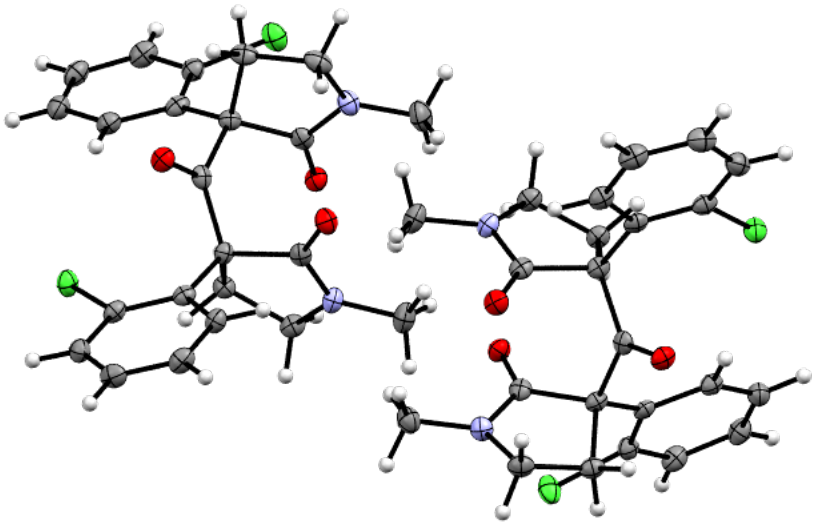

Table 4.2. Crystal data and structure refinement for **4.11d**.

Bond precision: C-C = 0.0027 A Wavelength=1.54178

Cell: a=8.3651(2) b=15.8542(3) c=16.0938(3)

alpha=103.010(1) beta=98.028(1) gamma=90.894(1)

Temperature: 100 K

Calculated Reported

Volume 2056.77(7)

Space group P -1

Hall group -P 1

Moiety formula C23 H22 Cl2 N2 O3

Sum formula C23 H22 Cl2 N2 O3

Mr 445.32

Dx,g cm-3 1.438

Z 4 4

Mu (mm-1) 3.077

F000 928.0

F000' 933.32

h,k,lmax 10,19,19

Nref 7361

Tmin,Tmax 0.650,0.750

Tmin' 0.515

Correction method= # Reported T Limits: Tmin=0.650

Tmax=0.750 AbsCorr = MULTI-SCAN

Data completeness= 0.952 Theta(max)= 69.484

R(reflections)= 0.0320(5947) wR2(reflections)= 0.0869(7361)

S = 1.110 Npar= 545

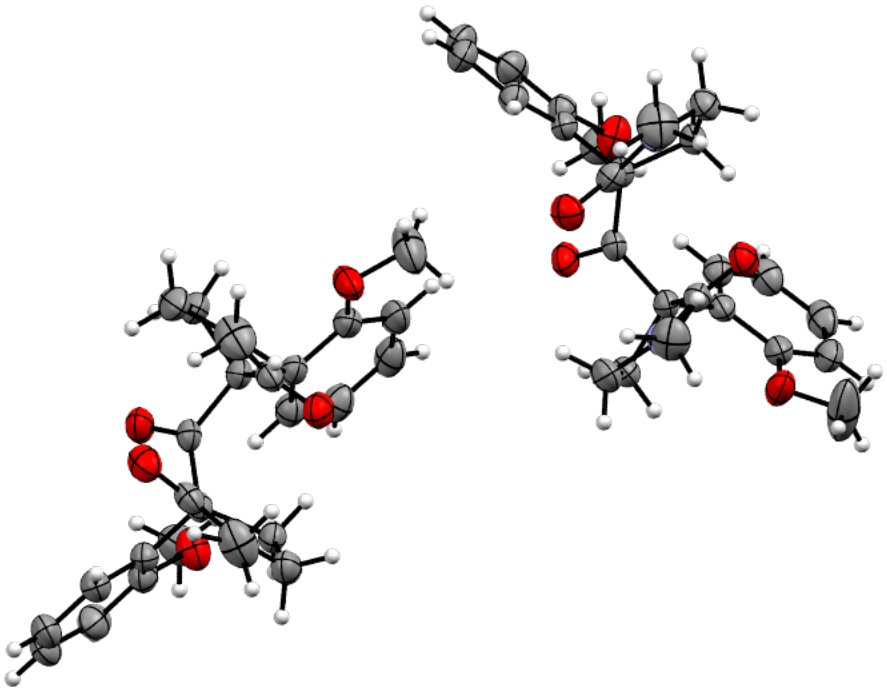

Table 4.3. Crystal data and structure refinement for **4.11f**.

Bond precision: C-C = 0.0030 A Wavelength=1.54178

Cell: a=15.4150(11) b=7.2655(6) c=19.3811(13)

alpha=90 beta=92.331(5) gamma=90

Temperature: 100 K

Calculated Reported

Volume 2168.8(3)

Space group P 21/c

Hall group -P 2ybc

Moiety formula C24 H28 N2 O6

Sum formula C24 H28 N2 O6

Mr 440.48

Dx,g cm-3 1.349

Z 4

Mu (mm-1) 0.802

F000 936.0

F000' 939.03

h,k,lmax 18,8,23

Nref 4037

Tmin,Tmax 0.490,0.750

Tmin' 0.908

Correction method= # Reported T Limits: Tmin=0.490

Tmax=0.750 AbsCorr = MULTI-SCAN

Data completeness= 0.968 Theta(max)= 70.952

R(reflections)= 0.0557(2779) wR2(reflections)= 0.1587(4037)

S = 1.005 Npar= 295

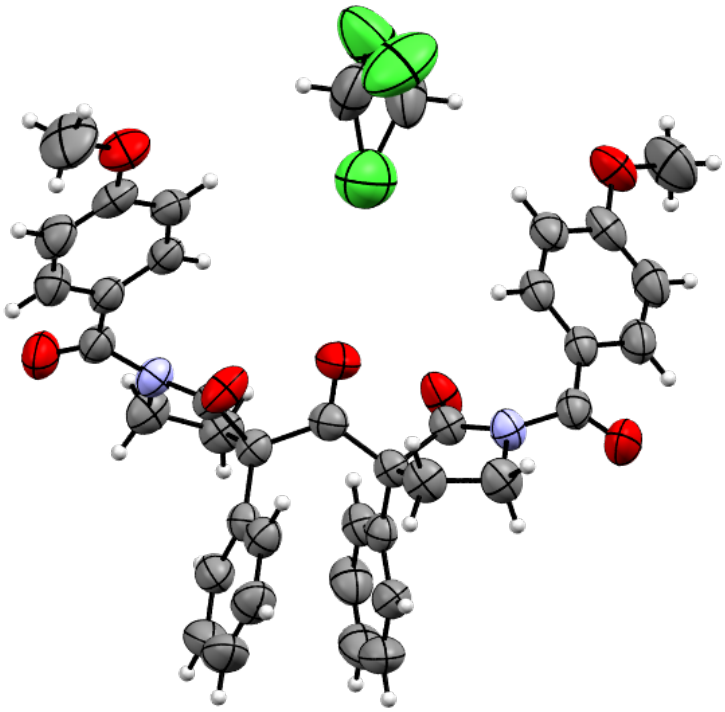

Table 4.4. Crystal data and structure refinement for **4.20** ($CDCl_3$ co-crystal).

Bond precision: C-C = 0.0039 A Wavelength=1.54178

Cell: a=19.6360(14) b=15.2276(11) c=13.0169(10)

alpha=90 beta=112.999(4) gamma=90

Temperature: 293 K

Calculated Reported

Volume 3582.8(5)

Space group C 2/c

Hall group -C 2yc

Moiety formula C37 H32 N2 O7, C H Cl3

Sum formula C38 H33 Cl3 N2 O7

Mr 736.01

Dx,g cm-3 1.364

Z 4

Mu (mm-1) 2.750

F000 1528.0

F000' 1536.60

h,k,lmax 23,18,15

Nref 3306

Tmin,Tmax 0.530,0.750

Tmin' 0.333

Correction method= # Reported T Limits: Tmin=0.530

Tmax=0.750 AbsCorr = MULTI-SCAN

Data completeness= 0.970 Theta(max)= 70.091

R(reflections)= 0.0601(2289) wR2(reflections)= 0.1932(3306)

S = 1.106 Npar= 234

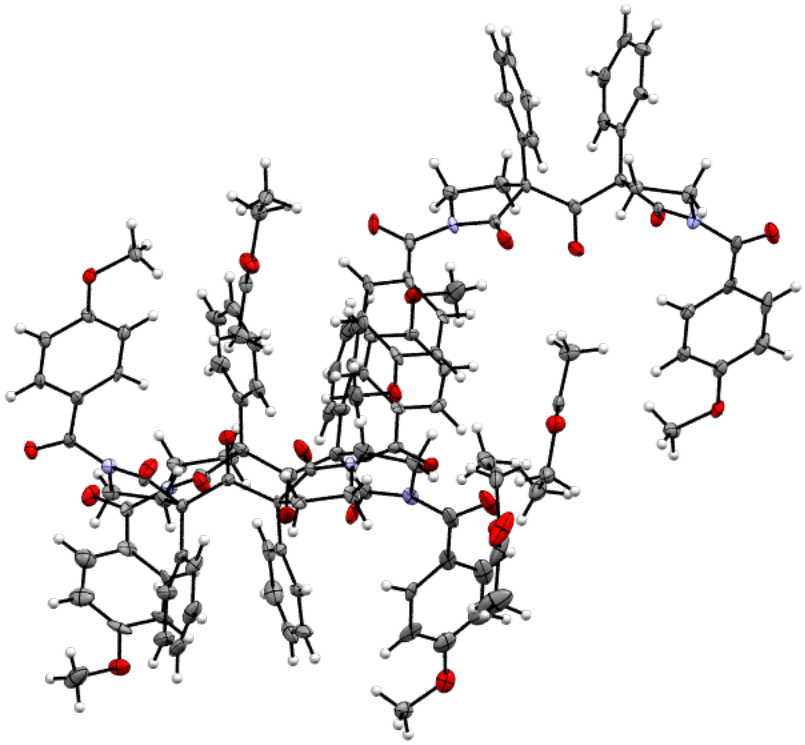

Table 4.5. Crystal data and structure refinement for **4.20** (EtOAc co-crystal).

Bond precision: C-C = 0.0126 A Wavelength=1.54178

Cell: a=19.3591(4) b=45.7078(10) c=12.9274(3)

alpha=90 beta=115.472(1) gamma=90

Temperature: 100 K

Calculated Reported

Volume 10327.0(4)

Space group C c

Hall group C -2yc

Moiety formula C41 H40 Cl0 N2 O9

Sum formula C41 H40 Cl0 N2 O9

Mr 704.75

Dx,g cm-3 1.360

Z 12

Mu (mm-1) 0.789

F000 4464.0

F000' 4478.36

h,k,lmax 22,54,14

Nref 15545

Tmin,Tmax 0.570,0.750

Tmin' 0.789

Correction method= # Reported T Limits: Tmin=0.570

Tmax=0.750 AbsCorr = MULTI-SCAN

Data completeness= 1.59/0.80 Theta(max)= 69.956

R(reflections)= 0.1091(12949) wR2(reflections)= 0.2815(15545)

S = 1.036 Npar= 1418

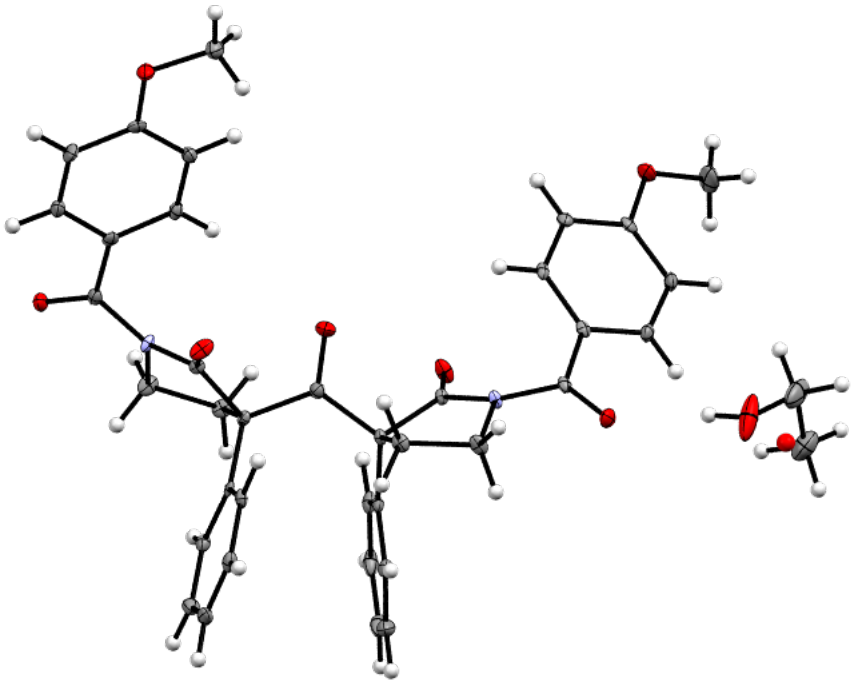

Table 4.6. Crystal data and structure refinement for **4.20** (EtOH co-crystal).

Bond precision: C-C = 0.0030 A Wavelength=1.54178

Cell: a=18.3925(3) b=14.5726(3) c=12.6603(2)

alpha=90 beta=103.375(1) gamma=90

Temperature: 100 K

Calculated Reported

Volume 3301.26(10)

Space group P 21/c

Hall group -P 2ybc

Moiety formula

C37 H32 N2 O7, 0.926(C2 H6 O),

0.074(O)

Sum formula C38.85 H37.56 N2 O8

Mr 660.49

Dx,g cm-3 1.333

Z 4

Mu (mm-1) 0.764

F000 1394.7

F000' 1399.12

h,k,lmax 22,17,15

Nref 6182

Tmin,Tmax 0.500,0.750

Tmin' 0.682

Correction method= # Reported T Limits: Tmin=0.500

Tmax=0.750 AbsCorr = MULTI-SCAN

Data completeness= 0.995 Theta(max)= 69.531

R(reflections)= 0.0567(4940)

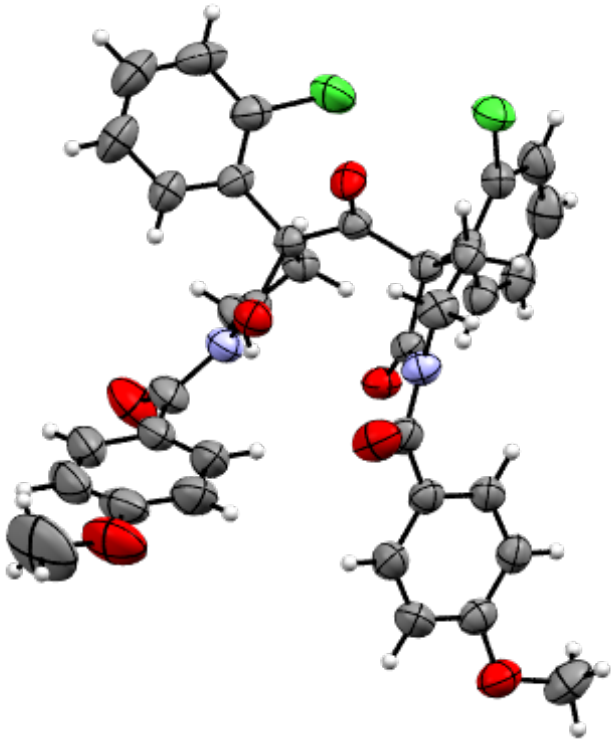

Table 4.7. Crystal data and structure refinement for **4.28d** (reactive polymorph).

Bond precision: C-C = 0.0042 A Wavelength=1.54178

Cell: a=28.2314(3) b=28.2314(3) c=21.6709(3)

alpha=90 beta=90 gamma=120

Temperature: 298 K

Calculated Reported

Volume 14958.0(4) 14958.0(4)

Space group R -3 R -3 :H

Hall group -R 3 -R 3

Moiety formula C37 H30 Cl2 N2 O7

Sum formula C37 H30 Cl2 N2 O7

Mr 685.53

Dx,g cm-3 1.370

Z 18

Mu (mm-1) 2.202

F000 6408.0

F000' 6439.76

h,k,lmax 32,34,26

Nref 6266

Tmin,Tmax 0.650,0.750

Tmin' 0.613

Correction method= # Reported T Limits: Tmin=0.650

Tmax=0.750 AbsCorr = MULTI-SCAN

Data completeness= 0.991 Theta(max)= 69.994

R(reflections)= 0.0472(4690) wR2(reflections)= 0.1502(6266)

S = 1.046 Npar= 435

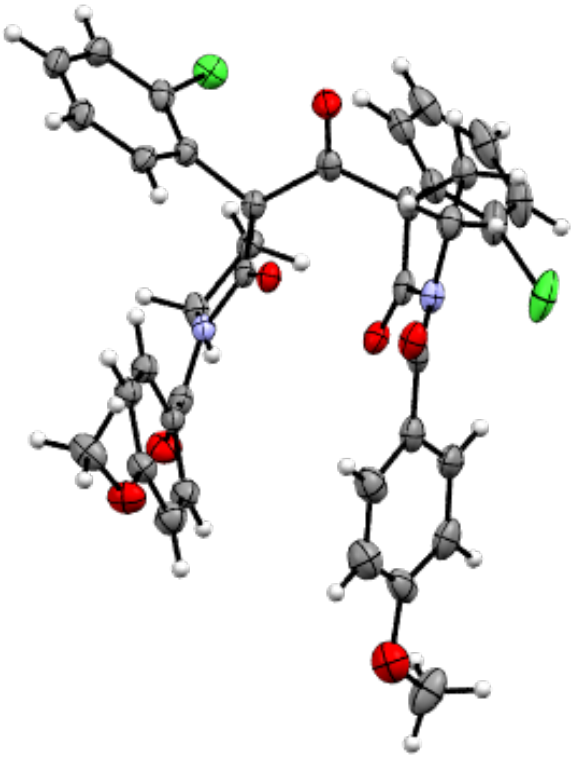

Table 4.8. Crystal data and structure refinement for **4.28d** (unreactive polymorph).

Bond precision: C-C = 0.0061 A Wavelength=1.54178

Cell: a=13.1482(6) b=14.7869(7) c=16.3314(7)

alpha=90 beta=90.461(2) gamma=90

Temperature: 100 K

Calculated Reported

Volume 3175.1(2) 3175.1(2)

Space group P 21/c P 21/c

Hall group -P 2ybc -P 2ybc

Moiety formula C37 H30 Cl2 N2 O7

Sum formula C37 H30 Cl2 N2 O7

Mr 685.53

Dx,g cm-3 1.434

Z 4

Mu (mm-1) 2.305

F000 1424.0

F000' 1431.06

h,k,lmax 15,17,19

Nref 5992

Tmin,Tmax 0.610,0.740

Tmin' 0.794

Correction method= # Reported T Limits: Tmin=0.610

Tmax=0.740 AbsCorr = MULTI-SCAN

Data completeness= 0.987 Theta(max)= 70.542

R(reflections)= 0.0743(4642) wR2(reflections)= 0.1608(5992)

S = 1.098 Npar= 435

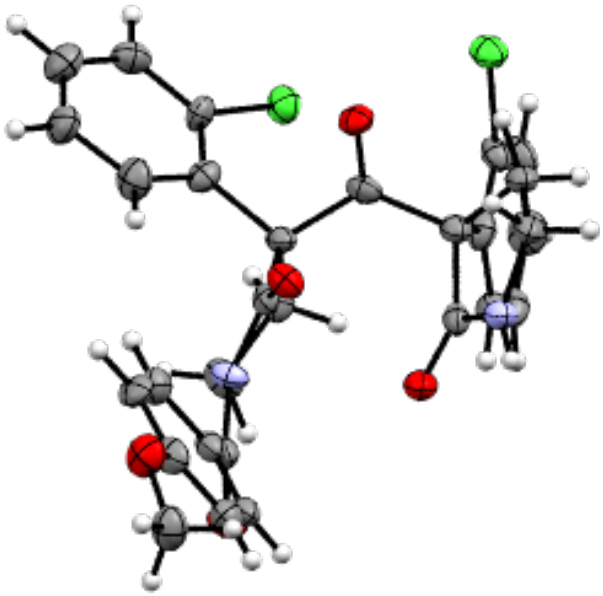

Table 4.9. Crystal data and structure refinement for **4.29d**.

Bond precision: C-C = 0.0088 A Wavelength=1.54178

Cell: a=14.8617(8) b=10.0463(7) c=17.6899(11)

alpha=90 beta=103.410(4) gamma=90

Temperature: 100 K

Calculated Reported

Volume 2569.2(3)

Space group P 21/c

Hall group -P 2ybc

Moiety formula C29 H24 Cl2 N2 O5

Sum formula C29 H24 Cl2 N2 O5

Mr 551.40

Dx,g cm-3 1.426

Z 4

Mu (mm-1) 2.642

F000 1144.0

F000' 1150.12

h,k,lmax 18,12,20

Nref 4763

Tmin,Tmax 0.630,0.750

Tmin' 0.768

Correction method= # Reported T Limits: Tmin=0.630

Tmax=0.750 AbsCorr = MULTI-SCAN

Data completeness= 0.967 Theta(max)= 70.650

R(reflections)= 0.0759(2459) wR2(reflections)= 0.2336(4763)

S = 0.963 Npar= 344

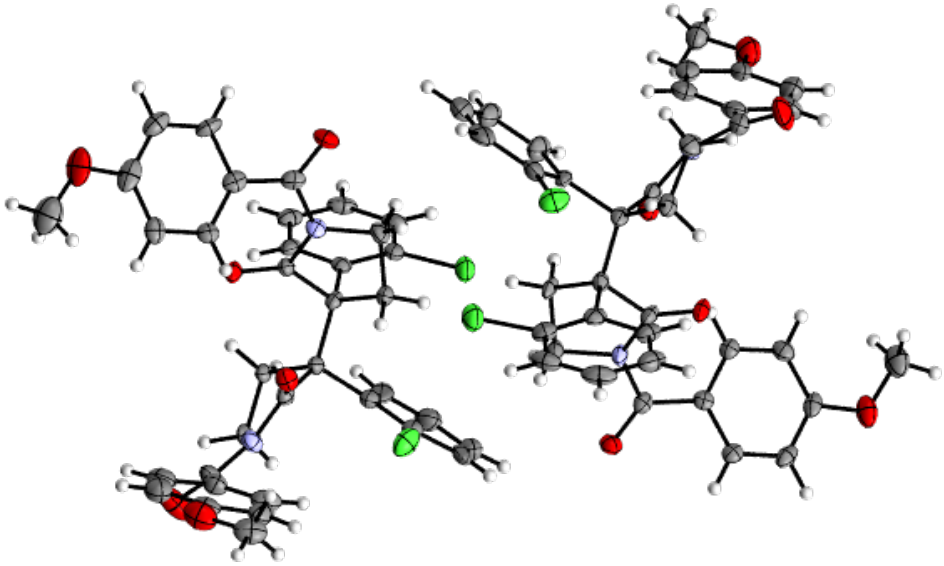

Table 4.10. Crystal data and structure refinement for **4.30d**.

Cell: a=13.3122(3) b=20.4330(5) c=22.1795(5)

alpha=90 beta=90 gamma=90

Temperature: 100 K

Calculated Reported

Volume 6033.0(2)

Space group P n a 21

Hall group P 2c -2n

Moiety formula C36 H30

Cl2 N2 O6

Sum formula C36 H30 Cl2 N2 O6

Mr 657.52

Dx,g cm-3 1.448

Z 8

Mu (mm-1) 2.374

F000 2736.0

F000' 2757.53

h,k,lmax 15,23,26

Nref 9886

Tmin,Tmax 0.796,0.909

Tmin' 0.491

Correction method= Not given

Data completeness= 1.68/0.86 Theta(max)= 69.977

R(reflections)= 0.0607(9196) wR2(reflections)= 0.1753(9886)

S = 1.025 Npar= 835

4.6 Spectra Relevant to Chapter Four:

Taming Radicals in the Solid State: Discovery and Total Synthesis of Psychotriadine

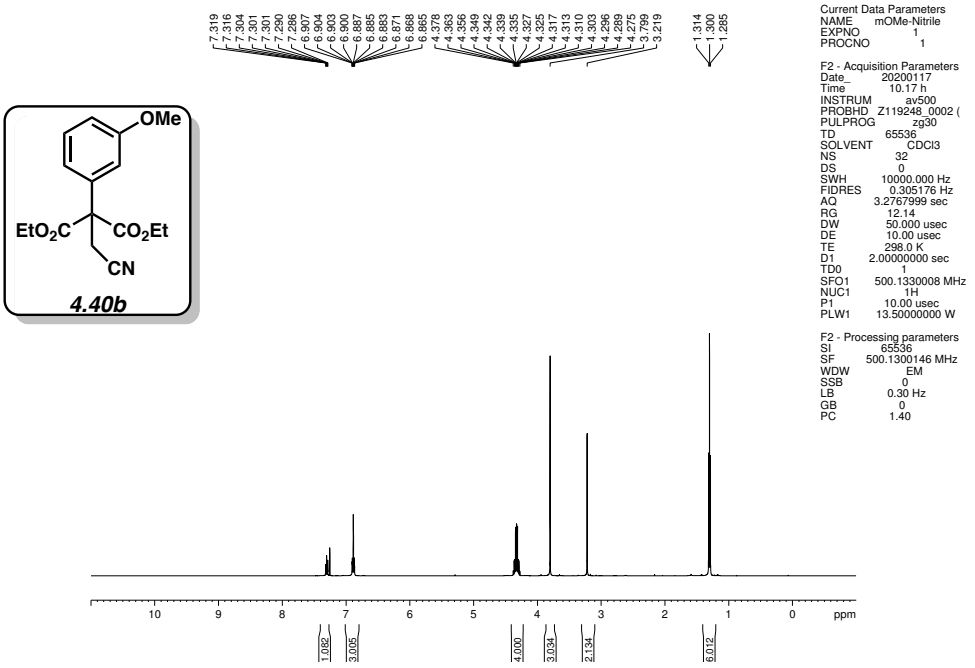

Figure 4.15 ^{1}H NMR (500 MHz, $CDCl_3$) of compound **4.40b**.

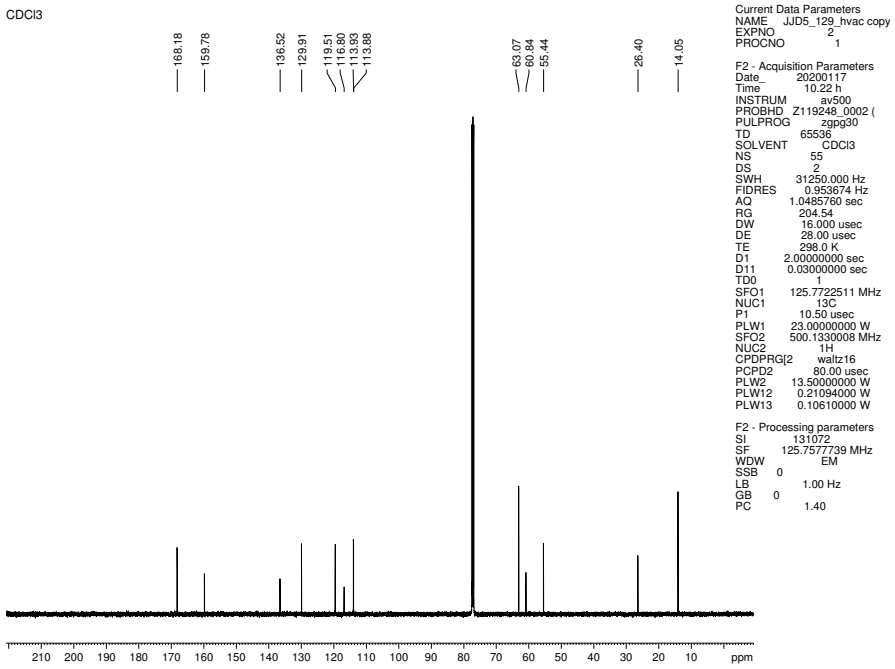

Figure 4.16 ^{13}C NMR (125 MHz, $CDCl_3$) of compound **4.40b**.

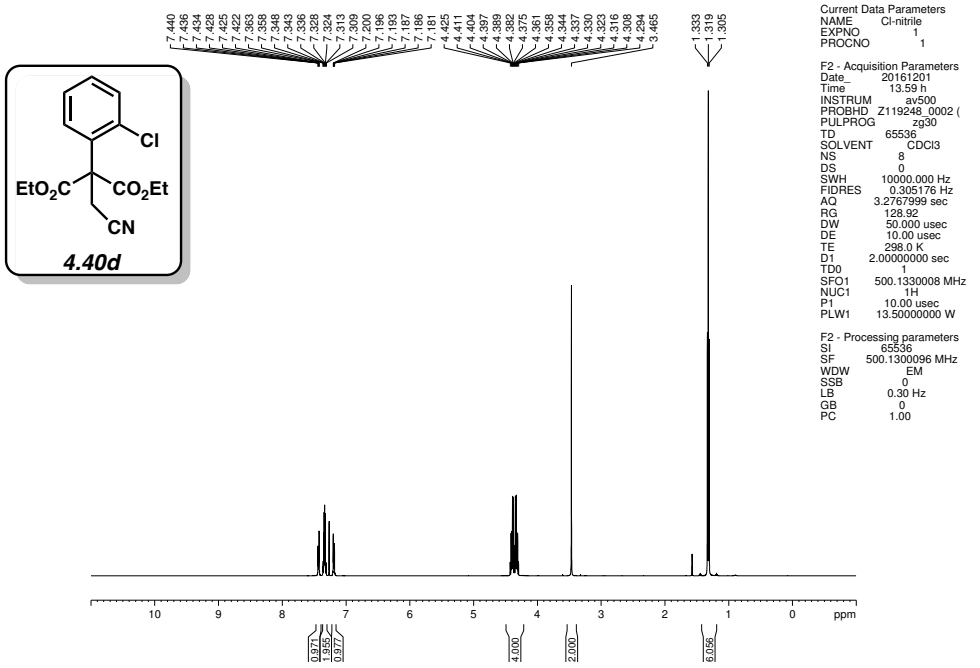

Figure 4.17 ^{1}H NMR (500 MHz, $CDCl_3$) of compound **4.40d**.

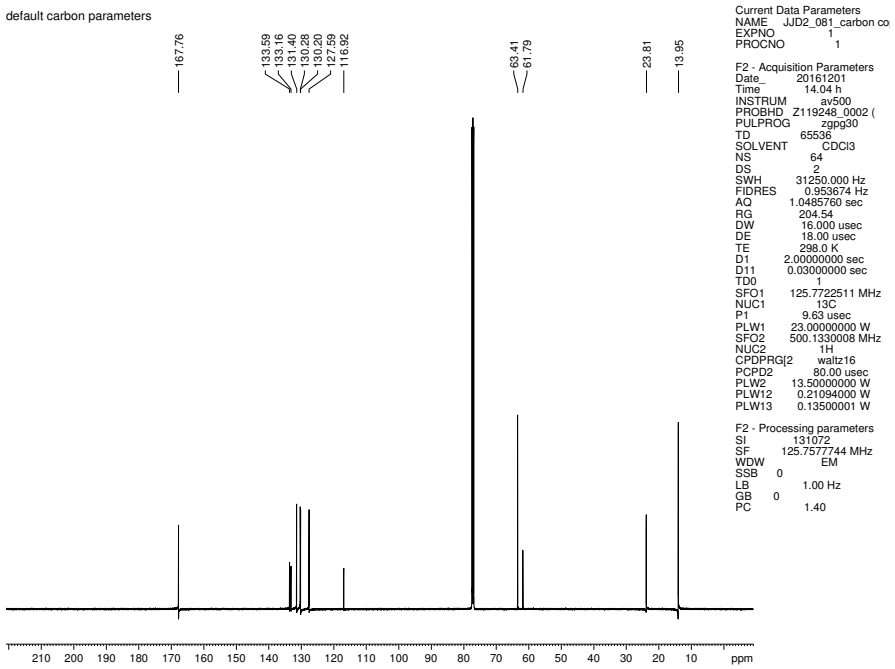

Figure 4.18 ^{13}C NMR (125 MHz, $CDCl_3$) of compound **4.40d**.

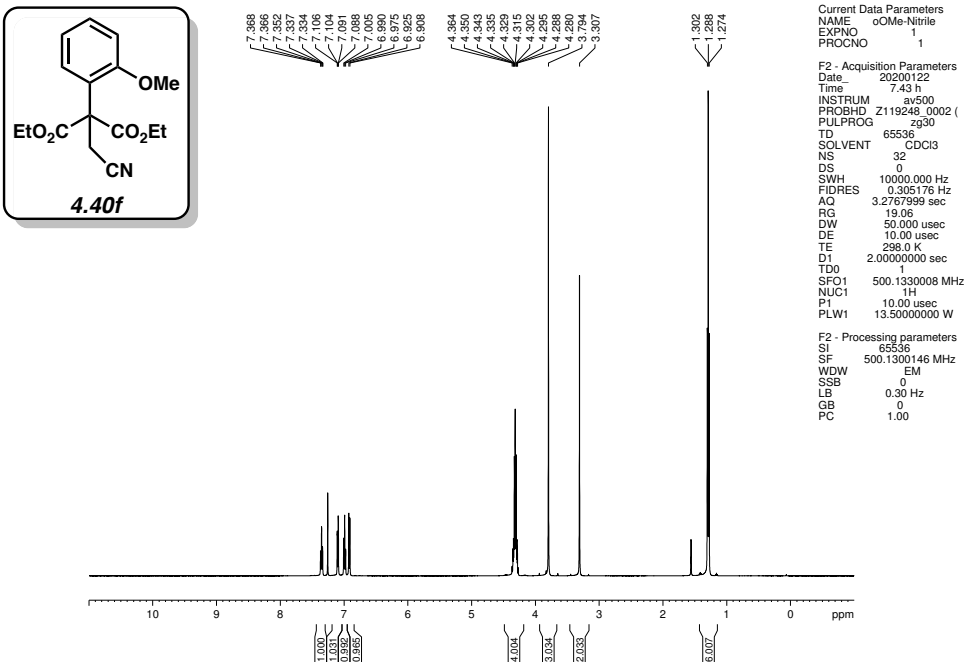

Figure 4.19 ^{1}H NMR (500 MHz, $CDCl_3$) of compound **4.40f**.

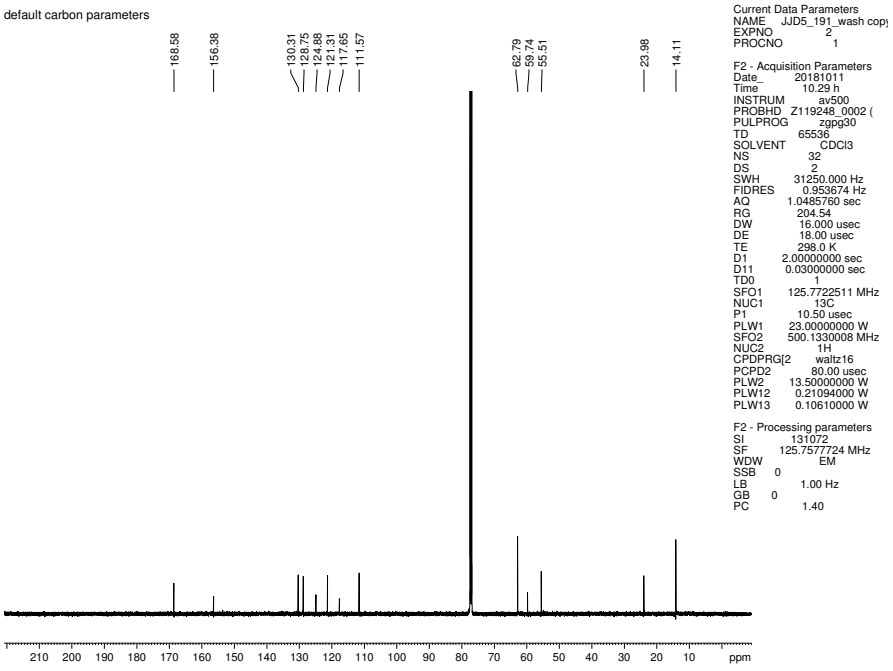

Figure 4.20 ^{13}C NMR (125 MHz, $CDCl_3$) of compound **4.40f**.

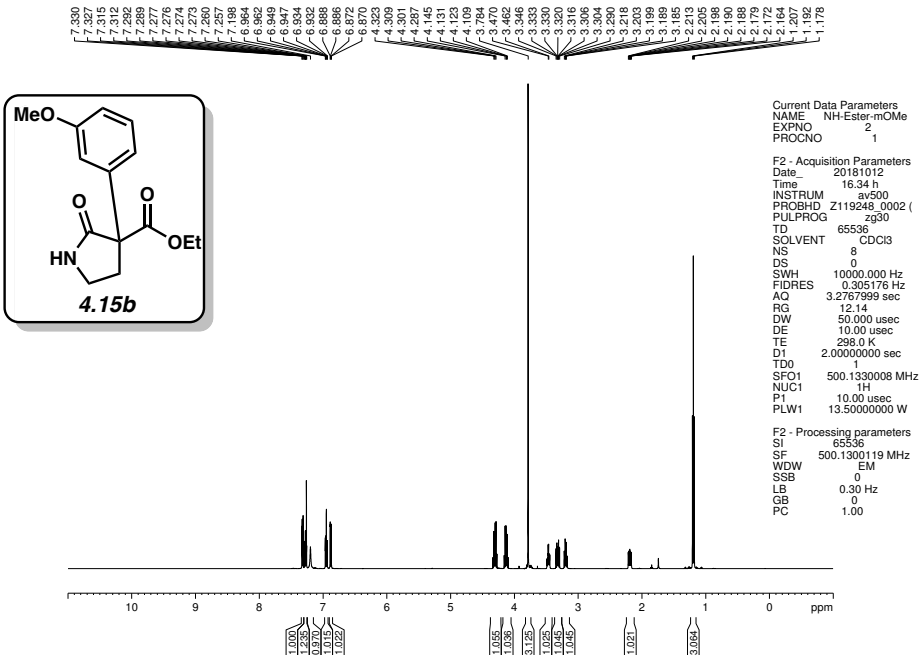

Figure 4.21 ^{1}H NMR (500 MHz, $CDCl_3$) of compound **4.15b**.

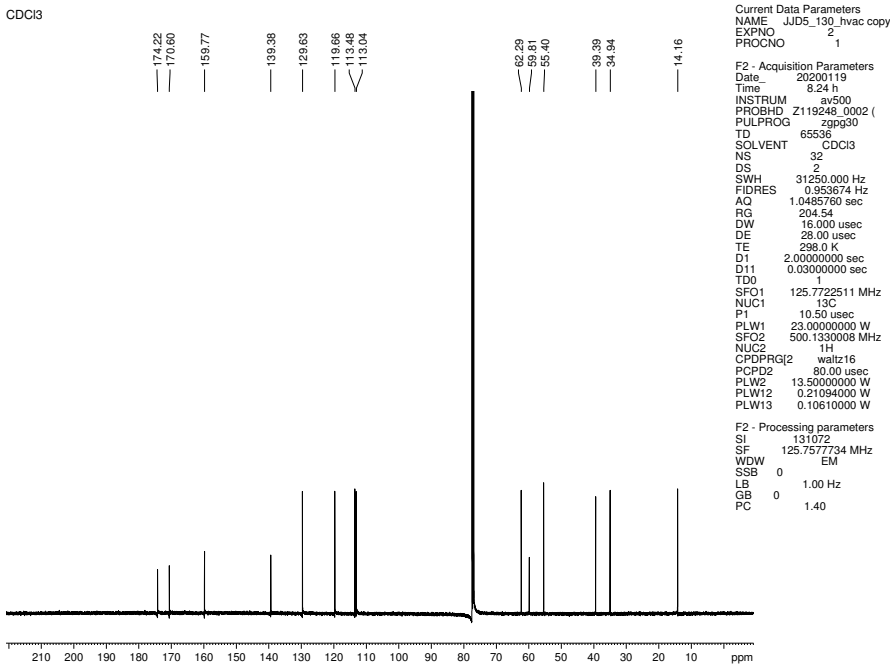

Figure 4.22 ^{13}C NMR (125 MHz, $CDCl_3$) of compound **4.15b**.

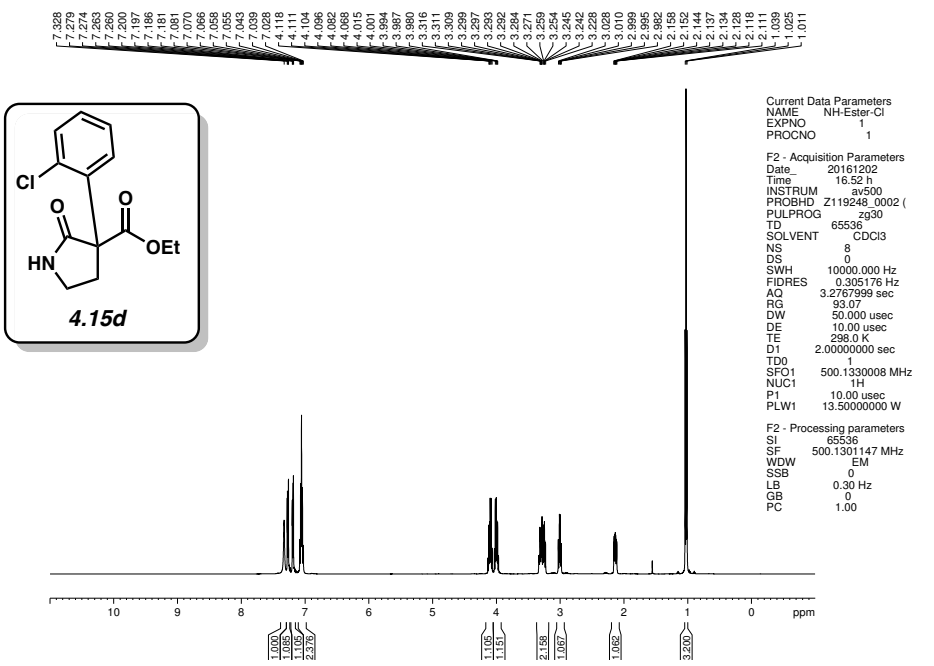

Figure 4.23 ^{1}H NMR (500 MHz, $CDCl_3$) of compound **4.15d**.

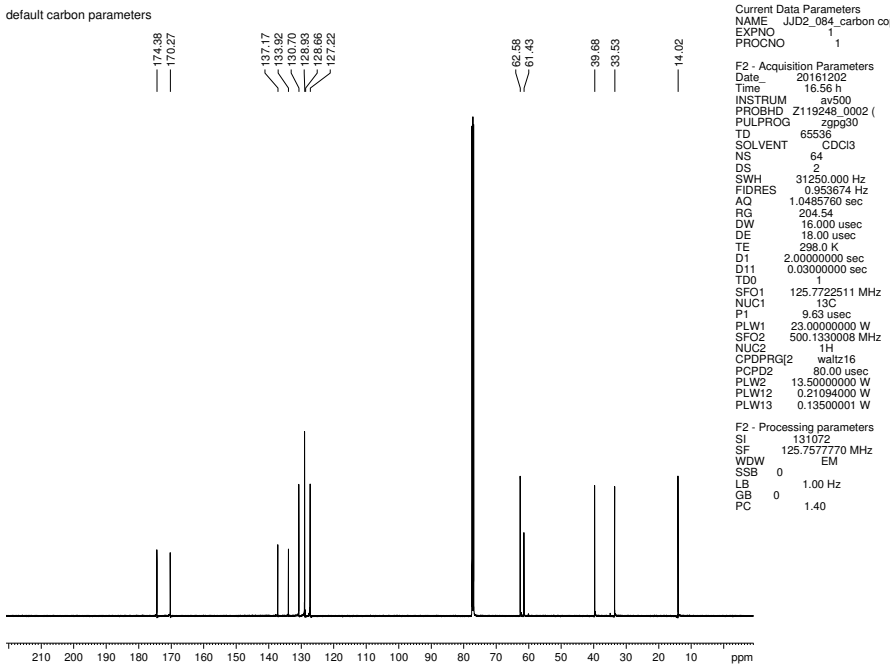

Figure 4.24 ^{13}C NMR (125 MHz, $CDCl_3$) of compound **4.15d**.

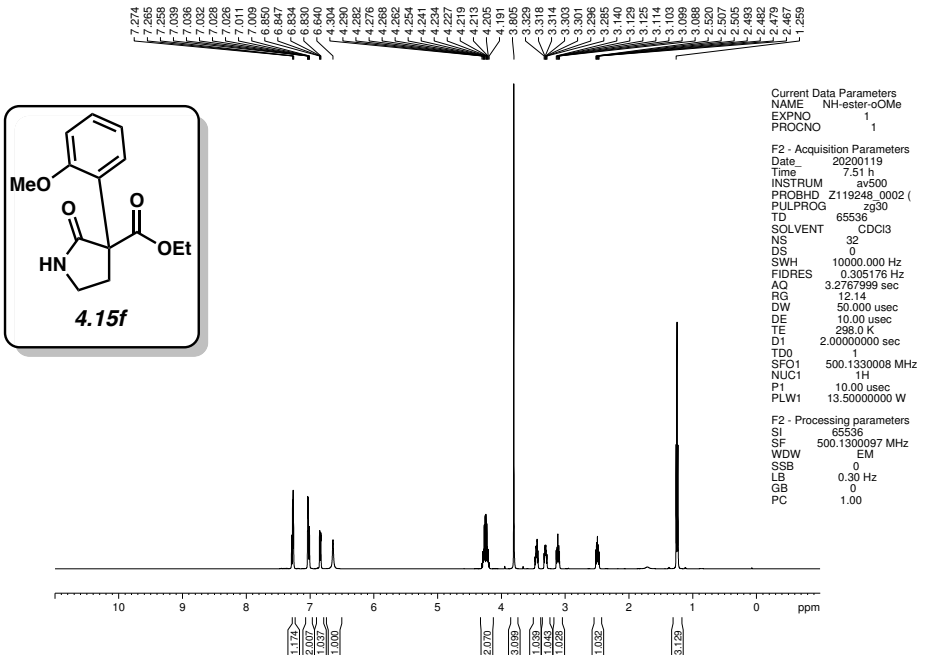

Figure 4.25 ^{1}H NMR (500 MHz, $CDCl_3$) of compound **4.15f**.

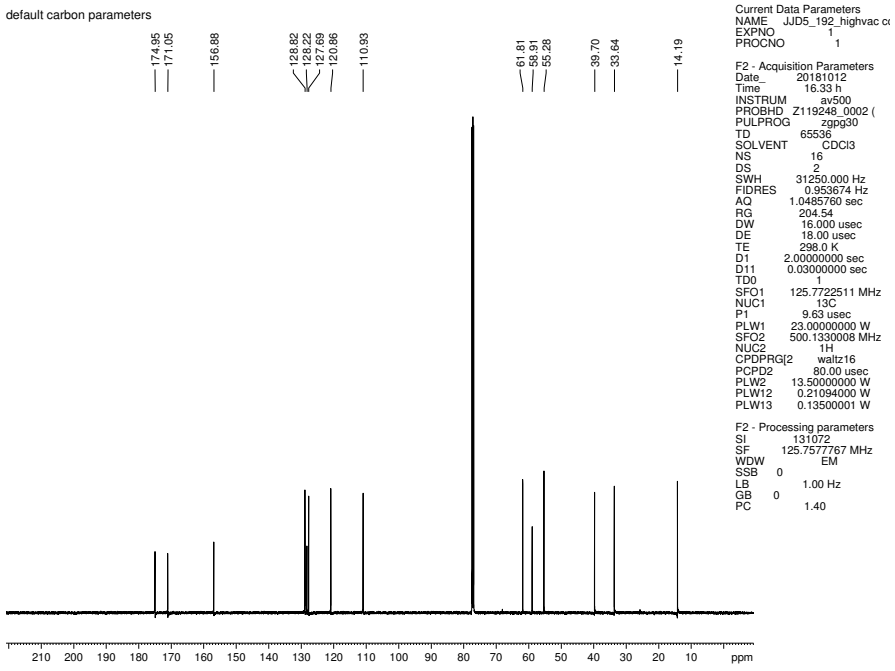

Figure 4.26 ^{13}C NMR (125 MHz, $CDCl_3$) of compound **4.15f**.

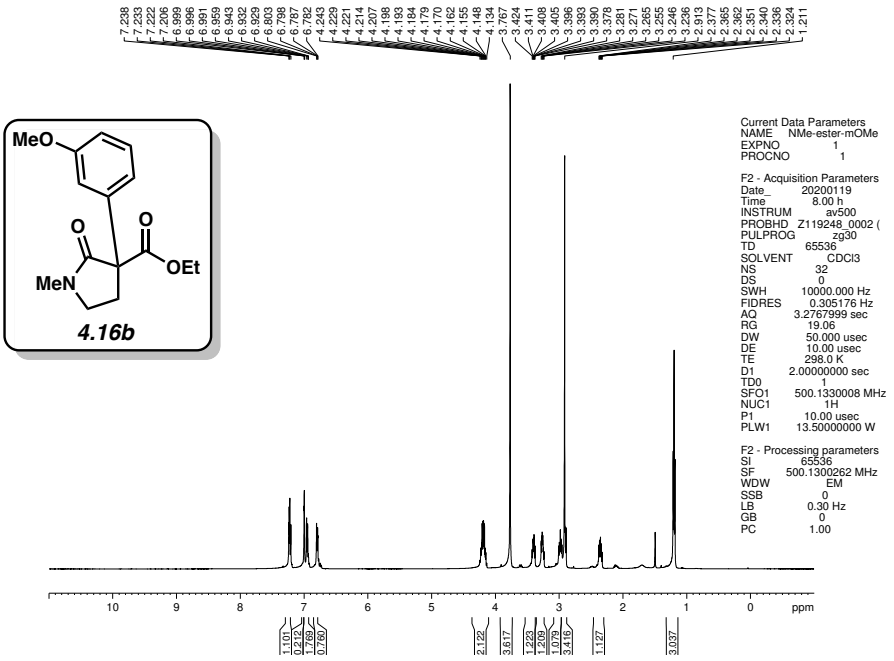

Figure 4.27 ^{1}H NMR (500 MHz, $CDCl_3$) of compound **4.16b**.

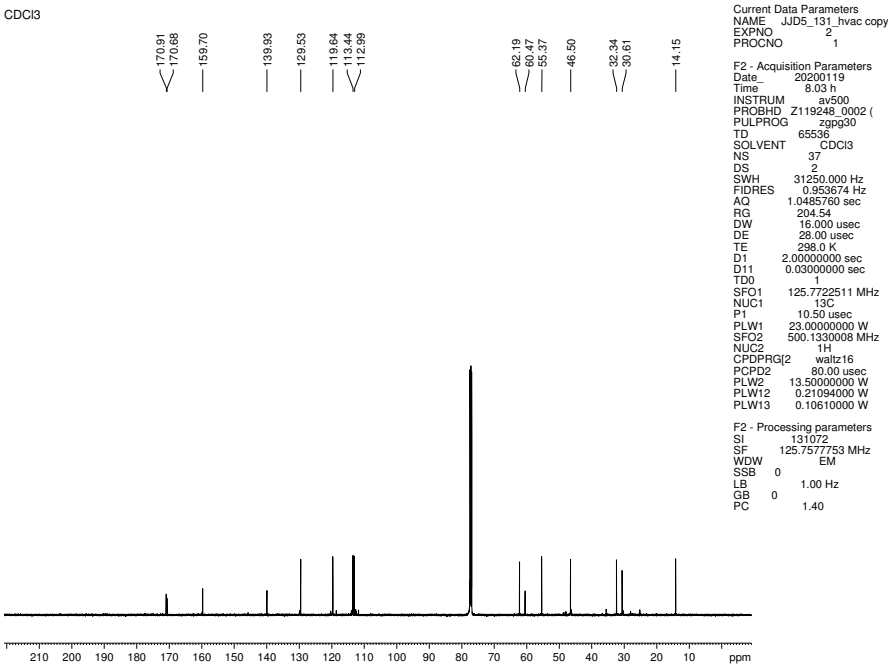

Figure 4.28 ^{13}C NMR (125 MHz, $CDCl_3$) of compound **4.16b**.

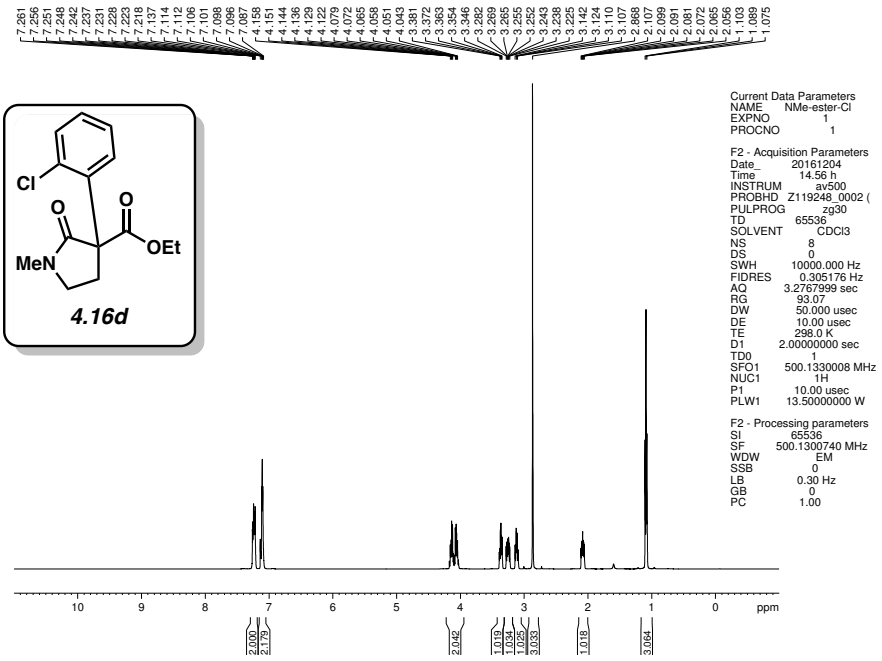

Figure 4.29 ^{1}H NMR (500 MHz, $CDCl_3$) of compound **4.16d**.

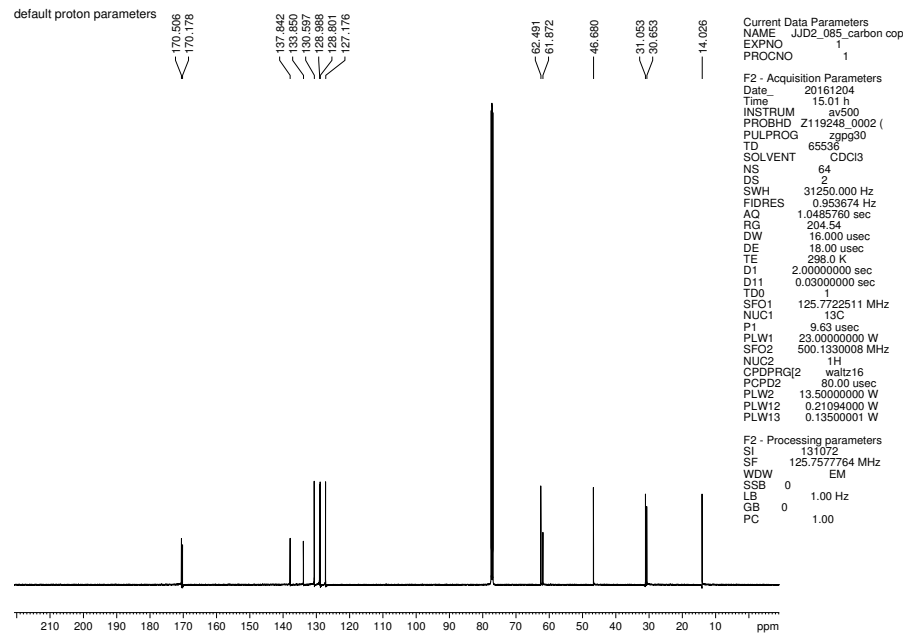

Figure 4.30 ^{13}C NMR (125 MHz, $CDCl_3$) of compound **4.16d**.

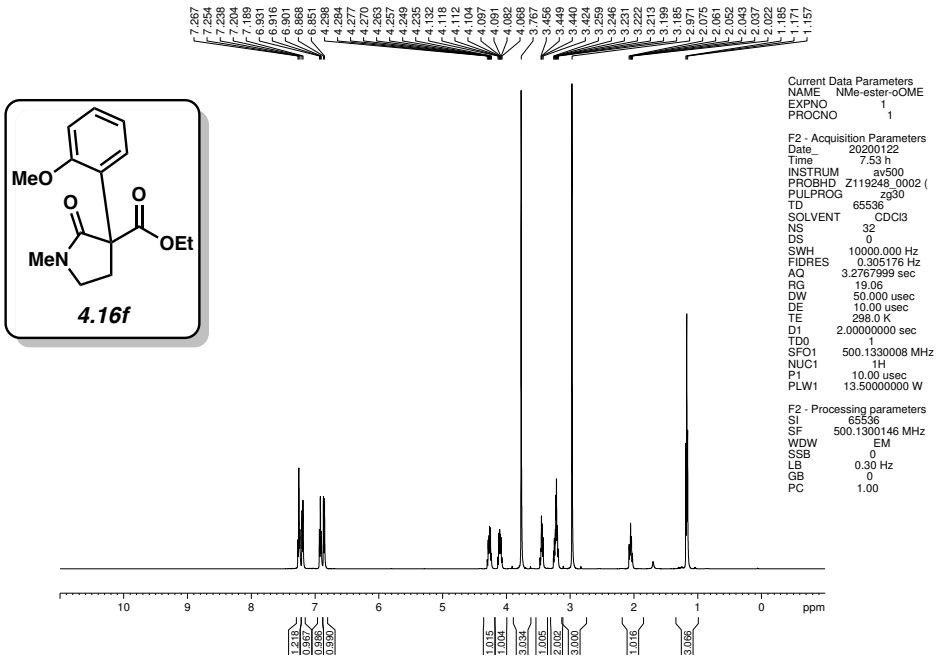

Figure 4.31 ^{1}H NMR (500 MHz, $CDCl_3$) of compound **4.16f**.

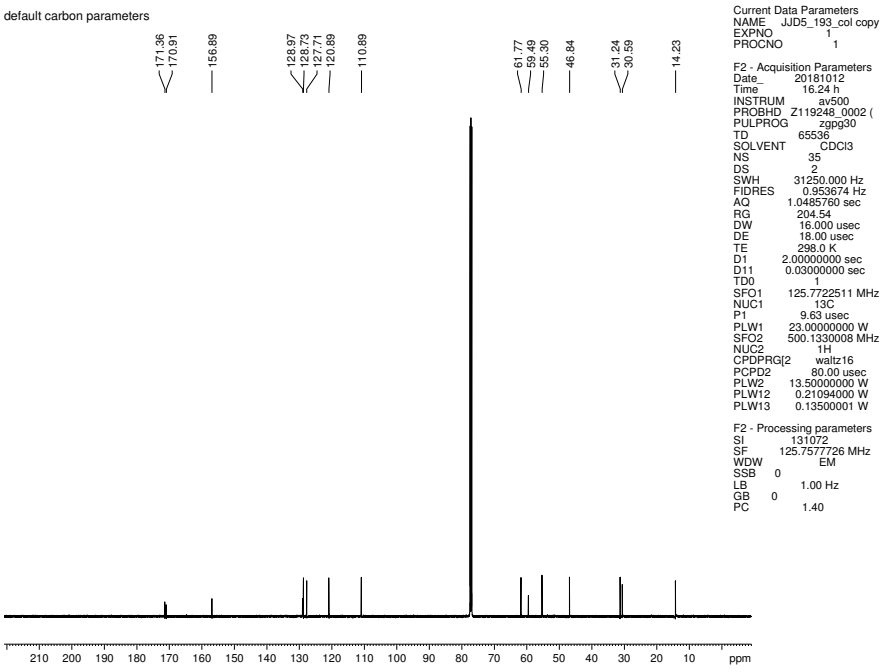

Figure 4.32 ^{13}C NMR (125 MHz, $CDCl_3$) of compound **4.16f**.

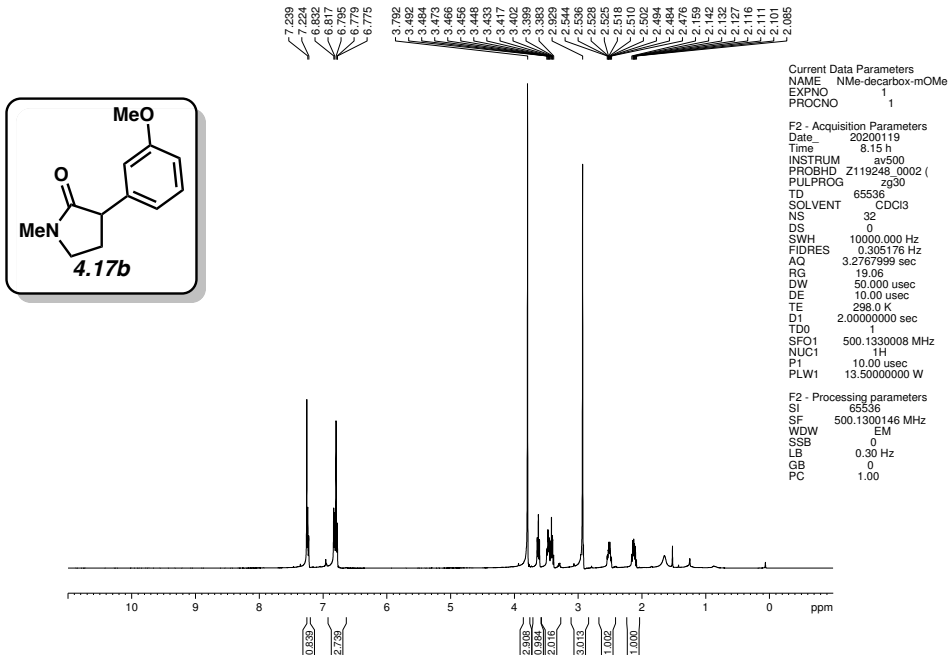

Figure 4.33 ^{1}H NMR (500 MHz, $CDCl_3$) of compound **4.17b**.

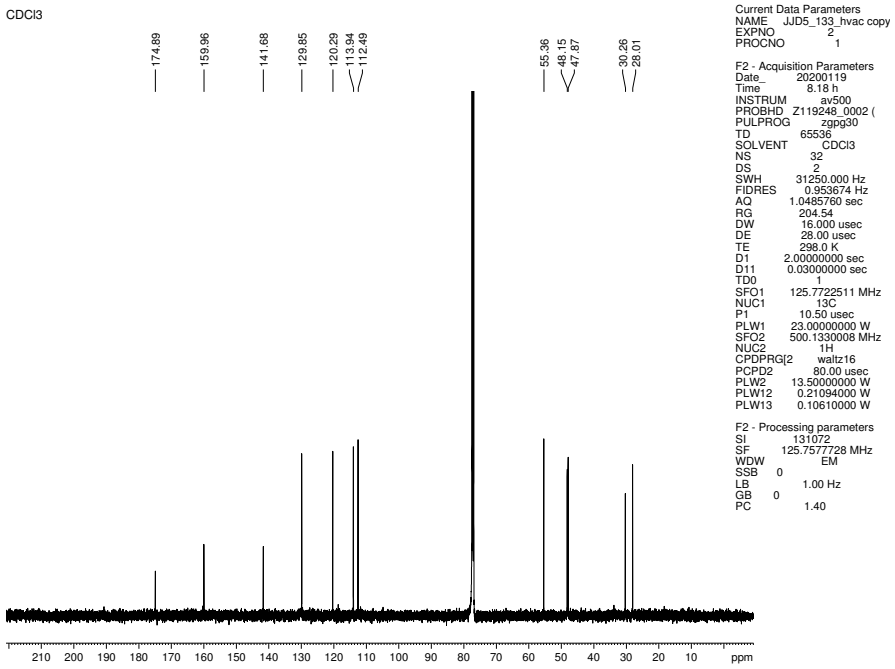

Figure 4.34 ^{13}C NMR (125 MHz, $CDCl_3$) of compound **4.17b**.

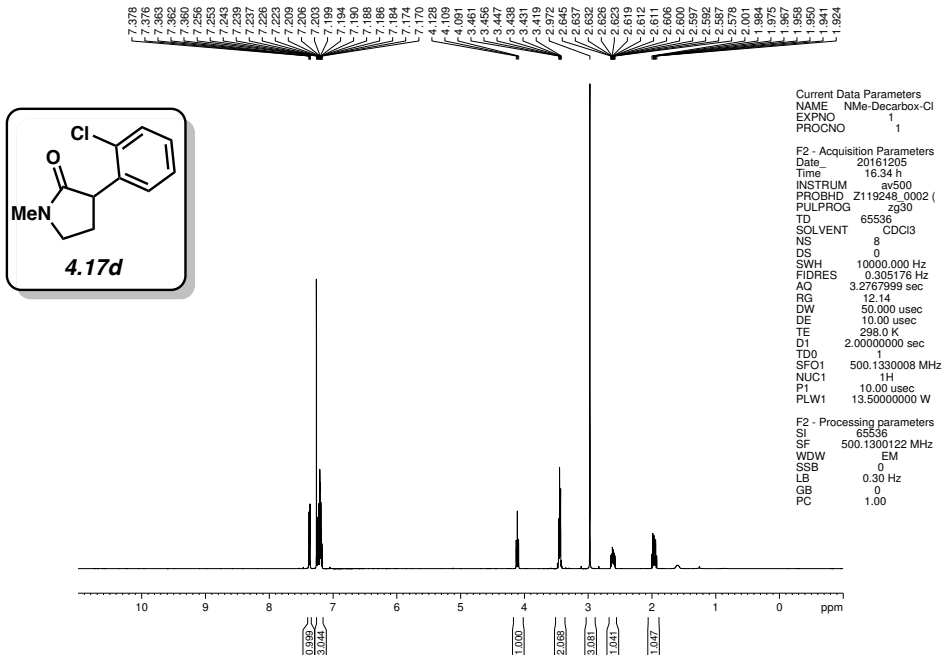

Figure 4.35 ^{1}H NMR (500 MHz, $CDCl_3$) of compound **4.17d**.

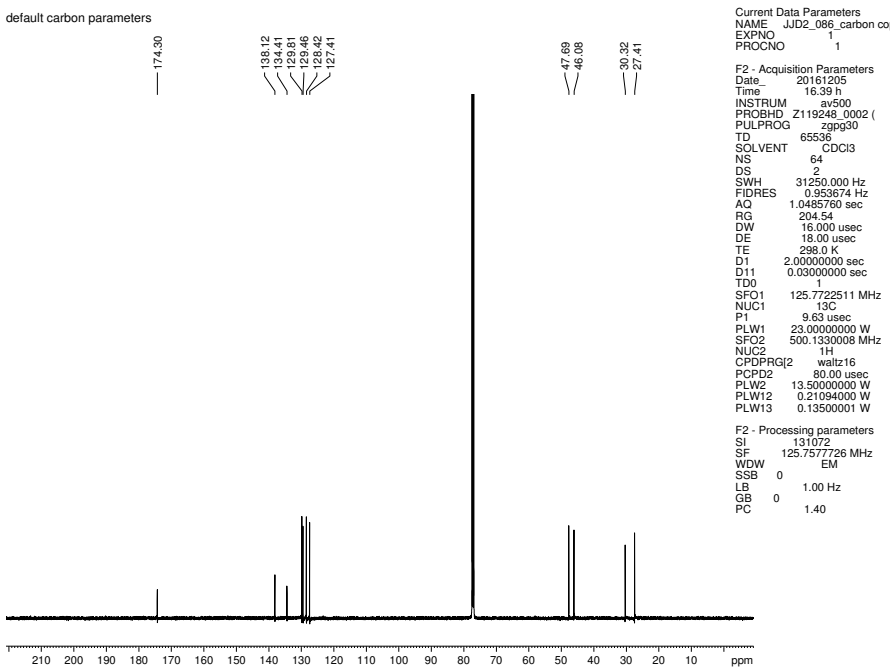

Figure 4.36 ^{13}C NMR (125 MHz, $CDCl_3$) of compound **4.17d**.

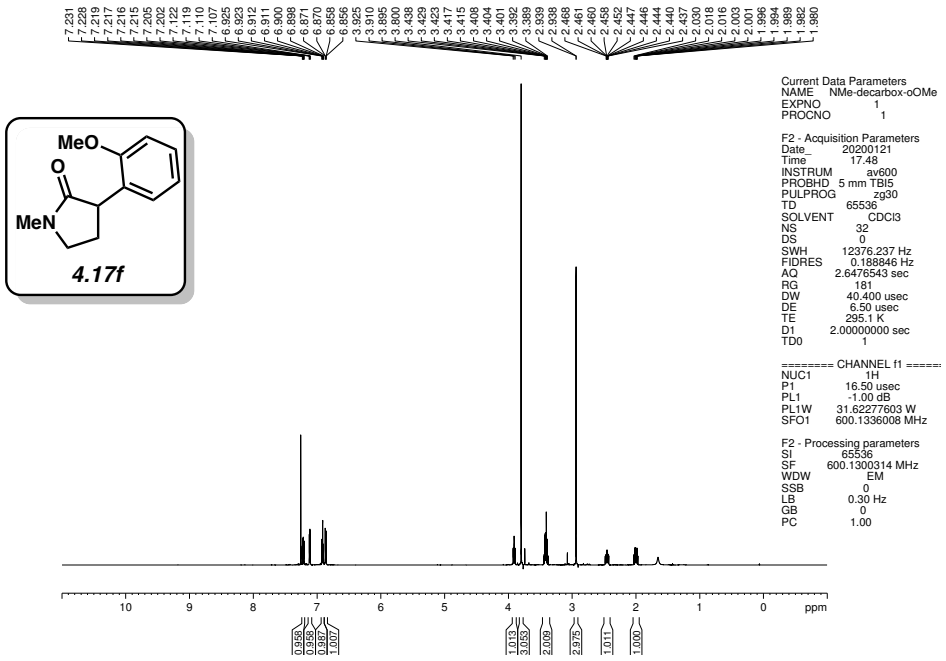

Figure 4.37 ^{1}H NMR (500 MHz, $CDCl_3$) of compound **4.17f**.

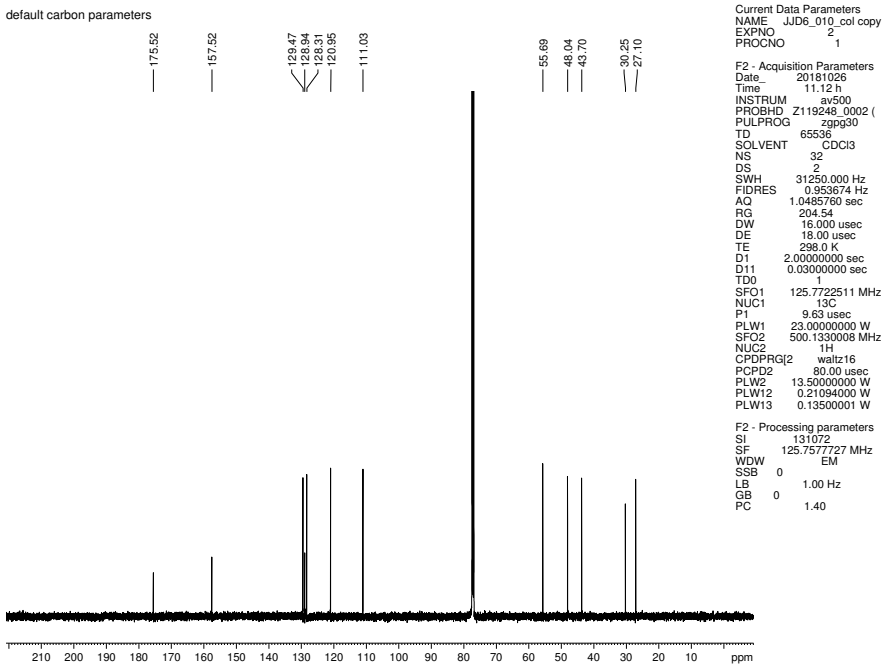

Figure 4.38 ^{13}C NMR (125 MHz, $CDCl_3$) of compound **4.17f**.

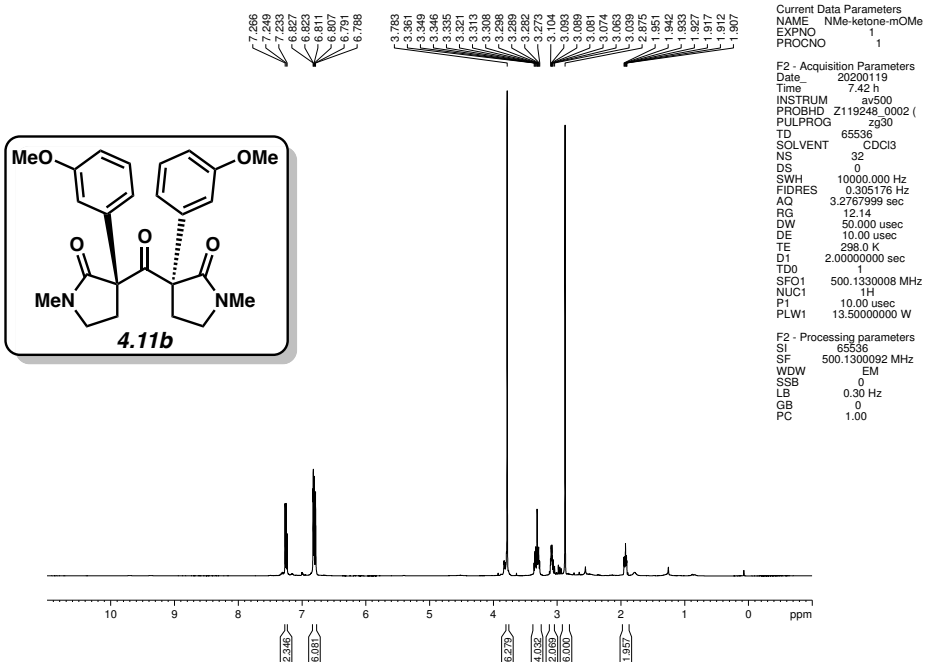

Figure 4.39 ^{1}H NMR (500 MHz, $CDCl_3$) of compound **4.11b.**

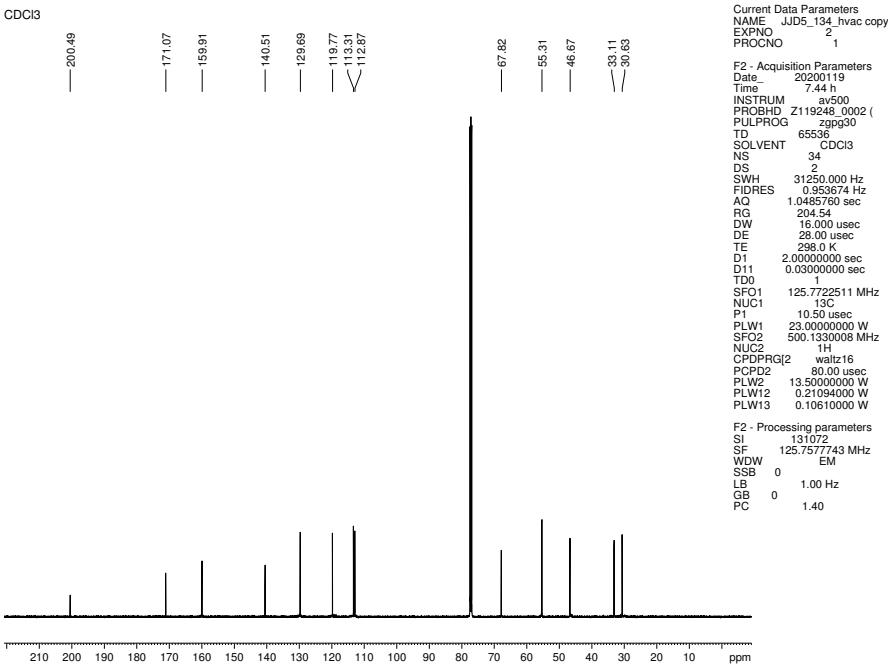

Figure 4.40 ^{13}C NMR (125 MHz, $CDCl_3$) of compound **4.11b**.

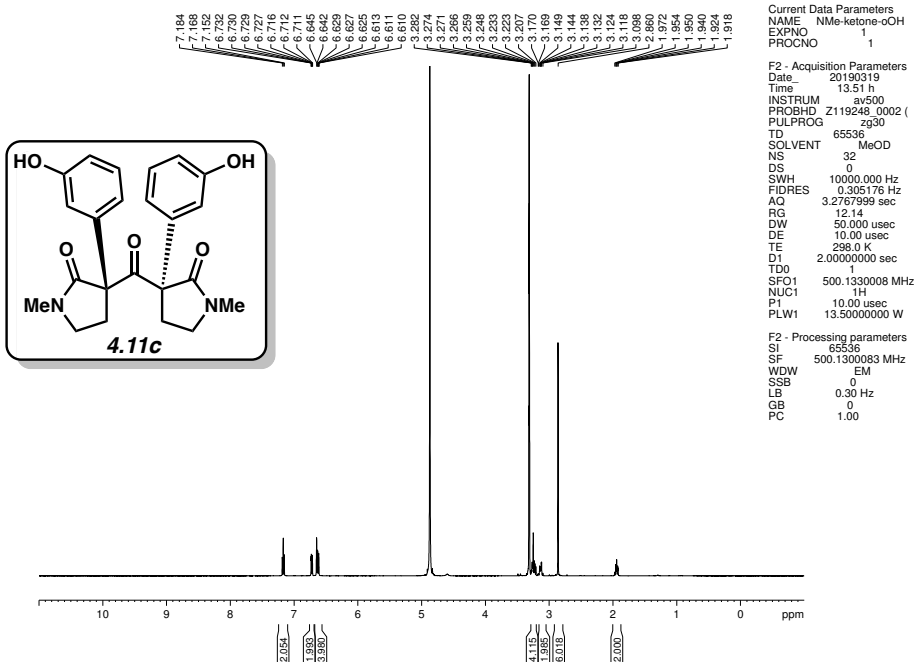

Figure 4.41 ^{1}H NMR (500 MHz, MeOH-d_4) of compound **4.11c**.

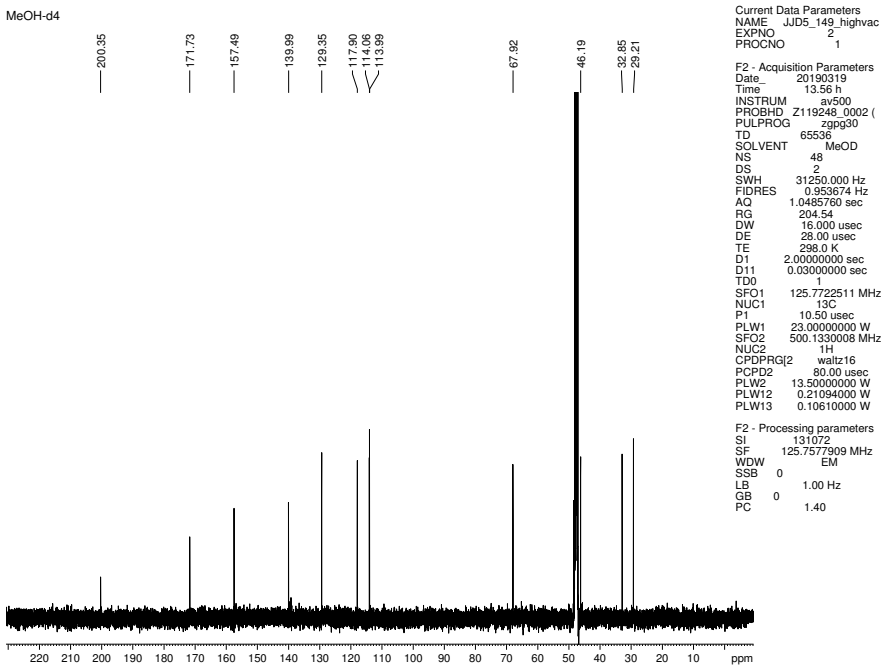

Figure 4.42 ^{13}C NMR (125 MHz, MeOH-d_4) of compound **4.11c**.

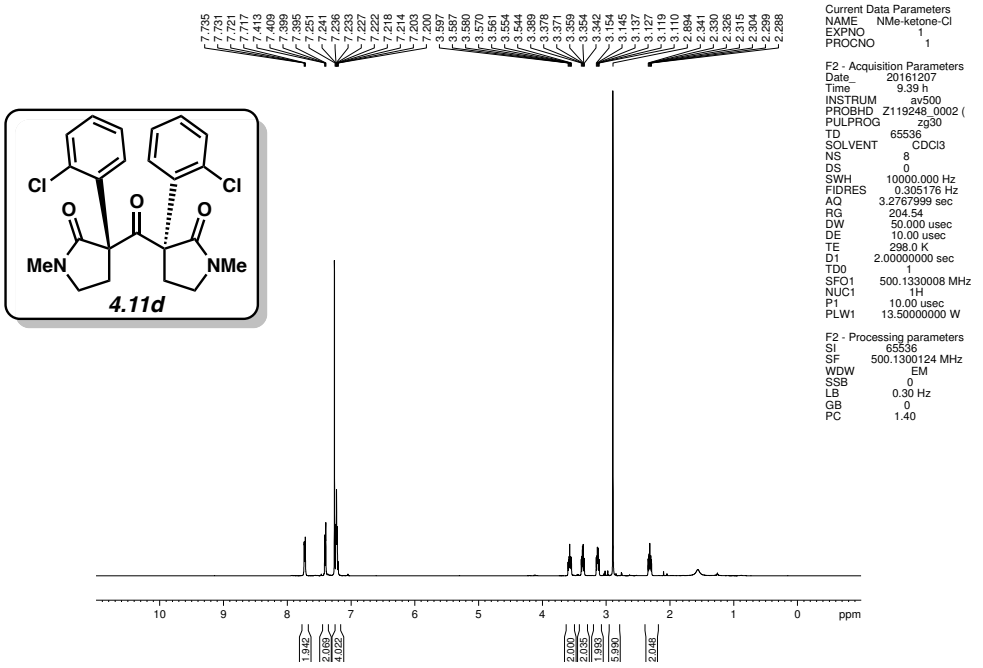

Figure 4.43 ^{1}H NMR (500 MHz, $CDCl_3$) of compound **4.11d**.

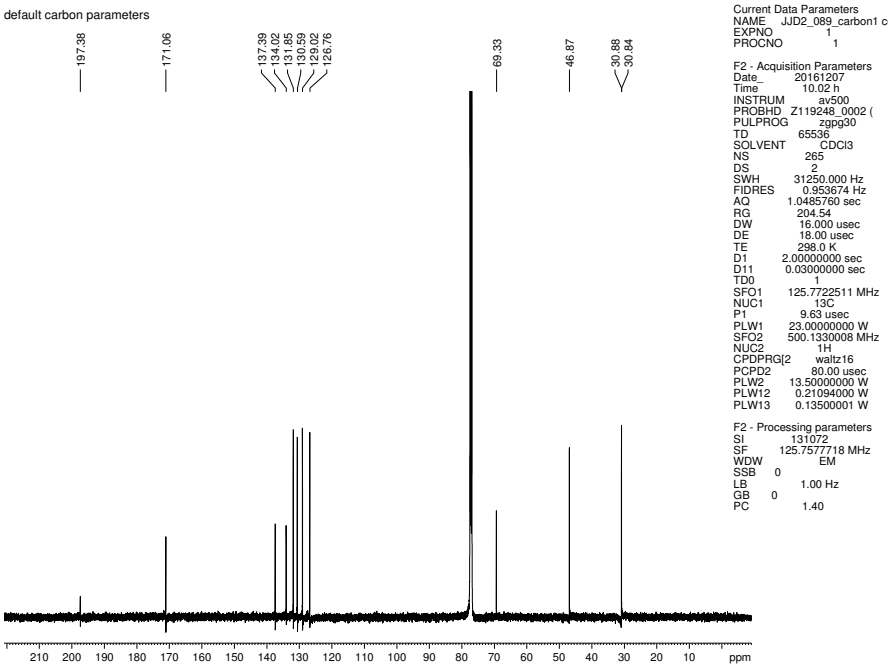

Figure 4.44 ^{13}C NMR (125 MHz, $CDCl_3$) of compound **4.11d**.

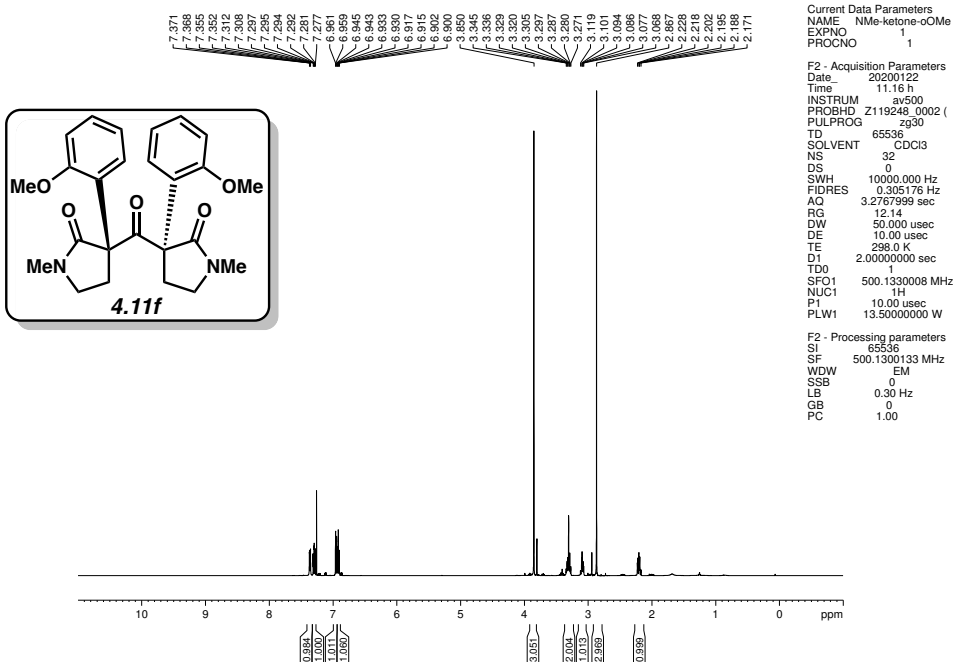

Figure 4.45 ^{1}H NMR (500 MHz, $CDCl_3$) of compound **4.11f**.

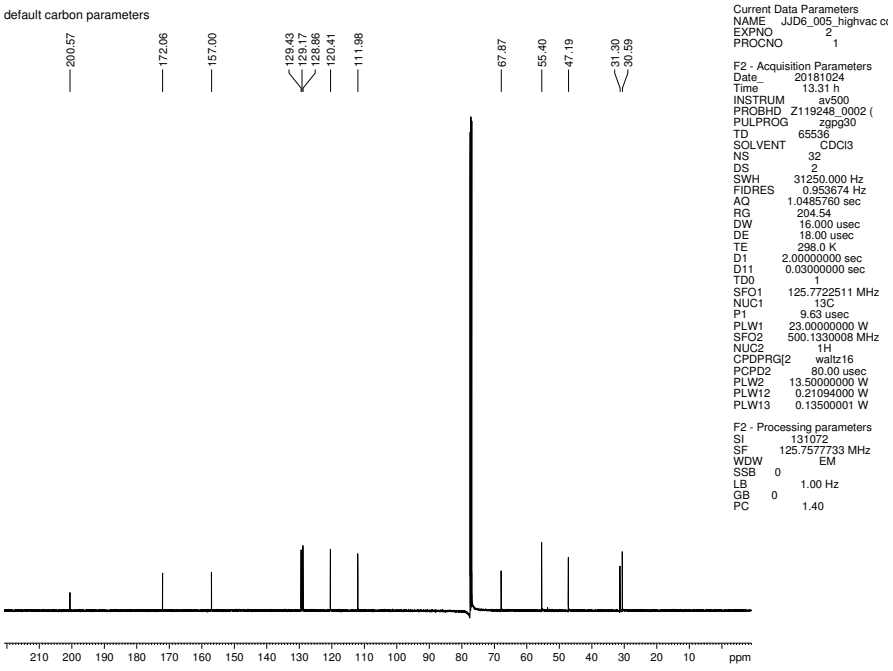

Figure 4.46 ^{13}C NMR (125 MHz, $CDCl_3$) of compound **4.11f**.

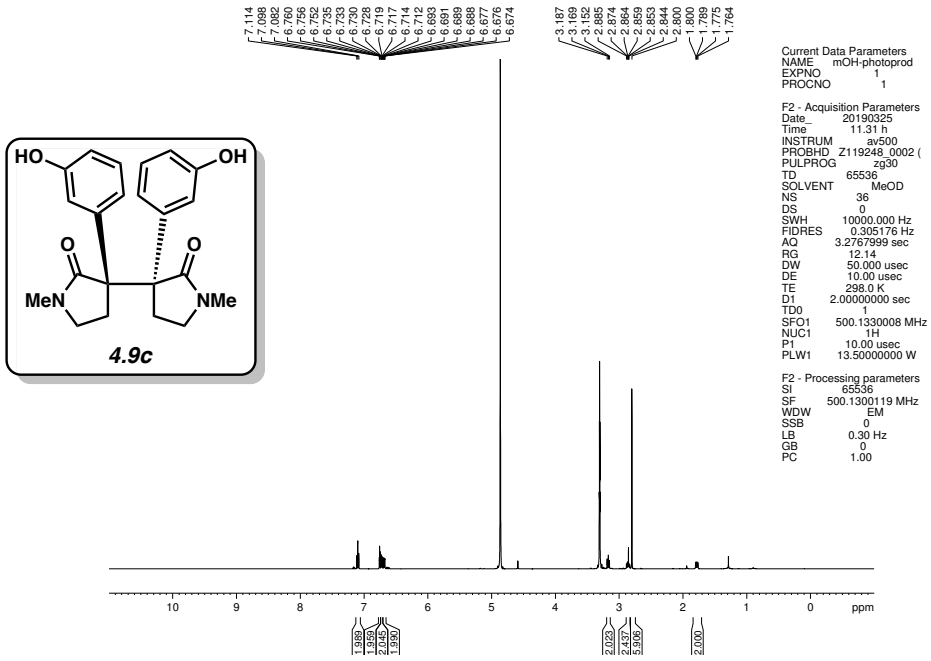

Figure 4.47 ^{1}H NMR (500 MHz, MeOH-d_4) of compound **4.9c**.

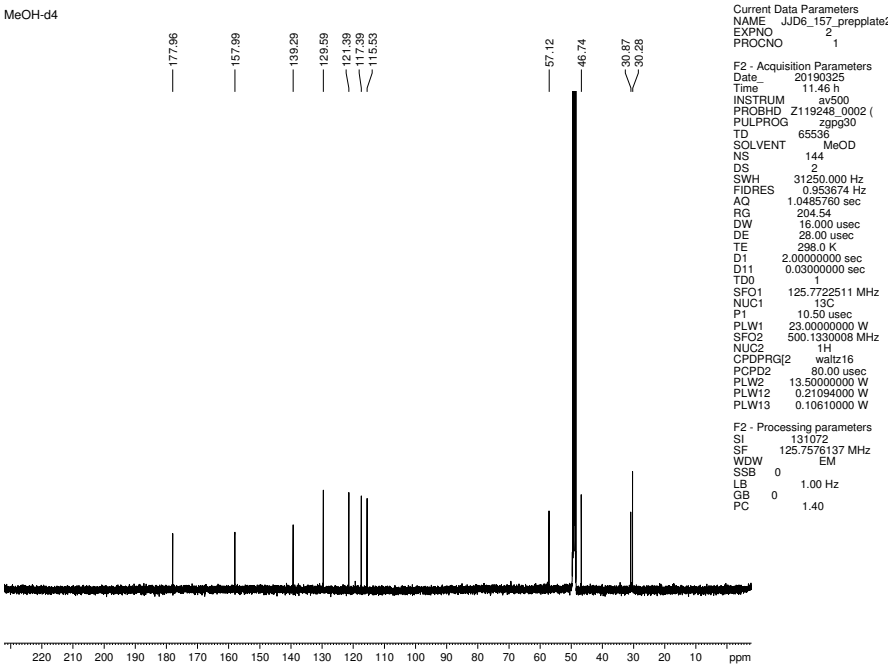

Figure 4.48 ^{13}C NMR (125 MHz, MeOH-d_4) of compound **4.9c**.

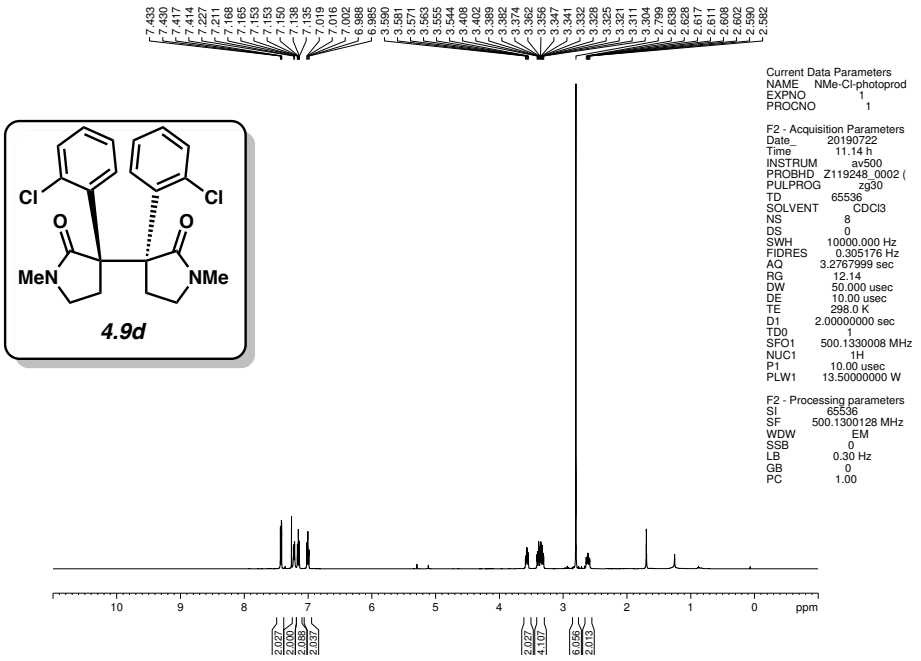

Figure 4.49^{1}H NMR (500 MHz, $CDCl_3$) of compound **4.9d**.

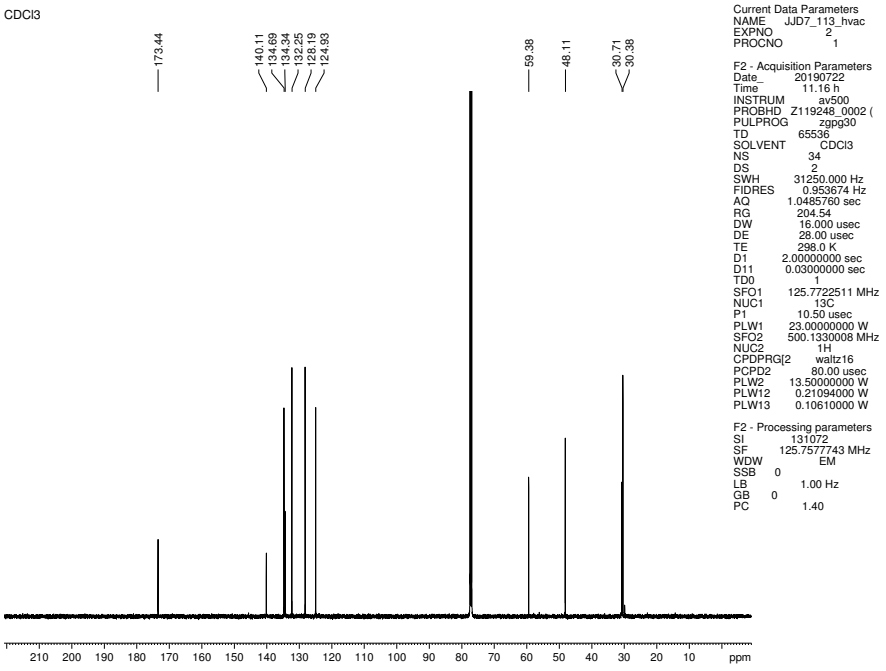

Figure 4.50^{13}C NMR (125 MHz, $CDCl_3$) of compound **4.9d**.

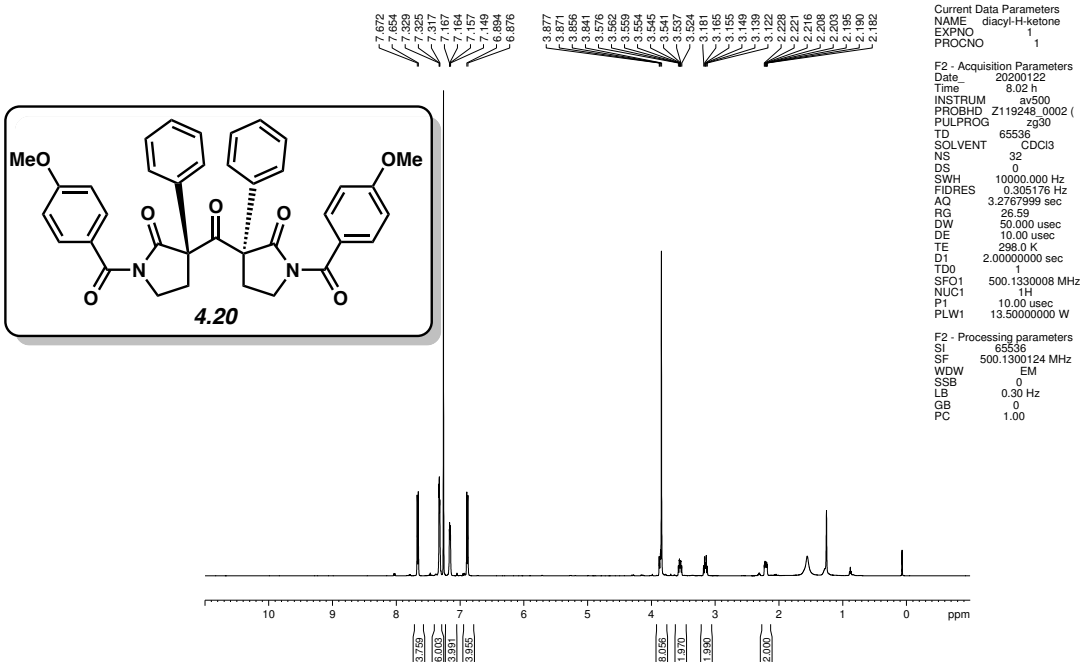

Figure 4.51 ^{1}H NMR (500 MHz, $CDCl_3$) of compound **4.20**.

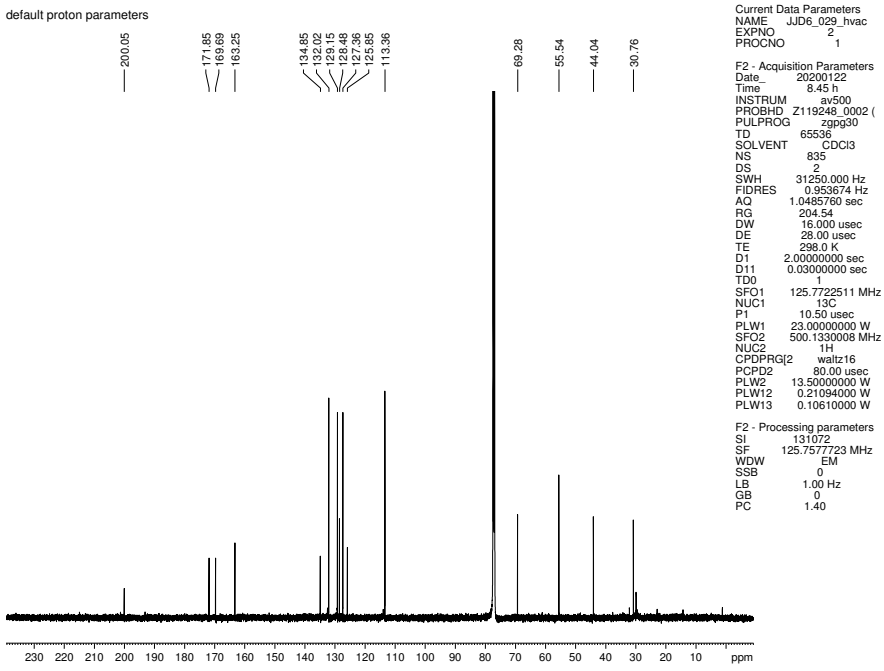

Figure 4.52 ^{13}C NMR (125 MHz, $CDCl_3$) of compound **4.20**.

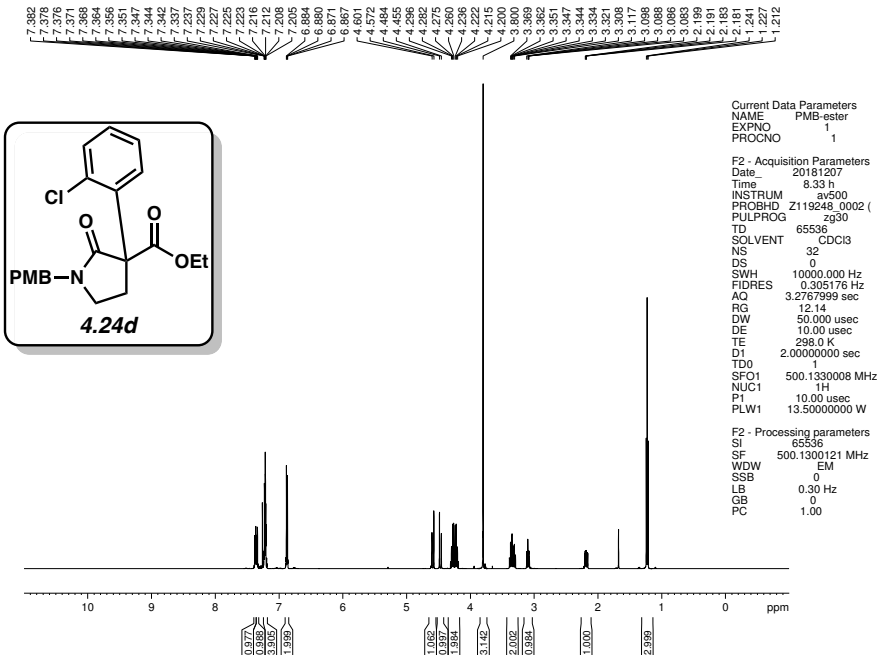

Figure 4.53 ^{1}H NMR (500 MHz, $CDCl_3$) of compound **4.24d**.

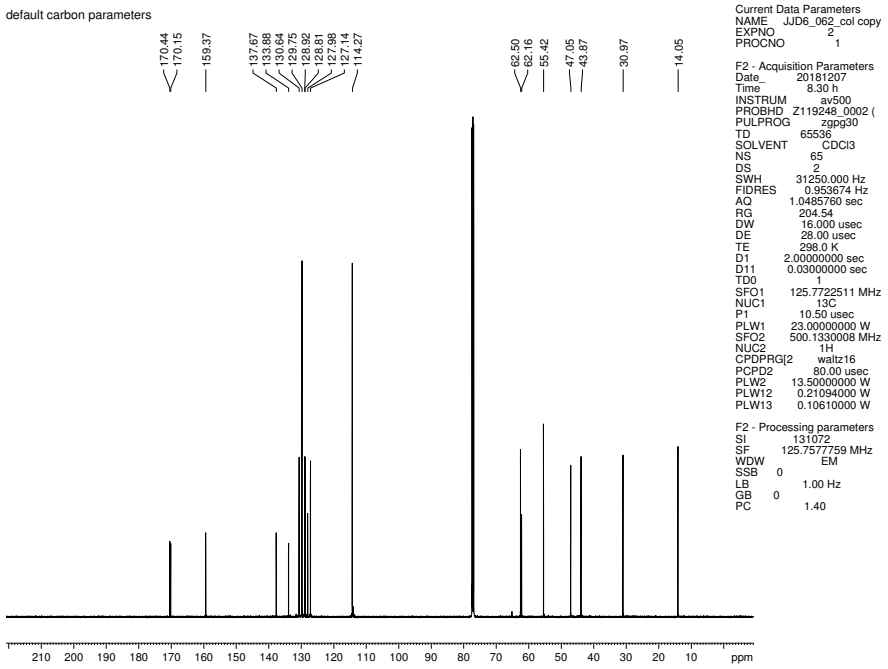

Figure 4.54 ^{13}C NMR (125 MHz, $CDCl_3$) of compound **4.24d**.

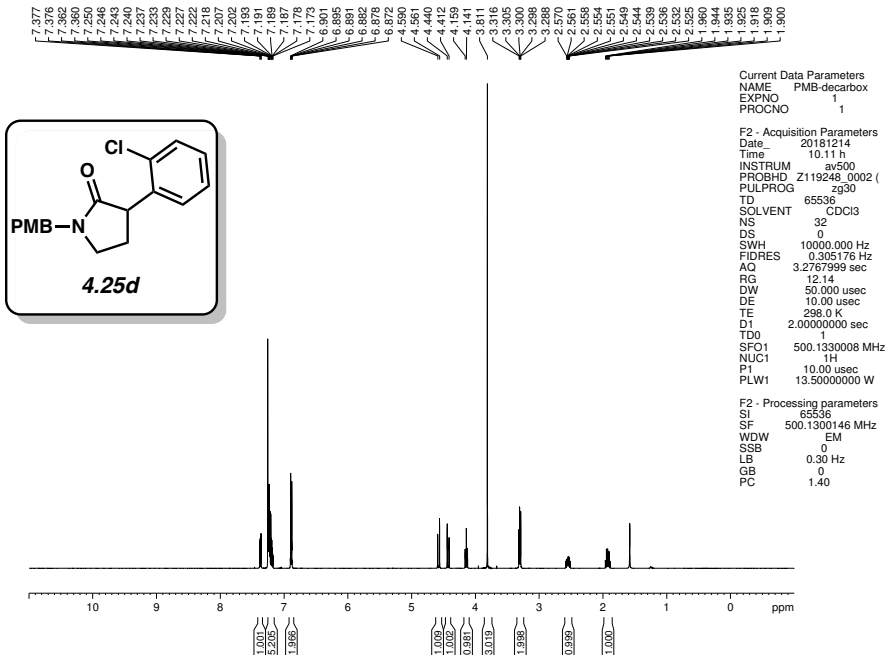

Figure 4.55 ^{1}H NMR (500 MHz, $CDCl_3$) of compound **4.25d**.

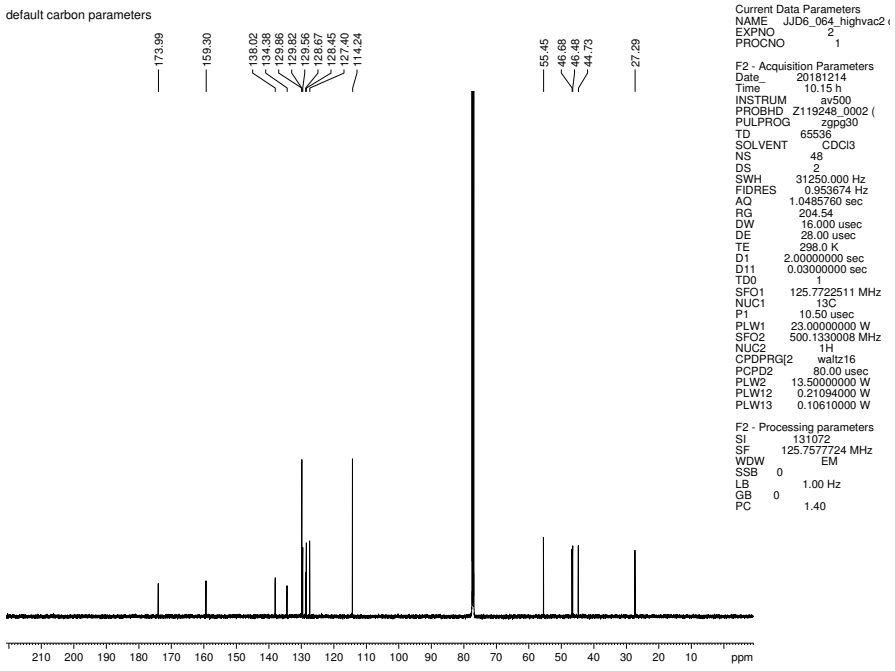

Figure 4.56 ^{13}C NMR (125 MHz, $CDCl_3$) of compound **4.25d**.

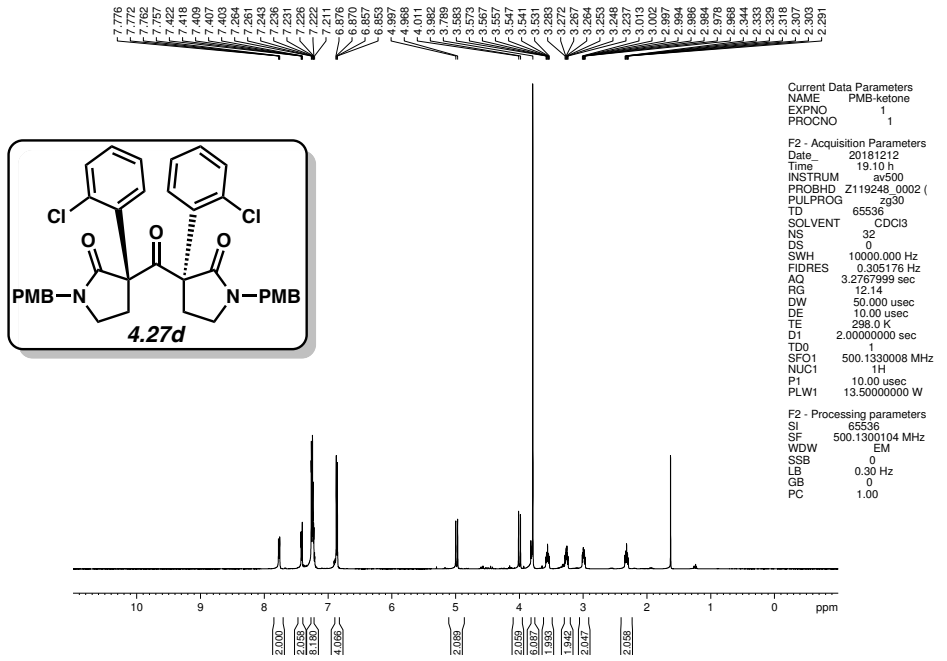

Figure 4.57 ^{1}H NMR (500 MHz, $CDCl_3$) of compound **4.27d**.

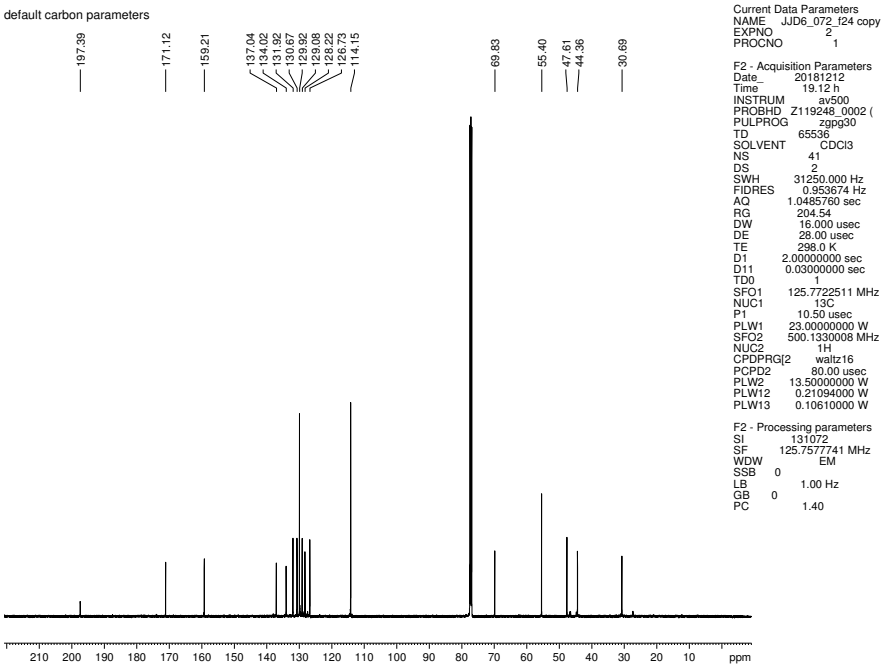

Figure 4.58 ^{13}C NMR (125 MHz, $CDCl_3$) of compound **4.27d**.

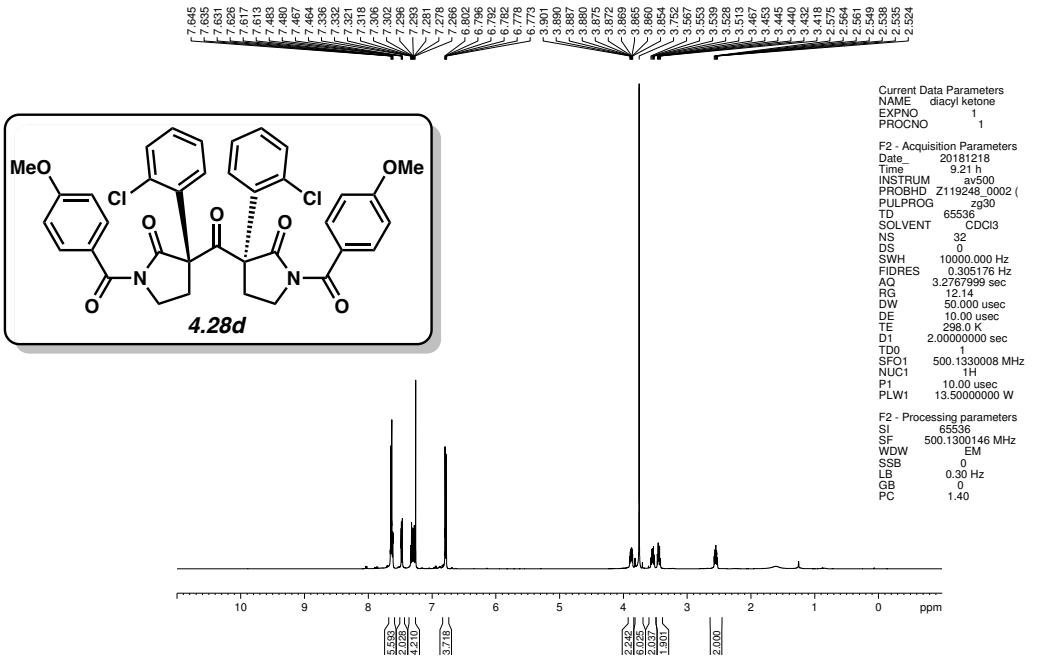

Figure 4.59 ^{1}H NMR (500 MHz, $CDCl_3$) of compound **4.28d**.

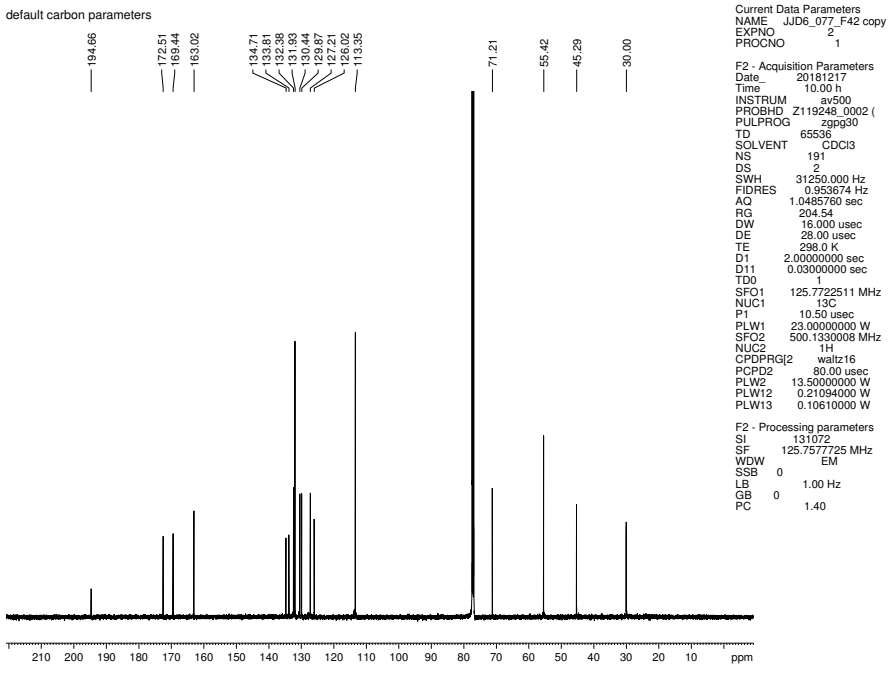

Figure 4.60 ^{13}C NMR (125 MHz, $CDCl_3$) of compound **4.28d**.

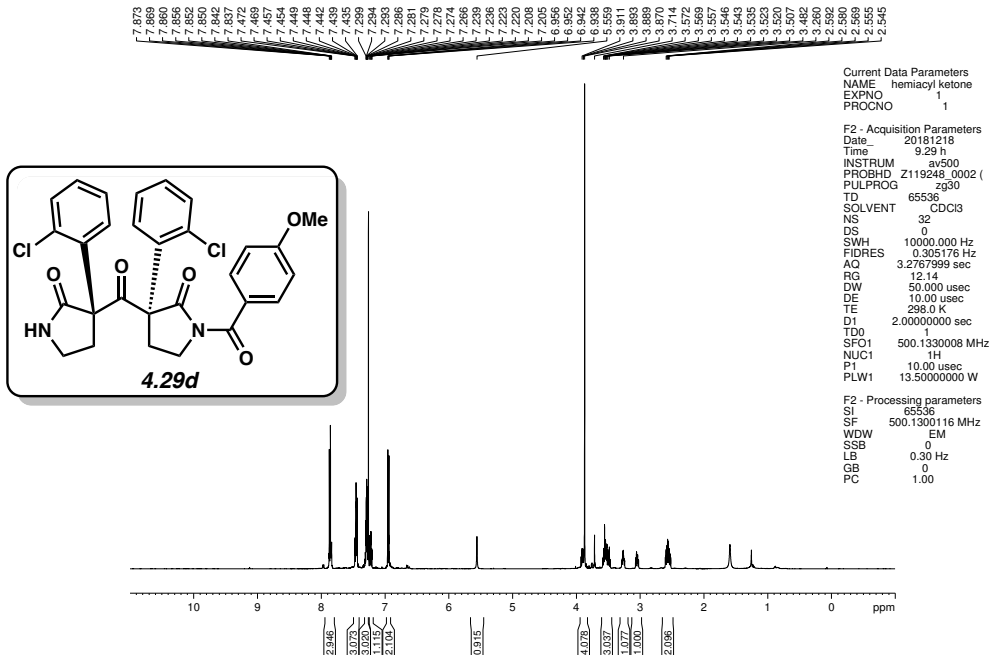

Figure 4.61 ^{1}H NMR (500 MHz, $CDCl_3$) of compound **4.29d**.

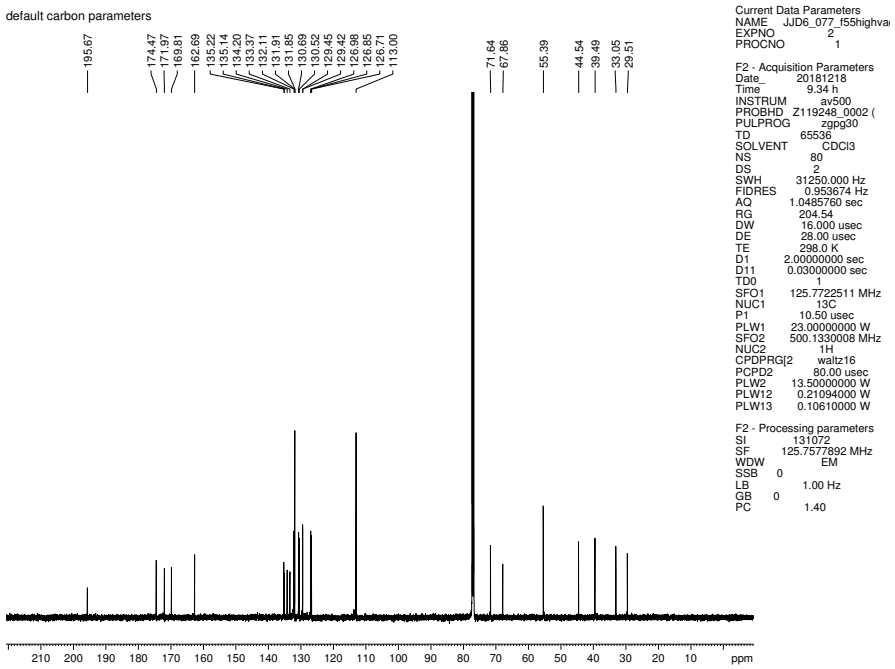

Figure 4.62 ^{13}C NMR (125 MHz, $CDCl_3$) of compound **4.29d**.

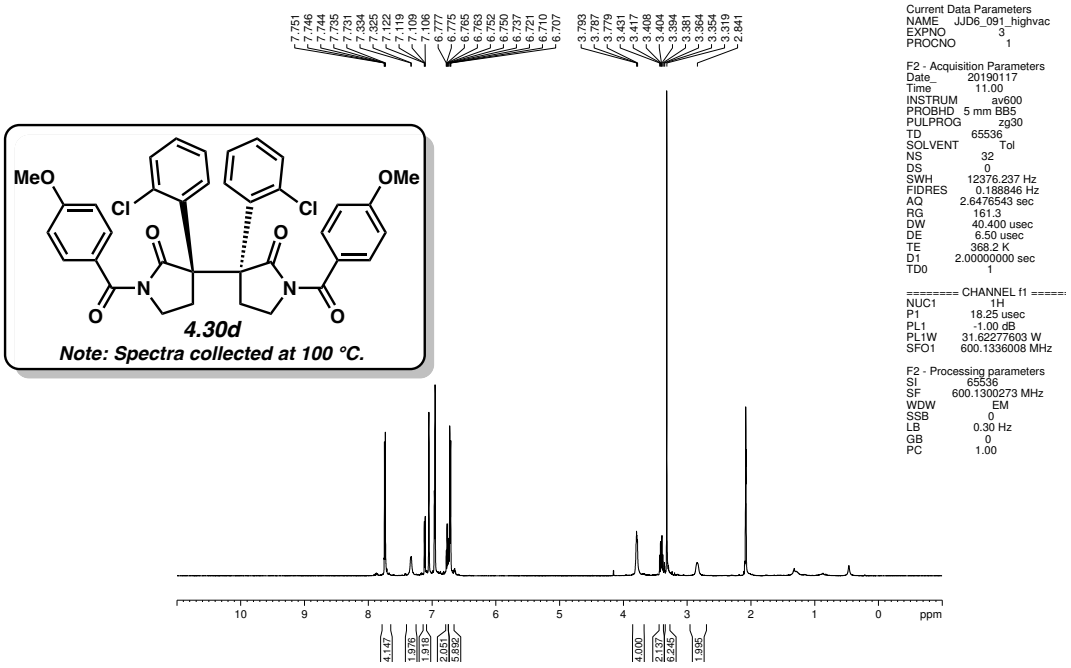

Figure 4.63 ^{1}H NMR (500 MHz, PhMe-d_8) of compound **4.30d**.

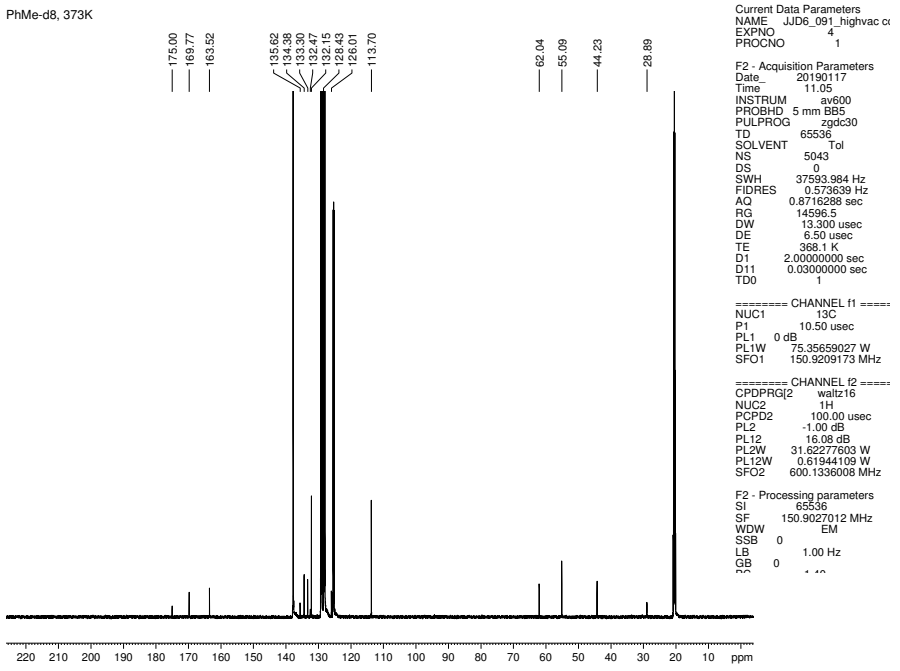

Figure 4.64 ^{13}C NMR (125 MHz, PhMe-d_8) of compound **4.30d**.

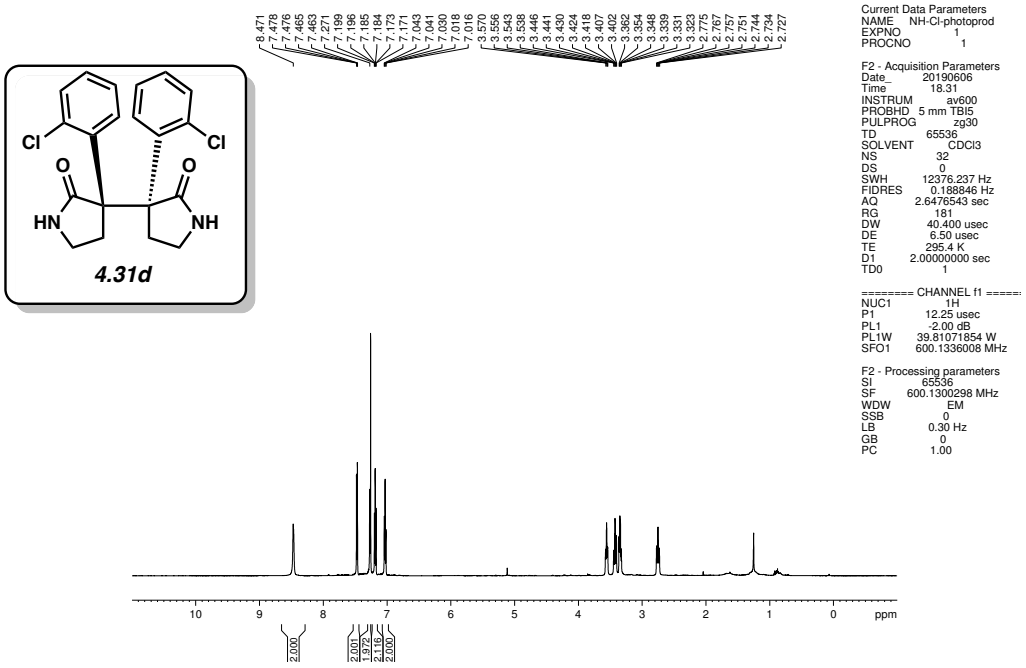

Figure 4.65 ^{1}H NMR (500 MHz, $CDCl_3$) of compound **4.31d**.

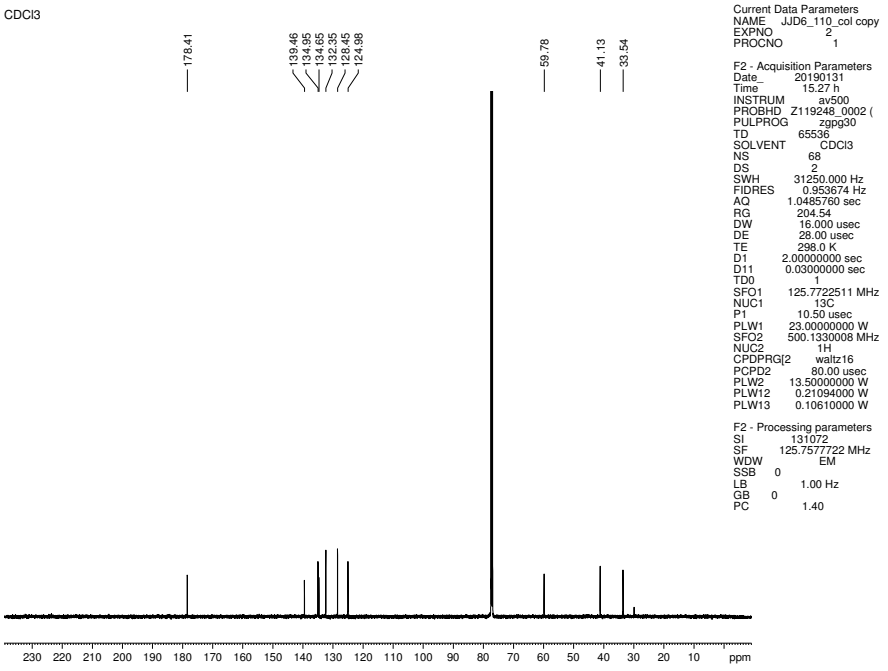

Figure 4.66 ^{13}C NMR (125 MHz, $CDCl_3$) of compound **4.31d**.

4.7 Notes and References

(1) For reviews of photochemical reactions being used in organic synthesis, see, (a) Prier, C. K.; Rankic, D. A.; MacMillan, D. W. C. *Chem. Rev.* **2013**, *113*, 5322–5363. (b) Kärkäs, M. D.; Porco, J. A.; Stephenson, C. R. J. *Chem. Rev.* **2016**, *116*, 9683–9747. (c) Bach, T.; Hehn, J. *Angew. Chem., Int. Ed.* **2011**, *50*, 1000–1045. (d) Nicholls, T. P.; Leonori, D.; Bissember, A. C. *Nat. Prod. Rep.* **2016**, *33*, 1248–1254.

(2) For reviews of photochemical reactions conducted in the solid state, see, (a) Dotson, J. J.; Perez-Estrada, S.; Garcia-Garibay, M. A. *J. Am. Chem. Soc.* **2018**, *140*, 8359–8371. (b) Ramamurthy, V.; Venkatesan, K. *Chem. Rev.* **1987**, *87*, 433–481. (c) Ramamurthy, V.; Sivaguru, J. *Chem. Rev.* **2016**, *116*, 9914–9993.

(3) (a) Hernandez-Linares, M. G.; Guerrero-Luna, G.; Perez-Estrada, S.; Ellison, M.; Ortin, M.-M.; Garcia-Garibay, M. A. *J. Am. Chem. Soc.* **2015**, *137*, 1679–1684. (b) Mortko, C. J.; Garcia-Garibay, M. A. *J. Am. Chem. Soc.* **2005**, *127*, 7994–7995. (c) Ng, D.; Yang, Z.; Garcia-Garibay, M. A. *Org. Lett.* **2004**, *6*, 645–647. (d) Natarajan, A.; Ng, D.; Yang, Z.; Garcia-Garibay, M. A. *Angew. Chem., Int. Ed.* **2007**, *46*, 6485–6487.

(4) For reviews on vicinal quaternary stereocenter construction, see, (a) Peterson, E. A.; Overman, L. E. *Proc. Natl. Acad. Sci. U.S.A.* **2004**, *101*, 11943–11948. (b) Long, R.; Huang, J.; Gong, J.; Yang, Z. *Nat. Prod. Rep.* **2015**, *32*, 1584–1601. (c) Liu, Y.; Han, S.; Liu, W.; Stoltz, B. M. *Acc. Chem. Res.* **2015**, *48*, 740–751.

(5) For reviews on the isolation and synthesis of bis(cyclotryptamine) alkaloids, see, (a) May, J. A.; Stoltz, B. *Tetrahedron* **2006**, *62*, 5262–5271. (b) Schmidt, M. A.; Movassaghi, M. *Synlett* **2008**, 313–324. (c) Steven, A.; Overman, L. E. *Angew. Chem. Int. Ed.* **2007**, *46*, 5488–5508.

(d) Trost, B. M.; Osipov, M. *Chem. Eur. J.* **2015**, *21*, 16318–16343. (e) Xu, J.-B.; Cheng, K.-J. *Molecules* **2015**, *20*, 6715–6738.

(6) The fifth scaffold, not depicted, has only been observed in a higher oxidation state and possesses opposite relative stereochemistry compared to **4.4**–**4.7**. For this scaffold, see, Verbitski, S. M.; Mayne, C. L.; Davis, R. A.; Concepcion, G. P.; Ireland, C. M *J. Org. Chem.* **2002**, *67*, 7124–7126.

(7) Eccles, R. G. *Druggists' Circular and Chemical Gazette* **1888**, *32*, 65.

(8) (a) Robinson, R.; Teuber, H. J. *Chem. Ind. (London)* **1954**, 783–784. (b) Manske, R. H. *Alkaloids* **1965**, *8*, 581–589.

(9) While this structure has never been isolated from a natural source, a structure with this ring system (albeit the *meso* isomer) was reported synthetically. For further details, see the following reference. Hall, E. S.; McCapra, F.; Scott, A. I. *Tetrahedron* **1967**, *23*, 4131–4141.

(10) When a ketone bearing an *ortho*- amine was synthesized, spontaneous condensation of the amine onto the ketone to form the corresponding spirocyclic aminal was observed.

(11) Although direct amination of the methoxy-substituted arene may be challenging, **4.9f** could also be converted to the corresponding aryl triflate, which should be more reactive toward cross-coupling.

(12) The common synthetic route used to access of ketones **4.11** was adapted from studies previously reported by our group. For details see the following reference: Resendiz, M. J. E.; Natarajan, A.; Garcia-Garibay, M. A. *Chem. Commun.* **2008**, 193–195.

(13) Dotson, J. J.; Garg, N. K.; Garcia-Garibay, M. A. *Tetrahedron* [Online early access]. DOI: 10.1016/j.tet.2020.131181. Published Online: Apr 10, 2020. https://www.sciencedirect.com/science/article/abs/pii/S0040402020303161?via%3Dihub.

(14) Note that starting material remained after irradiation. The yield based on remaining starting material is 54%.

(15) The loss of mass balance was attributed to unidentified, insoluble decomposition products.

(16) The yield of disproportionation was determined based on the yield of **4.17**.

(17) Note that starting material (**4.11d**) remained after irradiation. The yield based on remaining starting material is 17% (**4.9d**) and 24% (**4.17d**).

(18) Even substrates that exclusively undergo disproportionation upon solution-phase irradiation show full suppression of the disproportionation pathway in the crystalline solid state. For more details, see, Choe, T.; Khan, S. I.; Garcia-Garibay, M. A. *Photochem. Photobio. Sci.* **2006**, *5*, 449–451.

(19) Anslyn, E. V.; Dougherty, D. A. *Modern Physical Organic Chemistry*; University Science Books: Sausalito, CA, 2006; pp. 1–992.

(20) Consistent with our experimental results, this repulsive interaction results in diminished recombination yields for ketones with larger *ortho*- moieties.

(21) The topochemical principle states that reactions in the crystalline solid state will favor pathways that feature a minimum amount of atomic or molecular movement. For further discussion of the topochemical principle, see reference 2c and the following book: Schmidt, G. M. J.; et al. in *Solid State Photochemistry* (Ed.: Ginsburg, D.) Verlag Chemie: Weinheim, **1976**, pp, 1–280.

(22) We were also interested in a directed C–H amination of **4.9c**; however, we recognized that the *meta* hydroxy moieties would need to be reductively cleaved to provide the bis(pyrrolidinoindoline) alkaloids. Functionalization of **4.9a** would lead to a more ideal synthesis and was therefore prioritized in these studies.

(23) For select examples of transition metal-catalyzed activation of C(sp^2)–H bonds *ortho* to an amide directing group, see, (a) Qiu, F.-C.; Yang, W.-C.; Chang, Y.-Z.; Guan, B.-T. *Asian J. Org. Chem.* **2017**, *6*, 1361–1364. (b) Wykypiel, W.; Lohmann, J.-J.; Seebach, D. *Helvetica Chimica Acta* **1981**, *64*, 1337–1346. (c) Yeung, C. S.; Zhao, X.; Borduas, N.; Dong, V. M. *Chem. Sci.* **2010**, 331–336.

(24) For a review of directed aromatic lithiation of tertiary amides, see: Beak, P.; Snieckus, V. *Acc. Chem. Res.* **1982**, *15*, 306–312.

(25) Formation of the carbanion was determined by quenching with D_2O followed by NMR spectroscopic analysis.

(26) **4.20** was easily prepared in one step from a ketone previously reported by our group. For details, see reference 12.

(27) Since we anticipated that aryl halides would be ideal latent electrophiles for metal-catalyzed amination, we pursued the synthesis of chloro- and bromoketones **4.27d** and **4.27e**.

(28) The occurrence of a new, more stable polymorph that precludes formation of the desired polymorph is well-known and is often referred to as the "disappearing polymorph problem." For further discussion of this topic, see the following reviews: (a) Cruz-Cabeza, A. J.; Bernstein, J. *Chem. Rev.* **2014**, *114*, 2170–2191. (b) Snider, D. A.; Addicks, W.; Owens, W. *Advanced Drug Delivery Reviews* **2004**, *56*, 391–395.

(29) While highly irreproducible, several successful crystallizations to provide the reactive polymorph were accomplished when they were conducted in a different lab room, using new glassware, and new lab coat to avoid contamination of the unreactive polymorph. In these instances, small quantities of the reactive polymorph were used to seed crystallization.

(30) Larger scale transformations were not attempted. However, we surmise that the inherent scalability of suspension photochemistry would permit increased scale up without loss of reaction performance. See the following references for the use of crystalline suspensions to scale up the solid-state photodecarbonylation reaction. (For examples, see reference 3a and Verman, M.; Resendiz, M. J. E.; Garcia-Garibay, M. A. *Org. Lett.* **2006**, *8*, 2615–2617).

(31) Dapprich, S.; Komáromi, I.; Byun, K. S.; Morokuma, K.; Frisch, M. J. *J. Mol. Struct.* **1999**, *461*, 1–21.

(32) Vreven, T.; Byun, K. S.; Komáromi, I.; Dapprich, S.; Montgomery, J. A.; Morokuma, K.; Frisch, M. J. *J. Chem. Theory Comput.* **2006**, *2*, 815–826.

(33) This type of QM/MM strategy to model a reaction in the crystalline solid state was reported in the following reference: Keating, A. E.; Shin, S. H.; Houk, K. N.; Garcia-Garibay, M. A. *J. Am. Chem. Soc.* **1997**, *119*, 1474–1475.

(34) Chai, J.-D.; Head-Gordon, M. *Phys. Chem. Chem. Phys.* **2008**, *10,* 6615–6620.

(35) We favor the employment of a molecular mechanics method to describe the low-level layer (over semi-empirical methods or quantum chemical calculations with very small basis sets) since the MM force field by definition includes a description of dispersion effects between all atoms in the MM region and between QM and MM regions. Indeed, this hybrid approach has been shown to be accurate in similar computational studies of solid-state transformations of stilbene where crystalline environment calculations were included in the low-level layer (see reference 33).

(36) While we were able to successfully identify the transition state geometries for the disproportionation pathway, the calculated barriers did not agree with experimental results and the values ranged dramatically from 3 to 17 kcal/mol. We hypothesize that other factors

that are not accounted for in our computational model might be playing a role in determining the activation barrier. Our computational model was able to reflect the experimental results for recombination, but must be further tuned to model disproportionation successfully.

(37) We do not consider the ordering of barriers for **4.10d–f** to be meaningful as they fall within a 0.7 kcal/mol range and are therefore within computational error of one another.

(38) For a review of catalytic amination of aryl halides, see, Heravi, M. M.; Kheilkordi, Z.; Zadsirjan, V.; Heydari, M.; Malmir, M. *J. Organomet. Chem.* **2018**, *861*, 17–104.

(39) Unfortunately, despite extensive efforts, **4.33** could not be fully purified and was, therefore, carried forward directly in the subsequent step.

(40) Note that the double azidation reaction to convert **4.9e** to **4.33** was challenging to enact and resulted in < 35% yield (based on ^{1}H NMR analysis of the semi-pure material). As such, the reductive cyclization to convert **4.33** into **4.36** likely took place in > 75% yield.

(41) The observed ^{1}H and ^{13}C NMR and spectra of **4.36** were not identical to the published spectra of bhesine (**4.38**). We hypothesized that we may have either produced an aminal isomer of **4.38** or subtle changes in solvent acidity may have shifted the ^{1}H and ^{13}C resonances. For the first isolation of **4.38**, see, Balayer, A.; Sévenet, T.; Schaller, H.; Haudi, A. H. A.; Chiaroni, A.; Riche, C.; Païs, M. *Nat. Prod. Lett.* **1993**, *2*, 61–67.

(42) Oxdation conditions adapted from: Higuchi, K.; Sato, Y.; Tsuchimochi, M.; Sugiura, K.; Hatori, M.; Kawasaki, T. *Org. Lett.* **2009**, *11*, 197–199.

(43) Verotta, L.; Pilati, T.; Tató, M.; Elisabetsky, E.; Amaor, T. A.; Nunes, D. S.; *J. Nat. Prod.* **1998**, *61*, 392–396.

(44) Frisch, M. J.; Trucks, G. W.; Schlegel, H. B.; Scuseria, G. E.; Robb, M. A.; Cheeseman, J. R.; Scalmani, G.; Barone, V.; Mennucci, B.; Petersson, G. A.; Nakatsuji, H.; Caricato, M.; Li,

X.; Hratchian, H. P.; Izmaylov, A. F.; Bloino, J.; Zheng, G.; Sonnenberg, J. L.; Hada, M.; Ehara, M.; Toyota, K.; Fukuda, R.; Hasegawa, J.; Ishida, M.; Nakajima, T.; Honda, Y.; Kitao, O.; Nakai, H.; Vreven, T.; Montgomery, J. A.; Peralta, J. E.; Ogliaro, F.; Bearpark, M.; Heyd, J. J.; Brothers, E.; Kudin, K. N.; Staroverov, V. N.; Kobayashi, R.; Normand, J.; Raghavachari, K.; Rendell, A.; Burant, J. C.; Iyengar, S. S.; Tomasi, J.; Cossi, M.; Rega, N.; Millam, J. M.; Klene, M.; Knox, J. E.; Cross, J. B.; Bakken, V.; Adamo, C.; Jaramillo, J.; Gomperts, R.; Stratmann, R. E.; Yazyev, O.; Austin, A. J.; Cammi, R.; Pomelli, C.; Ochterski, J. W.; Martin, R. L.; Morokuma, K.; Zakrzewski, V. G.; Voth, G. A.; Salvador, P.; Dannenberg, J. J.; Dapprich, S.; Daniels, A. D.; Farkas; Foresman, J. B.; Ortiz, J. V.; Cioslowski, J.; Fox, D. J. Gaussian 09; Gaussian Inc.: Wallingford, CT, 2009.

CHAPTER FIVE

A High Yielding and Divergent Paradigm for the Synthesis of D_{2h}-Symmetric Octakis-Substituted Pentiptycenequinones

Adapted from: Geeta S. Vadehra, Xing Jiang, Jordan J. Dotson, Gong M. Chu, and Miguel A. Garcia-Garibay*.

Org. Lett. **2017**, *19*, 1838–1841.

5.1 Abstract

With a rigid fused polyaromatic framework and a well-defined, highly symmetric molecular geometry, pentiptycenes are appealing building blocks for a variety of materials applications. Unfortunately, their use has been limited by the lengthy syntheses of their functionalized derivatives. This communication describes a highly efficient, brief, divergent paradigm for the preparation of octakis-substituted pentiptycene derivatives that starts with the preparation of an octakis(bromo)-compound, which can be used as a Pd(0)-catalyzed coupling partner with suitable organometallic nucleophiles to install a range of groups in high yields at the peripheral 2,3,6,7,14,15,19,20 positions, including methyl, allyl, vinyl, alkynyl, aryl, heteroaryl, and even bulky 4-triphenylmethyl-phenyl substituents.

5.2 Introduction

Pentiptycenes are a family of compounds with five benzene rings fused to two bicyclo[2.2.2]octatrienes, which may be viewed as extended triptycenes.[1] Their rigid framework can be used to build geometrically regular structures with substituents attached along the central

ring[2,3] or by taking advantage of the peripheral positions,[4] as illustrated by the R-groups in Scheme 5.1. With five non-coplanar aromatic rings creating protuberances and cavities of unequal size, it is difficult for pentiptycenes to form densely packed structures, which renders them useful for the design of low-density materials[5] for applications in sensors,[3] molecular machines[6] and supramolecular chemistry.[7]

In general, the pentiptycene core is conveniently obtained by Diels-Alder reactions between *p*-benzoquinone with two equivalents of anthracene (Scheme 5.1). The resulting pentiptycenequinones are highly versatile intermediates for the synthesis of linearly conjugated polymers and other substituted analogs.[2] By contrast, the preparation of peripherally substituted structures has been extremely challenging. The Diels-Alder reaction requires the use of substituted anthracenes,[4,8] which are not readily available and have a low solubility that makes them difficult to manipulate. To our knowledge, there is only one example of a peripherally octakis-substituted pentiptycene, which was prepared by this strategy using tetramethoxyanthracene (Scheme 5.1, R = OMe).[4] However, even after optimization, this product is obtained in a relatively low yield (16%).[3] By contrast, the divergent procedure reported below provides a wide range of functionalities with overall yields in the range of ca. 50% to 75% from pentiptycenequinone **5.1**. Considering the potential of the peripherally substituted structures for applications that rely on precise geometric design, and aware of a highly improved selective multibromination of triptycenes,[9,10] we set out to explore a three-step divergent functionalization strategy that starts from the readily available pentiptycene quinone **5.1**.

Scheme 5.1 Our approach to the synthesis of peripherally functionalized pentiptycenequinones.

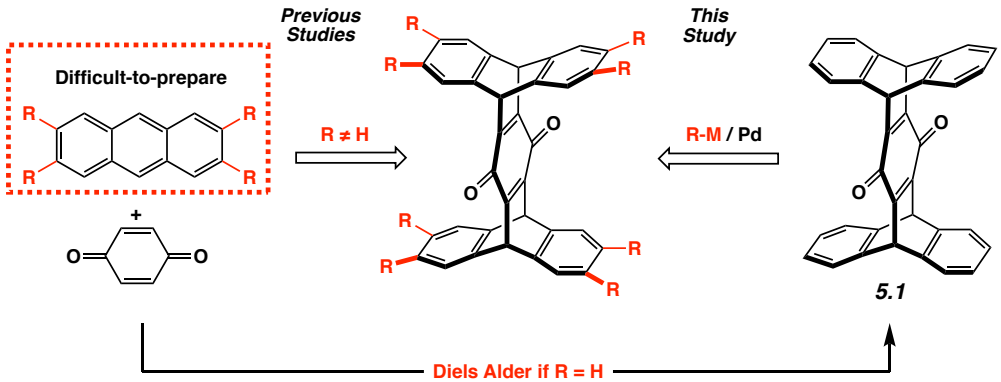

5.3 Results and Discussion

Considering the potential of the peripherally substituted structures for applications that rely on precise geometrical design, and aware of a highly improved selective multibromination of triptycenes, [10,11] we set out to explore a three-step divergent functionalization strategy that starts from the readily available pentiptycene quinone **5.1**. Our synthetic procedure for peripheral funcionalization of the pentiptycene scaffold is detailed in Scheme 5.2. Since the parent quinone structures are likely to be sparingly soluble in many organic solvents, we envisioned the temporary introduction of solubilizing butyl groups by reduction and alkylation of the central quinone ring. This was achieved in two steps and 98% overall yield to obtain the significantly more soluble dibutyl diether **5.2**. The key eight-fold regioselective bromination was achieved using molecular bromine in the presence of iron filings in refluxing chloroform. The ^{1}H NMR of the crude product mixture revealed the octabrominated product **5.3** with no side products and was isolated in 80–90% yield. As we noticed that the Lewis acid formed *in situ* leads to the cleavage of the ether linkage, it was important to limit the amount of Br_2 to 8 eq. to prevent deprotection and maximize the isolated yield. Since we envisioned pentiptycene **5.3** as a promising precursor to a variety of palladium cross-coupling reactions we set out to explore a number of organometallic partners to

couple alkyl, allyl, vinyl, aryl and heteroaryl groups covering a range of functional groups and steric bulk (Table 5.1).

Scheme 5.2 Bromination/cross-coupling strategy for peripheral functionalization of pentiptycenequinones.

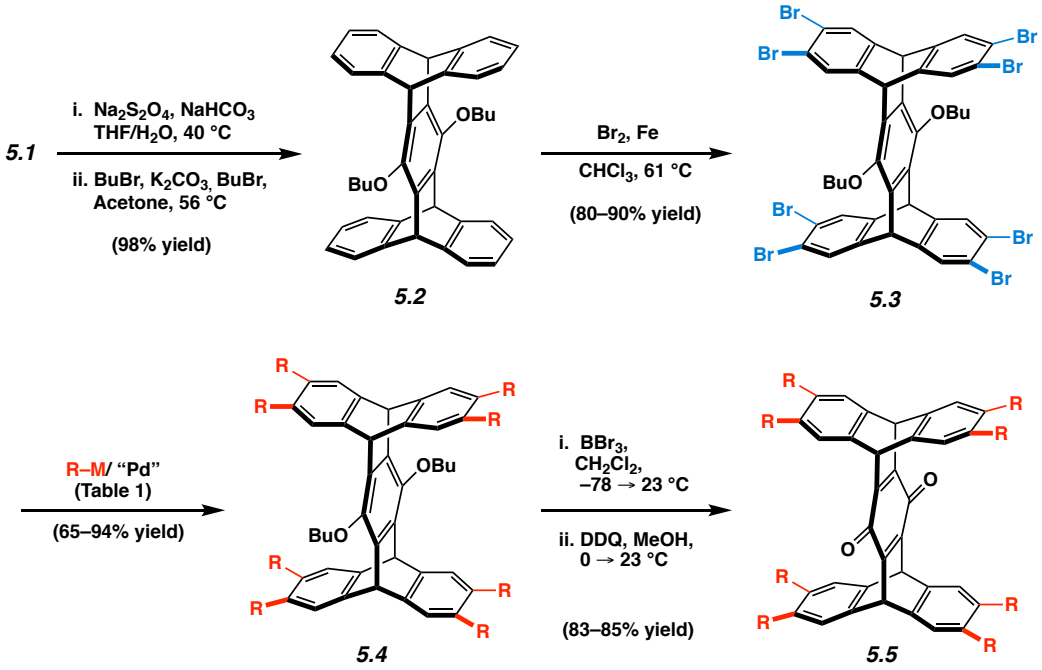

Table 5.1. Isolated yields of Pd-coupling reactions of octakis(bromo)-pentiptycene **5.3** with various coupling partners.[a]

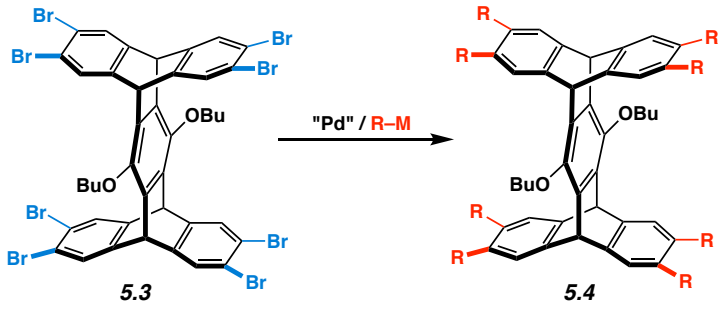

Product	R =	Coupling Partner	Yield (%)
5.4a		$AlMe_3$	94
5.4b	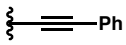	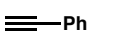	77
5.4c	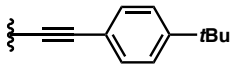	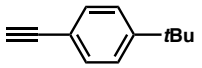	65
5.4d		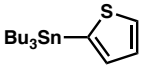	76
5.4e	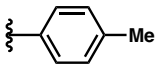	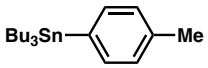	83
5.4f		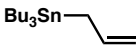	70
5.4g		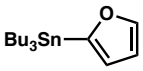	65
5.4h		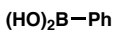	93
5.4i	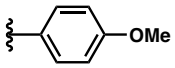	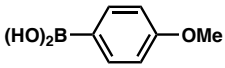	69
5.4j	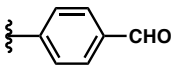	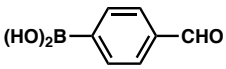	74
5.4k	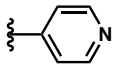	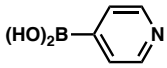	91
5.4l	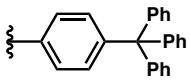	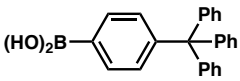	85
5.4m		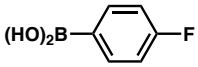	82
5.4n		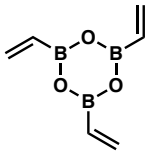	91
5.4o	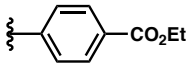	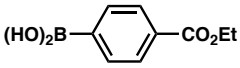	76

[a] Please see experimental section for reaction conditions.

To our satisfaction, we were able to conduct reactions of compound **5.3** to the octamethylpentiptycene (**5.4a**) in a 150 mg scale to complete conversion in ca. 12 h in an excellent yield of 94%. We showed that Sonogashira reactions in analogous scale work well in ca. 48 h

using phenyl- and tolylacetylene as the coupling partners to give the octaarylethynyl compounds (**5.4b**, **5.4c**). Stille couplings using 2-(tributylstannyl)thiophene, 4-(tributylstannyl)toluene, allyltributylstannane, and 2-(tributylstannyl)furan were shown to give derivatives **5.4d**–**5.4g** in good to excellent yields in ca. 16 h. Considering the accessibility of boronate nucleophiles, we analyzed a range of Suzuki-Miyaura couplings with vinyl, aryl, and heteroaryl groups that gave efficient access to pentiptycences **5.4h**–**5.4o** in a time frame of 12–16 h, except for **5.4n**, which was obtained in only 4 h after which the reaction was stopped to prevent decomposition. The aryl groups explored included examples with electron neutral (**5.4h**), donating (**5.4i**), and withdrawing groups (**5.4j**, **5.4k**, **5.4m**, and **5.4o**), as well the relatively large and bulky octakis(4-triphenylmethyl-phenyl) derivative (**5.4l**).

All reactions were conveniently monitored by following changes in the pentiptycene bridgehead signal in the ^{1}H NMR spectrum. It evolves from a singlet at 5.50 ppm in the case of **5.3** into multiple signals for partially reacted intermediates until it becomes a new singlet in the range of in 5.52- to 5.93 ppm for the final product, depending on the substituent (except in the case of **5.4a** where the corresponding signal occurs at higher field, at 5.47 ppm). In addition to ^{13}C NMR analysis (and ^{19}F NMR in the case of **5.4m**), the identity of all the coupling products was also supported by high-resolution mass spectra acquired by ESI or MALDI-TOF methods. Excellent results were obtained for all compounds with molecular masses in the range of 687.4-1781.7 amu. However, in the case of **5.4l**, with a molecular mass of 3119.4 amu, an exact mass could only be obtained after removal of the butoxy group and oxidation to quinone **5.5l** (Scheme 5.2). The eight-fold transformations occurred in isolated yields that range from 65% to 94%, indicating individual steps that occur with average individual efficiencies that vary from 95% to 99%, respectively. It should be noted that there are limitations to any single type of reaction. For

example, while the octathienyl pentiptycene **5.4d** was obtained in good yields by a Stille coupling, attempts to prepare the same compound by the Suzuki-Miyaura procedure using 2-thiopheneboronic acid as a coupling partner led to a quantitative protodeboronation of the latter.

The structural significance of the iptycenes in Table 5.1 comes from their potential in a variety of applications. For example, 4-pyridyl (**5.4k**) and 4-(ethoxycarbonyl)phenyl (**5.4o**) substitutions may serve as ligands in metal-organic frameworks,[12] and the 4-phenyl-carboxaldehyde derivative **5.4j** should be ideal for the preparation of imine-based covalent organic frameworks and dynamic combinatorial synthesis.[13,14] As a proof of concept, we showed that refluxing **5.4j** with aniline provides the corresponding octaimine **5.4p** in a remarkably clean transformation (Scheme 5.3).

Scheme 5.3. Efficient Schiff-Base formation from octaaldehyde **5.4j**.

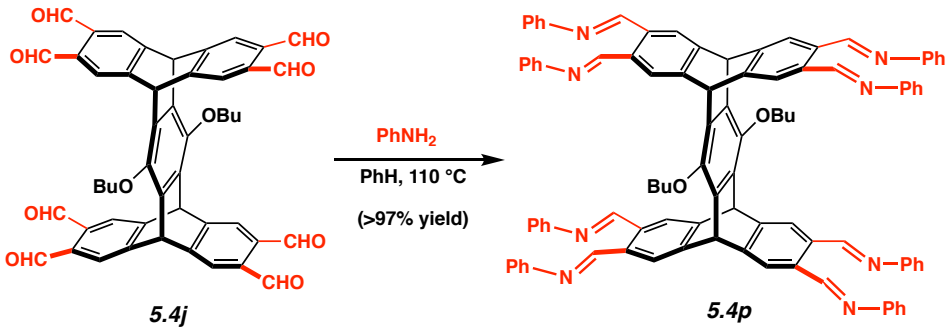

Having obtained the peripherally substituted dibutoxypentiptycenes we explored their transformation into the synthetically more versatile pentiptycenequinones. Knowing that conditions needed for the removal of the butoxy group and oxidation of the intermediate hydroquinone could compromise a variety of the substituents, we selected the octamethyl, octaphenyl, and octakis(4-triaphenylmethyl-phenyl) derivatives **5.4a**, **5.4h** and **5.4l** (Scheme 5.2) to demonstrate the potential of this reaction. The transformation was achieved consistently in ca.

85% isolated yields in one-pot procedures consisting of ether cleavage under Lewis acidic conditions followed by DDQ mediated oxidation (Scheme 5.2). The pentiptycenequinones **5.5a**, **5.5h** and, **5.5l** were sufficiently soluble for chromatographic purification and all structures were confirmed by ^{1}H NMR, ^{13}C NMR, and FTIR spectroscopic methods, as well as by high-resolution mass spectrometry (either MALDI-TOF or ESI) as noted in the experimental section.

Single-crystal X-ray diffraction analysis of **5.5h** revealed packing in the space group P_1 with two benzene molecules and one molecule of **5.5h** per unit cell. The phenyl groups rotate out of conjugation with the pentiptycene blade, forming dihedral angles that range from 45.8° to 53.5°. Molecules pack in layers orthogonal to the direction of the carbonyl axis, with the peripheral phenyl groups from one molecule projecting towards the groove of another, and benzene molecules located in the proximity of the quinone carbonyls, between the adjacent pentiptycene layers (Figure 5.1). We note that the excellent overall yield for the formation of pentiptycenequinone **5.5l** with a molecular mass of 3005.3 amu and a severely sterically crowded structure (Figure 5.2) highlights the remarkable potential of this method.

Figure 5.1. (Left) ORTEP diagram of pentiptycenes quinone **5.5h** with ellipsoids shown at 50% probability and (right) packing interactions between adjacent molecules in the lattice. Benzene molecules are shown in red.

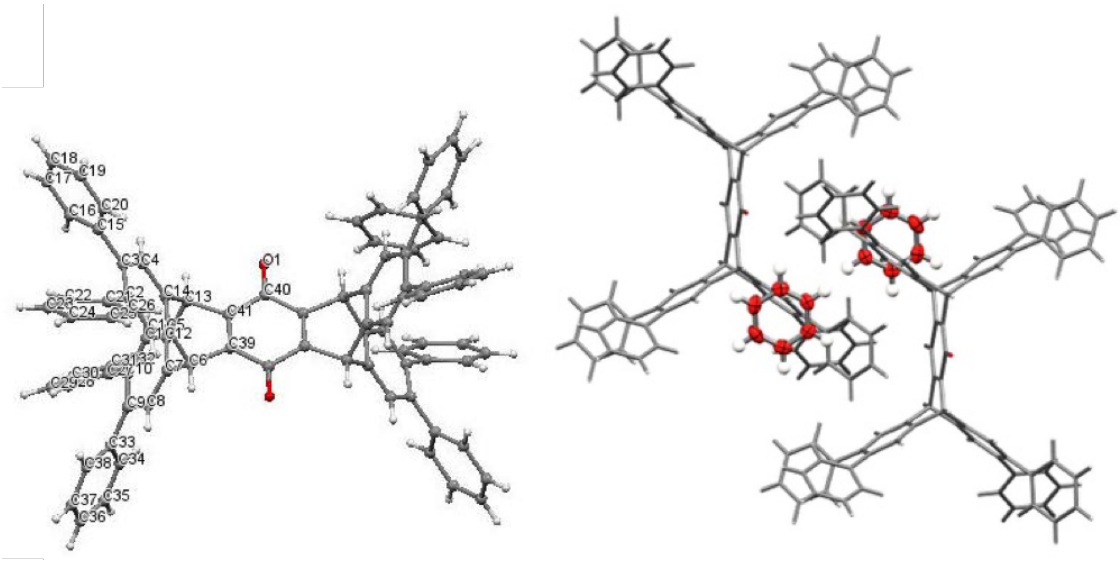

Figure 5.2. Line structure and space-filling model of pentiptycene quinone **5.5e** with eight 4-triphenylmethyl-phenyl groups in the periphery of the structure illustrating the power of the method.

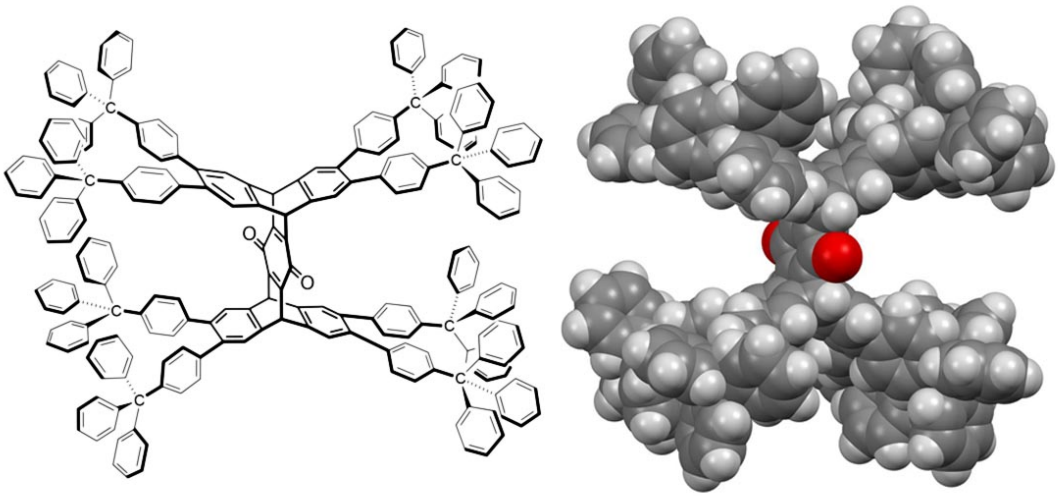

5.4 Conclusion

In conclusion, the strategy described in this communication was successful because of the remarkable efficiency of the two key steps and will make it possible to prepare a wide range of peripherally substituted pentiptycene derivatives that will help explore and develop a wide range of chemical and materials science applications.

5.5 Experimental Section

5.5.1 Materials and Methods

All reactions were performed under an inert atmosphere of argon unless otherwise stated. Chemicals were purchased from commercially available sources and used without further purification unless otherwise noted. Nuclear magnetic resonance (NMR) spectra for ^{1}H were obtained at 300, 400, or 500 MHz as noted using Bruker NMR spectrometers. All ^{13}C NMR measurements were carried out at 500 MHz. Chemical shifts are reported in ppm on the δ-scale using the residual natural abundance isotopes of the solvents as references. $CDCl_3$ was calibrated at δ7.26 and δ77.16 for ^{1}H and ^{13}C NMR spectroscopy, respectively. High-resolution mass spectrometry was performed using electrospray ionization with a time of flight (ESI-TOF), DART or MALDI mass spectrometer, as noted. 2,4,6-trivinylcyclotriboroxane-pyridine complex **5.6** and 4-tetraphenyliodide **5.7** were prepared according to previously reported literature procedures.[15,16]

5.5.2 Experimental Procedures

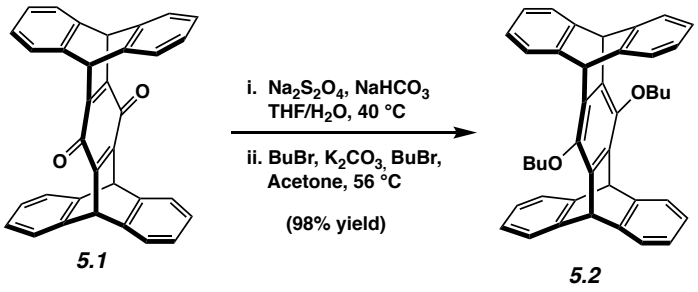

5.1 *5.2*

Pentiptycenedihydroquinone 5.2. Pentiptycene quinone **5.1** (800 mg, 1.74 mmol, 1.0 equiv) was suspended in THF (8 mL). Sodium dithionite (2.6 g, 14.77 mmol, 8.5 equiv) was dissolved in H_2O (12 mL). The aqueous solution was added to the suspended starting material and the biphasic mixture was heated to 40 °C while stirring vigorously for 1.5 hours or until suspended solid in organic layer had completely dissolved and yellow color had paled. The reaction was cooled to room temperature and transferred to a separatory funnel. The aqueous layer was removed and the organic layer was washed with sat. aq. NaCl (3 x 25 mL) and dried with Na_2SO_4. The solvent was removed under reduced pressure to yield off-white solid. This solid, along with freshly dehydrated K_2CO_3 (1.2 g, 8.686 mmol, 5.0 equiv) and a catalytic amount of 18-crown-6 (5 mg) was suspended in anhydrous acetone (75 mL) in a dry round-bottom flask. Bromobutane (940 µL, 8.68 mmol, 5.0 equiv) was added and the reaction was heated to reflux for 14 hours. The reaction was cooled to room temperature and the solvent was removed under reduced pressure. CH_2Cl_2 (50 mL) was added and the mixture was filtered. Solid was washed thoroughly with CH_2Cl_2 until filtrate no longer contained product by TLC analysis. Combined organics were washed with H_2O (3 x50 mL), dried with $MgSO_4$, and evaporated under reduced pressure to yield the crude product. The crude product was purified by flash column chromatography (25% CH_2Cl_2 in hexane gradient to 50% CH_2Cl_2 in hexane) to yield the pure product as a white powder (979 mg, 98%). m.p. 284.1-

286.0 °C. ^{1}H NMR (400 MHz, $CDCl_3$): δ = 7.31 (dd, *J*= 5.3, 3.2 Hz, 8H), 6.93 (dd, *J*= 5.4, 3.2 Hz, 8H), 5.64 (s, 4H), 3.91 (t, *J*= 6.7 Hz, 4H), 1.99 (m, 4H), 1.72 (m, 4H), 1.14 (t, *J*= 7.4 Hz, 6H); ^{13}C NMR (125 MHz, $CDCl_3$): δ = 146.2, 145.5, 136.4, 125.2, 123.7, 76.1, 48.5, 32.8, 19.9, 14.3; IR (cm^{-1}): 3067, 3018, 2955, 1480, 1459, 1376, 1301, 1257, 1067, 1024, 751, 554; HRMS (ESI) calcd for $C_{42}H_{39}O_2$ $[M+H]^+$ 575.2950, found 575.2946.

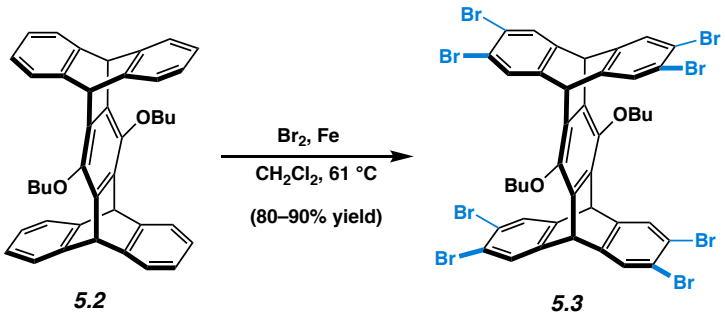

5.2 *5.3*

Pentiptycenedihydroquinone 5.3. A flame dried 10 mL Schlenk flask was charged with compound **5.2** (70 mg, 0.122 mmol, 1.0 equiv) and iron filings (9 mg, 0.16 mmol, 1.3 equiv). The reaction flask was evacuated and backfilled with argon three times. Anhydrous CH_2Cl_2 (8 mL) was added and the reaction was stirred for five minutes until the starting material was fully dissolved. Freshly distilled Br_2 (55 µL, 1.06 mmol, 8.7 equiv) was added, and the reaction was heated to reflux under an argon atmosphere for 90 minutes. The reaction was cooled first to room temperature and then to 0 °C. K_2CO_3 (~50 mg) was added and the reaction was allowed to warm to room temperature and continue stirring for 10 hours. The solvent was removed under reduced pressure. Solid was taken up in hot chloroform (~75 mL) in order to dissolve the maximum amount of solid. The suspension was filtered through a short silica pad. The solvent was removed under reduced pressure to yield the crude product as a pale yellow solid. Solid was then washed with acetone and a minimal amount of cold CH_2Cl_2 followed by collection by centrifugation to yield

the product as a white powder (116 mg, 80–90% yield). A melting point determination was not possible because the solid decomposed when heated to 350 °C. ^{1}H NMR (400 MHz, $CDCl_3$): δ = 7.55 (s, 8H), 5.50 (s, 4H), 3.87 (t, *J*= 8.9 Hz, 4H), 1.94 (m, 4H), 1.70 (m, 4H), 1.15 (t, *J*= 9.7 Hz, 6H) ; ^{13}C NMR (125 MHz, $CDCl_3$): δ = 146.4, 145.0. 135.5, 128.9, 121.5, 76.6, 46.7, 32.8, 19.9, 14.3; IR (cm^{-1}): 2951, 2866, 1465, 1436,1359, 1266, 1065, 1028, 917, 858, 786, 532; HRMS (MALDI-TOF) calcd for $C_{42}H_{30}Br_8O_2$ $[M]^+$ 1205.5631, found 1205.5664.

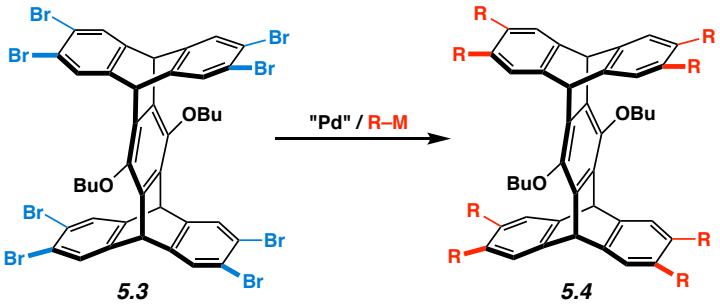

5.3 *5.4*

Product	R =	Coupling Partner	Yield (%)
5.4a	Me	$AlMe_3$	94
5.4b	Ph	Ph	77
5.4c	*t*Bu	*t*Bu	65
5.4d	S	Bu_3Sn S	76
5.4e	Me	Bu_3Sn Me	83
5.4f		Bu_3Sn	70
5.4g	O	Bu_3Sn O	65
5.4h	Ph	$(HO)_2B$ Ph	93
5.4i	OMe	$(HO)_2B$ OMe	69
5.4j	CHO	$(HO)_2B$ CHO	74
5.4k	N	$(HO)_2B$ N	91
5.4l	Ph, Ph, Ph	$(HO)_2B$ Ph, Ph, Ph	85
5.4m	F	$(HO)_2B$ F	82
5.4n			91
5.4o	CO_2Et	$(HO)_2B$ CO_2Et	76

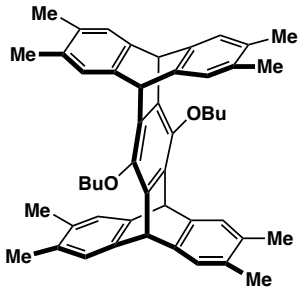

5.4a

Pentiptycene 5.4a. A flame dried 50 mL Schlenk flask and condenser system was charged with **5.3** (150 mg, 0.124 mmol, 1.0 equiv). The flask was evacuated and backfilled with argon three times. Anhydrous THF (24 mL) was added and the suspension was thoroughly degassed. $PdCl_2(PPh_3)_2$ (35 mg, 0.0498 mmol, 40 mol%) was added and the mixture was further degassed. The reaction was heated to 60 °C and allowed to stir for 30 min. $AlMe_3$ (2M in Hexanes, 1 mL, 1.99 mmol, 16 equiv) was added and the reaction was heated to reflux for 12 hours. The reaction was cooled down to 0 °C and 2 M HCl was added dropwise until bubbling ceased. The organics were washed with sat. aq. NaCl (3x), dried over $MgSO_4$, and evaporated under reduced pressure. The product was purified by flash column chromatography (15% CH_2Cl_2 in Hexane) to yield the product as white solid (80 mg, 94%). A melting point determination was not possible because the solid decomposed when heated to 350 °C. ^{1}H NMR (400 MHz, $CDCl_3$): δ = 7.04 (s, 8H), 5.47 (s, 4H), 3.88 (t, *J*= 6.7 Hz, 4H), 2.07 (s, 24H), 1.98 (m, 4H), 1.71 (m, 4H), 1.14 (t, *J*= 7.3 Hz, 6H); ^{13}C NMR (125 MHz, $CDCl_3$): δ = 145.8, 143.4, 136.8, 132.7, 125.0, 75.9, 47.6, 32.9, 19.9, 19.5, 14.4; IR (cm^{-1}): 2959, 2918, 2852, 1463, 1261, 1068, 1026, 860, 799, 556; HRMS (ESI) calcd for $C_{50}H_{55}O_2$ $[M+H]^+$ 687.4202, found 687.4228.

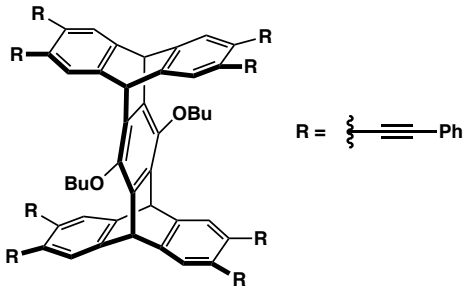

5.4b

Synthesis of 5.4b. To a 100 mL round-bottom flask were added anhydrous DMF (5 mL), Et_3N (1 mL), **5.3** (120.6 mg, 0.100 mmol, 1.0 equiv), and PPh_3 (15.7 mg, 0.060 mmol, 0.6 equiv). The resulting mixture was cooled down to –78 °C before it was connected to vacuum for 30 min. It was then allowed to warm up to room temperature under Argon atmosphere. Phenylacetylene (490 mg, 4.80 mmol, 48 equiv), $Pd(PPh_3)_4$ (34.7 mg, 0.030 mmol, 30 mol%) and CuI (5.7 mg, 0.030 mmol, 30 mol%) were added into the reaction flask, and the mixture was cooled down in a dry ice-acetone bath before it was connected to vacuum again for 5 min. The flask was then gradually heated up and the reaction was stirred at 65 °C under argon for 48 hours. A 1:1 water-acetone mixture (20 mL) was added to quench the reaction and the crude product was collected by filtration. The obtained solids were further washed with excess of water and acetone (106 mg, 77%) after solvent removal. A melting point determination was not possible because the solid decomposed when heated to 350 °C. ^{1}H NMR (400 MHz, $CDCl_3$): δ = 7.53 (s, 8H), 7.50 (m, 16H), 7.30 (m, 24H), 5.67 (s, 4H), 3.99 (t, *J*= 6.4 Hz, 4H), 2.06-2.00 (m, 4H), 1.87-1.79 (m, 4H), 1.23 (t, *J*= 7.3 Hz, 6H); ^{13}C NMR (125 MHz, $CDCl_3$): δ = 146.4, 144.3, 135.6, 131.8, 128.45, 128.43, 127.0, 123.5, 123.4, 93.2, 88.6, 76.5, 47.8, 33.0, 20.1, 14.4; IR (cm^{-1}): 2936, 2860, 1596, 1493, 1460, 1255, 1060, 1027, 912, 752, 688, 564, 529, 456; HRMS (ESI) calcd for $C_{106}H_{70}O_2Na$ $[M+Na]^+$ 1397.5268, found 1397.5284.

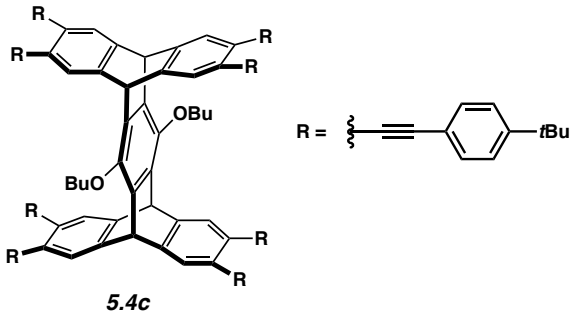

5.4c

Pentiptycene 5.4c. To a 15 mL round-bottom flask was added **5.3** (30.0 mg, 0.0249 mmol, 1.0 equiv), dry DMF (5 mL), and Et_3N (1 mL). The mixture was freeze-pump-thawed (1x). $Pd(PPh_3)_4$ (28.8 mg, 24.9 μmol, 1.0 equiv), CuI (8.5 mg, 44.6 μmol, 2.0 equiv) PPh_3 (25.5 mg, 97.2 μmol, 3.9 equiv) and 4-*tert*butylphenyl acetylene (0.82 mL, 3.98 mmol, 159 equiv) were added to the suspension. The reaction was freeze-pump-thawed again (1x), heated to 65 °C for 48 hours, and then cooled to room temperature. The solvent was then removed under reduced pressure leaving a crude brown solid. The crude product was purified via flash column chromatography (1% CH_2Cl_2 in Hexanes) to yield the pure product as light brown solid (29.6 mg, 65%). A melting point determination was not possible because the solid decomposed when heated to 350 °C. ^{1}H NMR (500 MHz, $CDCl_3$): δ = 7.51 (s, 8H), 7.44 (d, *J* = 8.4 Hz, 16H), 7.33 (d, *J* = 8.6 Hz, 16H), 5.65 (s, 4H), 3.97 (t, *J* = 6.5 Hz, 4H), 2.06 – 1.99 (m, 4H), 1.88 – 1.77 (m, 4H), 1.31 (s, 72H), 1.23 (t, *J* = 7.3 Hz, 6H); ^{13}C NMR (125 MHz, $CDCl_3$): δ = 151.6, 146.3, 144.2, 135.6, 131.5, 127.0, 125.4, 123.5, 120.6, 93.2, 88.1, 76.5, 47.7, 34.9, 33.0, 31.3, 20.1, 14.4; IR (cm^{-1}): 3036, 2959, 1504; HRMS (MALDI-TOF) calcd for $C_{138}H_{134}O_2$ $[M+Na]^+$ 1846.028, found 1846.033.

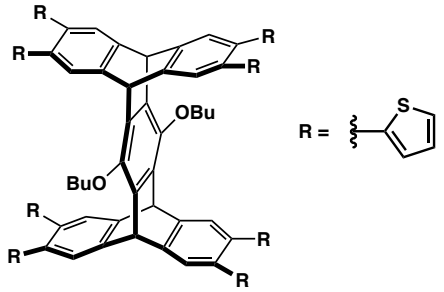

5.4d

Pentiptycene 5.4d. To a 15 mL round-bottom flask was added DMF (3 mL), **5.3** (30.0 mg, 0.0248 mmol, 1.0 equiv) and 2-tributylstannyl thiophene (79μL, 0.249 mmol, 10 equiv). The suspension was thoroughly degassed by the freeze-pump-thaw method (2x). $PdCl_2(PPh_3)_2$ (7 mg, 0.010 mmol, 40 mol%) was added and the reaction was further degassed via one more round of freeze-pump-thaw and backfilled with argon. The reaction was heated to 130 °C for 16 hours and then cooled to room temperature. The solvent was evaporated under reduced pressure to yield a brown solid/film. The solid was taken up in CH_2Cl_2 (20 mL). The solution was washed with H_2O, dried over $MgSO_4$, and concentrated under reduced pressure. The solid was purified via flash column chromatography (25% CH_2Cl_2 in hexane) to yield the product as a off-white solid (23.4 mg, 76%). A melting point determination was not possible because the solid decomposed when heated to 350 °C. ^{1}H NMR (400 MHz, $CDCl_3$): δ = 7.51 (s, 8H), 7.20 (dd, *J*= 5.1, 1.2 Hz, 8H), 6.89 (dd, *J*= 5.1, 3.5 Hz, 8H), 6.76 (dd, *J*= 3.6, 1.2 Hz, 8H), 5.78 (s, 4H), 4.01 (t, *J*= 6.7 Hz, 4H), 1.98-2.05 (m, 4H), 1.69-1.78 (m, 4H), 1.11 (t, *J*= 7.4 Hz, 6H); ^{13}C NMR (125 MHz, $CDCl_3$): δ = 146.4, 144.6, 142.7, 136.1, 131.2, 127.2, 126.9, 126.5, 126.0, 76.5, 47.7, 32.8, 20.0, 14.3; IR (cm^{-1}): 3105, 2959, 2928, 2889, 1489, 1273, 1249, 1035, 907, 849, 830, 694; HRMS (MALDI-TOF) calcd for $C_{74}H_{54}O_2S_8$ $[M]^+$: 1230.1890, found 1230.1852.

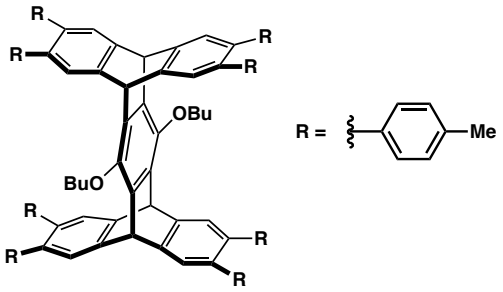

5.4e

Pentiptycene 5.4e. To a 10 mL Schlenk flask was added **5.3** (30.0 mg, 0.0249 mmol, 1.0 equiv) and DMF (3.5 mL). The mixture was freeze-pump-thawed (2x). $PdCl_2(PPh_3)_2$ (7.1 mg, 10.1 μmol, 40 mol%) was added to the mixture and the reaction was freeze-pump-thawed again (1x). Finally, 4-(tributylstannyl)toluene (103 mg, 270 μmol, 11 equiv) was added and the reaction was freeze-pump-thawed (1x). The reaction was heated for 16 hours at 95 °C under argon, then cooled to room temperature and concentrated under reduced pressure, leaving the crude mixture as a brown solid. The crude product was purified via flash column chromatography (10% CH_2Cl_2 in Hexanes) to yield a glassy white solid. This was rinsed with cold Hexanes to yield the product as a white solid (26.8 mg, 83%). A melting point determination was not possible because the solid decomposed when heated to 350 °C. ^{1}H NMR (500 MHz, $CDCl_3$): δ = 7.38 (s, 8H), 6.95 (d, *J* = 8.2 Hz, 16H), 6.92 (d, *J* = 8.2 Hz, 16H), 5.77 (s, 4H), 3.98 (t, *J* = 6.4 Hz, 4H), 2.27 (s, 24H), 2.01-1.95 (m, 4H), 1.79- 1.72 (m, 4H), 1.09 (t, *J* = 7.4 Hz); ^{13}C NMR (125 MHz, $CDCl_3$): δ = 146.4, 144.4, 138.8, 137.5, 136.5, 135.9, 129.9, 128.6, 126.1, 76.2, 48.0, 32.9, 21.3, 20.1, 14.3; IR (cm^{-1}): 3036, 2959, 1504; HRMS (MALDI-TOF) calcd for $C_{98}H_{86}O_2$ $[M+H]^+$ 1295.671, found 1295.673.

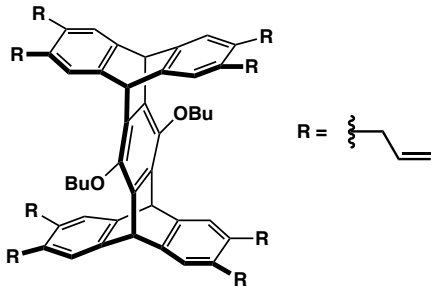

5.4f

Pentiptycene 5.4f. To a 5 mL round-bottom flask was added **5.3** (34.5 mg, 0.0286 mmol, 1.0 equiv) suspended in DMF (3.5 mL). The suspension was degassed via freeze-pump-thaw method (2x). Allyltributylstannane (89µL, 0.286 mmol, 10 equiv) was added and the suspension was cooled to –78 °C and stirred under vacuum for 5 minutes, followed by being backfilled with argon. $PdCl_2(PPh_3)_2$ (8.0 mg, 0.011 mmol, 38 mol%) was added and the suspension was stirred under vacuum at –78 °C for 5 more minutes and backfilled with argon. The reaction was heated to 95 °C for 14 hours. The reaction was allowed to cool to room temperature. The solvent was removed under reduced pressure. The reaction mixture was filtered through a short silica pad followed by purification by flash column chromatography (25% CH_2Cl_2 in Hexanes) to yield a white solid product with tin impurities. Solid was washed with hexane and collected by centrifugation to yield the pure white solid product. The remainder of the product was crystallized from hexane wash by slow evaporation to a minimal amount of solvent and cooling in the refrigerator for 12 hours to complete the crystallization. Crystals were added to the original solid to yield the pure product as white solid (17.9 mg, 70%). A melting point determination was not possible because the solid decomposed when heated to 350 °C. ^{1}H NMR (400 MHz, $CDCl_3$): δ = 7.09 (s, 8H), 5.81(ddt, *J*= 16.7 Hz, 10.4 Hz, 6.5 Hz, 8H), 5.52 (s, 4H), 4.94-4.99 (m, 16H), 3.87 (t, *J*= 7.0 Hz, 4H), 3.24 (d, *J*=6.5 Hz, 16 H), 1.92-1.99 (m, 4H), 1.58-1.67 (m, 4H), 1.10 (t, *J*= 7.3 Hz, 6H); ^{13}C NMR (125 MHz, $CDCl_3$): δ = 146.0, 143.9, 137.2, 136.6, 134.4, 124.7, 115.9, 76.0, 47.7, 37.1, 32.7, 19.7,

14.3; IR (cm^{-1}): 3078, 3005, 2960, 2932, 1638, 1467, 1265, 1071, 1028, 995, 906, 734, 558; HRMS (ESI) calcd for $C_{66}H_{71}O_2$ $[M+H]^+$ 895.5454, found 895.5490.

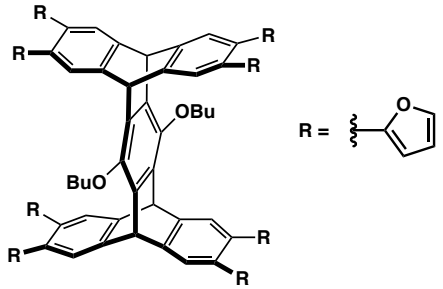

5.4g

Pentiptycene 5.4g. To a 10 mL round-bottom flask was added DMF (3 mL) and **5.3** (30.6 mg, 0.0254 mmol, 1.0 equiv). The suspension was deoxygenated via freeze-pump-thaw method (2x). 2-tributylstannyl furan (80μL, 0.254 mmol, 10 equiv) was added and the suspension was further deoxygenated with one more cycle. $PdCl_2(PPh_3)_2$ (7.1 mg, 0.010 mmol, 40 mol%) was added and the reaction was further degassed via one final round of freeze-pump-thaw and backfilled with argon. The reaction was heated to 130 °C for 16 hours before being cooled to room temperature. The crude reaction mixture was evaporated under reduced pressure to yield the crude product as a brown solid/film. The solid was purified by flash column chromatography (35% CH_2Cl_2 in hexane gradient to 40% CH_2Cl_2 in hexane) to yield the product as white solid still containing aliphatic impurities by NMR. The product was further purified by trituration with Hexanes and finally collected by centrifugation to yield the pure product as white solid (18.1 mg, 65%). A melting point determination was not possible because the solid decomposed when heated to 350 °C. ^{1}H NMR (400 MHz, $CDCl_3$): δ = 7.60 (s, 8H), 7.37 (dd, *J*= 1.8, 0.8 Hz, 8H), 6.34 (dd, *J*= 3.4, 1.8 Hz, 8H), 5.89 (dd, *J*= 3.3, 0.8 Hz, 8H), 5.77 (s, 4H), 4.00 (t, *J*= 6.7 Hz, 4H), 1.98-2.06 (m, 4H), 1.70-1.80 (m, 4H), 1.14 (t, *J*= 7.4 Hz, 6H); ^{13}C NMR (125 MHz, $CDCl_3$): δ = 153.0, 146.3, 144.7, 141.7, 136.0, 126.5, 124.3, 111.4, 108.2, 76.4, 47.9, 32.9, 20.0, 14.3; IR (cm^{-1}): 3118, 2958, 2931, 1499,

1457, 1274, 1155,1008, 905, 809, 731, 594; HRMS (ESI) calcd for $C_{74}H_{55}O_{10}$ $[M+H]^+$ 1103.3795, found 1103.3790.

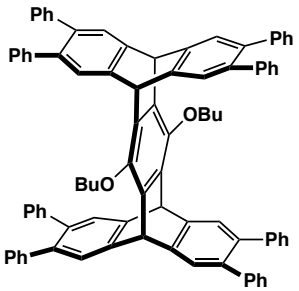

5.4h

Pentiptycene 5.4h. A flame dried 50 mL Schlenk flask was charged with phenylboronic acid (162 mg, 1.33 mmol, 16 equiv) and K_3PO_4 (563 mg, 2.65 mmol, 32 equiv). The flask was evacuated and backfilled with argon three times. Anhydrous THF (12 mL) was added and reaction was degassed with argon. $Pd(P\textit{t}Bu_3)_2$ (17 mg, 0.033 mmol, 40 mol%) was added and the reaction was further degassed. **5.3** (100 mg, 0.083 mmol, 1.0 equiv) was added and the reaction was further degassed. The reaction mixture was heated to 40 °C and stirred for 14 hours. The reaction was cooled to room temperature. The reaction mixture was washed with saturated NH_4Cl solution (3x20 mL), dried with $MgSO_4$ and concentrated under reduced pressure to yield the crude product. The crude product was purified by flash column chromatography (30% CH_2Cl_2 in Hexane gradient to 40% CH_2Cl_2 in Hexane) to yield the product as white solid (91 mg, 93%). A melting point determination was not possible because the solid decomposed when heated to 350 °C. ^{1}H NMR (400 MHz, $CDCl_3$): δ = 7.45 (s, 8H), 7.15-7.14 (m, 24H), 7.05-7.02 (m, 16H), 5.84, (s, 4H), 4.02 (t, *J*= 6.4 Hz, 4H), 2.05-1.97 (m, 4H), 1.81-1.72 (m, 4H), 1.09 (t, *J*= 7.3 Hz, 6H) ; ^{13}C NMR (125 MHz, $CDCl_3$): δ = 146.5, 144.6, 141.6, 137.8, 136.5, 130.1, 127.9, 126.4, 126.1, 76.3, 48.0, 32.9, 20.1, 14.3; IR (cm^{-1}): 3021, 2923, 2855, 1600, 1464, 1276, 1248, 1072, 763, 700, 574; HRMS (ESI) calcd for $C_{90}H_{74}NO_2$ $[M+NH_4]^+$ 1200.5714, found 1200.5734.

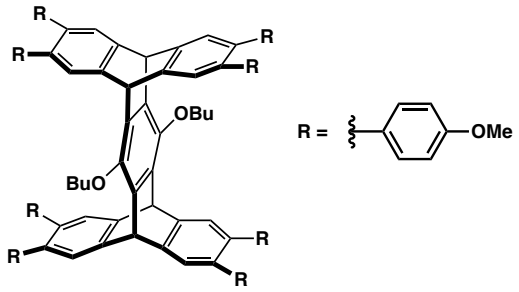

5.4i

Pentiptycene 5.4i. To a 15 mL pressure tube was added THF (5mL), H_2O (2mL), **5.3** (29.3 mg, 0.0243 mmol, 1.0 equiv), 4-methoxyphenylboronic acid (118 mg, 0.777 mmol, 32 equiv), and K_2CO_3 (137 mg, 0.992 mmol, 41 equiv). The suspension was thoroughly degassed by sparging with Argon. $Pd(PPh_3)_4$ (11.5 mg, 9.9 μmol, 47 mol%) was added and the reaction was further degassed, before being sealed under argon. The reaction was heated to 95 °C for 14 hours and then cooled to room temperature. The aqueous layer was removed and the organics were washed with sat. aq. NaCl, dried over $MgSO_4$ and evaporated under reduced pressure. The crude product was purified by flash column chromatography (70% CH_2Cl_2 in hexane to 100% CH_2Cl_2) to yield pale yellow solid. Solid was suspended in acetone/MeOH mixture and collected via centrifugation (2x) to yield the pure product as a white powder (23.7 mg, 69%). A melting point determination was not possible because the solid decomposed when heated to 350 °C. ^{1}H NMR (400 MHz, $CDCl_3$): δ = 7.38 (s, 8H), 6.95 (d, *J* = 8.8 Hz, 16H), 6.70 (d, *J*= 8.8 Hz, 16 H), 5.78 (s, 4H), 4.00 (t, *J*= 6.5 Hz, 4H), 3.75 (s, 24H), 1.97-2.04 (m, 4H), 1.71-1.81 (m, 4H), 1.10 (t, *J*=7.3 Hz, 6H); ^{13}C NMR (125 MHz, $CDCl_3$): δ = 158.2, 146.4, 144.3, 137.1, 136.5, 134.2, 131.1, 126.0, 113.4, 76.2, 55.3, 48.0, 32.9, 20.1, 14.3; IR (cm^{-1}): 2958, 2932, 2834, 1608, 1513, 1464, 1291, 1244, 1177, 1034, 908, 831, 732, 558; HRMS (MALDI-TOF) calcd for $C_{98}H_{86}O_{10}$ $[M]^+$ 1422.6221, found 1422.6220.

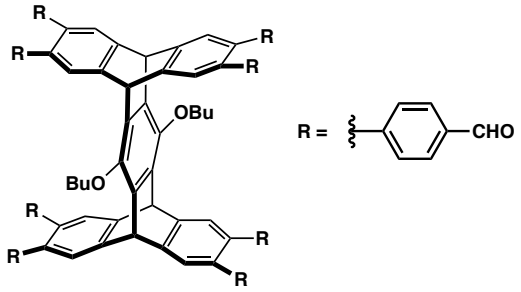

5.4j

Pentiptycene 5.4j. To a 10 mL pressure tube was added THF (6mL), H_2O (2mL), **5.3** (30.0 mg, 0.0249 mmol, 1.0 equiv), freshly recrystallized 4-formylphenylboronic acid (45 mg, 0.299 mmol, 12 equiv), and K_2CO_3 (138 mg, 1.00 mmol, 42 equiv). The suspension was thoroughly degassed by sparging with Argon. $Pd(PPh_3)_4$ (11.5 mg, 0.010, 40 mol%) was added and the reaction was further degassed, before being sealed under argon. The reaction was stirred in a pressure tube at 95 °C for 15 hours before being cooled to room temperature. The aqueous layer was removed and the organics were washed with sat. aq. NaCl, dried over $MgSO_4$, and evaporated under reduced pressure. The crude product was purified by flash column chromatography (CH_2Cl_2 to 5% diethyl ether in CH_2Cl_2) to yield the product as white solid (26.1 mg, 74%). A melting point determination was not possible because the solid decomposed when heated to 350 °C. ^{1}H NMR (400 MHz, $CDCl_3$): δ = 9.95 (s, 8H), 7.70 (d, *J* = 8.4 Hz, 16H), 7.52 (s, 8H), 7.18 (d, *J*= 8.2 Hz, 16 H), 5.93 (s, 4H), 4.06 (t, *J*= 6.6 Hz, 4H), 2.01-2.08 (m, 4H), 1.70-1.79 (m, 4H), 1.08 (t, *J*=7.4 Hz, 6H); ^{13}C NMR (125 MHz, $CDCl_3$): δ = 191.8, 147.0, 146.7, 145.3, 137.0, 136.2, 134.9, 130.6, 129.7, 126.1, 76.0, 48.0, 32.8, 20.0, 14.3; IR (cm^{-1}): 2959. 2828, 1699, 1602, 1465, 1209, 1168, 830; HRMS (MALDI-TOF) calcd for $C_{98}H_{70}O_{10}$ $[M]^+$ 1406.4969, found 1406.4902.

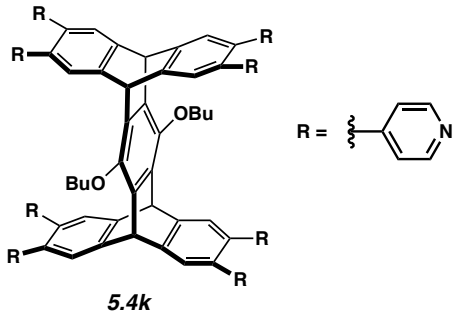

5.4k

Pentiptycene 5.4k. To a 15 mL pressure tube was added THF (6 mL), H_2O (2 mL), **5.3** (29.9 mg, 0.0248 mmol, 1.0 equiv), 4-pyridinylboronic acid (111.8 mg, 0.793 mmol, 3.2 equiv), and K_2CO_3 (137 mg, 0.992 mmol, 40 equiv). The suspension was thoroughly degassed by sparging with Argon. $Pd(PPh_3)_4$ (11.5 mg, 9.9μmol, 46 mol%) was added and the reaction was further degassed, before being sealed under argon. The reaction was heated to 90 °C for 12 hours. The reaction was allowed to cool to room temperature. The aqueous layer was removed and the organics were washed with sat. aq. NaCl, dried over $MgSO_4$ and concentrated under reduced pressure. The crude material was purified by flash column chromatography (1% Et_3N in CH_2Cl_2 gradient to 1% Et_3N and 8% MeOH in CH_2Cl_2) to yield a white solid containing 1:1 ratio of the desired product to triethyl ammonium. Solid was freebased by dissolving in CH_2Cl_2 and washing with $NaHCO_3$ and drying over $MgSO_4$. The solvent was removed under reduced pressure to yield the product as white solid (26.9 mg, 91%). A melting point determination was not possible because the solid decomposed when heated to 350 °C. ^1H NMR (400 MHz, $CDCl_3$): δ = 8.45 (d, *J* = 5.8 Hz, 16H), 7.48 (s, 8H), 6.94 (d, *J*= 6.1 Hz, 16 H), 5.92 (s, 4H), 4.04 (t, *J*= 6.6 Hz, 4H), 2.00-2.08 (m, 4H), 1.70-1.79 (m, 4H), 1.09 (t, *J*=7.3 Hz, 6H); ^{13}C NMR (125 MHz, $CDCl_3$): δ = 149.9, 148.2, 146.8, 145.7, 136.0, 135.6, 126.0, 124.6, 76.7, 47.9, 32.8, 20.0, 14.3; IR (cm^{-1}): 3025, 2958, 2872, 1598, 1465, 826, 730, 578; HRMS (MALDI-TOF) calcd for $C_{82}H_{63}N_8O_2$ $[M+H]^+$ 1191.5074, found 1191.5106.

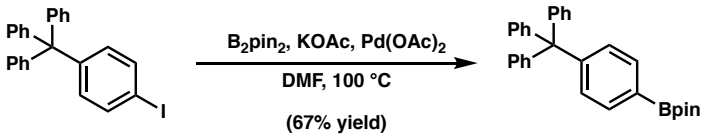

5.8 *5.9*

Synthesis of Tetraphenylmethyl-Bpin 5.9.[17] To a 25 mL round-bottom flask was added tetraphenylmethyl iodide (300mg, 0.672mmol, 1.0 equiv), B_2Pin_2 (295mg, 1.16 mmol, 1.7 equiv) and KOAc (198 mg, 2.016 mmol, 3 equiv) were taken up in DMF (16mL). The suspension was deoxygenated by the freeze-pump-thaw method. $Pd(OAc)_2$ (7.5 mg, 0.0336 mmol, 5 mmol%) was added, and the solution was further deoxygenated. The reaction was heated to 100 °C for 12 hours. The reaction mixture was filtered through a celite pad. The solvent was removed under reduced pressure. The solid was taken up in ether/water mixture. The aqueous layer was removed and the organics were washed with aqueous NH_4Cl (3x). The organics were dried over $MgSO_4$ and concentrated under reduced pressure to yield pale brown solid as crude product. The crude product was purified by flash column chromatography (20% CH_2Cl_2 in hexane) to yield a white solid. Solid was triturated with MeOH to remove the remaining B_2Pin_2 reagent to yield the pure product as white solid (202 mg, 67%). m.p. 241-243 °C; ^{1}H NMR (400 MHz, $CDCl_3$): δ = 7.69 (d, *J*= 8.4 Hz, 2H), 7.24-7.15 (m, 17H), 1.33 (s, 12H); ^{13}C NMR (125 MHz, $CDCl_3$): δ = 150.1, 146.8, 134.1, 131.3, 130.7, 127.6, 126.0, 83.9, 65.3, 25.0; IR (cm^{-1}): 3083, 2976, 1609, 1492, 1397, 1381, 1144, 750, 701; HRMS (DART) calcd for $C_{31}H_{32}BO_2$ $[M+H]^+$ 447.2495, found 447.24787.

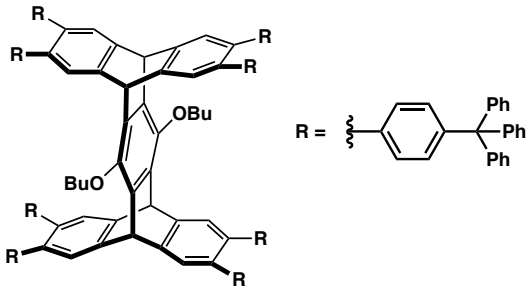

5.4l

Synthesis of 5.4l. To a 20 mL pressure tube was added THF (9 mL), H_2O (3 mL), **5.3** (65 mg, 0.054 mmol, 1.0 equiv), **5.9** (289 mg, 0.647 mmol, 12 equiv) and K_2CO_3 (298 mg, 2.16 mmol, 40 equiv). The suspension was thoroughly degassed by sparging with Argon. $Pd(PPh_3)_4$ (25 mg, 0.0216, 40 mol%) was added and the reaction was further degassed, before being sealed under argon. The reaction was stirred in a pressure tube at 95 °C for 13 hours. The aqueous layer was removed and the organics were dried over $MgSO_4$ and evaporated under reduced pressure. Solid was then taken up in the biphasic CH_2Cl_2-H_2O mixture. The organic layer was washed with H_2O (3x), dried, once again, over $MgSO_4$, and concentrated under reduced pressure. The crude brown solid was purified by flash column chromatography (20% CH_2Cl_2 in Hexanes) to yield a white solid, which contained a mixture of the desired product **5.4l** and **5.9**. Boronic ester **5.9** could then be removed by triturating solid with Hexanes and filtered until filtrate was clean by TLC to yield the pure **5.4l** as white solid. (143 mg, 85%). A melting point determination was not possible because the solid decomposed when heated to 350 °C. ^{1}H NMR (400 MHz, $CDCl_3$): δ = 7.42 (s, 8H), 7.09-7.16 (m, 120H), 6.94 (d, *J*= 8.6 Hz, 16H), 6.84 (d, *J*= 8.5 Hz, 16H), 5.77 (s, 4H), 3.99 (t, *J*= 6.3 Hz, 4H), 2.01-1.95 (m, 4H), 1.78-1.69 (m, 4H), 1.06 (t, *J*= 7.4 Hz, 6H); ^{13}C NMR (125 MHz, $CDCl_3$): δ = 146.8, 146.4, 144.9, 144.5, 139.1, 137.5, 136.4, 131.3, 130.6, 129.2, 127.5, 126.0, 125.7, 76.2, 64.8, 48.0, 32.9, 20.1, 14.3; IR (cm^{-1}): 3056, 3028, 2927, 1597, 1491, 1446, 1034, 830, 748, 699; HRMS (MALDI-TOF) calcd for $C_{242}H_{182}O_2$ $[M]^+$ 3119.4140 , found 3119.464.

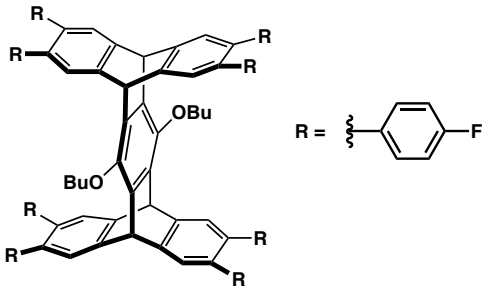

5.4m

Synthesis of 5.4m. To a 10 mL pressure tube was added THF (5 mL), H_2O (2 mL), **5.3** (28.7 mg, 0.0238 mmol, 1.0 equiv), 4-fluorophenylboronic acid pinacol ester (60.5 µL, 0.286 mmol, 12 equiv) and K_2CO_3 (132 mg, 0.952 mmol, 40 equiv). The suspension was thoroughly degassed by sparging with Argon. $Pd(PPh_3)_4$ (11.0 mg, 9.5µmol, 40 mol%) was added and the reaction was further degassed, before being sealed under argon. The reaction was stirred in a pressure tube at 95 °C for 15 hours. The aqueous layer was removed and the organic layer was washed with sat. aq. NaCl, dried over $MgSO_4$, and evaporated under reduced pressure to yield the crude product. The solid was purified by flash column chromatography (30% CH_2Cl_2 in hexane) to yield a white solid mixture of the product and unreacted pinacol ester starting material. This semi-pure material was washed with hexane and collected by centrifugation to yield the pure product as white solid (25.8 mg, 82%). A melting point determination was not possible because the solid decomposed when heated to 350 °C. ^{1}H NMR (400 MHz, $CDCl_3$): δ = 7.40 (s, 8H), 6.84-6.88 (m, 16H), 6.94-6.98 (m, 16H), 5.82 (s, 4H), 4.02 (t, *J*= 6.7 Hz, 4H), 1.98-2.05 (m, 4H), 1.69-1.78 (m, 4H), 1.08 (t, *J*= 7.3 Hz, 6H); ^{19}F NMR (376 MHz, $CDCl_3$): δ = -116.4 (tt, *J*= 8.6 Hz, 5.2 Hz); ^{13}C NMR (125 MHz, $CDCl_3$): δ = 161. 8 (d, *J*= 246.3 Hz), 146.5, 144.7, 137.2 (d, *J*= 3.3 Hz), 136.8, 136.4, 131.5 (d, *J*= 7.9 Hz), 126.0, 115.1 (d, *J*= 21.3 Hz), 76.4, 47.9, 32.9, 20.0, 14.3; IR (cm^{-1}): 2959, 2832, 1605, 1511, 1466, 1226, 1158, 835, 542; HRMS (MALDI-TOF) calcd for $C_{90}H_{62}F_8O_2$ $[M]^+$ 1326.4622, found 1326.4596.

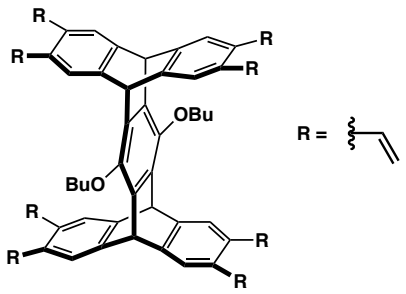

5.4n

Synthesis of 5.4n. **5.3** (70 mg, 0.058 mmol, 1.0 equiv), 2,4,6-trivinylcyclotriboroxane-pyridine (84 mg, 0.348 mmol, 6 equiv) and K_2CO_3 (64 mg, 0.464 mmol, 8 equiv) were suspended in a biphasic mixture of THF (3 mL), dimethoxyethane (1.5 mL) and H_2O (0.75 mL) in a 10 mL pressure tube. The mixture was thoroughly degassed with argon. PPh_3 (15 mg, 0.058 mmol, 1.0 equiv) and $Pd(OAc)_2$ (5.2 mg, 0.023 mmol, 40 mol%) was added and the reaction was further degassed. The pressure tube was closed and stirred in sand bath at 70 °C for 4 hours. The reaction could be visually monitored as was completed once all solids had gone into solution and reaction resembled a biphasic solvent system. At this point, the reaction was cooled to room temperature. The aqueous layer was removed and the organics were evaporated under reduced pressure. The residue was dissolved in the biphasic mixture of ethyl acetate (40 mL) and sat. aq. NaCl (30 mL). The aqueous layer was removed and the organics were washed with sat. aq. NaCl two more times before being dried with Na_2SO_4 and concentrated under reduced pressure. The residue was taken up in a 1:1 mixture of CH_2Cl_2 and Hexanes and ***quickly*** flushed through a silica plug.[18] The mixture was then concentrated under reduced pressure to yield pale yellow solid as crude product. The crude material could then be recrystallized from Hexanes to yield the pure product as white solid (41.2 mg, 91%). A melting point determination was not possible because the solid decomposed when heated to 350 °C. ^{1}H NMR (400 MHz, $CDCl_3$): δ = 7.40 (s, 8H), 6.87 (dd, *J*= 17.4, 11.0 Hz, 8H), 5.64 (s, 4H), 5.50 (dd, *J*= 17.4, 1.2 Hz, 8H), 5.21 (dd, *J*= 11.0, 1.2 Hz, 8H), 3.96 (t, *J*= 6.8

Hz, 4H), 2.06-1.98 (m, 4H), 1.78-1.65 (m, 4H), 1.14 (t, *J*= 7.4 Hz, 6H); ^{13}C NMR (125 MHz, $CDCl_3$): δ = 146.0, 144.5, 136.1, 134.8, 133.4, 121.5, 115.9, 76.3, 48.0, 32.8, 19.8, 14.3; IR (cm^{-1}): 2954, 2927, 2867, 1624, 1463, 1425, 1271, 1247, 1067, 1029, 986, 903, 750, 555; HRMS (ESI) calcd for $C_{58}H_{55}O_2$ $[M+H]^+$ 783.4202, found 783.4224.

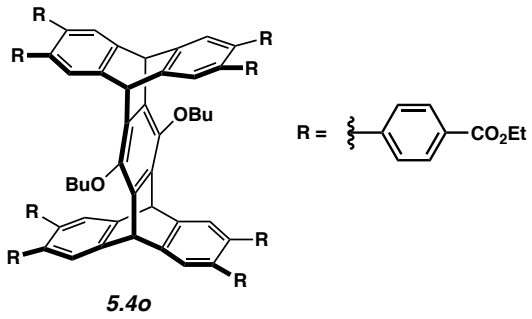

5.4o

Synthesis of 5.4o. To a 10 mL pressure tube was added **5.3** (30.4 mg, 25.2 μmol, 1.0 equiv), 4-ethoxycarbonylphenyl-boronic acid (90.1 mg, 464 μmol, 18 equiv), K_2CO_3 (156 mg, 1.13 mmol, 45 equiv), and $Pd(PPh_3)_4$ (13.0 mg, 11.3 μmol, 45%) followed by THF (6 mL) and water (2 mL). The suspension was degassed by the freeze-pump-thaw method (1x). The reaction vessel was sealed and heated at 90 °C for 16 hours and then cooled to room temperature. THF (20 mL) was added and the organic layer was washed with sat. aq. NaCl, dried over magnesium sulfate, and concentrated under reduced pressure to yield a brown solid. The crude mixture was purified by flash column chromatography (10% EtOAc in Hexane) to yield **5.4o** as a white solid (33.9 mg, 76%). A melting point determination was not possible because the solid decomposed when heated to 350 °C. ^{1}H NMR (500 MHz, $CDCl_3$): δ = 7.84 (d, *J* = 8.5 Hz, 16H), 7.48 (s, 8H), 7.08 (d, *J* = 8.5 Hz, 16H), 5.89 (s, 4H), 4.34 (q, *J* = 7.1 Hz, 16H) 4.04 (t, *J* = 6.6 Hz, 4H) 2.07–1.98 (m, 4H), 1.79–1.66 (m, 4H), 1.37 (t, *J* = 7.1 Hz, 24H), 1.08 (t, 6H); ^{13}C NMR (125 MHz, $CDCl_3$): δ = 166.6, 146.6, 145.6, 145.1, 137.1, 136.3, 130.0, 129.5, 128.9, 126.1, 76.6, 61.1, 48.0, 32.8, 20.0, 14.5,

14.3; IR (cm^{-1}): 3044, 2958, 1713, 1608; HRMS (MALDI-TOF) cacld for $C_{114}H_{102}O_{18}$ $[M+Na]^+$ 1781.6965, found 1781.6905.

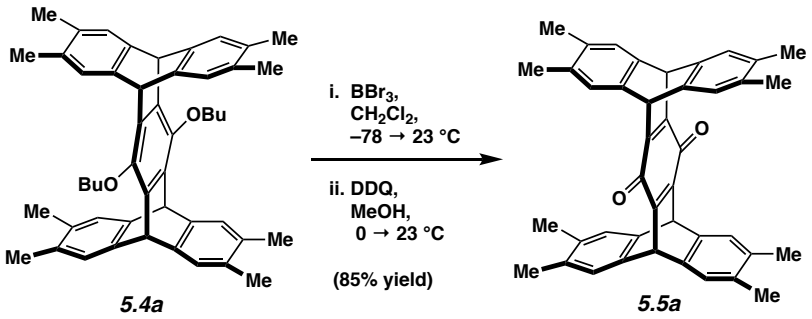

Synthesis of 5.5a. A flame dried 25 mL round-bottom was charged with pentiptycene **5.4a** (50 mg, 0.073mmol, 1.0 equiv), dissolved in anhydrous CH_2Cl_2 (19 mL). The solution was cooled to –78 °C. BBr_3 (510 μL, 0.51 mmol, 1M in CH_2Cl_2, 7.0 equiv) was added dropwise. Upon completion of addition dry ice bath was removed and the reaction was allowed to gradually warm to room temperature and stir until TLC showed complete dealkylation (45 minutes). The reaction was then cooled to 0 °C. MeOH (100 μL) was added dropwise. DDQ (41 mg, 0.18 mmol, 2.5 equiv). The reaction was allowed to warm to room temperature, and stir for a further 20 minutes. Aqueous sodium bicarbonate was added and stirred. Sufficient CH_2Cl_2 was added to fully dissolve all solids. The biphasic mixture was extracted with CH_2Cl_2. The organics were dried over $MgSO_4$. The crude product was purified by flash column chromatograph (35% CH_2Cl_2 in Hexane) to yield the product as orange solid (35 mg, 85%). A melting point determination was not possible because the solid decomposed when heated to 350 °C. ^1H NMR (400 MHz, $CDCl_3$): δ = 7.10 (s, 8H), 5.57 (s, 4H), 2.09 (s, 24H); ^{13}C NMR (125 MHz, $CDCl_3$): δ = 180.4, 151.6, 141.7, 133.3, 125.6, 46.6, 19.5; IR (cm^{-1}): 2965, 1644, 1594, 1471, 1457, 1301, 1199, 902, 750, 728, 570; HRMS (ESI) calcd for $C_{42}H_{37}O_2$ $[M+H]^+$ 573.2794, found 573.2786.

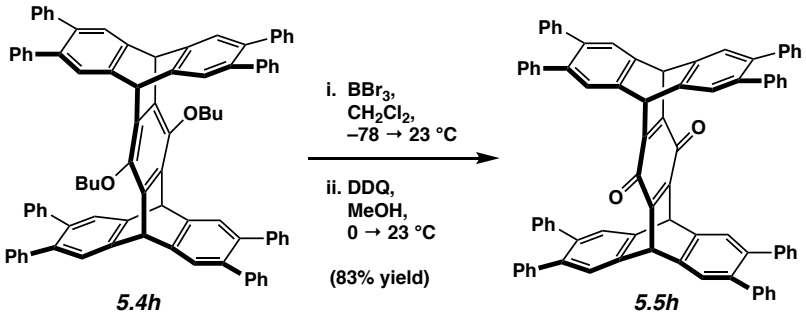

Synthesis of 5.5h. A flame dried 15 mL round-bottom was charged with pentiptycene **5.4h** (32 mg, 0.027 mmol, 1.0 equiv), dissolved in anhydrous CH_2Cl_2 (7 mL). The solution was cooled to –78 °C. BBr_3 (190 μL, 0.190 mmol, 1M in CH_2Cl_2, 7.0 equiv) was added dropwise. Upon completion of addition, the dry ice bath was removed and the reaction was allowed to gradually warm to room temperature and stir until TLC showed complete dealkylation (65 minutes). The reaction was then cooled to 0 °C. MeOH (100 μL) was added dropwise. DDQ (12.3 mg, 0.054 mmol, 2.0 equiv) was added and the reaction was allowed to warm to room temperature, and stir for a further 20 minutes. Aqueous sodium bicarbonate was added and stirred. Sufficient CH_2Cl_2 was added to fully dissolve all solids. The biphasic mixture was extracted with CH_2Cl_2. The organics were dried over $MgSO_4$. The crude product was purified by flash column chromatograph (40% CH_2Cl_2 in Hexane) to yield the product as orange solid (24 mg, 83%). A melting point determination was not possible because the solid decomposed when heated to 350 °C. ^{1}H NMR (400 MHz, $CDCl_3$): δ = 7.50 (s, 8H), 7.15 (m, 24H), 7.03 (m, 16H), 5.94 (s, 4H); ^{13}C NMR (125 MHz, $CDCl_3$): δ = 180.0, 151.2, 142.8, 141.1, 138.2, 130.0, 128.0, 126.8, 126.7, 47.0; IR (cm^{-1}): 2920, 2851, 1641, 1592, 1463, 1129, 910, 758, 698, 584, 565, 525; HRMS (ESI) calcd for $C_{82}H_{53}O_2$ $[M+H]^+$ 1069.4045, found 1069.4027.

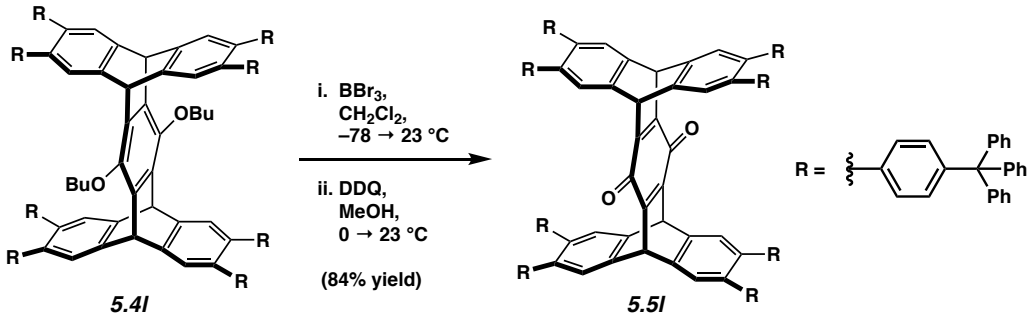

5.4l *5.5l*

Synthesis of 5.5l. A flame dried 10mL Schlenk flask was charged with pentiptycene **5.4l** (45 mg, 0.0144 mmol, 1.0 equiv) dissolved in anhydrous CH_2Cl_2 (3 mL). The solution was cooled to –78 °C. BBr_3 (101 µL, 0.101 mmol, 1M in CH_2Cl_2, 7.0 equiv) was added dropwise. Upon completion of addition, the reaction was allowed to gradually warm to room temperature and stir until TLC showed complete dealkylation (2 hours and 35 minutes). The reaction mixture was then cooled to 0 °C and MeOH (~50 µL) was added slowly. DDQ (6.5 mg, 0.029 mmol, 2.0 equiv) was added and ice bath was removed in order to allow the reaction to warm to room temperature, and stir for a further 20 minutes. Aqueous sodium bicarbonate was added and stirred. Sufficient CH_2Cl_2 was added to fully dissolve all solids. The biphasic mixture was extracted with CH_2Cl_2 (2x) and the combined organics were dried over $MgSO_4$. The crude product was purified by flash column chromatography (30% CH_2Cl_2 in Hexane) to yield the product as orange solid (37 mg, 84%). A melting point determination was not possible because the solid decomposed when heated to 350 °C. ^{1}H NMR (400 MHz, $CDCl_3$): δ = 7.48 (s, 8H), 7.16-7.08 (m, 120H), 6.94 (d, *J*= 8.6 Hz, 16H), 6.83 (d, *J*= 8.6 Hz, 16H), 5.87 (s, 4H) ^{13}C NMR (125 MHz, $CDCl_3$): δ = 180.0, 151.1, 146.8, 145.2, 142.7, 138.7, 137.9, 131.3, 130.7, 129.1, 127.5, 126.4, 126.0, 64.8, 47.0; IR (cm^{-1}): 2921, 2851, 1648, 1594, 1491, 1403, 1371, 1181, 1083, 831, 735, 700; HRMS (MALDI-TOF) calcd for $C_{2342}H_{164}O_2$ $[M]^+$ 3005. 2731, found 3005.277.

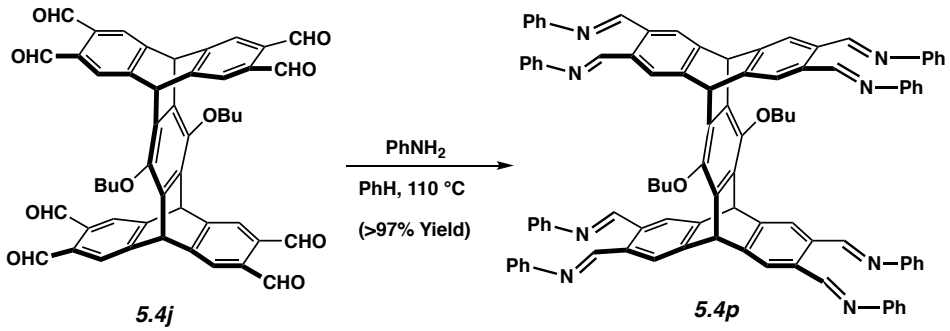

5.4j *5.4p*

Pentiptyceneimine 5.4p. Solid **5.4j** (11.4 mg, 0.0081 mmol, 1.0 equiv) was suspended in benzene (7 mL). Aniline (47.2µL, 0.518 mmol, 64 equiv) was added and the reaction was heated to reflux through a Soxhelet extractor with a layer of $MgSO_4$ for 12 hours. The reaction mixture was concentrated under reduced pressure to show clean conversion to **5.4p** by NMR with an estimate yield ≥97%.

5.6 Spectra Relevant to Chapter Five:

A High Yielding and Divergent Paradigm for the Synthesis of D_{2h}-Symmetric Octakis-Substituted Pentiptycenequinones

Adapted from: Geeta S. Vadehra, Xing Jiang, Jordan J. Dotson, Gong M. Chu, and Miguel A. Garcia-Garibay*.

Org. Lett. **2017**, *19*, 1838–1841.

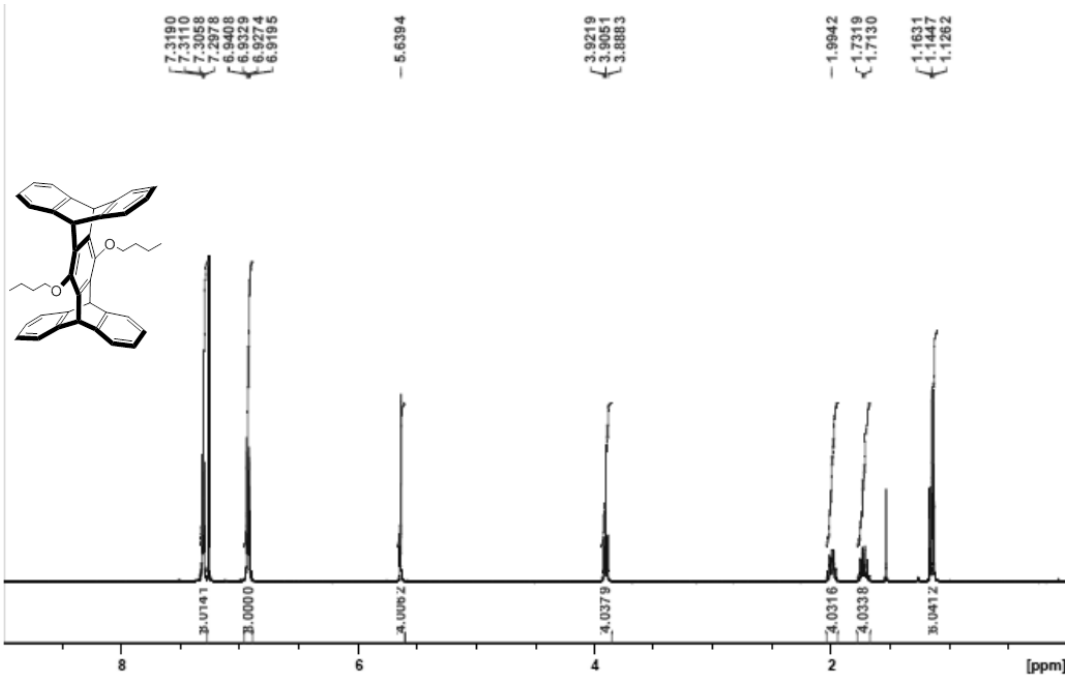

Figure 5.3 ^{1}H NMR (400 MHz, $CDCl_3$) of compound **5.2**.

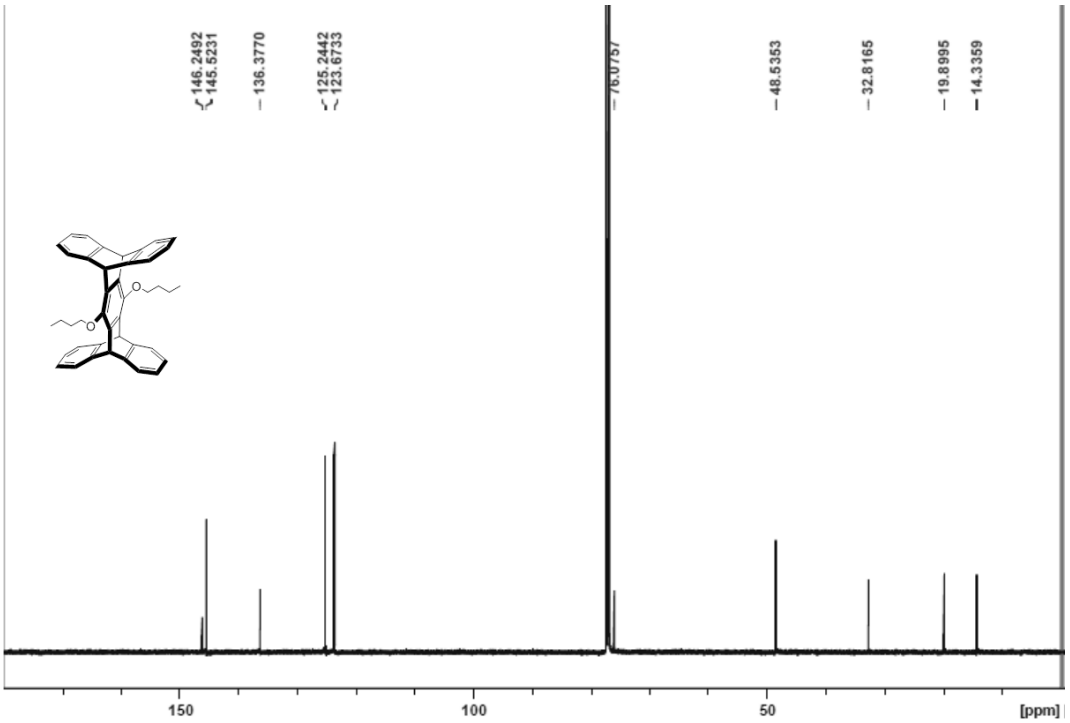

Figure 5.4 ^{13}C NMR (125 MHz, $CDCl_3$) of compound **5.2**.

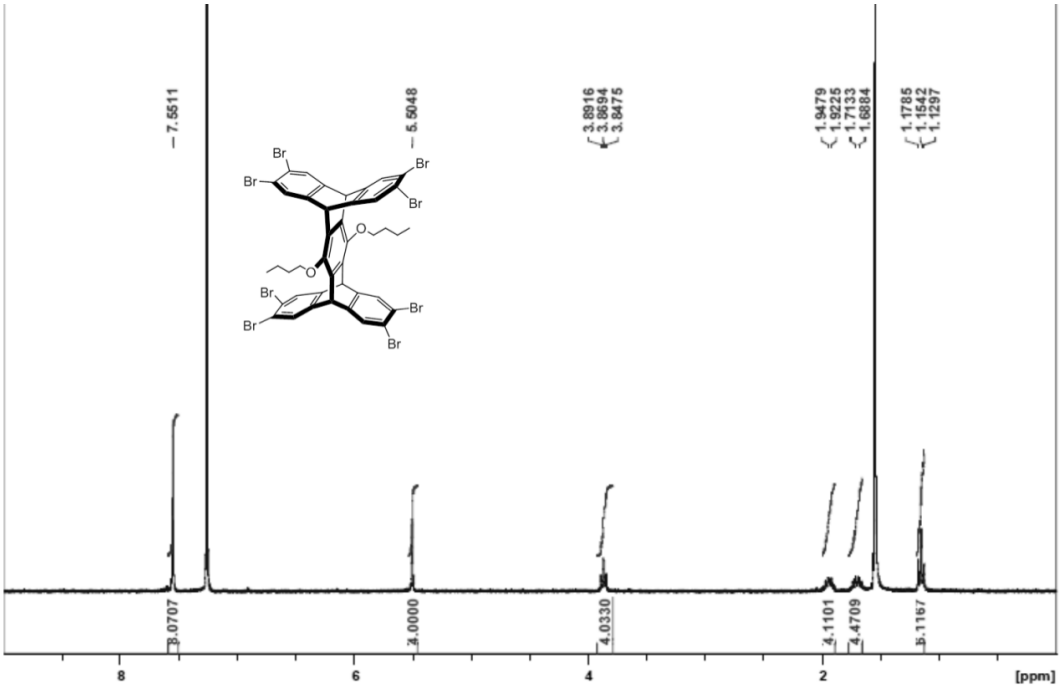

Figure 5.5 ^{1}H NMR (400 MHz, $CDCl_3$) of compound **5.3**.

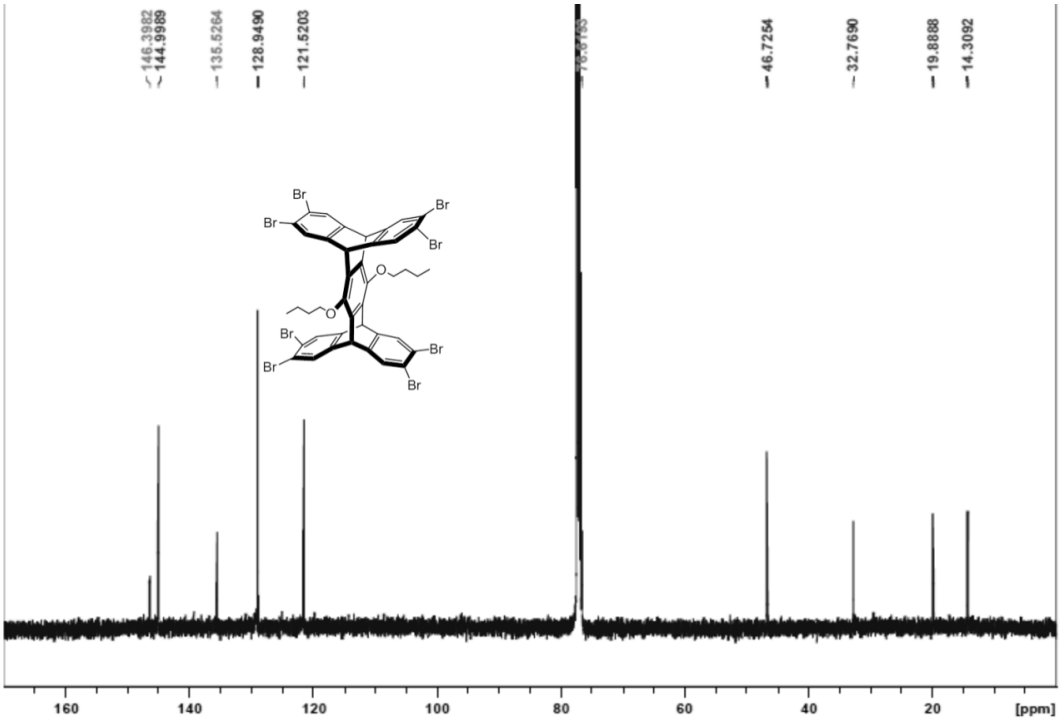

Figure 5.6 ^{13}C NMR (125 MHz, $CDCl_3$) of compound **5.3**.

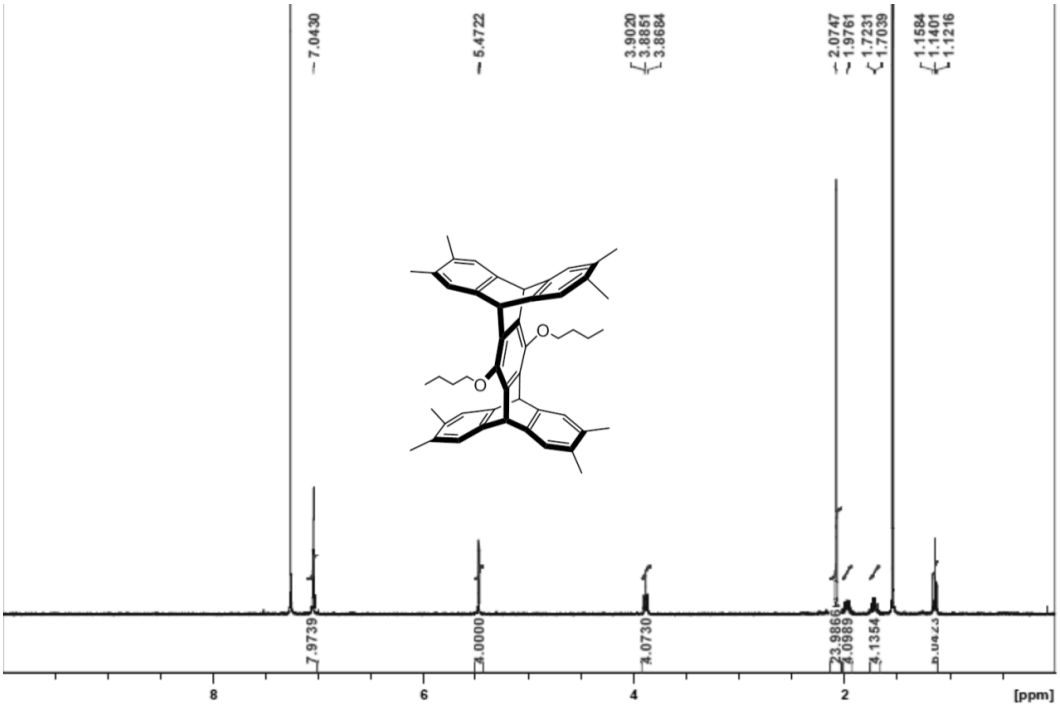

Figure 5.7 ^{1}H NMR (400 MHz, $CDCl_3$) of compound **5.4a**.

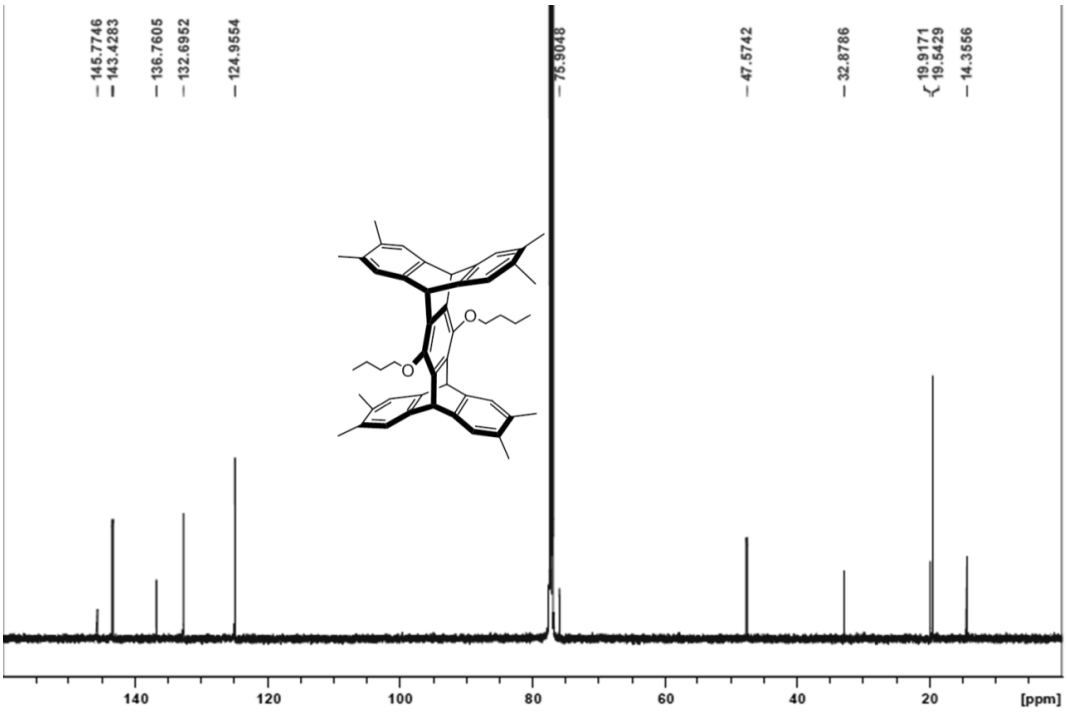

Figure 5.8 ^{13}C NMR (125 MHz, $CDCl_3$) of compound **5.4a**.

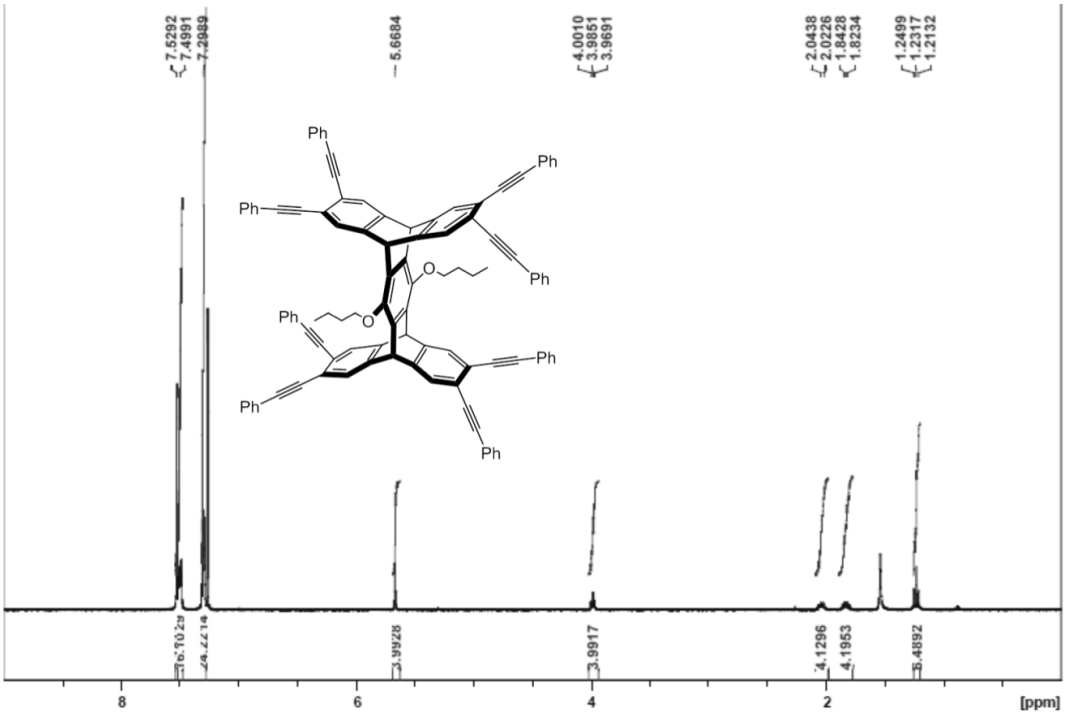

Figure 5.9 ^{1}H NMR (400 MHz, $CDCl_3$) of compound **5.4b**.

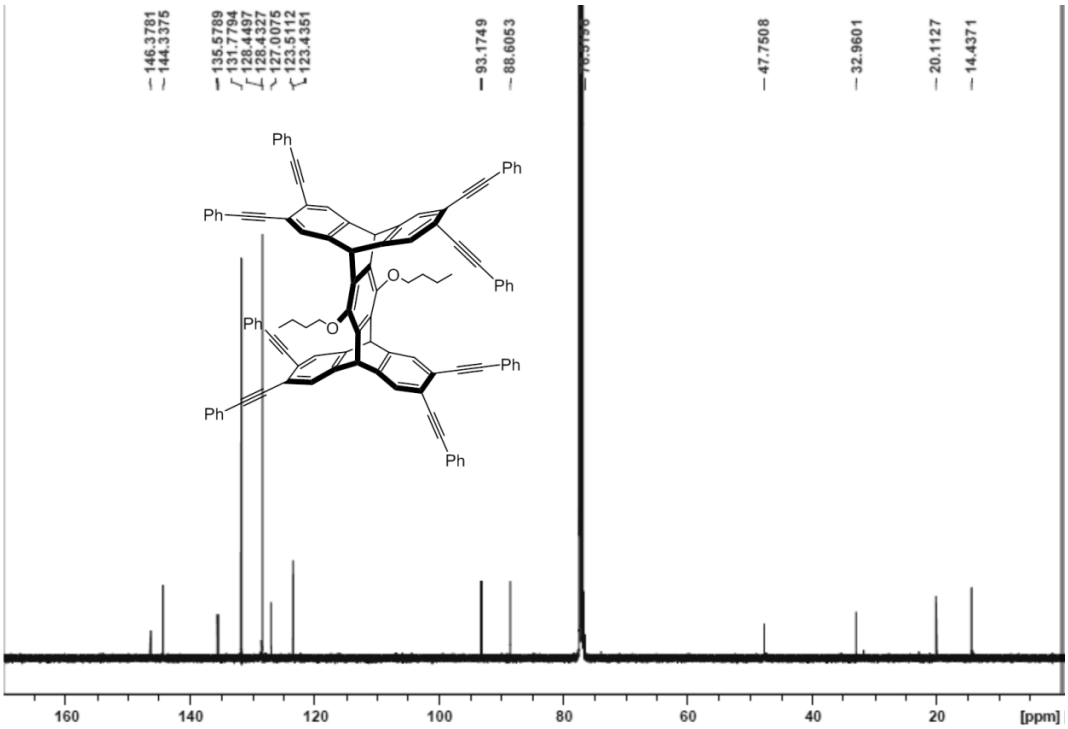

Figure 5.10 ^{13}C NMR (125 MHz, $CDCl_3$) of compound **5.4b**.

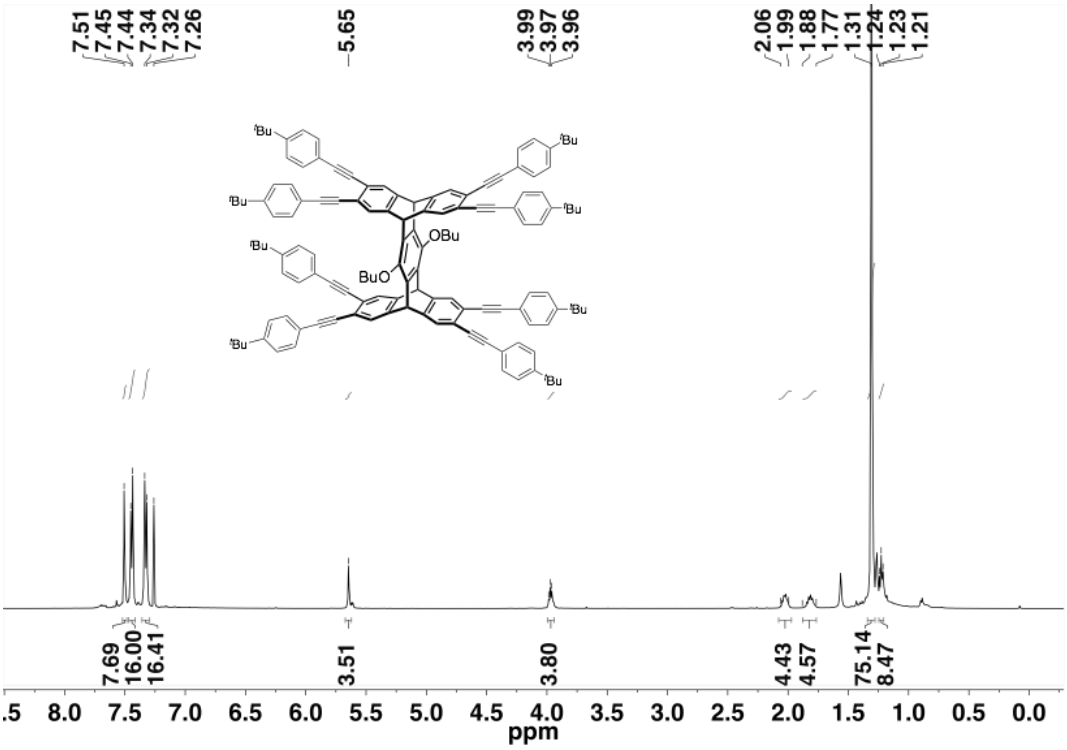

Figure 5.11 ^{1}H NMR (500 MHz, $CDCl_3$) of compound **5.4c**.

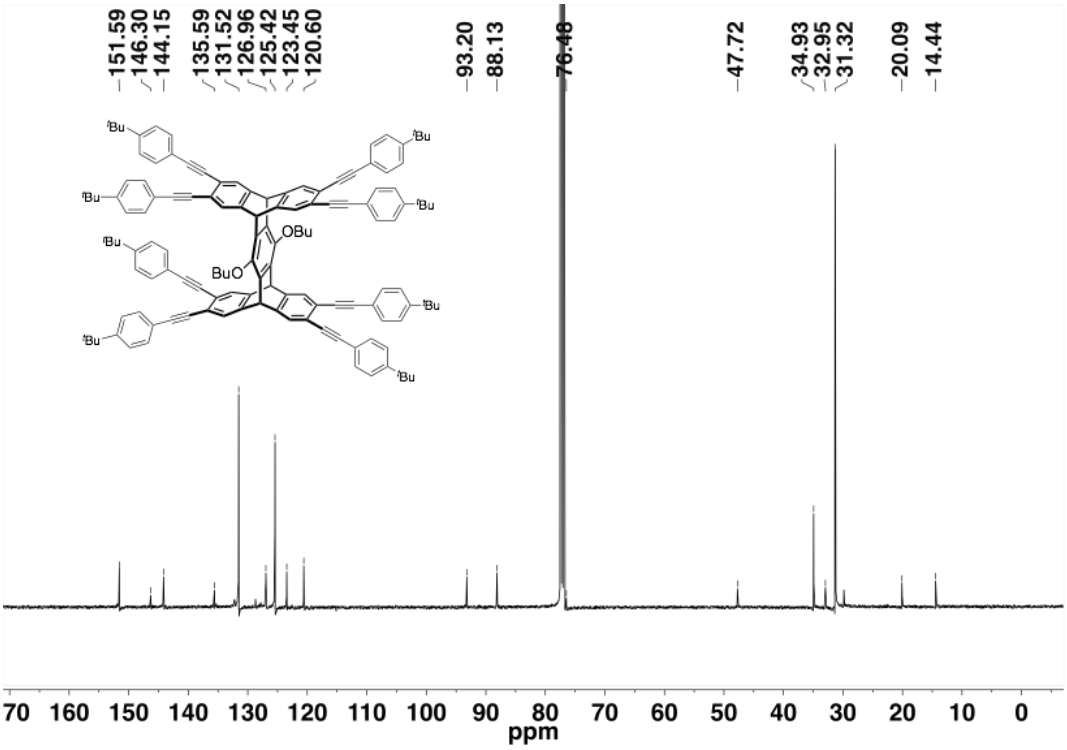

Figure 5.12 ^{13}C NMR (125 MHz, $CDCl_3$) of compound **5.4c** .

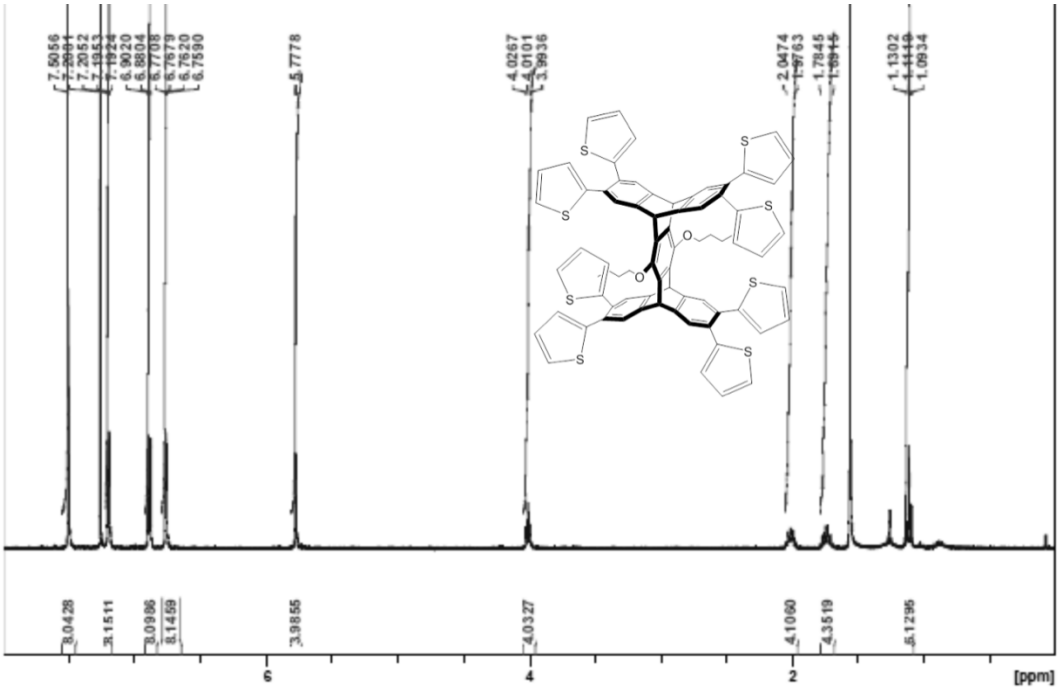

Figure 5.13 ^{1}H NMR (400 MHz, $CDCl_3$) of compound **5.4d**.

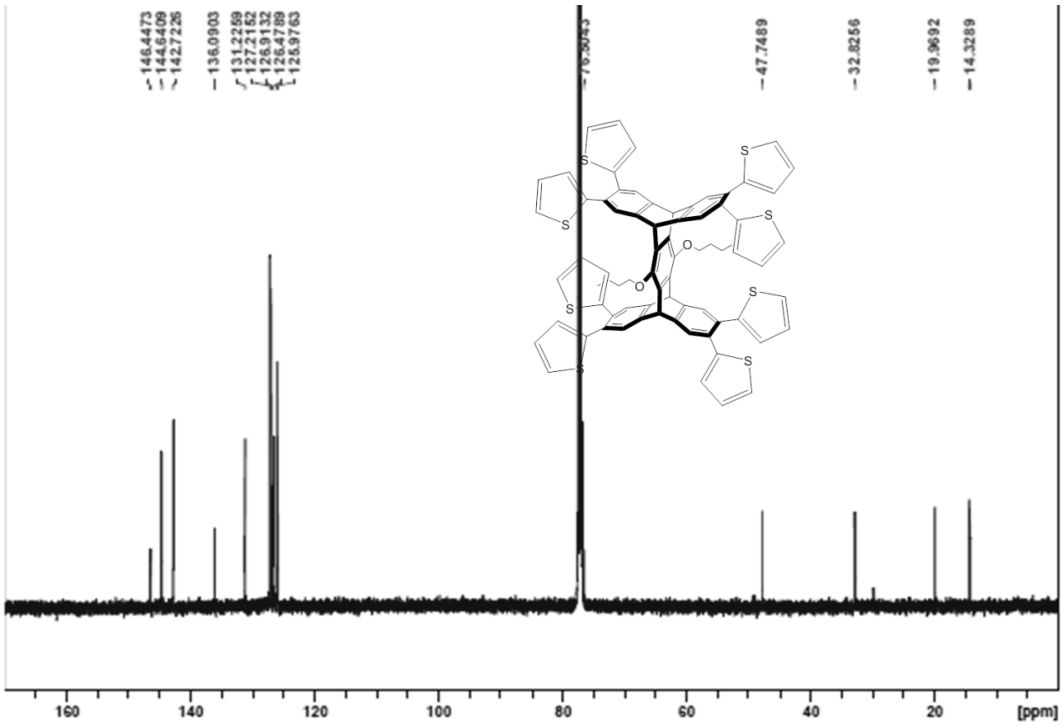

Figure 5.14 ^{13}C NMR (125 MHz, $CDCl_3$) of compound **5.4d**.

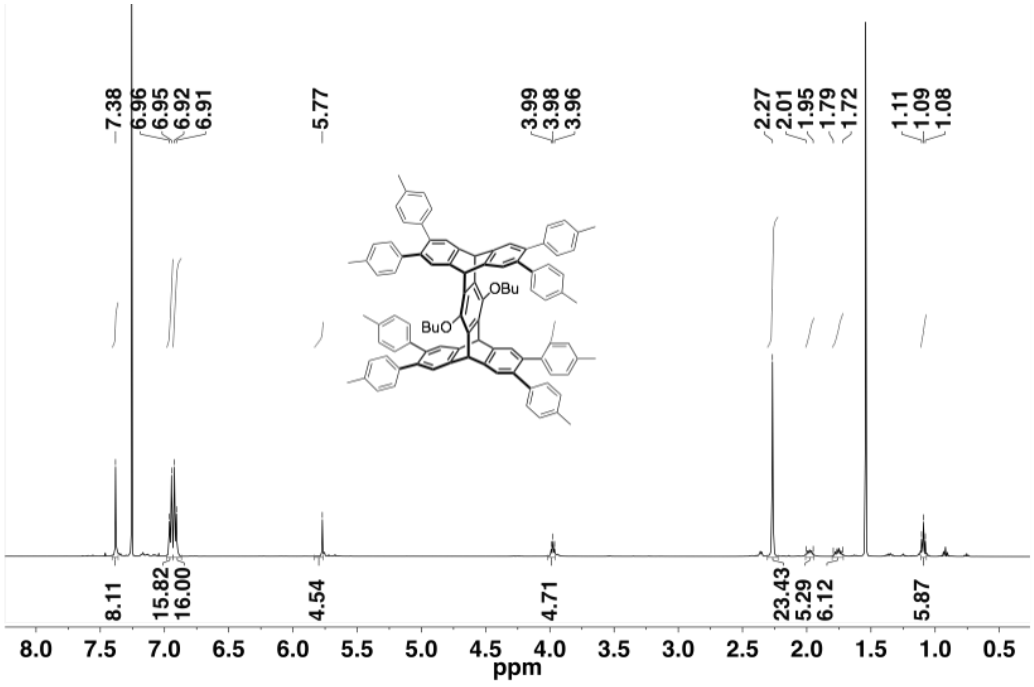

Figure 5.15 ^{1}H NMR (500 MHz, $CDCl_3$) of compound **5.4e**.

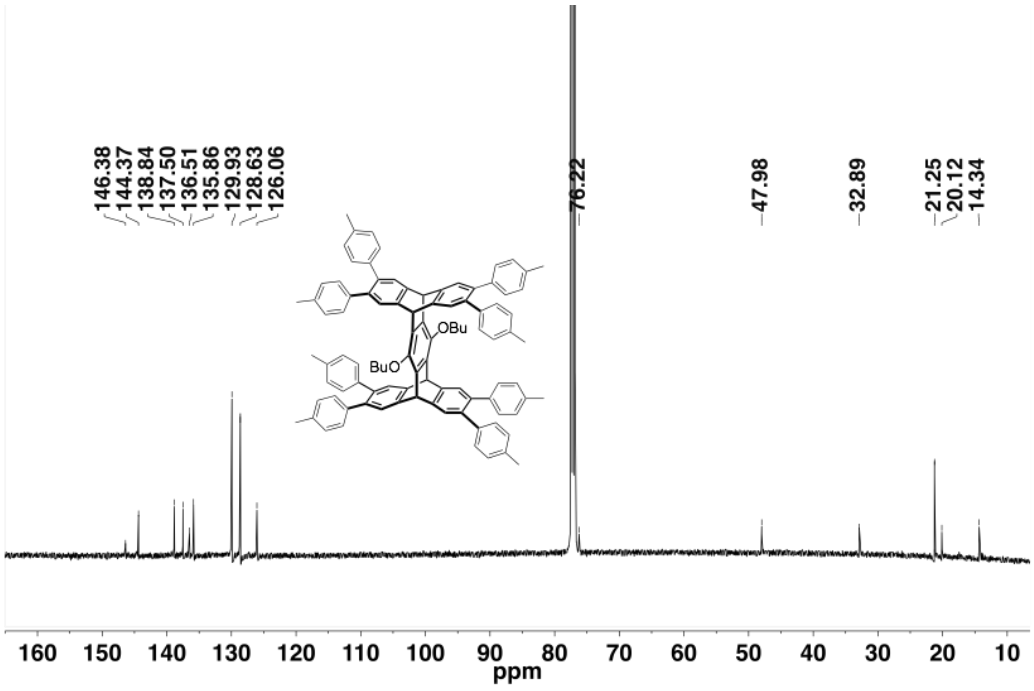

Figure 5.16 ^{13}C NMR (125 MHz, $CDCl_3$) of compound **5.4e**.

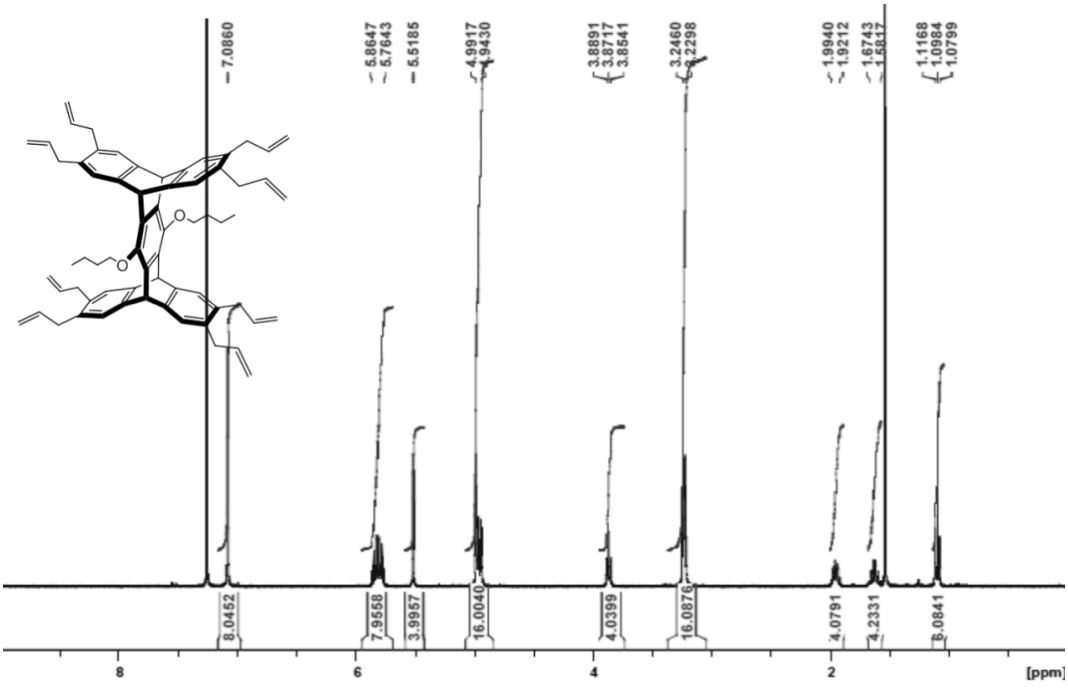

Figure 5.17 ^{1}H NMR (400 MHz, $CDCl_3$) of compound **5.4f**.

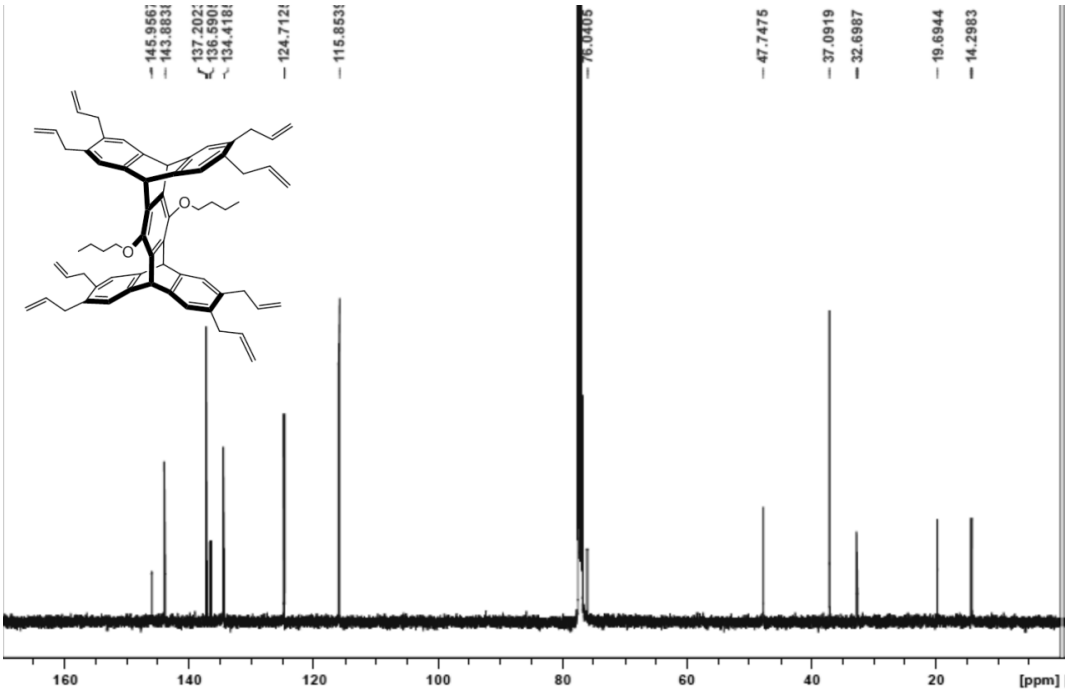

Figure 5.18 ^{13}C NMR (125 MHz, $CDCl_3$) of compound **5.4f**.

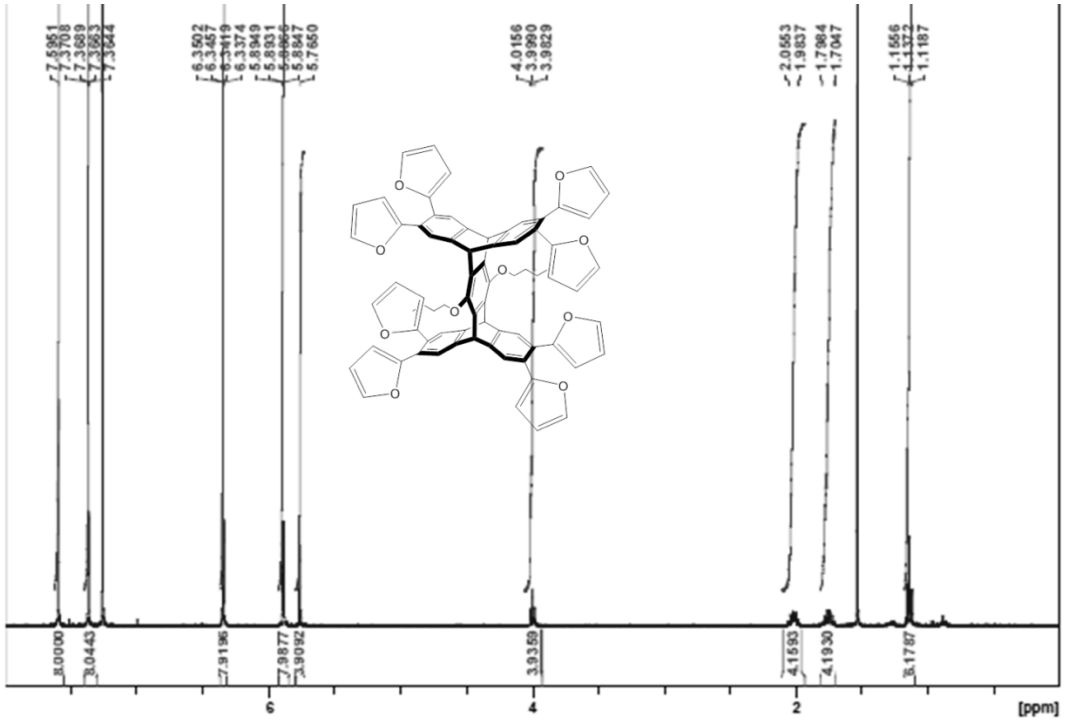

Figure 5.19 ^{1}H NMR (400 MHz, $CDCl_3$) of compound **5.4g**.

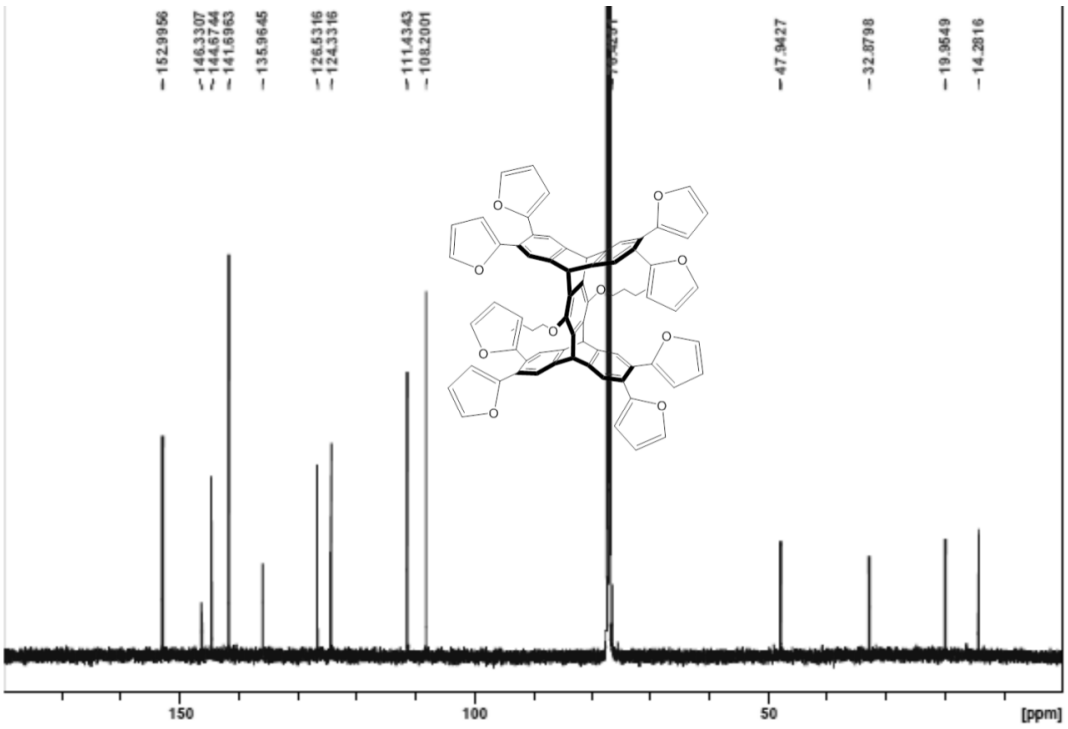

Figure 5.20 ^{13}C NMR (125 MHz, $CDCl_3$) of compound **5.4g**.

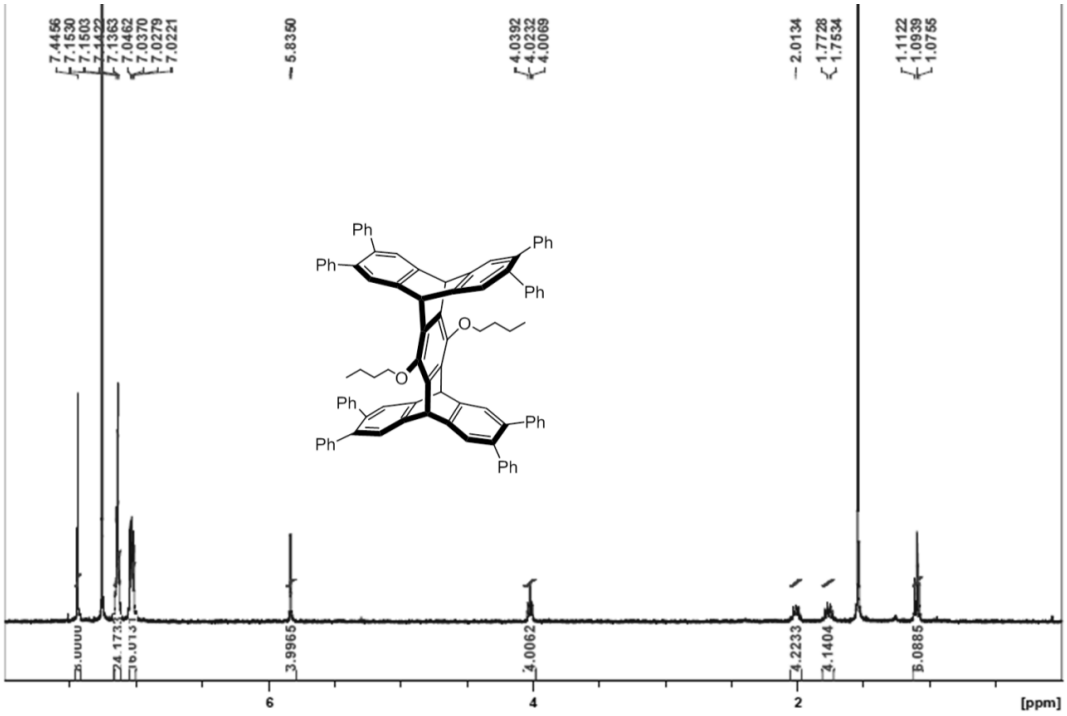

Figure 5.21 ^{1}H NMR (400 MHz, $CDCl_3$) of compound **5.4h**.

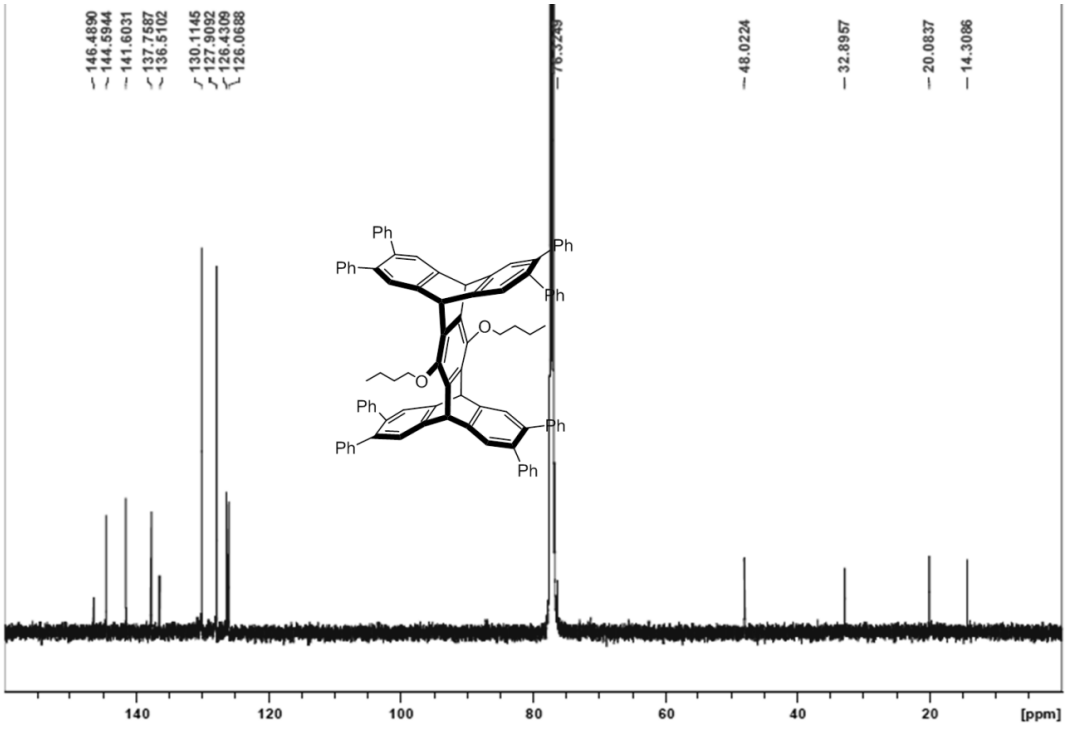

Figure 5.22 ^{13}C NMR (125 MHz, $CDCl_3$) of compound **5.4h**.

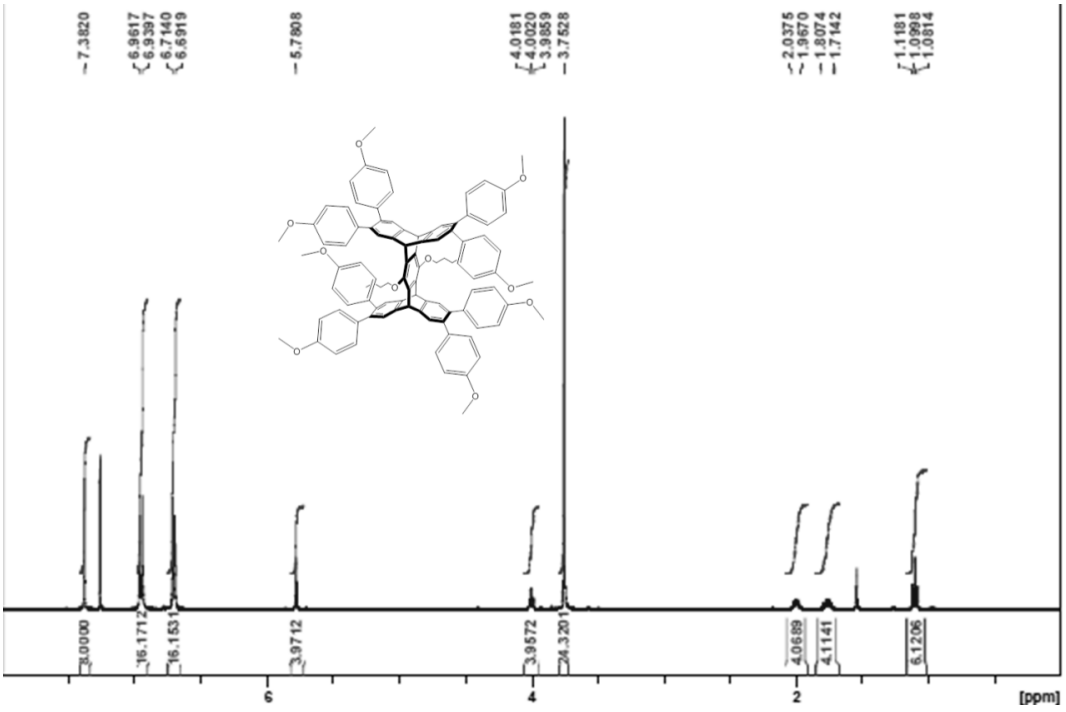

Figure 5.23 ^{1}H NMR (400 MHz, $CDCl_3$) of compound **5.4i**.

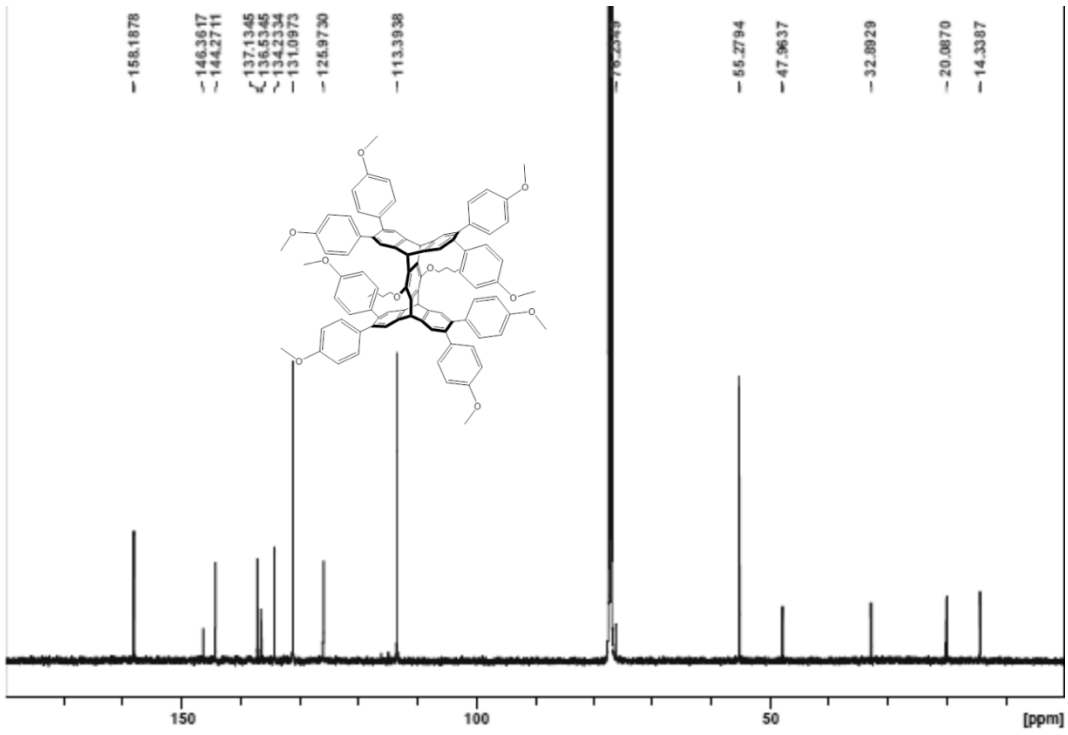

Figure 5.24 ^{13}C NMR (125 MHz, $CDCl_3$) of compound **5.4i**.

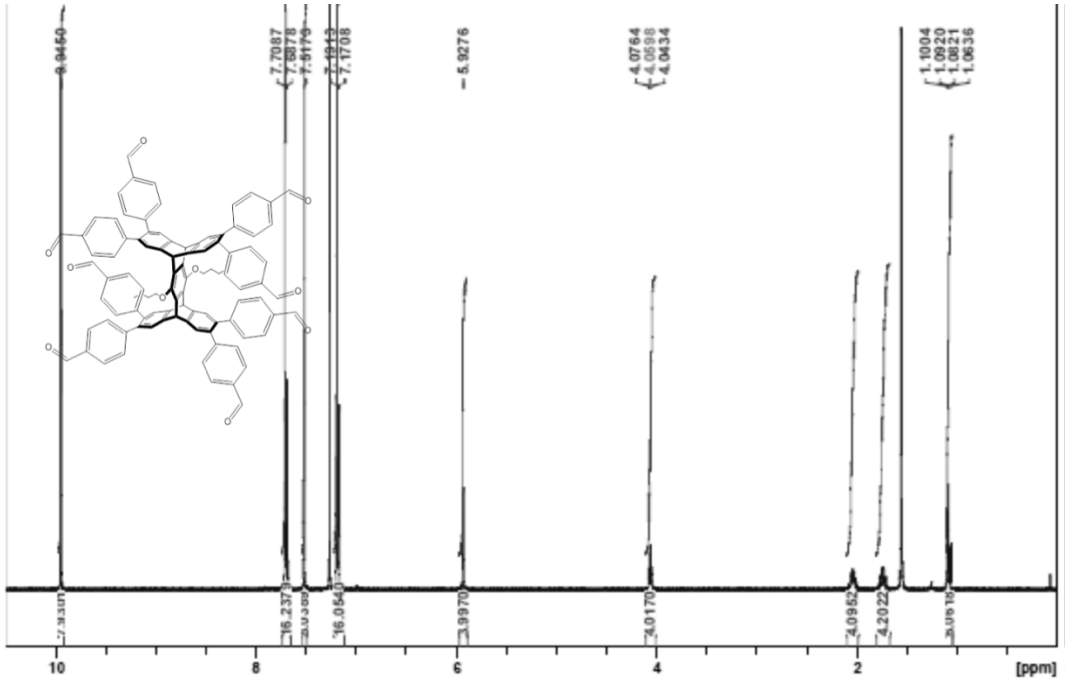

Figure 5.25 ^{1}H NMR (400 MHz, $CDCl_3$) of compound **5.4j**.

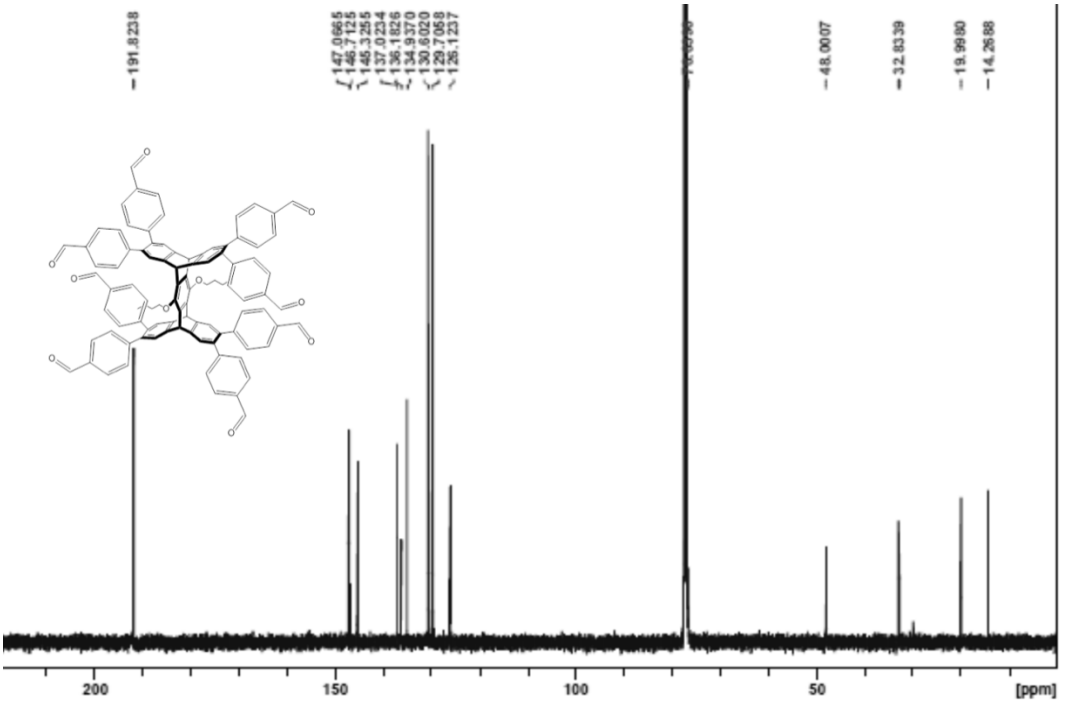

Figure 5.26 ^{13}C NMR (125 MHz, $CDCl_3$) of compound **5.4j**.

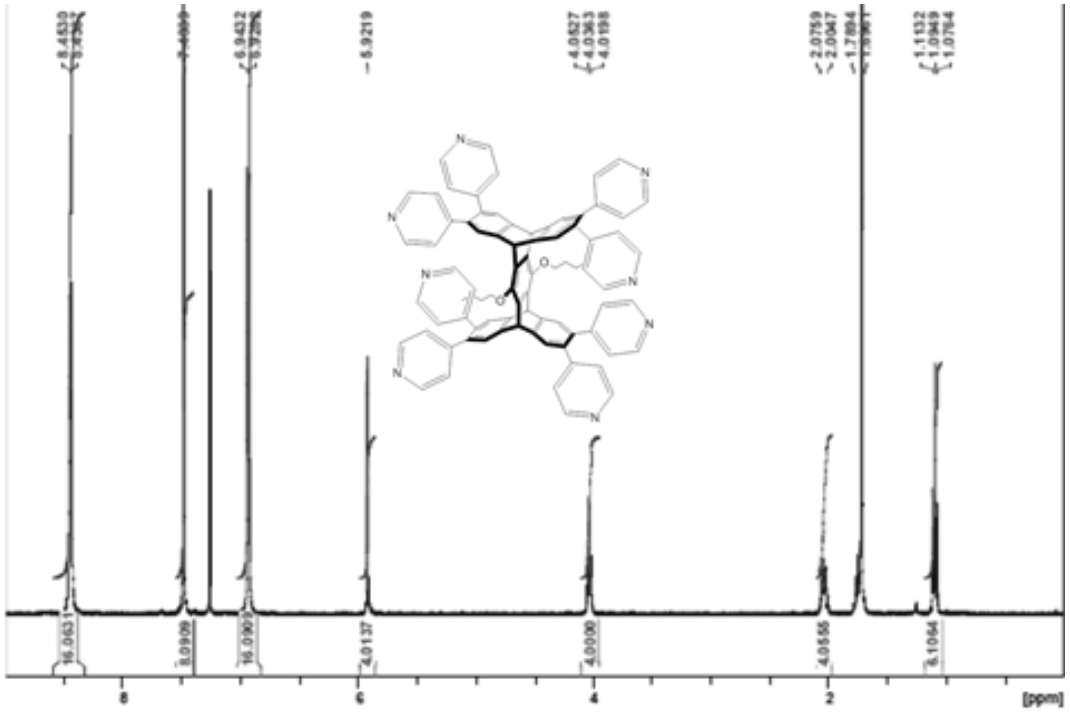

Figure 5.27 ^{1}H NMR (400 MHz, $CDCl_3$) of compound **5.4k**.

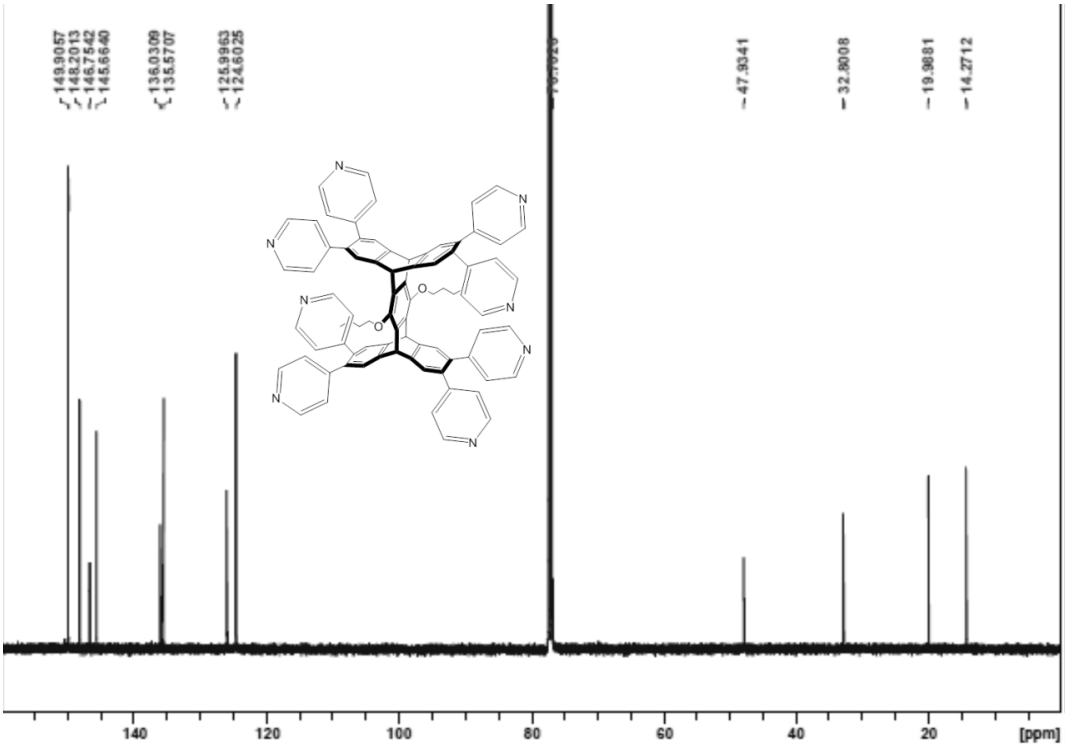

Figure 5.28 ^{13}C NMR (125 MHz, $CDCl_3$) of compound **5.4k**.

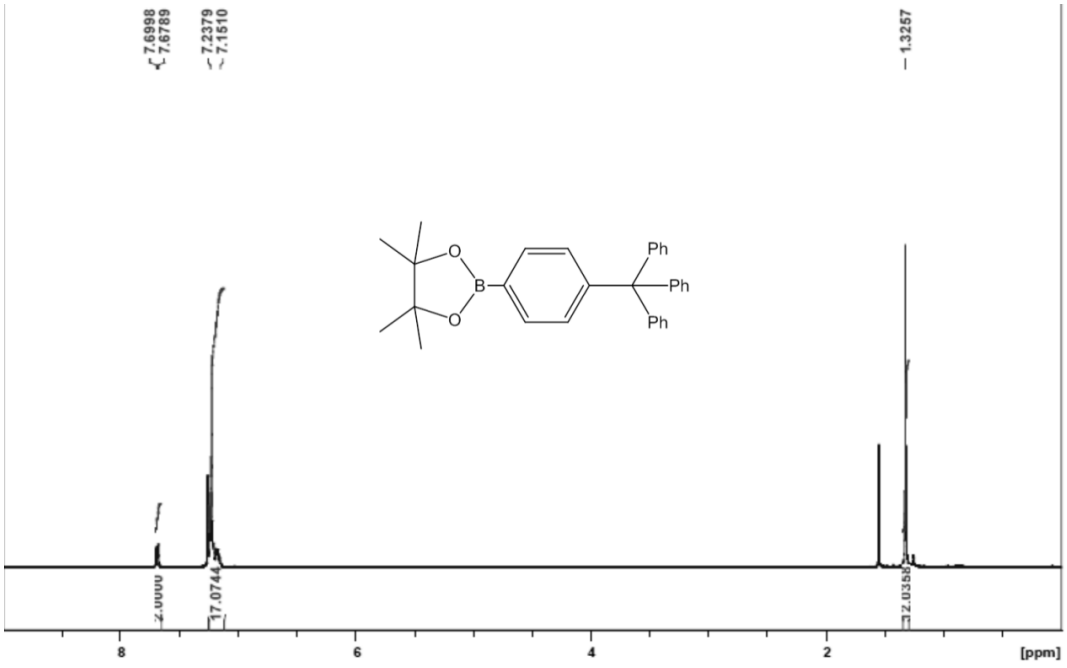

Figure 5.29 ^{1}H NMR (400 MHz, $CDCl_3$) of compound **5.9**

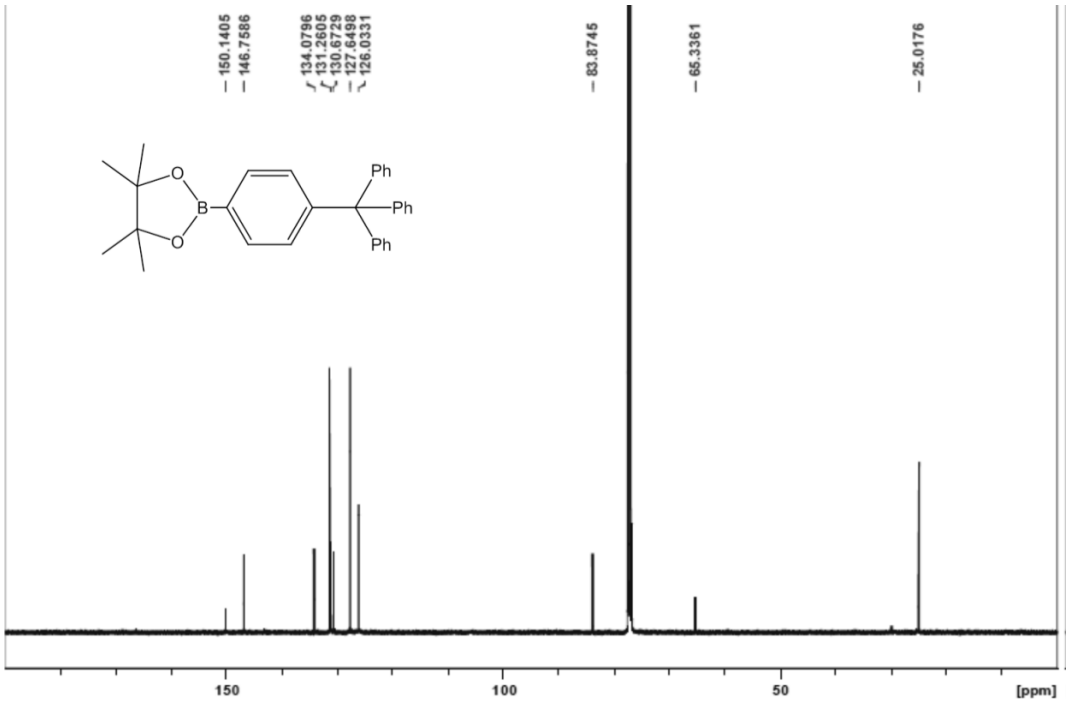

Figure 5.30 ^{13}C NMR (125 MHz, $CDCl_3$) of compound **5.9**

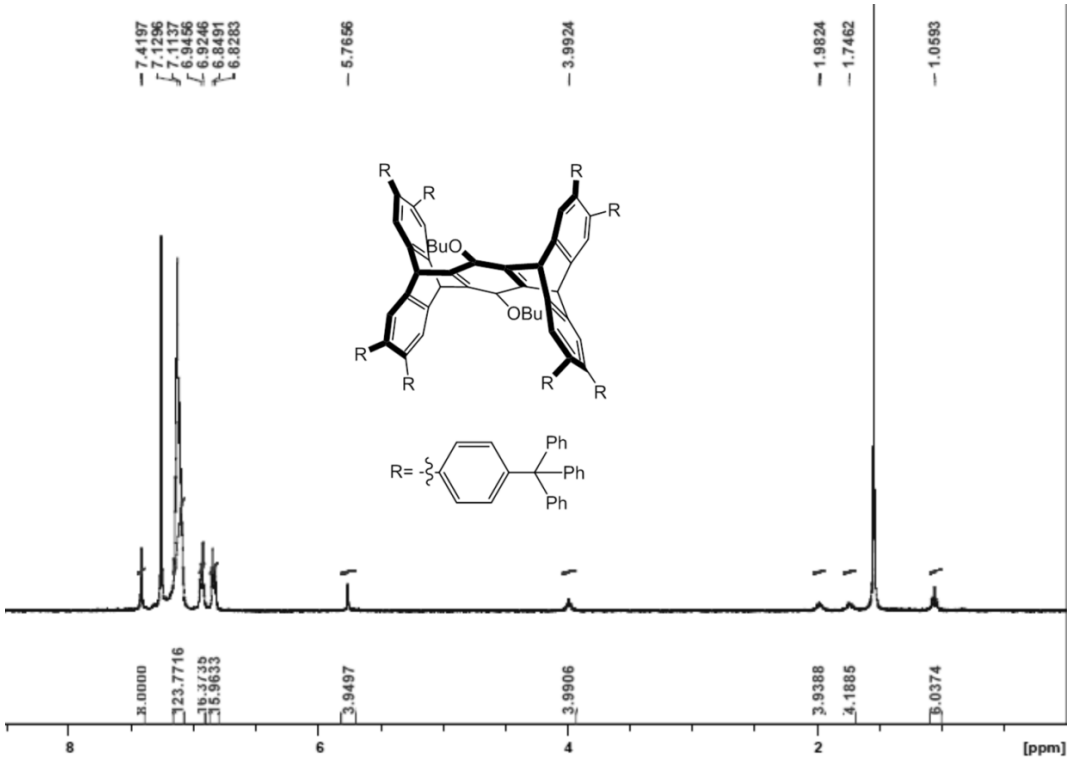

Figure 5.31 ^{1}H NMR (400 MHz, $CDCl_3$) of compound **5.4l**

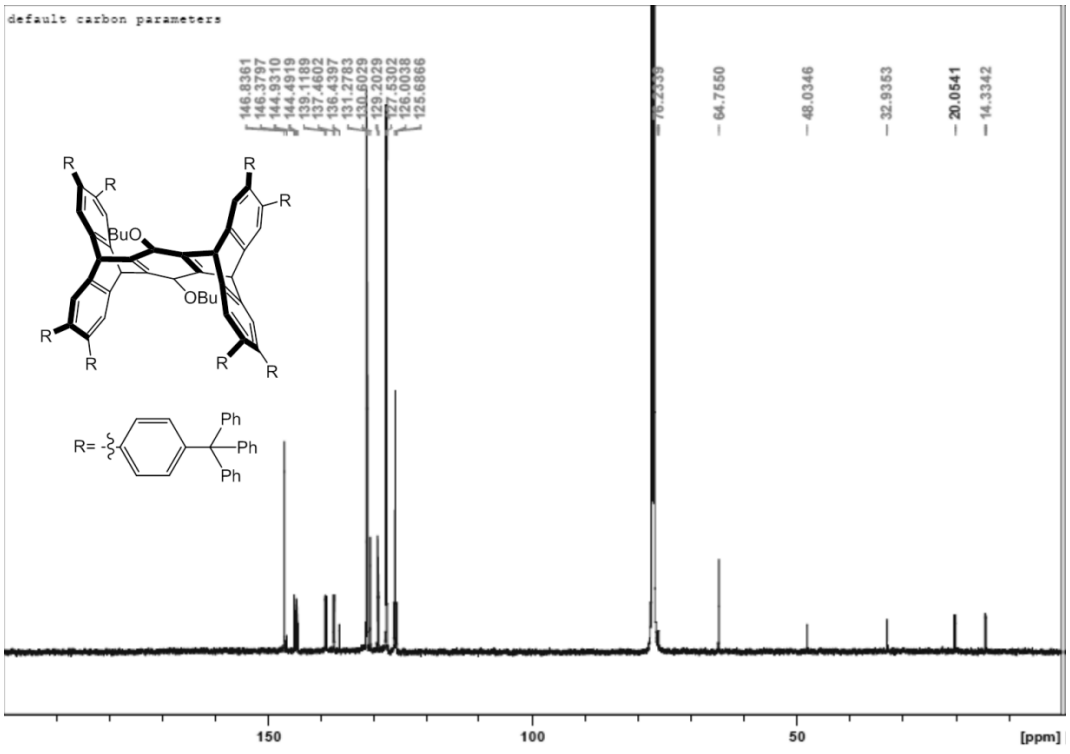

Figure 5.32 ^{13}C NMR (125 MHz, $CDCl_3$) of compound **5.4l**

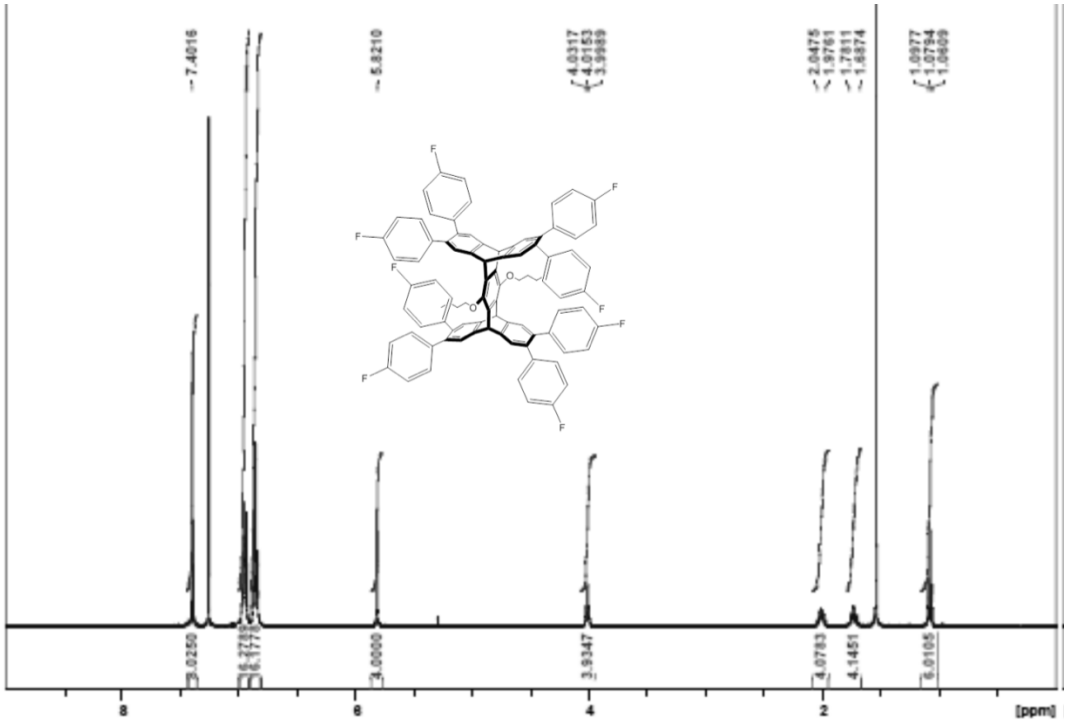

Figure 5.33 ^{1}H NMR (400 MHz, $CDCl_3$) of compound **5.4m**

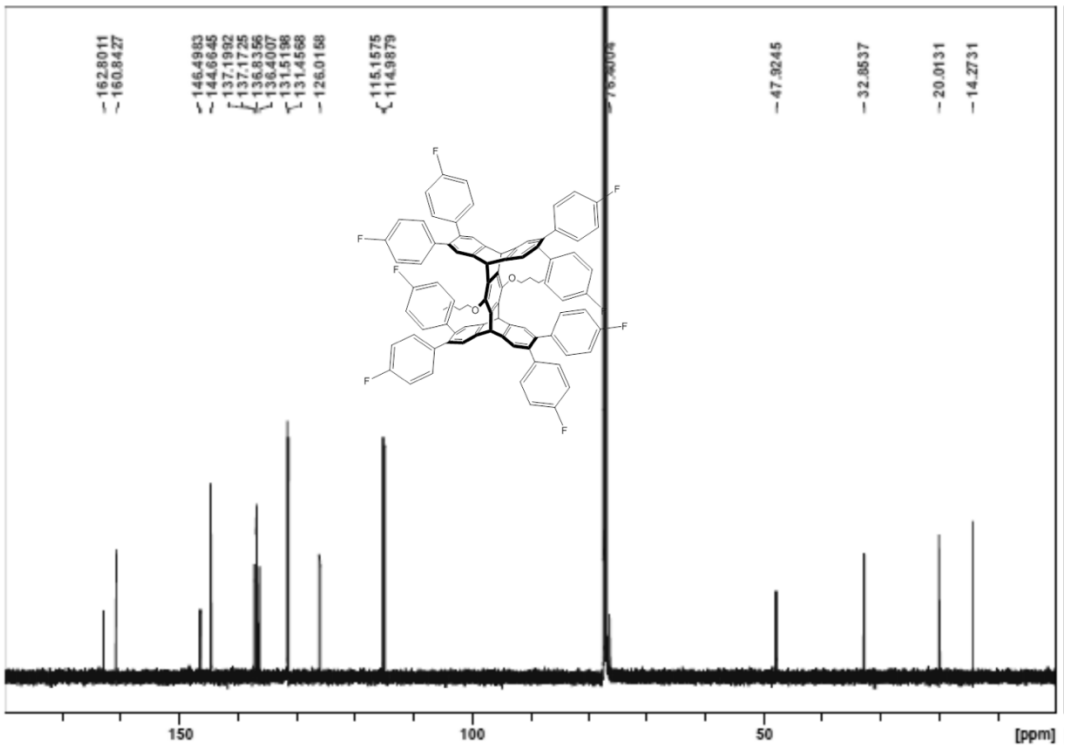

Figure 5.34 ^{13}C NMR (125 MHz, $CDCl_3$) of compound **5.4m**

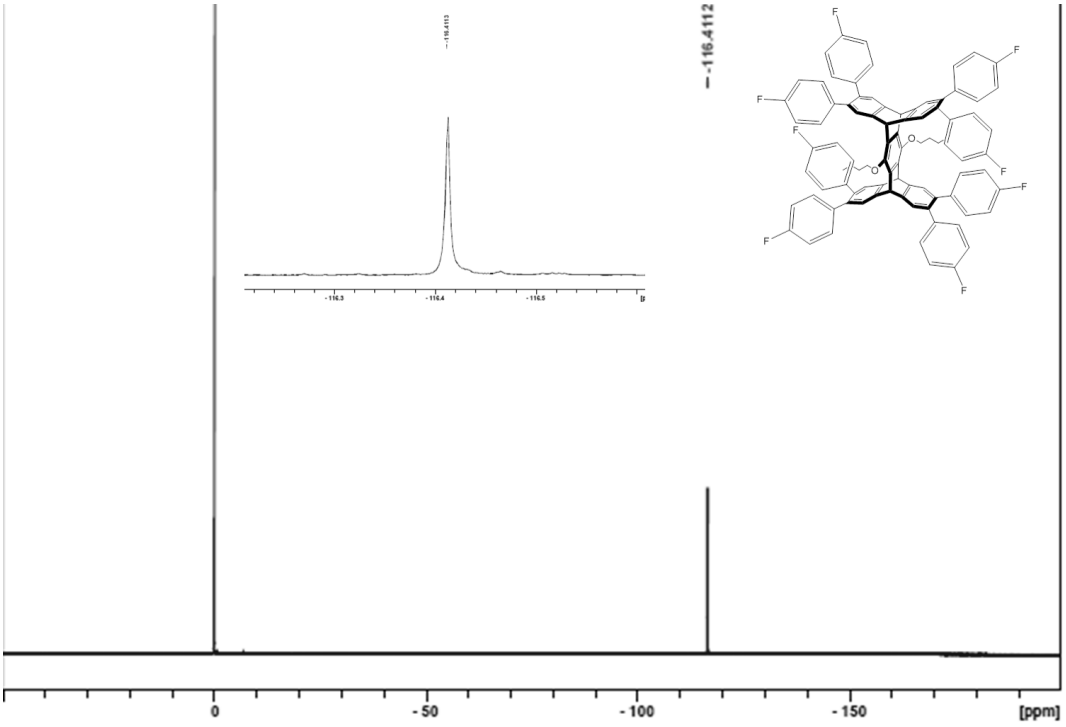

Figure 5.35 ^{19}F NMR (376 MHz, $CDCl_3$) of compound **5.4m** (proton decoupled)

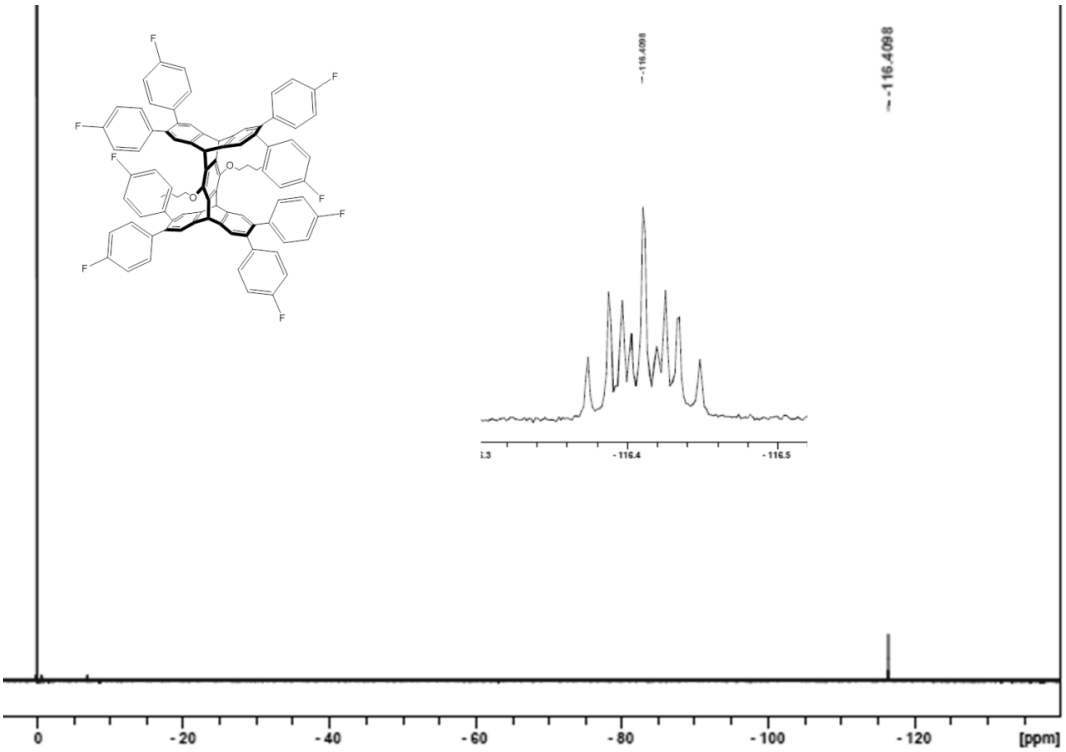

Figure 5.36 ^{19}F NMR (376 MHz, $CDCl_3$) of compound **5.4m.**

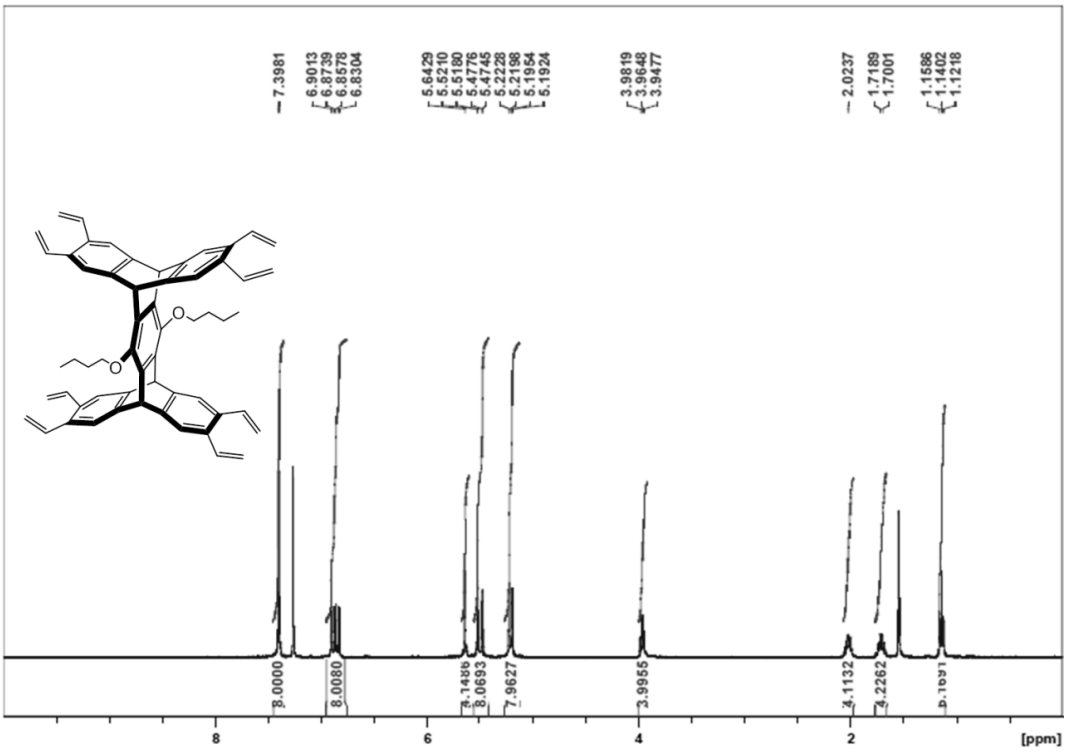

Figure 5.37 ^{1}H NMR (400 MHz, $CDCl_3$) of compound **5.4n**

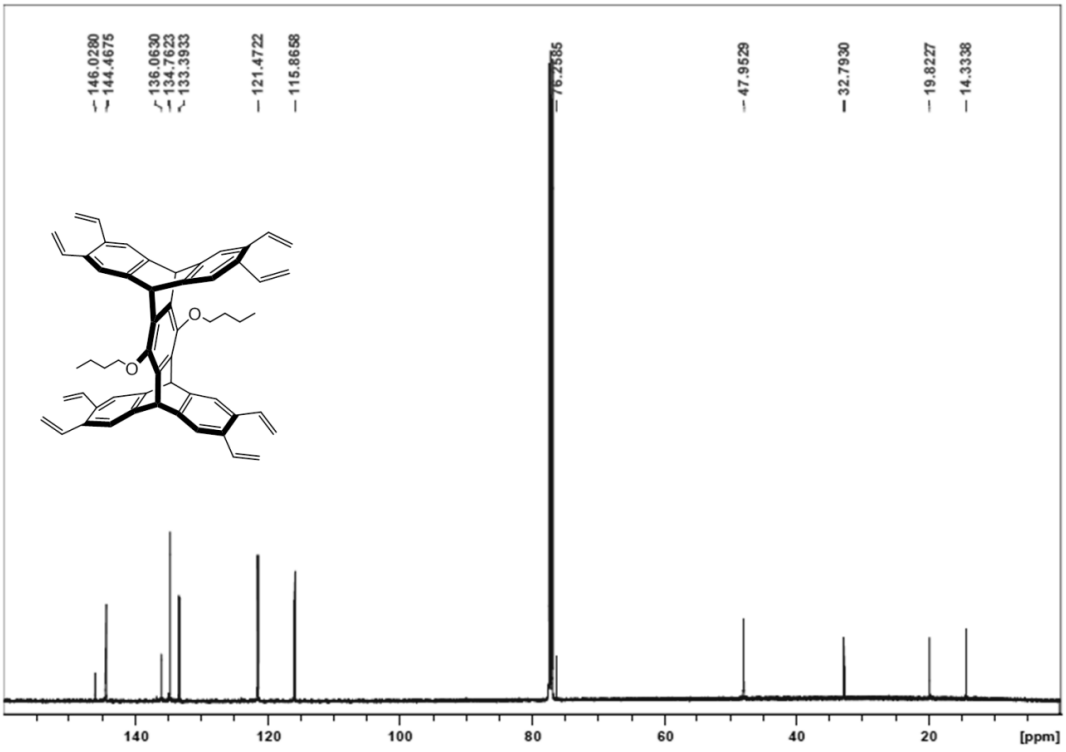

Figure 5.38 ^{13}C NMR (125 MHz, $CDCl_3$) of compound **5.4n**

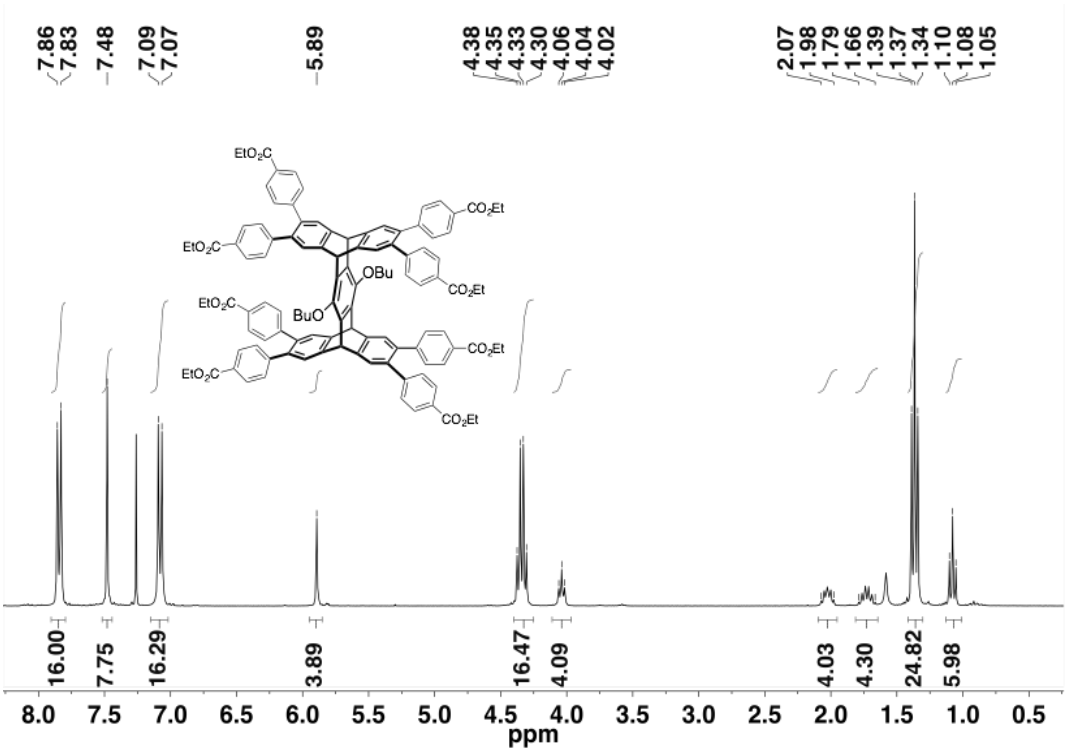

Figure 5.39 ^{1}H NMR (300 MHz, $CDCl_3$) of compound **5.4o**

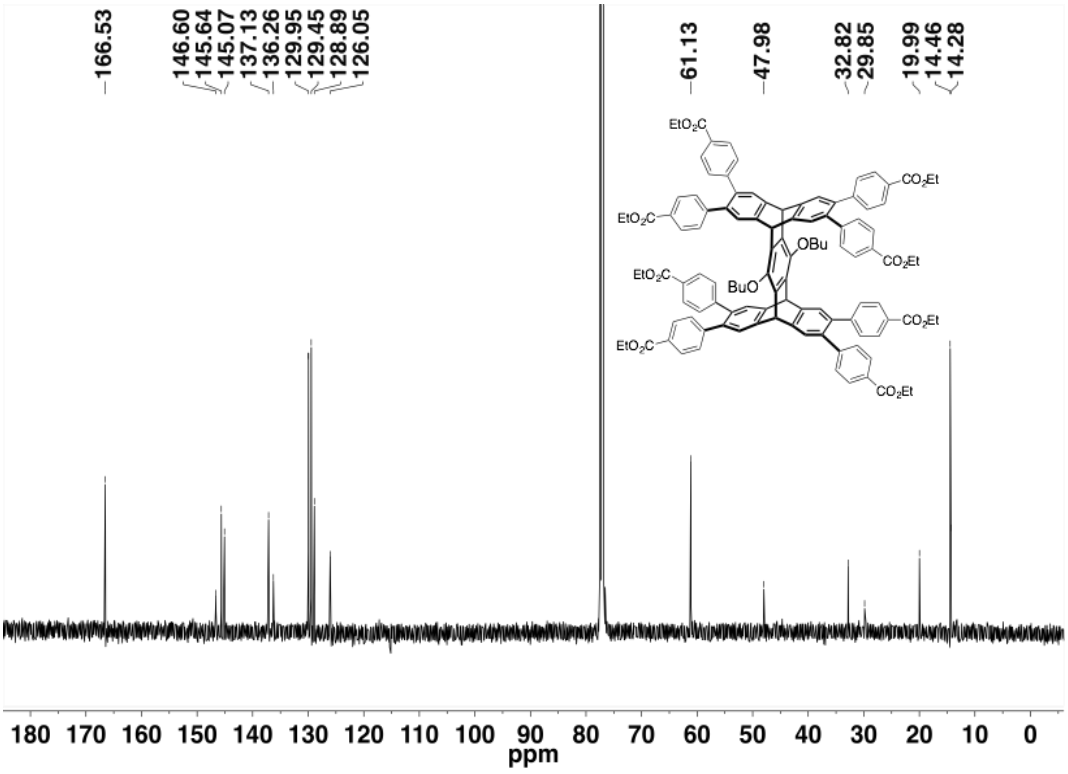

Figure 5.40 ^{13}C NMR (125 MHz, $CDCl_3$) of compound **5.4o**

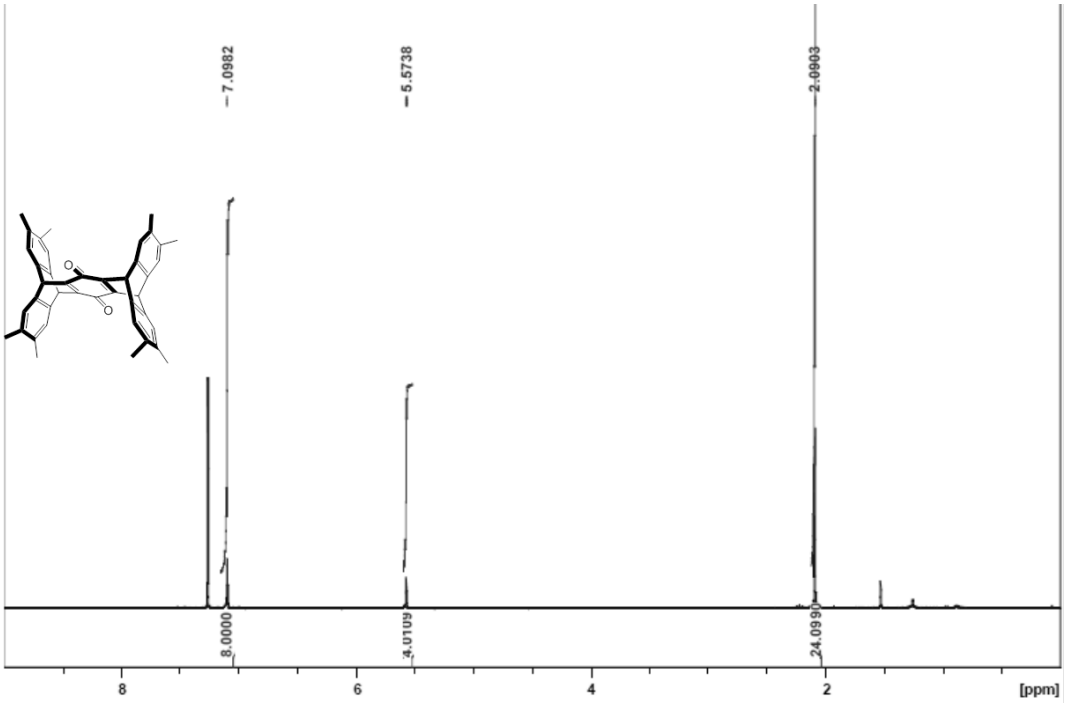

Figure 5.41 ^{1}H NMR (400 MHz, $CDCl_3$) of compound **5.5a**

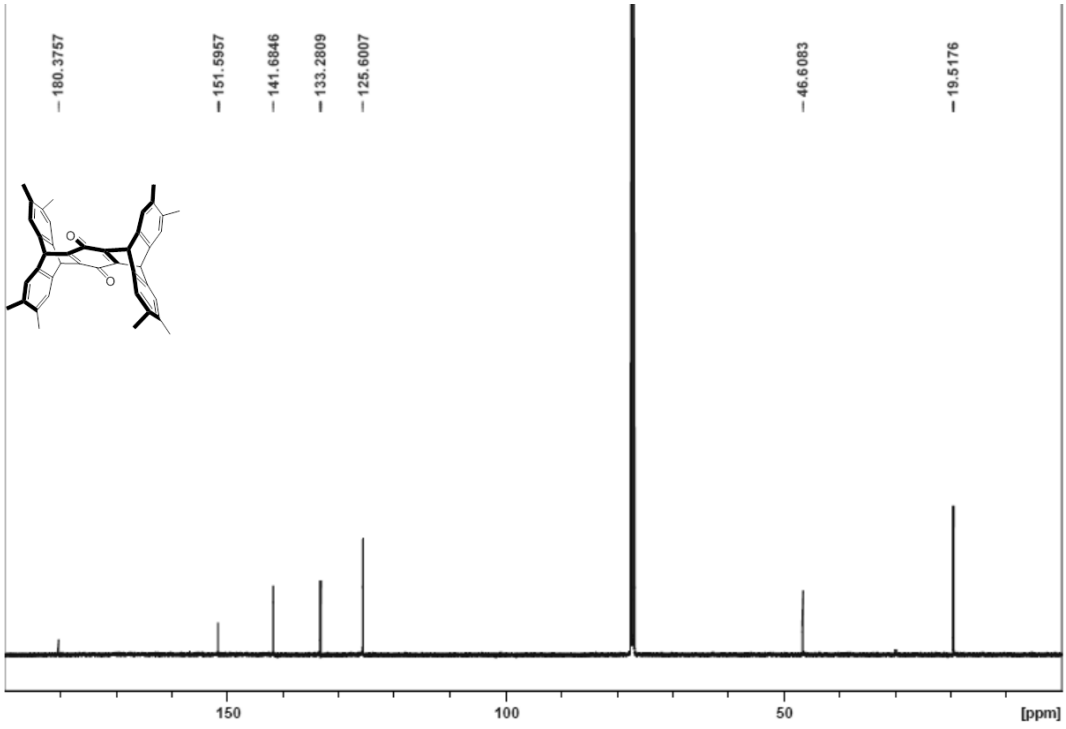

Figure 5.42 ^{13}C NMR (125 MHz, $CDCl_3$) of compound **5.5a**

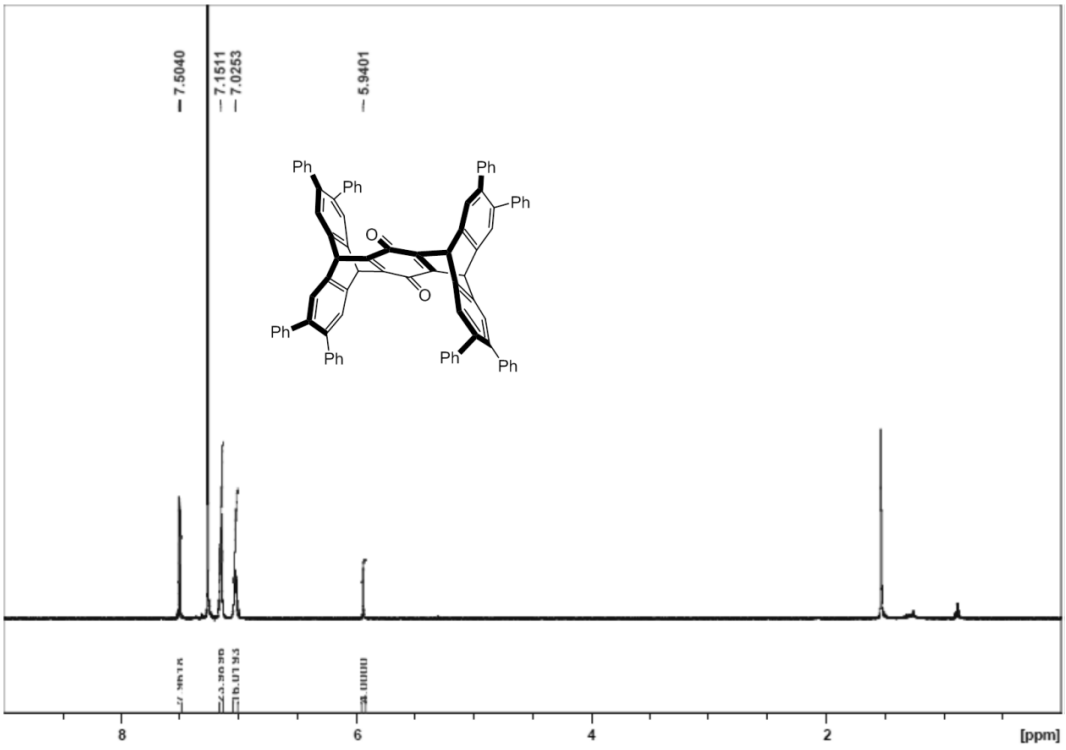

Figure 5.43 ^{1}H NMR (400 MHz, $CDCl_3$) of compound **5.5h**

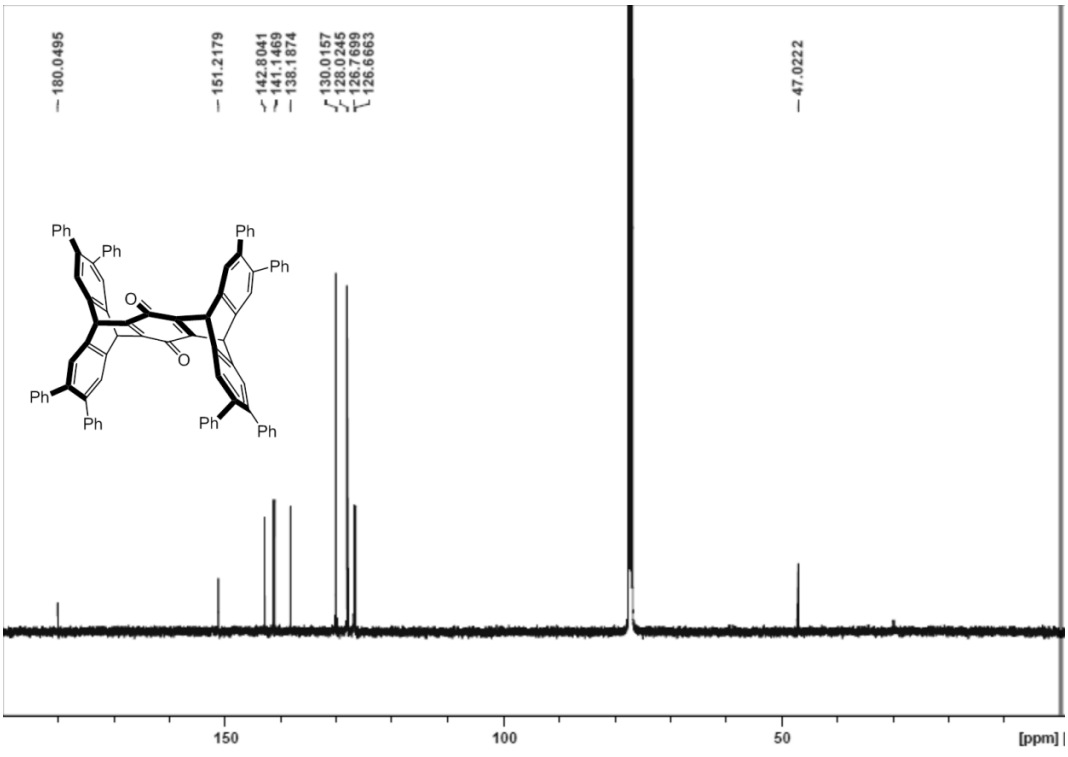

Figure 5.44 ^{13}C NMR (125 MHz, $CDCl_3$) of compound **5.5h**

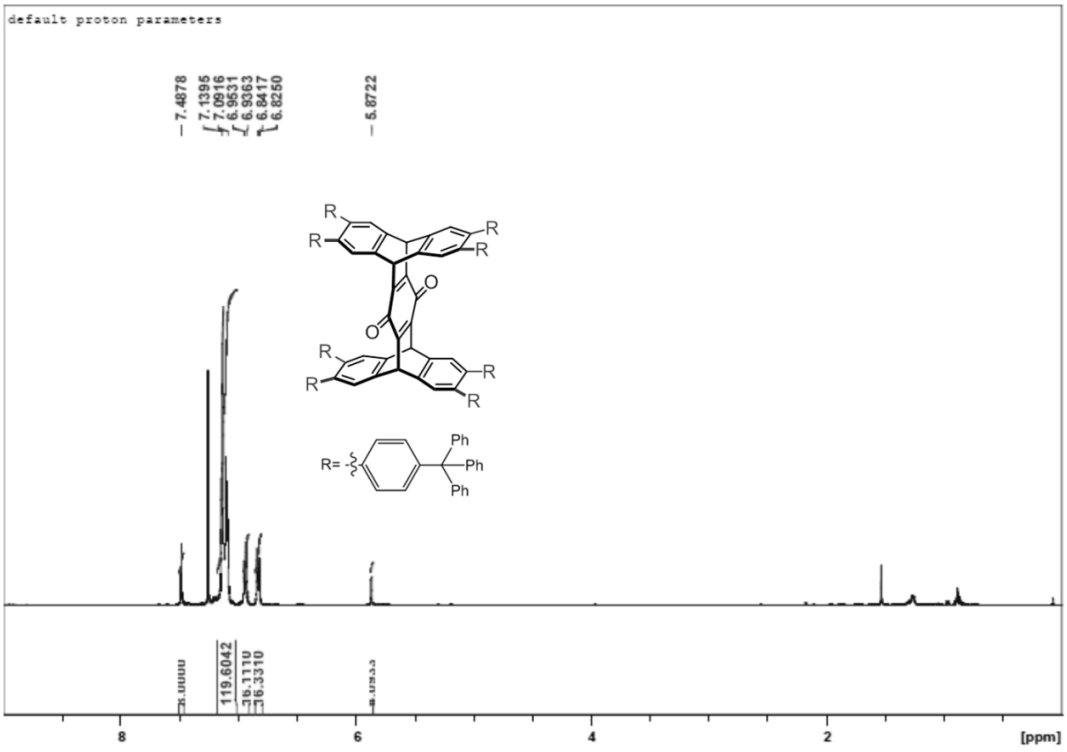

Figure 5.45 ^{1}H NMR (500 MHz, $CDCl_3$) of compound **5.5l**

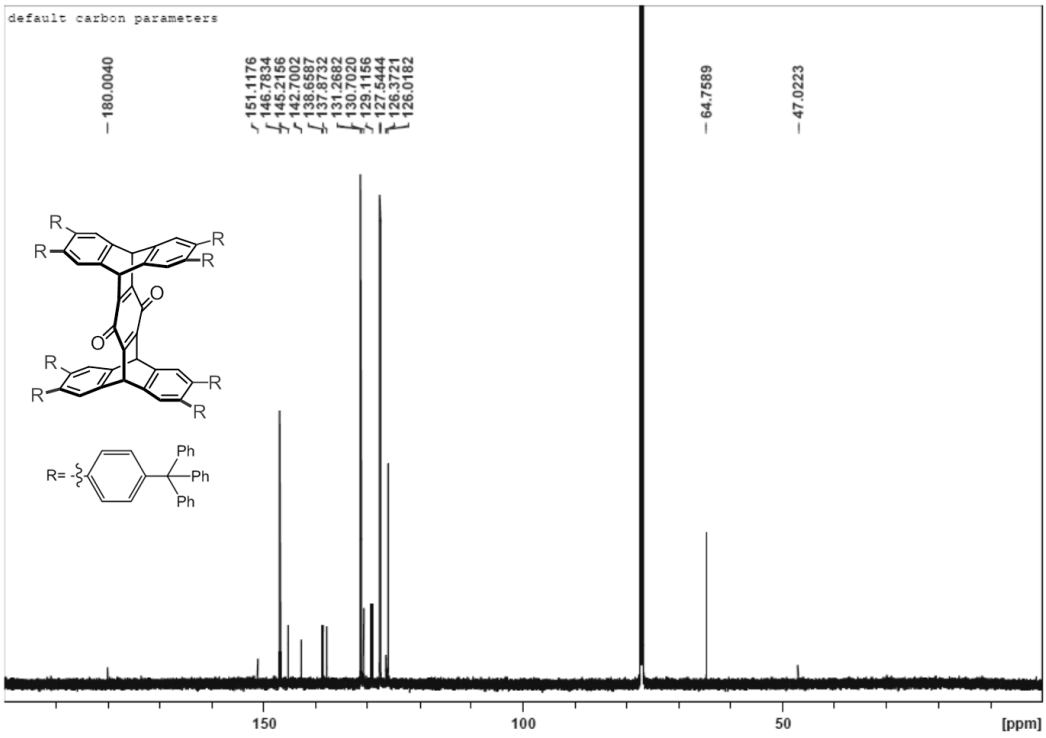

Figure 5.46 ^{13}C NMR (125 MHz, $CDCl_3$) of compound **5.5l**

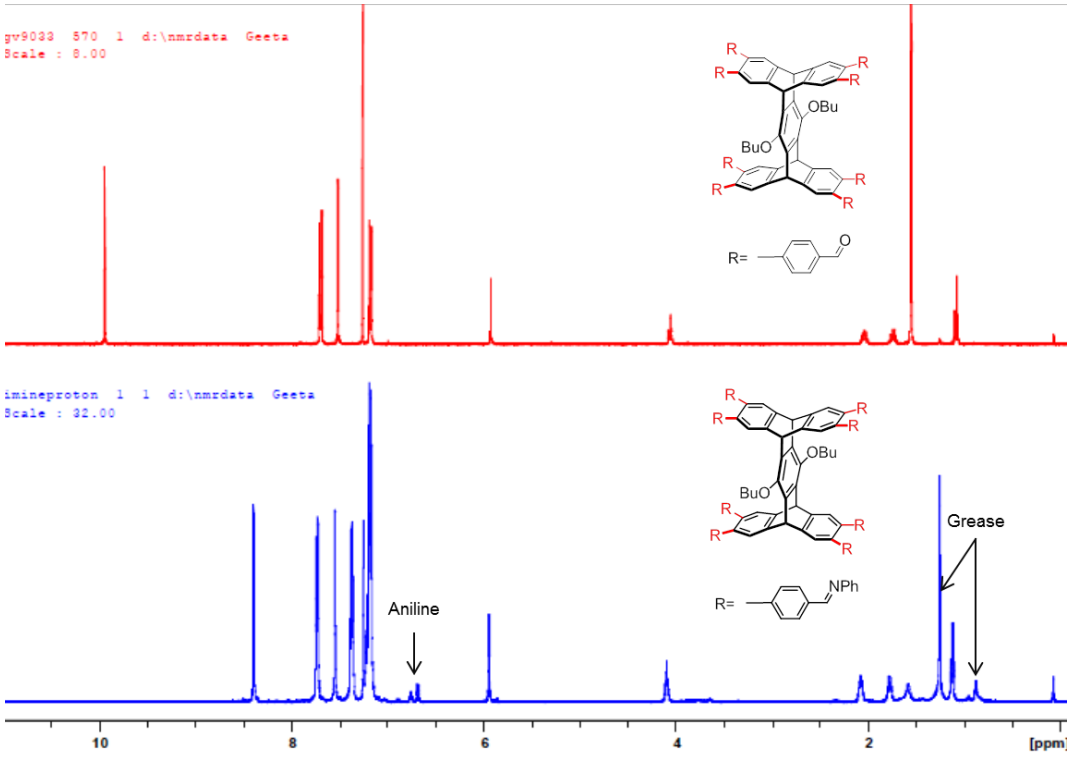

Figure 5.47 ^{1}H NMR (400 MHz, $CDCl_3$) of compound **5.4p**.

5.7 Notes and References

(1) Hart, H.; Bashir-Hashemi, A.; Luo, J.; Meador, M. A. *Tetrahedron* **1986**, *42*, 1641–1654.

(2) (a) Breen, C.; Rifai, S.; Bulovic, V.; Swager, T. M. *Nano Lett.* **2005**, *5*, 1597–1601. (b) Yang, J.-S.; Yan. J.-L. *Chem. Commun.* **2008**, *13*, 1501–1512.

(3) (a) Thomas, S. W.; Joly, G. D.; Swager, T. M. *Chem. Rev*. **2007**, *107*, 1339–1386. (b) Yang, J.-S.; Swager, T. M. *J. Am. Chem. Soc*. **1998**, *120*, 5321–5322. (c) Yang, J.-S.; Swager, T. M. *J. Am. Chem. Soc*. **1998**, *120*, 11864–11873. (d) Lin, C.-J.; Chen, C.-Y.; Kundu, S. M.; Yang, J.-S. *Inorg. Chem.* **2014**, *53*, 737–745. (e) Ghosh, K. R.; Saha, S. K.; Gao, J. P.; Wang, Z. Y. *Chem. Commun.* **2014**, 716–718.

(4) Cao, J.; Lu, H.-Y.; Chen, C.-F. *Tetrahedron* **2009**, *65*, 8104–8112.

(5) (a) Crane, A.; White, N.; MacLachlan, M. *Cryst. Eng. Comm.* **2015**, *17*, 4912–4918. (b) Tsui, N. T.; Paraskos, A. J.; Torun, L.; Swager, T. M.; Thomas, E. L. *Macromolecules* **2006**, *39*, 3350–3358.

(6) (a) Hughs, M.; Jimenez, M.; Khan, S.I.; Garcia-Garibay, M. A. *J. Org. Chem.* **2013**, *78*, 5293–5302. (b) Sun, W.-T.; Huang, Y.T.; Huang, G.-J.; Lu, H.-F.; Chao, I.; Huang, S.-L.; Huang, S.-J.; Lin, Y.-C.; Ho, J.-H.; Yang, J.-S., *Chem. Eur. J*. **2010**, *16*, 11594–11604. (c) Kao, C.-Y.; Lu, H.-F.; Chao, I.; Yang, J.-S. *Org. Lett.* **2014**, *16*, 6100–6103. (d) Ma, Y-X.; Meng, Z.; Chen, C.-F. *Org. Lett.* **2014**, *16*, 1860–1863.

(7) (a) Cao, J.; Zhu, X.-Z.; Chen, C.-F. *J. Org. Chem.* **2010**, *75*, 7420–7423. (b) Cao, J.; Lu, H.-Y.; Xiang, J.-F.; Chen, C.-F. *Chem. Commun*. **2010**, 3586–3588. (c) Supur, M.; Kawashima, Y.; Ma, Y.-X.; Ohkubo, K.; Chen, C.-F.; Fukuzumi, S. *Chem. Commun*. **2014**, 15796–15798. (d) Jiang, Y.; Chen, C.-F. *Eur. J. Org. Chem*. **2011**, *32*, 6377–6403. (e) Mosca, L.; Koutník, P.; Lynch, V. M.; Zyryanov, G.V.; Esipenko, N.A.; Anzenbacher, P. *Cryst. Growth. Des*. **2012**,

12, 6104–6109. (f) Cao, J.; Guo, J.-B.; Li, P.-F.; Chen, C.-F. *J. Org. Chem.* **2011**, *76*, 1644–1652. (g) Cao, J.; Lu, H.-Y.; You, X.-J.; Zheng, Q.-Y.; Chen, C.-F. *Org. Lett.* **2009**, *11*, 4446–4449. (h) Cao, J.; Jiang, Y.; Zhao, J.-M.; Chen, C.-F. *Chem. Commun.* **2009**, 1987–1989.

(8) Ma, Y.-X.; Meng, Z.; Chen, C.-F. *Synlett* **2015**, *26*, 6–30.

(9) Shalaev, V. K.; Getmanova, E. V.; Skvarchenko, V. R. *Zh. Org. Khim*. **1976**, *12*, 191.

(10) (a) Hilton, C. L.; Jamison, C. R.; Zane, H. K.; King, B. T. *J. Org. Chem*. **2009**, *74*, 405–407. (b) Kissel, P.; Murray, D. J.; Wulftange, W. J.; Catalano, V. J.; King, B. T. *Nat. Chem.* **2014**, *6*, 774–778. (c) Lee, C.-H.; Filler, R.; Lee, J.; Li, J.; Mandal, B. K. *Renew. Energy* **2010**, *35*, 1592–1595. (d) Ghanem, B. S.; Hashem, M.; Harris, K. D. M.; Msayib, K. J.; Xu, M.; Budd, P. M.; Chaukura, N.; Book, D.; Tedds, S.; Walton, A.; McKeown, N. B. *Macromolecules* **2010**, *43*, 5287–5294. (e) Xie, T. Z.; Guo, K.; Huang, M.; Lu, X.; Liao, S. Y.; Sarkar, R.; Moorefield, C. N.; Cheng, S. Z. D.; Wesdemiotis, C.; Newkome, G. R. *Chem. Eur. J.* **2014**, *20*, 11291–11294.

(11) Shalaev, V. K.; Getmanova, E. V.; Skvarchenko, V. R. *Zh. Org. Khim*. **1976**, *12*, 191.

(12) (a) Segura, J. L.; Mancheño, M. J.; Zamora, F. *Chem. Soc. Rev.* **2016**, *45*, 5635–5671. (b) Waller, P. J.; Gándara, F.; Yaghi, O. M. *Acc. Chem. Res.* **2015**, *48*, 3053–3063. (c) Uribe-Romo, F. J.; Hunt, J. R.; Furukawa, H.; Klöck, C.; O'Keeffe, M.; Yaghi, O. M. *J. Am. Chem. Soc.* **2009**, *131*, 4570–4571. (d) Zhang, G.; Presly, O.; White, F.; Oppel, I., Mastalerz, M. *Angew. Chem., Int. Ed.* **2014**, *53*, 1516–1520.

(13) Ghanem, B. S.; Hashem, M.; Harris, K. D.M.; Msayib, K. J.; Xu, M.; Budd, P.M.; Chaukura, N.; Book, D.; Tedds, S.; Walton, A.; McKeown, N. B. *Macromolecules* **2010**, *43*, 5287–5294.

(14) Corbett, P. T.; Leclaire, J.; Vial, L.; West, K. R.; Wietor, J.-L.; Sanders, J. K. M.; Otto, S. *Chem. Rev.* **2006**, 106, 3652–3711.

(15) Kerins, F.; O'Shea, D. *J. Org. Chem.*, **2002**, *67*, 4968–4971.

(16) Li, Q.; Rukavishnikov, A.; Petukhov, P.; Zaikov, T.; Keana, J. *Org. Lett.*, **2002**, *21*, 3631–3634.

(17) Kamkaew, A.; Barhoumi, R.; Burghardt, R.; Burgess, K. *Org. Biomol. Chem.*, **2011**, *9*, 6513–6518.

(18) It should be noted that the octavinyl derivative proved to be sensitive to a variety of conditions including high heat, light and SiO_2. As a result, attempts to completely purify the product by traditional column chromatography resulted in drastically depressed yields.